Determination of soil shear modulus at low strain level using an innovative pressuremeter probe : Application to cyclic pile design.

Alexandre Lopes dos Santos

École des Ponts ParisTech

UNIVERSITÉ PARIS-EST

Dissertation presented for the degree of

Doctor of Université Paris-Est

Specialty: Geotechnics

Doctoral school: Sciences, Ingénierie et Environnement (SIE)

Determination of soil shear modulus at low strain level using an innovative pressuremeter probe. Application to cyclic pile design

---

by

Alexandre LOPES DOS SANTOS

Thesis defended June 3rd 2020

Examination committee:

Mr.	**BENOIT Jean**	University of New Hampshire	Referee
Mr.	**EMERIAULT Fabrice**	Université Grenoble Alpes	Referee
Mr.	**FRANK Roger**	École des Ponts Paristech	President
Mr.	**BREUL Pierre**	Université Clermont Auvergne	Examiner
Mr.	**CANOU Jean**	École des Ponts Paristech	Examiner
Ms.	**PALIX Elisabeth**	EDF Renouvelables	Examiner
Mr.	**PUECH Alain**	Fugro France	Examiner
Mr.	**CUIRA Fahd**	Terrasol	Invited
Mr.	**DUPLA Jean-Claude**	École des Ponts Paristech	PhD Supervisor

ABSTRACT

Many civil engineering structures are subjected to cyclic loading of environmental types (e.g. waves or earthquakes) or industrial types (e.g. rails or roads). Some of these constructions are supported by deep foundations (piles), which must resist the vertical or transversal components of the cyclical efforts. In general, this results in degradation of the bearing capacity of the piles by modifying the properties of the soil-structure interface, which should be considered for design. In France, current design methods of deep foundations are based primarily on the results of pressuremeter tests and concern only the monotonous loads. On the other hand, the existing methods enabling the design of piles under axial or lateral cyclic loads are based on soil parameters obtained from laboratory tests, and this approach does not fit in the French daily practice.

This thesis is inserted in the context of the National Project ARSCOP ("*improvement of the ground investigation and the design of geotechnical structures with the use of pressuremeter*"). Its main objective is the development of a new methodology for the design of deep foundations under cyclic loads using the pressuremeter test. However, it has been found that it is not possible to obtain significant soil parameters for the design of this type of structure, namely soil shear moduli at small strain levels, using the pressuremeter testing equipment and the procedures currently available. In this work, we propose the use of an innovative pressuremeter probe, developed by a partner, as well as the testing procedures necessary to reach the proposed goal.

As a first step, we defined a laboratory testing program for the validation of the measurement capabilities of this new device. Tests were carried out in a calibration chamber, in dry Fontainebleau sand specimens, reconstituted at different density indices. Emphasis was placed on determining the shear modulus in a range of small strains, between 10^{-4} and 10^{-2}. Tests have also been carried out to assess the behavior of the soil under repeated cyclic loading. The second part consisted in validating the measurement capabilities of this probe from *in situ* tests. Two reference test sites were chosen, Dunkirk and Merville (dense sands and overconsolidated clays, respectively), on which the soil characteristics, assessed using different ground investigation methods, were previously known. Results of full-scale cyclic axial pile load tests carried out at these sites were also available.

The results obtained with the new pressuremeter device according to the methodology developed in this thesis were then used to illustrate possible engineering applications, with emphasis on the design of piles under axial cyclic loading. The validation was made by comparison with the behavior measured in the pile loading tests available on the reference sites.

RÉSUMÉ

De nombreux ouvrages de génie civil sont soumis à des sollicitations cycliques de type environnementales (houles, séismes) ou industrielles (routiers, ferroviaires). Une partie de ces ouvrages sont réalisés sur fondations profondes (pieux), qui doivent donc reprendre les composantes verticales ou transversales des efforts cycliques. Cela entraîne, en général, une dégradation de la capacité portante des pieux par modification des propriétés de l'interface sol-structure, phénomène qui doit être pris en compte dans le dimensionnement. En France, les méthodes actuelles de dimensionnement des fondations profondes sont basées principalement sur les résultats des essais pressiométriques et ne concernent que les sollicitations monotones. En revanche, les méthodes existantes permettant le dimensionnement des pieux sous charges cycliques, axiales ou transversales, sont basées sur des paramètres de sol obtenus par essais de laboratoire, et ce type d'approche ne s'inscrit pas dans la pratique quotidienne française.

Cette thèse s'inscrit dans le cadre du Projet National ARSCOP (« nouvelles Approches de Reconnaissance de Sols et de Conception des Ouvrages géotechniques à l'aide du Pressiomètre »). Elle a pour principal objectif le développement d'une nouvelle méthodologie de dimensionnement des fondations profondes sous chargement cyclique à partir du pressiomètre. Cependant, il a été constaté que l'obtention des paramètres du sol significatifs pour le dimensionnement de ce type d'ouvrage, notamment les modules de cisaillement sous faibles taux de distorsion, n'est pas possible avec le matériel d'essai pressiométrique et les procédures actuellement disponibles. Dans ce travail, nous proposons l'utilisation d'une sonde pressiométrique innovante, développée par un partenaire, ainsi que la réalisation de procédures d'essai spécifiques, nécessaires pour atteindre l'objectif proposé.

Dans une première partie, nous avons défini un programme d'essais en laboratoire pour la validation des capacités de mesure de ce nouveau dispositif. Des essais ont été réalisés en chambre d'étalonnage, sur des massifs de sable de Fontainebleau sec, reconstitués à différents indices de densité. L'accent a été mis sur la détermination du module de cisaillement dans une plage de faibles déformations, comprise entre 10^{-4} et 10^{-2}. Des essais ont également été menés pour l'évaluation du comportement du sol sous chargement cyclique répété. Une deuxième partie a consisté à valider les capacités de mesure de cette sonde à partir d'essais *in situ*. Deux sites d'essai ont été choisis, Dunkerque et Merville (sables denses et argiles surconsolidées, respectivement), sur lesquels les caractéristiques du sol, évaluées à partir de différentes méthodes d'investigation, étaient connues. Des essais de chargements cycliques axiaux de pieux à échelle réelle avaient également été réalisés sur ces sites.

Les résultats obtenus avec le nouveau dispositif pressiométrique suivant la méthodologie développée dans cette thèse ont ensuite été utilisés pour illustrer les possibles applications à l'ingénierie, en particulier pour le dimensionnement des pieux sous chargement cyclique axial. La validation a été faite par comparaison avec le comportement mesuré dans les essais de chargement de pieux disponibles sur les sites de référence.

ACKNOWLEDGEMENTS

This work was carried out within the scope of a CIFRE Industry-Academia convention between Fugro France and Laboratory Navier at École des Ponts ParisTech, supported by the French National Association for Research and Technology (ANRT). The work was partly funded by the French Project ARSCOP. I would like to express my gratitude to every person who contributed to make this project a reality.

I would like to thank Dr. Jean-Claude Dupla for supervising this work, supporting and helping me to find the best direction for my thesis, for his patience and for teaching me to be patient and persevere with the experiments. I am grateful to Jean Canou, who co-supervised this work and provided precious and rigorous scientific advice.

Special thanks to Dr. Alain Puech, my Fugro supervisor, who guided me with mastery throughout the project and encouraged me in the most difficult moments. His advice was fundamental for the completion of this work and a source of inspiration for becoming the professional I want to be.

I would like to thank Pierre Vergobbi, Fugro France Director, representing all colleagues who have warmly welcomed me in the company. Special thanks to my GeoConsultancy workmates, who were very supportive since my arrival. I would like to express my gratitude to Michel Garnier for sharing his deep practical experience with the pressuremeter test, and to Jean-François Barral for the support provided during the *in situ* campaigns.

I would like to thank CERMES technical staff, Emmanuel De Laure, Baptiste Chabot, Marine Lemaire, Xavier Boulay and Loïc Lesueur for the support with the laboratory experiments. Many thanks to Thanh Tung Nguyen and Mohamad Abdulrahman Hussein for the useful work developed during their master's research internship, and to Ahn Kyeung-Hye for the work done during her research initiation project.

Thanks to Fahd Cuira and Dr. Philippe Reiffsteck, members of the supervising committee, who followed the development of this work and provided valuable contributions to its progress. I'd also like to thank all the partners of ARSCOP project for the rich and passionate discussions we shared.

Many thanks to Francis Cour, whose ingenious insights were a key to the success of this work. Thanks for encouraging me "getting down to business" and for showing me how to transform notebook sketches into reality.

I strongly appreciate and am grateful for the detailed reviewing of this manuscript by the referees, Prof. Fabrice Emeriault and Prof. Jean Benoit. I also acknowledge the very kind participation of Prof. Roger Frank, president of the examination committee, Prof. Pierre Breul and Elisabeth Palix, examiners.

Last, but not least, many thanks to those who have been with me all this way long. To my childhood friends, even though they still don't know what I do. To my wife Larissa for her love, friendship, unlimited support and encouragement during all the steps of this work. To my parents and my brother, my deep foundations, who have been and will always be by my side.

LIST OF SYMBOLS AND ABBREVIATIONS

Latin symbols

Symbol	Meaning	Units
a	Internal radius of a thick cylinder (cylindrical cavity expansion)	[m]
A	Cyclic pressure amplitude of series performed with the pressuremeter	[Pa]
A_b	Cross-sectional area of the pile tip	[m^2]
B	Pile diameter	[m]
b	External radius of a thick cylinder (cylindrical cavity expansion)	[m]
C_u, s_u	Undrained shear strength	[Pa]
D_{ef}	Equivalent embedment depth of the pile	[m]
D_t	Degradation factor	[-]
E	Young modulus (linear elasticity)	[Pa]
E_b	Elasticity modulus of the pile	[Pa]
E_M	Ménard modulus	[Pa]
E_{uo}	Elasticity modulus evaluated from unloading curve	
E_{ro}	Elasticity modulus evaluated from reloading curve	
f	Frequency of a regular cyclic loading	[Hz]
f_{soil}	Soil-structure interaction coefficient that depends only on the soil type (AFNOR, 2012)	[-]
G	Shear modulus (linear elasticity)	[Pa]
G_0 or G_{max}	Maximum shear modulus	[Pa]
G_c	Cyclic shear modulus calculated between two apexes of a loop	[Pa]
G_R	Shear modulus during reload	[Pa]
G_U	Shear modulus during unload	[Pa]
G_{UR}	Shear modulus for unload-reload (equivalent to G_c)	[Pa]
G_P	Pressuremeter modulus	[Pa]
$G_{corr}(p_{r,c})$	Shear modulus corrected for probe compliance	[Pa]
$G_{meas}(p_{r,c})$	Shear modulus evaluated from test in soil in a loop starting at a $p_{r,c}$ pressure	[Pa]
G_{ref}	Reference shear modulus obtained for a reference stress p'_{ref}	[Pa]
G_s	Soil elementary secant shear modulus	[Pa]
$G_{syst}(p_{b,L_i})$	Equivalent probe stiffness obtained in the compliance test, for a loop performed at a given p_{b,L_i} pressure	[Pa]
G_t	Soil elementary tangent shear modulus	[Pa]
h	Depth below the pile head	[m]
I_D	Soil density index	[-]
I_r	Rigidity index ($I_r = G/s_u$)	[-]
k_n	Normal stiffness of an interface	[N/m^3]
k_q	Initial slope of the tip resistance mobilization function (q-z)	[N/m^3]
k_t	Initial slope of the skin friction mobilization function (t-z)	[N/m^3]
k_p	Bearing capacity factor (for shallow or deep foundations)	[-]
L	Pile length	[m]
N	Number of cycles	[-]
N_{eq}	Equivalent number of cycles that leads to a given damage level	[-]
P or p	Net pressure applied to the cavity wall	[Pa]
$p_{b,Li}$	Probe internal pressure at start of loop i	[Pa]

Symbol	Meaning	Units
$p_{cav}, p_{cav,u}$	Pressure applied to the cavity wall before the beginning of the unload	[Pa]
$p_{cav,r}$	Pressure applied to the cavity wall before the beginning of the reload	[Pa]
p'_{cav}	Effective pressure applied to the cavity wall ($p'_{cav} = p_{cav} - u$)	[Pa]
p_l	Pressuremeter limit pressure	[Pa]
p^*_l	Pressuremeter net limit pressure	[Pa]
p^*_{le}	Pressuremeter equivalent net limit pressure	[Pa]
p_1, p_2	Cavity pressures delimiting the beginning and the end of the "pseudo elastic" phase in pressuremeter tests	[Pa]
p_f	Pressuremeter creep pressure	[Pa]
p'	Mean effective stress	[Pa]
p_0	Pressure at an infinite distance from the cavity walls	[Pa]
p_{ave}	Average cavity pressure applied during pressuremeter cyclic loading	[Pa]
p_{min}	Minimum cavity pressure applied during pressuremeter cyclic loading	[Pa]
p_{max}	Maximum cavity pressure applied during pressuremeter cyclic loading	[Pa]
p_{ref}	Reference stress	[Pa]
Q_c, Q_{cyc}	Half amplitude defined for a regular cyclic loading	[N]
Q_{ave}, Q_{mean}	Mean load defined for a regular cyclic loading	[N]
Q_{max}	Maximum load defined for a regular cyclic loading	[N]
Q_{min}	Minimum load defined for a regular cyclic loading	[N]
$Q_{(h)}$	Effort at a depth *h* below the pile head	[N]
Q_0	Effort at the pile head	[N]
Q_b	Effort at the pile base	[N]
$q_{b,ult}$	The maximum value of the tip resistance depending on the type of soil and pile	[Pa]
q_b	The pile tip resistance	[Pa]
$q_{s,ult}$	The maximum value of the unit skin friction depending on the type of soil and pile	[Pa]
q_s	The pile axial unit skin friction	[Pa]
R	Ultimate bearing capacity	[N]
R_p	Radius of the plastic zone around the cavity	[m]
S	Area of the foundation	[m^2]
S_b	Area of the pile tip	[m^2]
s_0	Displacement at the pile head	[m]
s_b	Relative displacement between the soil and the pile tip	[m]
s_s	Relative displacement between the soil and the pile shaft	[m]
T	Period of a regular cyclic loading	[s]
V	Probe volume	[cm^3]
V_1, V_2	Probe volume associated to the beginning and the end of the "pseudo elastic" phase in pressuremeter tests	[cm^3]
V_c	Half amplitude of the vertical cyclic loading applied at the pile head	[N]
V_m	Mean vertical cyclic loading applied at the pile head	[N]
V_{uc}	Pile ultimate resistance to static compression	[N]
V_{ut}	Pile ultimate resistance to monotonic tension	[N]
u	Pore pressure	[Pa]
u_r	Displacement at a radial distance *r* from the cavity wall	[m]

Greek symbols

Symbol	Meaning	Units
α	Ménard "rheological coefficient" for soil-structure interaction formulas	[-]
$\alpha_{pile-soil}$	Soil-structure interaction coefficient that depends on the soil and the pile type (AFNOR, 2012)	[-]
δ_{cv}	Friction angle at the soil–pile interface	[°]
$\varepsilon_{c,max}$ *or* ε_a	Maximum cavity strain at a given unload-reload loop	[-]
$\varepsilon_{c,min}$ *or* ε_a	Minimum cavity strain at a given unload-reload loop	[-]
ε_c	Cavity strain (equals $\Delta r/R_0$)	[-]
ε_s	Axial strain in triaxial undrained test (Jardine, 1992)	[-]
ε_v	Volumetric strain	[-]
ε_θ	Orthoradial strain	[-]
φ'	Soil internal friction angle	[°]
ϕ	Probe external diameter	[m]
γ	Shear strain in an element of soil under homogeneous conditions	[-]
γ_{av}	Average shear strain in the soil mass around the cavity	[-]
γ_c	Shear strain at the cylindrical cavity wall	[-]
ν	Poisson's coefficient	[-]
σ_h' ; σ_h	Horizontal effective and total stress, respectively	[Pa]
σ'_{h0}	Horizontal effective stress at-rest	[Pa]
σ_{av}'	Average effective stress around the cavity (used similarly to *p'*)	[Pa]
σ_r' ; σ_r	Radial stress, effective and total, respectively	[Pa]
σ'_{r0}	Effective radial stress applied to an interface	[Pa]
σ_v' ; σ_v	Vertical effective and total stress, respectively	[Pa]
σ_θ' ; σ_θ	Ortho-radial stress, effective and total, respectively	[Pa]
$\Delta\sigma'_r$	Variation in the effective radial stress applied to an interface	[Pa]
τ_{cy}	Cyclic shear stress	[Pa]
$\tau_{max,stat}$	Maximum shear stress under monotonic loading	[Pa]
τ_{rf}	Interface friction	[Pa]

Abbreviations

Abbreviation	Meaning
AFNOR	French standards association. *Association Française de Normalisation*
API	American Petroleum Institute
ARSCOP	French joint industry project on improvements on the pressuremeter test. *nouvelles Approches de Reconnaissance des Sols et de Conception des Ouvrages géotechniques avec le Pressiomètre*
ASTM	American society for testing material
CEN	European committee for standardization. *Comité Européen de normalisation*
CFMS	French Society for Soil Mechanics and Geotechnical Engineering
CNS	Constant normal stiffness test
CPT	Cone Penetration Test
CU	Control unit
DSS	Direct simple shear test
EC7	Eurocode seven
EPWP	Excess pore water pressure
FEM	Finite element model
ICL	Imperial College of London
ICP	Imperial College pile design method
LCPC	Past *Laboratoire Central des Ponts et Chaussées*. Currently *Université Gustave Eiffel*
LVDT	Linear Variable Differential Transformer
NGI	Norwegian Geotechnical Institute
SOLCYP	French joint industry project on piles under cyclic loading. *Sollicitations cycliques sur pieux*
PWP	Pore water pressure
SPT	Standard Penetration Test
PIP	Pushed-in pressuremeter test
SBP	Self-bored pressuremeter test
PMT	Ménard Pressuremeter test

Term definition

Abbreviation	Meaning
Loop	Single unload-reload path
Cycle	Series of sequentially repeated loops
Pressure-hold step	Step in which the cavity pressure is kept constant during a certain period of time
Creep	Deformation of the soil over time under a constant stress field. This definition is different from the usual “pressuremeter creep pressure”
Time-dependent behavior	Behavior that varies as a function of the duration of the applied load. It can be originated by creep, consolidation, plastic flow, or others.
Virgin loading	Loading path at which soil experiments a given stress state for the first time
Pre-sheared	Soil that has experienced a higher loading level with respect to the current loading.

SUMMARY

GENERAL INTRODUCTION

Most civil engineering structures are subjected to variable actions, generically qualified as cyclic loads. For an important part of these structures, such as bridges and buildings, the ratio between variable and permanent actions is relatively small and do not lead to a consequence in design. However, recent developments in the domains of transportation and renewable energy, have led to a growth in the construction of highly optimized structures in rough environments, both offshore and onshore. This is specially the case of wind turbines and offshore platforms. For these structures, the cyclic component of loading is significant, and its transmission to the structure's foundation can lead to a modification of the soil-structure interaction properties. As a consequence, a reduction in the bearing capacity and changes in stiffness may take place and must be taken into account for design.

The design of deep foundations under cyclic loading, in axial or transversal directions, requires two sets of parameters: the first is identical to the one used for the design of piles under monotonic loads; the second is specific to cyclic repeated loads. Design methods for monotonic loads are well established and included in the most renowned design standards, such as the Eurocode 7. They are based either on *in situ* or on laboratory tests, for which the choice may vary according to local practice. French practice concerning pile design is mainly based on *in situ* tests, especially the Ménard pressuremeter, for which a detailed calculation method is standardized and available for engineers. On the other hand, the determination of cyclic pile design parameters is currently widely developed only through laboratory tests, as described in SOLCYP recommendations (Puech and Garnier, 2017). Despite cyclic pressuremeter tests have

been mentioned as a potentially adequate approach, there are only few developments on this subject and no technical recommendations are available for practitioners.

Pressuremeter tests are cylindrical cavity expansion tests which basically provide deformation and failure parameter for the soil. When the test is performed according to current standards, the resulting parameters are the so-called Ménard pressuremeter modulus E_M and the pressuremeter limit pressure p_l. The Ménard modulus is determined under monotonic conditions or in a single unloading-reloading loop. It can be associated to a shear strain level of approximately 10^{-2} and is much lower than the actual elasticity modulus of the soil, defined at very small strains. The limit pressure is conventionally defined as the pressure leading to doubling the cavity volume, corresponding to very high strains, frequently associated to failure. French researchers and practitioners were able to establish robust foundation design methods based on direct semi-empirical correlations between these parameters and soil-structure interaction parameters. These design rules were calibrated on large databases of full-scale foundation load tests performed on sites characterized with standard pressuremeter tests. They provide a satisfying evaluation of ultimate bearing capacity and load-displacement response of current foundations under monotonic loading.

The response of some geotechnical structures in service is however mainly controlled by the soil stiffness in small shear strain range, from 10^{-4} to 10^{-3}. This is especially true for foundations under cyclic loading, not covered by the traditional design approach with the pressuremeter. Yet, the determination of stiffness parameters in this strain range cannot be done using standard Ménard testing equipment and procedures and currently calls for high quality laboratory tests. Some more sophisticated pressuremeter type probes, equipped with punctual cavity strain measurement sensors, can provide measurements in the small strain range, but they cannot expand at sufficiently large deformations to bring most soils to failure. In practice, this reflects a lack of testing equipment able to measure, in the same test, moduli at small strains, and plasticity properties, at intermediate and high strains.

This Ph.D. thesis has been developed within the context of the French National Project ARSCOP ("*improvement of the ground investigation and the design of geotechnical structures with the use of pressuremeter*"), which is a collaborative research and development project gathering public and private actors of the French geotechnical

community, aiming at improving pressuremeter testing equipment, implementation protocols and procedures for design applications. The main objective of this thesis is to contribute to the development of a new methodology for the design of deep foundations under cyclic axial loadings using the pressuremeter test. In this work, it is demonstrated that the use of an innovative pressuremeter probe, coupled with enhanced testing and interpretation procedures, make it possible to assess soil properties representative to cyclic pile design. Focus is put on the determination of the soil shear modulus at small strain level and its dependency on shear strain and average stress levels. This document is divided in four chapters.

Chapter one presents a bibliographic review on pressuremeter testing and its application to geotechnical design. The general aspects of the traditional approach based on Ménard pressuremeter tests are presented, as well as its intrinsic limitations with respect to more recent engineering needs. Then, the theoretical background related to the determination of the elastic properties of soil from cavity expansion tests is reviewed and confronted to the practical aspects that have historically rendered difficult their obtention from pressuremeter tests.

Chapter two starts by presenting the limitations of the most common pressuremeter probes with respect to the objectives proposed within this work. Then, an innovative probe considered as being potentially able to bridge this gap is selected. In this chapter, the experimental procedures performed in the laboratory to validate the measurement capabilities of this probe are presented. The experimental setup is described, including the probe itself, specific calibration devices developed during this thesis and the laboratory calibration chambers. The tested reference soil (Fontainebleau sand) as well as the testing procedures are detailed.

Chapter three describes a further step of this validation program, which consisted in evaluating the previously mentioned equipment and procedures to perform *in situ* tests under real operational conditions. Two sites have been chosen for carrying out this investigation campaign: Dunkirk (dense sands) and Merville (overconsolidated clays). In this chapter, the experimental procedures, equipment and set up specific to the *in situ* application are presented. The geotechnical characterization of both sites is described based on previous ground characterization campaigns presented in the literature.

Chapter four is dedicated to the application of the results obtained in Chapter 3 to pile axial design. Focus is put on the evaluation of pile head stiffness, local load transfer relationships and overall pile stability under cyclic loading.

Three appendixes complement the content of the described chapters. **Appendix A** presents the existing pressuremeter testing equipment, its evolution since its invention, the applicable testing standards and its limitations with respect to the goals of this work. **Appendix B** presents qualification tests performed using the pressuremeter probes most commonly used in French practice, aiming at verifying their applicability for assessing soil properties at small strain levels. Finally, **Appendix C** presents the results of the *in situ* tests performed according to the procedures developed in this thesis at Dunkirk and Merville reference sites.

This manuscript ends with a general conclusion and a presentation of perspectives for future research.

CHAPTER 1

BIBLIOGRAPHIC REVIEW OF PRESSUREMETER TESTS AND THEIR APPLICATION TO GEOTECHNICAL DESIGN

1.1 GENERAL ASPECTS

Design methods for foundations under monotonic loads are well established and included in the most renowned design standards, such as the Eurocode 7 CEN (2004), (2007). They are based either on *in situ* or on laboratory tests, for which the choice may vary country by country. de Cock and Legrand (1997) summarized the most common investigation tests used in European practice on pile design. In France, pile design is mainly based on *in situ* tests, especially the Ménard pressuremeter test (Frank, 2017), for which the detailed calculation method is described in the national application standard (AFNOR, 2012). This is also valid for the design of shallow foundations (AFNOR, 2013a). One of the main advantages frequently put forward regarding the use of the pressuremeter test for foundation design is that it gives both a failure and a deformation parameter of the soil. While the failure parameter enables the determination of the ultimate limit capacity of the structures, the deformation parameter can be used to assess the serviceability state and to perform settlement calculations.

At present, however, the design of certain structures cannot be done using the standard pressuremeter test. According to Puech and Garnier (2017), the determination of the parameters required for the design of piles under cyclic loading is currently widely developed most through laboratory tests. Despite cyclic pressuremeter tests have been pointed out to be a potentially adequate approach for obtaining parameters on site (Puech and Brucy (1982), Little and Briaud (1988)), there are only few developments on this topic and no technical recommendations are available for practitioners.

A brief review of the general aspects on pressuremeter tests as well as a review of the existing methods for the design of foundations under monotonic and cyclic loads are presented in the next sections. Focus is given on French practice and on the assessment of soil moduli using this investigation method, and how this parameter is used in the design.

1.1.1 General aspects of the pressuremeter test

According to Baguelin *et al.* (1978), the concept of an *in situ* cavity expansion test in soil was first proposed by Kögler in 1933. However, the apparatus nowadays known as the pressuremeter and most of the traditional procedures that enable obtaining soil parameters applicable to the design of geotechnical structures were due to the work of Louis Ménard (1956), who applied for the first patent of the pressuremeter in 1955.

The general principle of the pressuremeter test is to insert a cylindrical probe equipped with an expandable flexible membrane into a borehole and to expand the probe according to a predefined loading program. The soil responds to the applied load, yielding a cavity pressure versus cavity volumetric strain curve, also called cavity expansion curve. This curve can be interpreted through an analytical theoretical background, enabling the determination of deformability and strength properties of the tested soil. The curve can also be interpreted within a semi-empirical framework, considering the geological context of the site and taking into account existing correlations, in order to obtain design parameters for geotechnical structures, such as foundations, retaining walls and embankments.

Since its invention, the pressuremeter has proven to be a useful tool for geotechnical site investigation, no matter the approach used for its interpretation: theoretical or semi-empirical. After Ménard's invention, different testing equipment have been developed as well as different probe insertion techniques, loading protocols and interpretation methods. The Ménard pressuremeter test is one amongst other cylindrical cavity expansion tests, reason for which, in this text, the term "pressuremeter test" is therefore generalized to "cavity expansion test" covering a wider domain, such as that of the flexible dilatometers. According to Ladanyi (1987), the first dilatometer tests were described in 1964 and in 1966.

Cylindrical cavity expansion tests are performed according to the simplified scheme shown in Figure 1.1a. A simplified cross-section and a photo of a standard pressuremeter probe are presented in Figure 1.1b and c. Carrying out a standard pressuremeter test requires the following successive steps:

- Drilling a borehole in the ground;
- Inserting a cylindrical expandable membrane (probe) into the cavity formed by the borehole;
- Carrying out the probe expansion by means of a pressure-volume control unit (C.U.) connected to the probe via tubing;
- Keeping records of cavity pressure and cavity volumetric deformation during the expansion test.

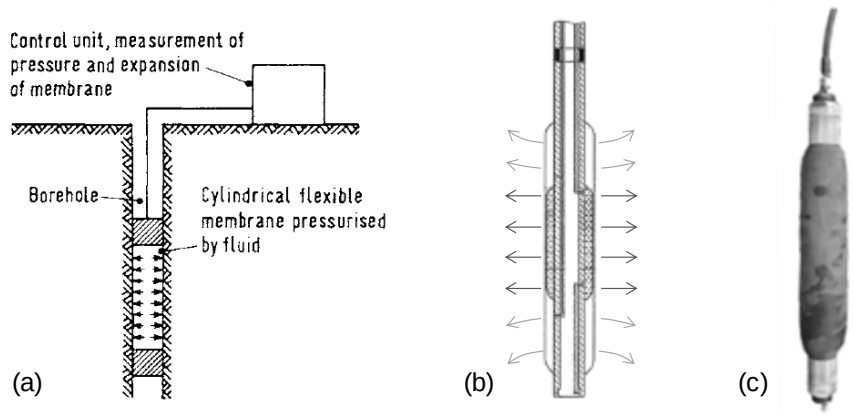

Figure 1.1 – General principle of a cylindrical cavity expansion test. Adapted from Mair and Wood (1987)

This general procedure can be applied both for soils and rocks since the testing equipment, the loading protocol and the interpretation procedures are adapted to the type of soil or rock to be tested. Three main categories of pressuremeter tests can be distinguished according to the probe installation method:

- Pre-bored tests (usually called Ménard tests, or simply PMT), in which the probe is inserted into a pre-drilled cavity in the soil. The main references are presented by Baguelin et al. (1978), Mair and Wood (1987), Briaud (1992) and Clarke (1995);
- Self-boring tests (SBP), in which the cavity is created by the probe itself, as it advances into the soil. The self-boring pressuremeter was first conceived in France (Jézéquel, 1968, according to Baguelin *et al.* (1978)) but got great

acceptance in England (Wroth and Hughes, 1972) especially for tests in clays. This system was conceived to mitigate the problems of disturbance of the initial state due to borehole drilling;

- Pushed-in tests (PIP), in which the probe is pushed into the ground. First developments took place in France in 1982 with the pressio-penetrometer for offshore applications and further with the works of Withers et al. (1986) about the full displacement pressuremeter, a Dutch and British cooperation.

Two main types of probes exist. They can be distinguished according to the number of expandable cells: tri-cellular probes (generally called Ménard probes), and monocellular probes. Independently from how the probe is mechanically assembled, the assessment of cavity deformation can be done in two ways:

- By measuring the volume of a low compressibility fluid (such as water or oil) injected into the measuring cell;
- By local displacement measurement using sensors installed inside the probe. Different technologies exist for those sensors (calipers, "feeler arms", inductance).

In both cases, the assessment of cavity stress and strain is not direct and requires probe calibration and supplementary corrections to account for the system compressibility, membrane inertia, hydraulic head and eventually pressure losses. Standard procedures for probe calibration and corrections are given by AFNOR (2015).

The pressure-volume control units are devices that enable injecting the pressurized fluid into the probe and controlling it according to the desired testing protocol. These devices have significantly evolved since the invention of cavity expansion tests, passing from manual control to full automatization, comprising data acquisition. *Appendix A* presents a review on the devices most commonly used at present.

The loading program can be either pressure or volume controlled, by application of successive increments, or at a constant rate of pressure or volume change. In the case of the Ménard pressuremeter test, the loading program is standardized and is applied in 60 seconds pressure-hold steps, as presented in Figure 1.2(a) (AFNOR, 2015). The soil response is presented in Figure 1.2(b), from which one can distinguish three phases: phase (P1) a recompression part on the beginning of the expansion curve, phase (P2) a

quasi-linear portion usually called “pseudo-elastic” part, and phase (P3) a plastic phase, characterized by volumetric changes over the constant-load steps (time dependent). The increase in volume variations over time that can be observed by analyzing the usually called “creep curve” (2) defines the so-called pressuremeter creep pressure, p_f. It should be noted that in pressuremeter practice, the simplified definition of one single value of “creep pressure” to the soil is conflictual with respect to the rheological definition of creep in terms of material mechanics, which in this case corresponds to the variation of the strain state at constant stress field. The Ménard pressuremeter modulus E_M is calculated from the slope of the “pseudo-elastic” phase (phase P2 in curve (1), limited by pressure and volume values p_1, V_1 and p_2, V_2). The conventional pressuremeter limit pressure p_l is calculated as the pressure corresponding to doubling the initial cavity volume. It can be either directly measured or calculated by extrapolation. Detailed methods for deriving those parameters are given by AFNOR (2015). The testing procedure can also include one unload-reload loop, to be performed according to AFNOR (1999).

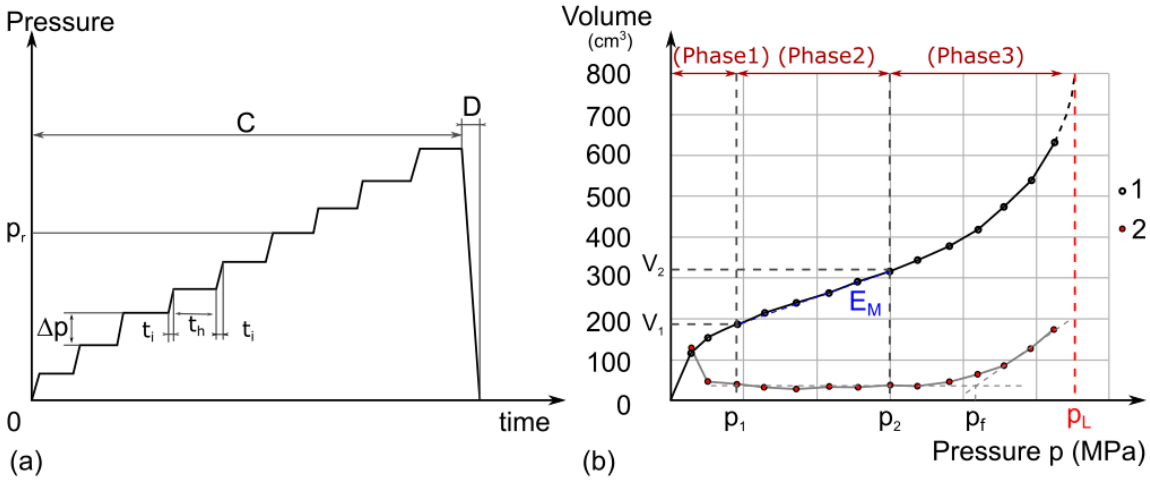

Figure 1.2 – (a) Ménard pressuremeter test loading program. (b) Representation of the general soil response to Ménard pressuremeter tests. Adapted from AFNOR (2015).

Other loading protocols exist for flexible dilatometer tests according to AFNOR (2013b), including the possibility to perform more than one pressure loop, to vary the pressure-change ratio, and to perform longer pressure-hold steps to assess creep or consolidation properties. According to this standard, the choice of the loading program should be done in function of the engineering properties needed.

1.1.2 General aspects of the traditional foundation design approach using pressuremeters

The application of pressuremeter test results to the design of shallow and deep foundations began a few years after the invention of the test by Ménard. It was found at that time that the derivation of intrinsic soil mechanics properties, such as cohesion, friction angle and moduli, using the pressuremeter was not satisfactory. According to Baguelin *et al* (1978), Ménard and his co-workers have postulated that the cavity expansion loading test could be considered as an analogue of a reduced scale foundation test. Based on this insight, numerous full-scale foundation tests have been performed on sites where pressuremeter tests were also available. By cross correlating the pressuremeter test results with the foundation behavior, it was concluded that the pressuremeter parameters could be directly used for the determination of the foundation bearing capacity. In this manner, the first design equations and charts relating pressuremeter results and bearing capacity of foundations appeared in the early 60's (Ménard and Rousseau (1962), Ménard (1963), (1965)). The design rules presented in the technical document established by Ménard (1967), most known as the "D60 notice", gained great acceptance amongst practitioners and form the basis of the method still present in the French standards for the application of the Eurocode 7. AFNOR (2012), (2013a) includes a table presenting a conventional soil classification criterion according to values of pressuremeter limit pressure. For soil-structure interaction problems including settlement calculation, semi-empirical approaches exist directly based on the use of the Ménard modulus. Those relationships usually include the so-called "rheology coefficient" (α, Table 1.1 and Table 1.2), which is an empirical parameter first introduced by Ménard and Rousseau (1962) for replacing the elasticity modulus by the pressuremeter modulus in the analytical solution of a semi-spherical foundation. According to these authors, α can be expressed as a relationship between pressuremeter modulus and unload-reload modulus.

Frank et al. (2019) present the design methods currently used for shallow and deep foundations in France. The relevant parameters that can be obtained using pressuremeter tests are synthesized in the next sections. There are many other methods for the evaluation of foundation behavior based on other types of *in situ* or laboratory tests. These methods are not discussed in this work.

Table 1.1 – "Rheological coefficient" α used for empirical settlement calculation using the Ménard pressuremeter modulus

Type	Peat	Clay		Silt		Sand		Gravel	
	α	E_M/p_l	α	E_M/p_l	α	E_M/p_l	α	E_M/p_l	α
OC, dense		> 16	1	> 14	2/3	> 12	1/2	> 10	1/3
NC	1	9 - 16	2/3	8 - 14	1/2	7 - 12	1/3	6 - 10	1/4
UC, loose		7 - 9	1/2	5 - 8	1/2	5 - 7	1/3		

OC – overconsolidated; NC – normally consolidated; UC – underconsolidated or disturbed

Table 1.2 – "Rheological coefficient" α for rocks

State	α
Slightly fractured	2/3
Normal	1/2
Extremely fractured	1/3
Extremely altered	2/3

1.1.2.1 Shallow foundations

The use of pressuremeter tests for the design of shallow foundations is detailed in the French national application standard of the EC7 by AFNOR (2013a). Pressuremeter test results are used to (1) calculate the equivalent embedment depth of the foundation, (2) calculate the soil's ultimate bearing capacity and (3) calculate settlements. The ultimate bearing capacity is directly related to the net limit pressure (eq. 1.1):

$$R = Sk_p p^*_{le} \tag{1.1}$$

in which S is the area of the foundation, p^*_{le} is the soil's equivalent net limit pressure and k_p is a bearing capacity factor that depends on the conventional type of soil, on the shape of the foundation, and on its embedment depth. Formulas for calculating this coefficient are presented in the same standard.

The evaluation of settlements can be done either by (1) estimating soil's Young modulus using available correlations and then applying elastic solutions for shallow foundations or (2) by direct application of Ménard's empirical approach, which is detailed by AFNOR (2013a), Appendix H. Indicative values of the relationship between the elastic modulus and the Ménard modulus are suggested in the same document and presented in Table 1.3

Alternative approaches have been recently developed to account for the strain-dependent behavior of soils. Hoang et al. (2018) propose that the ratio between

soil's Young's modulus and Ménard pressuremeter modulus be a function of the strain level. This approach results in mathematical relationships between E/E_M and the strain level, for different types of soils. The method has been validated through field measurements of the performance of a raft foundation.

Table 1.3 – Indicative values of soil's Young modulus representative for foundation settlement correlated to Ménard pressuremeter modulus (after AFNOR (2013a))

Soil type	Condition	E/E_M
Clays	Normally consolidated	4.5
	Overconsolidated	3.0
Silts	Normally consolidated	4.5
	Overconsolidated	3.0
Sands	Loose	4.5
	Dense	3.0
Gravel	Loose	6.0
	Dense	4.5

1.1.2.2 Deep foundations

Similarly, the French national application standard of the EC7 for deep foundations, AFNOR (2012), defines the design rules for pile foundations based on pressuremeter tests. Pressuremeter parameters are used to calculate (1) the equivalent embedment depth of the pile, D_{ef}, (2) the ultimate skin friction and tip resistance, and (3) to estimate the stiffness of mobilization functions ("t-z" and "p-y") for soil-structure interaction problems involving axial and transversal displacements (AFNOR (2012), Appendixes L and I, respectively). Aspects related to modelling the axial behavior of piles are discussed in section 1.1.2.3.

The ultimate tip resistance is calculated according to eq. (1.2):

$$R = S_b k_p p_{le}^* \tag{1.2}$$

in which S_b is the cross-section of the pile tip, p_{le}^* is the equivalent net limit pressure near the pile tip and k_p is a bearing capacity factor that depends on the conventional types of soil (similar ones for shallow foundations), and on the type of pile.

The ultimate axial unit skin friction q_s is calculated according to eq. (1.3):

$$q_s = \min\left(\alpha_{pile-soil} \cdot f_{soil}; q_{s,ult}\right) \tag{1.3}$$

in which $\alpha_{pile-soil}$ is a coefficient that depends on the soil and on the pile type, f_{soil} is a coefficient that depends only on the soil type and $q_{s,ult}$ is the maximum value of the unit skin friction, which depends on the type of soil and pile. f_{soil} is a function of the soil's limit pressure, according to eq. (1.4):

$$f_{soil} = (a \cdot p_l^* + b)\left(1 - e^{-c \cdot p_l^*}\right) \tag{1.4}$$

in which *a*, *b* and *c* are parameters that depend on the soil type. Tabulated values for those parameters are presented in AFNOR (2012), Appendix F.

Other parameters can affect the limit capacity of a pile. A complete bibliographic review of the effects of different parameters on the foundation response, such as time after pile installation, previous loading history, mode of loading and loading rate is presented in the SOLCYP recommendations (Puech and Garnier (2017)).

1.1.2.3 Theoretical aspects concerning the modelling of the axial behavior of deep foundations

Pile-soil interaction is usually modelled using one of the following approaches: (1) the load transfer method; (2) the elastic continuum method; (3) numerical modelling, such as the Finite Element Method (FEM).

The load transfer method consists in modelling the pile as a series of elastic elements supported by discrete non-connected (independent) springs. The resistance due to the soil shaft skin friction is represented by axial "*t-z*" springs while the tip bearing is represented by a "*q-z*" spring at the pile base. Those non-linear springs are local representations of the global soil reaction, including the interface and the continuum behavior, as a function of the relative soil-pile displacement. Further details concerning this method are provided in section 1.1.2.4. The method was developed in the 50's (Seed and Reese (1957), Gambin (1963a), Cambefort (1964), and Coyle and Reese (1966)).

The elastic continuum method, presented by Poulos and Davies (1968), is based on the elasticity theory. Solution is obtained by writing the pile-soil equilibrium equation and considering displacement compatibility between them. Pile displacements can be calculated using pile compressibility properties, and soil displacements can be

calculated using Mindlin equations. This method presupposes that the intrinsic elasticity properties of the soil are known.

The finite element method is more complete (and more complex). It consists in discretizing the problem into elements of known properties and known boundary conditions. The soil-structure interaction problem is solved for obtaining equilibrium taking all boundary conditions and all material properties into account. This method is more complex than the others because the properties of the different materials and interfaces (pile, soil and interface properties) must be well characterized prior to any calculation, which is frequently not the case in practical applications. Still, if all the parameters are reliably known, the FEM can be used as a reference solution to validate the other methods.

1.1.2.4 The load-transfer method for monotonic loading

Figure 1.3 presents the force equilibrium around an infinitesimal pile segment. The pile-soil interaction problem can be described by differential equations (1.5) and (1.6):

$$dQ_{(h)} = -\pi B q_{s_{(s_s(h))}} dh \tag{1.5}$$

$$ds_s(h) = -\frac{Q_{(h)}}{E_b S} dh \tag{1.6}$$

in which $Q_{(h)}$ is the axial load at a given pile depth h, B is the pile diameter, q_s is the mobilized skin friction, $s_s(h)$ is the relative pile-soil displacement at a depth h, E_b is the pile's Young modulus and S is its cross-sectional areal. Replacing eq. (1.6) in (1.5) leads to the governing equation (1.7):

$$E_b S \frac{d^2 s_s(h)}{dh^2} - \pi B q_{s_{(s_s(h))}} = 0 \tag{1.7}$$

Equation (1.7) can be solved if the relationship between the shaft skin friction and the relative shaft-soil displacement, or the "t-z" curve, is known. The boundary conditions of the local soil-structure interaction problem are the load applied at the pile head and the "q-z" curve (tip mobilization curve).

In this manner, this method requires that "t-z" and "q-z" springs are known and well calibrated to simulate the complete soil-structure interaction problem. Those curves can be (1) derived from elasticity theory, (2) be fully empirical or semi-empirical or (3) be derived from measurements on full scale instrumented pile load tests. Different types of mobilization curves with different degrees of complexity and number of soil parameters are available in literature.

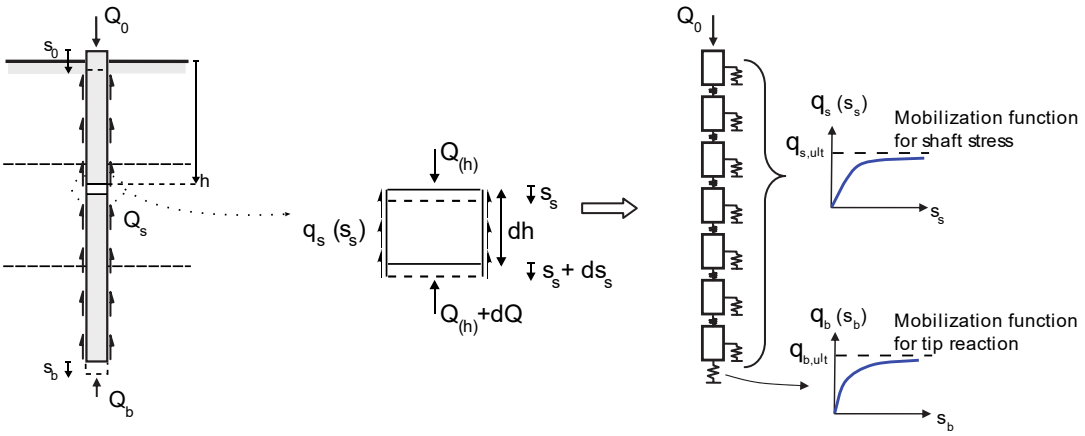

Figure 1.3 – Principle of the load transfer method for axially loaded single piles (figure after Bohn et al. (2017)

In Figure 1.3, s_s and s_b are, respectively, the pile displacements at the shaft and the tip, minus the free ground movements at these same positions, if they exist; $q_{s,ult}$ and $q_{b,ult}$ are the ultimate skin friction and the ultimate tip resistance, respectively.

1.1.2.5 Available load-transfer curves

AFNOR (2012) suggests the use of load transfer curves for piles under monotonic axial loads that have been calibrated on the basis of full-scale pile tests. Frank and Zhao (1982) define relationships between the Ménard modulus, the soil type (classified into fine or coarse) and the stiffness of the mobilization function, k_t for the skin friction and k_q for the tip resistance (Figure 1.4). This method has gained great acceptance in the French practice.

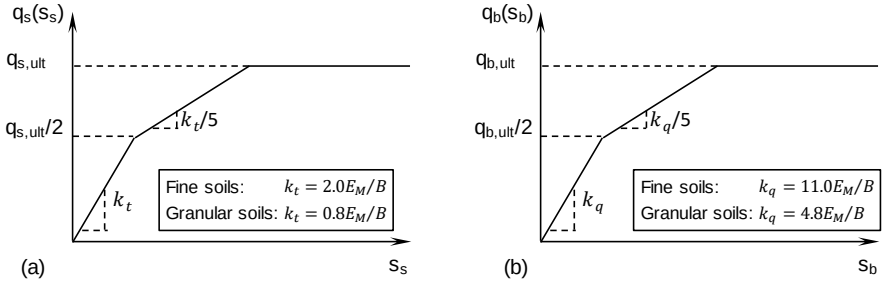

Figure 1.4 – (a) Skin friction; (b) tip resistance mobilization function calibrated from Ménard pressuremeter modulus (after AFNOR (2012))

Other mobilization functions exist; some of them are obtained from analytic elastic solutions and depend on intrinsic soil properties such as the initial shear modulus. Randolph and Wroth (1978) and Baguelin and Frank (1980) have presented bi-linear mobilization functions for which the stiffness is dependent on soil's elasticity properties. The interaction between the pile shaft and the soil can be written as:

$$s_s = \frac{q_s B}{2G}\,\zeta = \frac{q_s B}{2G}\ln\left(\frac{2.5L(1-\nu)}{B/2}\right) \tag{1.8}$$

where the parameters s_s, q_s and B are the same as previously defined, L is the pile length, G is the shear modulus and ν the Poisson's coefficient of the soil. ζ depends on pile geometry and soil elastic properties, as defined above. The pile base mobilization function is derived from linear elasticity solution for a rigid punch, and can be written as:

$$s_b = \frac{q_b A_b (1-\nu)}{2BG}\eta \tag{1.9}$$

where s_b is the relative pile-soil displacement at the pile tip, A_b is the cross-sectional area of the pile tip. The coefficient η has been introduced to take into account the effect of the pile base penetration into the ground. The slope of the mobilization functions can be directly related to the soil shear modulus by coefficients k_t and k_q, depending only on the pile geometry and on the soil's Poisson's coefficient, as follows:

$$\frac{dq_s}{ds_s} = \frac{2G}{B}\frac{1}{\zeta} = k_t G \tag{1.10}$$

with:

$$k_t = \frac{2}{B\ln\left(\frac{2.5L(1-\nu)}{B/2}\right)} \tag{1.11}$$

$$k_q = \frac{8G}{\pi B(1-\nu)\eta} \tag{1.12}$$

Kraft et al. (1981) obtain non-linear theoretical mobilization functions including shear modulus degradation as a function of the stress level. The initial slope of the curve is the same as that described by equations (1.11) and (1.12).

According to Randolph (2013), theoretical methods linking the initial load transfer gradient to the maximum shear modulus of the soil should be privileged where those values are available. However, there has been a historical difficulty in obtaining reliable values of maximum shear modulus from *in situ* or laboratory tests. The lack of geotechnical information to be used as an input for these curves encouraged practitioners to give preference to load-transfer curves that have been calibrated on parameters that are easier to obtain in practice, such as those by Frank and Zhao (1982). A variation of this method has been recently tested including a wider pile load test database and non-linear mobilization functions, as presented by Abchir et al. (2016), with an application to piles under monotonic loading.

Lopes (2013) synthesizes some of the existing mobilization functions described in the literature and classify them according to the type of geotechnical parameters that need to be used as input. Some of them, such as those proposed by API (2000), have a predefined curvature depending only on failure parameters. Bohn et al. (2017) developed two types of functions based on the analysis of 50 instrumented pile load tests. The proposed curves depend only on the ultimate shaft and base resistance parameters. They have been validated through a database of 72 pile load tests and the authors conclude that their performance can be considered satisfying when no pressuremeter parameters are available.

1.2 ENGINEERING NEEDS FOR ADVANCED DESIGN

1.2.1 Limits of the traditional design approach in current practice

The traditional foundation design approach using standard pressuremeter tests is based on direct correlations established on the basis of full-scale load tests, most of them performed in France. The establishment of the direct correlations between pressuremeter parameters and foundation design parameters happened within a very specific historical context. According to Frank (2017), starting from the early 1970s, the urgent need for updated specifications for foundations design was at the origin of this intensive research work in France. At that time, after the works of Ménard (1967), pressuremeter tests had already reached such a maturity in this country that they were pointed out as the most promising tool for foundation design at that time. This justified

the investment on the development of the extensive pile load-test database and the traditional design approach in this country.

Briaud (2013) presents some perspectives on the use of pressuremeter tests beyond the traditional existing approach. The author discusses about special pressuremeter testing procedures that can be performed to provide soil parameters in problems such as for assessing time-dependent behaviour, lateral dynamic loading of piles, prediction of the lateral deflection of retaining walls or liquefaction. The procedures proposed, also semi-empirical, confirm that soil response under other types of pressuremeter loading can be correlated to foundation behaviour under similar loading. Despite promising, the acceptance of these innovative procedures by practitioners would require it to be validated from several applications and then to be standardized, case by case.

Despite the existing traditional design approach is robust and of great acceptance in France, it has experienced difficulties to be exported to other countries. Benoît and Howie (2014) present an overview of the use of pressuremeter tests in North America and conclude that more full-scale loading and monitoring of foundations are required to verify and to promote the traditional PMT design approach within the local community of practitioners. According to the authors, the pressuremeter technique has been insufficiently (and sometimes inappropriately) used in North America and a revival of its use would be profitable, especially because modern numerical analysis methods require more sophisticated soil parameters.

From the feedback presented in literature about the application of Ménard pressuremeter tests at an international level it can be concluded that, despite successful on its native country, the traditional design approach still faces difficulties to be exported. This approach presents the disadvantage of having been validated using the specific Ménard testing equipment and procedures and an extension of its applicability to other types of probes and testing protocols would require a similar validation program. However, it is improbable that the historical context that enabled establishing the cross-correlations that are on the basis of the traditional design rules will be repeated elsewhere worldwide, which freezes the perspectives for improvements in testing equipment and protocols, despite they have shown to be promising. On this context, extending and validating the application of the direct / empirical pressuremeter approach to other engineering problems that require determining soil stiffness at other

strain domains seems not feasible. Approaches in which the pressuremeter test is used to obtain intrinsic properties of soils that can be further used as an input for design purposes should be prioritized.

1.2.2 General aspects on recent engineering needs for design: from ultimate limit state to serviceability

According to Frank (2014), despite not yet very common, taking the load-displacement response of foundations into account is getting more and more necessary in order to integrate structural and geotechnical design. According to this author, the Eurocode 7 (CEN, 2004) provides a design framework favorable for the dialogue between geotechnical and structural engineers. On this context, geotechnical design is evolving. In traditional approaches, based only on limit equilibrium, the serviceability limit state was usually not verified. Instead, ground movements were kept to acceptable values by imposing relatively high safety factors with respect to the service load. In that manner, foundations were frequently considered as simple infinitely stiff supports.

In problems in which soil-structure interaction needs to be accounted for, this approach is no longer acceptable. In that case, the foundation response to structural loading affects the global response of the structure. Thus, in this case the structural design requires foundation load-displacement behavior to be accurately characterized. The prediction of the structure performance under service loads relies on the accurate prediction of its foundation performance.

For special structures, such as offshore wind turbines founded on piles, structural design is strongly dependent on soil-structure interaction behavior. Due to the slenderness of the structure, design to dynamic and cyclic loading is important. The performance of the structure and its durability is highly dependent on an accurate prediction of the global stiffness of the foundation system. In this case, providing accurate deformability properties can play an important role in the design of the structure. Only few developments exist on what concerns the use of pressuremeter for this specific application. This subject is presented in the next section.

1.2.3 The design of piles under cyclic loading

Puech and Brucy (1982) use cyclic pressuremeter tests to evaluate the axial response of offshore foundations. The authors propose a pressuremeter testing procedure including a large number of cycles to simulate the effect of a storm loading on offshore piles (Figure 1.5a). Through the cyclic tests performed using a self-boring pressuremeter in soft clays at Cran experimental site in France (Figure 1.5,a), the authors study the evolution of cyclic pressuremeter parameters, such as the cyclic shear modulus G_c or the secant shear modulus G_M, defined in Figure 1.5b, as a function of the number of cycles. They try to correlate the pressuremeter test results to the observed behavior of a full scale axially loaded driven pile.

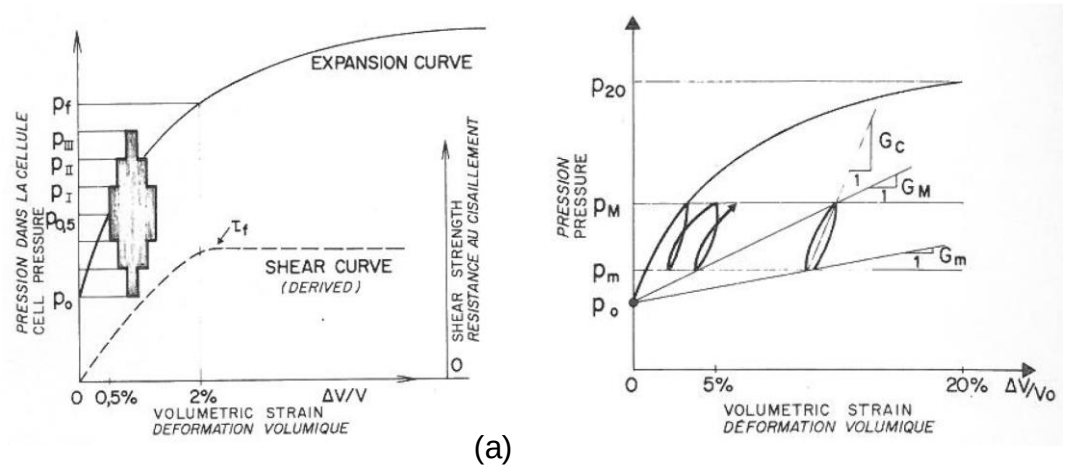

Figure 1.5 – (a) Principle of a cyclic pressuremeter test simulating a storm loading; (b) definitions of cyclic shear modulus as defined by Puech and Brucy (1982)

The authors observed that the cyclic shear modulus G_c generally stabilized after about ten cycles. They have also noticed an increase in the rate of volumetric strain accumulation related to an increase in the average pressure of the cyclic series, and the effect of the cyclic amplitude on the decrease of G_c. It is concluded that it is possible to determine representative values of soil shear modulus using the self-boring pressuremeter on site. The authors underline the advantages of using pressuremeter tests for assessing both static and cyclic soil properties for the design of piles.

Briaud et al. (1984) and Little and Briaud (1988) try to correlate cyclic pressuremeter tests to the behavior of laterally loaded piles. The authors compare the evolution of cyclic parameters evaluated from series of repeated cycles performed with the pressuremeter and those evaluated from full scale laterally loaded piles. Those parameters are the evolution of cyclic and secant pressuremeter shear modulus, and the

creep exponents. It has been noticed that these parameters were generally higher when calculated from the pile response than when calculated from the pressuremeter cavity response. Two main reasons are found to justify this observation: (1) during pile lateral loading, the cylindrical cavity is loaded asymmetrically (while one side of the pile is pushed against the soil, there is a gap opening at the other side), which is different to the symmetrical pressuremeter loading. The pile section is thus less confined that the soil around a pressuremeter probe; (2) the cyclic pressuremeter tests performed by the authors were pressure-controlled, while not all the pile sections are submitted to stress-controlled cycles. Based on previous studies, the authors note that for pressuremeter tests in soils, the resistance degradation is more rapid under displacement-controlled tests than under pressure-controlled conditions.

More recently, Puech and Garnier (2017) have presented recommendations on the choice of the most suitable investigation tests for the determination of cyclic parameters for the design of piles under cyclic loading. The authors note that the standard Ménard testing procedures do not enable assessing shear modulus at adequate strain rates needed for the design of piles under cyclic loads (small strain domain). The interest of performing multiple series of cycles using pressuremeters, for simulating the effects of storm or repeated loading on soil, is highlighted. According to the authors, these data can be interpreted in terms of the accumulation of irreversible strains and evolution of the shear moduli with the number and severity of the cycles. There are currently no practical recommendations on how to apply pressuremeter test results to the design of deep foundations under cyclic loading. Some fundamental aspects concerning the behavior of these structures is presented in section 1.2.3.1.

1.2.3.1 On the behavior of piles under cyclic loading

The SOLCYP Recommendations on the design of piles under cyclic loading (Puech and Garnier, 2017) present a synthesis of the most important international research works carried out regarding piles under cyclic axial loading starting in the 1970's. Some definitions and aspects specific to the behavior of piles under cyclic loading that will be important for within the framework of this Ph.D. thesis are summarized in the next sections.

a) Definitions

A regular cyclic load is usually defined by a mean load Q_{mean}, a cyclic component of the load Q_{cyc}, corresponding to half the amplitude, a period T (or frequency f) and a number of cycles N (Figure 1.6). The loading can be classified as *one-way* when there is globally no change in the direction of the action ($Q_{cyc} < Q_{mean}$), or *two-way* (or alternated), when there is a global reversal of the loading ($Q_{cyc} > Q_{mean}$).

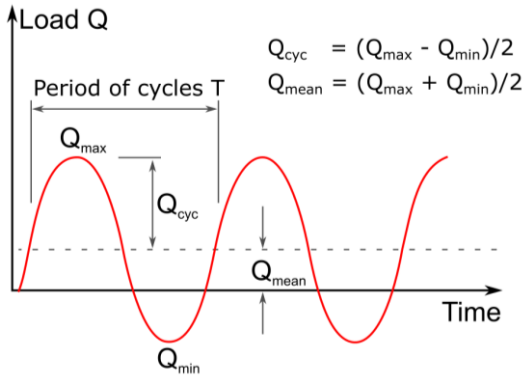

Figure 1.6 – Definitions for regular cyclic loading (after Tsuha et al. (2012))

Cyclic loads of natural origin such as wind loads, waves or storms are not regular. Instead, they are composed by a succession of random loads of irregular amplitude and random distribution over time. A key step for the design to cyclic loading is to convert random loading into a regular one, composed of a succession of series of cycles of constant amplitude. This is called the "idealized load" and this operation is done by the application of a counting method. For the case of structures subject to large numbers of cycles, it is possible to determine a series of reduced number of cycles of a given amplitude that generates the same effect on the structure (or soil) that would do a series of numerous cycles of different amplitude. Those are called the "equivalent load" and the "equivalent number of cycles" and they can only be obtained if there is knowledge of the constitutive model of the material and its intrinsic damage rules. A scheme on how cyclic loading can be taken into account for foundation design is presented in Figure 1.7.

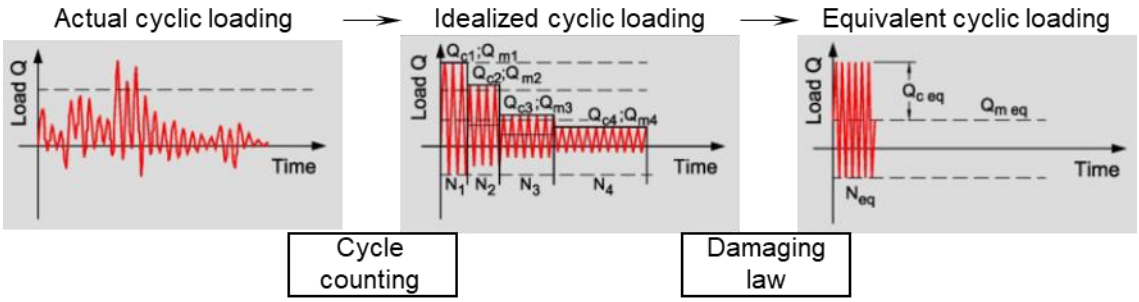

Figure 1.7 – Scheme on how real-world cyclic loading is accounted for when designing foundations. (adapted from Puech and Garnier (2017))

b) Pile response under axial cyclic loading

Axial cyclic loading effects on piles results most frequently in a reduction on the pile bearing capacity or an accumulation of head displacements due to the repeated loading, as compared to similar piles subjected to monotonic loading.

According to Puech and Garnier (2017), when a cyclic loading is applied to the pile head, the top layers undergo a stronger cyclic degradation than the deepest layers. The loss of shaft friction capacity of the top layers is, thus, compensated by the transfer of the applied load toward the bottom of the shaft. Friction degradation tends to propagate from the top toward the base of the pile.

Pile head response under axial cyclic loading depends on the magnitude of the load with respect to the pile axial capacity. It can be classified as stable, meta-stable or unstable. As illustrated in Figure 1.8, a stable (A) response means that the permanent relative cyclic displacement accumulation remains small, tending to stabilize quickly ($N < 100$), even after a very large number of cycles. An unstable (C) response means that the permanent relative cyclic displacement accumulation becomes significant for $N < 100$ and continue to grow in an accelerated manner. The pile evolves to cyclic failure. Between those two states, the metastable (B) response means that cyclic failure can occur for $N > 100$. For this case, permanent relative cyclic displacements seem to stabilize briefly, but then begin rising again and speeding up beyond around 100 cycles. Cyclic failure can be defined by a conventional value of the relative head displacement s_0/B. From this definition, the normalized pile loading can be plotted into the so-called stability diagrams (Poulos (1989a)), that enable distinguishing stability zones in function of the severity of the cyclic loading.

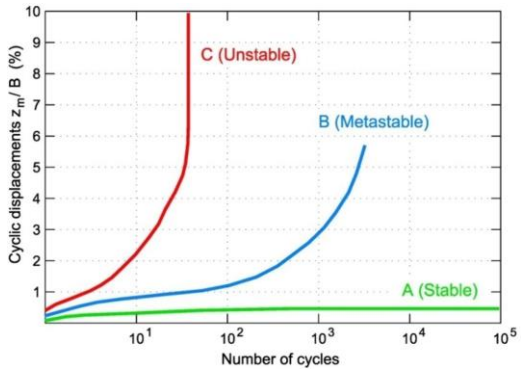

Figure 1.8 – Examples of pile head displacement accumulation in function of the number of cycles, corresponding to stable, metastable and unstable domains (figure after Puech and Garnier, 2017)

c) Cyclic stability diagrams

Cyclic stability diagrams are graphical representations of the three pile response domains (stable, meta-stable and unstable) in a plan relating the normalized component of the cyclic load (V_c/V_u) to the normalized component of the mean load (V_m/V_u). An example is illustrated in Figure 1.9. V_{uc} and V_{ut} are, respectively, the pile ultimate compression and tension resistance. The line separating the domains A and B is usually called the "zero damage line", defined for 1000 cycles. The line separating domains B and C is usually called the "failure line", defined for 100 cycles.

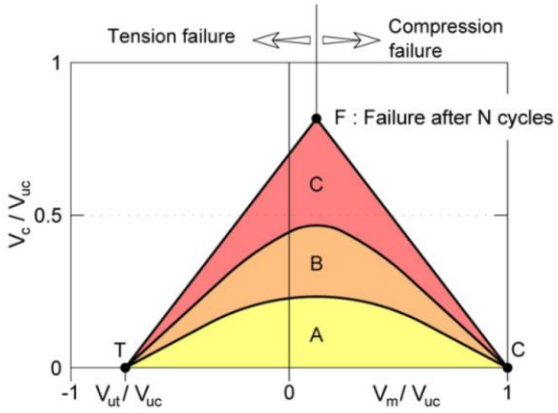

Figure 1.9 – Principle of a cyclic stability diagram (Poulos (1989a) figure after Puech and Garnier (2017))

The size of each stability zone depends on the type of soil and the pile and installation procedure. The extent of each zone needs to be calibrated on a basis of full-scale or model-scale tests for each specific case. These diagrams are useful for identifying whether a cyclic loading has or not a critical effect on the pile stability. More detailed analysis, including modelling the pile behavior under cyclic loading, may be required

in order to safely design piles in the meta-stable or unstable zones. The following section describes some of the existing methods.

1.2.3.2 Models for axial cyclic loading

Puech and Garnier (2017) present an overview and discussion of some operational approaches for design that have been used in engineering practice to model pile behavior under cyclic loading. These approaches and their main application domains are synthetized in Table 1.4.

Table 1.4 – Operational approaches to model pile behaviour under cyclic loading, according to Puech and Garnier (2017)

Approach	Method	Application domain
NGI	Total stress approach	Cohesive soils
ABC (ICL)	Effective stress approach	Sands and clays
RATZ, CYCLOPS	Cyclic t-z	Soils with significant softening (carbonate soils)
SCARP	Elastic continuum	Sands
SOLCYP	Effective stress approach	Sands

According to the authors, the behavior of piles under axial cyclic loading is mainly controlled by the response of the shaft, except for very short piles, in which the tip response is dominant. This last case, however, is poorly documented in literature and remains an exception in practice. All the described approaches focus on modelling the cyclic degradation of the soil-pile interaction and its propagation along the shaft. Each one requires specific input parameters that can be obtained from different procedures.

In all approaches, the skin friction evolution due to cyclic loading is considered to be caused by the displacements in the radial direction at the pile-soil interface. The origin of the mechanisms producing radial displacements differs in relation with the type of soil. In the case of fine-grained, saturated soils, these movements are mainly linked to the consolidation process which takes place after pile installation (in the case of pile driving, dissipation of excess pore water pressures (EPWP) and redistribution of total stresses). In the case of sands, radial displacements are essentially linked to soil's dilatancy properties (related to the state of density). However, Puech and Garnier (2017) note that independently of the state of density or consolidation, most sands and clays exhibit contracting behavior under cyclic loading. As a consequence of contractancy, a drop in the effective radial stress occurs, generating a drop in the effective shear stress at the pile-soil interface (i.e. the local shaft friction).

The NGI approach assumes that the local friction along the shaft can be assimilated to the undrained shear strength s_u as measured in the direct simple shear (DSS) device. Soil specimens must be conditioned to adequately simulate the representative zone around the pile, being then subjected to monotonic and cyclic undrained shear tests. The idealized cyclic loads are expressed in the form of contour diagrams representing the permanent and cyclic strains for a given number of cycles. The cumulative effects of the cyclic loads on pile bearing capacity can be considered by implementing the strain accumulation procedure based on diagrams relating the cyclic distortion as a function of the cyclic stress and the number of cycles. The input parameters for the NGI's approach are contour diagrams that can be obtained by DSS tests. In case of driven piles in which a remolded and reconsolidated zone is formed around the pile, the ICP method (Jardine *et al.*, 2005) can be used to deduce the stress paths to be imposed in the DSS test. For bored piles, it is suggested to simulate intact clay conditions.

The Imperial College of London (ICL) approach is an effective stress approach based on the two following principles: the interface failure criterion is governed by Coulomb's law, and interface slippage occurs when the effective radial stress is no longer capable of satisfying this criterion. It is assumed that slippage occurs at the interface itself (and not elsewhere within the soil medium), thus the friction resistance depends on an interface friction angle δ and a radial effective stress σ'_r. The interface friction angle can be assessed through ring shear tests, respecting the nature and the relative roughness of the interfaces. Indications on how to evaluate the radial effective stress in the case of driven piles are given by the ICP method (Jardine *et al.*, 2005), developed for the design of driven piles under static loading. The global reduction of the radial effective stress in function of the number of cycles can be estimated using the ABC method (after Jardine and Standing (2000), Jardine et al. (2005b)). This method is founded on the assumption that the drop in effective radial stresses can be obtained using undrained cyclic DSS tests. The following equation describes the relative drops in radial stress ($\Delta\sigma'_r/\sigma'_{r0}$) along the shaft:

$$\frac{\Delta\sigma'_r}{\sigma'_{r0}} = A\left(B + \frac{\tau_{cyc}}{\tau_{max,stat}}\right)N^C \qquad (1.13)$$

where τ_{cyc} is the cyclic shear stress, $\tau_{max,stat}$ is the maximum shear stress under monotonic loading, *N* is the number of cycles and *A*, *B* and *C* are material coefficients

defined by calibration based either on DSS laboratory tests or on pile loading tests (full scale or model scale). Samples must be consolidated under an effective stress equal to the effective radial stress acting at the walls of the pile after the dissipation of excess pore pressures generated due to the installation procedure. This stress level can be evaluated using the ICP method. If the laboratory device is not capable of performing undrained tests, it may be considered that the decrease in vertical stresses measured in drained conditions, is equivalent to the increase in excess pore water pressure (EPWP) in the corresponding undrained test. It has been reported in literature that the determination of parameters A, B and C may be difficult and sensitive to operator (Puech and Garnier, 2017).

The RATZ-CYCLOPS method (Randolph (1986), Erbrich et al. (2010)) is a load-transfer method in which the "*t-z*" curves include the local cyclic response. Compared to the other methods, this method presents the advantage to enable a cycle-by-cycle description of the load-transfer mechanism. The permanent accumulation of displacements is controlled by one parameter which defines the transition between the reversible and irreversible phases. The peak curves (Figure 1.10a) implicitly account for softening behavior, which limits its use for soil exhibiting this type of behavior (it was originally developed for cemented carbonate materials). RATZ input parameters can be calibrated based on Constant Normal Stiffness (CNS) tests. Its application on soil types other than carbonate soils is rare (Puech and Garnier, 2017).

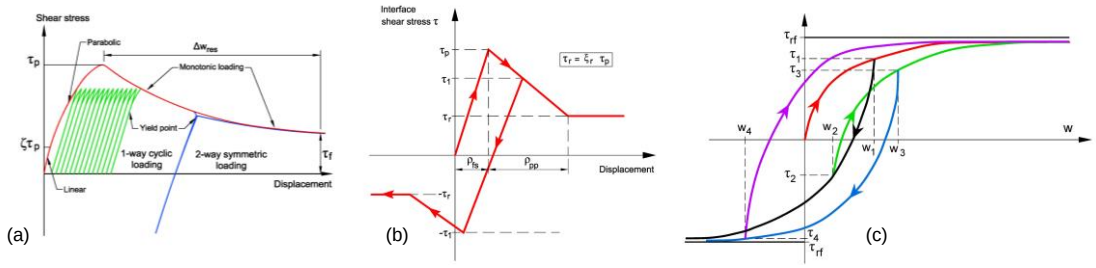

Figure 1.10 – (a) Example of cyclic "t-z" load transfer curve from the RATZ method; (b) interface model used in SCARP program; (c) principle of cyclic "t-z" curves according to TZC model (adapted from Puech and Garnier (2017)

The SCARP method proposed by Poulos (1989b) is a simplified formulation of the boundary element method, in which the soil medium is represented by an elastic continuum. The relative soil-pile slippage is simulated by introducing limiting values of shear stress to the interface, such as presented in Figure 1.10b, which also enables to account for softening. The model enables to take the following effects into

consideration: degradation of friction, of tip resistance and of soil's elasticity modulus; effect of the loading speed; accumulation of the permanent displacements under a non-zero mean load. The author defines a degradation factor D_t as the ratio between a property (such as the skin friction) after cyclic loading and this same property for static loading. The degradation of friction is modeled using two approaches: one works on the assumption that degradation occurs only if there is two-way displacement (relative pile-soil displacement); the other relates the relative amplitude of the cyclic displacement to the degradation factor after N cycles, $D_{t_{(N)}}$, according to eq. (1.14):

$$D_{t_{(N)}} = (1 - \lambda)\left(D_{t_{(N-1)}} - D_{t_{(\infty)}}\right) + D_{t_{(\infty)}} \tag{1.14}$$

in which $D_{t_{(N-1)}}$ is the degradation factor for N-1 cycles, $D_{t_{(\infty)}}$ is the degradation factor for very large number of cycles and λ is a model parameter. Based on model pile tests, the author concluded that the degradation of friction occurred only for relative displacements greater than 0.2% of the diameter *B* and that it tends to stabilize for relative amplitudes greater than 1.5% of *B*.

The permanent soil displacements S_P are calculated according to eq. (1.15):

$$S_P = BN^m e^{nX} \tag{1.15}$$

in which *B* is the permanent settlement under a low load level for the first cycle, *N* is the number of cycles, *X* is the reference load level (Q_{max}/Q_u), and *m* and *n* are two model parameters. These parameters were originally calibrated on the basis of model pile tests, some of them without a very clear definition in the software manual. Puech and Garnier (2017) presented a calibration of the parameters from back-analysis of full-scale pile tests in sands.

The SOLCYP project recommends two other approaches for the evaluation of the pile capacity degradation in function of the number of cycles: the "t-z envelope" curves and the "cyclic t-z" curves, briefly described in the next paragraph. The ultimate skin friction resistance is calculated with a total stress approach for non-cohesive soils. the soil-pile interface friction τ_{rf} is considered to be governed by eq. (1.16):

$$\tau_{rf} = \sigma_r' \, tan \, \delta_{cv} \tag{1.16}$$

where σ_r' is the effective radial stress acting on the pile shaft and δ_{cv} is the constant volume friction angle on the soil–pile interface. The cyclic shear paths mobilized along the pile interface are considered to be close to that obtained from CNS paths performed at similar stiffness. A database on CNS tests established within the SOLCYP project showed that these paths are always contracting independently on the state of density of the soil and confirmed that the degradation of interface friction has its origins, in fact, in a reduction in the normal effective stress level.

The SOLCYP CNS test database was interpreted giving origin to the so-called SOLCYP-DEG module, which can be used to determine the relative drop in normal stress $\left(\frac{\Delta\sigma'_{n\,cm0}}{\sigma'_{n\,cm0}}\right)$ resulting from a series of *N* cycles. Six input parameters are necessary: soil density index I_D, normal stiffness k_n, initial normal stress $\sigma'_{n\,cm0}$, cyclic series average shear stress ($\eta_{cm} = \frac{\tau_{cm}}{\sigma'_{n\,cm0}}$) and cyclic shear stress ($\Delta\eta = \frac{\Delta\tau}{\sigma'_{n\,cm0}}$). Puech and Garnier (2017) give further references on the choice of the parameters to characterize the soil-pile system, such as the interface friction angle, the initial normal stress and the normal stiffness (k_n). This last one is related to pile geometry and to soil's intrinsic shear modulus:

$$k_n = \frac{2G}{B/2} \tag{1.17}$$

where *G* is the soil's shear stiffness in the elastic domain (thus to be evaluated in the order of G_{max} to $G_{max}/2$, according to the authors) and *B/2* is the pile radius. *G* must be adjusted for stress level around the pile according to the following expression, where *p*' is the effective mean stress and the parameter *n* has a value between 0.5 and 0.7 for sands:

$$G \approx G_{ref}\left(\frac{p'}{p_{ref}}\right)^n \tag{1.18}$$

The drop in normal stress obtained using SOLCYP-DEG module can be directly applied to the ultimate skin friction of "t-z" curves. This is called the "t-z envelope" curve method (Figure 1.11). The degraded ultimate limit friction can be evaluated as:

$$\tau_{rf} = tan\ \delta_{cv}\ (\sigma'_{n0} - \Delta\sigma'_n) \tag{1.19}$$

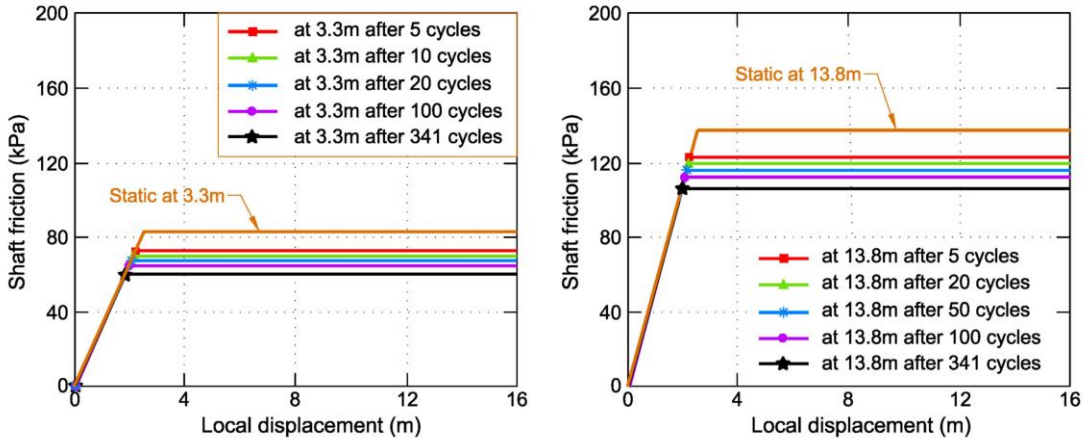

Figure 1.11 – Example of the evolution of the ultimate axial skin friction as a function of depth and the number of cycles obtained by coupling the SOLCYP-DEG approach with "t-z" curves (Puech and Garnier, 2017)

Another approach proposed within the context of the project SOLCYP is that of the "cyclic *t-z*" curves, entitled *TZC* law. Similar to the RATZ method, this approach enables modelling the cycle-by-cycle behavior of the pile. The function is non-linear and based on the principle that the shear stiffness decreases as the mobilized shear stress increases. The model parameters, described by Burlon et al. (2013), allow to describe the changes in stiffness as a function of the stress level at each load reversal. The principle of the proposed cyclic "t-z" curves is described in Figure 1.10c. The method can be coupled with the SOLCYP-DEG approach to degrade the limiting values of skin friction in function of the number of cycles. in this case, an iterative procedure is needed, in which the value of the limit skin friction should be updated at certain intervals of number of cycles. According to Puech and Garnier (2017), the use of this method for the prediction of displacements is still not reliable from a quantitative point of view but it can give interesting qualitative indications regarding the evolution of pile's behavior. On the other hand, the use of the method to predict the number of cycles leading to conventional failure is satisfactory.

For the SOLCYP approach, the drop in effective radial stresses is determined by direct shear tests with constant normal stiffness, CNS. To date, the method has only been developed for sands under drained conditions. The initial effective vertical stress is taken equal to the effective radial stress after pile installation. For bored piles, it may be accepted that this stress results from the pressure of the concrete before setting. For driven piles, it can be deduced from the ICP method. The constant normal stiffness

imposed during CNS tests must be comparable to that of the pile under investigation. It is a function of the pile diameter, the soil's elastic shear modulus G_{max} and the effect of pile installation on the effective radial stress.

Despite the fact that laboratory tests will help to obtain parameters related to the soil-pile interface behavior during cyclic loading, the pile installation effects and the soil shear modulus must be evaluated from other methods. The use of pressuremeters to characterize the *in situ* shear modulus appears as a potentially suitable solution.

1.2.4 Site characterization

Besides the use of pressuremeter results as direct input for foundation design (the traditional approach, section 1.1.2), other methods exist enabling the evaluation of elementary soil properties frequently necessary for engineering ground characterization.

Mair and Wood (1987) present many available methods for the derivation of soil properties from pressuremeter tests in clays, sands and weak rocks. These parameters are the shear modulus, the *in situ* total horizontal stress, strength properties (undrained shear strength for clays and weak rocks, and the friction and dilation angles for sands), and the coefficient of horizontal consolidation. The authors provide guidance concerning the use of these parameters for engineering design. It is stated that the greatest potential for pressuremeter tests lies in the measurement of shear modulus, especially obtained through unload-reload loops.

It is well known that soil does not behave as a linear elastic material (Duncan and Chang (1970), Hardin and Drnevich (1972a), (1972b)). The elastic domain is limited to a very small shear strain amplitude, from which behavior becomes non-linear. Ménard's observations (1961) already suggested the possibility to detect variations in soil modulus as a function of the strain amplitude using pressuremeters. This observation would be possible thanks to the use of a high-resolution equipment, for which the author gives no further details.

Atkinson and Sallfors (1991) and Tani (1995) indicate that the determination of shear moduli in the small strain domain is limited to refined laboratory tests with local strain

measurement and cannot be done *in situ* using the most common pressuremeter testing equipment. CFMS (2019) synthesized the recommended measurement domains for different types of tests with a focus on the characterization of shear modulus for the design of offshore wind turbines foundations (Figure 1.12). Assessing moduli at a shear strain range between 10^{-4} and 10^{-2} on site is currently reserved for flexible dilatometers (probes equipped with local strain-measurement sensors). Ménard pressuremeters are considered unable to provide measurements in the required measuring range for the design of offshore foundations.

Theoretical aspects related to the derivation of soil moduli from pressuremeter tests are presented in section 1.3.

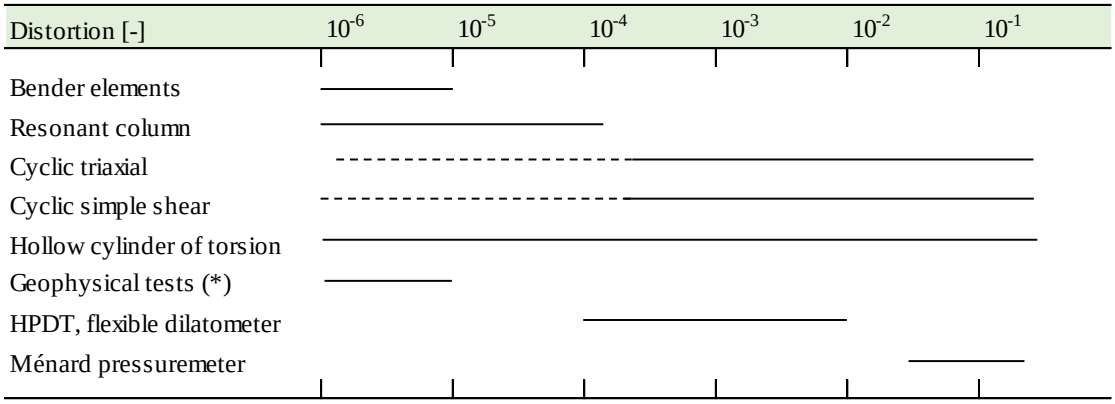

Figure 1.12 – Recommended range of measurement of soil shear modulus in function of shear strain for different in situ and laboratory tests (after CFMS (2019))

The derivation of other soil parameters such as shear strength or initial horizontal stress or consolidation state at rest using pressuremeters is generally much more sensitive to disturbance and is not a common practice for engineering design. The effects of disturbance are discussed on section 1.4.1.

Still, pressuremeter tests have been used to assess other properties related to the mechanical behavior of soils. For what concerns soil behavior under repeated loadings, Robertson (1982) discusses about the use of pressuremeter tests with series of repeated cycles for accessing soil's liquefaction properties. The author presents results from literature obtained for dense and loose sands. Two main conclusions are drawn. The first one is that the accumulated strains for pressuremeter tests with cyclic series of constant stress amplitude are greater for loose sand than for dense sand (Figure 1.13a). According to the author, this result is similar to what is obtained in drained triaxial tests

and highlights the potential for using PMT tests for accessing liquefaction properties. The second conclusion is that for cyclic tests performed in similar density sands, greater cyclic stress amplitude (which also implies greater strain amplitude) leads to greater strain accumulation (Figure 1.13b).

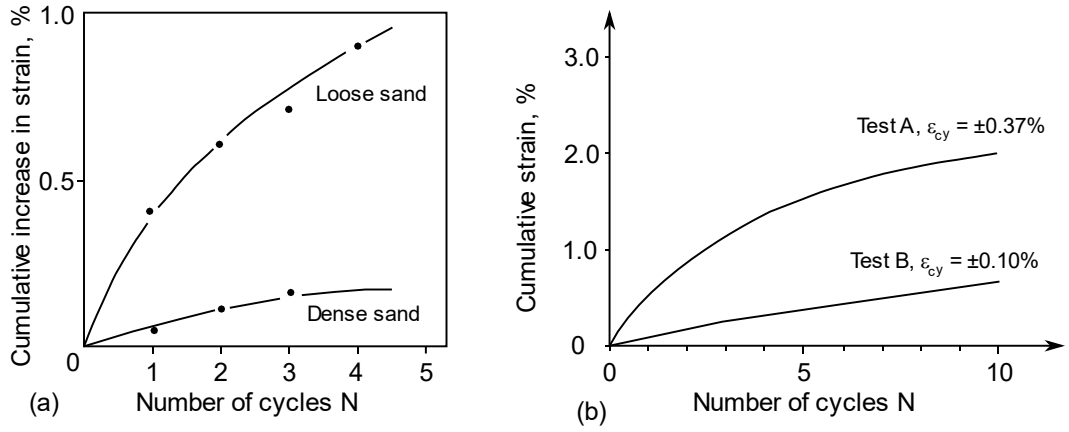

Figure 1.13 – (a) Strain accumulation for series of repeated cycles of constant stress amplitude in loose and dense sand; (b) strain accumulation for series of repeated cycles of variable stress amplitude in a similar density sand (adapted from Robertson (1982))

The author mentions that it is generally recognized in literature that the rise in EPWP during undrained cyclic loading is related to the cumulative volume changes during drained cyclic loading. Funded on this statement, it is concluded that it is reasonable to assume that the observed cumulative strain with cycles from slow pressuremeter testing can be related to the increase in pore-pressure during undrained cyclic loading and hence, to liquefaction potential.

Dupla (1995) studied the application of the cyclic cylindrical cavity expansion test for the evaluation of liquefaction properties of sands through physical models in calibration chamber. The author has shown strong evidence that the soil behavior under drained cyclic cylindrical cavity expansion is analog to the elementary behavior observed under undrained triaxial tests, which has opened perspectives to the establishment of correlations between those tests. Dupla and Canou (2003) obtained a correlation between the volume growth of cylindrical cavities upon drained cyclic pressure-controlled loading in sand and the elementary undrained behavior of the sand observed upon cyclic triaxial loading. This procedure was validated under controlled conditions in laboratory using reference sands and a mini-pressuremeter probe, adapted for laboratory tests.

1.2.5 Design of other structures

Any soil-structure interaction problem requires the characterization of soil deformability properties within a strain range representative of the problem. For the case of retaining walls, French practice is also based on established direct correlations between the horizontal coefficient of subgrade reaction and the pressuremeter modulus. This approach, however, is local, and enables only determining displacements on the retaining wall. The evaluation of displacements induced in the proximities of the retaining wall must be evaluated using finite elements or finite difference methods. The use of standard pressuremeter data is not directly suitable for this approach and soil deformability properties have to be characterized using other methods (AFNOR (2009)). Despite the influence of the non-linear behaviour of soils on the performance of geotechnical structures is known since a long time (Jardine et al. (1986)), it is still common practice to consider soil behaviour as linear elastoplastic. If so, since the strain level involved in retaining walls problems is relatively small, soil stiffness must be characterized from a range of small strains.

Wedekin et al. (2012) inquired international practitioners with respect to design practice in underground tunneling in soft ground. Amongst others, they were asked about preferences regarding geotechnical investigation techniques to be used for tunnel design. It was concluded that laboratory characterization tests and Standard Penetration Tests (SPT) were the most used techniques, and that pressuremeter tests were not much used in routine practice.

It will be shown in the next sections that there exist literature background showing that the pressuremeter test can be used for the determination of soil elastic properties covering the strain ranges required for the design of such structures.

1.3 THEORETICAL ASPECTS ON OBTAINING ELASTIC PROPERTIES FROM CAVITY EXPANSION TESTS

1.3.1 Linear elasticity

The loading imposed by a pressuremeter to the soil cavity wall can be assimilated to the expansion of a cylindrical cavity in an elastoplastic material. In this work, focus is mainly given to the elastic behavior whereas cavity expansion solutions including the plastic phase are not presented. These have been extensively discussed in literature such as by Baguelin et al. (1978), who present an overview of the pressuremeter theories and of the general relationships for the cavity expansion in any type of soil. Yu (2000) presents a more complete set of solutions including the cases of hardening/ softening soils, brittle rocks, time dependent behavior and the background for numerical implementation using the finite element method. In all these solutions, despite the increasingly complexity of the plastic behavior taken into account, the elastic domain is always considered as linear.

The solution in isotropic linear elasticity consists in writing the equilibrium equations for a thick-walled elastic cylinder and to further study the special case of an infinitely thick one. The equilibrium equation in cylindrical coordinates for the thick cylinder is presented in Figure 1.14, for an internal radius *a*, an external radius, *b*, and internal and external pressures *p* and p_0, respectively, can be written according to eq. (1.20):

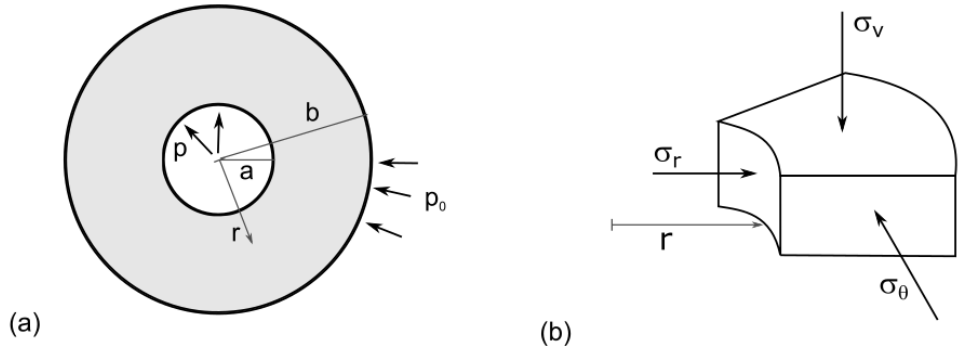

Figure 1.14 – (a) Scheme of thick cylinder under pressure; (b) stresses on an element at radius *r*

$$r\frac{d\sigma_r}{dr} + (\sigma_r - \sigma_\theta) = 0 \tag{1.20}$$

The boundary conditions in terms of radial stress are known and are $\sigma_r|_{r=a} = p$ at the internal wall of the cavity and $\sigma_r|_{r=b} = p_0$ at the external wall. Solving the differential

equation using the compatibility equations and the boundary conditions leads to the following solution for stresses:

$$\sigma_r = -\frac{p_0 b^2(r^2 - a^2)}{r^2(a^2 - b^2)} - \frac{pa^2(b^2 - r^2)}{r^2(a^2 - b^2)} \tag{1.21}$$

and:

$$\sigma_\theta = -\frac{p_0 b^2(r^2 + a^2)}{r^2(a^2 - b^2)} + \frac{pa^2(b^2 + r^2)}{r^2(a^2 - b^2)} \tag{1.22}$$

So, the radial displacement can be obtained as:

$$u_r = -r\varepsilon_\theta = \frac{p - p_0}{2G\left(\frac{1}{a^2} - \frac{1}{b^2}\right)}\left[\frac{1 - 2\nu}{b^2}r + \frac{1}{r}\right] \tag{1.23}$$

The special case of an infinite medium can be obtained by making *b* tend to infinite in the above equations, leading to:

$$\sigma_r = p_0 + (p - p_0)\left(\frac{a}{r}\right)^2 \tag{1.24}$$

$$\sigma_\theta = p_0 - (p - p_0)\left(\frac{a}{r}\right)^2 \tag{1.25}$$

$$u_r = \frac{p - p_0}{2G}\left(\frac{a}{r}\right)^2 r \tag{1.26}$$

A pressuremeter probe allows measuring the pressure and the radial displacement at the cavity wall ($r = a$). In this case, the latest equation can be rewritten as:

$$u_{r=a} = \frac{p - p_0}{2G}a \tag{1.27}$$

Differentiating *u* with respect to *p* leads to:

$$G = \frac{1}{2}\frac{dp}{du}a = \frac{1}{2}\frac{dp}{\frac{du}{a}} \tag{1.28}$$

This demonstration shows that it in the elastic domain the shear modulus can be calculated as half the slope of the pressuremeter expansion or contraction curve.

Early interpretation methods for obtaining a soil modulus from pressuremeter tests were based on linear elasticity. Soil behavior was considered to be linear elastic-perfectly plastic. The first propositions of Ménard (1957) were similar to what has been presented above. However, instead of evaluating variations in cavity radius, the author evaluated variations in cavity volume since conventional pressuremeter probes enable volumetric measurement. Both solutions are equivalent if the probe measuring cell expansion is considered as perfectly cylindrical, as presented by Cassan (1960). The first interpretation methods considered that the first linear portion of the test curve, the so-called the "pseudo-elastic" part, corresponds to the elastic behavior of the soil.

Instead of directly deriving shear modulus *G*, most solutions for pressuremeter tests focused on calculating a compression Young's modulus, *E (*Ménard (1957), Gibson and Anderson (1961)). The historical reason behind this is that the use of linear elasticity in soil mechanics was rising at that time, mainly for the estimate of foundations settlements. The pressuremeter appeared as a promising solution for assessing elasticity parameters on site, but the test has been wrongly assimilated to a compression test enabling direct assessment of modulus *E*. This idea has been quickly refuted by some authors, Gambin (1963b), stating that the cavity expansion was a pure shear test. The relationship between shear modulus *G* and Young's modulus *E* is given by elasticity theory (eq (1.29)).

$$E = 2G(1 + \nu) \tag{1.29}$$

Converting the shear modulus G into the compression modulus E implies making a hypothesis for the value of the Poisson's coefficient, ν, which cannot be measured in the test. This coefficient was frequently supposed to be equal 0.33 for sands. For matter of simplicity and standardization, practitioners have fixed this value as 0.33 for the calculation of the standard Ménard pressuremeter modulus (E_M), independently on the type of soil AFNOR (2015).

Ménard has further found that the slope of the "pseudo-elastic" portion of the pressuremeter curve does not yield an elastic modulus of the soil. Ménard (1961)

presents his first findings related to stiffness non-linearity. He is the first to suggest that it should be possible to measure soil's stiffness decay from cavity expansion tests. One year later, Ménard and Rousseau (1962) clarify the fact that soil moduli are dependent on shear strain and on the intensity and nature of the stress field. The authors suggest that there should be a "micro-strain" modulus, associated to very small strains, and which should describe the dynamic behavior of soils obtained from wave propagation tests. It was thought that this modulus should be close to the one obtained by performing an unload-reload loop during the pressuremeter test. It was suggested that the ratio between the standard pressuremeter modulus and the modulus obtained from unload-reload loop was dependent on the soil type. This ratio was later called the "rheological" coefficient (or "soil-structure" coefficient) and was used in formulas developed for calculating foundations settlement, as those presented in section 1.1.2.

It has been suggested that disturbance due to pre-boring should be one of the main reasons for which Ménard modulus was much lower than the elastic modulus. The self-boring pressuremeter has been proposed by the end of the 60's as a possible solution to this problem. However, practice has shown that even minimal disturbance due to probe insertion could perturb the initial portion of the curve in such a way that it would not correspond to soil's initial (maximum) shear modulus (discussion in paragraph 1.4.1). The only way to access the soil's shear modulus with minor disturbance from insertion methods, would be through unload-reload loops as stated by Wroth (1982) and confirmed by Lunne *et al.* (1989) and Howie (1991).

According to Wroth (1982), for pressuremeter tests with unload-reload loops, the unloading amplitude should be limited so as to avoid failure in extension and keep soil in the elastic domain. Analytical solutions for the maximum unloading amplitude in drained or undrained conditions are presented in Figure 1.15. The author observes some amount of hysteresis on the loop and recognizes that the position of the loop with respect to the expansion curve (the cavity pressure value before unloading) is important for the determination of the modulus for the drained cases. Those observations cannot be explained in the framework of linear elasticity.

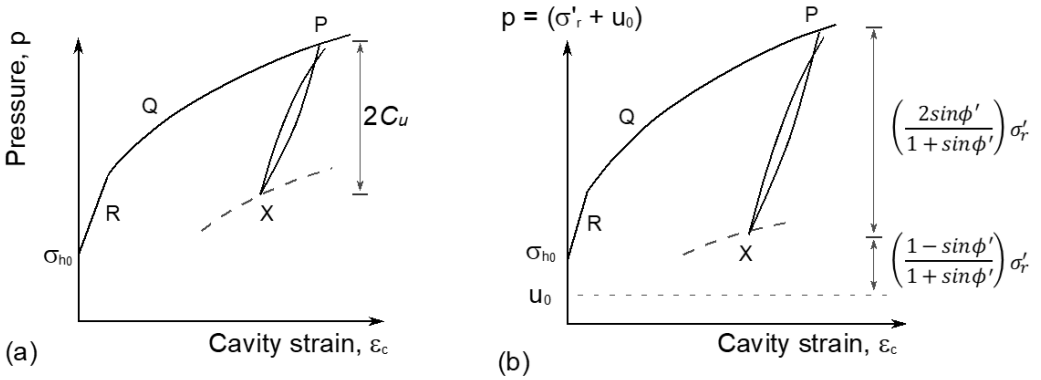

Figure 1.15 – Maximum amplitudes that can be applied in unload-reload loops: (a) clays; (b) sands (according to Wroth (1982))

In the 80's, with the increasing success of the use of numerical analysis for geotechnical problems and the development of calculation methods for taking into account the soil-structure interaction, it has been recognized that the small strain shear stiffness and the non-linear behavior of soils play an important role in the performance of structures (Jardine *et al.* (1986)). This new context required the determination of non-linear elasticity parameters from geotechnical investigation tests.

1.3.2 Non-linear elasticity

In 1972, three important studies dealt with the interpretation of undrained pressuremeter tests in clays. Ladanyi (1972), Palmer (1972) and Baguelin *et al.* (1972) propose methods for obtaining soil stress-strain response from pressuremeter tests (pre-bored – for the two first authors; and self-boring for the last). The main difference between these methods and the methods previously described is that there is no assumption concerning the type of behavior of the soil (elastic or elastoplastic). These three methods are based on the fact that for undrained expansion, the elementary volume being sheared remains constant. In this special case (no volume change), the strain field around the cavity can be described simply by the displacement of the cavity wall.

The procedure consists in obtaining the soil elementary stress-strain relation directly from the pressuremeter loading curve (inverse identification method). A non-linear response is obtained, making it possible to obtain the initial shear modulus and the peak undrained shear strength (Figure 1.16). Similar methods for obtaining the stress-strain response of sands, and so allowing for volume changes, were presented by Wroth and Windle (1975), Hughes et al. (1977), Manassero (1989). However, it has been shown that deriving stress-strain response from the virgin cavity expansion curve is very

sensitive to possible induced initial disturbance and these methods have relatively low acceptance in practice (section 1.4.1).

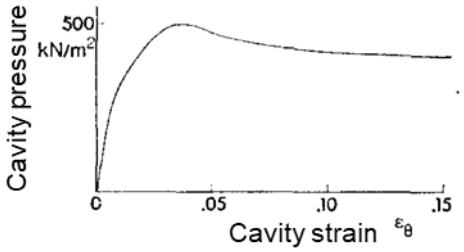

Figure 1.16 – Elementary shear curve of the soil obtained from an undrained pressuremeter test in clay (from Palmer (1972))

Hardin and Drnevich (1972a), (1972b) provide design equations and experimental laboratory methods for assessing soil behavior at small strains. This work reinforces the idea that the linear elasticity domain is very reduced in soils. Shear stiffness, actually, is dependent on stress and strain. These new findings could not yet be described by the existing pressuremeter theories.

Robertson (1982) observes that for drained pressuremeter tests, shear modulus should increase with increasing stress level and decrease with increasing strain level. The tests interpreted by the author contained relatively low amplitude cycles (strains of about 10^{-3}). This author observes that the modulus obtained from unload-reload loops in pressuremeter tests are about one fifth of the modulus obtained from resonant column tests or i*n situ* shear wave velocity tests, and attributes this to the difference in the magnitude of strain level between these two tests.

Briaud, Lytton and Hung (1983) propose a new method for obtaining stress and strain dependent soil moduli from pressuremeter tests with one unload-reload loop. These authors suggest that the unloading amplitude should be limited to about 0.7 times the maximum effective stress imposed by the pressuremeter before unloading. This should be enough to avoid the reloading curve to have a "S" shape as presented in Figure 1.17a. One should note that this proposition is different from the work carried out in parallel by Wroth (1982) (Figure 1.15).

Briaud *et al.* (1983) observe that the unload and the reload curves can be considered as hyperbolic and approximated by equation (1.30):

$$\frac{\varepsilon_v}{\Delta p} = a + b\varepsilon_v \tag{1.30}$$

in which ε_v is the volumetric strain calculated between any point of the loop and its origin (unload or reload), and Δp is the change in cavity pressure within this same interval. In the example of the loop defined by the points C – S presented in Figure 1.17a, the origin of the unload loop is point C, and the origin of the reload loop is point J. During unload, ε_v is calculated as the difference in volume between points D to C, E to C, …, J to C. Inversely, during reload, ε_v is calculated as the difference between points K to J, L to J, …, S to J. A straight line is obtained by plotting the reciprocal of the secant modulus ($\varepsilon_v/\Delta p$) against the volumetric strain ε_v. These authors suggest that cycling in this manner allows pressuremeter moduli to be obtained at any strain level, including the zero-strain level by extension of the regression line to zero strain.

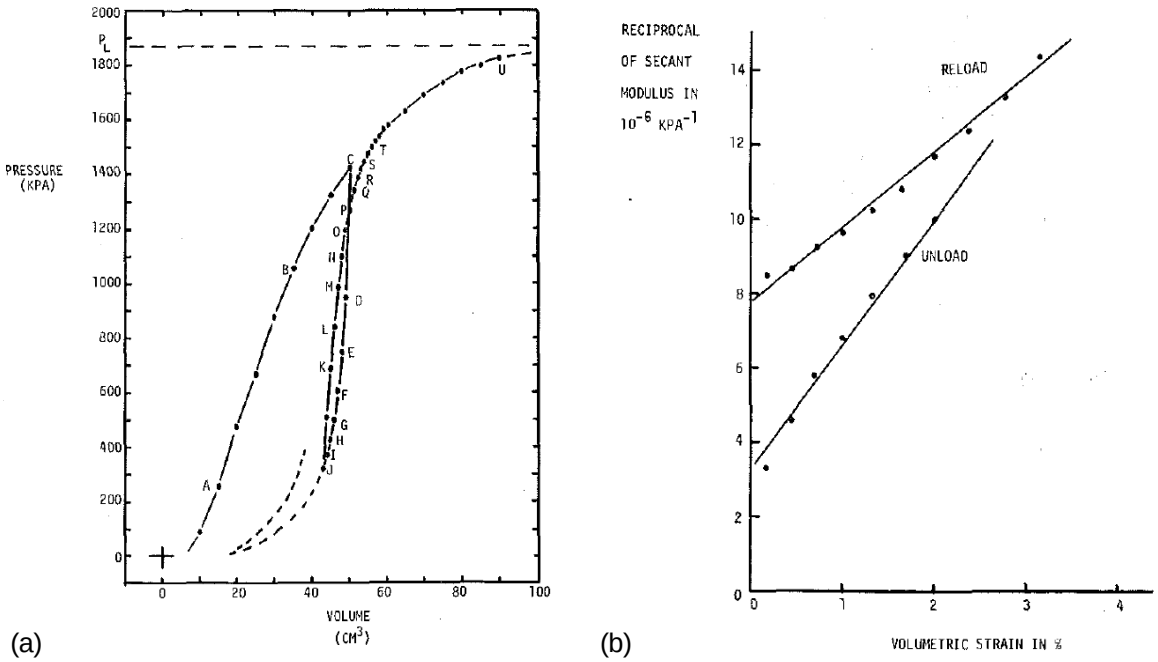

Figure 1.17 – (a) Pressuremeter test with one unload-reload loop; (b) plot of the reciprocal of the secant modulus as a function of volumetric strain (adapted from Briaud et al, 1983)

The authors also discuss the influence of stress level on modulus. It is recognized that if soil behaves elastically there will be no changes in average stress, because in this case, as radial stress increases, circumferential stress decreases by the same amount. The authors propose to obtain the coefficient of stress dependency *n* using eq. (1.31), which relates the ratio between the initial unload and the reload modulus to the cavity pressure at the start of the unload and of the reload.

$$\frac{E_{uo}}{E_{ro}} = \left(\frac{p_{cav,u}}{p_{cav,r}}\right)^{n} \tag{1.31}$$

However, there is a drawback in this interpretation procedure. It should be noted that, using the unload and reload pressures from the same loop ($p_{cav,u}$, associated with point C in Figure 1.17a and $p_{cav,r}$, associated with point J in the same figure) in order to describe modulus stress dependency is not consistent with the previous statement that, if soil behaves elastically, there are no average effective stress changes within the loop. For this reason, it seems not be possible to describe modulus stress dependency from only one unload-reload loop, and it should be necessary to perform more loops (at least three), beginning at different stress levels. Briaud (1992) suggests a testing procedure including loops performed at increasing cavity pressures. In this case, the coefficient *n* can be obtained by the relationship between the modulus and the average effective stress of each loop. The author considers that a reasonable estimate for the average effective stress, accounting for the radial, circumferential and vertical stresses, is given by eq. (1.32).

$$\sigma'_{av} = \frac{1}{3}\left(0.8p'_{cav,u} + \sigma'_{v}\right) \tag{1.32}$$

The author quotes the importance of measuring porewater pressure evolution during the test, since stiffness evolves with effective stresses, and not with total stresses.

Mair and Wood (1987) note that even though pressuremeter loops of limited amplitude are elastic, hysteresis is observed, which increases as loop amplitude increases. Authors suggest that the shear strain at which a modulus is calculated should always be indicated. It is also noted that in drained tests, the stress level at which the loop is performed has an influence on the value of the shear modulus (stress dependency). The effect of stress and strain levels on pressuremeter unload-reload loops is illustrated in Figure 1.18.

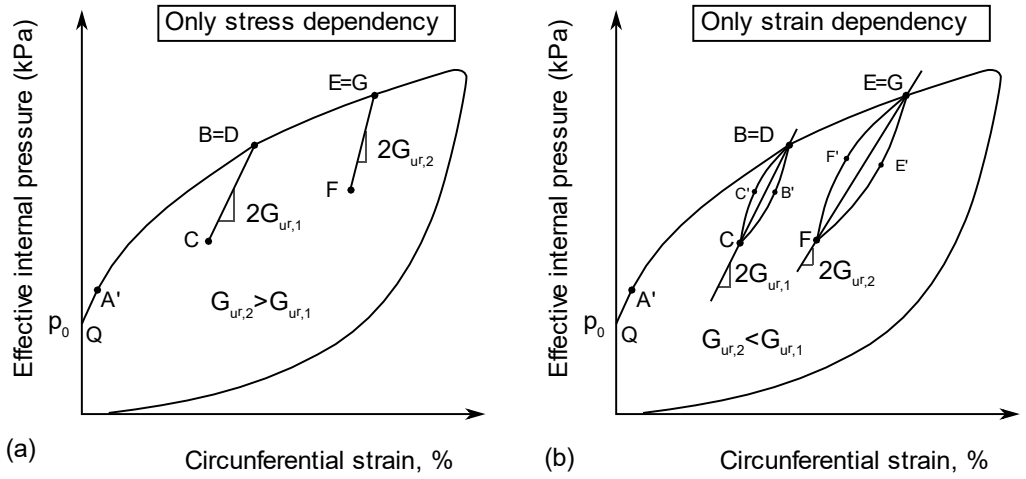

Figure 1.18 – Illustration of the stress and the strain effects on loop shape by considering them as isolated phenomena (Cunha, 1994).

Bellotti *et al.* (1989) present a review on sand behavior at small strains and apply it to the interpretation of self-boring pressuremeter tests in sands. The authors recall the notion of threshold shear strain, which is a value of the shear strain at which soil behavior changes from linear elastic, to non-linear elastic and finally to plastic. According to these authors, performing very small strain loop would result in quasi-zero hysteresis, and the slope of the cycle would be close to the maximum initial shear modulus of the soil.

The authors underline the fact that performing very small amplitude loops is delicate due to experimental difficulties such as the measurement resolution and hysteresis of sensors and soil creep, which can make these measurements unreliable. The authors note that the amount of creep increases as cavity pressure increases. Creep has to be managed before performing an unload-reload loop. If a sufficiently long stress-hold load step is not performed before reversing the loading direction (i.e. loading direction is reversed without performing a stress hold step), then the shear modulus can only be calculated between the two apexes of the loop.

Bellotti *et al.* (1989) consider that elementary soil moduli can be obtained from unload-reload loops. Adjustments are required for the average stress and strain state around the cavity at the time when the loop is performed. The average plane strain effective stress, σ'_{av}, can be calculated according to eq. (1.33). The associated elementary shear strain corresponds to the average shear strain within the plastic zone at the start of the unloading, γ_{av}, and it can be calculated according to eq. (1.34):

$$\sigma'_{av} = \sigma'_{h0} + \alpha(p'_c - \sigma'_{h0}) \tag{1.33}$$

$$\gamma_{av} = \beta \Delta\gamma_c \tag{1.34}$$

where σ'_{h0} is the horizontal at-rest stress, p'_c is the cavity pressure at the beginning of the unloading, $\Delta\gamma_c$ is the strain amplitude of the loop. The values of α and β are obtained by integration of stresses and strains in the plastic zone, from the cavity wall to the limit of the plastic radius, as follows:

$$\sigma'_{av} = \frac{\int_a^{R_p} s' \frac{dr}{r}}{\int_a^{R_p} \frac{dr}{r}} = \frac{\left(\frac{1}{2\sin\varphi'} - \frac{p'_0}{p'_c}\frac{1+\sin\varphi'}{2\sin\varphi'}\right)p'_c}{\ln\left\{\left[\frac{p'_c}{p'_0(1+\sin\varphi')}\right]^{1+\sin\varphi'/2\sin\varphi'}\right\}} \tag{1.35}$$

and:

$$\gamma_{av} = \frac{\int_a^{R_p} \frac{\Delta\gamma}{r} dr}{\int_a^{R_p} \frac{dr}{r}} = \frac{1}{2}\Delta\gamma_c \frac{\left[1 - \left(\frac{a}{R_p}\right)^2\right]}{\ln\frac{R_p}{a}} \tag{1.36}$$

with:

$$\frac{R_p}{a} = \left[\frac{p'_c}{p'_0(1+\sin\varphi')}\right]^{(1+\sin\varphi')/2\sin\varphi'} \tag{1.37}$$

$$\Delta\gamma_c = 2(\varepsilon_b - \varepsilon_a) \tag{1.38}$$

ε_b and ε_a are the cavity strains reached at the loop apexes.

Withers *et al.* (1989) present a review on the theoretical background of cavity expansion tests applied to the interpretation of the cone-pressuremeter (a push-in type probe). Authors present important practical observations concerning derivation of moduli from pressuremeter tests. Besides effective mean stress and loop stress-amplitude dependency, authors state that moduli should be dependent on the strain level and the creep rate at the start of unloading.

Lunne, Lacasse and Rad (1989) discuss about the evaluation of soil stiffness using different ground investigation techniques. The authors note that the stress-strain curves directly derived from pressuremeter tests are often not reliable mainly because of

disturbance, error in the estimated or measured reference stress state, instability of the numerical differentiation, partial drainage and large variation of the strain rate with radial distance from the cavity. This should lead to inconsistencies in the derivation of moduli from the virgin cavity expansion curve. Performing unload-reload loops would be the most reliable way to access soil's moduli. According to authors' experience, different types of pressuremeter and different installation techniques (Ménard pre-bored and pushed-in) may give a reliable evaluation of soil's elastic moduli if issued from unload-reload loops properly programmed. This means that, to minimize disturbance effects on the unload-reload loops, they should be performed at a later stage of the loading phase.

Schnaid (1990) presents a flowchart for the interpretation of cone-pressuremeter tests for obtaining shear moduli. The author suggests that besides the theoretical cavity expansion theory, some practical aspects must be taken into account in test interpretation, such as (1) the consideration of the probe membrane compliance and (2) the effect of the probe finite dimensions on the test results. Section 1.4 deals with these aspects.

In regard to shear modulus increase with effective stress, the author underlines the differences between stress-adjustment formulas found in literature. Examples are given by Robertson (1982), that considers the mean effective stress around the cavity ($p' = 1/3\ (\sigma_r' + \sigma_\theta' + \sigma_z')$), and other authors (Fahey and Randolph (1985), Bellotti *et al.* (1989) and Yu (1990)) who consider the mean plane-strain effective stress to control shear stiffness in unload-reload loops ($s' = 1/2\ (\sigma_r' + \sigma_\theta')$). Schnaid suggests to obtain *p*' from eq. (1.39) by expressing the vertical effective stress as a function of the radial and the ortho-radial effective stresses ($\sigma_z' = (\sigma_r'\sigma_\theta')^{1/2}$).

$$\sigma_{av}' = \frac{\sigma_r'}{3}\left[1 + \frac{1-\sin\varphi'}{1+\sin\varphi'} + \left(\frac{1-\sin\varphi'}{1+\sin\varphi'}\right)^{\frac{1}{2}}\right] \tag{1.39}$$

Byrne, Salgado and Howie (1991) propose a method of analysis to predict the maximum shear modulus of a soil from unload loops performed with self-bored pressuremeters. The method considers stress and void ratio changes during pressuremeter loading and the non-linear stress-strain response upon unloading. A finite element model is used to obtain the relationship between soil's maximum shear

modulus and shear modulus evaluated from one unload-reload loop. A chart is proposed for this, as presented in Figure 1.19. The method needs the horizontal effective stress at rest to be known. Results obtained by *in situ* and laboratory calibration chamber tests using self-boring and full-displacement probes are compared to those obtained with resonant column and cross hole tests showing a good agreement since disturbance and anisotropy are compensated through proposed coefficients.

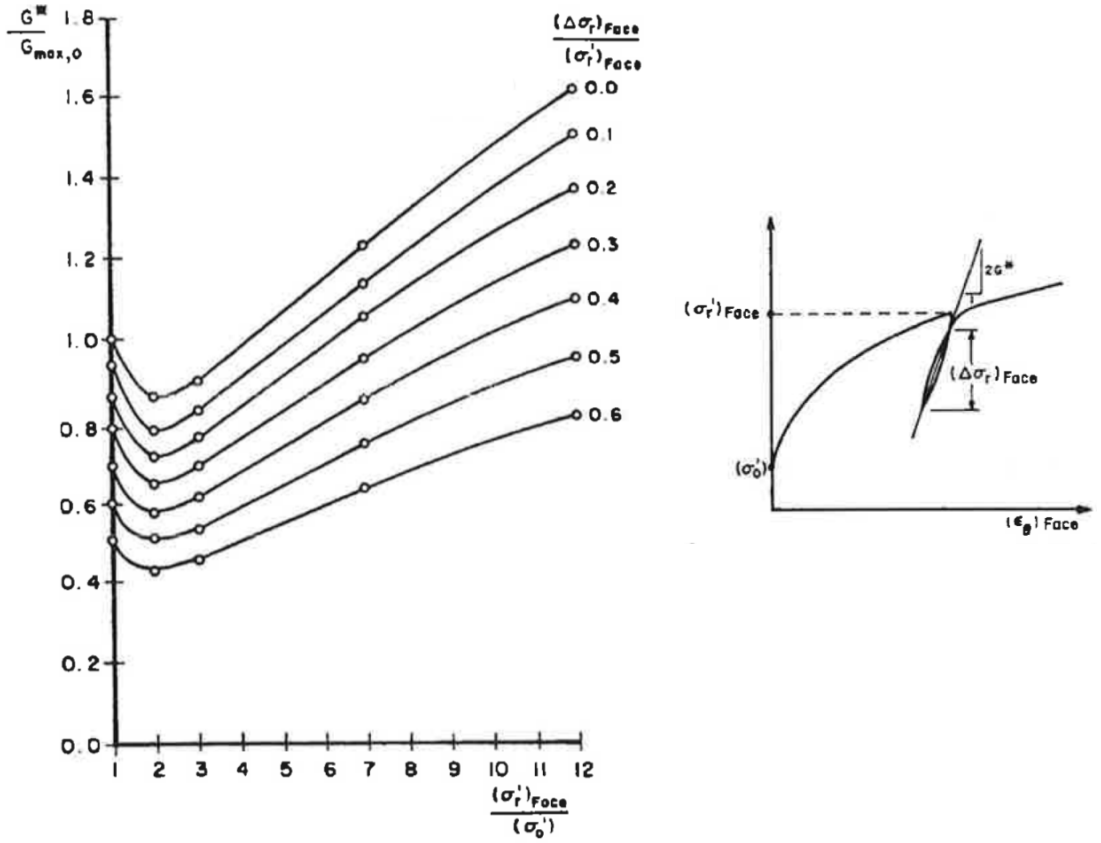

Figure 1.19 – Chart for determination of G_{max} of soils based on the evaluated shear modulus from one unload-reload loop (after Byrne et al. (1991)

Wood (1990) presents a review on the theoretical background linking elementary soil's tangent and secant moduli obtained from undrained triaxial tests to pressuremeter modulus (defined according to Figure 1.20 a, b and c, respectively). This author uses the assumptions of Palmer (1972) and shows that it is possible to relate the soil's secant modulus G_s to pressuremeter modulus G_p using eq. (1.40), and how to link cavity strain ε_c to soil elementary strain ε_s with eq. (1.41). This leads to the important conclusion that, despite the pressuremeter modulus seems to be a secant soil modulus, it is not. In fact, it is the tangent to a pressuremeter curve that actually corresponds to soil's secant modulus.

$$G_s = G_P + \varepsilon_c \, dG_P/d\varepsilon_c \tag{1.40}$$

$$\varepsilon_s = \left(2/\sqrt{3}\right)\varepsilon_c \tag{1.41}$$

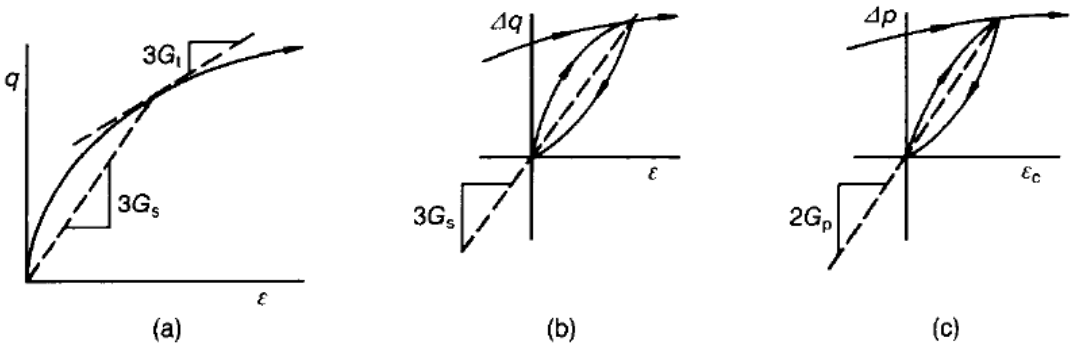

Figure 1.20 – (a) Definitions of tangent and secant (Gt and Gs) modulus in undrained triaxial compression tests; (b) secant modulus Gs in unload-reload loop in undrained triaxial test; (c) pressuremeter modulus GP deduced from unload-reload loop in undrained pressuremeter test according to Wood (1990)

However, the differentiation of the experimental curve in order to obtain tangent moduli data can add major uncertainty to results. The author adopts a curve fitting procedure. It is underlined that soil creep makes the interpretation of unload-reload loops difficult due to the superposition of time dependent phenomena and elasticity.

Jardine (1992) proposes an integral form of equation (1.40), which allows to calculate an equivalent pressuremeter curve from triaxial tests. Based on triaxial tests with specimens instrumented with local strain sensors, the author obtains a relationship between the cavity strain and the elementary strain for which both moduli, G_s and G_p, are equal. The equi-stiffness curves yield eq. (1.42):

$$\varepsilon_s = \frac{\varepsilon_c}{1.2 + 0.8 * log10\,(\varepsilon_c/10^{-5})} \tag{1.42}$$

The author states that undrained pressuremeter curves (G_p-ε_p) may be transformed into elementary (G_s-ε_s) curves by using eq. (1.42). Graphical representation of the variation of G_p, G_s and G_t with strain is given in Figure 1.21

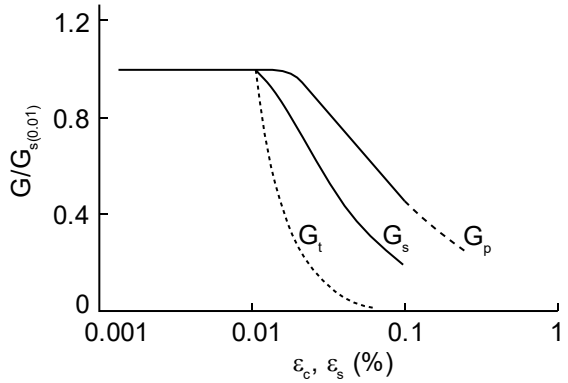

Figure 1.21 – Tangent, secant and pressuremeter moduli, plotted against strain (adapted from Jardine, 1992)

Furthermore, the author confirms Muir Wood's comment on the complications of obtaining shear moduli due to creep before unloading. It is stated that their current experience consists in pausing the test until a sufficiently low creep rate is achieved (reduced to the order of about 1% compared with the subsequent shearing rate).

Fahey and Carter (1992) simulate pressuremeter tests in sands using the finite element method with a hyperbolic constitutive model. The non-linear, stress dependent behavior of soil is considered. The pressuremeter shear modulus can be obtained from any secant segment drawn from the origin of the non-linear loop. Authors state that shear modulus derived from the cavity pressure versus cavity radial strain curve is a weighted average of the stiffness of all the soil elements around the cavity. The model proposed enables to conclude that the unload and the reload initial shear modulus may not be the same, even for a loop where no plastic yielding has taken place during unloading. According to the authors, within one loop, the initial reload shear modulus is higher than the unload modulus, and the rate of tangent modulus decay is faster on the reload path than on the unload path. This conclusion is opposite to that obtained by Briaud et al. (1983), who considers maximum shear modulus to be lower on the reload curve than on the unload one. When performing loops at increasing stress levels, the initial shear stiffness increases.

Bolton and Whittle (1999) present a solution for the undrained expansion of a cylindrical cavity in a non-linear elastic perfectly-plastic soil. A power law is used to describe stiffness decay with strain. Authors suggest that the power law coefficients can be obtained by fitting a power law curve to the reloading path obtained in an unload-reload loop. Elementary shear stress-strain response is described as presented in Figure 1.22.

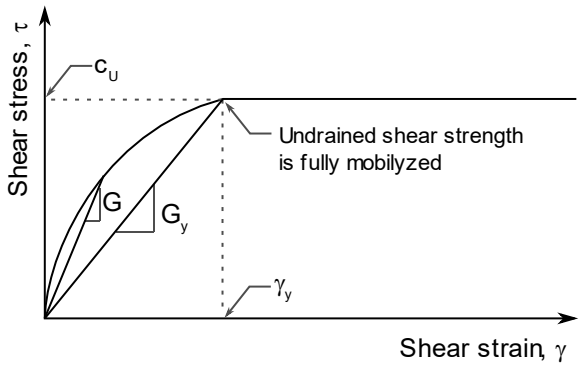

Figure 1.22 – Elementary non-linear stress-strain response as proposed by Bolton and Whittle (1999) (figure adapted)

The model is based on Palmer's (1972) solution for undrained behavior conditions. The later implies that all elements within the soil mass around the probe experience the same stress-strain relationship. Authors propose a power law to describe the stress-strain behavior:

$$\tau = \alpha\gamma^{\beta} \tag{1.43}$$

It is proposed that non-linear elasticity coefficients α and β can be obtained by fitting a power law curve on data obtained from unload-reload loops, where soil behavior is fully elastic. Previous equation can be rewritten as:

$$\tau_c = \eta\beta\gamma_c^{\beta} \tag{1.44}$$

where $\alpha = \eta\beta$. Thus, the secant shear modulus can be derived as:

$$G_s = \eta\beta\gamma_c^{\beta-1} = \alpha\gamma_c^{\beta-1} \tag{1.45}$$

and the tangential shear modulus as:

$$G_t = \eta\beta^2\gamma_c^{\beta-1} = \alpha\beta\gamma_c^{\beta-1} \tag{1.46}$$

Whittle and Liu (2013) present an extension of this method for drained behavior conditions. Authors' proposition relies on the fact that during unload-reload loops, soil behavior is elastic and that no volume changes take place. However, the method does not take into account the fact that the shear modulus may vary within the soil mass since both stress and strain levels vary with the radial distance from the cavity wall. The authors present the example of a test performed in sands and containing five unload-

reload loops initiated at different stress levels. The effective stress state around the cavity at the beginning of each loop is calculated as:

$$\sigma'_{av} = \frac{1}{2}(\sigma'_r + \sigma'_\theta) \cong \frac{p'_{cav}}{1 + sin\varphi'} \tag{1.47}$$

It is proposed that shear modulus should be adjusted to an average stress according to the power law of eq. (1.48). The exponent *n* can be obtained by plotting $G_{measured}$ against σ'_{av} for a chosen strain level:

$$G_{ref} = G_{measured}\left(\frac{\sigma'_{ho}}{\sigma'_{av}}\right)^n \tag{1.48}$$

Values can then be adjusted to any reference stress by calculating the stress adjustment parameter α_{ref} for each loop:

$$\alpha_{ref} = \alpha\left(\frac{\sigma'_{ref}}{\sigma'_{av}}\right)^n \tag{1.49}$$

The adjusted secant shear modulus can be obtained using eq. (1.50). The same procedure can be applied for calculating the adjusted tangent modulus.

$$G_{s,ref} = \alpha_{ref}\gamma^{\beta-1} \tag{1.50}$$

However, the exponent *n* also depends on the strain level. Authors isolate stress and strain dependency by plotting secant shear modulus against mean effective stress for the five loops performed. Then, the exponents of the power law are plotted against shear strain. The authors observe that exponent *n* decreases with an increase of the strain. This diverges from what has been observed from laboratory studies (Oztoprak and Bolton (2013)). Whittle et al. (2017) recognized that obtaining the power law exponent evolution with strain is one of the major difficulties related to the test. A simplified procedure is proposed by the authors, in which the power law exponent *n* is calculated only for an arbitrary shear strain rate of 10^{-3} and then applied to the whole curve.

Briaud (2013) compares values of maximum shear modulus of soil G_{max} evaluated by hyperbolic extension of the virgin pressuremeter expansion curve with values obtained using empirical correlations between other *in situ* tests, such as CPT and SPT. The author concludes that estimating G_{max} by hyperbolic fit of the virgin PMT curve is not

accurate. This result confirms that deriving elasticity properties from the initial cavity expansion curve (without performing unload-reload loops) is difficult. Reasons for this may be superposition of elasticity and plasticity during the first expansion stage and disturbance due to probe insertion, which is the subject of the next section.

1.4 PRACTICAL ASPECTS THAT MAY INFLUENCE THE TEST RESULTS

1.4.1 Disturbance of the initial state

All of the existing insertion methods, self-boring, pre-boring or pushed-in, cause a certain level of disturbance to the initial state of the soil. In the case of self-boring installation, indeed disturbance is minimized with respect to other methods. However, the application of the self-boring technique is limited to a few types of soils and soft rocks. The effect of soil disturbance on the pressuremeter measurements has been extensively discussed in literature.

Aubeny et al. (2000) analyze the effect of installation disturbance on the evaluation of soil shear strength parameters from self-boring and push-in type pressuremeters using advanced finite element constitutive model to simulate the effect of probe insertion in low plasticity clays. It is concluded that for both types of probes, the installation effects have a major influence on the strength properties derived from the first expansion test. On the other hand, it is shown that shear strength can be reliably obtained from the contraction curve (unloading) assuming prior membrane expansion to large strains.

Silvestri (2004) analyses the effect of overpushing a self-boring probe or overcutting the soil on the derivation of soil stress-strain curves from tests in clays. It is also concluded that the installation has a major effect on the stress-strain curves derived from the virgin expansion and that contraction curves performed after large cavity strains have been reached yield more accurate results.

Houlsby and Withers (1988) analyzed tests performed with the cone pressuremeter in clays. When comparing the results obtained with the displacement pressuremeter with

those obtained with a self-boring one, on a same site, the authors obtained good agreement when interpreting the unload phase of the test, both for strength and stiffness.

Benoit and Clough (1986) assessed the influence of disturbance parameters such as cutter position and dimension and cutting rate on the results of self-boring pressuremeter tests in soft clays with respect to the determination of the *in situ* horizontal stress, shear strength and moduli. Tests performed on slightly overcut pockets resulted in overestimated undrained shear strength and an underestimated horizontal stress at rest; high cutting rates resulted in similar errors. The authors report difficulties in deriving initial moduli from disturbed tests ("S-shaped curves"). Authors observed that moduli obtained from cycles were smaller than initial moduli from undisturbed tests, but did not relate this to the degree of disturbance.

Huang et al. (1991) performed a series of self-boring pressuremeter tests in clay specimens reconstituted in a calibration chamber. Initial controlled level of disturbance was imposed to some of the tests in order to verify its influence on the derivation of soil parameters. Authors concluded that initial modulus (derived from the early beginning of the cavity expansion curve) and the undrained strength were very sensitive to disturbance. The origin of the disturbing factor (overpushing or overcutting) and stress history of the clay (normally or overconsolidated) have different incidence on the error obtained on the soil properties derived. It was also concluded that disturbance had minor influence on the shear modulus derived from unload-reload loops.

Hughes and Robertson (1985) discuss the application of the push-in pressuremeter test for assessing sand properties. They present a summary of the stress paths of σ_r and σ_θ followed during the tests, including the installation process, for self-boring, pre-boring and displacement type probes (Figure 1.23). Despite the initial state suffers different amounts of disturbance as a function of the probe insertion mode, it is concluded that unload-reload loops are not, to a large extent, influenced by the installation method.

Fahey and Randolph (1984) study the effect of installation disturbance on parameters such as *in situ* lateral stress, friction angle, dilation angle and shear modulus, derived from self-boring tests in sands. Authors employ different types of shoes and cutter geometries deliberately causing drilling disturbance so that to evaluate its influence on the obtained parameters. Their conclusion is that shear modulus obtained via unload-

reload modulus is the least influenced parameter. The unload-reload loops were performed after significant cavity expansion.

This same conclusion is obtained by Robertson and Hughes (1986) by simulating the effects of initial state of disturbance in sand. The authors performed two self-boring tests at the same testing depth. The first one was started from an undisturbed state and the second was performed after full deflation of the probe after the end of the first test (disturbed state). It was noticed that the slope of the first expansion was very different in both tests (points A-B and F-G, respectively, in Figure 1.24). However, the unloading curves (D-E and G-H) were very similar in both cases. This result evidences that the incidence of disturbance effect is more pronounced on the first expansion curve than on the contraction curve performed after the cavity has undergone high deformations. If unload-reload loops are programmed in this manner, the disturbance effects can be erased. This same conclusion is reported by Lunne et al. (1989) and Tani (1995). Recently, Whittle et al. (2017) compared results obtained on chalk, on the same testing site, with three different types of pressuremeters, using three different installation methods. It is concluded that the installation method has no influence on the elastic modulus evaluated, provided that the loops are performed after having failed the soil around the cavity, creating a zone of plasticity extending to a distant radius within the soil mass.

Haberfield (1997) analyses pressuremeter tests in weak rocks and cemented sands and draws a similar conclusion regarding the determination of elastic moduli. According to the author, shear modulus should be determined from unload-reload loops at pressures greater than the uniaxial compressive strength of the rock (after having failed it).

Combarieu and Canépa (2001) evaluated the influence of the mode of drilling on the conventional Ménard reload modulus in soils. The conventional modulus is measured by unloading the cavity before soil failure (before the conventional pressuremeter creep pressure p_f is reached), and thus, at a relatively low expansion rate. This method differs from the previously mentioned methods. These authors used adequate and inadequate tools and methods for creating the borehole in various types of soils (plastic clays, silts and sands) with different amounts of disturbance, and compared the resulting moduli obtained. It is concluded that an unload-reload loop cannot erase the effect of the boring

quality. This conclusion is complementary to the previous ones that stated that previously dilating the cavity mitigates the probe installation effects.

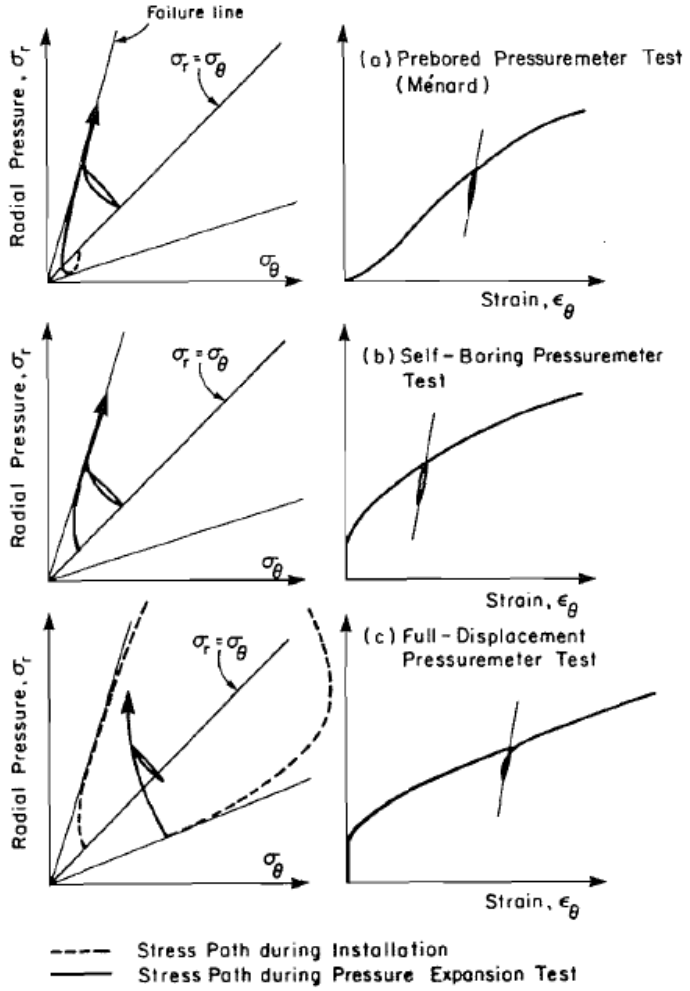

Figure 1.23 – Stress paths during pressuremeter tests including the installation process, according to Hughes and Robertson (1985)

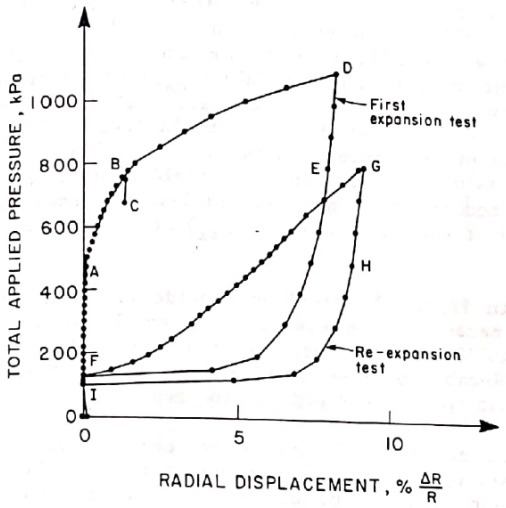

Figure 1.24 – Simulation of soil disturbance effects by repeating a test a same depth. Unload curves are similar despite the inflation curves are very different (after Robertson and Hughes (1986))

Table 1.5 – Bibliographic synthesis on the influence of disturbance effects on the determination of soil parameters from pressuremeter tests

Author	Soil	Probe	Parameter	Conclusion
Aubeny et al. (2000)	Clays	SBP PIP	Shear strengh	Reliable on contraction curve (but need more tests to confirm). Contraction after significant cavity expansion.
Silvestri (2004)	Clays	SBP	Shear strengh	Reliable results on contraction curves. Contraction after significant cavity expansion.
Houlsby and Withers (1988)	Clays	SBP PIP	Shear strength Moduli	Independency of the insertion method if the contraction curve is interpreted. Contraction after significant cavity expansion.
Benoit and Clough (1986)	Clays	SBP	Shear strength At-rest pressure Moduli	Initial moduli are influenced by disturbance. Overcutting or fast cutting rates resulted in overestimated undrained shear strength and an underestimated horizontal stress at-rest
Hughes and Robertson (1985)	Sands	PIP	Moduli	Moduli are not disturbed by the insertion mode. Contraction after significant cavity expansion.
Robertson and Hughes (1986)	Sands	SBP	Shear strength Moduli	The contraction curve is not influenced by the insertion mode. Contraction after significant cavity expansion.
Huang et al. (1991)	Clays	SBP	Shear strength Moduli	The early beginning of the expansion curve is highly influenced by disturbance. Moduli derive from unload-reload loops seem to be insensitive to disturbance and to stress rate.
Whittle et al. (2017)	Chalk	SBP PIP PBP	Moduli	Moduli are not disturbed by the insertion mode. Loops performed after significant cavity expansion.
Combarieu and Canépa (2001)	Clays Silts Sands	PBP	Moduli	Moduli are influenced by the boring technique. Contraction before soil failure.
Fahey and Randolph (1984)	Sands	SBP	Shear strength Moduli At-rest pressure	Moduli obtained via unload-reload loops were the least influenced parameters
Jézéquel et al. (1968)		PBP	Shear strength Moduli	Disturbance effects on the limit pressure depend on the type of soil and on the boring technique. Ménard modulus is very sensitive to cavity wall disturbance. Contraction curves are not discussed.

1.4.2 Probe insertion

In the case of pre-bored tests, besides the quality of the drilling and the disturbance of the cavity walls, there is a concern related to the stability of the borehole walls. For certain types of soils, remarkably loose granular ones, dry or under the phreatic level, and soft clays, the use of adequate support fluid, such as bentonite mud, is necessary to keep the cavity walls stable after drilling and before the probe insertion. The drilling techniques have to be carefully chosen in function of the ground conditions. The borehole advancement rate also has to be adjusted in function of the soil strength and drainage conditions, which have a significant influence on the capability of the cavity walls to stand stable while the test is not effectively performed. For very coarse non-

cohesive soils, such as gravels, keeping a borehole stable maybe just impossible. In this case, the insertion technique has to be adapted (pushed-in or driven slotted tube, for example).

Jézéquel et al. (1968) highlight some critical aspects regarding the influence of the drilling technique on the quality of the test and conclude that test results are dependent on the drilling method. Recommendations for establishing an adequate borehole for various types of soils were presented in the LCPC (1971) operation manual and are still present in the current European standard AFNOR (2015). It should be noted, however, that these recommendations are not sufficient to ensure repeatable borehole quality, as stated by Briaud et al. (1985). These authors highlight that there is a high level of operator's know-how involved in this practice.

Efforts have been undertaken to mitigate problems due to boring difficulties, such as the invention of self-boring slotted tubes (Arsonnet *et al.*, 2005) and new drilling techniques (Cour, 2016). Those, however, still present little acceptance in practice and does not represent a significative amount of tests performed. Reiffsteck et al. (2012) present the most current tools used for drilling boreholes for geotechnical testing purposes, including pressuremeter tests.

Another difficulty related to the test regards the position of the probe into the borehole. In multi-layered soils, in terrains where geological shear bands can be present or in any other heterogenous ground formation, care has to be taken in relation to the precise depth of the probe. If the probe is placed straddling between two or more layers of different stiffnesses or strength, the cavity expansion will not be cylindrical as presupposed by most interpretation methods. The pressuremeter test operator needs to use parallel investigation methods, or previous knowledge of the terrain, to place the probe in ground formations that are relatively homogeneous. Reiffsteck et al. (2012) mention that it is important to use borehole drilling parameters (drilling logging) to validate the pertinence of the pressuremeter tests performed. Figure 1.25 presents some specific cases in which the probe position can affect the test interpretation, and, in some cases, configurations for which the test results should not be taken into account. Cour and Lopes (2018a) suggest that the drilling parameters should be analyzed on site, before performing any tests, as a tool for helping the operator to decide where to place

the probe. Besides the fact that test results will not be interpretable, placing the probe in a zone of contrast of stiffness can cause damages to it.

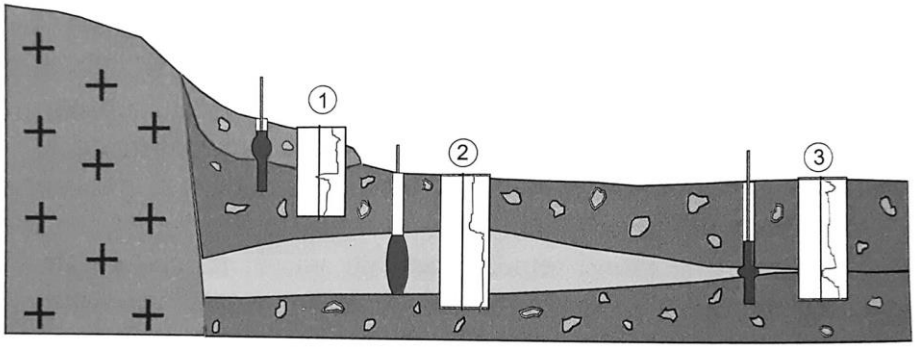

Figure 1.25 – Specific cases where the probe position can affect the testing results, according to Reiffsteck et al. (2012). Tests 1 and 3 should not be considered for further interpretation

Besides a careful analysis of geological conditions before inserting the probe, drilling quality and operator's experience are of major importance to ensure a cylindrical cavity is really formed. In some cases, it can be very difficult to obtain a smooth cavity wall. Reiffsteck et al. (2012) present some examples of difficulties associated to borehole creation. Drilling mud is used for three main reasons: (1) help stabilizing the cavity walls; (2) help evacuating the drilling cuttings from the cavity; and (3) help lubricating and cooling the drilling tool. Failing on the control of the mud quality, its injection pressure or the flow-rate can result in prejudice to the cavity quality, as illustrated in Figure 1.26.

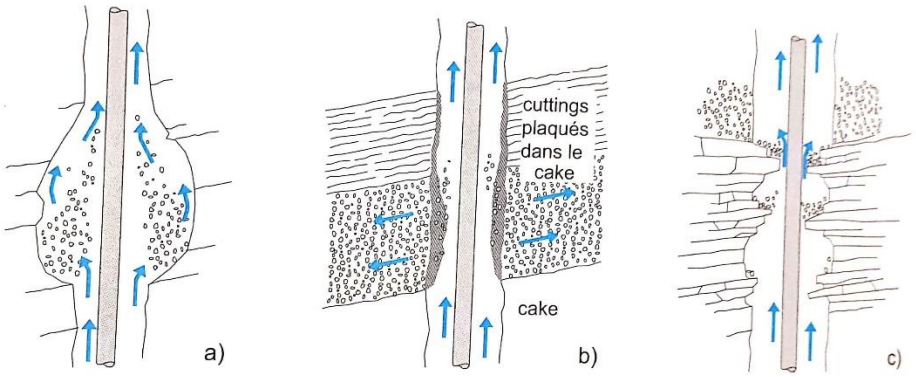

Figure 1.26 – Examples of drilling problems: (a) erosion due to excessive mud flow rate; (b) mud cake accumulation in the cavity walls due to excessive pressure; (c) cavity constriction due to low mud pressure in a plastic soil (after Reiffsteck et al. (2012))

1.4.3 Drainage conditions

The drainage boundary conditions during a pressuremeter test cannot be controlled. For a pressuremeter test performed in a given soil, the level of drainage (fully drained, fully undrained or partially-drained) will depend only on the rate of loading with respect to the soil permeability (or consolidation coefficient). Baguelin et al. (1978) stated that only in some specific cases, such as in coarse sand and gravels, the assumption of full drainage is reasonable. In most cases, how much drainage occurs, if any, can be only speculated. The only way to follow up the generation of excess pore water pressures (EPWP) during the test is by incorporating pore pressure transducers onto the probe membrane. Benoit and Clough (1986) present typical plots obtained in clays using self-boring pressuremeter equipped with pore pressure transduces. The authors comment that the evaluation of consolidation coefficient from EPWP dissipation tests using pressuremeter test resulted in the order of 10 times higher than those obtained from conventional oedometer tests in laboratory. It is underlined that this can be justified by the fact that horizontal permeability is higher than the vertical permeability, and that the presence of thin sandy layers could have contributed to faster drainage on site.

If the drainage conditions are to be taken into account for the test interpretation, additional soil investigation is necessary as for obtaining permeability parameters. Rangeard et al. (2003) quantify, using numerical finite element analyses, how soil permeability can significantly change the interpreted parameters from pressuremeter tests.

Some existing probes implement local pore pressure transducers, which enables measuring pore water pressure (PWP) at the soil-membrane interface. The use of this measurement in practice, is reserved to few cases and remains complex due to some reliability problems. Mair and Wood (1987) described problems related to the sensor itself (such as de-saturation), but also to water flowing adjacent to the membrane and pore pressure dissipation due to the development of tension cracks near the interface. Assessing variations of PWP is still the subject of recent researches and developments ongoing within the framework of the National Project ARSCOP. Measuring PWP would be the only straightforward way to distinguish if time-dependent measurements in pressuremeter tests are originated from creep or from consolidation.

1.4.4 Effect of the limited probe length

Cylindrical cavity expansion interpretation methods suppose that the cavity under expansion is infinite in the plane direction. However, real probe dimensions are finite. To some extent, it is expected that measurements performed with shorter probes (small ratio of length over diameter) will be closer to a spherical cavity expansion, and for longer probes, to a cylindrical cavity expansion.

The purpose of the three-cellular probes originally conceived by Ménard was to eliminate the end effects and ensure that stress and strain fields within the soil at the level of the central measuring cell were plane-strain and axisymmetric.

Briaud et al. (1985) conclude that single-cell probes with a length to diameter ratio of 6.5 can reproduce results obtained by tri-cellular probes. Schnaid (1990) quantifies the influence of the *L/D* ratio on the assessment of the limit pressure in sands by testing cone-pressuremeter probes of variable lengths in a calibration chamber. The author focuses on strength properties and concludes that the measured limit pressure decreases as the *L/D* ratio increases. There are no conclusions on whether longer or shorter probes are better for assessing soil properties, but the author considers that corrections must be applied in any cases.

Shuttle and Jefferies (1995) performed finite element calculations comparing infinitely long probes and probes presenting a *L/D* ratio of 6, which is, according to the authors, the most common dimension of self-boring pressuremeters. The influence of the length to diameter ratio of the probe on the uncertainty in the evaluation of the undrained shear strength, the total horizontal pressure at-rest and the rigidity index $I_r = G/s_u$ is quantified. It is concluded that interpreting the test with finite dimensions using infinite cavity expansion theory can result in an uncertainty of about 20% on I_r.

Ajalloeian and Yu (1998) highlight the influence of the probe finite dimensions specially on the determination of strength properties of sands. There is no focus on the determination of moduli and these authors state that the interpretation methods must take the finite probe dimensions into account instead of making the assumption of an infinite cavity expansion.

Whittle (1999) contradicts most works on the influence of the finite pressuremeter length on the determination of soil properties. This author contests the applicability of finite element calculations to represent real pressuremeter tests and highlights that the most widely accepted solutions for pressuremeter tests (Gibson and Anderson (1961), Palmer (1972)) do not take the finite probe length into consideration. It seems that there is no general agreement on this subject.

1.4.5 Creep and time-dependent phenomena

Wood (1990) and Jardine (1992) highlight how soil creep can affect the measurement of shear modulus through unload-reload loops. According to these authors, the superimposition of continuing outward creep deformation and inward unloading can lead to falsely high or even negative apparent initial unloading moduli. It may be difficult to precisely identify the start of an unloading or reloading process.

Withers et al. (1989) suggested using stress-controlled tests and enabling enough time to creep effects decrease before performing unload loops. The result of a cone pressuremeter test in sands at 4.9 m depth shows that creep can be observed during the complete test (Figure 1.27). Authors do not propose a precise criterion for the evaluation of stabilization of creep rate before unloading. It can be noticed that all loops are closed.

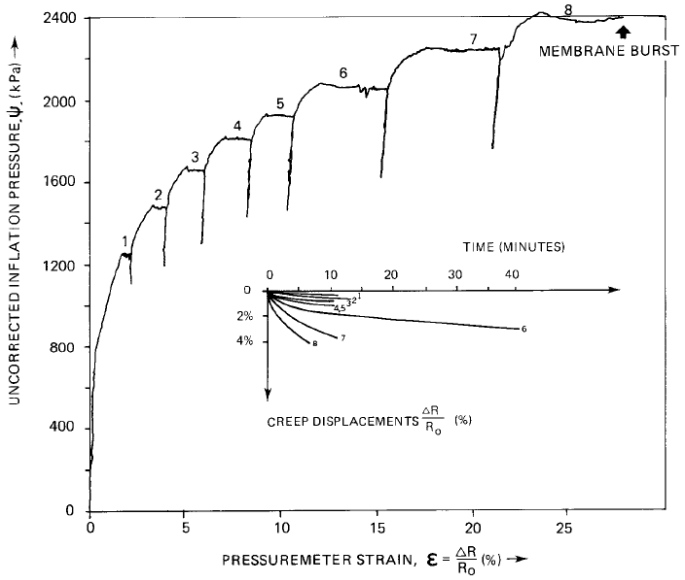

Figure 1.27 – Cone pressuremeter test in sands illustrating creep along the entire test range (after Withers et al. (1989))

Howie (1991) presents an analogy between the influence of the shearing rate in triaxial tests and shearing rate in pressuremeter tests (Figure 1.28a). The author equally describes the creep and relaxation effects during pressuremeter tests in sands (Figure 1.28b). This indicates that the test results are dependent on the rate of loading.

Clarke and Smith (1992) put in evidence the difference between loops being performed without and with a pressure hold before unloading, as it can be seen in Figure 1.30a and b, respectively. The work concerns self-boring pressuremeter tests in weak rocks. From the figure, it can be noticed that if enough time is provided to allow for creep phenomena decrease, loops are closed (despite hysteretic).

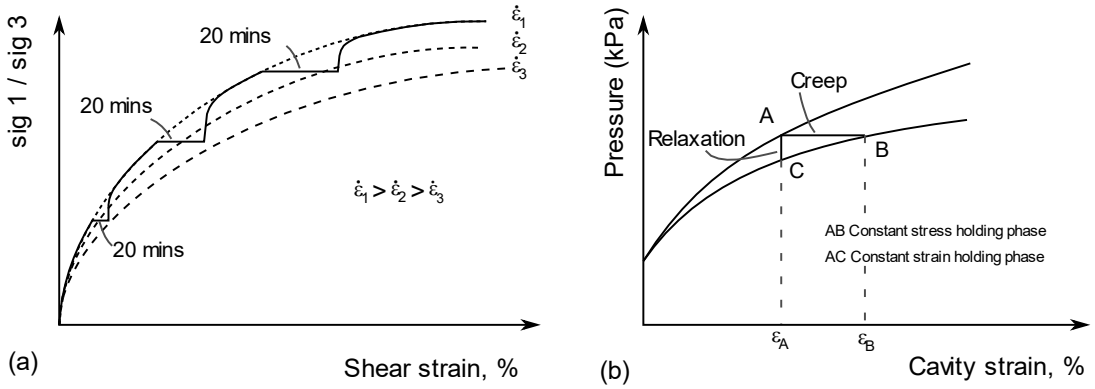

Figure 1.28 – (a) Analog strain rate contours obtained in triaxial tests; (b) comparison of creep and relaxation effects in pressuremeter tests (adapted from Howie (1991))

Nutt (1993) states that a creep-rate criterion of $\dot{\varepsilon_c} = 0.03\%/\text{min}$ at the end of the pressure-hold step is usually sufficient for successful unload loops. The author presents results of pressuremeter tests in which the rate of shearing was varied during the test, confirming the analogy previously cited by Howie (1991). From this fact, it can be concluded that the conventional limit pressure depends on the loading rate. The magnitude of this dependency, however, seems to be of less importance, as it had already been shown by Baguelin et al. (1978) when comparing tests following conventional Ménard procedure with strain-controlled tests (Figure 1.29). The slope of the quasi-linear portion of the curves seems not to be affected by the loading rate.

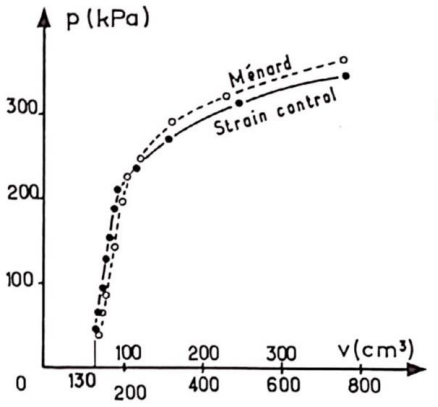

Figure 1.29 – Comparison between pressuremeter tests performed following Ménard's procedure (stress-controlled) and strain-controlled procedure (after Baguelin et al. (1978))

Benoit and Clough (1986) arrive to the same conclusion when interpreting self-boring tests in clays: the pressuremeter expansion rate does not strongly affect moduli calculated from the initial portion of the test curve, but faster expansion rates lead to higher values of undrained shear strength.

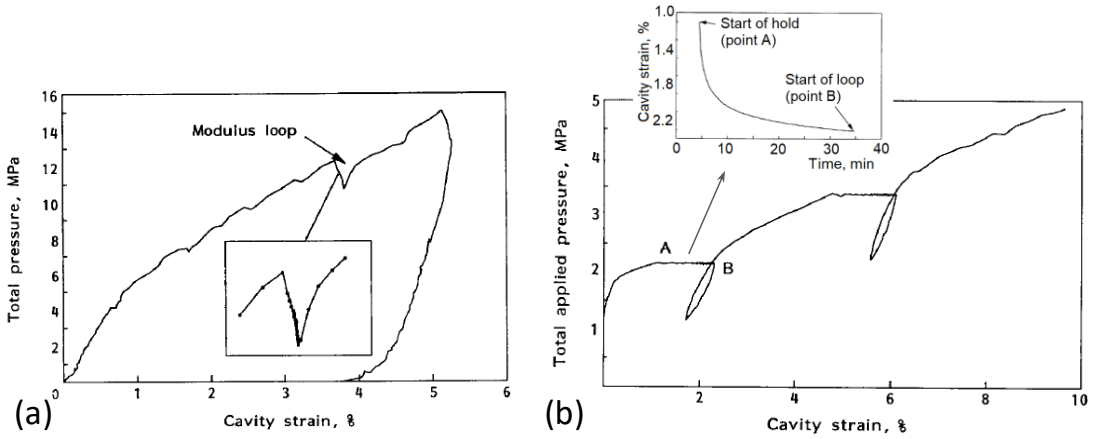

Figure 1.30 – (a) Test in mudstone 24.6 m depth without pressure-hold steps before unloading; (b) test in sandstone at 17.6 m depth including pressure-hold steps showing (after Clarke and Smith (1992))

Time dependent behavior has been captured in pressuremeter tests performed in all types of soils, even in dry sands. This enables concluding that the time dependent behavior in cavity expansion may have two distinct origins: creep and consolidation. Creep is related to the occurrence of deformations under a constant effective stress field, while consolidation is an excess pore water pressure problem depending on drainage conditions, which results in changes in the effective stress field.

1.4.6 Difficulties related to the testing equipment

The determination of soil's shear modulus requires assessing cavity strains with a high level of accuracy. This requirement, however, faces different technological limits regarding the membrane geometry and its stability over time, the representativeness of the measurements and parasite phenomena that may disturb measurements.

Baguelin et al. (1978) stated that besides the role of ensuring axisymmetric plane-strain conditions, the guard cells in three-cellular probes play also the role of keeping the measuring cell from changing in length. Otherwise, the rubber membrane would also tend to expand axially, filling the empty annulus between the probe and the soil cavity. Axial deformations of the measuring cell imply that part of the injected volume is lost and do not contribute to the cylindrical expansion. Figure 1.31a illustrates this phenomenon. The authors also tested the effect of variation of pressure in the guard cells on the measurement made on the central cell. With an "E" type probe inserted into a calibration tube and inflated to a pressure of 1000 kPa against it, the guard cells were progressively deflated while pressure was kept constant in the measuring cell. The corresponding result is presented in Figure 1.31b. It can be concluded that in tri-cellular probes, a variation in the differential pressure may induce measurement errors.

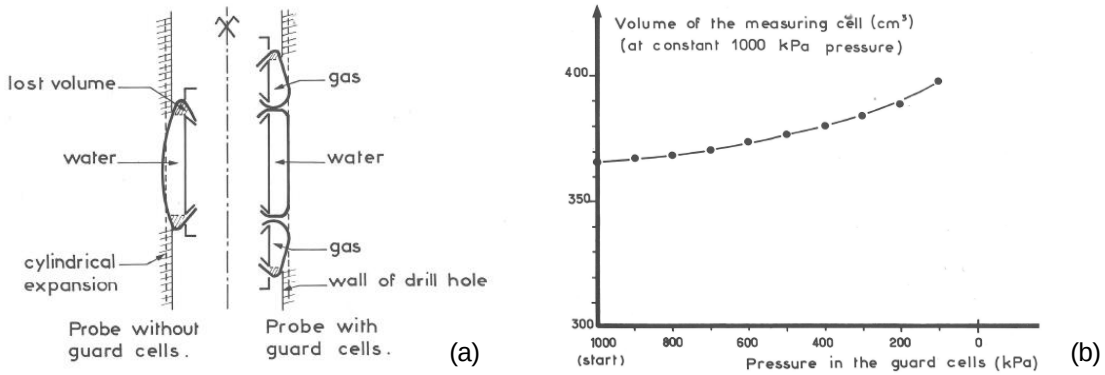

Figure 1.31 – (a) Deformation of the rubber-membrane cells with and without the presence of guard cells; (b) increase in volume of the measuring cell at constant pressure due to the deflation of the guard cells (after Baguelin et al. (1978))

Those measurement errors seem to be inherent to the behavior of thin rubber membranes. Elton (1981) analyzed the influence of the stiffness of the rubber membrane on the interpretation of the test results. He reported an unusual volumetric expansion of the rubber membranes assembled on OYO type probes. It seems that the origin of this phenomenon is related to small heterogeneities of the rubbers forming the

membranes, which makes the expansion not to be perfectly symmetric. Membrane expands randomly, without any imposed geometry.

Kjartanson (1986) uses an OYO Elastometer 100 pressuremeter to assess creep properties of ice performing tests under controlled conditions in the laboratory. On this type of probe, radial displacements are measured by caliper arms connected to an LVDT transducer. The author calibrated the probe using calibration tubes of different diameters in order to identify the membrane compressibility coefficients, and their variation with the membrane thickness and its variation over time. The author concludes that both corrections for thickness variation and for drift in time should be taken into account for creep tests interpretation. The membrane used was made of rubber, 70 mm outside diameter, 4 mm thickness.

Howie (1991) describes other sources of uncertainties inherent to measurement systems based on caliper arms. The probe used by the author was equipped with the same type of strain arms than the Cambridge Self Boring Pressuremeter. This type of sensor bears on the internal walls of the probe membrane. Time dependent drift on measurement by strain arms was also detected for this probe but there are no discussions on whether the source of the problem is the rubber membrane or the sensor itself. According to the author, another limitation of the strain arms measuring system is that the latter bear onto a small area on the rubber membrane and that it is possible that a punctual particle movement induces measurement error. It is stated that averaging measurements from the three arms should damp this source or error.

Fahey and Jewell (1990) evaluated the effect of inaccuracies in the strain-measuring system in the evaluation of shear modulus through self-boring pressuremeter tests. They evaluate the behavior of strain measurement arms when performing unloading and reloading loops with the probe placed into a steel cylinder. It resulted that the displacement transducers measured a variation even for an outer diameter imposed (membrane in contact with the steel cylinder). The authors concluded that one of the origins of the errors was the internal friction between the components of the strain arms. A mechanical solution is proposed to minimize the error, but it is not possible to eliminate it completely. Results of a compliance test performed are presented in Figure 1.32.

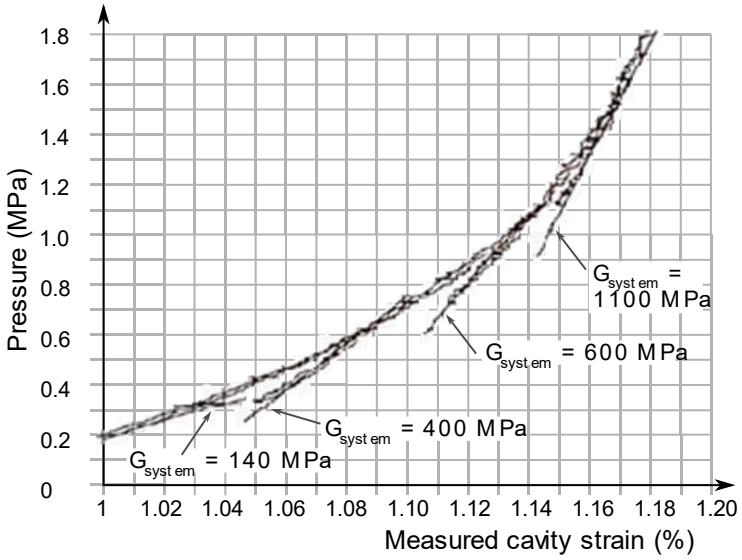

Figure 1.32 – Compliance test of a self-boring pressuremeter probe (loops performed with the probe inside calibration cylinder, constant radius). Adapted from Fahey and Jewell (1990)

By interpreting the loops performed in the compliance test, the authors obtain the so-called "system stiffness", which corresponds to the apparent deformation measured by the sensors at constant external diameter. The system stiffness varies according to the loading path, whether it is a first load or an unload-reload loop. The system stiffness increases as pressure increases.

According to the authors, system compliance can be corrected by applying equation (1.51). This equation is derived from the association of springs in series. It results that the inverse of the corrected shear modulus G_{corr} is equals to the difference between the inverse of the measured shear modulus G_{meas} and that of the system stiffness G_{sys}.

$$\frac{1}{G_{corr}} = \frac{1}{G_{meas}} - \frac{1}{G_{sys}} \tag{1.51}$$

Schnaid (1990) identifies the same phenomena in another type of probe, a cone pressuremeter that enables both local measurement by strain arms and volumetric measurement. The author performed a compliance test similar to that proposed by Fahey and Jewell (1990). Membrane compliance manifests in both systems but is more accentuated in the volumetric measurement one.

Cunha (1994) presents a typical compliance calibration curve for a UBC self-boring pressuremeter implementing a rubber membrane thinner than that used by Howie (1991). Results are presented in Figure 1.33a. The author established a power law relation between the probe equivalent stiffness, G_{sys}, and the internal pressure before

unloading, p_c. With this established law (Figure 1.33b), it becomes possible to evaluate G_{sys} for any probe pressure developed during a test.

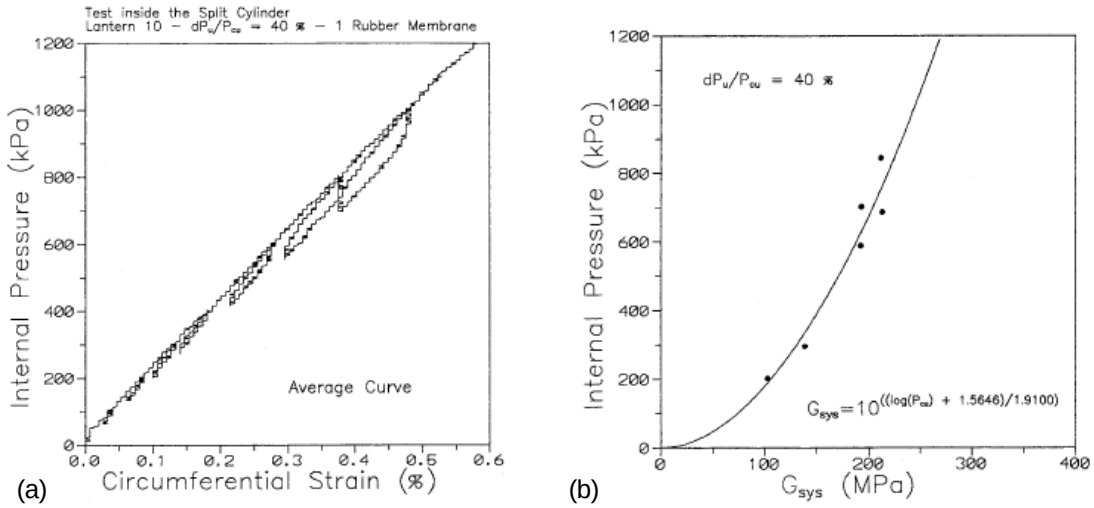

Figure 1.33 – (a) Result of a typical compliance test for an UBC self-boring pressuremeter (b) establishment of a relationship between probe equivalent stiffness and internal pressure before unloading (after Cunha (1994))

For what concerns the testing equipment, few were the technological evolutions with respect to the inflatable membrane. It is known, however, that membrane behavior is an important source of measurement errors and limitations on the pressuremeter tests. Cour (2006) patented a restraining sheath for improving the geometry of the measuring cell of tri-cellular pressuremeter probes during inflation. The sheath is installed around the rubber membrane that seals the expandable cell. This sheath has the capacity to expand freely up to a limiting diametrical profile from which it opposes to any additional deformation, thus controlling the geometry of the probe. Tri-cellular pressuremeter probes implementing this technology have already been used by practitioners, as presented by Jacquard et al. (2013). They can reach enough radial expansion levels in order to assess the soil's conventional pressuremeter limit pressure. However, despite presenting an improved measurement capability, these new generation probes still suffer from some of the problems inherent to tri-cellular probes, such as the sensitivity to variations in differential pressure (Figure 1.31). The use of the restraining sheath has been extended to monocellular probes, with the advantage that they can be controlled using simplified control units and they can be easily used for tests including cyclic sequences. A monocell probe implementing a restraining sheath has been first presented by Cour and Rouet (2017). It is pointed out as a potential

solution for performing tests with an improved measurement accuracy and with an extended expansion capacity even at high pressures.

SUMMARY AND PARTIAL CONCLUSIONS

The present chapter was dedicated to a bibliographic study on the state of practice concerning the use of cylindrical cavity expansion tests for the design of foundations. It has been shown that soil parameters can be obtained using this type of tests either through empirical or theoretical approaches. The French practice in foundation engineering is currently based on the use of standard Ménard pressuremeter tests within a semi-empirical approach. The development of this approach was favored by the historical context: invention of the pressuremeter by Louis Menard in the 60's at a time where an urgent need for new foundation design methods was identified in France. Those methods are now well established, they are robust and have proved their reliability for the applications for which they have been validated. Pressuremeter testing procedures are standardized (ISO) and pressuremeter based design methods are recognized by EC7. However, this approach has little acceptance at an international level and there are few chances that the same historical context that enabled promoting pressuremeter in France comes to happen at a larger international scale. This aspect presents a barrier for expanding the possibilities of this test.

Advanced soil-structure interaction problems require a more sophisticated characterization of the deformation properties of soils that cannot be done using traditional Ménard pressuremeter testing. Assessing soil shear moduli at low strain levels is beyond the scope of standard pressuremeter tests. This explains why this test fails to provide reliable data (i.e. deformation moduli) which could be easily used for numerical modelling applied to e.g. the evaluation of the performance of retaining walls or underground tunneling.

In this Ph.D. thesis a particular focus will be given, to the design of foundations under cyclic loading. Currently, cyclic design requires specific parameters which can be obtained from laboratory tests but are outside the capabilities of standard pressuremeter testing equipment and procedures. However, it was shown in the literature review that performing tests using more sophisticated expansion probes could enable assessing

shear modulus at lower strain ranges and open a new way to obtain data representative of the cyclic response of soils. These probes, usually referred to as flexible dilatometers (Appendix A.3), are of more complex implementation than pressuremeters and cannot reach the failure domain, necessary for the evaluation of the bearing capacity of foundations.

The theoretical background concerning the interpretation of cavity expansion tests, was found sufficiently developed to support a reliable assessment of soil parameters at small strains. It seems at present that it is essentially a lack of recognized testing procedures and adapted equipment that prevents practitioners using pressuremeter tests to characterize soil behavior within the framework of non-linear elasticity.

Recent developments in the domain of expandable membranes have brought a promising solution for increasing the measurement accuracy of pressuremeter probes. This technology presents the advantage of improving measurements at small strains without limiting its performance at high expansion rates. They can enable, in a same test, the characterization of soil properties in both the small and the large strain domains.

Within the framework of this Ph.D. research work, the use of an innovative monocell pressuremeter probe is proposed as a potential solution for improving the application of pressuremeter tests for soil-structure interaction design. Focus is put on the design of deep foundations under cyclic loading. Considering the limitations and the implementation difficulties evidenced by the state of the art presented herein, the objectives of the following work are to (1) identify and understand the source of the problems in the standard testing equipment that makes it unsuitable for performing the special testing procedures mentioned; (2) validate the measurement capabilities of an innovative pressuremeter probe that has been identified as a possible solution for the problem; (3) to define and validate testing protocols that enable to obtain the soil parameters representative for the design of foundations under axial cyclic loading; (4) to verify that the parameters obtained using the proposed equipment and procedures are suitable for the design of such structures. Validation will be done by comparing results obtained using the proposed approach with results obtained adopting the traditional Ménard one, in sites where soils have been characterized using both methods.

CHAPTER 2

SELECTION OF THE PRESSUREMETER PROBE AND LABORATORY VALIDATION

INTRODUCTION

The bibliographic study has highlighted that obtaining soil parameters representative of the design of foundations under cyclic loading using pressuremeters is feasible from a theoretical point of view. The main difficulties rely on the practical aspects involving the testing equipment. An adequate probe for this task should be able to provide accurate measurements in the small strain domain and reach sufficiently large strains in a same test, assessing, thus, elasticity and failure parameters. It should also favor the application of series of repeated cycles.

The state of practice on the pressuremeter and dilatometer probes showed that there is currently no testing equipment capable of satisfying these criteria. While Ménard pressuremeters can provide parameters at large strains that have proved efficient for designing foundations under monotonic loads, their performance is insufficient for the derivation of elastic properties. On the other hand, using more sophisticated dilatometer probes enables obtaining soil moduli at low strains. These probes, however, cannot reach the failure domain.

This chapter starts with a qualification of the most common pressuremeter probes with regards to their application to the design of piles under cyclic loading. For this application, focus is given on assessing shear stiffness at a shear strain range between 10^{-4} and 10^{-2}. The use of an innovative probe is proposed as a potential solution for the problems encountered with the standard equipment. An experimental protocol is proposed to validate in the laboratory the measuring capabilities of this probe within the quoted range of interest and the testing procedures necessary to reach the goals of

this research. The laboratory testing devices, the procedures and the soil used are described. The results obtained from tests performed in large specimens of dry sand reconstituted in two different calibration chambers are presented, as well as the parametric study carried out on the influence of the density index of the sand. The conclusions are positive and lead to a further validation program *in situ*.

2.1 EXPERIMENTAL SETUP

2.1.1 Selection of the pressuremeter probe

2.1.1.1 On the applicability of standard pressuremeter probes

There are few recent studies related to the measurement accuracy of the most used standard tricellular pressuremeter probes. The possibility of using the commercially available equipment for the objectives of this research would present an obvious advantage. However, it implies extending its application domain to non-standard tests, which requires validation, absent in literature.

An experimental procedure using the tricellular probes most used in French practice (after Jacquard and Varaksin (2018)) was implemented. The main objective was to verify if these probes could be used for assessing soil parameters representative for the design of piles under cyclic loading. Several calibration tests were performed aiming at verifying the accuracy of these devices when submitted to special testing protocols.

The testing program performed, and the results obtained are presented in *Appendix B*. The following conclusions referring to the applicability of this type of probe could be drawn:

- Measurements performed with tricellular probes have shown to be very sensitive to differential pressure variations. The system becomes more sensitive at higher volumetric expansion of its measuring cell. This implies that measurement accuracy decreases with the increase in cell volume, which penalizes measurements at high expansion rates and may prevent from performing loops of small amplitude;

- It was found that another source of measurement error was caused by the progressive dissolution of gas into water. The problem appears, especially during depressurization, when gas bubbles can appear and lead to erroneous volumetric measurements;
- Coaxial tubing presents relatively low compressibility coefficients and does add uncertainty to measurements due to volume losses. However, tubing behavior cannot be decoupled from that of the whole system which implies that it must be calibrated with the complete setup assembled (probe, tubing, controller);
- The internal diameter of the water circuit of the coaxial tubing most commonly used in practice is relatively small (3mm). The water head losses that take place when there is water flow cannot be neglected, especially for a long tubing;
    - Water head loss depends on the viscosity of the fluid being used (water or water with anti-freeze fluid) and on the temperature. It is difficult, if not impossible, to calibrate this effect for practical applications;
    - The main problem related to pressure losses along coaxial tubing is that, in tricellular devices, two fluids must be controlled simultaneously: gas and water. This task may be very complex, especially during loading step changes, during loading reversals or when high flow-rates take place;
    - The consequence is that it is difficult to precisely control the differential pressure inside the probe, and that measurements done on the control unit, at the ground level, can be misleading. This problem becomes critical when using long tubing.

- The standard probe calibration procedure assumes that the measuring cell expands as a perfect cylinder and that the volume losses due to system self-compressibility are linear with pressure. None of these assumptions could be verified through the calibration tests performed. Instead, it was observed that some of the standard probe properties as defined by AFNOR (2015) (the conventional volume of the measuring cell and the system compressibility coefficient) were sensitive to the external diameter and the probe pressure itself. These parameters are used for further test interpretation and thus, they can add unnecessary uncertainty to the test results. A more rigorous calibration procedure must be adopted;

- The external rubber membrane of the Ménard type probes tested presented severe wear after few calibration tests. In some cases, the probe burst during calibration tests. It seems useless to perform more rigorous calibrations with probes with such a short lifetime. Improvements to the inflatable membrane are necessary.

Application of enhanced membrane technology, such as implemented in the FC60®, has brought significant improvements but they are masked by the other parasite phenomena inherent to tricellular probes. Operating with three cells is definitely a major drawback for tests including unload and reload loops or series of repeated cycles. It is difficult to keep differential pressure constant while reversing pressure, which penalizes the accuracy of those probes on assessing cavity strains.

2.1.1.2 The Monocell Francis Cour® (FC) probe

The restraining sheath technology implemented in the tricellular probes of type FC-60 was originally conceived to prevent membrane bursting at high pressures and high expansion rates. It has been found that by adjusting the restraining sheath geometry, it was possible to obtain a proportional relationship between the probe diameter and the injected volume of water. This new possibility has allowed to remove the central measuring-cell and to design a simpler probe that operates with only one water cell, the *Monochambre Francis COUR*® (Monocell FC) probes.

The Monocell FC probe, schematized in Figure 2.1a, is basically composed of a cylindrical core, a mandrel in which all the membranes are set and an external protection. The core is a rigid steel tube to which the water line is connected. The mandrel is a thin steel tube over which the membranes are crimped. Three membrane layers are used as illustrated in Figure 2.1b: an impervious thin rubber membrane, which defines the measuring cell; the textile restraining sheath, which controls the thin rubber membrane geometry and resists to any traction load; and an external polyurethane membrane (Figure 2.1c) which protects the textile sheath from abrasion due to the contact with the soil. A photo of the fully inflated probe showing the textile sheath is presented in Figure 2.1c, and a photo presenting the external polyurethane sheath is presented in Figure 2.1d. Yet, an external metallic protection can be used against damage in coarse soils, as in standard probes. Probe components are basically

the same as those of the FC 60 tricellular probe presented in Appendix A. The main difference is that the central cell no longer exists and that there is only one fluid circuit.

The textile restraining sheath is the main innovation of this probe in comparison with other monocellular probes currently existing. It is fabricated by cylindrical weaving of so-called hybrid cables, patented by Cour (2014), which are a combination of elastic yarns (elastomer) and very high strength yarns (kevlar, high-density polyethylene or other). They have the particularity of being able to elongate more than one hundred per cent under a very low stiffness (the elastomer's stiffness). The resistance of the high-strength yarns mobilizes as the hybrid cable reaches its limit elongation, quickly increasing the cable's stiffness. The quick increase in stiffness limits the capacity of elongation and imposes a maximum length for the cable. This can be seen in Figure 2.2a. The detail of the mobilization of the high-strength yarns is presented in Figure 2.2b and the cable loading curve is presented in Figure 2.2c. Weaving the restraining sheath using the hybrid cables allows imposing the geometry of the probe during its inflation. Due to this conception, probe limits in pressure and in maximum expansion are only dependent on the strength properties of the restraining sheath yarns. The thin rubber membrane defining the measuring cell does not contribute to probe resistance and has the only role of providing water tightness. The sheath strength can be adjusted by increasing yarn density or cable strength.

The simplified hydraulic circuit presents the advantage of enabling adopting control units that use no pressurized gas (only water). Operating with only one fluid is advantageous for cyclic loading. Another advantage is that the tubing is dedicated only to water, providing a larger internal diameter which reduces water head losses.

The membrane improvements and the enhanced lifetime enable implementing a more rigorous calibration procedure.

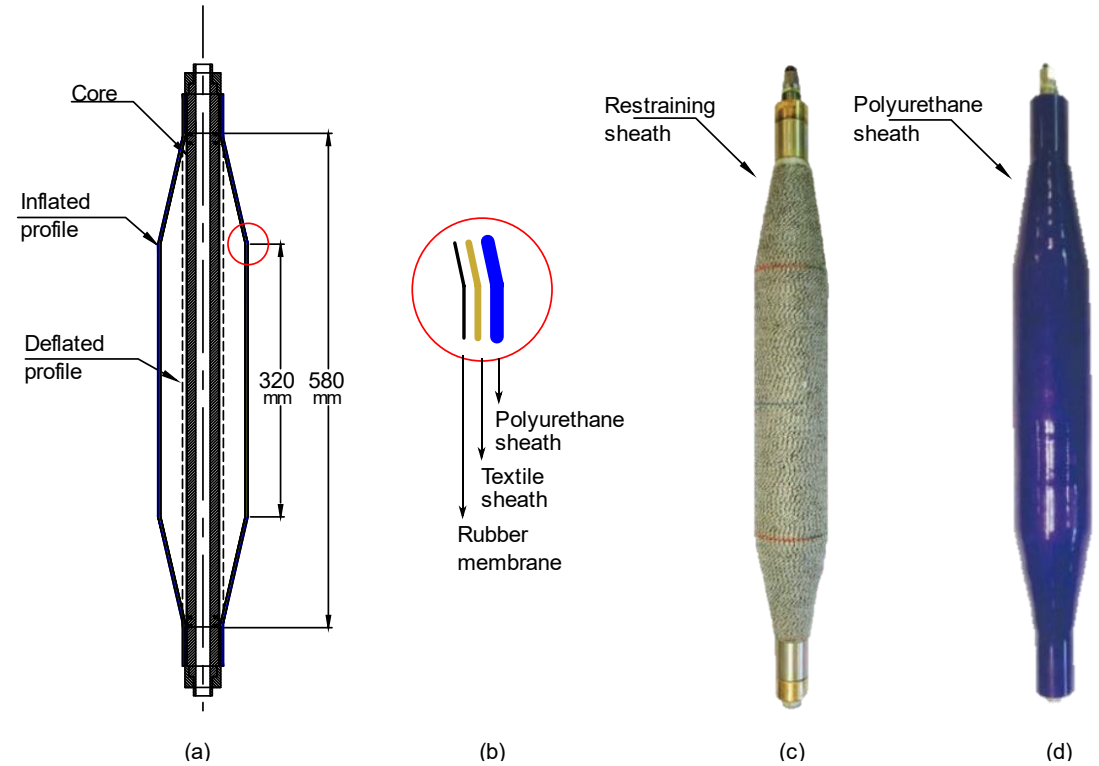

Figure 2.1 – (*a*) Monocell FC® probe scheme; (b) scheme of the layers composing the inflatable membrane; (*c*) photo of the probe fully inflated showing the restraining sheath; (*d*) photo of the probe fully inflated with the protective PU external sheath. Dimensions in millimetres

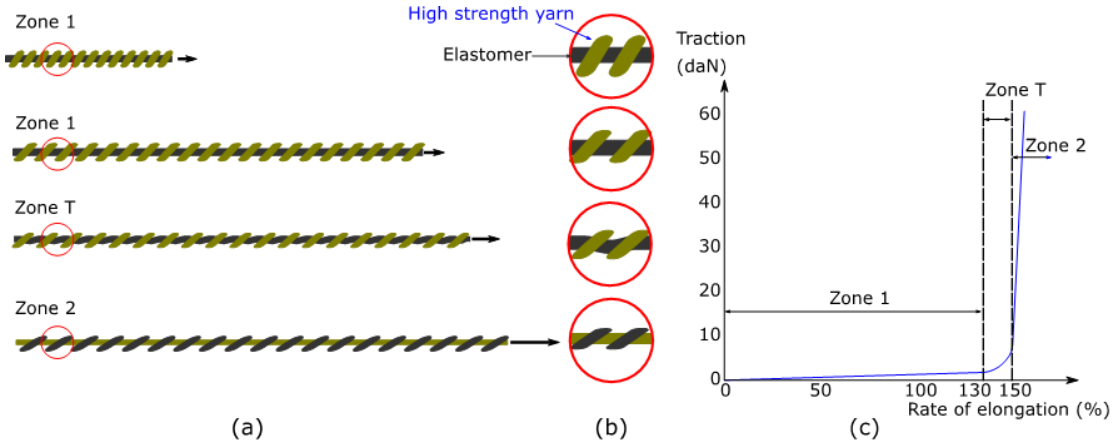

Figure 2.2 – Working principle of the hybrid cables, which are used for manufacturing the restraining sheath for Monocell probes. From Cour (2014)

2.1.2 The pressure-volume controller and calibration cylinders

The development of the experimental procedures required an adapted setup for using the Monocell FC probe in the laboratory. The experimental setup (Figure 2.3) was composed of:

- An advanced pressure volume controller (GDS Instruments), used to control the probe inflation. The pressure and volume measurement resolutions of the controller are of 1 kPa and $1 \cdot 10^{-3}$ cm^3, respectively. Maximum flow-rate provided by the controller is of approximately 1 cm^3/s. Its maximum operational volume capacity is of about 600 cm^3. The reservoir of the controller needs to be refilled if higher volumes are needed;
- The GDS output tubing is equipped with a bypass (Figure 2.4) which allows to refill the reservoir without having to open the probe circuit and risking desaturating it. Two valves allow isolating each circuit: the probe circuit and the refilling circuit;
- The controller is connected to the probe via a reinforced tubing of 2 m length and 4 mm internal diameter, with a very high stiffness (designed to support up to 74 MPa internal pressure), in order to minimize volume losses due to system self-dilation. The resulting volume loss was less than 1.0 cm^3/MPa. Other sets of tubing were tested but presented less satisfactory properties;
- A quick connector is placed on the probe head (Figure 2.3 detail a). This connector allows connecting and disconnecting the probe to the rest of the circuit without desaturating it. A supplementary pressure transducer is placed near the probe head to allow measuring the water pressure near the probe. A purge valve is installed on the probe head;
- The probe was calibrated using a set of steel calibration tubes (Figure 2.5) following the procedures given in item 2.3.1. Special devices developed for specific calibration tests are presented in items 2.1.3 and 2.1.3.2.
- Data acquisition is performed through a portable computer and a *LabView* standalone app developed specially for this application by the Geotechnical team of Navier laboratory (CERMES). Acquisition frequency is set to one data point per second;

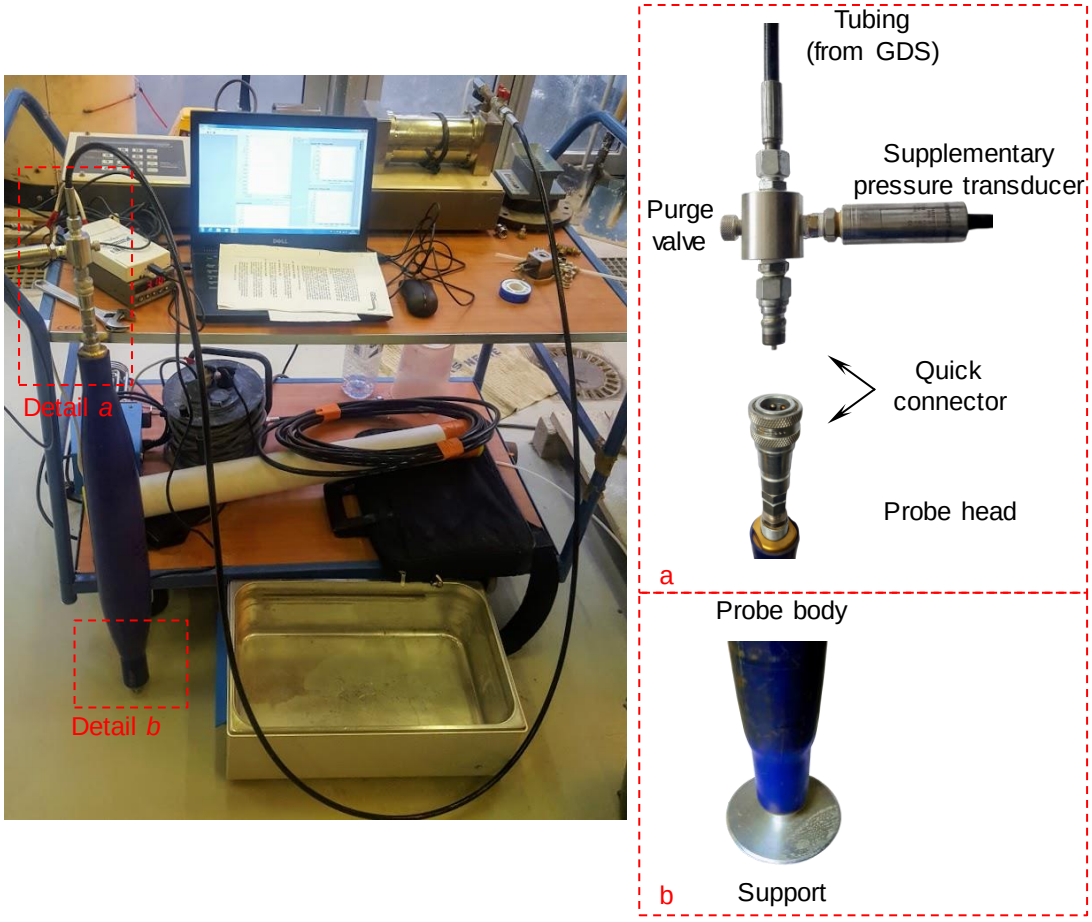

Figure 2.3 – Experimental setting for the first probe calibration tests and details of the hydraulic connectors at the probe head and the supplementary pressure transducer

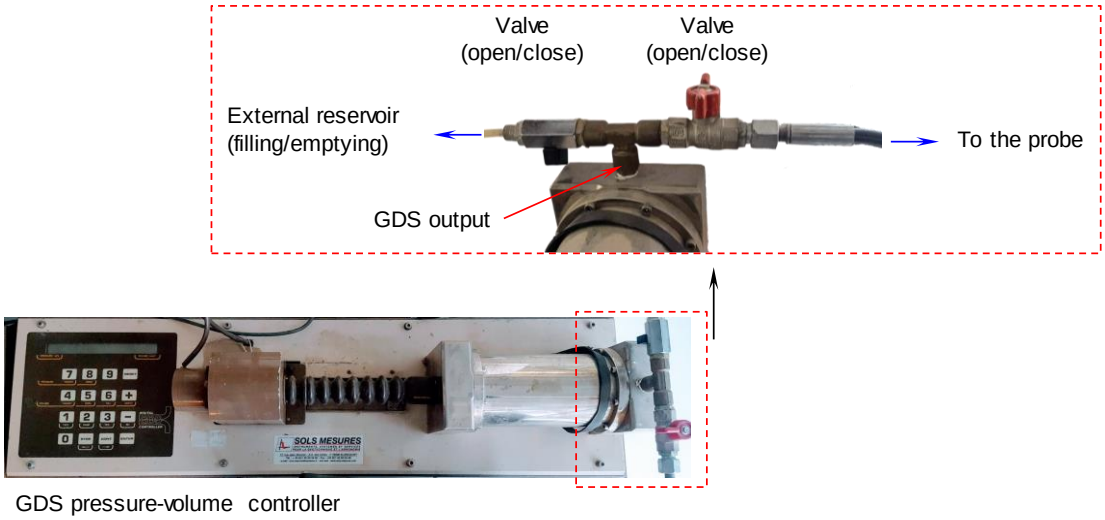

Figure 2.4 – Detail of the hydraulic connectors in the GDS controller output

Figure 2.5 – Steel calibration tubes of internal diameter 60 mm, 66 mm, 75 mm and 85 mm

Besides the equipment presented above, two specific devices were developed in the laboratory to check the probe calibration procedure and its membrane sensitivity to external variations of pressure. The use of these devices was only necessary in order to validate the probe measuring capabilities in the context of the laboratory study, and its use is not required for further *in situ* applications.

2.1.3 Specific probe calibration devices

2.1.3.1 The instrumented thick cylinder (ITC)

One straightforward way to verify the calibration procedure is to compare the evaluated radial displacements assessed using volumetric measurements (evaluated according to eq. (2.4)) to those obtained through external sensors, such as strain gauges. In order to make this verification possible, a specific setup was developed at Navier laboratory (CERMES) using a thick polyurethane cylinder instrumented with two pairs of strain gauges, internal and external, fixed symmetrically with respect to the cylinder's axis. The following method was used to assemble the setup:

- The polyurethane surfaces were sanded and then cleaned with ethanol before gluing the strain gauges;
- A temporary support was conceived for holding and gluing the strain gauges in the interior of the cylinder. The support was fabricated with a metallic rod on which a plastic foam was attached, providing a relatively soft surface. Details are presented in Figure 2.6;

- The strain gauges were temporarily fixed over the soft surface on the rod using adhesive tape. Glue was applied to the gauge's face, and then the rod was inserted into the polyurethane tube without touching its walls (Figure 2.7);
- Once the center of the rod reached the adequate position, it was carefully pushed against the tube's walls and slightly turned to ensure that the entire surface of the strain gauge got in contact with it. The soft surface enables applying uniform pressure to the strain gauge and avoid that air bubbles stay trapped during the installation process. The rod was held in position until the glue dries (Figure 2.8). The temporary support was removed using a cutter;
- The external gauges were manually fixed.

A scheme of the assembled device and a photo during a test are presented in Figure 2.9. The internal gauges are in contact with the outer probe membrane and thus allow directly comparing strain measurements. The external gauges were installed for two main reasons: (1) to serve as a control group to ensure that the internal gauges were not damaged due to shearing against the probe's membrane during pressurization and (2) to enable an evaluation of the polyurethane tube deformability properties based on cavity expansion theory. Technical characteristics of the polyurethane tube are: shore 800R, 70 mm internal diameter, 15 mm thick and 500 mm high.

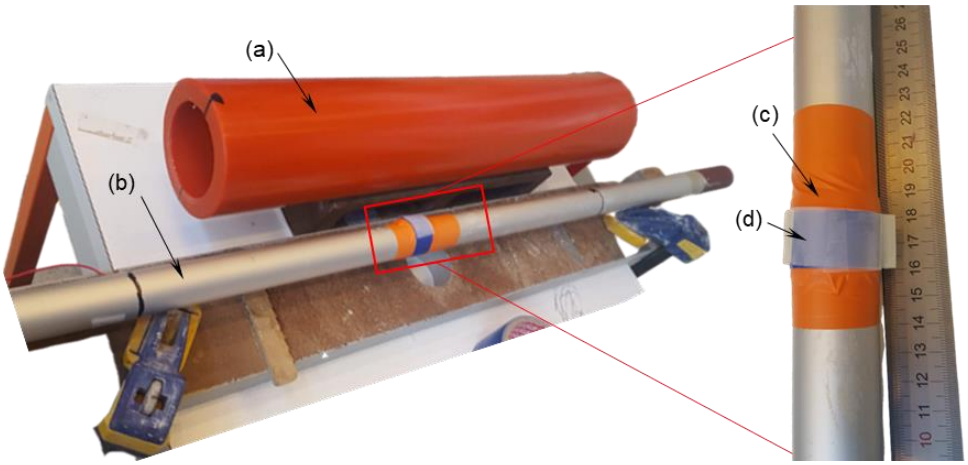

Figure 2.6 – Details on the development of the instrumented thick polyurethane cylinder. (a) The polyurethane tube; (b) metallic rod used for installing the internal strain gauges; (c) plastic foam attached to the rod; (d) adhesive tape used for temporarily support the strain gauge

Figure 2.7 – Placing the strain gauge over the temporary support before applying glue

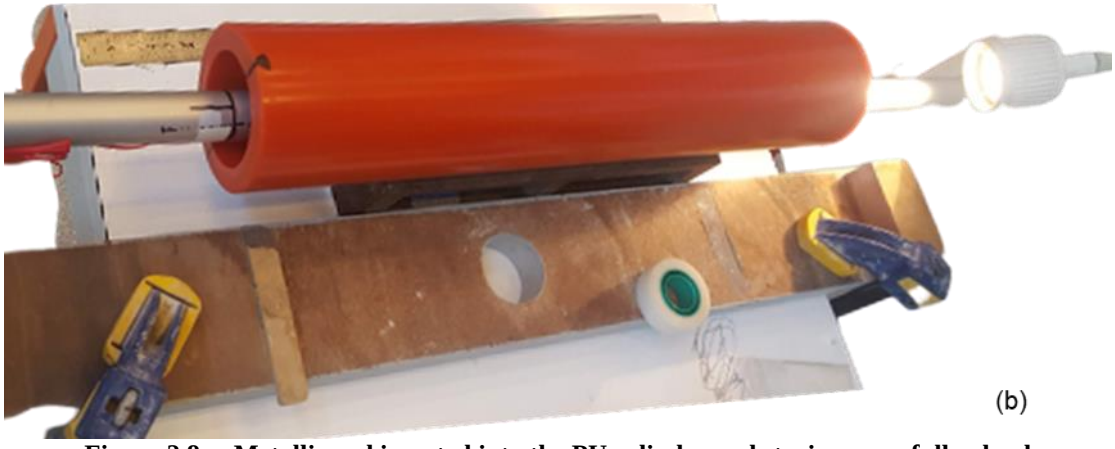

Figure 2.8 – Metallic rod inserted into the PU cylinder and strain gauge fully glued

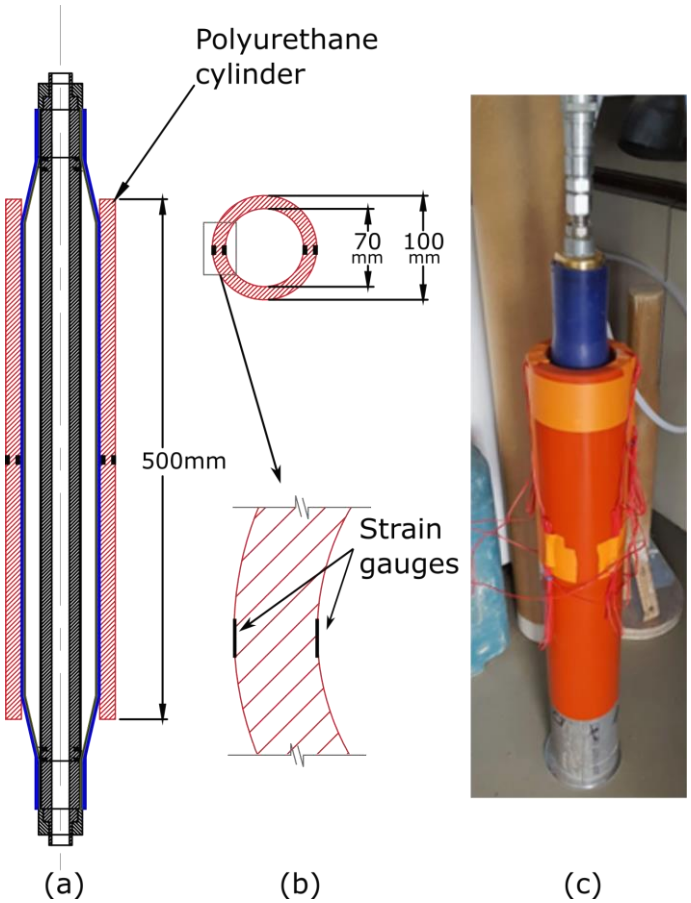

Figure 2.9 – Thick polyurethane cylinder equipped with two internal and two external strain gauges. (a) cross section; (b) detail of the strain gauges installation; (c) photo of the device under test

2.1.3.2 The hydrostatic calibration chamber (HCC)

The Monocell FC probe is composed of three membrane layers, each one having independent and complementary functions (water tightness, geometry control and protection). Besides the standard open-air calibration procedure, calibrating the probe's membrane sensitivity to an external pressure variation was also necessary to eliminate doubts in test interpretation. The Hydrostatic Calibration Chamber (HCC) was conceived in order to enable the application of a known external pressure to the probe's membrane and to verify that the variations on this pressure could be precisely detected by the probe control unit.

Hydrostatic conditions are necessary for this verification because in a calibration chamber filled with soil, the radial stress distribution may depend on several factors, such as the ratio between the horizontal and vertical stresses (K_0) and any possible disturbances from this initial state. The presence of the probe inside the soil specimen

can be a cause of such disturbance. If so, the stresses imposed at the chamber's boundaries are not homogeneous inside the soil specimen and it may be difficult to verify if the values of pressure measured by the probe controller are correct. Hydrostatic conditions eliminate the source of uncertainty due to stress distribution.

The HCC is a metallic cylindrical cell of internal diameter 162 mm, 3.4 mm thick. One of the chamber bases is equipped with hydraulic connectors that enable filling up the cell and pressurizing the water inside. An independent connector allows controlling the probe. The probe and the chamber are controlled using independent GDS type controllers. An air-water interface cell is used to provide supplementary volume for controlling the chamber. A schematic view of the HCC designed is presented in Figure 2.10 including the controllers. A photo of the fully assembled chamber is presented in Figure 2.11a and the details of the hydraulic connection on its top plate are presented in Figure 2.11b.

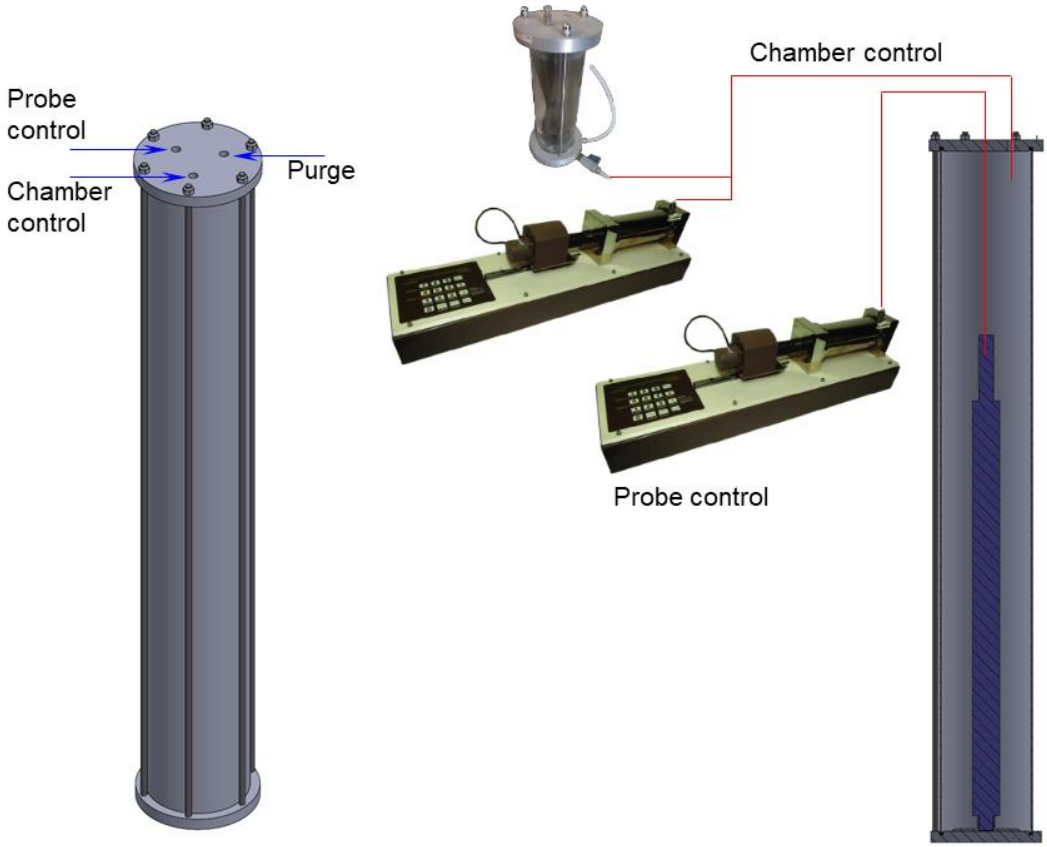

Figure 2.10 – View of the Hydrostatic Calibration Chamber (HCC) designed for special calibration tests

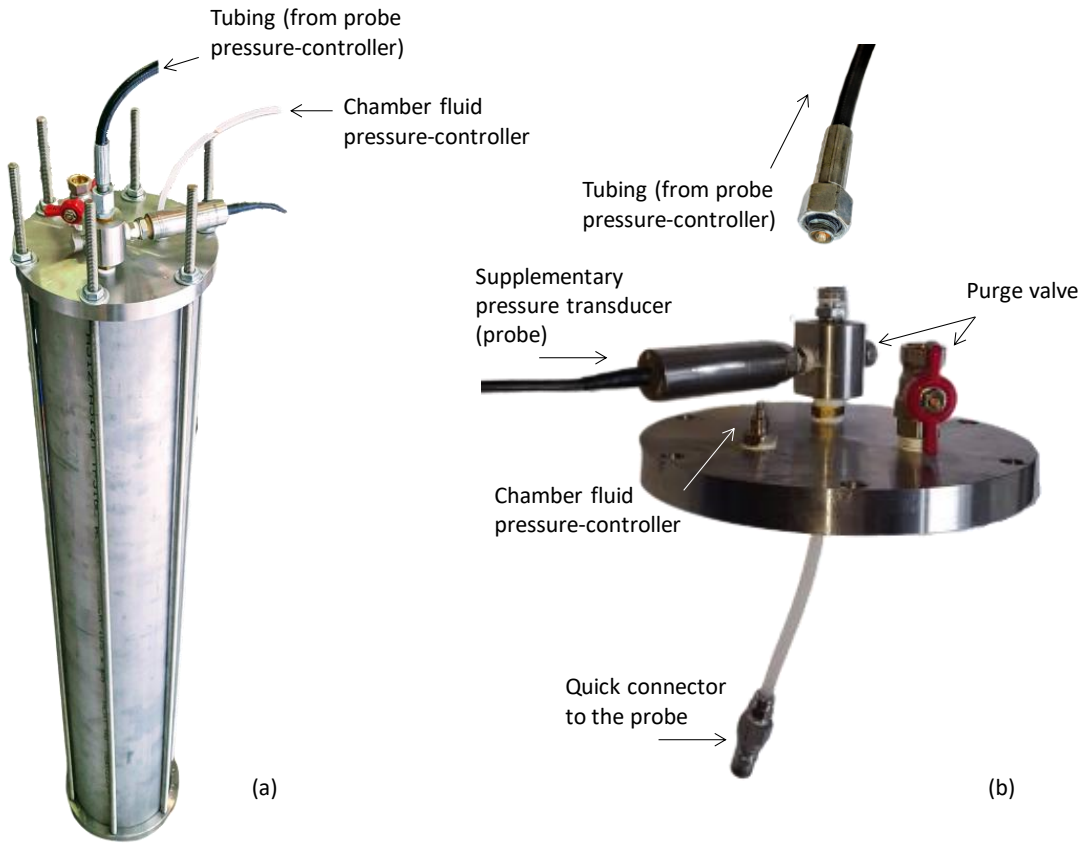

Figure 2.11 – (a) view of the hydrostatic calibration chamber fully assembled; (b) details of the hydraulic connections on the chamber's top enclosure.

2.1.4 The calibration chambers

Calibration chambers are experimental devices that enable the implementation of physical models capable of representing a real-world problem under controlled conditions in the laboratory. The boundary conditions in the reduced model (stress state and degrees of freedom) and the properties of the soil specimen are chosen so that to be representative of a slice of the full-scale problem (or, in some cases, a full reduced-scale of it). The interest of performing tests in a calibration chamber are that (1) most of the uncertainties that would be faced in tests on site are mastered, (2) it is simpler to perform parametric studies and (3) the global cost of the tests is inferior with respect to *in situ* tests.

Two different calibration chambers have been used for this research. The first one is the historical *Navier Géotechnique* (CERMES) Calibration Chamber, that has been first presented by Dupla (1995). This calibration chamber enables controlling both the vertical and the horizontal pressures acting on the soil specimen. It will be denoted *PCC* on the following text. Dupla and Canou (2003) used it in the context of the

investigation of the applicability of cyclic pressuremeter tests for assessing liquefaction properties of sands. For that work, a mini pressuremeter was used. Amongst numerous other works, the device has been further used by Le Kouby (2003) and Tali (2011) for the study of model piles under cyclic loading in sand, and by Muhammed (2015), in clays. Soil specimens of 524 mm in diameter and 700 mm high can be reconstituted in the *PCC* either by pluviation or by manual compaction for sands. The device is mainly composed of (1) a lower piston, movable in rotation and in translation over rails, which allows the application of the vertical stress, and (2) a metallic cylindrical enclosure for the application of the horizontal (radial) stress, (3) a membrane surrounding the soil specimen, (4) an upper base and a cover. A scheme and a photo are presented in Figure 2.12. The reaction frame over the chamber was not used on the present work.

The second type of calibration chamber used herein can be considered as a simplification of the previously described one. The main difference is that the soil specimen is in direct contact with the cylindrical metallic enclosure and it is not surrounded by a membrane. The vertical stress is controlled by a flexible hydraulic cushion placed between the soil specimen and the chamber coverage. The horizontal stress applied to the specimen is a function of the vertical stress and of the soil's K_0 coefficient. The test conditions are similar to those of an oedometer test. The device has been first used by Le (2014) for the study of soil-mix columns and more recently by Kerner (2018) for studying monopile behavior under cyclic loading. A schematic and a photo of the described apparatus are presented in Figure 2.13. In the subsequent text it will be denoted *KCC (K_0 Calibration Chamber)*. Its internal diameter is 550 mm and it is 730 mm height.

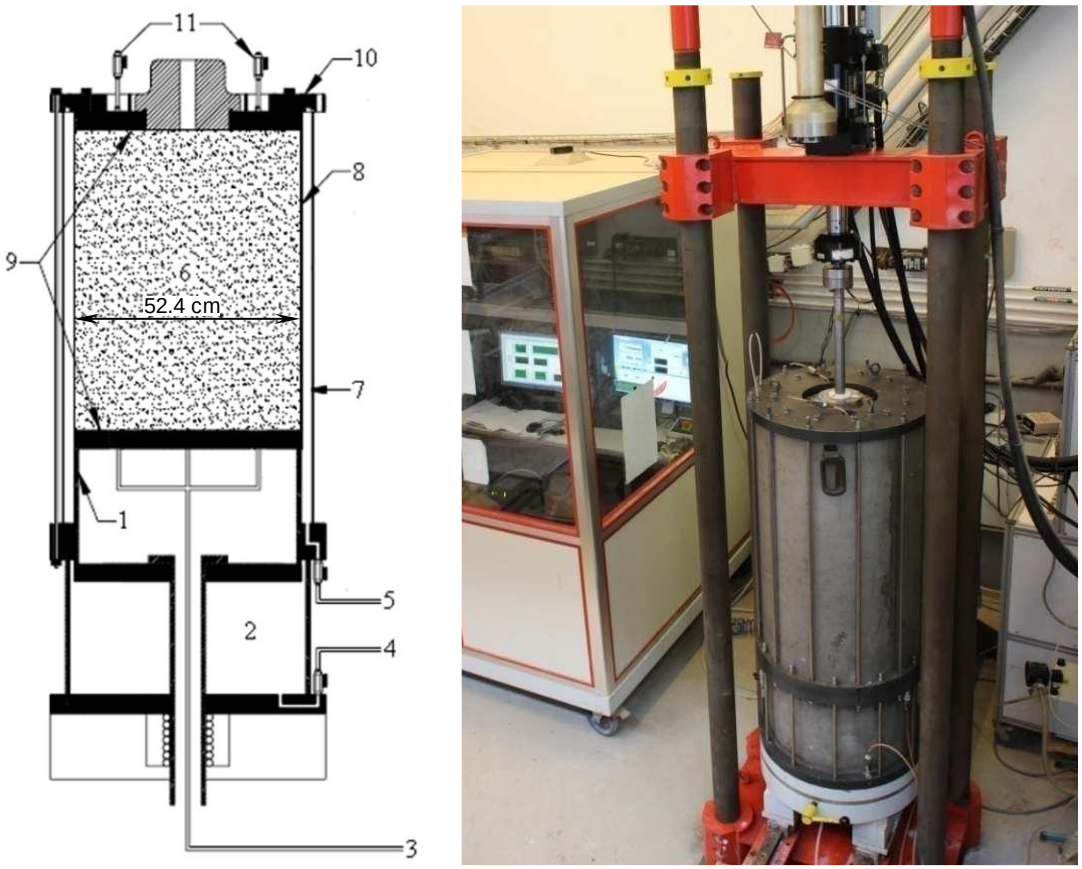

1 – Piston
2 – Pressurization chamber
3 – Connection to the specimen
4 – Vertical stress control
5 – Horizontal stress control
6 – Soil specimen
7 – Cylindrical enclosure
8 – Neoprene membrane
9 – Top and dow n bases
10 – Cover
11 – Drainage

Figure 2.12 – Scheme and photo of the CERMES Calibration Chamber (*PCC*) (adapted from Tali (2011) and Muhammed (2015))

Modelling using *KCC* instead of *PCC* presents the advantage of much faster assembly of the soil specimen. The equivalence between the two models must be verified since the radial boundary condition is different. This was done by comparing results obtained in both chambers and is presented in section 2.7.

In any case, the influence of the limited dimension of the calibration chamber in the obtained results should be investigated. For the pressuremeter tests aiming to assess soil properties at small strains, this verification can be done either by analytical solutions or through finite element models.

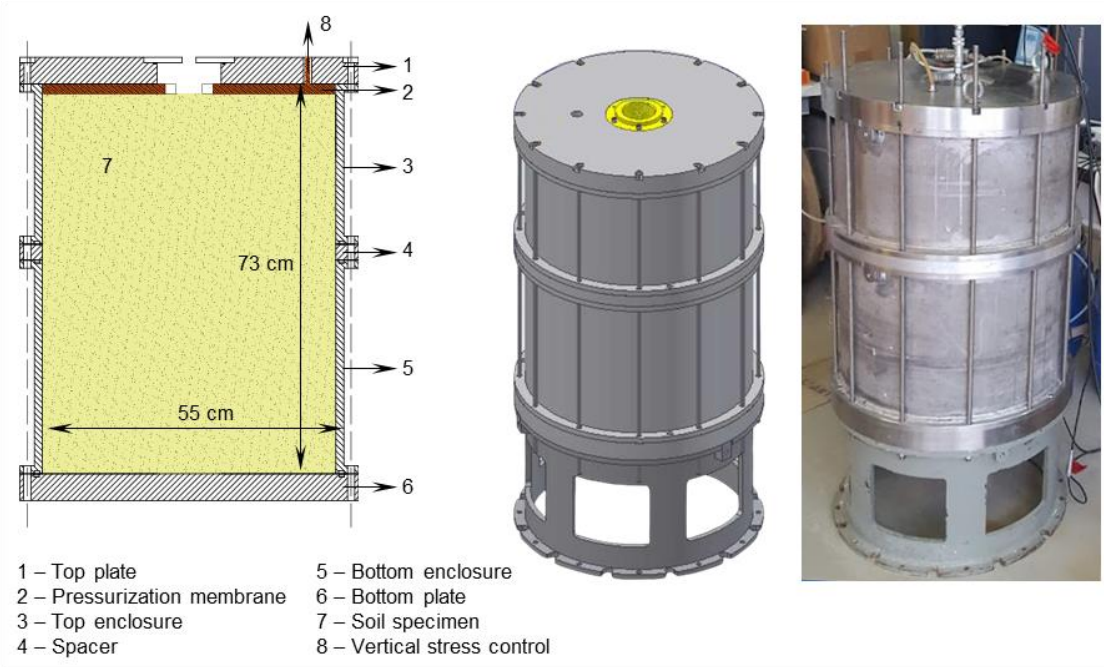

Figure 2.13 – Schematic, 3D model and photo of the K_0 Calibration Chamber (KCC)

2.2 TESTED SOIL

Fontainebleau sand (NE34) was selected for the calibration chamber study. This is a well-known reference silica sand widely used in France for benchmark purposes. Its grains are beige colored and have a sub-rounded shape. The main properties of this sand are summarized in Table 2.1. The grain size distribution curve and a view from scanning electron microscope (after Tali (2011)) are presented in Figure 2.14.

Table 2.1 – Grain size properties of Fontainebleau sand NE34 (after Kerner (2018)**)**

e_{min}	e_{max}	U_c	D_{50} (mm)	ρ_s (g/cm^3)
0.56	0.88	1.5	0.21	2.65

Fontainebleau sand mechanical properties were studied in the laboratory through triaxial tests (Andria-Ntoanina, 2011). The evolution of basic parameters in function of the density index are presented in Table 2.2. The coefficient of horizontal pressure at rest K_0 can be evaluated, as a first approximation, using Jaky's formula ($K_0 = 1 - \sin \varphi'$).

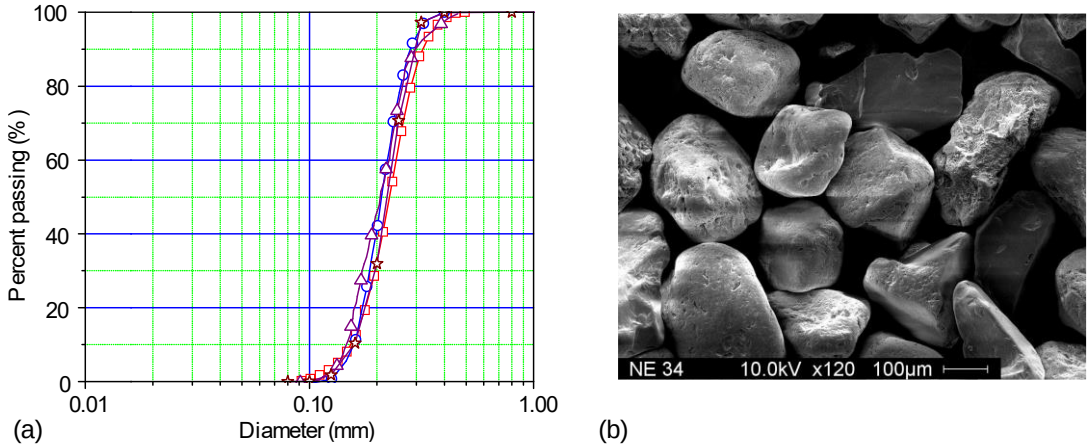

Figure 2.14 – (a) Fontainebleau sand grain size distribution curve from various studies and (b) electronic microscope view (after Tali (2011))

Table 2.2 – Fontainebleau sand strength properties

I_D	e	φ' (°)	ψ (°)	K_0
0.50	0.720	34	5	0.44
0.70	0.656	37	10	0.40
0.90	0.592	39	14	0.37

The influence of stress and strain levels on the deformability properties of this sand was studied by Delfosse-Ribay et al. (2004) using resonant column and cyclic triaxial tests. The authors showed that the power law in eq. (2.1) accurately represented the increase of the shear modulus of this sand with the confining stress for specimens isotropically consolidated:

$$G_{max} = 200\frac{(2.17-e)^2}{1+e}\sigma_c'^{0.47} \tag{2.1}$$

where: e is the current void ratio; and σ_c' [MPa] is the effective consolidation stress (specimens consolidated under an isotropic stress state). This expression is plotted in Figure 2.15*a* for three different density indices.

Delfosse-Ribay *et al*. (2004) studied the variation of Fontainebleau sand shear modulus versus strain for a consolidation stress of 0.3 MPa. The authors did not study the variation of the normalized stiffness decay in function of the consolidation stress. Examples of relationships between shear modulus and shear strain taking the consolidation stress into account are available in the literature (Zhang et al. (2005) , Oztoprak and Bolton (2013))

Oztoprak and Bolton (2013) studied the shear modulus degradation of sands through a large database of tests, including the one performed by Delfosse-Ribay et al. (2004). They proposed a model which is described by eq. (2.2). In this formulation, the effect of the effective stress on the stiffness degradation is considered through eq (2.3), which was calibrated by the authors using multiple variable regression analyses. The parameter γ_r is the characteristic reference shear strain that corresponds to the strain level at which shear modulus G_s is reduced to 50% of G_{max}. According to this formula, γ_r varies linearly with the average effective stress, p', and depends on the sand uniformity coefficient, void ratio and density index. Equation (2.2) has been plotted in Figure 2.15*b* considering Fontainebleau sand properties and a density index of 0.70 for various consolidation stresses.

$$\frac{G_s}{G_{max}} = \frac{1}{\left[1 + \left(\frac{\gamma - \gamma_e}{\gamma_r}\right)^a\right]} \tag{2.2}$$

$$\gamma_r(\%) = 0.01 U_c^{-0.3} \left(\frac{p'}{p_a}\right) + 0.08 e I_D \tag{2.3}$$

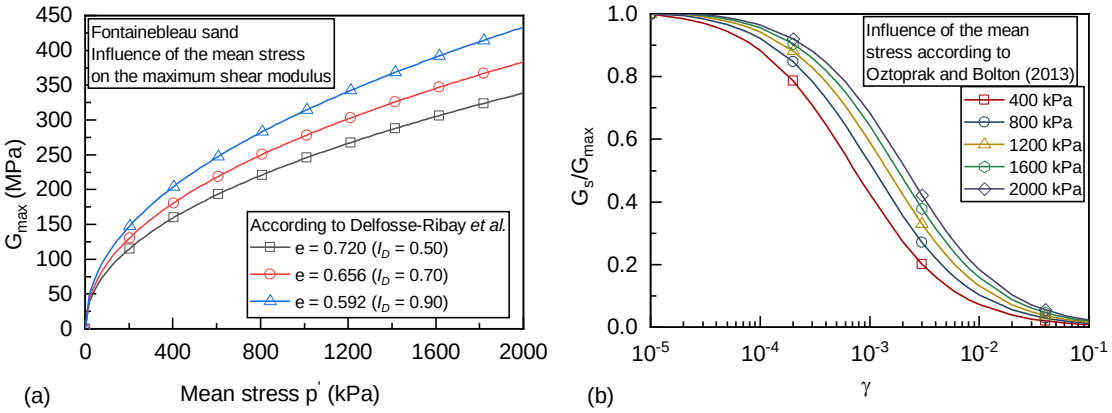

Figure 2.15 – (a) Elementary values of Fontainebleau sand of maximum shear modulus as a function of the effective isotropic consolidation stress ; (b) normalized shear stiffness decay in function of shear strain for various values of mean effective stress *p'* for I_D = 0.70

In pressuremeter tests, the initial state is anisotropic (K_0 condition) and, as cavity pressure increases and plastification develops around the cavity, stress anisotropy increases. Payan *et al.* (2016) showed that sands submitted to anisotropic stress state present higher values of G_{max} if compared to sands under isotropic stress state. Authors showed that stress anisotropy effect on maximum shear modulus is more pronounced on sands with high angularity grains and high coefficient of uniformity. The authors proposed a model to evaluate the ratio between $G_{max(isotropic)}$ and $G_{max(anisotropic)}$. The

application of the proposed model considering Fontainebleau sand properties results in the fact that anisotropy effects on maximum shear modulus are inferior to 3%. This is consistent with the fact that sand grains have a sub-rounded geometry. Stress anisotropy effects on shear stiffness of Fontainebleau sand will be considered as negligible in the present work.

2.3 EXPERIMENTAL PROTOCOLS

2.3.1 Probe calibration procedure

As in standard pressuremeters, the cavity's radial expansion and the cavity pressure imposed by the probe are evaluated from readings of water volume and water pressure on a control unit located at the ground surface. The following corrections must be accounted for when interpreting raw measurements: pressure corrections due to the vertical distance between the controller and the probe (hydrostatic pressure); probe membrane self-resistance correction; volume losses caused by the system compressibility. Probe calibration is fundamental in order to transform raw measurements of water pressure and volume variations into a cavity pressure versus cavity radial strain curve. The next sections describe in detail the calibration procedure proposed for the Monocell FC probe within the context of this work.

2.3.1.1 Open-air Calibration

Open air calibration consists in inflating the probe under free boundary condition (atmospheric pressure around the probe) following the same procedure as for an expansion test in the soil (vertical position, same inflation rate). The interpretation of this test allows obtaining the membrane self-resistance which must be accounted for when calculating the pressure effectively applied to the soil cavity. This procedure is similar to what is currently done in pressuremeter and dilatometer practice.

2.3.1.2 Diametrical Calibration

Another boundary condition to be verified by calibration tests is the relationship between the probe volume V and its external diameter ϕ. A calibration procedure that enables assessing this relationship requires using at least three steel tubes (or more) of

different internal diameters. The calibration tubes should cover the complete range of diameters reached by the probe during the expansion test in a soil.

The calibration test is performed by placing the probe inside a thick-walled steel tube with known internal diameter ϕ_1. The probe is pressurized while keeping records of its internal pressure and volume. After the membrane is in full contact with the tube wall, the measurements of volume variations in function of pressure increases enable evaluating the compressibility of the whole system, including the controller device, the line carrying water and the probe with its membranes. By repeating this test using calibration tubes of different diameters ϕ_i, it is possible to establish a relationship between the volume V injected into the probe and its external diameter ϕ. This relationship can be written as $\phi = f(V)$. This procedure is schematized in Figure 2.16.

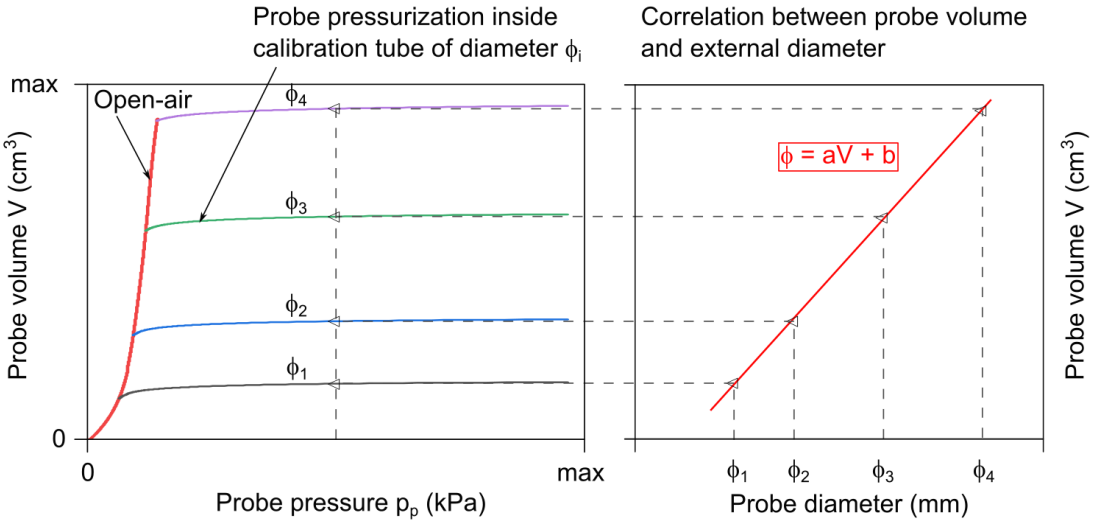

Figure 2.16 – Scheme of the calibration procedure using several diameters of calibration tubes and establishment of a relation between probe volume and external diameter

A particularity of the Monocell FC probe is that, for any constant internal pressure, the relationship between the injected volume and the diameter is linear. This is verified by calibration tests that will be presented in section 2.3.1. Therefore, the external diameter of the probe, ϕ, can be calculated by a linear equation in function of the probe volume V and pressure p_b, as presented in eq. (2.4). In this equation, the parameters a and b are calculated by the least square method, as presented in the right-hand side of Figure 2.16.

$$\phi(V, p_b) = a(p_b) \times V(p_b) + b(p_b) \tag{2.4}$$

Coefficient a is related to probe geometry and its external dressing (if using metallic stripes or not). Coefficient b is related to system compressibility. Their variation in

function of probe pressure is obtained by calculating $a(p_b)$ and $b(p_b)$ for all the pressure range reached in the calibration tests. For tests in soil, the external probe diameter corresponds to the cavity diameter. It can be easily converted to the cavity radius. The variation of the cavity radius gives the cavity strain.

It is important to note that this calibration procedure is valid for the limit conditions of a pre-bored test: the probe is placed in a pre-formed cavity. The self-boring condition, in which the probe is fully surrounded by soil would require a different calibration procedure.

Calibrating the probe using this procedure presents two main advantages: the first is that the membrane compressibility and its variation with the external diameter is automatically taken into account. The second is that the membrane behavior is verified on its entire working domain and no hypotheses are made regarding its geometry during inflation. In standard pressuremeter calibration practice, the central cell is supposed to inflate as a perfect cylinder, which has been shown to add unnecessary uncertainties to test interpretation.

2.3.1.3 ***Membrane compliance calibration***

Once the probe has been calibrated for its external diameter, a membrane compliance test is performed. The bibliographic study has shown that membrane compliance takes place in most types of probes, which implies that additional measurement corrections should be done when unload-reload loops are performed. The compliance calibration procedure adopted herein is the same as described by Fahey and Jewell (1990). It consists in placing the probe inside a calibration tube of diameter close to that of the borehole to be done in soil (60 mm in the present case) and performing a loading program including unload and reload loops at increasing pressure levels. The procedure is schematized in Figure 2.17a. Probe is inflated until reaching contact with the tube walls and then its pressure p_b is increased to reach an established value of pressure, $p_{b,L1}$ (probe internal pressure for loop 1). A pressure-hold step of at least one minute is performed to avoid any superposition of time dependent phenomena originated from the membrane, and then the probe is unloaded by a pressure amplitude of approximately 0.4 times $p_{b,L1}$. Another pressure-hold step is performed and then the probe is reloaded to a pressure $p_{b,L2}$ ($p_{b,L2} > p_{b,L1}$). This procedure is repeated for different values of $p_{b,Li}$,

chosen in order to correspond to the unload-reload loops that will be further performed in the test in soil. The loading rate should be close to that employed in the test in soil. The effect of membrane compliance manifests as additional volume losses within each unload-reload loop, as can be seen in Figure 2.17b.

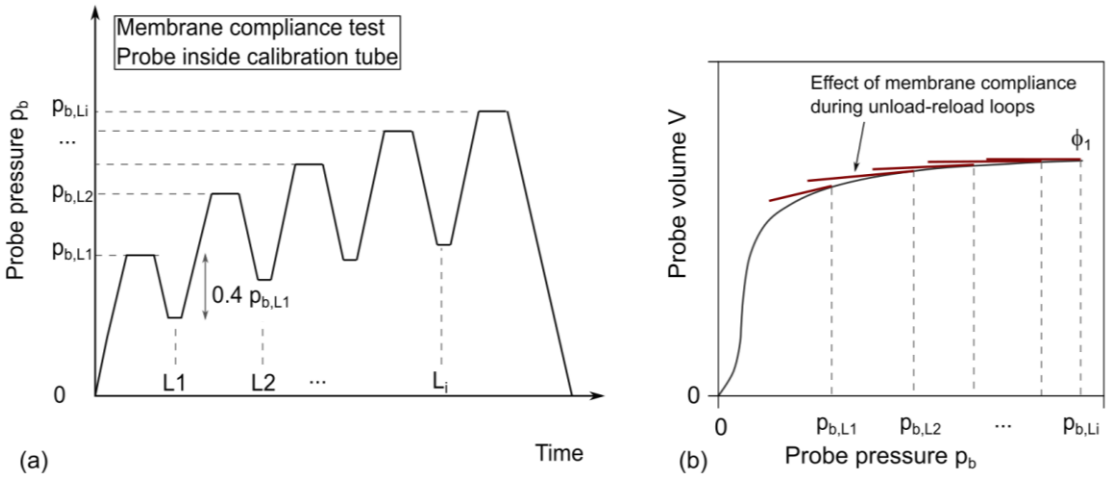

Figure 2.17 – (a) Scheme of the loading program of a membrane compliance calibration test; (b) expected result showing the effect of membrane compliance

2.3.1.4 Interpretation of raw measurements

The first step in the interpretation of the raw measurements is to correct for hydrostatic pressure in order to account for the vertical distance between the probe and the pressure transducer. The pressure inside the probe measuring cell p_b is equal to the raw pressure p_r measured at the control unit plus the hydrostatic pressure due to the water column above the probe. In the laboratory, probe and controller were at a same vertical position and this correction is negligible. Once the probe pressure is calculated, equation (2.4) is used to evaluate its external diameter for all measured values of V, yielding a curve probe pressure p_b versus diameter ϕ., as illustrated in Figure 2.18. As it can be seen, each calibration test can be considered as an iso-diameter curve, within which the probe pressure and volume vary at constant external diameter.

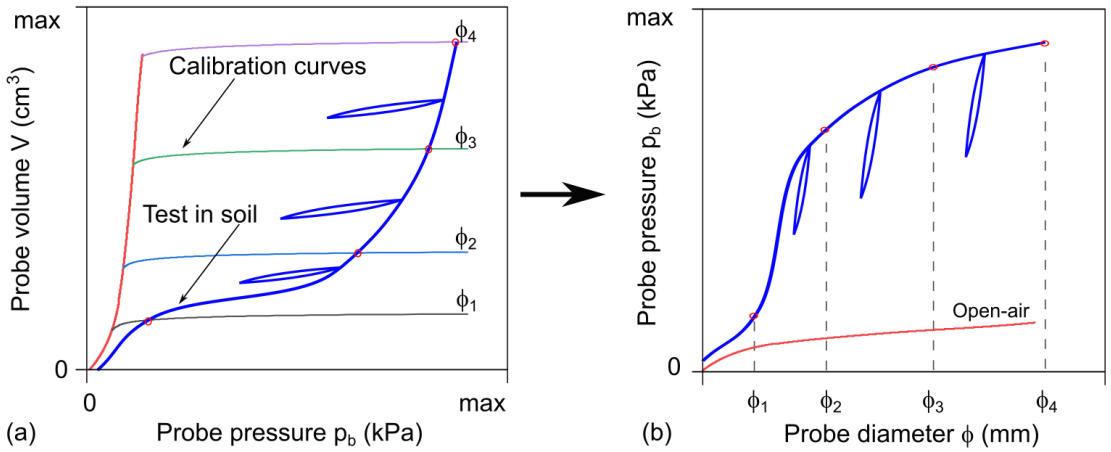

Figure 2.18 – Principle of the interpretation of a test in soil: from volume to diameter

The next step is to apply membrane inertia correction. This leads to a curve relating the external diameter of the probe and the external pressure, i.e. the pressure applied to the cavity wall. The cavity radius is obtained as half the diameter. The initial cavity radius R_0 can be calculated using the procedure presented in AFNOR (2013b) and illustrated in Figure 2.19a. The initial cavity diameter is considered as intersection between the extension of the straight line portion of the test curve and the pressure at which the probe is in contact with the soil. Cavity radial strains ε_c can be calculated as the ratio between variations in probe radius, Δr, and the initial radius, $\Delta r/R_0$, as illustrated in Figure 2.19b.

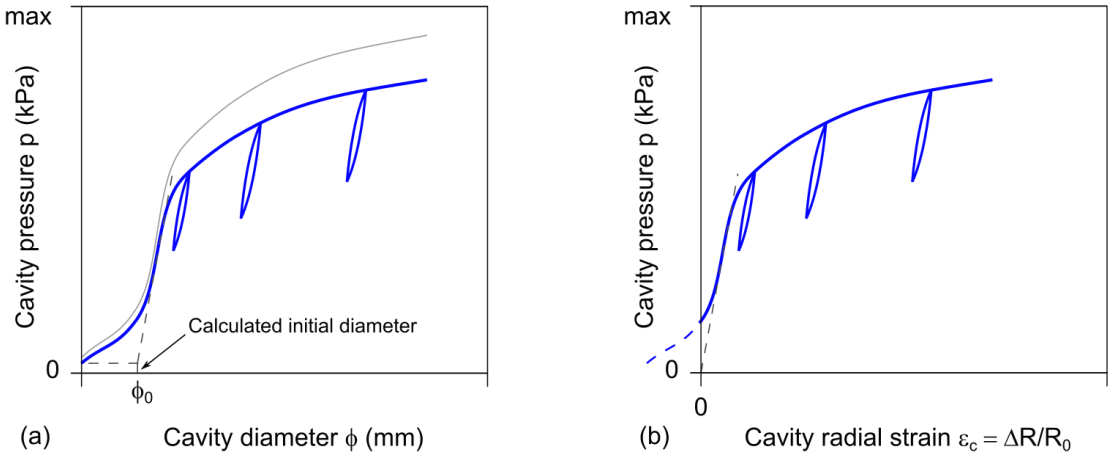

Figure 2.19 – (a) membrane inertia correction and calculation of the initial cavity diameter; (b) curve recalculated in terms of cavity radial strain

As a last interpretation step, it is needed to correct each of the unload-reload loops presented in Figure 2.19b from membrane compliance.

To do so, the membrane compliance test is interpreted using equation (2.4) following the previously presented procedures, as if it were a test in soil. As a result, a fictive

cavity expansion curve is obtained (the system curve), as presented in Figure 2.20a. The slope calculated within the interpreted points of each unload-reload loop is related to the amount of compliance (volume loss) that takes place during the unloading process. The system modulus G_{syst} of each loop is calculated as half the slope obtained in each loop. G_{syst} is dependent on the probe pressure before unloading, $G_{syst}(p_{b,L_i})$. A plot of G_{syst} as a function of p_{b,L_i} enables determining the so-called "compliance law", illustrated in Figure 2.20b.

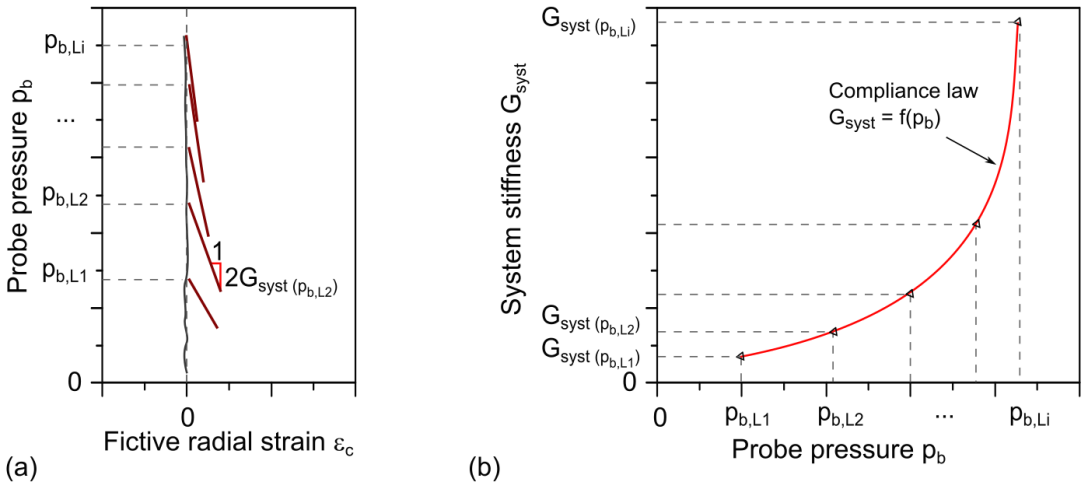

Figure 2.20 – (a) Scheme of an interpreted compliance test; (b) plot of the evolution of system stiffness in function of probe pressure and establishment of the compliance law

The compliance law is further applied to correct shear modulus evaluated from loops starting at any pressure p_b in tests in soil by the application of eq. (2.5), which is an extension of the formula proposed by Fahey and Jewell (1990). The result obtained by the application of this equation to one loop is schematized in Figure 2.21.

$$\frac{1}{G_{corr}(p_b)} = \frac{1}{G_{meas}(p_b)} - \frac{1}{G_{syst}(p_b)} \tag{2.5}$$

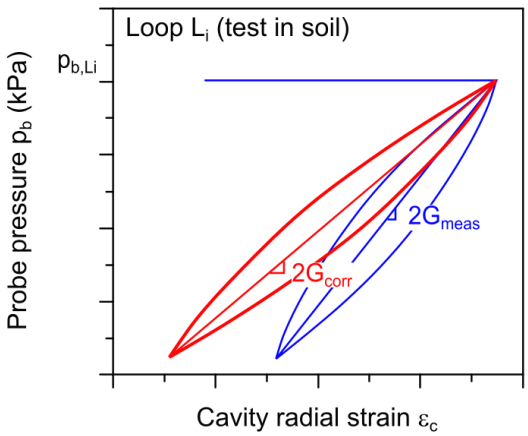

Figure 2.21 – Principle of the application of the compliance correction for one unload-reload loop

All the steps involved in the interpretation of a test, from raw measurement to the derivation of shear moduli from unload-reload loops are presented in Figure 2.22. Further details on the specific procedures used to derive shear modulus at small strain levels are presented in section 2.6.2.1.

Step	Action	Param	Procedure
1	Raw measurements	p_r V	Readings on the control unit
2	Hydrostatic correction	p_b V	$p_b = p_r + \gamma_w z$
3	Application of diametrical calibration	p_b ϕ	Calibration tests Eq. (2.1)
4	Probe self resistance correction	p ϕ	Open-air calibration
5	Calculating cavity strains	p ε_c	Calculating $\varepsilon_c = \Delta R/R_0$
For each loop :			
6	Loop interpretation	G_{meas}	Theoretical calc. $G = 1/2\ dp/d\varepsilon_c$
7	Membrane compliance correction	G_{corr}	$\frac{1}{G_{corr}} = \frac{1}{G_{meas}} - \frac{1}{G_{syst}}$

Figure 2.22 – Steps involved in the interpretation of a pressuremeter test using the Monocell FC probe

2.3.2 Specific calibration procedures

2.3.2.1 Testing procedures using the instrumented thick cylinder

One test was performed in the instrumented thick cylinder (ITC1) according to the following procedure: the probe was placed inside ITC and inflated until getting in contact with the cylinder wall. The probe was pressurized to 530 kPa and series of cycles of amplitude 30, 60 and 120 kPa were performed without a stress-hold step. Then, a program including pressure-hold steps of at least 30 seconds at pressure levels 770 kPa, 830 kPa, 954 kPa, 1254 kPa, 1554 kPa and 1854 kPa followed by loops of pressure amplitude equal to 0.4 times the maximum pressure before unloading was performed. The pressure hold step at 1854 kPa lasted for 360 seconds for studying the creep of polyurethane. It was followed by small amplitude volume-controlled loops of 1.0 cm^3 and 2.0 cm^3. Probe was deflated, and a similar procedure was repeated, with minor modifications, for verifying repeatability. The first two loops of the second series were performed without a previous pressure hold step. Simultaneous recordings of gauge strains, probe pressure and probe volume were performed at a data acquisition frequency of one point per second. Figure 2.23 illustrates the loading protocol performed into the thick cylinder.

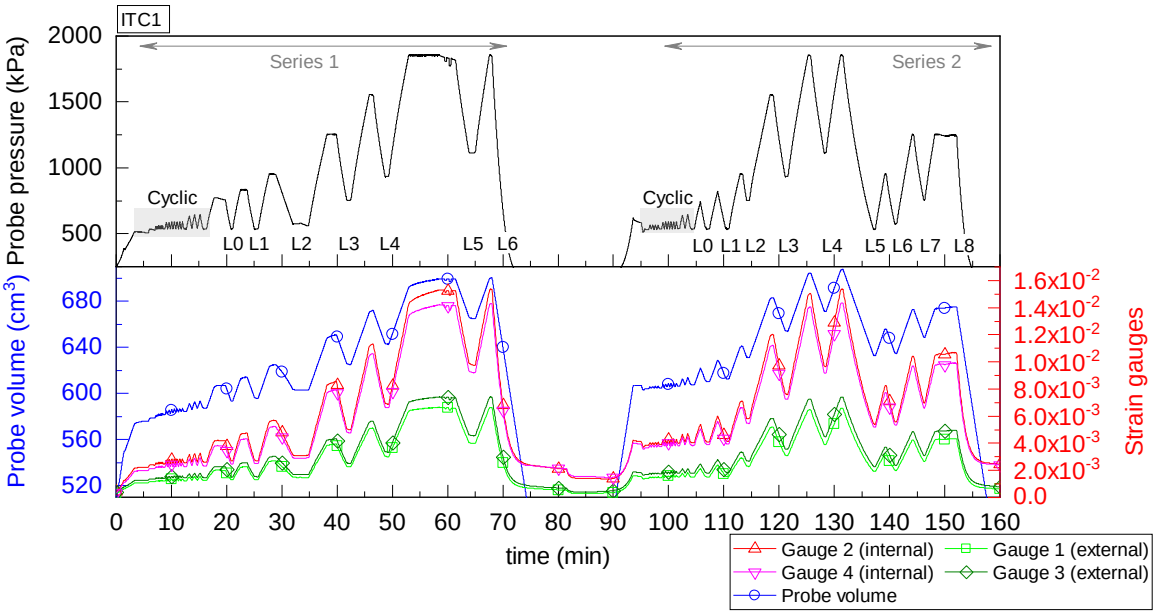

Figure 2.23 – Loading protocol performed for pressuremeter testing inside the instrumented thick cylinder

2.3.2.2 Testing procedures using the hydrostatic chamber

Two different protocols were used to verify the membrane sensitivity to external pressure variations. The first one (protocol HCC 1, Figure 2.24) consisted in applying an external pressure to the probe by pressurizing the hydrostatic chamber and measuring the probe pressure while its volume was kept constant. The chamber was pressurized at pressure-hold steps of 100 kPa lasting for 60 seconds, until reaching a pressure of 600 kPa. It was then depressurized with shorter hold-steps.

The second protocol (protocol HCC 2, Figure 2.27) consisted in pressurizing the probe and measuring the chamber pressure variation at constant volume. The difference between the two procedures is that in the second case, the probe volume increases and thus, an increasing difference between probe pressure and chamber pressure is expected due to changes in membrane inertia. This procedure enables verifying if membrane self-resistance correction using open-air calibration is valid. Probe was pressurized at a constant flow-rate and pressure-hold steps were performed at each 100 kPa increments from 300 kPa until reaching 700 kPa.

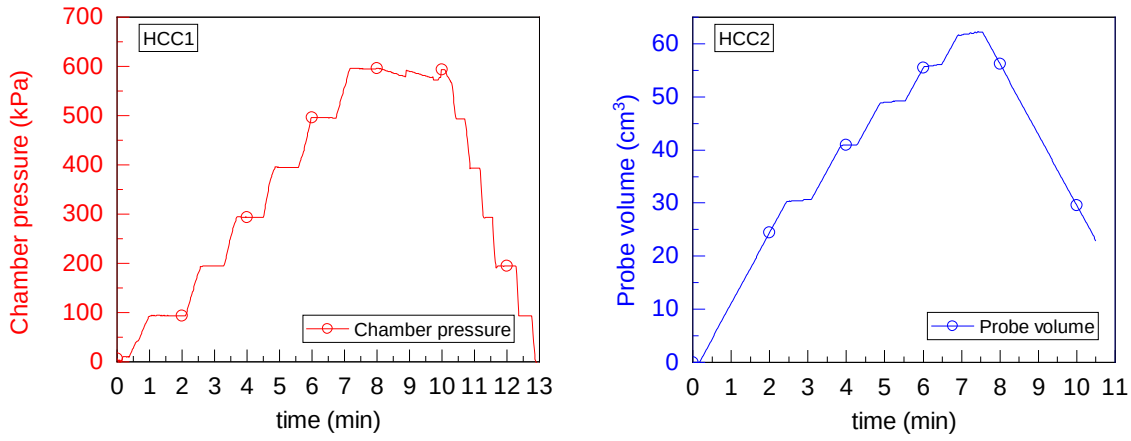

Figure 2.24 – Membrane calibration protocols 1 and 2 in the hydrostatic calibration chamber. (a) Chamber pressure is increased while keeping probe volume constant; (b) Probe volume (and pressure) pressure is increased while keeping the chamber volume constant

2.3.3 Testing procedures in the calibration chambers

An initial stage of tests was required for the investigation of the influence of some factors on the results obtained in calibration chambers. This first stage enabled overcoming certain experimental difficulties, improving the soil specimen consolidation procedure, the geometrical characteristics inside the chamber and eliminating uncertainties on the results obtained. In this work, focus will be given to the results obtained after the experimental procedure was fully developed, which led to this chapter's conclusions. Some observations made during the development phase are discussed.

2.3.3.1 Setting up the calibration chambers

The first tests were performed into the K_0 calibration chamber (*KCC*) according to the configuration presented in Figure 2.25a. The setup procedure is illustrated in Figure 2.26 and composed by the following steps: (a) the probe is placed inside the *KCC* and kept in vertical position by a support screwed to its toe; (b) Fontainebleau sand is placed in ten centimeters thick layers and manually compacted to achieve the desired density index (0.50, 0.70 or 0.90, according to the test); (c) this process is repeated until the specimen reaches the chamber height, leaving 1.5 cm free space for placing the pressurization cushion above of it; (d) the pressurization system is placed on the top of the soil specimen, then the chamber is closed. This installation procedure corresponds to an ideal probe insertion, leading to an undisturbed initial state. The probe is fully surrounded by soil, and there are no empty spaces corresponding to the borehole. The complete experimental set-up is presented in Figure 2.26(e), including pressure-volume controllers and data acquisition unit.

The influence of the boundary conditions of the *KCC* has been studied through two other experimental variants. The first one consisted in eliminating friction between the sand specimen and the chamber wall, as schematized in Figure 2.25b. This was done by greasing the chamber wall and then covering it with a plastic film, as presented in Figure 2.27 (a). Specimen compaction was performed as previously described.

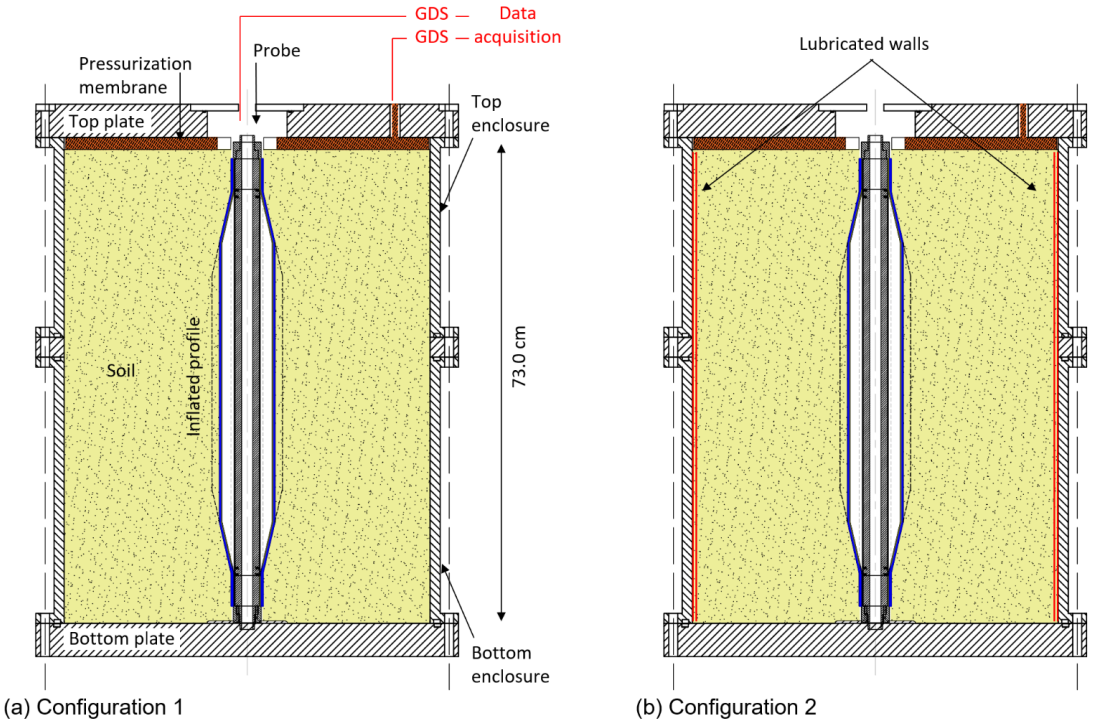

Figure 2.25 – Scheme of the probe installation in KCC. (a) Configuration 1 fully filled with soil; (b) configuration 2, same geometrical configuration but with lubricated wall

Figure 2.26 – (a) Probe inside KCC, (b) manual compaction of 10 cm sand layer, (c) end of compaction, (d) installation of the pressurization cushion, (e) fully assembled set up.

Figure 2.27 – (a) Lubrification of the chamber wall and installation of a plastic film; (b) compaction of the sand layers; (c) installation of the pressurization cushion

The second proposed modification consisted in adding wooden discs inside the chamber in order to simulate the geometric condition of a real pre-bored test. In this case, there is an empty annulus (a cylindrical cavity) between the probe and the soil, above and below the beveled parts of the probe. A scheme is presented in Figure 2.28 and the setup is illustrated in Figure 2.29. The installation procedure consisted in placing the probe inside the calibration chamber and then, inserting wooden discs in the chamber. All the empty spaces between the discs and the chamber walls were sealed. A thin latex membrane was fitted around the probe membrane and then fixed to the upper wooden disc to avoid sand grains to pass through the empty annulus in between these two parts. Fontainebleau sand was added in layers of ten centimeters and manually compacted to achieve the desired density index and 42 cm high. Then, wooden discs were inserted so as to complete the calibration chamber. A latex membrane was also placed between the first wooden disc and the probe to avoid sand grains to move upwards in the cavity direction. The flexible hydraulic pressurization system was placed between the last wooden disc and the chamber cover, and then the chamber was closed. The first experiments showed that this configuration enabled better simulating real test conditions.

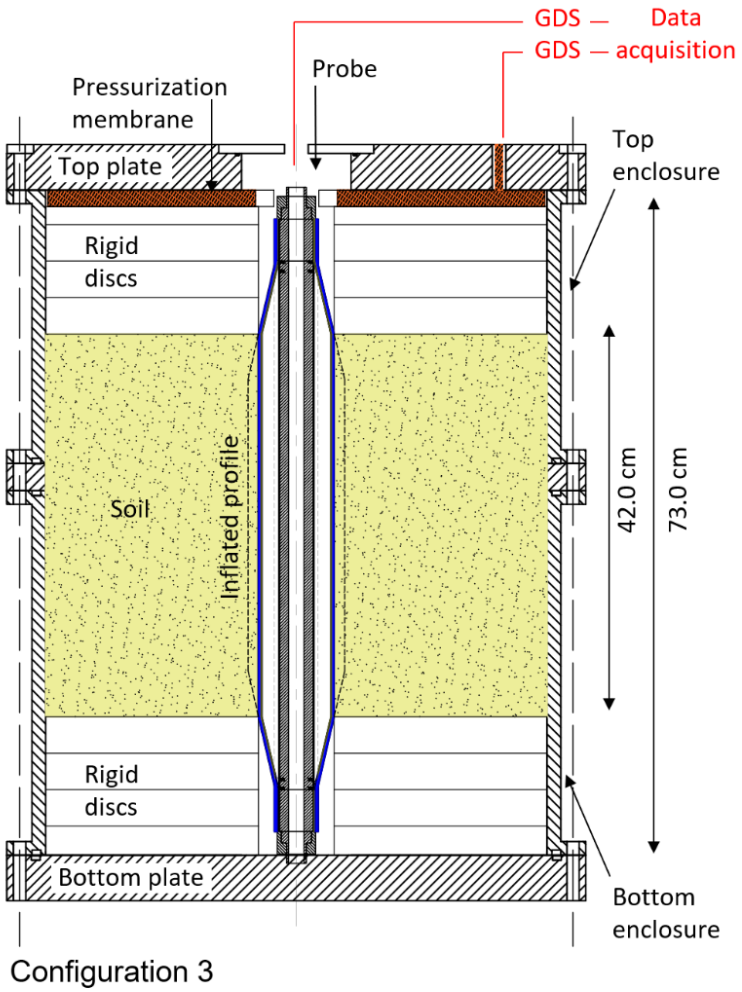

Figure 2.28 – Scheme of the modified boundary conditions used in the *KCC* (configuration 3)

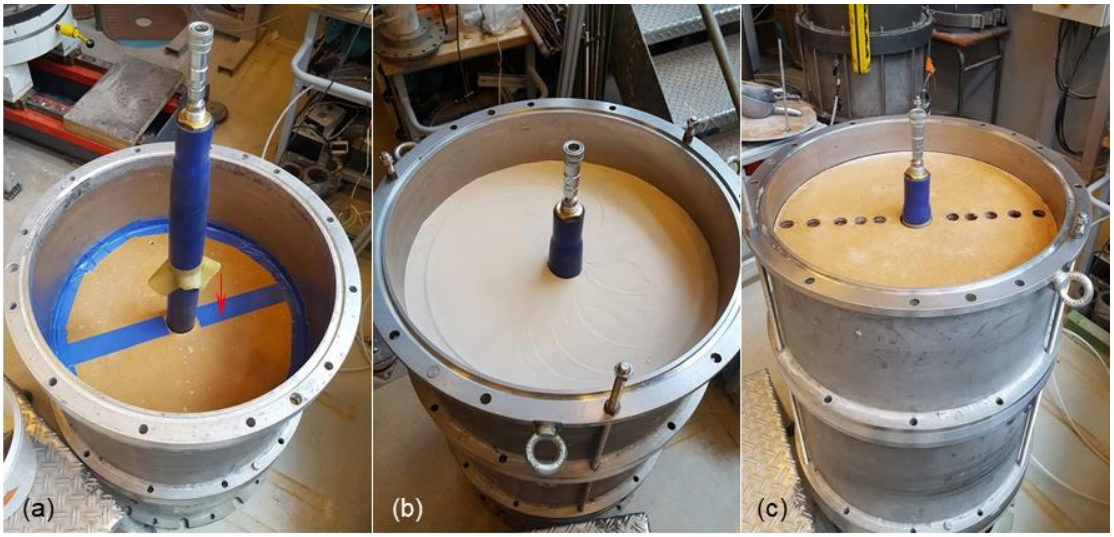

Figure 2.29 – Modification of the chamber limit conditions to simulate the geometry of a borehole. (a) Installation of wooden discs on the bottom of the chamber, and setting up a rubber membrane for tightening the empty annulus, (b) manual compaction of 42 cm heigh specimen, (c) setting up the wooden discs in the top of the chamber.

The configuration of the calibration chamber *PCC* is illustrated in Figure 2.30. The reconstitution procedure of the sand specimen is presented in Figure 2.31 and in Figure 2.32 and consisted in the following steps: a mold is placed over the chamber's base. A neoprene membrane is placed inside the mold and kept tight against its wall through the application of a negative pressure (partial vacuum). The probe is centered over the base. Soil specimen is compacted using the same procedure as previously described. Figure 2.32 shows (a) the soil specimen on the mold, (b) the installation of the top plate and (c) the soil specimen fully surrounded by the neoprene membrane, standing up thanks to the partial vacuum applied. Figure 2.33 shows the metallic confinement tube placed around the soil specimen. The resulting annular space is filled with water, which enables applying the horizontal stress to the soil specimen. In this case, vertical and horizontal pressures are independent and manually controlled by the pressurized air regulator connected to air-water reservoirs. Probe is controlled by the same GDS device previously presented. Data acquisition was done using a specific *LabView* application.

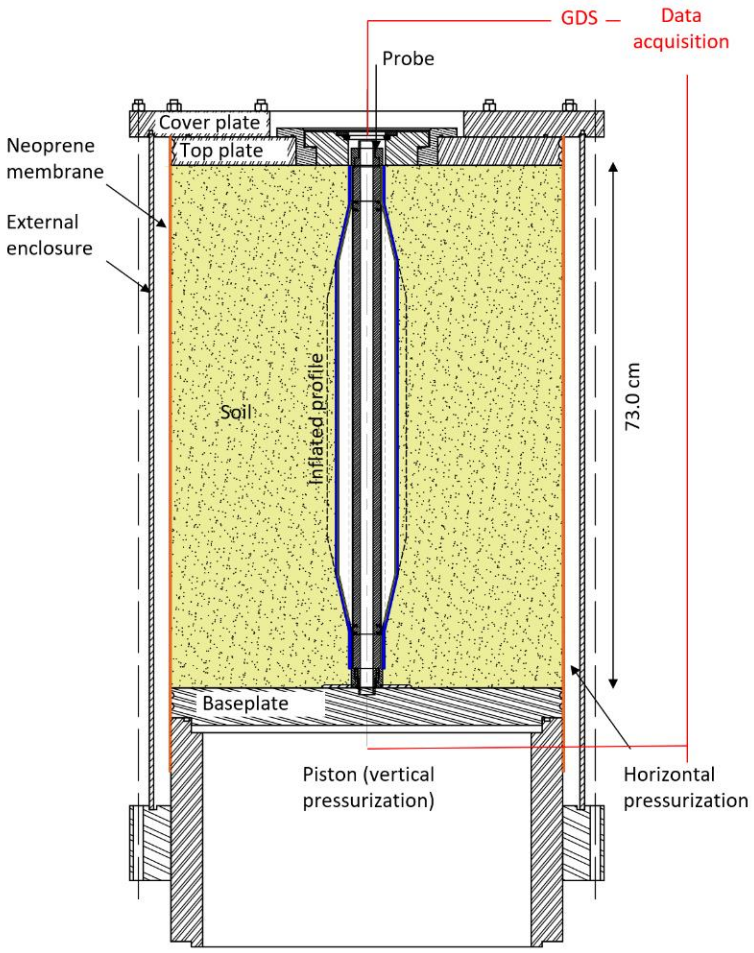

Figure 2.30 – Configuration of the tests performed in *PCC*

Figure 2.31 – Calibration chamber (*PCC*) set-up: (a) detail of the lower base (vertical pressurization); (b) mold set-up over the inferior base and the neoprene membrane that surrounds the soil specimen; (c) detail of the probe centred in the mold

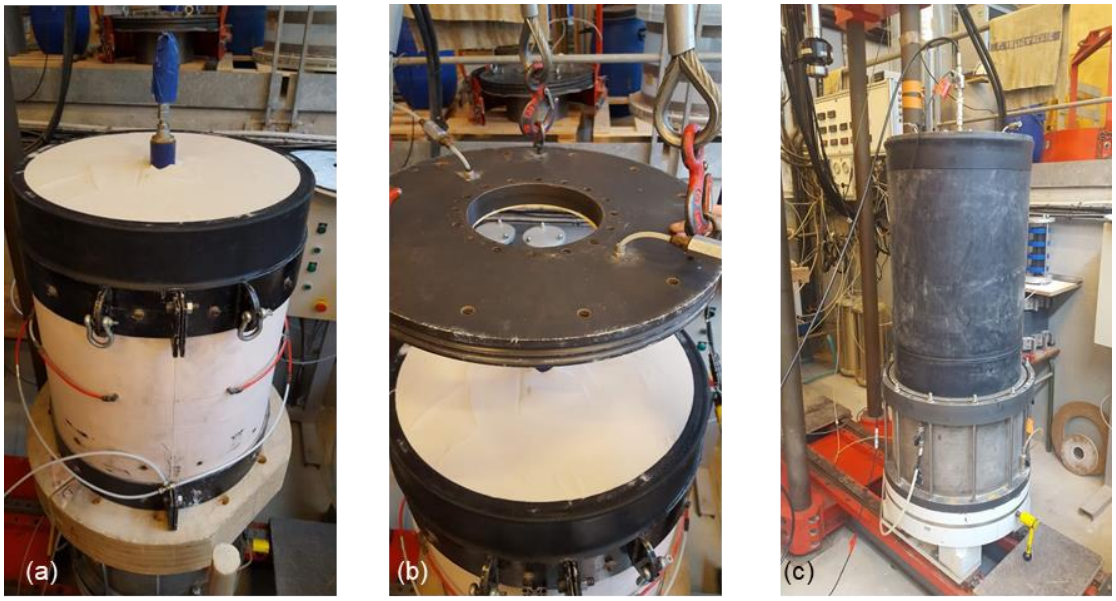

Figure 2.32 – Calibration chamber (*PCC*) set-up: (a) Detail of the soil specimen after manual compaction), (b) set-up of the upper base on the top of the soil specimen; (c) assembled soil specimen surrounded by the neoprene membrane under vacuum;

Figure 2.33 – External cylindrical enclosure set-up and detail of the empty space between the specimen and the enclosure, used for horizontal pressurization.

2.3.3.2 Consolidation procedure for the sand specimen

Two consolidation procedures were tested. In the first four tests in *KCC* (referenced *KCC* 1 to 4) the consolidation procedure nº 1 was performed by increasing the vertical chamber stress while the probe circuit was kept closed (no volume variations in the probe). In this procedure, presented in Figure 2.34a, the probe pressure is a response to variations in chamber pressure. The second consolidation procedure (nº 2) consisted in increasing the probe pressure in steps in order to equalize the chamber horizontal pressure, as presented in Figure 2.34b.

It was observed that the consolidation procedure nº 1 did not yield ratios between the vertical chamber pressure and the horizontal probe pressure consistent with the expected K_0 coefficient for Fontainebleau sand. In fact, at low pressures, probe membranes are relatively compressible, as has been shown by Clarke (1995). As a consequence, when the chamber is pressurized, even if the probe water volume is kept constant, the soil in contact with the membrane will compress it, resulting in convergence within the soil specimen. Convergence induces radial stress to decrease within the soil specimen, similar to a convergence-confinement problem in tunnels,

which makes this consolidation procedure inadequate for the desired application. Consolidation procedure n° 2 avoids this problem to happen by simultaneously equalizing the horizontal pressure at the probe contact.

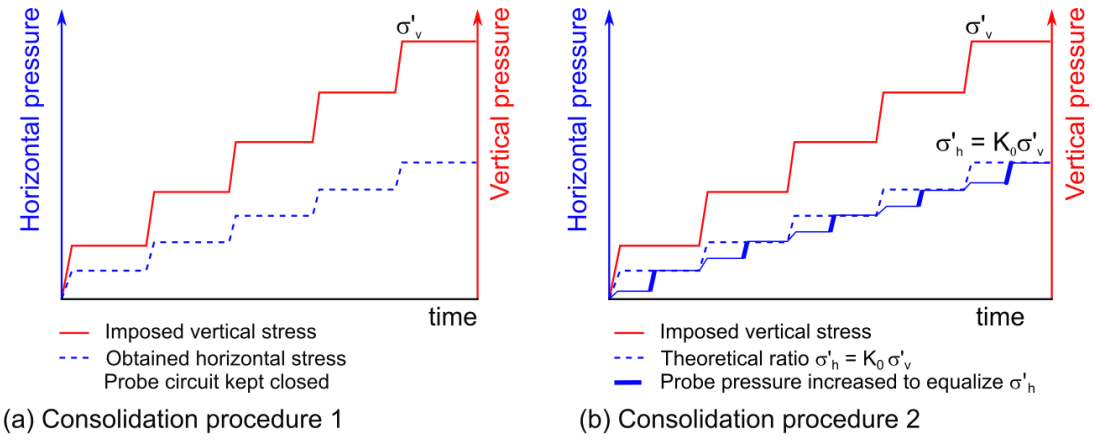

Figure 2.34 – Soil specimen consolidation procedures: (a) the chamber pressure is increased while the probe volume is kept constant (probe pressure is a response to chamber pressure); (b) probe pressure is increased to equalize the horizontal pressure in the chamber

2.3.3.3 Loading programs

Two distinct loading protocols were applied, one for assessing shear stiffness at small strains, and the other to evaluate the soil behavior under repeated cyclic series. The first protocol is called "*loop procedure*". It is composed of five unload-reload loops, all preceded by a pressure hold step, performed at increasing levels of cavity pressure, p_{cav}. Loop stress amplitudes $\Delta p_{cav,i}$ were defined as approximately 0.4 times p_{cav}. This procedure is illustrated in Figure 2.35*a*.

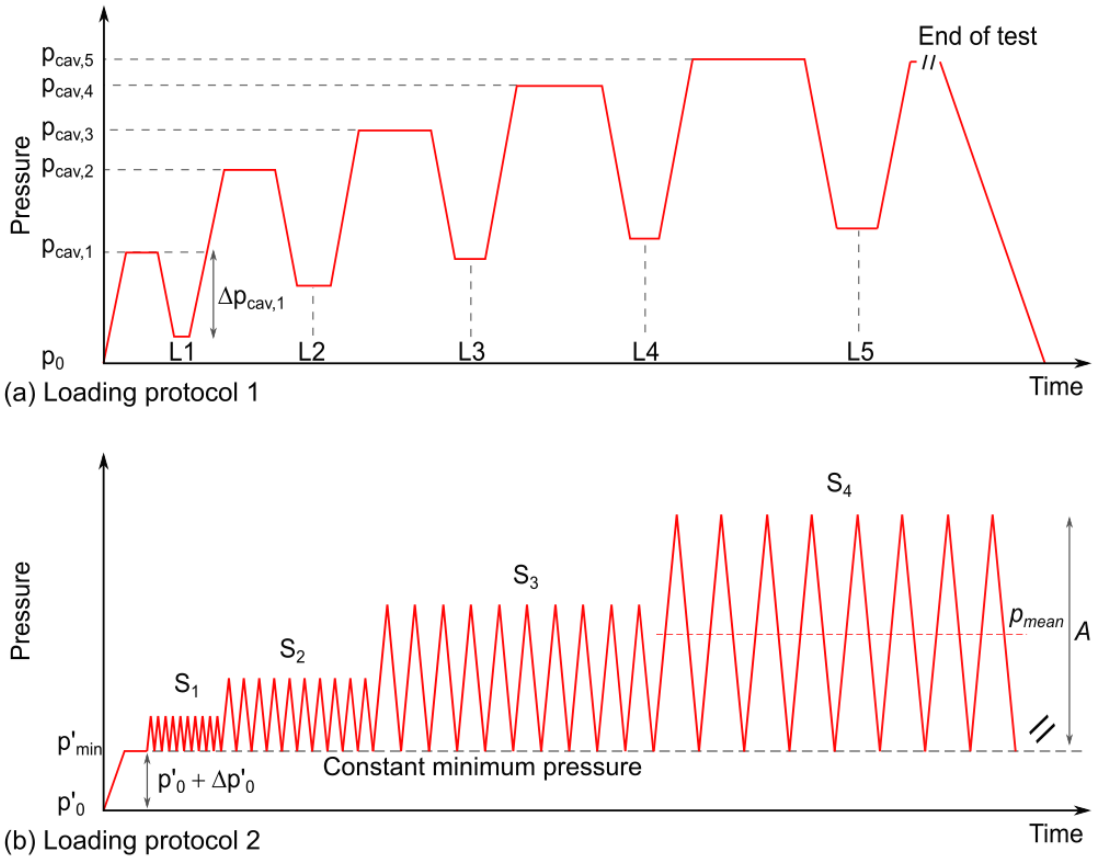

Figure 2.35 – (a) Scheme of the loading protocol for assessing elasticity properties (protocol 1), including unload-reload loops at variable stress levels and preceeded by stress hold steps; (b) loading protocol for assessing cyclic properties (protocol 2), including series of repeated cycles of variable amplitude

The second procedure is called "*cyclic*" procedure. It is composed of a series of repeated cycles of increasing amplitudes (Figure 2.35b). Starting from the radial stress at rest p_0, the probe pressure is increased by $\Delta p'_0$ = 20 kPa to reach a minimum pressure, p'_{min} defined as the minimum pressure of the cyclic series. This is done for preventing the probe from losing contact with the soil specimen. Then, series of increasing amplitudes *A* are performed, as illustrated in Figure 2.35*b*. The shape of the load variations over time is triangular due to its easier implementation in the GDS controller. It is considered that applying other loading patterns, such as sinusoidal, was not necessary at this stage of the research.

2.3.3.4 Important experimental observations

A series of preliminary tests were performed during the development of the final experimental program, aiming at fully understanding the physical model and at identifying and adjusting any parameters that could differ from tests on site. The first

adjustments were made on *KCC* due to its faster implementation. Four specimens were assembled, as summarized in Table 2.3.

It was observed that the test results obtained with geometric configuration 1 did not correspond to that of a pre-bored test, and tests could not be interpreted using the calibration procedure developed in section 2.3.1.

Table 2.3 – Preliminary testing program performed in *KCC* for adjusting the experimental procedure

Specimen	Geometric configuration	I_D	Loading protocol	Consolidation procedure	σ'_v (kPa)	K_0
KCC1	1	0,70	2	1	var	0,40
KCC2	1	0,70	2	1	var	0,40
KCC3	2	0,70	2	1	var	0,40
KCC4	3	0,70	1	1	var	0,40

The tests performed in *KCC* (tests KCC1 to KCC4) have provided important insights for the definition of the final testing protocol. Some of them are presented in the next sections. It is considered that the following experimental observations lead to interesting discussion.

a) Hysteresis and recovery of the maximum shear stiffness

A loop-into-loop procedure was performed in *KCC* 4 specimen. Result is presented in Figure 2.36. Cavity was initially loaded, and then unloading and reloading loops of increasing amplitude were performed. Result is presented in Figure 2.36, where it can be seen that the behaviour is hysteretic, and that soil seems to recover its maximum stiffness after each load reversal (i.e. the same initial unloading slope is obtained). There is an accumulation of irreversible strains within the loops, which may be due to superposition of creep. In this case, a sufficiently long pressure hold-step has not been performed before this procedure. This result illustrates the fact that the initial shear modulus of the soil is associated to the initial slope of the unload path, and as the loop amplitude increases, the shear modulus decreases. When the loading direction is reversed, soil recovers its maximum stiffness, which degrades as the soil is sheared in the reversed direction.

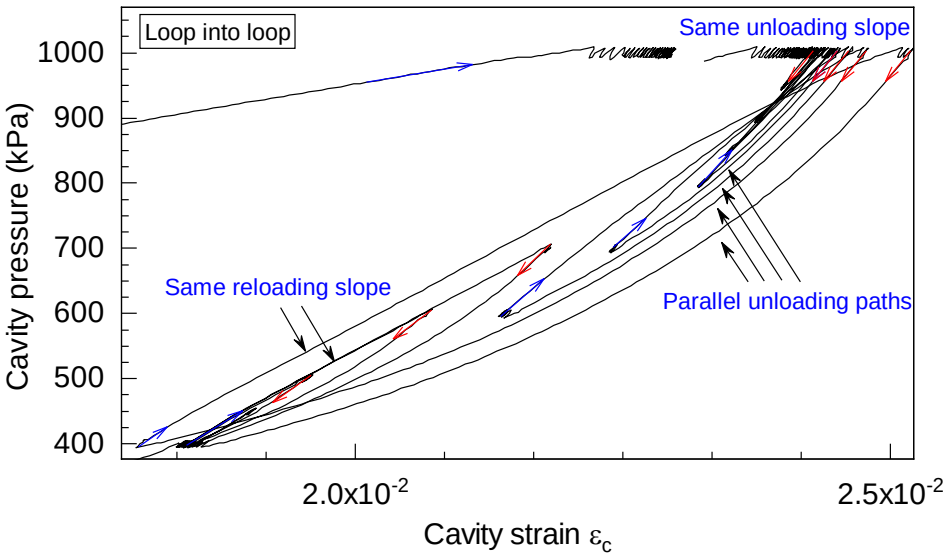

Figure 2.36 – Loop-into-loop procedure performed in KCC 4

b) Importance of the pressure-hold step prior to unloading

In order to better understand the superposition of creep and elasticity during cyclic loading, two unload-reload loops were performed at the same stress level according to the following procedure: the first loop was performed without a pressure-hold step and the second, after 20 minutes creep. The result is presented in Figure 2.37. It can be observed that the initial unloading slope of the loop performed without pressure-hold step is negative and that the loop is opened: there are accumulations of plastic strains within the loop. The second loop is closed. This result evidences the importance of performing a sufficiently long pressure-hold step before reversing the loading direction.

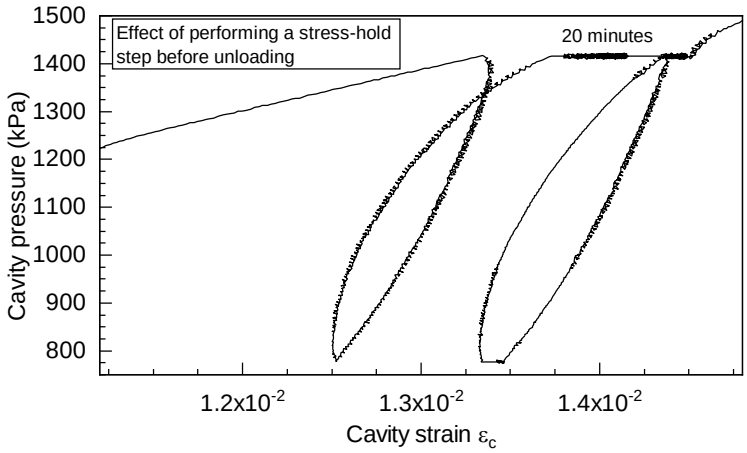

Figure 2.37 – Two unload-reload loops performed at same stress level, one immediately after loading, and the second after 20 minutes pressure-hold

2.3.3.5 Validation of KCC boundary conditions

A validation test was performed in order to verify if the difference in boundary conditions between *KCC* and *PCC* can affect test results. A cyclic test comprising 6 series of different amplitudes was performed in both chambers. As for having similar horizontal stress conditions, the vertical pressure in KCC was adjusted so that to obtain the same horizontal stress than in PCC1 (applied σ'_v = 875 kPa, to obtain σ'_h = 350 kPa for Fontainebleau sand K_0 = 0.40). The test results are presented in Figure 2.38. It can be observed that the soil response obtained was very close in both cases. Further interpretation of these tests will be presented in section 2.7.

This result enables validating that tests performed on *KCC* are equivalent to those performed in *PCC* and that the differences in boundary conditions between the two calibration chambers do not influence the results. It also enables confirming that the ratio between vertical and horizontal stresses in Fontainebleau sand can be adequately evaluated using Jaky's formula for this application.

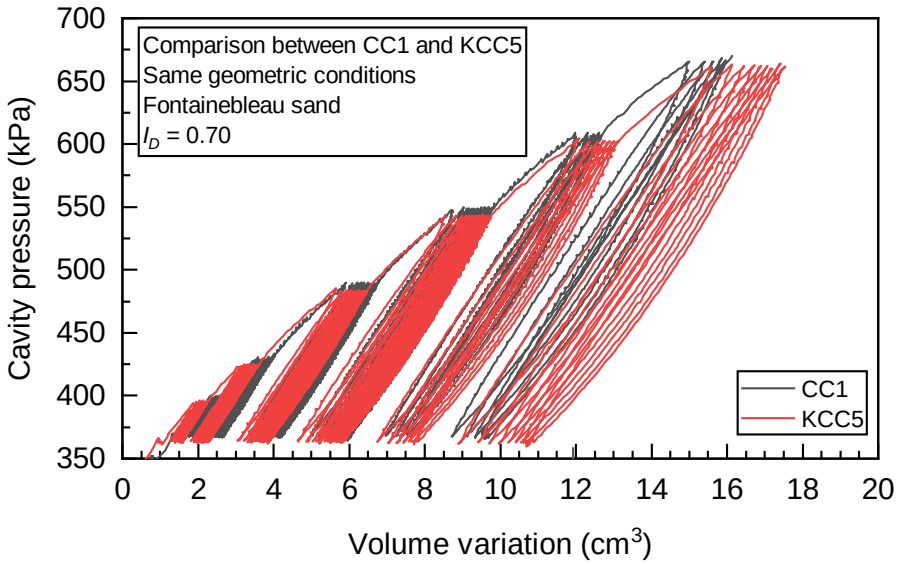

Figure 2.38 – Comparison between cyclic tests performed in *PCC* and *KCC* under same geometrical configurations

2.4 RESULTS AND VALIDATION OF PROBE CALIBRATION TESTS

2.4.1 Probe calibration

In the laboratory, the Monocell FC probe was calibrated using the experimental setup presented in section 2.1.2. After verifying that the system was fully saturated, the first calibration step was open-air pressurization. The second step was to calibrate the probe using tubes of internal diameter 60 mm, 66 mm, 75 mm and 85 mm. In the laboratory tests, maximum pressure was limited to 2.0 MPa, due to pressure-volume controller limitation. After the maximum pressure was reached, the probe was deflated. Both loading and unloading portions of the curve were recorded.

The calibration procedure presented in section 2.3.1 was repeated three times for each calibration tube in order to evaluate the repeatability of this process. Results of the diametrical and open-air calibration tests performed in the laboratory are presented in Figure 2.39. In this figure, the curve plotted in red corresponds to open air inflation (probe was inflated freely in open-air). The other curves correspond to the probe inflation inside a calibration cylinder. It can be noticed that before touching the calibration cylinder wall, probe inflation follows a path similar to that of open-air inflation. When the membrane gets in contact with the cylinder, pressure begins to increase quickly.

From the repeated calibration curves, it can be noticed that there are small volume variations for the first contact between the probe and the calibration cylinders. This can be explained by the fact that the first loading may be affected by interaction between the probe membranes and the calibration tube which can add uncertainty (for example, if the probe is not perfectly centered in the tube). These uncertainties are considerably reduced on the unload path. For the interpretation of the laboratory tests, it has been chosen to keep the unload calibration curves, presented in Figure 2.40, since unload loops are to be interpreted further.

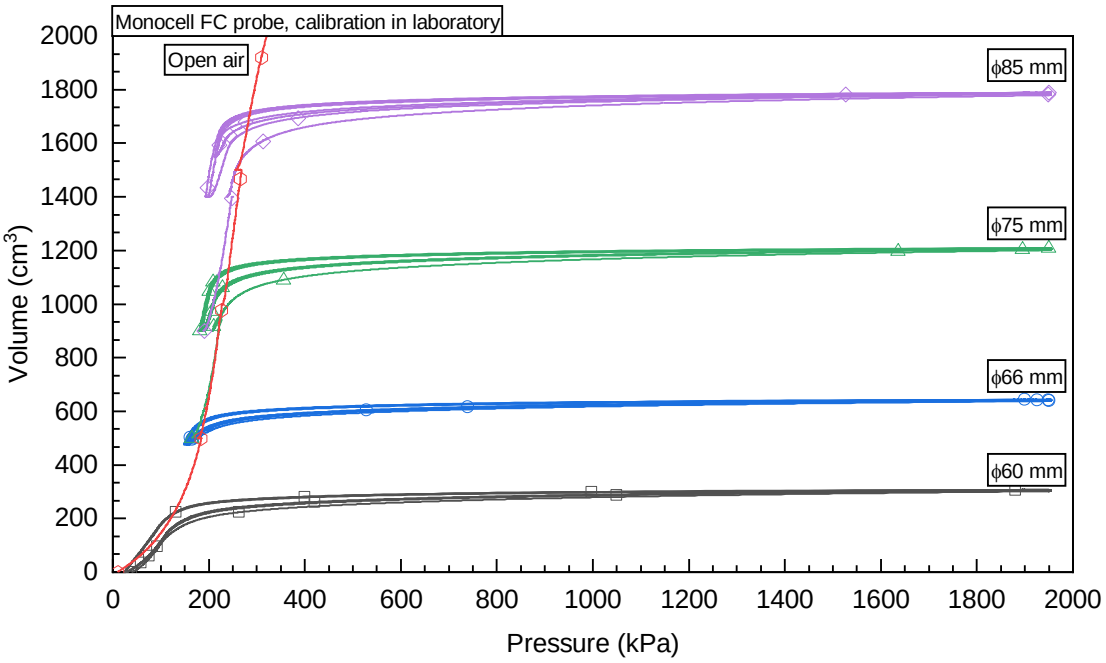

Figure 2.39 – Open-air and diametrical calibration curves of the Monocell FC probe

Figure 2.40 presents one example of the linear relationship between the calibration diameter and the injected volume, obtained for a raw pressure of 1000 kPa. For a given pressure, this relation can be described by two coefficients, *a(p)* and *b(p)* (eq. (2.4)), which are respectively the slope and the intercept of the regression line obtained through the calibration. In this way, probe external diameter ϕ can be written as a function of its actual volume and internal pressure.

The second coefficient, *b*, is related to system compressibility. Variations in function of probe pressure are obtained by calculating *a(p)* and *b(p)* for the whole pressure range reached in the calibration tests. All calculated values are presented in Figure 2.41.

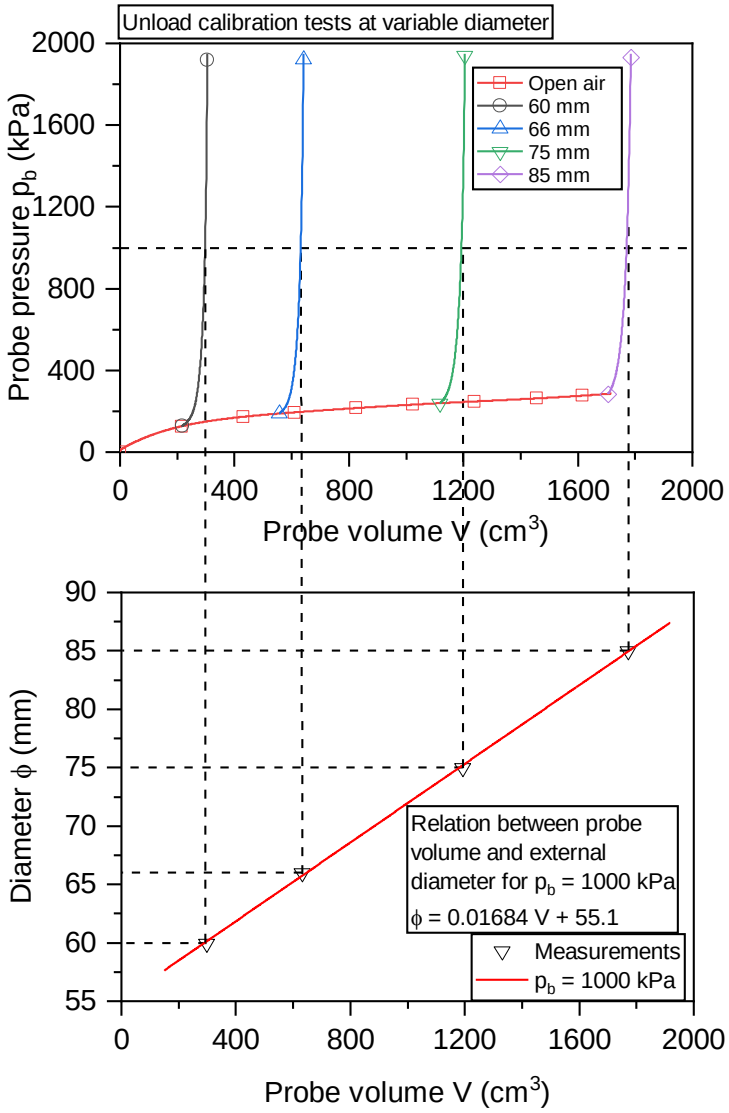

Figure 2.40 – Probe unload calibration test with four different diameter steel-tubes and open-air calibration. Example of the linear relation between volume and diameter

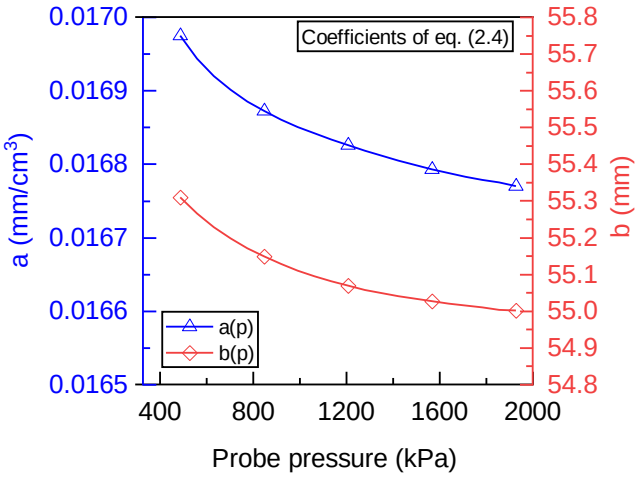

Figure 2.41 – Probe coefficients evolution in function of the probe pressure

Results of the compliance test performed with the Monocell FC probe are presented in Figure 2.42*a*. The unloading compliance curves are linear. For each unload loop, G_{sys} is calculated by linear regression on the unload curve. The negative system moduli obtained mean that the probe behaves in a stiffer way in the first calibration than in the compliance test. System moduli $G_{sys}(p_c)$ increase in absolute value as the pressure before unloading increases. It tends to infinity (meaning no compliance correction) as the unload pressure tends to the maximum pressure reached in the calibration tests (2000 kPa). The compliance law relating system moduli and probe pressure is presented in Figure 2.42*b*.

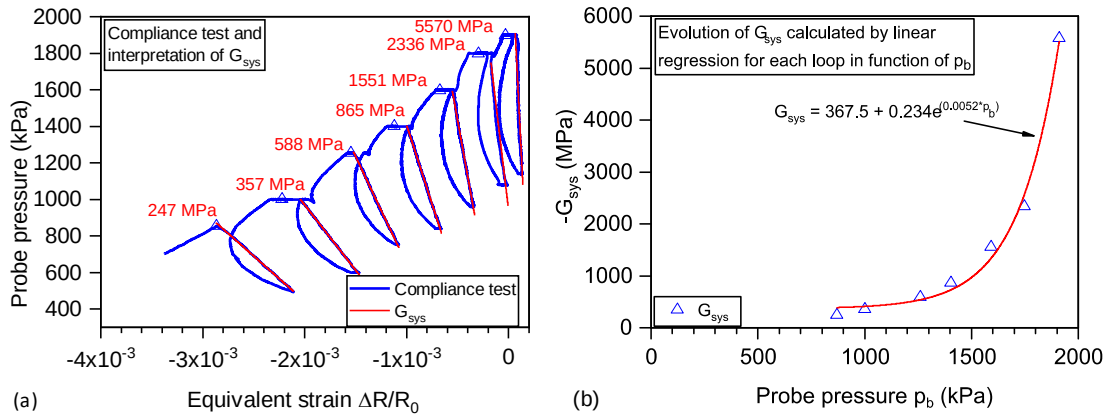

Figure 2.42 – (a) Compliance test performed with the monocell FC probe in laboratory; (b) Interpretation of the compliance test and the obtained "compliance law"

2.4.2 Validation of the calibration procedure

Tests in the instrumented thick cylinder and in the hydrostatic calibration chamber were used to validate the probe calibration procedure.

2.4.2.1 Validation using ITC

Figure 2.43 presents a comparison between strains evaluated using the probe volumetric measurements interpreted according to the calibration procedure described and strains directly measured with one of the internal strain gauges in a range from 0 to $3 \cdot 10^{-3}$. One of the internal gauges failed, possibly because of glue failure, and has not been interpreted. As previously stated, the external gauges were not interpreted. They served as a control group to ensure that the internal gauges were not damaged

Within the range of strain measurements up to $3 \cdot 10^{-3}$, the relative difference between measurements obtained using both setups were inferior to ±7,5%. The exception was

for loops performed at pressures less than 800 kPa, for which errors could reach ±15% for strain ranging from 0 to $1 \cdot 10^{-3}$, as it can be seen in loops *L0* and *L1* on the second test series. These loops were performed without previous pressure-hold steps. This result means that measurement accuracy increases as probe pressure increases and confirms that measurements at pressures lower than 800 kPa must be interpreted with precautions. At low pressures, the interaction between the layers of the probe's membranes may lead to excessive compliance and low repeatability. As pressure increases, the different membrane components behave homogeneously, drastically reducing compliance and repeatability problems, as it can be seen by the quick increase in G_{sys}. This may be a limiting factor when testing soft soils or soils near ground surface using this configuration of restraining sheath.

The external measurement experiment validates the calibration procedure, the correction methodology for membrane compliance and the probe measuring capabilities out of soil.

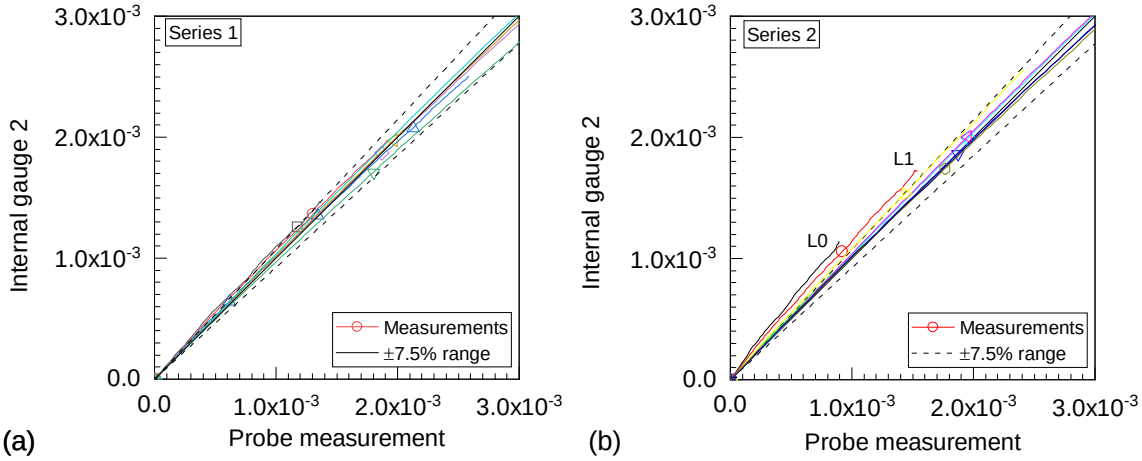

Figure 2.43 – External measurement verification. Comparison between strains assessed via strain gauge and probe measurements

2.4.2.2 Validation using HCC

Results obtained in the hydrostatic calibration chamber are presented in Figure 2.44. The following conclusion can be drawn: when pressuring the chamber and keeping the probe volume constant (protocol 1), an error of 4% was observed between the increments in chamber pressure and the increments in probe pressure, as it can be seen in Figure 2.44a. When following protocol 2 (probe pressurization while keeping the chamber volume constant), an increasing difference between the probe and the chamber pressure is observed. This is caused by the membrane self-resistance, that increases as

probe volume increases. It can be seen from Figure 2.44b that the difference between probe pressure and chamber pressure is equal to the probe self-resistance when inflated in open-air. This result validates the applicability of the standard procedures for pressure correction to the Monocell FC probe.

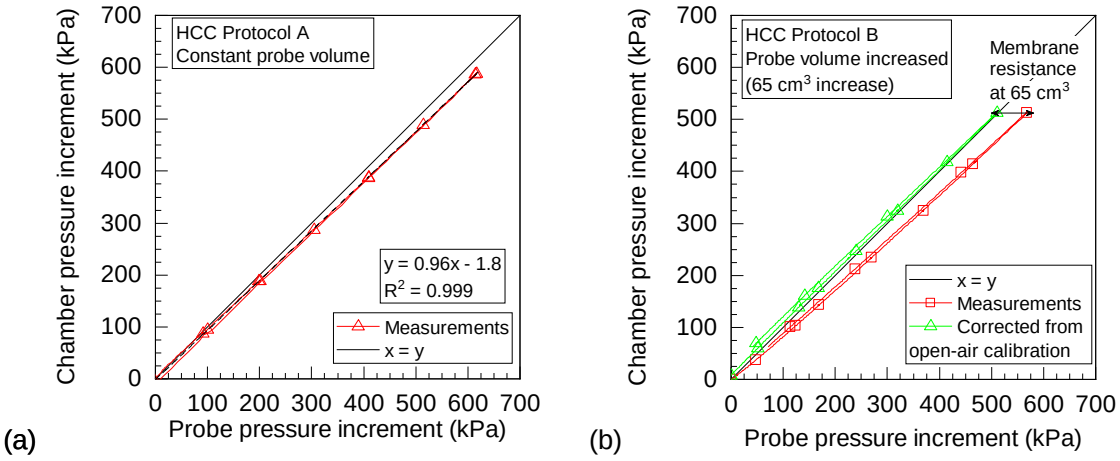

Figure 2.44 – Results for membrane inertia calibration in the hydrostatic calibration chamber. (a) Chamber pressurization with probe at constant volume; (b) probe pressurization (increasing volume) and chamber at constant volume

2.5 VALIDATION OF THE APPLICABILITY OF THE PHYSICAL MODEL

2.5.1 Preliminary evaluation of the boundary conditions effects

A preliminary evaluation of the influence of the calibration chamber boundary conditions on the laboratory test results in comparison to *in situ* tests was performed by comparing the results of the analytical solutions for the cavity expansion of a thick cylinder and that of an infinite cylinder. Linear elasticity was considered on this first approach. The thickness of the cylinder was imposed equal to the radius of the calibration chamber. The assumption of linear elastic behavior (no plasticity) is consistent at this stage, since the interest of the laboratory program is to validate the probe capacity to determine soil's elasticity properties through unload-reload loops. The influence of the calibration chamber boundary conditions with regard to the determination of plasticity properties has been studied by Schnaid and Houlsby (1990) and Salgado et al. (1998). In that case, it is recognized that results are significantly

influenced by the size of the calibration chamber. Assessing plasticity properties with the pressuremeter in calibration chamber is not within the scope of this work.

The analysis procedure consists in calculating the cavity expansion curve of a thick elastic cylinder. The curve obtained is interpreted as if it was issued from an infinite cavity expansion. The error is calculated as the relative difference between modulus evaluated from the thick cylinder and the infinite cavity expansion. Analytical solutions for thick and infinite cylinders are given in chapter 1 (Equation 1.23).

The numerical results obtained considering p_0 = 300 kPa, p = variable; a = 3.3 cm; b = 25 cm; G = 50 MPa; ν = 0.30 are presented in Figure 2.45*a*. The values of these parameters were chosen in order to be consistent with Fontainebleau sand properties and the stress level of the tests performed in the calibration chambers, which will be discussed in the forthcoming sections.

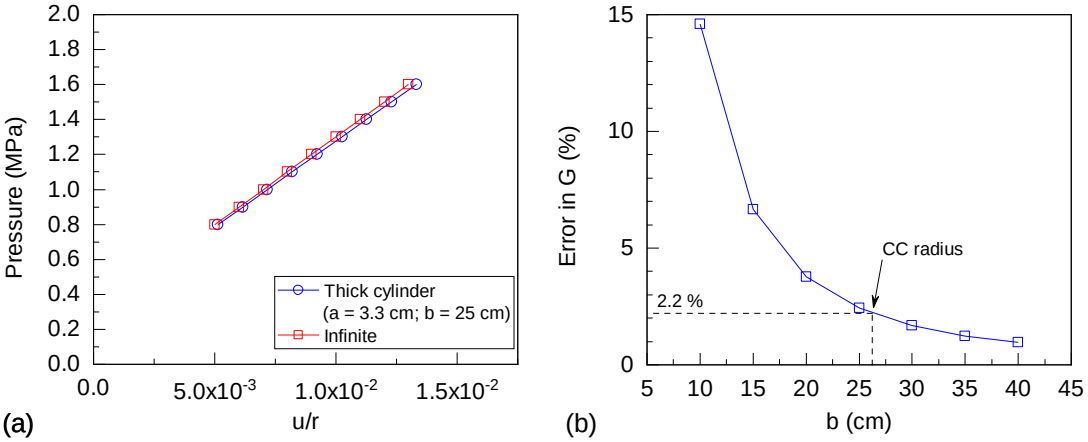

Figure 2.45 – (a) Comparison between the expansion curve of a thick cylinder of external radius 25 cm and a cavity in infinite media. (b) Evaluation of the error in measured shear modulus in function of the external radius of the thick cylinder.

It can be seen that the thick cylinder curve lies under the infinite one, meaning that it is not as stiff. If infinite cavity expansion theory is used to derive G from both cases (half of the slope of the expansion curve), a 2.4% difference is obtained. The result is only sensitive to geometrical parameters (a and b) and to Poisson's ratio. A sensitivity analysis was performed to investigate the influence of the diameter of the calibration chamber, b, considering that the internal radius a = 3.3 cm is constant (approximately the probe diameter at the beginning of a test). The result is presented in Figure 2.45*b*. When b tends to infinity, the error tends to zero (the thick cylinder approaches a cavity in an infinite media).

The Navier Laboratory (*CERMES*) calibration chambers have internal radius of 26.2 and 27.5 cm. This study indicates that errors in soil stiffness derived from tests carried out in these calibration chambers is inferior to 3%.

This first result is in favor of calibration chamber testing in the laboratory. However, it presents two limitations. The first is that the analytic solution for thick cylinder may be representative only for the case of *PCC*. There is no analytic solution for the case of *KCC* (zero radial displacement at the chamber boundaries). The second is that this approach does not account for changes in the stress state in the soil specimen due to the constrained boundary conditions. Disturbances on the stress state due to the proximity of the boundary conditions can affect the measured shear modulus. These effects can be investigated through numerical analysis, either by finite difference or finite element modelling.

2.5.2 Finite element evaluation of chamber size effects

The influence of the calibration chamber boundary conditions was evaluated using the finite element method. Two models were built, both in axisymmetric conditions considering an internal radius of 3 cm. One simulates the geometry of the *KCC* and the other simulates infinite boundary conditions, as presented in Figure 2.46. Pressuremeter tests with unload-reload loops were simulated for both models. The loops were interpreted and compared. The error is evaluated as the relative difference between the results obtained in the two cases. *PLAXIS* software was used with two different constitutive models: linear elastic (Hooke's law), and non-linear elastic, stress hardening with Mohr-Coulomb plasticity yield criterion (commercially known as *Generalized Hardening Soil Model*). The first one enables verifying if the *KCC* boundary conditions can introduce errors because of the constraint in radial displacement at the metallic rigid enclosure. Besides this, the second model enables verifying if the increase in stress near the boundaries of the calibration chamber can lead to significant hardening to disturb the measurements of shear moduli.

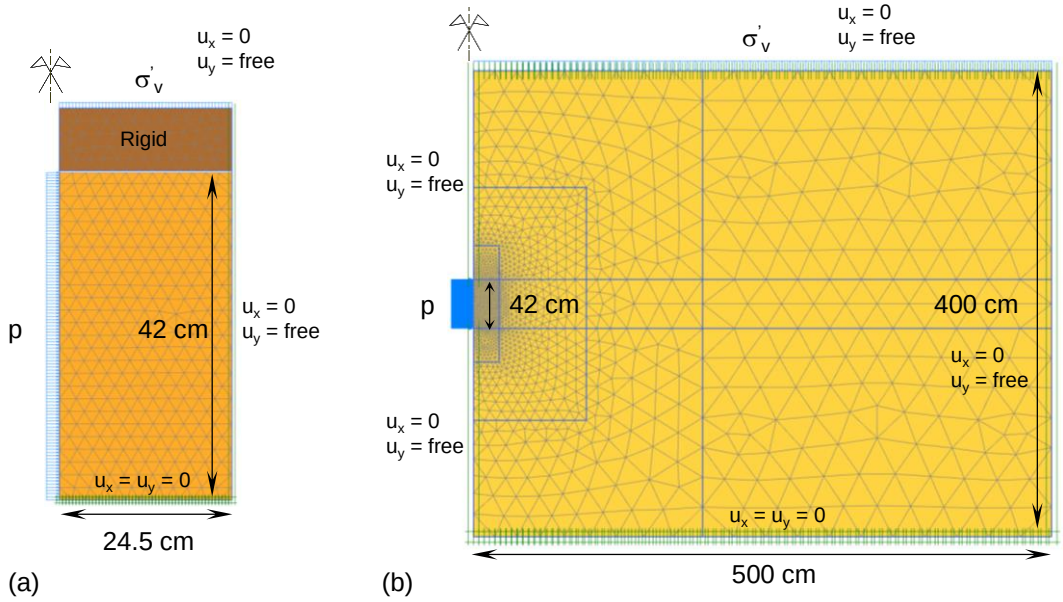

Figure 2.46 – Finite element axisymetric models for investigating the influence of the boundary conditions of the *KCC* in comparison to the real case. (a) *KCC* model; (b) infinite model

For the linear elastic constitutive model, the following parameters were adopted: E = 100 MPa, ν = 0.3. The cavity expansion curves obtained for the two geometric conditions are presented in Figure 2.47. The interpretation of these curves shows that shear stiffness in *KCC* is overestimated by 3%.

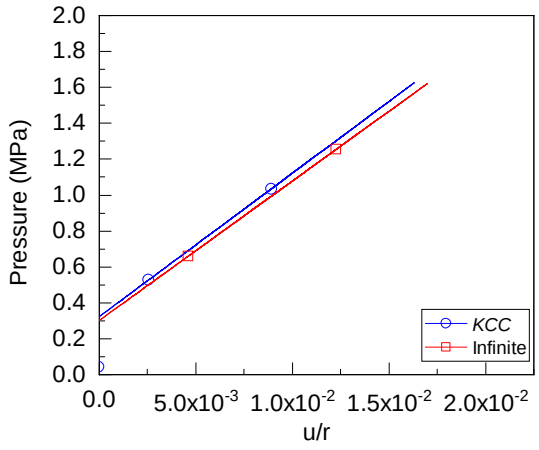

Figure 2.47 – Comparison between cavity expansion curves obtained in constrained conditions and infinite conditions using linear elastic constitutive model

The same analysis was carried out for the more advanced constitutive model. Given parameters were: E_{50} = 33 MPa, E_{oed} = 33 MPa, E_{ur} = 100 MPa, G_0 = 139 MPa, $\gamma_{0.7} = 1.0\ 10^{-3}$, ν_{ur} = 0.3, m = 0.46, p_{ref} = 300 kPa, φ = 37°, ψ = 9°, c = 0 kPa. The vertical stress was imposed σ'_v = 750 kPa. These parameters have been chosen in order to be consistent with what had been further performed in calibration chamber. In the

numerical model, the variation of elasticity modulus in function of average stress *p'* is considered through equation (2.6) and its variation with the strain level according to equation (2.7). Details on the numerical implementation of the constitutive model are given in PLAXIS (2015) . The cavity expansion curves obtained for the two geometries are presented in Figure 2.48*a*. Five unload-reload loops were performed at increasing stress levels, similarly to what has been further performed in the calibration chamber.

$$E_{ur} = E_{ur}^{ref}\left(\frac{(p' + p_c)/2}{p^{ref}}\right) \tag{2.6}$$

$$G_s = \frac{1}{1 + 0.385\left|\frac{\gamma}{\gamma_{0.7}}\right|} \tag{2.7}$$

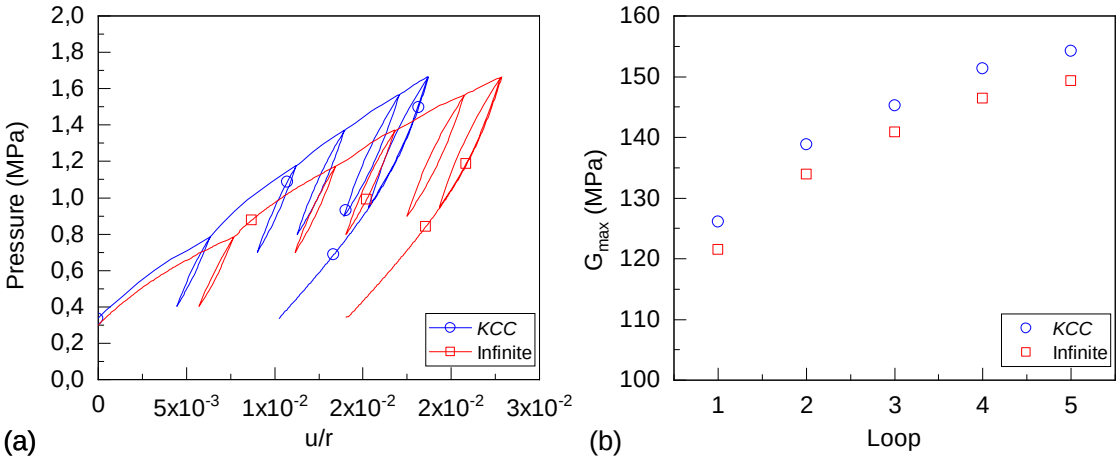

Figure 2.48 – Comparison between cavity expansion curves obtained in constrained conditions and infinite conditions using non-linear elastic-plastic strain hardening constitutive model

It can be seen from the above results that the development of plasticity leads to an increase in the difference between the virgin loading curve obtained by the two models, which is consistent with what has been previously presented in literature: since plasticity develops, results in *KCC* diverges from *in situ* results.

Each unload loop can be interpreted using Briaud et al. (1983) method. This method has been presented in Chapter 1 and is further used to interpret tests in calibration chamber. It enables the estimation of the maximum shear modulus of the soil at the beginning of the unloading process. Values of the initial shear modulus for each loop are presented in Figure 2.48*b*. It can be noticed that the relative error between the *KCC* model and the infinite condition is constant and inferior to 4%.

The analysis presented confirms that modelling the full scale pressuremeter test based on calibration chamber testing is straightforward. The response to be measured in *PCC* is expected to be about 3% softer than it would be under the real infinite boundary conditions. In *KCC*, it is expected to be 4% stiffer than *in situ*. For a given chamber geometry, the error was found to be constant even at increasing stress levels. It will be considered, for all practical purposes, within the present study, that this magnitude of error can be neglected and that the physical model can be considered as representative of the full-scale problem. This conclusion is valid for the interpretation of unload-reload loops (elastic behavior).

2.6 PRESENTATION OF RESULTS OBTAINED. EVALUATION OF SHEAR STIFFNESS AT SMALL STRAINS

This section presents the results of the tests performed in *KCC* aiming at determining soil shear moduli at low strain level. The section is divided in seven parts. First, the testing program including three soil specimens of different density index and one repeatability test is presented. The interpretation procedure is then illustrated based on one typical case. The repeatability test is then presented, as well as the influence of density index and cavity pressure on the results obtained. The results are then summarized and validated with respect to Fontainebleau elementary stiffness properties.

2.6.1 Testing program

Table 2.4 presents the testing program performed in the *KCC*. It should be noted that all tests were performed under geometric condition 3 (simulating the borehole geometry), consolidation procedure 2 (probe pressure increased simultaneously with chamber pressure) and loading program 1.

Table 2.4 –Testing program performed in KCC aiming at assessing shear moduli at small strains

Specimen	I_D	σ'_v (kPa)	K_0	Geometric condition	Loading protocol	Consolidation procedure	Loop	p_{cav} (kPa)	Δp_{cav} (kPa)
KCC6	0,70	750	0,40	3	1	2	L1	811	391
							L2	1208	555
							L3	1407	635
							L4	1607	715
							L5	1705	756
KCC7	0,90	810	0,37	3	1	2	L1	806	375
							L2	1212	554
							L3	1414	638
							L4	1611	718
							L5	1710	756
KCC8	0,70	750	0,40	3	1	2	L1	815	395
							L2	1210	556
							L3	1408	633
							L4	1604	717
							L5	1701	749
KCC11	0,50	680	0,44	3	1	2	L1	811	394
							L2	1204	554
							L3	1398	633
							L4	1593	716
							L5	1692	752

2.6.2 Results and analysis of a typical test

The interpretation of the test results in terms of shear modulus at small strain will be illustrated on the typical test performed in *KCC* 6, which can be considered representative of all the others. The first interpretation step is to transform raw measurements into a cavity pressure versus cavity radial strain curve (according to section 2.3.1). The result is illustrated in Figure 2.49. Then, each loop is corrected for membrane compliance. The example of loop L3 is presented in Figure 2.50a. The origin point of the unloading path is identified. To facilitate the analysis, the unload curve is isolated and plotted in a modified coordinates system in which the origin corresponds to zero strain, zero pressure (Figure 2.50b). It can be noted that the resulting curve is non-linear.

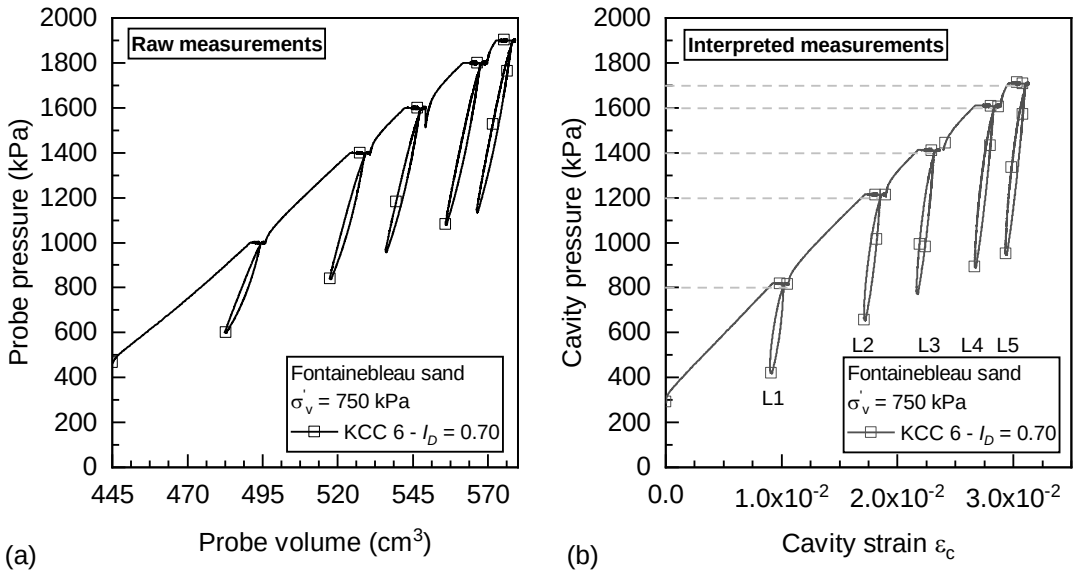

Figure 2.49 – Results of test performed in KCC 6. (a) Raw measurements; (b) interpreted measurements

The maximum shear modulus G_{max} of the soil can be evaluated from each loop using the methods proposed by Briaud *et al.* (1983) and Byrne *et al.* (1991) presented in Chapter 1.The degradation of the secant shear modulus in function of the shear strain of the soil at the cavity wall, γ_c, can also be evaluated, as it can be seen in Figure 2.50b and as will be detailed in the following sections.

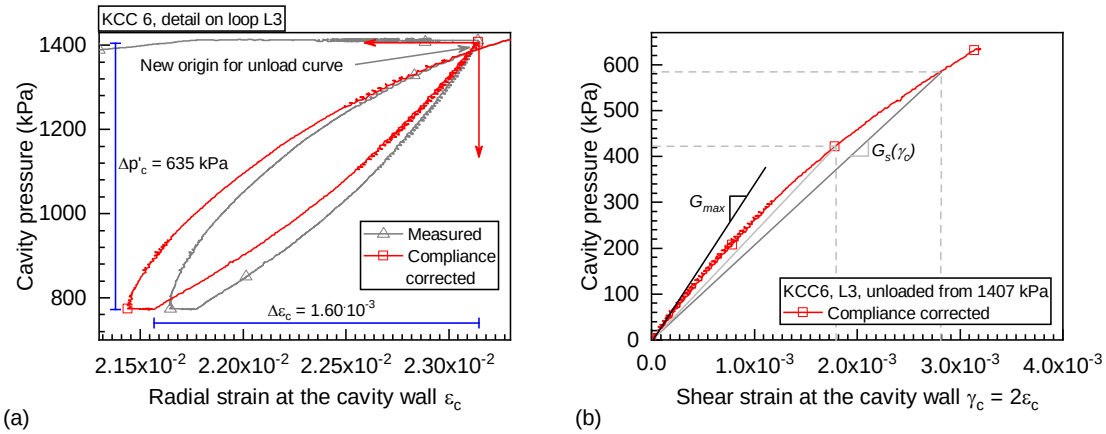

Figure 2.50 – Detail in the interpretation of loop L3 from test in KCC 6; (a) membrane compliance correction and values of loop stress and cavity strain amplitude; (b) detail on the unload path after coordinate changes with indication of derivation of maximum and secant shear modulus

2.6.2.1 Evaluating the maximum shear modulus G_{max}

The method proposed by Briaud *et al.* (1983) considers that the relationship between the inverse of the secant shear stiffness and the cavity shear strain is linear. The maximum shear modulus can be obtained as the intersection between the straight line

fitted to the calculated points and the ordinate axis. Figure 2.51 illustrates the application of this method to loop L3 in KCC 6.

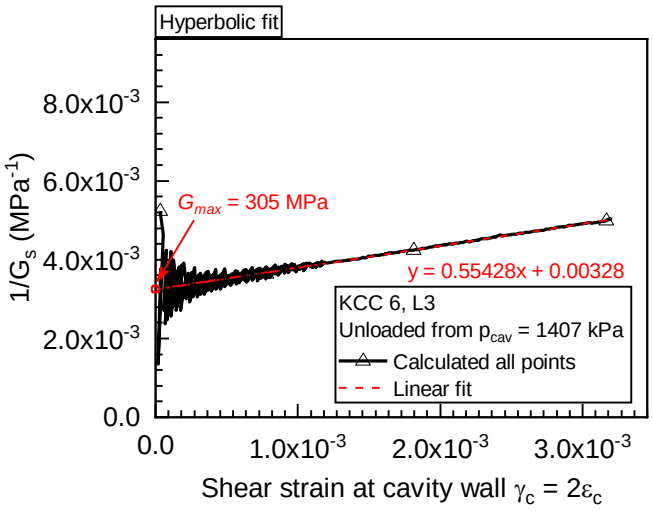

Figure 2.51 – Example of hyperbolic fit for the unload path of loop L3 performed in KCC6. Maximum shear modulus is equal to the intercept between the fitted line and the ordinate axis

The method proposed by Byrne *et al.* (1991) requires calculating the shear modulus evaluated at full loop amplitude, and inserting loop properties into a chart (see Chapter 1, Figure 1.19). Numerical application for loop L3 in *KCC* 6, in which the maximum pressure before unloading p_{cav} is 1407 kPa, the loop stress amplitude Δp_{cav} = 635, the loop strain amplitude $\Delta\varepsilon_c$ is $1.60 \cdot 10^{-3}$ and the associated shear modulus is $G_s(\Delta\varepsilon_c)$ = 198 MPa (Figure 2.50a), leads to the following chart inputs: ratio between the pressure before unloading and the initial stress at rest p_{cav} / σ'_{h0} = 4.7, ratio between loop amplitude and pressure before unloading $\Delta p_{cav} / p_{cav}$ = 0.45. The ratio obtained between pressuremeter modulus and maximum shear modulus G_s/G_{max} is 0.67, yielding G_{max} = 297 MPa.

2.6.2.2 Evaluating secant shear modulus decay

As presented in Figure 2.50b, pressuremeter secant shear modulus G_s can be evaluated in function of cavity radial strain, ε_c as half the slope between all the measured points and the loop origin, resulting in a secant pressuremeter modulus decay curve of type $G_s = f(\varepsilon_c)$.

However, the strain level associated to pressuremeter secant shear moduli cannot be directly compared to that associated to soil elementary shear moduli, as it has been presented in *Chapter 1* (Wood, 1990). Cavity radial strains must be transformed into

equivalent elementary shear strains. There are two straightforward ways to do this based on experimental data: as proposed by Bellotti *et al.* (1989) for sands and by Jardine (1992), for clays. For the current case, it can be shown that both approaches yield similar results within the range of interest of average shear strains, as illustrated in Figure 2.52.

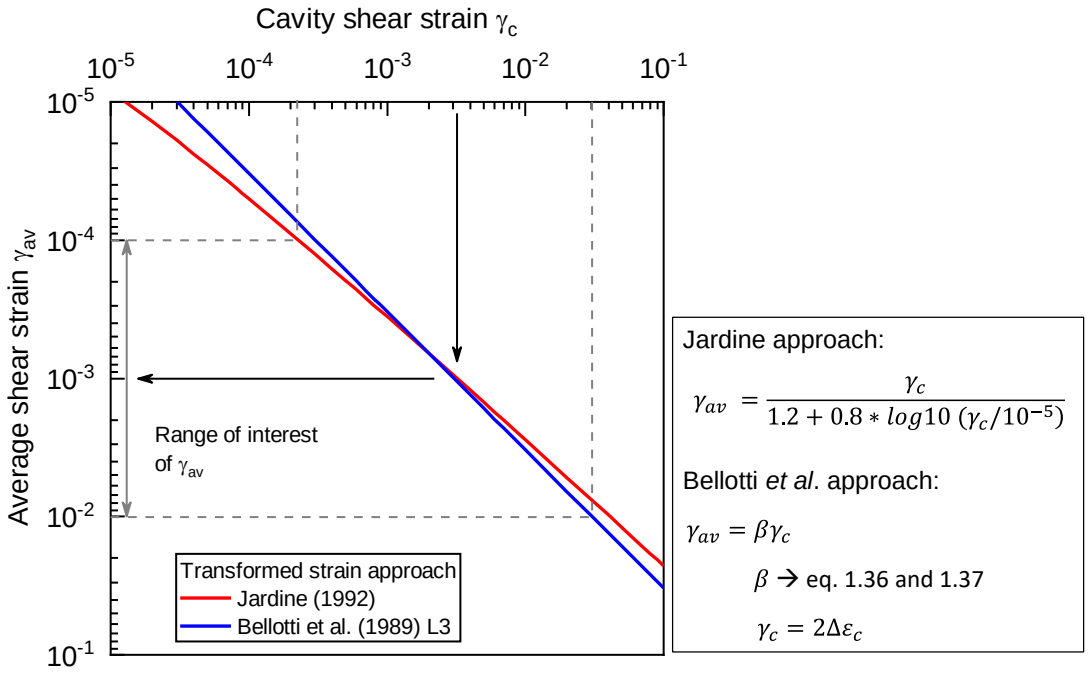

Figure 2.52 – Comparison between the transformed strain approach using both Bellotti et al. (1989) and Jardine (1992) methods

The application of Bellotti *et al.* equation (1.36) for loop 3 (p_{cav} = 1400 kPa, p'_0 = 300 kPa, ϕ'= 37°), and considering that $\gamma_c = 2\,\varepsilon_c$ leads to a constant transformation coefficient $\gamma_{av}/\gamma_c = 0.329$, represented by the blue line in Figure 2.52. The application of Jardine's transformed strain approach (eq. 1.42) leads to a ratio between the transformed shear strain and the cavity wall shear strain, γ_{av}/γ_c, varying between 0.50 and 0.28 within the range of interest of measurement ($10^{-4} < \gamma_{av} < 10^{-2}$), represented by the red line in the previous figure. It can be seen that the application of both approaches is very similar in this case, because the level of plasticity developed around the cavity is relatively low. This was also verified for the other loops. Thus, for simplicity, Jardine's approach was chosen.

Figure 2.53 presents a plot of G_s in function of the cavity strain γ_c further transformed into an average strain, γ_{av}, also for the third unload loop (L3).

It should be noticed that for small strain increments, even minimal measurement noise will be highly amplified when deriving shear moduli and exploring the results may require data smoothing. It can be observed in Figure 2.53 that the hyperbolic fitting proposed by Briaud *et al.* (1983) can be used for this purpose without distorting the results. The hyperbolic curve fitted is represented by the red smooth line

The relative error due to smoothing can be evaluated by comparing G_s calculated from the fitted curve and that calculated directly from the measurement points after strain transformation. Relative errors are systematically inferior to ±7.5% from a cavity average shear strain of approximately $2 \cdot 10^{-4}$. From a cavity strain of $4 \cdot 10^{-4}$, relative errors are inferior to 1%. Thus, it is considered that the probe can effectively provide measurements from $\gamma_c > 2 \cdot 10^{-4}$ (plotted in green line in Figure 2.53) and for smaller strain ranges, shear modulus cannot be assessed without curve fitting or smoothing, and this is to be considered an extrapolation range. Measurements needing smoothing or extrapolation are plotted in color magenta.

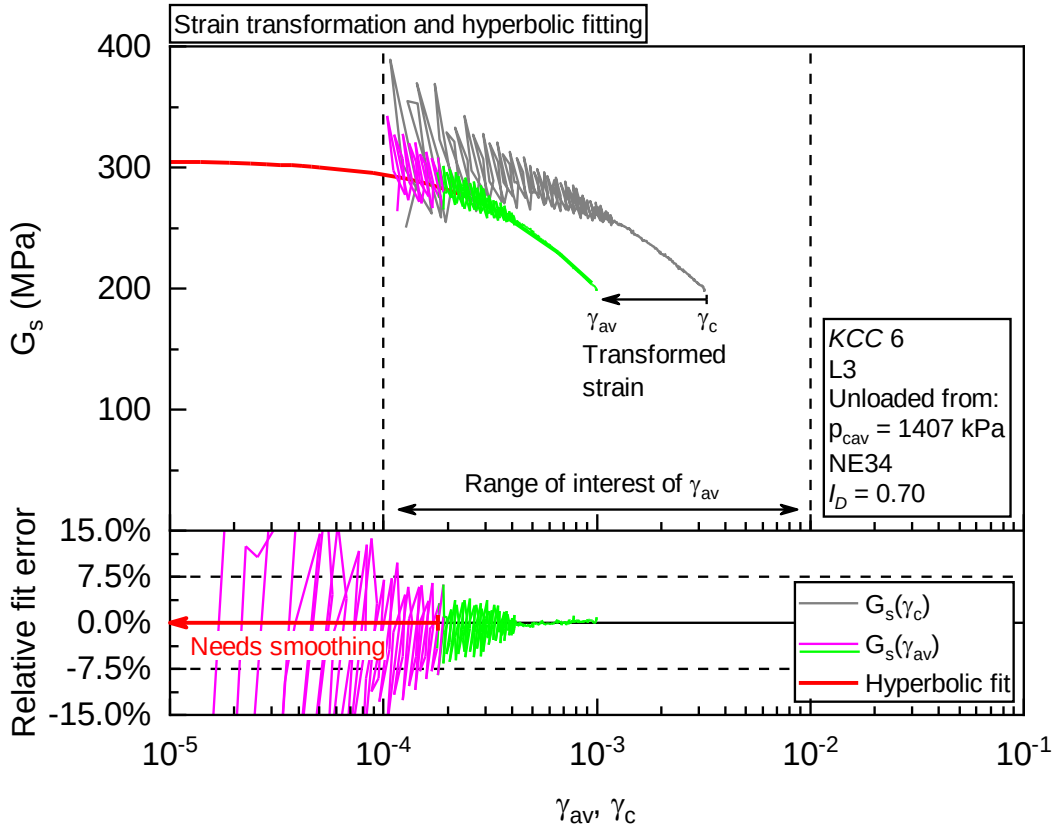

Figure 2.53 – Example of the strain transformation and the derivation of Gs in function of γ_{av} for the third unload loop in *KCC* 6, including the relative fit errors.

2.6.3 Repeatability test

A repeatability test was performed to validate the experimental procedure. A sand specimen of same characteristics that the one used in KCC 6 was reconstituted in KCC 8 following the same protocol as previously described. The same loading program and interpretation procedure were applied. Figure 2.54 presents both test results superposed with the detail of the third unload-reload loop. It can be seen that the resulting behavior observed is very similar for both tests.

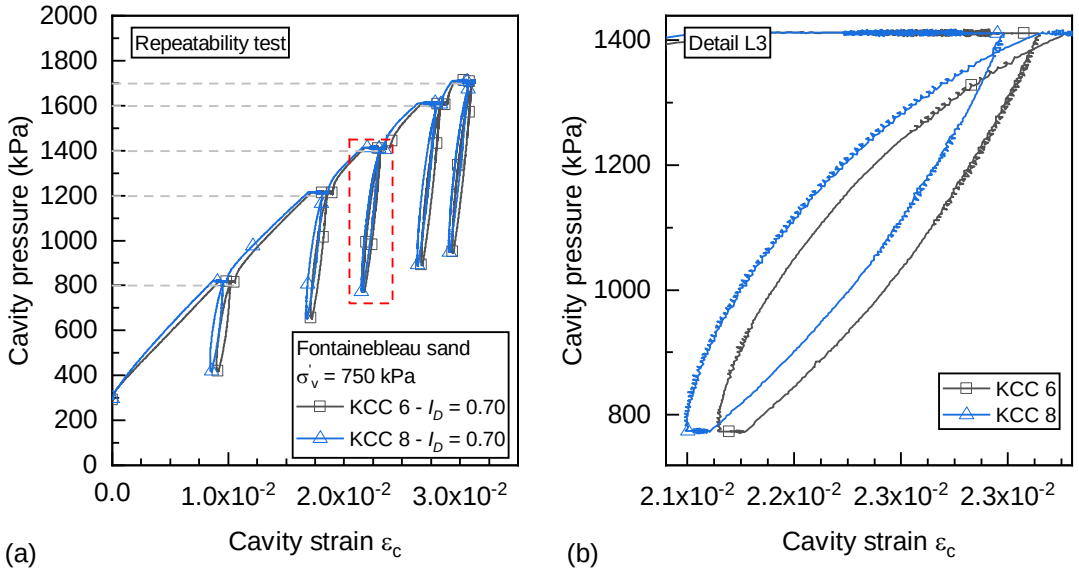

Figure 2.54 – Comparison between test in KCC 6 and KCC 8 of same density index. (a) Whole test; (b) loop L3

The derivation of maximum shear modulus and the hyperbolic fit of loop L3 in KCC 6 and 8 are presented in Figure 2.55. Results plot very close to each other, and the difference between the evaluated G_{max} is inferior to 2%.

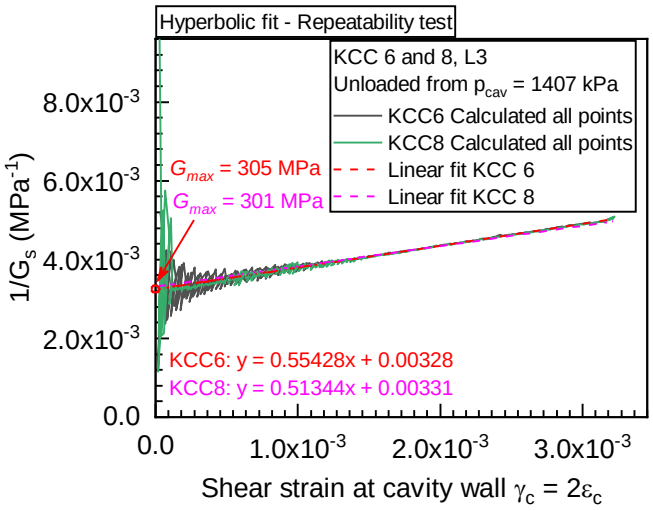

Figure 2.55 – Comparison between loop L3 in KCC 6 and 8

The derivation of secant shear modulus in function of average shear strain for both loops is presented in Figure 2.56. This result is considered satisfactory.

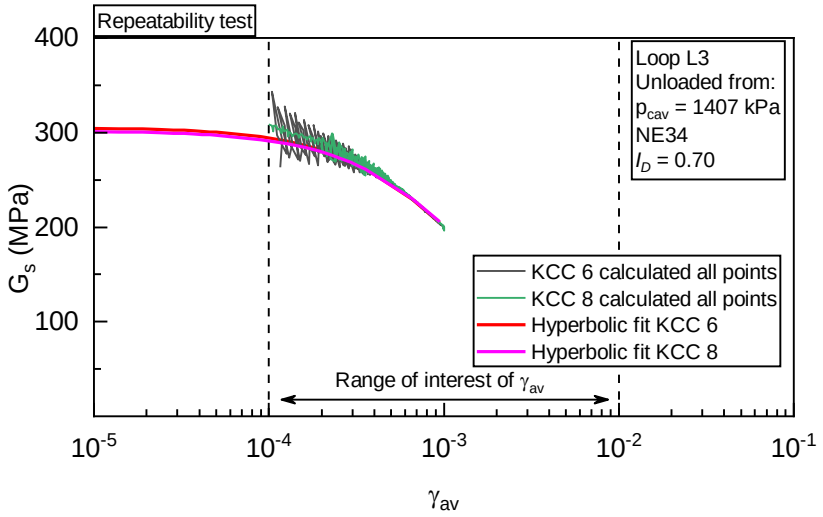

Figure 2.56 – Comparison between derived degradation curve of secant shear modulus from loop L3 performed in KCC 6 and KCC 8 tests

As will be shown in the summary tables presented in section 2.6.6, the maximum difference between the evaluated values of G_{max} happens in the first loop and it is of about 11%. For the other loops, less than 5% difference was observed. The reason for which the difference is higher in the first loop is probably related to the fact that measurement accuracy is lower at lower probe pressures, as it has been discussed in section 2.4.2.1.

2.6.4 Influence of the density index I_D

The influence of the density index I_D of the sand on the results obtained is presented in Figure 2.57. It can be observed that specimens of higher density index presented a stiffer behavior. These measurements are in accordance with the expected behavior of dry sands, and they confirm that the test can capture the influence of sand density on its response. It can also be observed that the repeatability tests (KCC 6 and 8) are well superposed, confirming that the testing procedure yields repeatable results. The influence of the density index on sand response will be quantified in the next section.

2.6.5 Influence of the cavity pressure before unloading

The influence of the cavity pressure level for loops *L1* to *L5* can be observed by analyzing Figure 2.58. It can be seen that an increase in the cavity pressure before unloading leads to an overall increase of the slope of the unload curve. This result confirms that increasing probe pressure before unloading leads to an increase in the average effective stress in the soil around the cavity, leading to an increase in shear modulus. It can also be observed that loops starting from higher pressure levels present a longer quasi-linear portion, while loops performed from lower pressure values tend to be non-linear from its early beginning. These results also confirm the importance of adjusting the loop pressure-amplitude in function of the cavity pressure before unloading, and confirm that the ratio chosen in this research, $\Delta p_{cav,i}/p_{cav,i} = 0.4$, was a good compromise in this case.

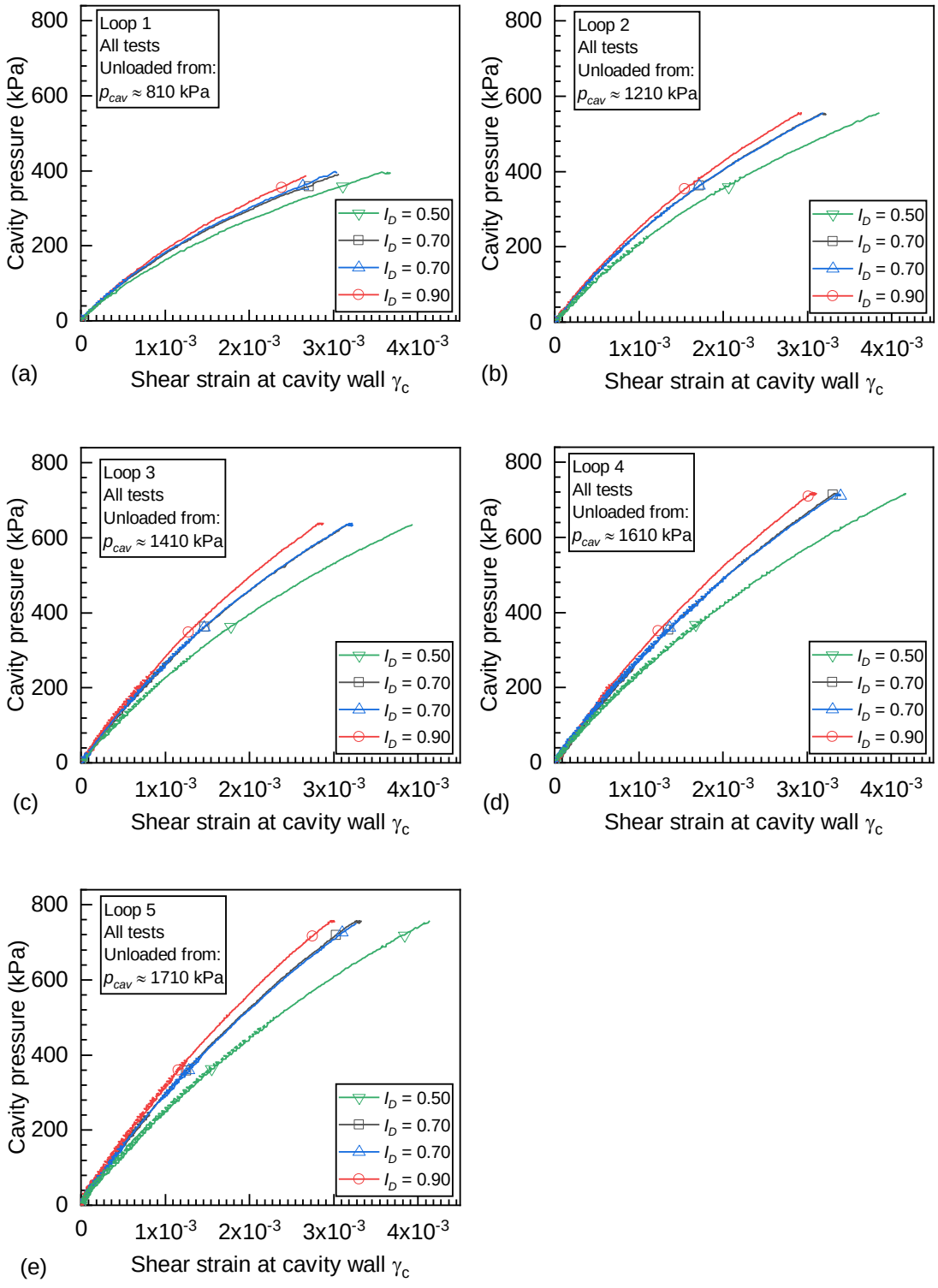

Figure 2.57 – Influence of the density index on the unload curve for loops L1 to L5

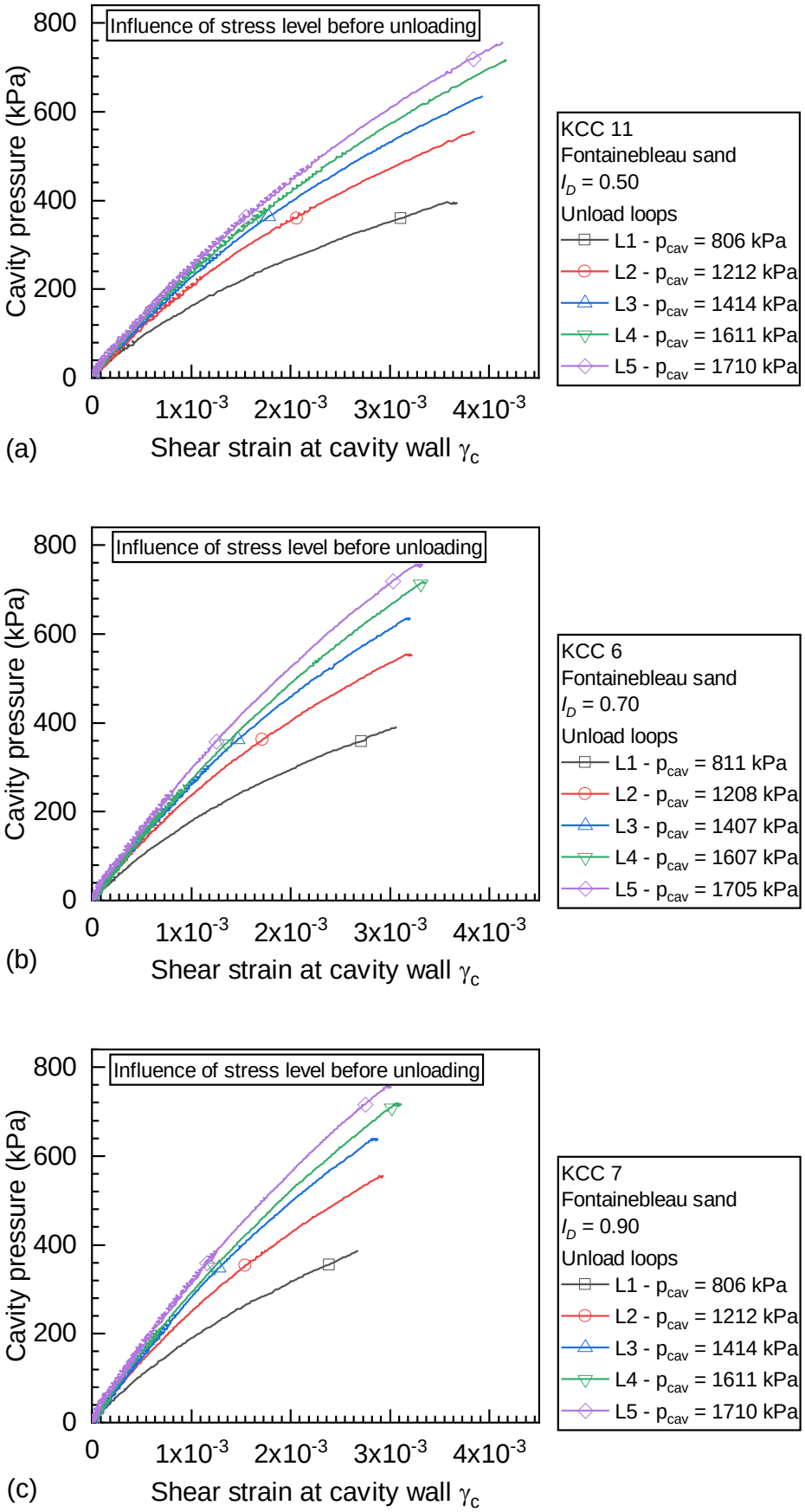

Figure 2.58 – Influence of the cavity pressure before unloading on the unloading curve

2.6.6 Summary of results

Results of the cavity expansion curves obtained in KCC 6, 7, 8 and 11 following the test protocol for measuring shear stiffness at small strains are presented in Figure 2.59. From a first inspection of these results, it is easy to confirm the influence of the density index on the curves obtained.

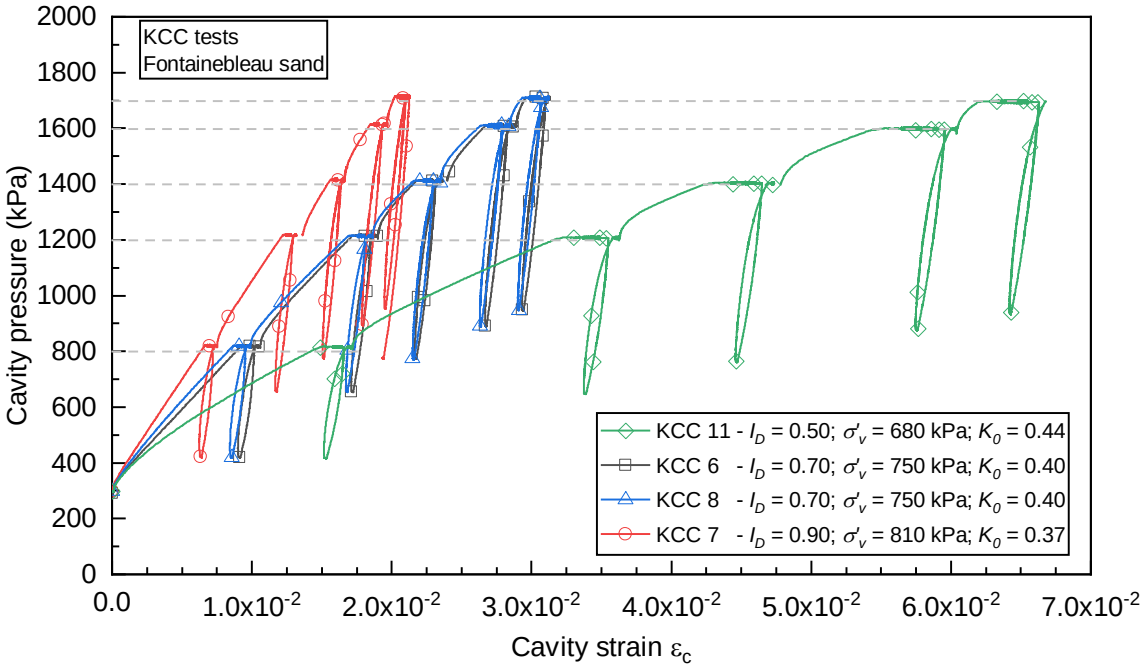

Figure 2.59 – Results of tests in KCC 6, 7, 8 and 11

The influence of the cavity pressure before unloading and of the density index on the maximum shear modulus derived using both methods described is illustrated in Figure 2.60. Both methods used for evaluating G_{max} yielded close results.

The influence of the density index and of the cavity pressure before unloading on the secant moduli of Fontainebleau sand NE34 assessed through the tests is presented, respectively, in Figure 2.61 and in Figure 2.62.

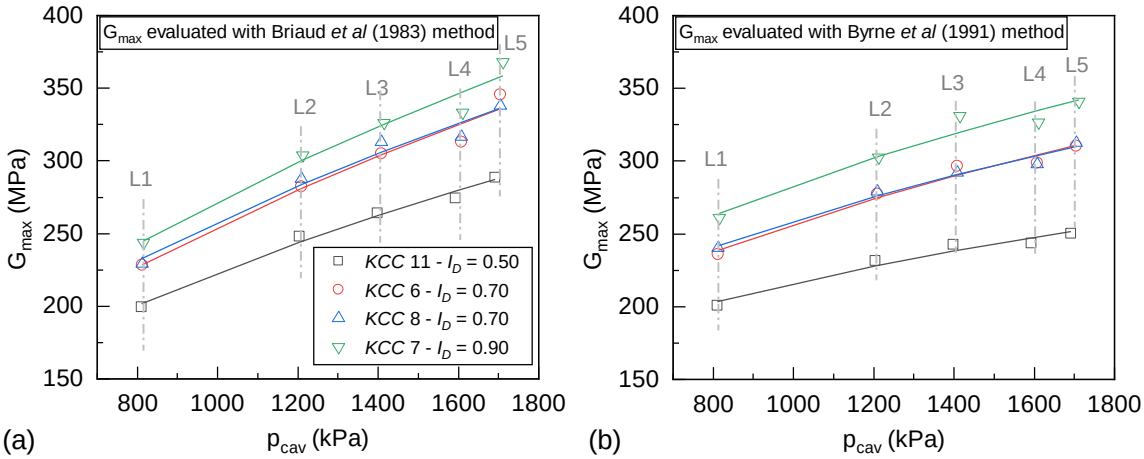

Figure 2.60 – Maximum shear modulus of fontainebleau sand evaluated for each unload loop using (a) Briaud *et al.* (1983) and (b) Byrne *et al.* (1991) methods

The hyperbolic parameters derived from the interpretation of all the unloading loops using the method of Briaud *et al.* (1983) are synthetized in Table 2.5.

Table 2.5 – Application of Briaud et al. (1983) method to the interpretation of the unload loops

		Hyperbolic fit			
	Loop	***p*$_{cav}$ (kPa)**	**a** (MPa^{-1}) 10^{-3}	**b** [-]	***G*$_{max}$ *(MPa)***
KCC11	L1	811	5.01	1.1725	199
(I_D = 0.50)	L2	1204	4.03	0.7732	248
	L3	1398	3.79	0.6207	264
	L4	1593	3.64	0.5343	274
	L5	1692	3.46	0.4912	289
KCC6	L1	811	4.38	1.1772	228
(I_D = 0.70)	L2	1208	3.54	0.6927	282
	L3	1407	3.28	0.5389	305
	L4	1607	3.20	0.4477	313
	L5	1705	2.89	0.4462	346
KCC8	L1	815	4.36	1.1223	229
(I_D = 0.70)	L2	1210	3.47	0.7286	288
	L3	1408	3.20	0.5716	313
	L4	1604	3.16	0.4664	317
	L5	1701	2.96	0.4322	338
KCC7	L1	806	4.10	1.1484	244
(I_D = 0.90)	L2	1212	3.29	0.6907	304
	L3	1414	3.06	0.4860	327
	L4	1611	3.00	0.4182	334
	L5	1710	2.72	0.4127	368

Table 2.6 presents the results obtained by the application of the chart proposed by Byrne *et al.* (1991) for all the unload loops.

Table 2.6 – Application of Byrne *et al.* (1991) method to the interpretation of the unload loops (all tests performed at σ'_{h0} = 300 kPa)

		Measured values				Application of Byrne *et al.* (1991) method			
		p_{cav} (kPa)	Δp_{cav} (kPa)	$\Delta\varepsilon_c$ x(10^{-3})	$G_s(\Delta\varepsilon_c)$ (MPa)	p_{cav}/σ'_{h0}	$\Delta p_{cav}/p_{cav}$	G_s/G_{max}	G_{max} (MPa)
KCC11	L1	811	394	1.83	108	2.7	0.49	0.54	201
	L2	1204	554	1.92	144	4.0	0.46	0.62	231
	L3	1398	633	1.96	162	4.7	0.45	0.67	243
	L4	1593	716	2.08	172	5.3	0.45	0.71	243
	L5	1692	752	2.06	183	5.6	0.44	0.73	250
KCC6	L1	811	391	1.53	127	2.7	0.48	0.54	236
	L2	1208	555	1.60	173	4.0	0.46	0.62	278
	L3	1407	635	1.60	198	4.7	0.45	0.67	297
	L4	1607	715	1.68	213	5.4	0.44	0.71	299
	L5	1705	756	1.66	227	5.7	0.44	0.73	310
KCC8	L1	815	395	1.52	129	2.7	0.48	0.54	240
	L2	1210	556	1.59	174	4.0	0.46	0.62	279
	L3	1408	633	1.61	196	4.7	0.45	0.67	292
	L4	1604	717	1.69	212	5.3	0.45	0.71	298
	L5	1701	749	1.63	230	5.7	0.44	0.74	313
KCC7	L1	806	375	1.30	144	2.7	0.47	0.55	261
	L2	1212	554	1.46	190	4.0	0.46	0.63	303
	L3	1414	638	1.44	222	4.7	0.45	0.67	331
	L4	1611	718	1.54	233	5.4	0.45	0.71	327
	L5	1710	756	1.50	251	5.7	0.44	0.74	341

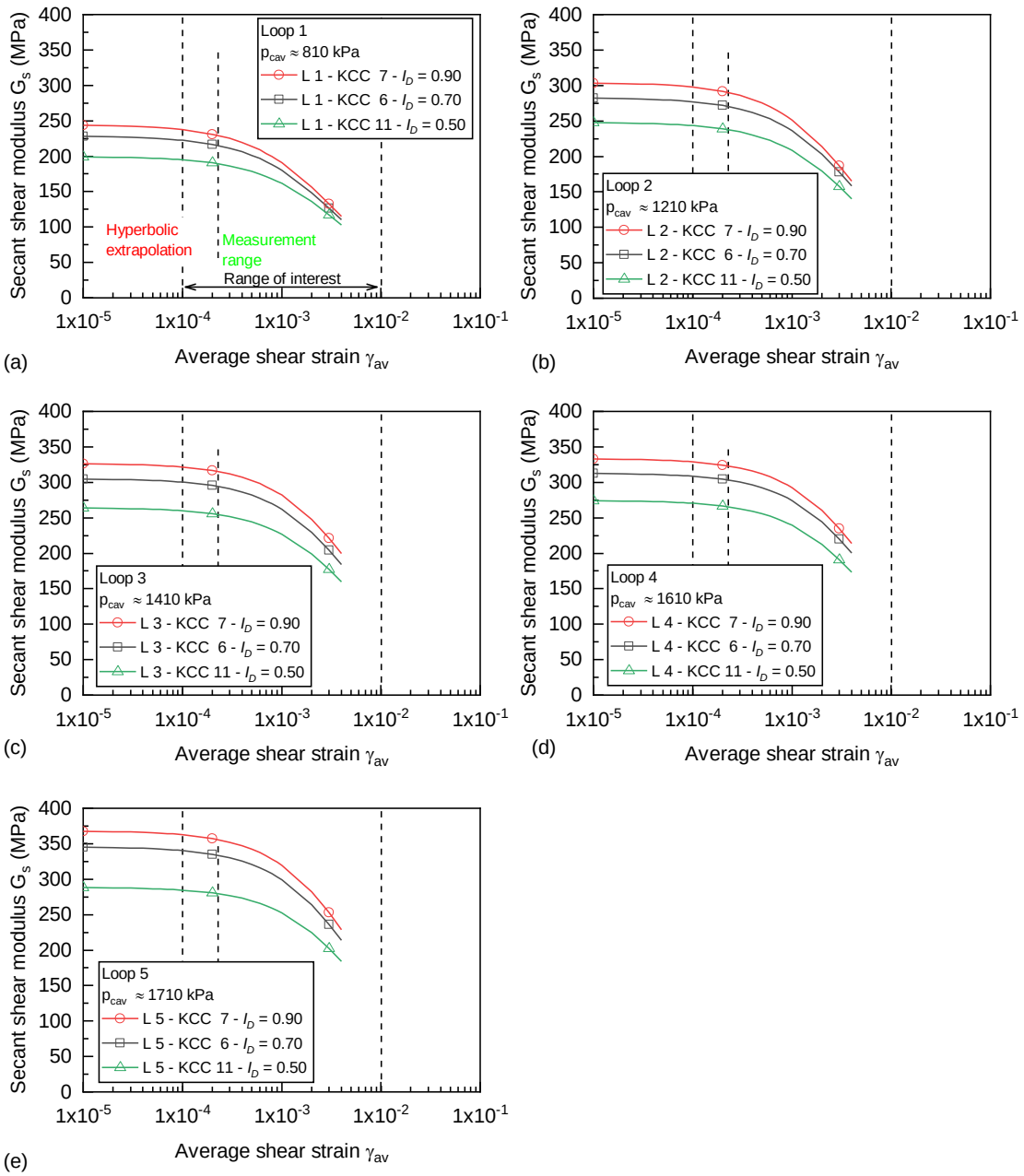

Figure 2.61 – Summary of the obtained degradation curves of the secant shear moduli versus the average shear strain obtained for all loops. Influence of the density index of the sand

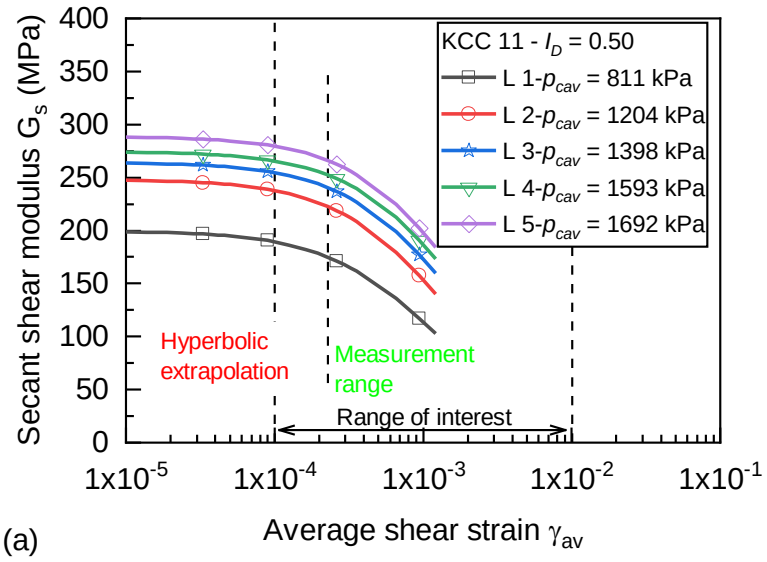

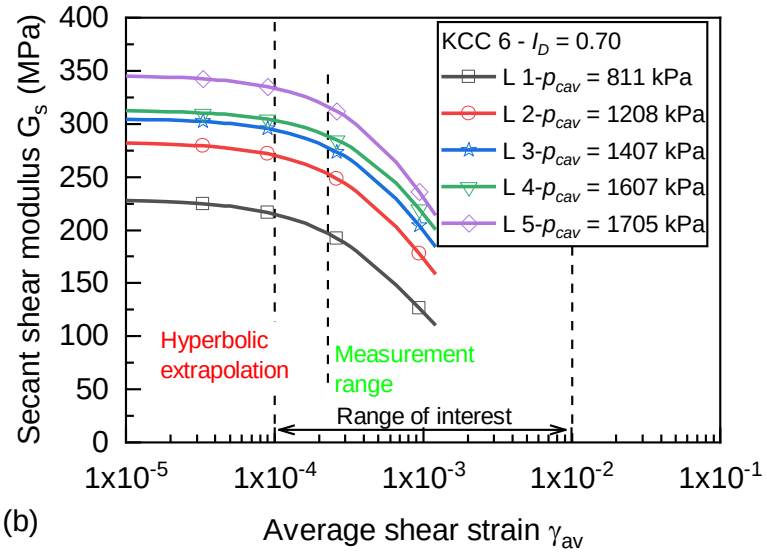

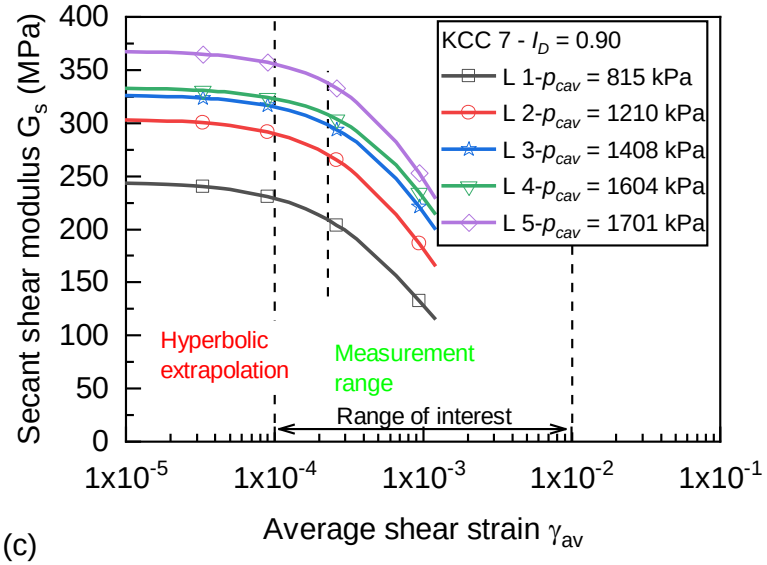

Figure 2.62 – Summary of the obtained degradation curves of the secant shear moduli versus the average shear strain obtained for all loops. Influence of the cavity pressure before unloading

These results confirm that pressuremeter tests performed with this probe are sensitive to changes in soil properties such as the density index. The next section presents a validation of the measured parameters with respect to intrinsic elasticity properties of Fontainebleau sand NE34.

2.6.7 Validation

The validation of the testing protocol is done by comparing measurements in *KCC* with Fontainebleau intrinsic properties that can be obtained through laboratory tests. The evolution of maximum shear modulus with the average stress was evaluated using Delfosse-Ribay et al. (2004) formulation, and the evolution of the shear modulus with the shear strain can be evaluated using Oztoprak and Bolton (2013) model, as presented in section 2.2.

Shear modulus in granular soils is dependent on the average state of stress. In pressuremeter tests, since the stress field is not homogeneous around the cavity, it is considered that shear modulus is dependent on an average stress state, which can be calculated according to the formulas previously presented in literature. However, there is no consensus amongst the many methods available. For the tests performed in calibration chamber, the pertinence of all the stress adjustment methods was investigated. Results are presented in Figure 2.63, Figure 2.64 and in Figure 2.65. Values calculated using the different methods found in literature are summarized in Table 2.7.

Based on the results presented, it can be seen that the values of maximum shear modulus evaluated from the pressuremeter test are in good agreement with those expected for Fontainebleau sand. For tests performed in *KCC* 6, *KCC* 8 and *KCC* 11, the relative difference between G_{max} evaluated from the pressuremeter and the intrinsic values for Fontainebleau sand are inferior to 10 %. For *KCC* 7, the maximum difference is of 15%.

The adjustment methods for stress level do not seem applicable for the tests carried out in the calibration chamber with the current configuration. For these tests, it seems that the soil stiffness during unloading is controlled by the maximum stress before unloading ($p' = p_{cav}$).

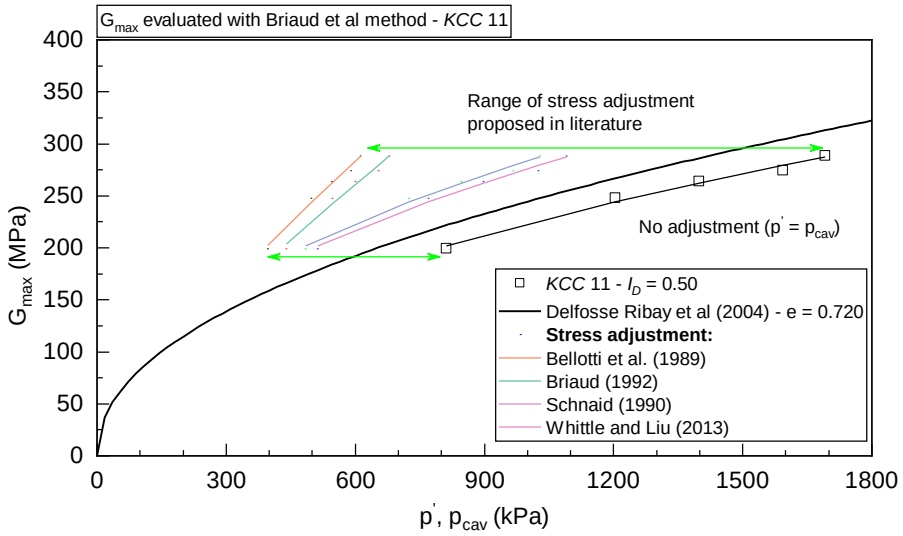

Figure 2.63 – Comparison between the maximum shear modulus evaluated with the pressuremeter in KCC 11 and the intrinsic values after Delfosse-Ribay et al. (2004) for ID = 0.50

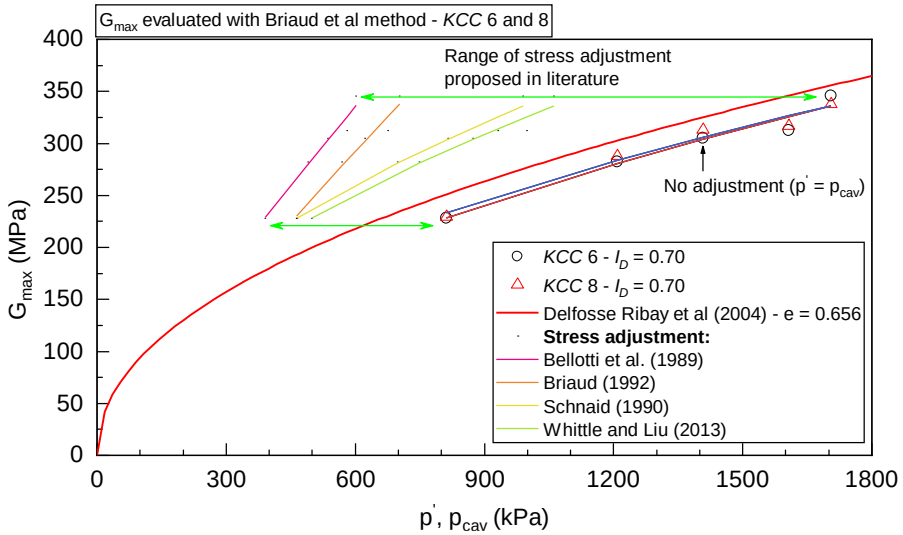

Figure 2.64 – Comparison between maximum shear modulus evaluated with the pressuremeter in *KCC* 6 and 8 and the intrinsic values after Delfosse-Ribay et al. (2004) for I_D = 0.70

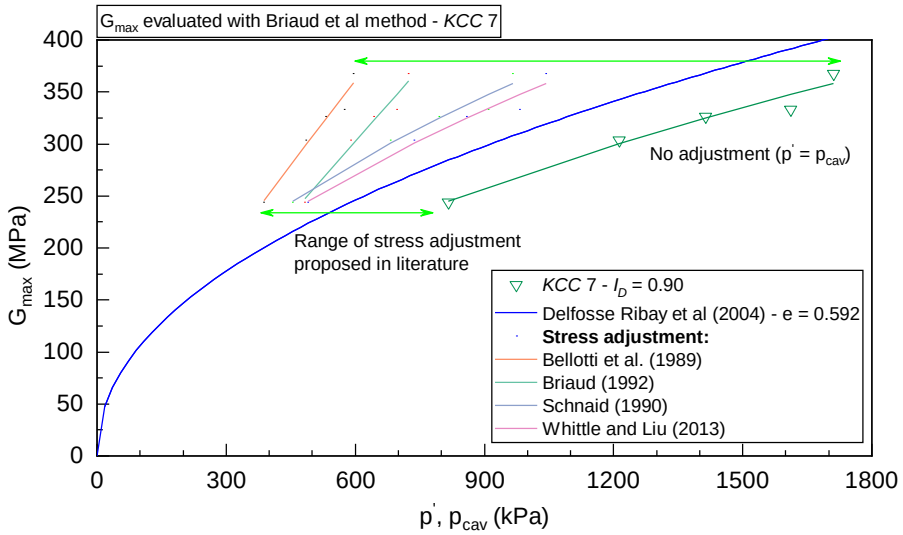

Figure 2.65 – Comparison between the maximum shear modulus evaluated with the pressuremeter in *KCC* 7 and the intrinsic values after Delfosse-Ribay et al. (2004) for I_D = 0.90

Table 2.7 – Cavity stress and average stress around the cavity for each unload loop

	Loop	p_{cav} (kPa)	Average stress around the cavity p' (kPa)			
			Bellotti *et al* (1989)	**Briaud (1992)**	**Schnaid (1990)**	**Whittle and Liu (2013)**
KCC 11	L1	811	400	443	490	520
	L2	1204	499	548	728	772
	L3	1398	545	600	846	897
	L4	1593	589	652	964	1022
	L5	1692	611	678	1023	1085
KCC 6 and 8	L1	811	394	466	473	507
	L2	1208	493	572	704	754
	L3	1407	538	625	820	879
	L4	1607	583	679	936	1003
	L5	1705	604	705	993	1064
KCC 7	L1	806	389	485	458	494
	L2	1212	489	593	689	744
	L3	1414	535	647	803	868
	L4	1611	578	700	915	989
	L5	1710	599	726	972	1050

A comparison between shear moduli decay assessed based on pressuremeter test results and intrinsic curves for Fontainebleau sand is presented in Figure 2.66.

Results for *KCC* 6 and *KCC* 11 (Figure 2.66 a and b) show a good agreement between the degradation curves evaluated with the pressuremeter and the theoretical ones for Fontainebleau sand. For KCC 7 (Figure 2.66 *c*) there is a small offset in the values of shear modulus. The origin of this error corresponds to the difficulties related to the stress level adjustment, which was more accentuated in this case, as illustrated in Figure 2.65. Despite this offset, the trends in shear moduli decay are similar to those expected for Fontainebleau sand. The results presented enable to conclude that it is possible to derive consistent and representative values of shear stiffness in a range of small strains using the proposed pressuremeter probe and associated testing procedures.

Instead of tracing the continuous shear modulus degradation curve, Lopes et al. (2019a) presents the results of test KCC 6 in a different manner. The authors calculated two moduli for each loop: one unload and one reload modulus, corresponding to the loop apexes. The obtained values were then adjusted using the same procedure presented herein.

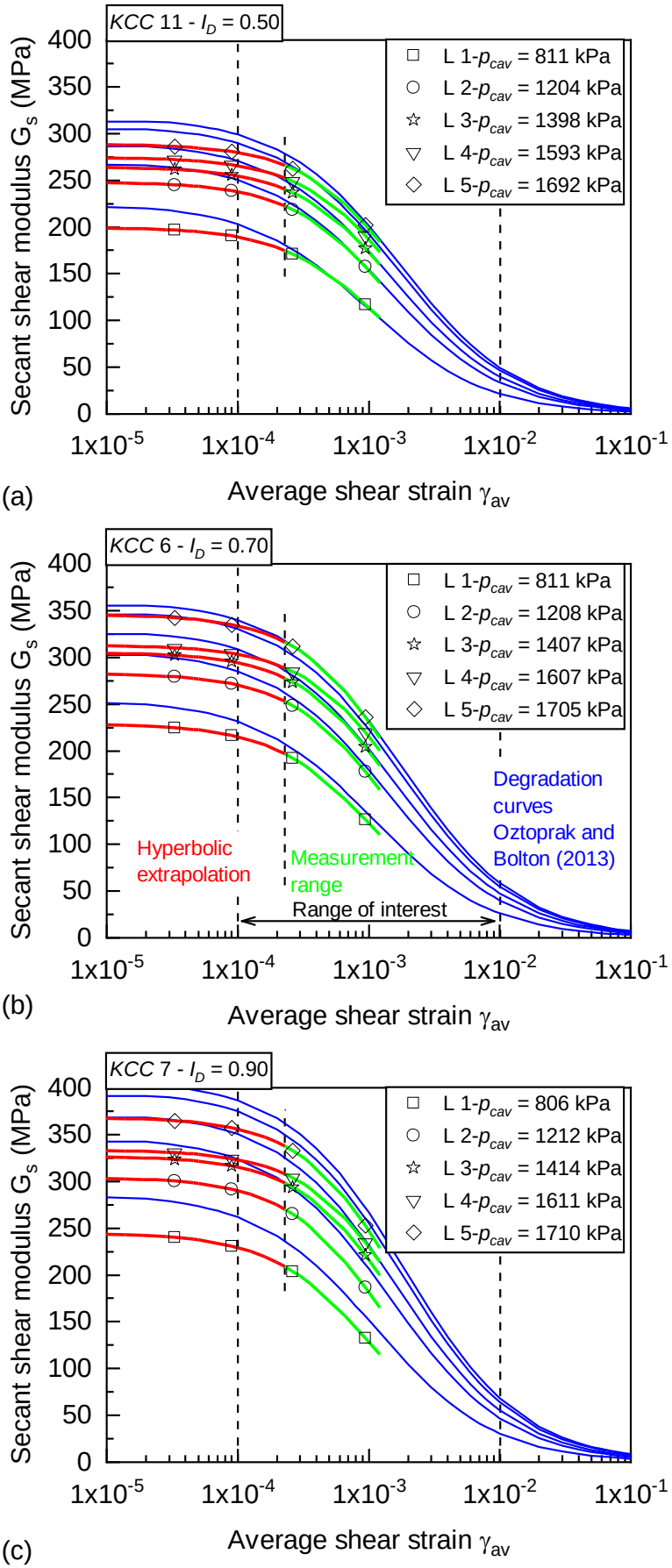

Figure 2.66 – Comparison between secant shear moduli decay in function of average shear strain assessed using the pressuremeter and the intrinsic curves for Fontainebleau sand

2.7 PRESENTATION OF RESULTS OBTAINED. ASSESSING CYCLIC PARAMETERS

This section presents the results of the cyclic tests performed in the PCC and in the KCC with the purpose of understanding the soil behaviour under cyclic loading using the pressuremeter. The section is divided in four parts. First, the testing program is presented. The interpretation procedure is then illustrated based on one typical case. Furthermore, the influence of density index, stress amplitude and average pressure of the cyclic series (as defined in Figure 2.35*b*) on the accumulation of plastic strains is studied.

2.7.1 Testing program

Table 2.8 presents the cyclic testing program performed in the two types of calibration chambers (*PCC* and *KCC*). It should be noted that test KCC 5 was performed using the same geometric conditions than test *PCC* 1 in order to evaluate the influence of the chamber boundary conditions on the test results. One should also note that complementary cyclic series were performed in PCC1 , as indicated by a (*). These series correspond to a post-failure solicitation and are aimed at verifying the changes in cyclic volumetric strain accumulation after pre-shearing the sand specimen.

Table 2.8 – Testing program performed in PCC and KCC aiming to assess cyclic properties

Specimen	I_D	σ'_{v0} (kPa)	K_0	Geometric Condition	Loading program	Consolidation procedure	Series	A (kPa)	p'_{min} (kPa)	N
PCC1	0,70	700	0,50 (imposed)	1 (PCC)	2	2	S1	30	370	20
							S2	60	370	22
							S3	120	370	21
							S4	180	370	17
							S5	240	370	5
							S6	300	370	5
							S7	360	370	5
					*		S8	15	1701	19
					*		S9	30	1687	12
					*		S10	60	1657	10
					*		S11	690	803	143
					*		S12	230	1256	17
					*		S13	180	1421	19
					*		S14	690	916	15
					*		S15	1220	374	11
					*		S16	500	559	28
					*		S17	720	347	14
					*		S18	555	336	10
					*		S19	400	755	10
					*		S20	400	1239	15
KCC5	0,70	875	0,40	1	2	2	S1	30	370	20
							S2	60	370	22
							S3	120	370	21
							S4	180	370	17
							S5	240	370	7
							S6	300	370	9
KCC9	0,70	750	0,40	3	2	2	S1	60	320	20
							S2	120	320	20
							S3	360	320	20
KCC10	0,90	810	0.37	3	2	2	S1	60	320	20
							S2	120	320	20
							S3	360	320	20
							S4	480	320	46
							S5	580	320	30

(*) Post failure cyclic series, to be detailed in section 2.7.2.4

2.7.2 Results and analysis of a typical test

The analysis of the accumulation of plastic strains due to cyclic loading will be illustrated on the tests *PCC* 1 and *KCC* 5 (Figure 2.67), series one to six.

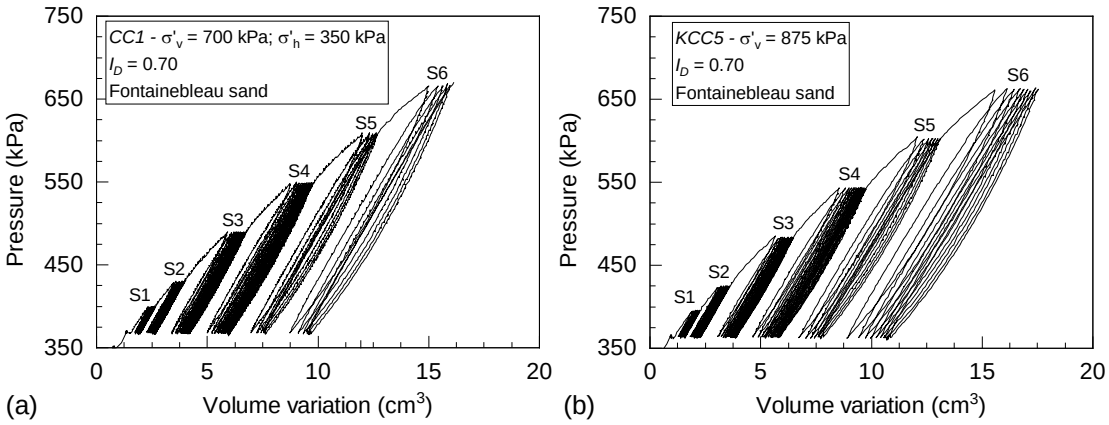

Figure 2.67 – Results of the cyclic series S1 to S7 in PCC1 and in KCC5

The cyclic series were interpreted in order to obtain the accumulation of volumetric strain in function of the number of cycles according to the scheme presented in Figure 2.68. The procedure consists in plotting the accumulated volume at the end of each cycle in function of the number of cycles. In this case, one cycle is defined by two points of minimum pressure, as presented in Figure 2.68.

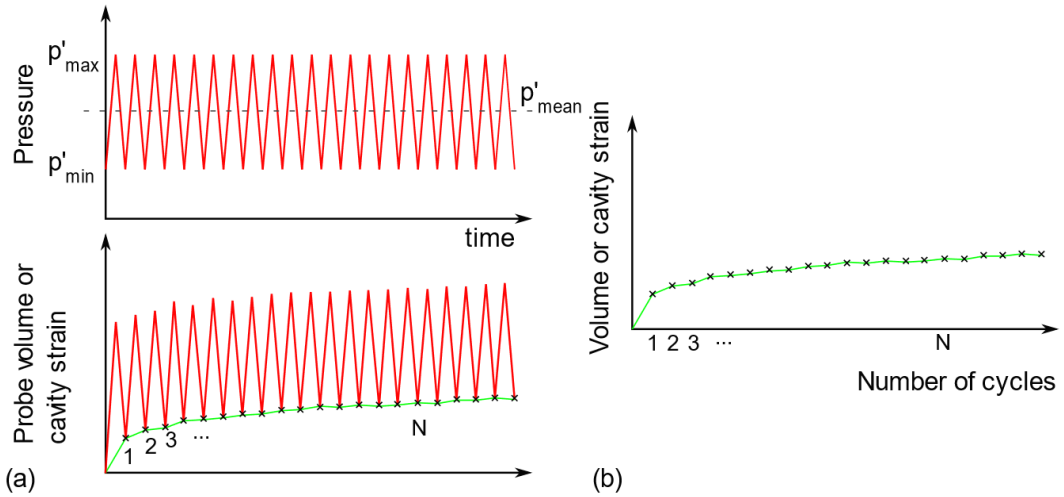

Figure 2.68 – Interpretation procedure for the determination of the accumulation of cavity strains in function of the number of cycles

Results corresponding to cyclic series S1 to S6 in *PCC* 1 and in *KCC* 5 are presented in Figure 2.69. From the results obtained, it can be seen that the volume variation in both tests are similar.

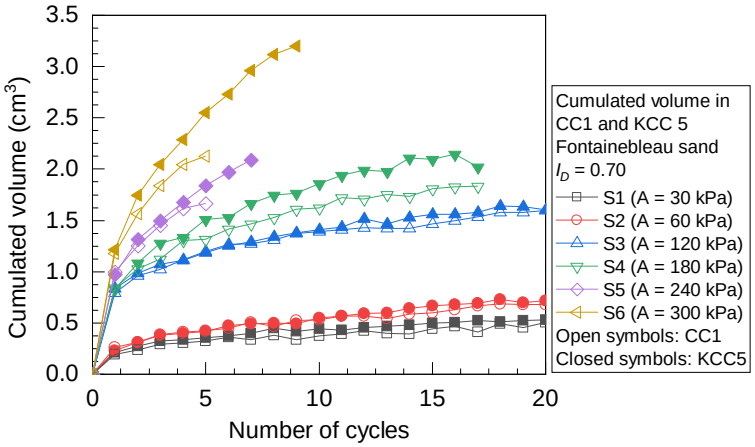

Figure 2.69 – Comparison between the accumulated volumes obtained in PCC1 and in KCC5

2.7.3 Influence of the density index

The influence of the density index I_D of the sand on the accumulation of volumetric strains during cyclic loading can be evaluated by comparing cyclic series performed in tests *KCC* 9 and *KCC* 10.

Results corresponding to cyclic series S1 to S3 performed in these tests are presented in Figure 2.70.

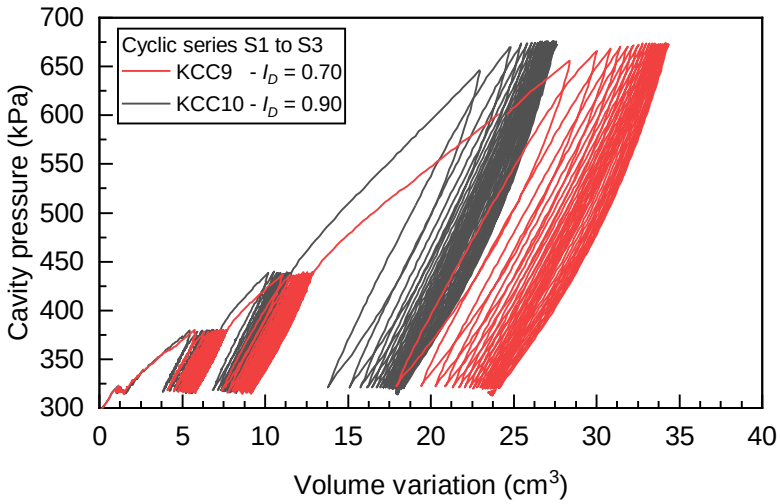

Figure 2.70 – Results obtained from the cyclic series performed in *KCC* 9 and *KCC* 10 tests

Figure 2.71 presents a comparison between series S1 to S3. All the curves were plotted relatively to the volume of the first cycle ($V_N - V_1$). It is observed that for the two smaller amplitude levels (60 and 120 kPa), volumetric accumulation is very similar in both specimens. For the 360 kPa amplitude series, the difference in behavior between the two specimens is evident. Lower accumulations are obtained for the denser specimen (KCC 10), as expected. These results are consistent with what has been published in

literature. Series of lower amplitude (60 kPa and 120 kPa) led to less accumulation and it is more difficult to distinguish the behavior between the two speciimens.

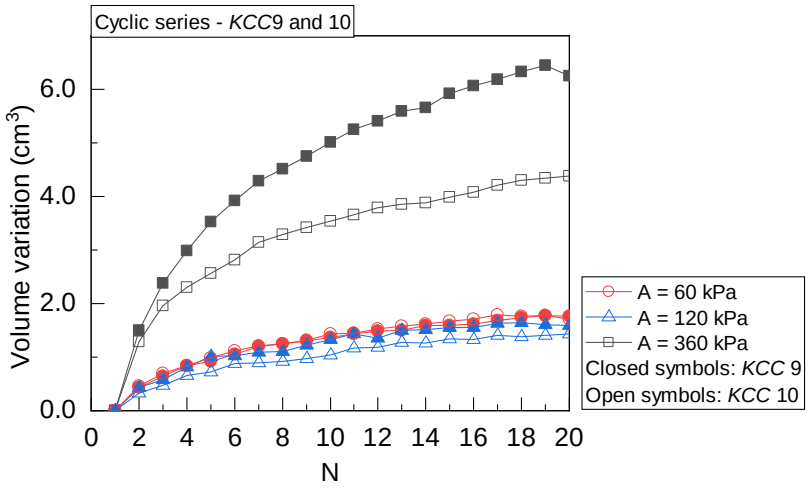

Figure 2.71 – Effect of the density index on volumetric accumulation during cyclic loading

2.7.4 Influence of the stress amplitude

2.7.4.1 Virgin loading

The influence of the cyclic amplitude in series performed according to loading protocol 2 is shown in Figure 2.72 (for I_D = 0.70) and in Figure 2.73 (for I_D = 0.90).

It was observed that despite the cyclic series S4 and S5 in KCC10 had a higher cyclic amplitude than series S3, they presented lower accumulation than series S3. The main reason for this is that the density of the specimen was modified after series S3, influencing the behavior observed in the subsequent series. The interpretation of series performed sequentially, one after the other, must be done with precaution: an apparent virgin loading (first expansion to a given cavity pressure) can have been modified by a previous loading of lower amplitude.

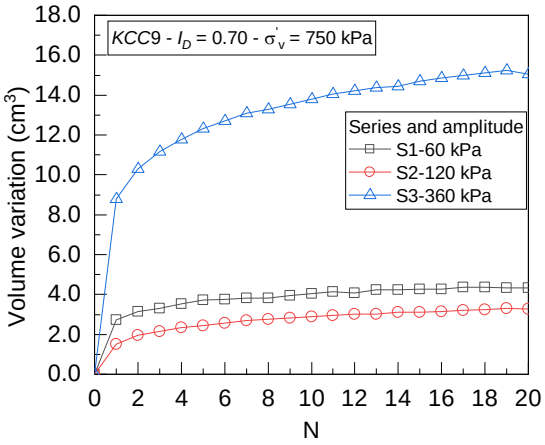

Figure 2.72 – Influence of the loop amplitude on the volumetric accumulation in *KCC*9

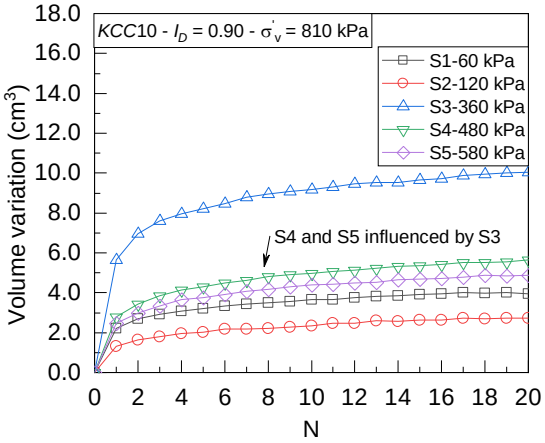

Figure 2.73 – Influence of the loop amplitude on the volumetric accumulation in *KCC*10

The influence of the cyclic amplitude of the six series performed in *PCC* 1 test is illustrated in Figure 2.74.

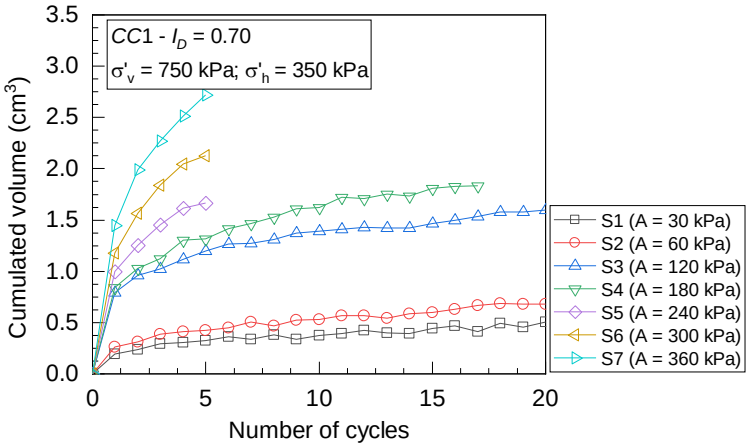

Figure 2.74 – Influence of the loop amplitude on the volumetric accumulation in *PCC*1

2.7.4.2 Investigation of post-failure cyclic loading

Test *PCC*1 was continued after the cyclic series S1 to S7 were performed and other cyclic series were performed after having pre-sheared the soil specimen. The complete

test with all successive sequences is presented in Figure 2.75 and the resulting cavity expansion curve is presented in Figure 2.76.

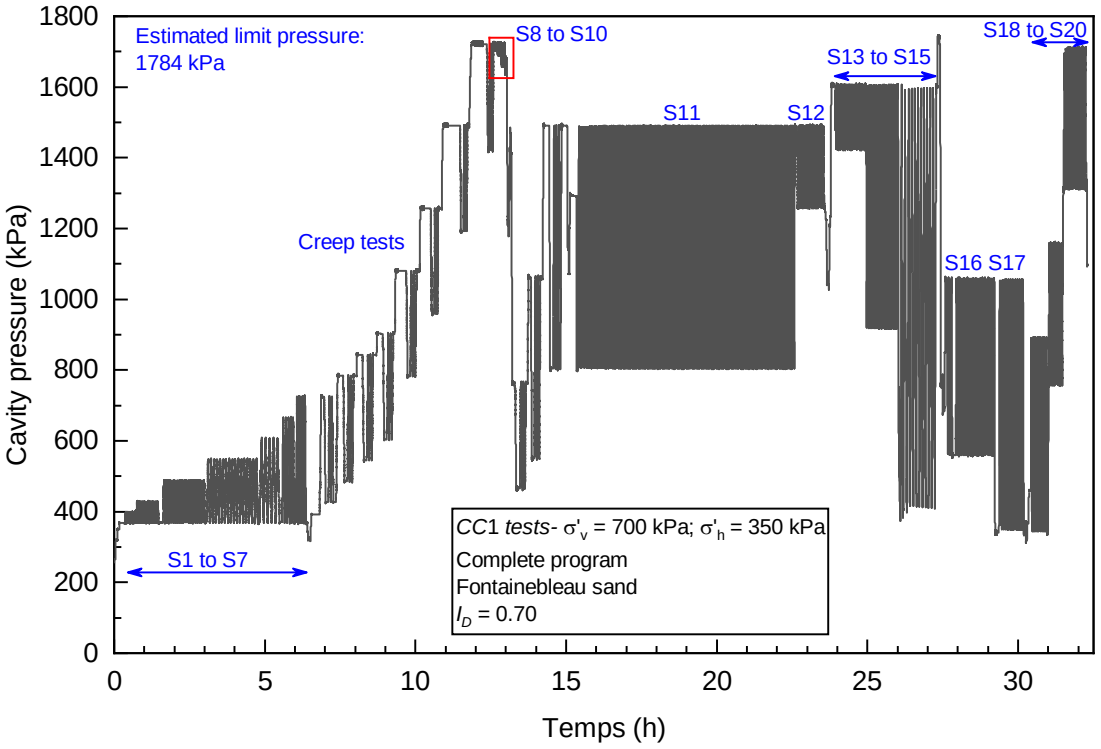

Figure 2.75 – Complete loading program performed in PCC1, including post-failure cyclic series

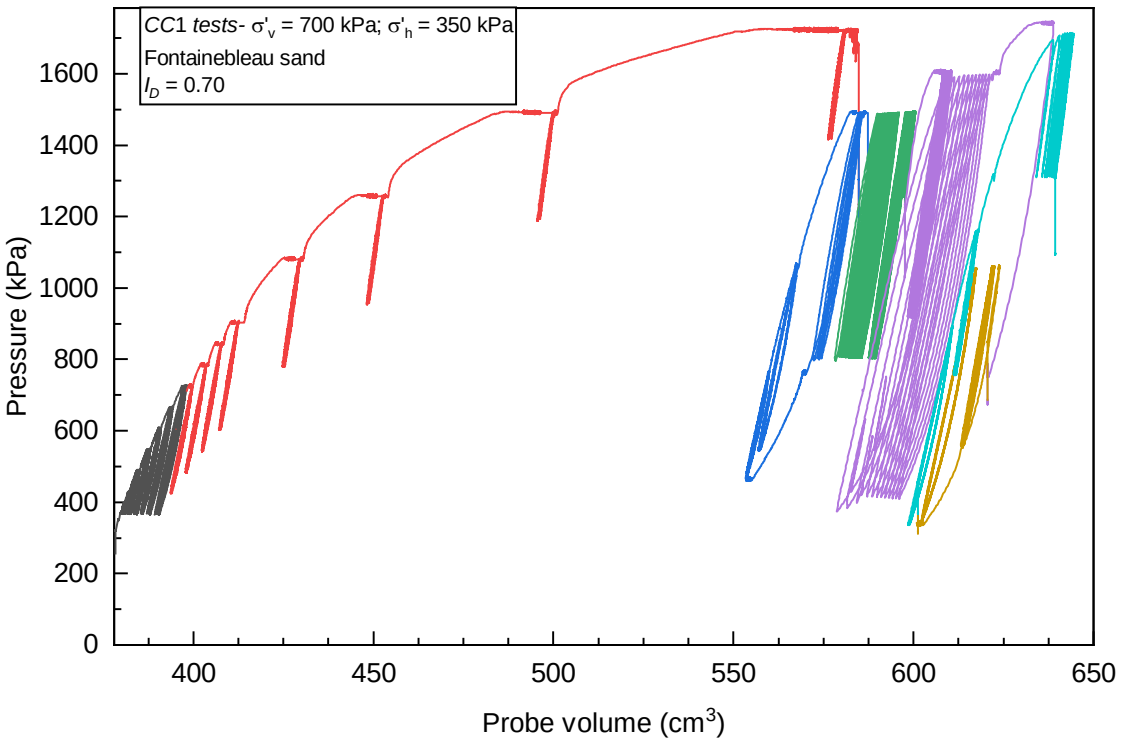

Figure 2.76 – Results obtained for all the cyclic series performed in PCC1

The volume variations obtained in all the cyclic series performed in PCC1 (series S1 to S20) are presented in Figure 2.77. From most series, the most significant volumetric accumulations take place between the fifth and the first loops.

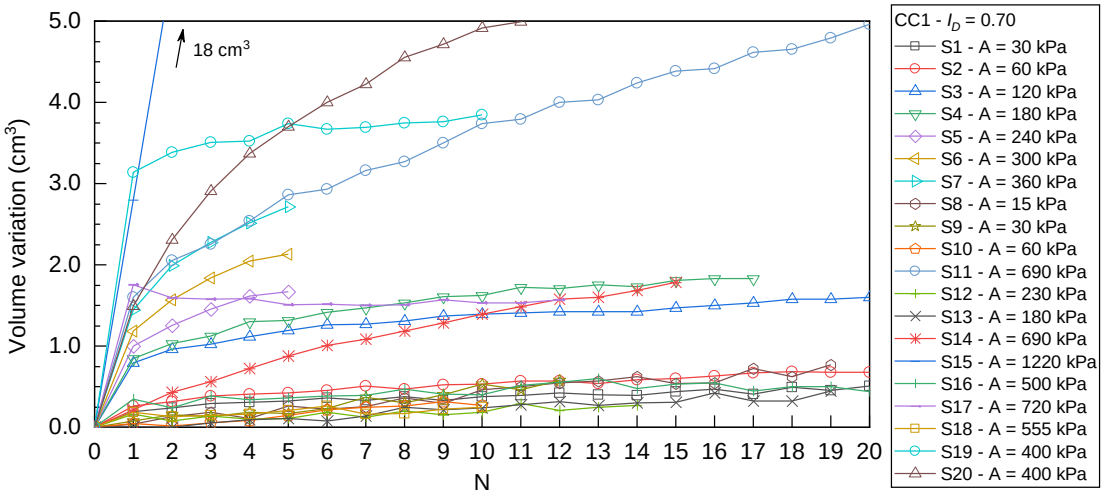

Figure 2.77 – Results of all the cyclic series performed in PCC1

The results obtained herein cannot be directly used as an input to characterize elementary soil parameters. However, they enable drawing interesting insights regarding sand behavior under cyclic cavity expansion loading. The mean pressure and half amplitude of each cyclic series, normalized by the specimen pressuremeter limit pressure, can be represented in an analogous cyclic stability chart, as presented in Figure 2.78. In this figure, the labels in front of each point represents the volume accumulated between the fifth and the first cycles, enabling an appreciation of the rate of volumetric accumulation. Each data point was colored in accordance to the rate of accumulation. The limit pressure of the soil specimen PCC1 was evaluated using theoretical solution for elasto-plastic thick cylinder (see, for example, Yu (2000)). Numerical application of this theory considering *PCC* dimensions, the horizontal stress imposed in the chamber and Fontainebleau sand properties, leads to a limit pressure equal to 1784 kPa, close to the maximum value measured presented in Figure 2.76.Three paths can be distinguished:

- Series S1 to S7, represented in Figure 2.78a: starting from the horizontal stress at-rest and performing cyclic series of increasing amplitudes generates a progressive increase in the rate of volumetric accumulation. It has been demonstrated that creep is present during all test, and it is likely that volume

accumulation in tests performed following this procedure has one component due to the cyclic loading but also one component due to soil creep;

- Series S13 to S15, represented in Figure 2.78b: this series was performed after having pre-sheared the soil specimen (i.e. after the probe had been previously expanded). Series S13 yielded few volumetric accumulation despite the high value of average pressure. On the other hand, Series S15 of lower average pressure but higher amplitude presented significant accumulation of permanent strains. The increase in amplitude accompanied by a decrease in average pressure leads to soil failure by extension, as it has been presented in the bibliographic review (Wroth, 1982).
- Figure 2.78c presents the increase in the rate of accumulation between series S18 to S20. These series had an approximately constant amplitude and an increasing average pressure. It can be noticed that series S18 presented much less accumulation than series S7 (Figure 2.78a) of similar amplitude and average pressure. This can be explained by the fact that S18 was preceded by pre-shearing. When the average pressure is progressively increased from S18 to S20, the rate of accumulation increases back again.

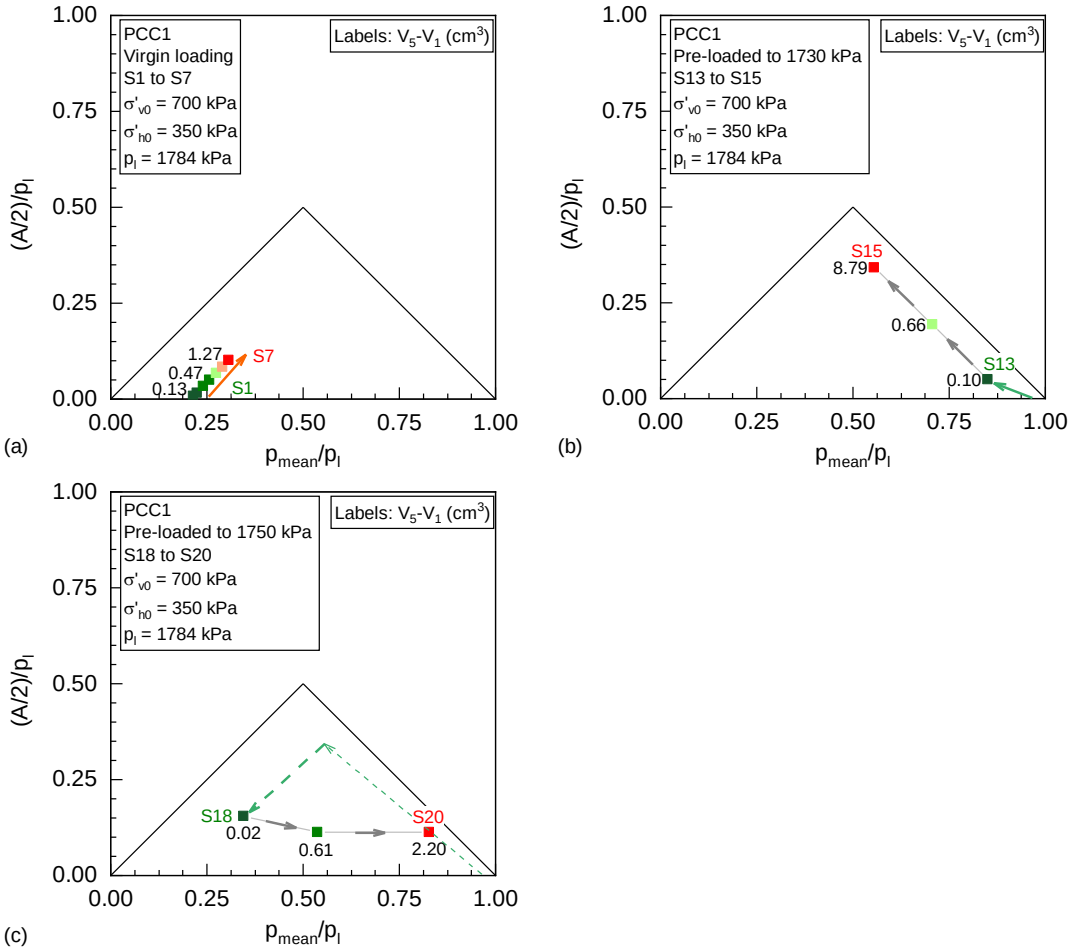

Figure 2.78 – Analogue of a cyclic stability chart presenting the accumulated volume in the first five cycles in series (a) S1 to S7, (b) S13 to S15, (c) S18 to S20

2.7.5 Validation

The present study did not focus on deriving elementary soil properties related to the accumulation of cyclic strains in the specimen and the testing protocols performed on this validation campaign did not target the determination of one specific parameter. The tests presented herein had the objective to validate if it was possible to identify a representative behaviour of sands under cyclic cavity expansion loading. The results presented in this work led to the positive conclusion that it is possible to distinguish the cyclic behaviour of sands presenting different properties and submitted to different stress states using the Monocell FC probe. If one specific parameter has to be determined from these tests to be used, for example, as an input for a constitutive model for numerical simulations or for establishing correlations with other soil parameters (such as those proposed by Dupla and Canou (2003)), the loading protocols should be

adapted. The present study showed that the Monocell FC probe would be suitable for those applications.

SUMMARY AND PARTIAL CONCLUSIONS

In this chapter, it has been shown that the most common pressuremeter probes cannot be used to reach the objectives fixed within the framework of this research. Some of the inherent sources of uncertainties present in the commercially available testing equipment were evidenced by a campaign of probe qualification tests. A new technology in probe membrane was found to be a potential solution for enabling assessing both the small strain and large strain domains from volumetric measurements of the expandable cell. The Monocell FC® probe is an innovative probe that implements improvements on the inflatable membrane, which help increasing the measurement accuracy, presenting a special interest for tests including unload-reload loops or series of repeated cycles. The capabilities of this new equipment needed to be further validated to any practical application.

The validation program performed in the laboratory comprised: (1) probe calibration according to a special protocol; (2) validation of this calibration protocol and (3) physical modelling using dry Fontainebleau sand specimens reconstituted in calibration chambers. The validity of the physical models was verified through analytical solution and numerical simulations and it was shown that the boundary conditions of the calibration chambers add only negligible errors to the results. Two different loading protocols were applied to the sand specimens: one to verify if it is possible to assess shear moduli at small strains with this probe, and the other including series of repeated cycles for investigating the soil behavior under cyclic cavity expansion solicitation.

A first series of tests enabled defining a testing loading program that accounts for the practical difficulties reported in literature concerning the evaluation of shear moduli at small strains. The proposed loading program comprises pressure-hold steps prior to any load direction reversal that are necessary for avoiding that time-dependent phenomena in soil superposes to elasticity properties. The proposed loop stress amplitude is such as it is sufficiently low to avoid soil failure by excessive unloading, but large enough to enable characterizing the non-linear behavior.

The application of methods proposed in literature for the evaluation of the maximum shear modulus of the soil for each unload loop and then evaluating the shear modulus decay in function of the shearing strain resulted in satisfactory results in an average strain range between $2 \cdot 10^{-4}$ and $1 \cdot 10^{-3}$. Comparison to Fontainebleau sand elementary properties gave close results, enabling validating the proposed procedure. It appears, however, that a consensus does not exist in the literature on how to calculate the average stress around the cavity for each loop. This study has shown that in *KCC*, the maximum cavity stress before unloading seems to control the soil specimen response during unloading. It is possible that the limit conditions of the calibration chamber have an influence on the development of the plastic zone around the cavity.

The application of cyclic loading to different soil specimens yielded results similar to what was expected from literature review. Accumulation of plastic strains due to cyclic loading was shown to be dependent on the following parameters: soil density, confining stress, cyclic amplitude, ratio between the average load and the horizontal stress at rest (if virgin loading). In soil specimens pre-sheared, it was possible to "re-activate" plastic accumulation by performing cycles of high amplitude. Plotting the results in a stability chart can provide meaningful insights related to the behavior of piles under cyclic loading.

The laboratory study presented herein points out the applicability of the innovative Monocell FC probe to reach the objectives fixed for this research. The testing conditions in the laboratory being optimal regarding measurement resolution and minimization of uncertainties, the next validation step consists in performing tests on site, under real operation conditions. This will be the subject of the next chapter.

CHAPTER 3

IN SITU INVESTIGATION

INTRODUCTION

The experimental results presented in chapter 2 enabled confirming that the Monocell FC ® probe presents a potential interest for assessing small strain and cyclic properties of soils in cavity expansion tests. The measuring capabilities of this probe have been validated under controlled conditions in the laboratory through tests performed in dry Fontainebleau NE34 sand specimens reconstituted in a calibration chamber. The testing conditions in the laboratory are optimal: use of high-resolution pressure-volume controllers that cannot be employed for current applications on site, short length of tubing, controlled environmental temperature and full knowledge of the tested soil and stress state. These conditions are favorable with respect to those encountered during real testing on site. For this reason, the applicability of the Monocell FC probe for *in situ* tests requires validation tests under real operational conditions.

In order to carry out the *in situ* validation campaign, two sites have been chosen based on their soil properties and on the existence of reference data gained from previously performed campaigns: Dunkirk (dense sands) and Merville (overconsolidated clays), both of them being located in the North of France. These sites present geologic-geotechnical characteristics analogous to marine sites where offshore piles have been historically installed, and therefore they present a special interest to the scientific community. These sites have been characterized by laboratory, *in situ* and geophysical tests. Full-scale pile load tests have also been carried out on these sites, including different pile installation techniques and different loading procedures (monotonic and cyclic).

This chapter presents the experimental testing procedures performed *in situ* under real conditions within the framework of the validation of the pressuremeter probe and testing protocols previously proposed in this work. The testing equipment and set up specific to the application on site will be presented. Geotechnical and geologic context of both testing sites, Dunkirk and Merville, will be described based on previous works presented in literature. Next, the testing program performed on each site will be presented, as well as the results obtained. Finally, the results will be validated by comparison to elementary soil properties given in the literature.

3.1 EXPERIMENTAL SETUP

The testing equipment used for *in situ* tests differs in some aspects from the one used in the laboratory. The main differences are: (1) the need of drilling equipment for creating the borehole; (2) the pressure volume controller; (3) the tubing length and (4) practical aspects related to being outdoor and working with heavy equipment. The high-resolution pressure-volume controller used in the laboratory is not adapted for these conditions.

On site, a 20-meter-long tubing was used, ten times longer than that used in the laboratory, but keeping the same mechanical properties. Concerning the set up on site, the pressure-volume controller and the data acquisition systems were installed inside a construction trailer for protection against environmental disturbance (direct incidence of sun, rain or wind), and in order to provide shelter for the operator. Details on the equipment and general implementation on site are presented in the next sections.

3.1.1 The pressure-volume controller

The control unit used for tests on site relies on the principle patented by Cour (2017) schematized in Figure 3.1, which consists in measuring the volume of water injected by weighting the water reservoir. This type of controller uses a hydraulic pump (1) connected to a water reservoir (2) to pressurize the probe. The water reservoir is placed on a digital scale (3). Once the initial weight of the system is known, the volume of water flowing out of the reservoir (injected into the probe) corresponds to the variation of mass on the reservoir during operation.

The injection pump is driven by an electric motor (4). The operator can control the speed of rotation of this engine and thus, the water flow-rate sent by the pump. The pump is connected to the probe using the tubing (5) (high-pressure circuit). A pressure transducer (6) is placed in the high-pressure circuit enabling the probe pressure to be measured. A valve (7) links the high-pressure to the low-pressure circuits (reservoir) and it enables deflating the probe. The operator controls deflation by defining the flow-rate passing through the valve. Both the digital scale and the pressure transducer are connected to a computer for data acquisition (8). The measurement resolution of the pressure transducer is less than 1 kPa and that of the digital scale of 0.5 g (corresponding to 0.5 cm^3).

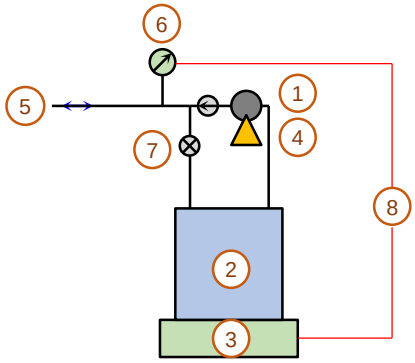

1 – Hydraulic pump
2 – Water reservoir
3 – Digital scale
4 – Electric motor
5 – Tubing (to the probe)
6 – Pressure transducer
7 – Deflation valve
8 – Computer (data acquisition)

Figure 3.1 – Principle of the pressure-volume controller patented by Cour (2017)

Different loading protocols can be performed by retro-controlling the flow-rate according to the instant response obtained by the system in terms of pressure or water flow-rate. All actions (inflating, deflating and choice of loading rates) are manually imposed by the operator. A photo of the device installed on site is presented in Figure 3.2.

Figure 3.2 – (a) Photo of the pressure-volume controller (principle patented by Cour (2017)) ; (b) view of the setup on site showing data acquisition;

3.1.2 Drilling the borehole

The borehole was drilled using a drilling rig made available and operated by *CEREMA Nord*. Photos of the machines used for creating the boreholes on both testing sites are presented in Figure 3.3. For the tests performed in Dunkirk, the testing pocket was drilled using a rotary tool of external diameter 60 mm with continuous injection of bentonite (Figure 3.4a). In Merville site, the testing pocket was drilled using a continuous auger of external diameter 63 mm without bentonite injection (Figure 3.4b). In both cases, the upper soil layers were temporarily supported by metallic casing.

Figure 3.3 – Drilling rigs used: (a) Dunkirk testing site; (b) Merville testing site

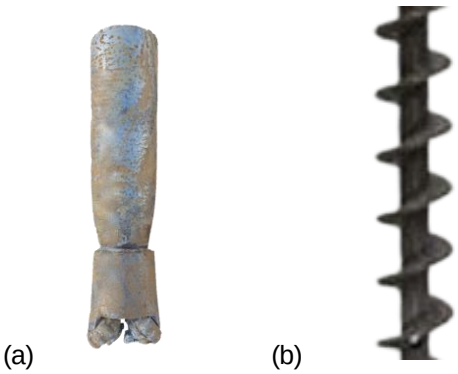

Figure 3.4 – Detail of the drilling bits used for creating the borehole on the experimental testing sites. (a) bicone roller bit with bentonite injection used for sands in Dunkirk; (b) continuous auger without bentonite injection for clays in Merville

3.1.3 Site organization

The control unit used comprises a digital scale that is sensitive to disturbances induced by vibrations. Data acquisition was done using a regular computer. A shelter was necessary for protecting the electronical components and the operator and adverse climate conditions. Tests were controlled from inside a construction trailer brought to the experimental sites. The trailer was installed near the borehole to minimize the tubing length necessary for the probe to reach the testing depths. The general setup for the tests performed in Dunkirk site is presented in Figure 3.5 and that for Merville site is presented in Figure 3.6. In both locations, electricity was provided by a gasoline power generator.

3.1.4 The probe

Some minor differences exist between the probe used for tests on site and that used in the laboratory. These differences are related to the mechanical assembly used in its connection to the rods enabling its insertion into the ground. A metallic conic tip is screwed to the probe toe to facilitate the insertion process. Regarding the membrane geometry and its properties during inflation, there are no differences with respect to that used in the laboratory. The same probe was used for tests in Dunkirk and in Merville sites, and photos of it inflated and assembled for *in situ* tests are presented in Figure 3.7a and in Figure 3.8a. The external polyurethane protective sheath was replaced from one site to the other, keeping identical properties.

During the insertion process, the tubing connecting the probe to the control unit was protected from friction against the cavity wall by being attached to the rods using an adequate adhesive tape. This is important to prevent the tubing from curling up and getting blocked and damaged during probe insertion or removal. Figure 3.7b shows the probe and the rods suspended by the drilling rig before its insertion into the borehole. Figure 3.8b shows the operators removing the rods from the ground after a test was finished.

Figure 3.5 – General view of the testing setup at Dunkirk site

Figure 3.6 – General view of the testing setup at Merville site

Figure 3.7 – (a) Photo of the probe assembled for the tests at Dunkirk site; (b) photo taken before probe insertion into the ground

Figure 3.8 – (a) Photo of the probe assembled for the tests at Merville site; (b) view of the probe connected to the steel rods prior to its insertion into the ground

3.2 GEOTECHNICAL PROPERTIES OF THE TESTING SITES

3.2.1 Flander's sands at Dunkirk site

Dunkirk testing site has been chosen due to the extensive ground characterization that has been undertaken in the region in the past decades. Several pile testing campaigns have been held in the near region because the encountered medium-dense to dense sand layer can be considered as a good analog to those found in offshore North Sea deposits. The site is of major interest for research related to offshore piling. Pile testing programs such as CLAROM (Brucy, Meunier and Nauroy, 1991), SOLCYP (Puech and Garnier, 2017) and PISA (Zdravković et al., 2018) contributed to increasing knowledge about that specific sand's mechanical behavior and its behavior in interaction with pile foundation. The pressuremeter tests presented herein were performed on the same site as the PISA and CLAROM pile tests. Its location is presented in Figure 3.9.

Figure 3.9 – Location of the Dunkirk testing site and of the pressuremeter testing campaign

3.2.1.1 Site stratigraphy

The site's stratigraphy is described by Chow (1997). It is composed of about 3 meters of hydraulic fill made of sand, below which a layer of normally consolidated Flandrian marine sand is found down to 30 meters depth. Ypresian marine clays are found below the sand layer.

CPT test profiles performed on the site (Zdravković et al., 2018)) are presented in Figure 3.10. The water table was identified at 4.0 meters depth by Chow (1997) and reevaluated at 5.4 meters depth by Zdravković et al. (2018), which attributed this difference to local site variability and more than 20 years spent between both campaigns.

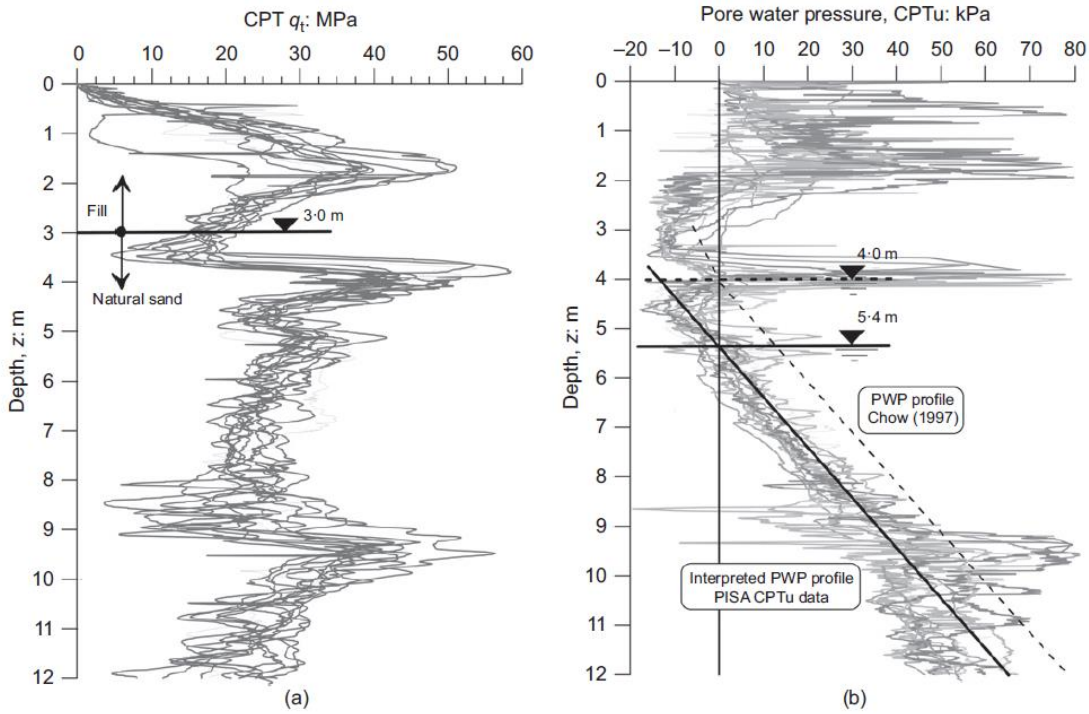

Figure 3.10 – CPT profiles at Dunkirk site. (a) CPT cone resistance; (b) excess pore water pressure measurements (after Zdravković et al., 2018)

3.2.1.2 Soil description

According to Kuwano (1999), Flandrian sand deposits are dense and formed of sub-rounded, medium-fine, quartz sand with shell fragments. Index properties for this sand are summarized in Table 3.1. The relative density of the natural sand deposit below the hydraulic fill has been estimated as approximately constant and equal to I_D = 0.75. Soil's bulk unity weight was estimated to be 17.1 kN/m^3 above the water table and 19.9 kN/m^3 below it. Chow (1997) evaluated the coefficient of earth pressure at rest on site using Jaky formulation as K_0 = 0.40. This proposition has been accepted by other researchers that worked on the same site (Zdravković et al., 2018). At present, there is no better estimative of K_0.

Table 3.1 – Index properties for Dunkirk sand after Kuwano (1999). G_s – specific gravity; e_{max} and e_{min} – maximum and minimum void ratio; C_U – coefficient of uniformity; D_{50} – particle diameter at which 50% of the sample's particles are smaller than

G_s	e_{max}	e_{min}	C_U	D_{50} (mm)
2.65	0.91	0.54	1.72	0.28

The Dunkirk sand grain size distribution curve and a microscope image using optical profiler were presented by Aghakouchak (2015) and reproduced in Figure 3.11.

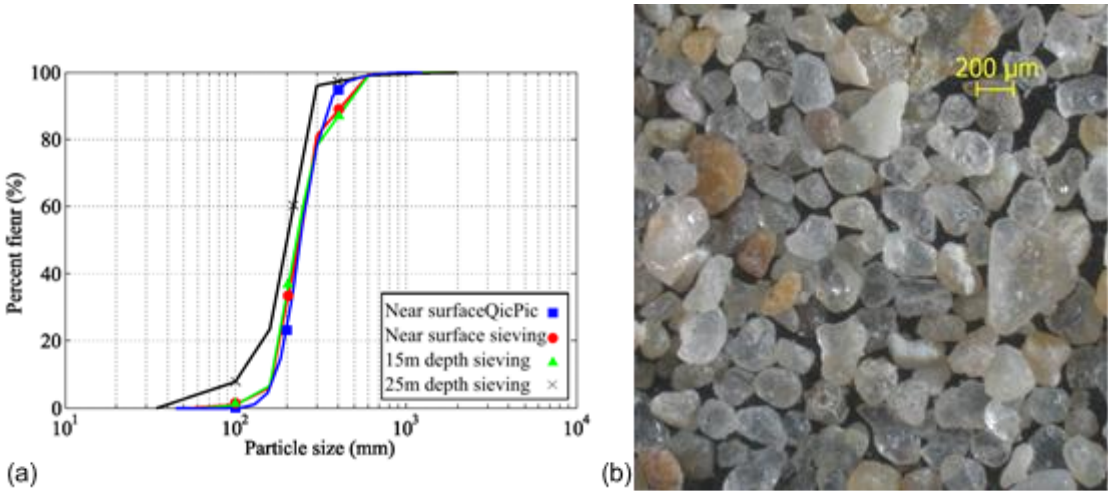

Figure 3.11 – (a) Flander's sand granulometric curve and (b) microscope image using optical profiler (after Aghakouchak, 2015)

3.2.1.3 Strength parameters

Kuwano (1999) characterized peak and critical state friction angles for Dunkirk sand (Figure 3.12). A value of 31.1° was obtained for the critical state friction angle. Aghakouchak (2015) obtained a close value of 32.1° for this same parameter.

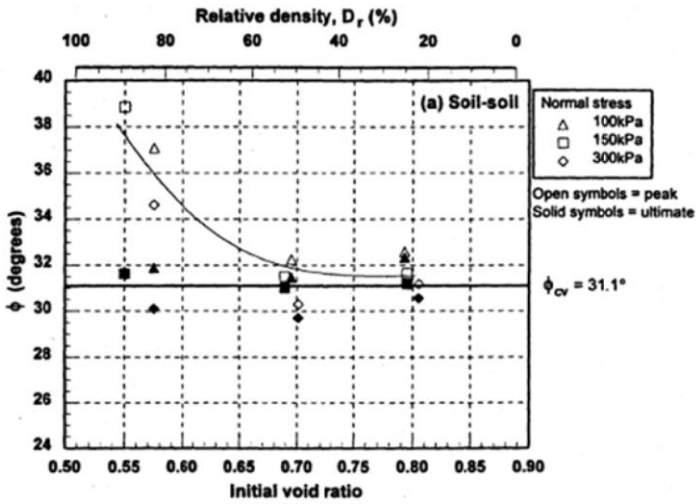

Figure 3.12 – Peak and critical state friction angles for Dunkirk sand (after Kuwano (1999))

3.2.1.4 Stiffness at small strains

Chow (1997) presented results of seismic cone penetration tests performed in a neighboring site. The author showed that a good correlation was obtained between the CPT tip resistance q_c and the maximum shear modulus of soil measured with seismic CPT tests (SCPT) using Baldi et al. (1989) equation (3.1).

$$G_{\max} = q_c[A + B\eta + C\eta^2] \tag{3.1}$$

where: $\eta = q_c\,(P_a\sigma'_v)^{-0.5}$, P_a is the atmospheric pressure (100 kPa), A = 0.0203, B = 0.00125, and C = 1.216·10^{-6}. This correlation will be used in *Chapter 4* for obtaining a profile of G_{max} on a neighboring site (Loon Plage).

Complementary SCPT tests were further presented by Zdravković et al. (2018), this time performed in the same site as the pressuremeter campaign performed in this Ph.D. thesis.

Dunkirk's sand elementary stiffness was characterized in the small strain domain using triaxial tests with local instrumentation. Zdravković et al. (2018) show that equation (3.2) can be considered satisfying for describing the evolution of the initial shear modulus of this sand, G_{max}, as a function of the average stress, *p'*:

$$G_{\max} = A \cdot p'_{ref} \cdot f(e) \cdot \left(p'/p'_{ref}\right)^n \tag{3.2}$$

in which $f(e) = (2.97 - e)^2/(1 + e)$, p'_{ref} is a reference stress. Parameters A and n were calibrated by these authors, obtaining n = 0.5 and A = 310 for isotropically consolidated specimens, or A = 470 for K_0 consolidated specimens. Equation (3.2) is plotted in Figure 3.13a for both values of A.

The authors further used equation (3.2) to evaluate a profile of initial (at-rest) shear modulus as a function of depth. This profile is presented in Figure 3.13b, together with measurements performed using seismic CPT.

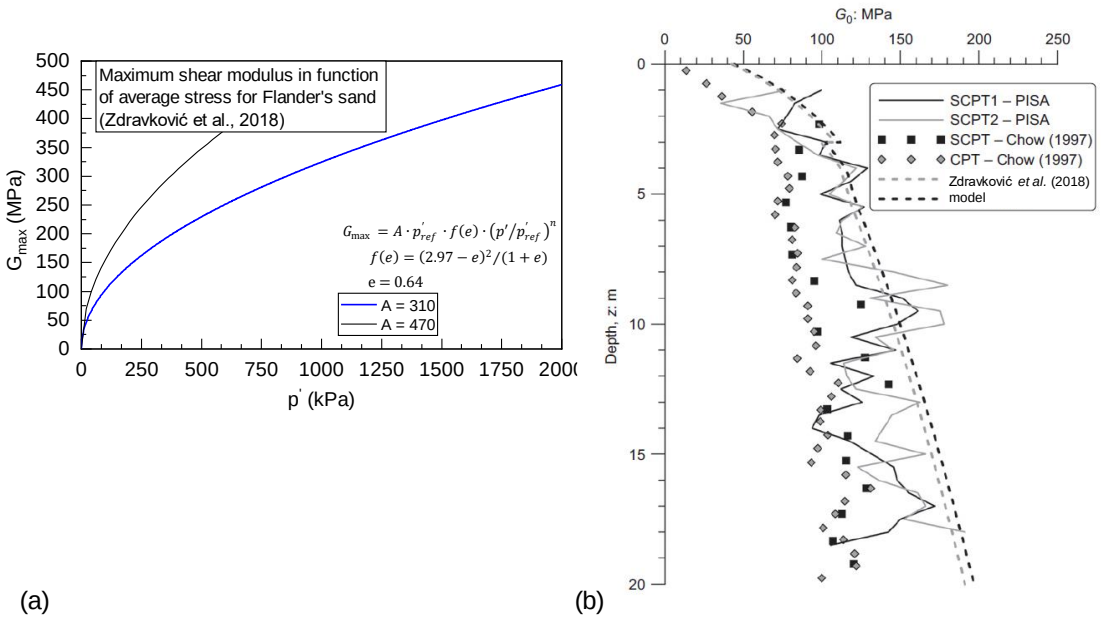

Figure 3.13 – Evolution of initial shear modulus in function of average confining stress for Dunkirk sand, adapted from Zdravković et al. (2018)

Aghakouchak (2015) presents degradation curves for the tangent drained Young's modulus measured in triaxial compression and extension tests using local instrumentation. Results are presented in Figure 3.14. It can be noticed that under extension tests, stiffness drops slower than when compared to compression tests. The author does not provide equations for the determination of the shear modulus in function of the shear strain and the average stress: the Oztoprak and Bolton (2013) model will be assumed valid for this case, as it was done in Chapter 2.

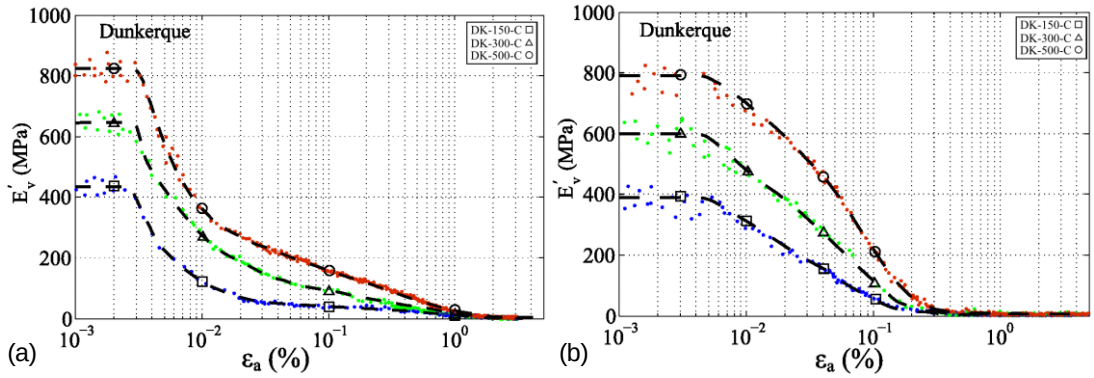

Figure 3.14 – Tangent Young's modulus degradation curves from drained K_0 tests in Dunkirk sand. (a) compression tests; (b) extension tests (after Aghakouchak (2015))

Aghakouchak (2015) measured the Poisson's ratio of the sand using axial and radial LVDT instrumentation. A value of $\nu = 0.27$ was obtained for Dunkirk sand over a range of axial strain between $0 < \varepsilon_a < 0.05\%$. This value is close to that reported by Kuwano (1999), who obtained $\nu = 0.33$.

3.2.1.5 Characterization using standard pressuremeter tests

Investigations using standard pressuremeter tests performed in the context of the SOLCYP project in a neighboring site are presented in Figure 3.15. On this site, CPT tip resistance in depths ranging from 6 to 12 meters are similar to those obtained on the site in which the current campaign was performed. Within this range of depths, values of Ménard modulus E_M vary between 10 to 30 MPa, with an average value of 18 MPa. This is equivalent to shear modulus G_M varying between 3.8 and 11.3 MPa, with an average of 6.8 MPa. Values of limit pressures range between 2.7 and 3.8 MPa.

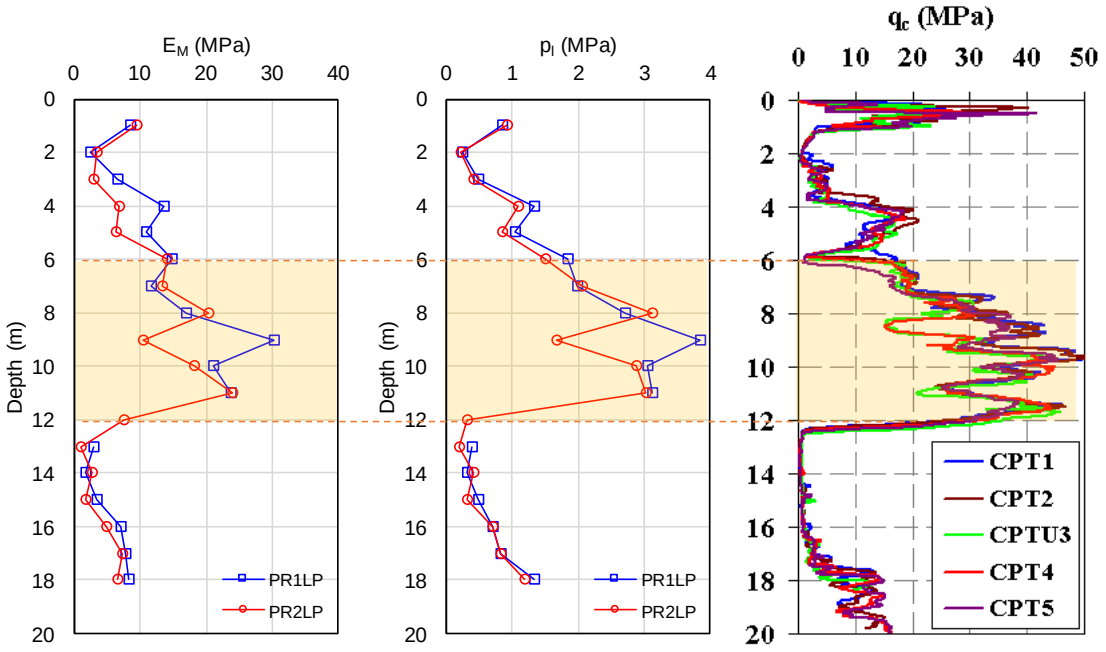

Figure 3.16 – Standard pressuremeter test results obtained in a neighboring site at Dunkirk (adapted from Benzaria,2013). The range of depths underlined in orange present soil properties expected to be similar to those encountered in the current testing site

3.2.2 Flander's clays at Merville site

Merville testing site held many campaigns of static pile tests since the 80's. The most recent pile testing campaign on the site was performed in the context of the SOLCYP project (Puech and Garnier, 2017), aiming at improving the design of piles under cyclic axial loads. The existing geotechnical characterization campaigns, composed of laboratory and *in situ* tests, geotechnical and geophysical, were summarized by Borel and Reiffsteck (2006). The site location, with a detail showing the location of the pressuremeter campaign performed in 2018, is presented in Figure 3.17.

Figure 3.17 – Location of the Merville testing site and of the pressuremeter testing campaign

3.2.2.1 Site stratigraphy

According to Borel and Reiffsteck (2006), the site's stratigraphy is described as follows: Flander's overconsolidated clay is found below an approximately 2-meter silt layer, and extends down to 42 meters depth, below which Landenian sands are found. Groundwater table fluctuates between 1.5 and 1.9 meters depth, into the silt layer. It is, however, difficult to estimate the phreatic level into the very impermeable, but micro-fissured, Flander's clay.

3.2.2.2 Soil description

Flander's clay is classified as very plastic. According to Borel and Reiffsteck (2006), Atterberg's limit tests performed on samples collected on the site resulted in plasticity index ranging from 40 to 69 %. Bulk unit weight ranges between 18.5 and 19.5 kN/m^3 for depths between 4 to 12 meters. Flander's clay's grain size distribution curve and a view from scanning electron microscopy are presented in Figure 3.18.

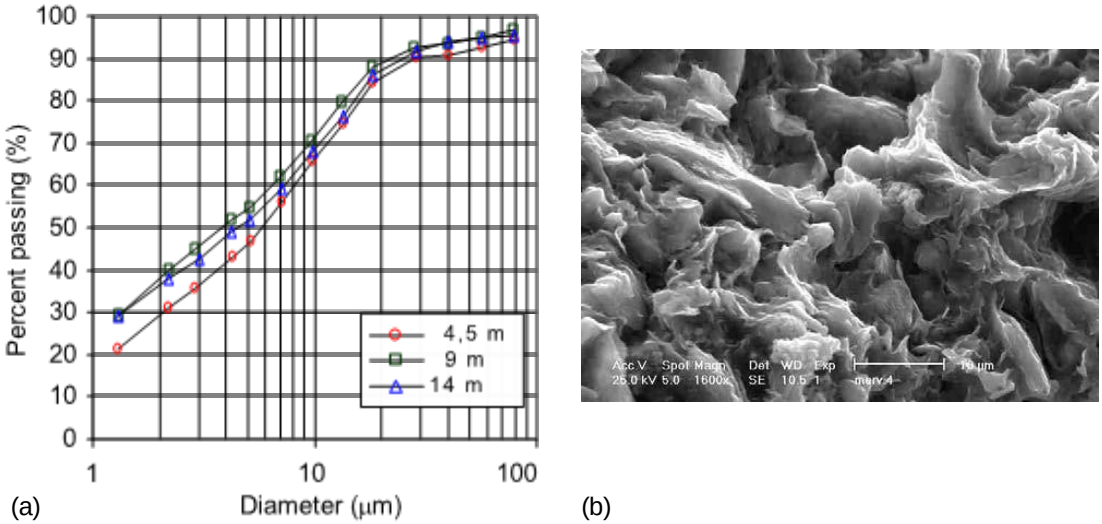

Figure 3.18 – (a) Flander's clay granulometric curve and (b) scanning electron microscopy view (after Borel and Reiffsteck, 2006)

3.2.2.3 Strength properties

Borel and Reiffsteck (2006) present a synthesis of laboratory test results used to characterize the strength properties of Flander's clays at Merville site. A profile of undrained shear strength obtained from undrained triaxial compression tests and from correlations between CPT, PMT and SPT tests is presented in Figure 3.19a.

Table 3.2 – Synthesis of Flander's clay strength parameters according to Borel (2000)

Triaxial CU+U				UU
φ' (°)	c' (kPa)	c_u (kPa)	λ (°)	c_u (kPa)
15 - 28	35 - 37	35 - 48	10 - 22	110 - 190

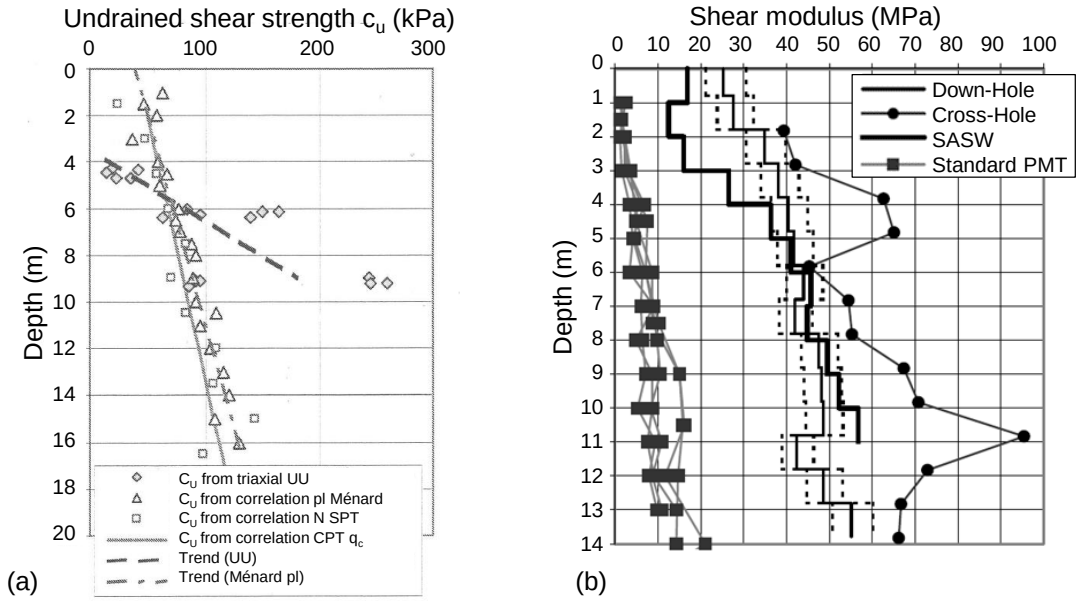

Figure 3.19 – (a) Profile of undrained shear strength obtained using undrained triaxial compression tests and from correlations with CPT, PMT and SPT tests (adapted from Borel and Reiffsteck,2006); (b) profile of shear modulus assessed at Merville testing site using different techniques (adapted from Ferber and Abraham, 2002)

3.2.2.4 Stiffness at small strains

Initial shear stiffness was assessed on site using cross-hole, down-hole and surface wave geophysical tests. Standard pressuremeter tests were also carried out in previous investigation campaigns. Ferber and Abraham (2002) presented a synthesis of shear moduli assessed on the site using different techniques (Figure 3.19b).

With respect to the results of the cross-hole test presented, it seems that the peak shear stiffness seen at eleven meters depth is a local phenomenon. In fact, none of the CPT penetration tests performed on site (as presented in Figure 3.21) present a peak at this depth that could justify this anomaly.

Borel and Reiffsteck (2006) suggest that shear modulus decay for Merville clay between 4 to 10 meters depth can be modelled using the hyperbolic relation described by eq. (3.3) considering $\gamma_r = \tau_{max}/G_{max} = 1.10^{-2}$, as illustrated in Figure 3.20.

$$\frac{G_s}{G_{max}} = \frac{1}{1 + \frac{\gamma}{\gamma_r}} \tag{3.3}$$

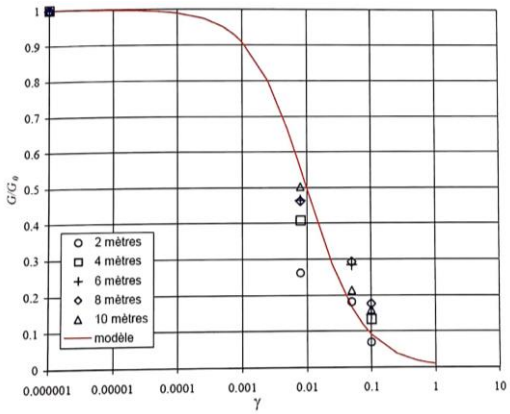

Figure 3.20 – General shear modulus decay trend evaluated at Merville site (after Borel and Reiffsteck, 2006)

3.2.2.5 Characterization using standard pressuremeter tests

Results of standard pressuremeter testing campaigns performed at the same site (Borel, 2000; Benzaria, 2013) are presented in Figure 3.21 as well as the profile of CPT tip resistance, q_t. CPT profiles present a quasi-linear increase from approximately from 1 MPa to 4 MPa in depths between 2 to 12 meters. Pressuremeter limit pressures also present a linear increase with depth, varying from approximately 0.4 to 1.5 MPa within this same depth. Ménard moduli present a higher scatter, but also a general trend of linear increase.

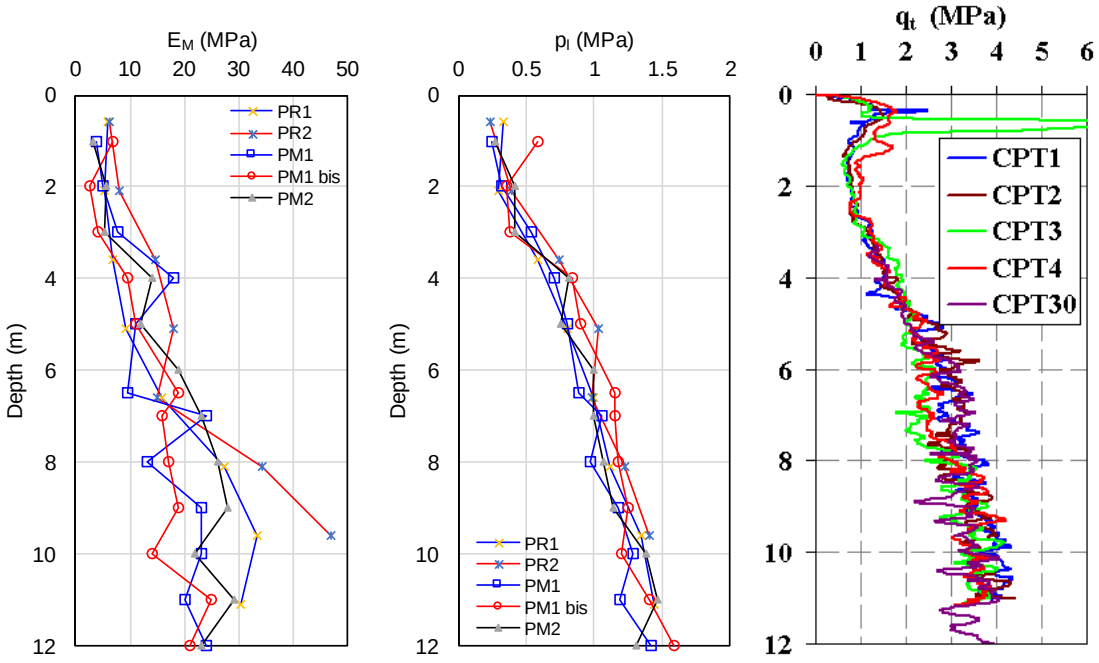

Figure 3.21 – Profiles of Ménard pressuremeter modulus, limit pressure and cone tip resistance at the Merville site (adapted from Benzaria, 2013)

3.3 EXPERIMENTAL PROTOCOLS

The testing procedures on site take place according to the following general sequence:

- Installation of the testing equipment on site and planning an adequate lay-out for the operations;
- Installation of the control unit inside the trailer, probe connection, verification that the circuits are saturated;
- Probe calibration using tubes of four different diameters 60 mm, 66 mm, 75 mm and 85 mm; Probe calibration procedure is similar to that presented in Chapter 2.
- Borehole drilling down to the first testing depth;
- Probe insertion and performance of the first test immediately after drilling;
- At the end of the test, probe is removed from the ground;
- Repetition of the last three steps for all the tests: drilling, inserting the probe, performing the test.

At the beginning of each working day, the probe was recalibrated using the smallest diameter tube to ensure the validity of the calibration procedure (reference calibration). A flowchart synthetizing all the required steps from probe calibration to test interpretation is presented in Figure 3.22. General aspects concerning the different loading programs performed are described in the next section. Details specific to each testing site, Dunkirk and Merville, will be presented in subsequent sections.

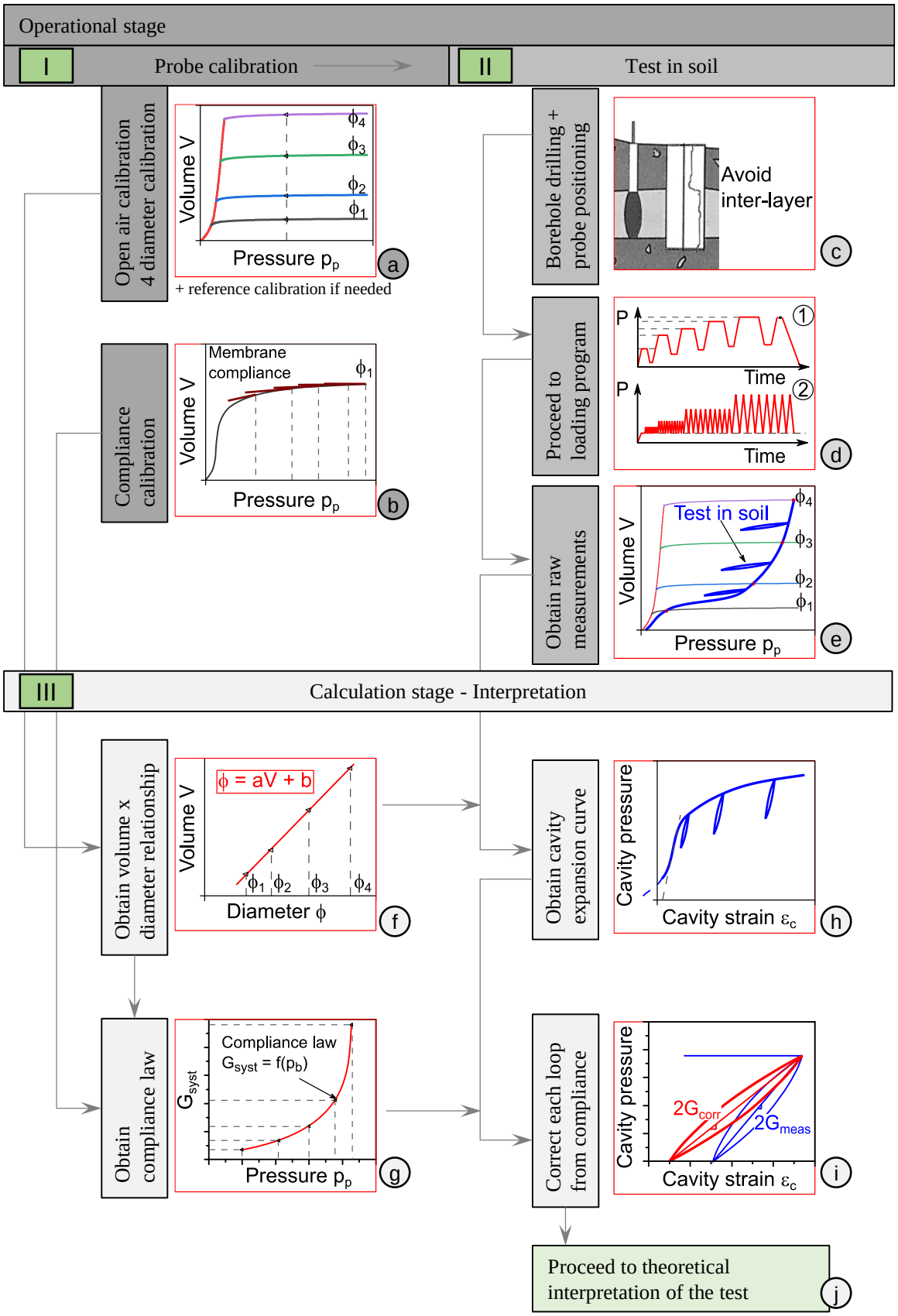

Figure 3.22 – Flowchart including the successive test steps, from probe calibration to test interpretation

3.3.1 Loading programs: general aspects

The testing depths were defined based on the previous knowledge of the site stratigraphy. Relatively deep tests in which higher limit pressures were expected were privileged in order to favor loops starting at pressures beyond 800 kPa (best working range of the Monocell FC probe, as presented in Chapter 2).

On both testing sites, two types of loading programs were performed, one for assessing soil stiffness at small strains, and the other for investigating soil behavior under series of repeated cycles. In principle, the loading programs performed were similar to those performed in the laboratory validation campaign, with some minor modifications to make them adequate for the *in situ* condition. The following sections describe the differences between the loading programs performed *in situ* and those performed in the laboratory.

3.3.1.1 Protocol for assessing shear stiffness at small strains

The loading protocol called "*protocol 1*", presented in *Chapter 2* section 2.3.3.3 (Figure 2.35a), was adapted for reducing test duration on site. Three loops were performed *in situ* instead of five in the laboratory. In principle, performing three loops is sufficient to characterize shear modulus evolution in function of the cavity pressure.

Loop amplitude was defined using the same criteria as in the laboratory, as approximately 0.4 times the cavity pressure before unloading ($\Delta p_{cav} = 0.4 \times p_{cav}$). At Merville, besides this procedure, some loops were performed with different amplitudes, with the purpose of investigating the influence of this parameter for clays.

The test procedure proposed herein brings a compromise aiming at solving the practical difficulties presented in the bibliographic review, which are mainly: (1) to avoid that time-dependent phenomena, such as creep and relaxation, superpose to the desired elasticity properties that can be evaluated during unload-reload loops. The superposition of these phenomena can lead to an overestimation of shear modulus or even to negative values (Wood (1990), Jardine (1992)). For this reason, sufficiently long pressure-hold steps must be performed before unloading the cavity walls; (2) with respect to any possible disturbance caused by drilling, it has been shown in the literature that the unload-reload loops performed after first expanding the cavity to a significant

expansion level are not sensitive to probe installation effects (Fahey and Randolph (1984), Hughes and Robertson (1985), Robertson and Hughes (1986), Houlsby and Withers (1988)). For this reason, the first loop is performed only after a plastic annulus has been created around the cavity (beyond of the "pseudo-elastic" domain). This combined intermediate procedure is illustrated in Figure 3.23 and consists in:

- Loading the cavity at a constant shearing rate up to a pressure $p_{cav,1}$ just at the end or after the so-called "pseudo-elastic" domain. Here, the radial strain rate was of approximately 6.10^{-3} mm/s;
- Performing a pressure-hold step for a sufficiently long time $\Delta t_{u,1}$ so that creep reduces to a considerably low value;
- Unloading at a constant shearing rate (or pressure-rate) until a pressure amplitude $\Delta p_{cav,1} \sim 0.4 \cdot p_{cav,1}$ is reached;
- Performing a pressure-hold step $\Delta t_{r,1}$ of sufficient duration to considerably reduce time-dependent phenomena after unloading;
- Reloading at a constant shearing rate (or pressure-rate) up to a pressure $p_{cav,2}$.
- Repeating this procedure for all unload-reload loops and then shearing at a constant rate up to achieving the soil conventional limit pressure. The suggested loading program is illustrated in Figure 3.23a.

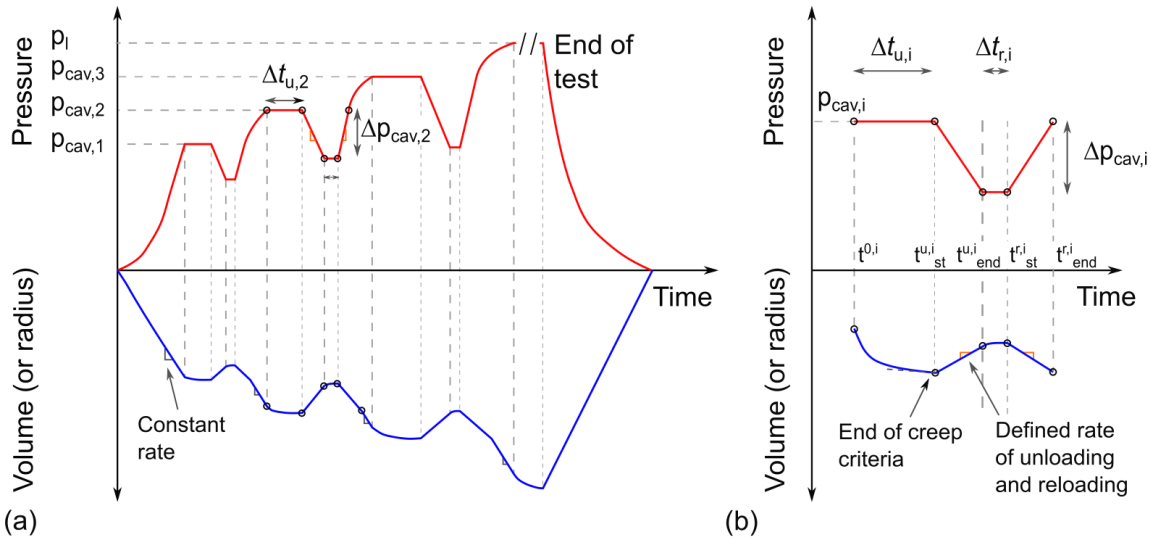

Figure 3.23 –Loading protocol 1 adapted for *in situ* tests. (a) Loading program including three unload-reload loops; (b) detail of the loading procedure within one loop

The detail of the unload-reload loop is presented in Figure 3.24b. The duration of each pressure-hold step must be adjusted to reach an "end of creep" criterion. This criterion is defined as reaching a sufficient reduction in creep rate so that time-dependent

behavior can be considered not to disturb the unload-reload loop (avoiding a negative slope and leading to approximately closed loops, as presented in Chapter 2). Thus, the duration of the pressure-hold step may vary in function of the amount of creep that takes place in each loop. In the tests performed herein, a reduction of the cavity expansion rate of approximately 10 to 15 times with respect to the beginning of the loop was adopted as an "end of creep" criterion (i.e. if at time $t^{0,i}$ at the beginning of the pressure-hold step probe is inflated at 6.10^{-3} mm/s, creep criterion was considered as satisfied at $t^{u,i}_{st}$ when inflation rate was reduced to 4.10^{-4} mm/s. In practice, during operation, the criterion was considered as satisfied when the injected volume got inferior to 1 cm^3 after 15 seconds of pressure-hold). The duration $\Delta t_{u,i}$ of the pressure-hold steps varied from 3 to more than 10 minutes.

Since no (or few) time-dependent behavior is expected to take place within the unload-reload loops, the rate of unloading and reloading can be adjusted to favor data acquisition (lower rates leading to more acquired points per loop).

By following this procedure, the cavity expansion response presented in Figure 3.24 is expected. The duration of one test is approximately one hour and fifteen minutes.

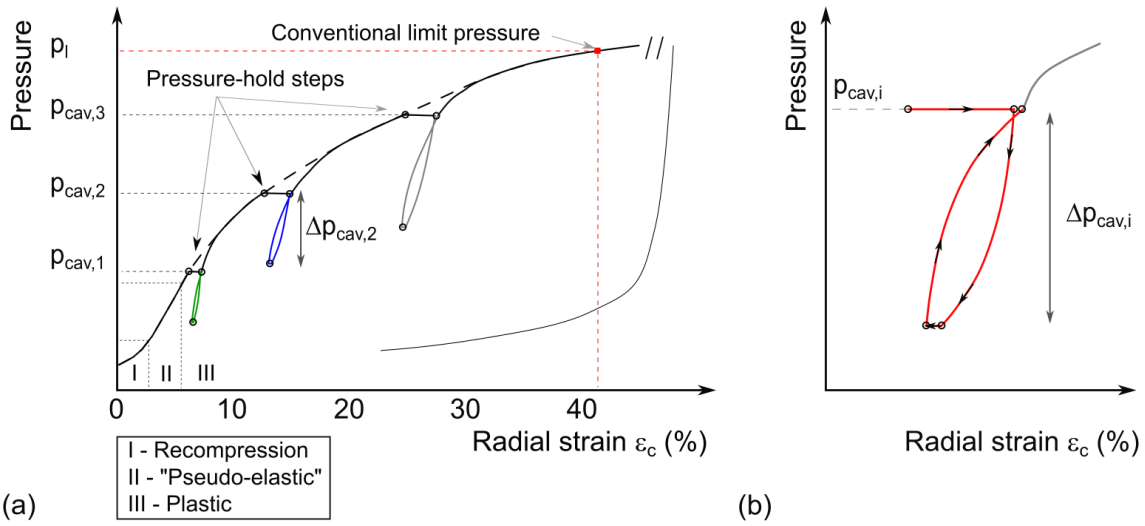

Figure 3.24 – (a) Expected cavity expansion response following protocol 1; (b) detail of a loop

The interpretation procedure for the derivation of shear moduli at small strains from each loop presented in Chapter 2 is summarized in Figure 3.25.

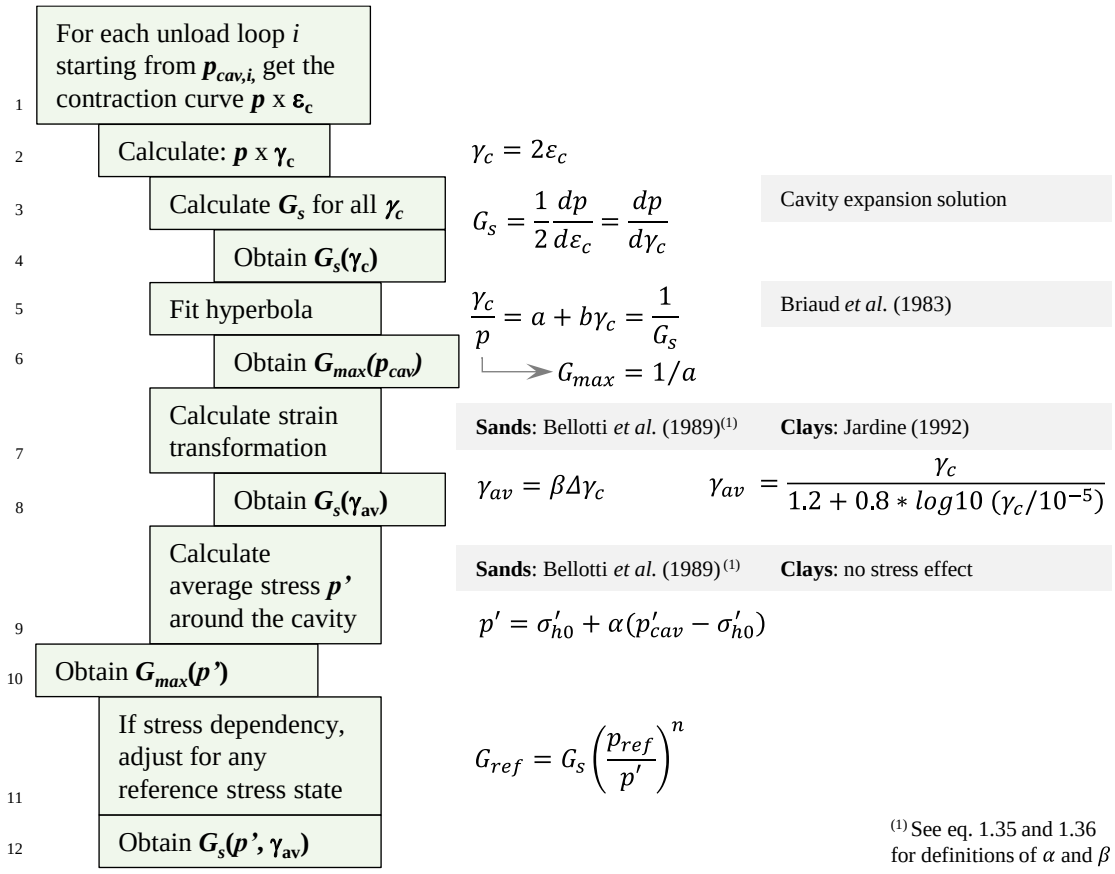

Figure 3.25 – Summary of the interpretation procedure for the loops performed according to loading protocol 1

3.3.1.2 Assessing cyclic parameters

The "cyclic procedure" denoted "*protocol 2*" in Chapter 2 (section 2.3.3.3, Figure 2.35b) was modified with respect to what has been performed in the laboratory. On site, p_{min} has been imposed at a higher value than the estimated horizontal stress at-rest. There are two reasons for this choice: the first is the recommendation of Briaud (1992) that any cyclic procedure should be started at a pressure level higher than 20% of the soil limit pressure ($p_{min} > 0.2\ p_l$). According to the author, starting cyclic series from lower values of p_{min} pressures may lead to unreliable results. The author does not explicit the reasons behind this recommendation, but it is possible that at low pressures, test results could be misleading due to soil disturbance caused by drilling and probe insertion. A second reason is that to favor a domain of high pressures, in which probe measurements are more reliable.

Cyclic procedures have also been performed after the soil has been pre-sheared, denoted "*protocol 2**", as illustrated in Figure 3.26. They will be detailed case-by-case with the presentation of the test results in the next section.

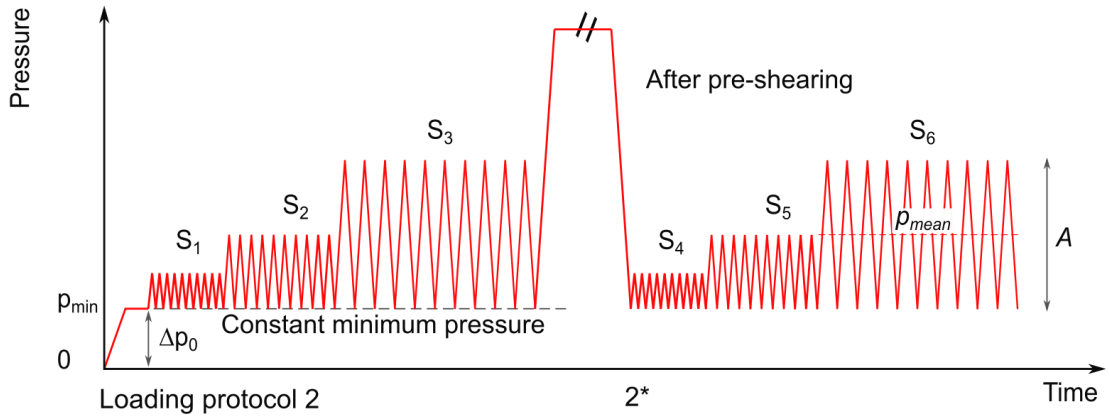

Figure 3.26 – Loading protocol 2 and 2* adapted for *in situ* tests

3.3.1.3 Other procedures

Monotonic tests controlled at a continuous rate of shearing have also been performed and are denoted “protocol 3”. At Merville site, one test following the standard Ménard procedure has also been performed.

3.3.2 Summary of tests performed at Dunkirk site

The pressuremeter testing campaign has taken place in Dunkirk between September 17th and 20th 2019. Eight tests, from 6 to 14 meters depth have been performed in one borehole. The upper sand layer (hydraulic fill) was cased. During the drilling operations, difficulties were found to insert the casing at depths between 4 to 5 meters, possibly due to the presence of gravels or blocks in the interface between man-made ground and the natural soil. Once the upper layer had been cased, the test pocket was drilled using a rotary tool of external diameter 60 mm and with continuous injection of bentonite. It was initially planned to advance casing along with the borehole in order to protect it from the possibility of closing and blocking the probe. However, after having lowered the casing tube to 8 meters depth, it got blocked and it was impossible to advance it any further.

Initially, two boreholes were planned to be performed on site in order to enable comparing test results performed at same depths. However, the drilling difficulties faced when inserting the casing into the first meters of fill delayed the operations, and only one borehole could be performed (BH1).

Table 3.3 – General testing program performed at Dunkirk site, borehole BH1

Test	Test depth (m)	Drilling depth (m)	Casing depth (m)	Date	Comments	Loading protocol
DKK6	6.0	6.4	5.0	17/09/2019	Difficulties during drilling process delayed the operations. Casing the first 4 meters of soil was difficult	1+2*
DKK7	7.0	7.4	5.0	18/09/2019		3+2*
DKK8	8.0	8.4	5.0	18/09/2019	Impossible to advance casing	1
DKK10	10.0	10.4	5.0	18/09/2019		2
DKK11	11.0	11.4	8.0	19/09/2019	Casing blocked	1
DKK12	12.0	12.4	8.0	19/09/2019		2
DKK13	13.0	13.4	8.0	19/09/2019		3
DKK14	14.0	14.4	8.0	19/09/2019	Significant change in sand properties detected during drilling operations. Test not interpreted	4(NI)

(NI) Non interpreted test due to different soil properties

3.3.3 Summary of tests performed at the Merville site

Tests at the Merville site have taken place between December 3rd and 6th 2018. A total of ten tests were performed into two boreholes, BH1 and BH2, located 3 meters apart in the horizontal plan. Depths between 9 to 15 meters were tested.

The upper silt layer was cased to avoid the groundwater table to penetrate the test cavity. Once the upper layer was cased, the test pocket was drilled using a continuous auger of external diameter 63 mm without injection of support fluid. Drilling advanced at a rate of one pressuremeter test per continuous drilling stage length.

No particular difficulties took place during the drilling operations. However, after the test in BH1 at 12 meters depth, it was difficult to remove the probe from the ground. In fact, the probe membrane adhered to the cavity walls and the probe could not deflate after the test end. When trying to remove it, its membrane was damaged and the probe needed to be replaced by a similar one. To avoid this problem to happen in the next tests, the following procedure was adopted: (1) probe membrane was greased before being inserted into the ground; (2) the cavity was partly filled with water after the end test for providing external pressure to help deflate the probe. The problem was solved. Most of the added water was evacuated during the next drilling step.

Table 3.4 presents the testing program performed in BH1 and Table 3.5 that in BH2.

Table 3.4 – General testing program performed at Merville testing site, borehole BH1

Test	Test depth (m)	Drilling depth (m)	Casing depth (m)	Date	Comments	Loading protocol
MVL9.1	9.0	9.4	4.0	03/12/2018		1
MVL10.1	10.0	10.4	4.0	04/12/2018		2
MVL11.1	11.0	11.4	4.0	04/12/2018		1
MVL12.1	12.0	12.4	4.0	04/12/2018	Difficulties to remove the probe after test. Probe damaged during removal, needed replacement	Ménard
	13.0				Test at 13m skipped due to possible disturbance	
MVL14.1	14.0	14.4	4.0	05/12/2018	Probe membrane greased and water added to the borehole after the end of the test to help removing probe	2
MVL15.1	15.0	15.4	4.0	05/12/2018	Difficulties to insert the probe: borehole closed after drilling. Need to drill twice	2

Table 3.5 – General testing program performed at Merville testing site, borehole BH2

Test	Test depth (m)	Drilling depth (m)	Casing depth (m)	Date	Comments	Loading protocol
MVL10.2	10.0	10.4	4.0	06/12/2018	Probe membrane greased and water added to the borehole after the end of each test	2
MVL11.2	11.0	11.4	4.0	06/12/2018		2*
MVL12.2	12.0	12.4	4.0	06/12/2018		1
	13.0					
MVL14.2	14.0	14.4	4.0	06/12/2018		3

3.4 PRESENTATION OF RESULTS OBTAINED. SHEAR STIFFNESS AT SMALL STRAINS

This section presents the results of the tests performed on both testing sites aiming at determining soil shear moduli at low strain level. The section is divided in two main parts, each one dedicated to one testing site. For each site, the parameters of the testing program is described, followed by a presentation of the results and analysis of a typical test. Then, a summary of all the test results and validation with respect to the properties of the soil are presented.

3.4.1 Tests in sands: Dunkirk site

3.4.1.1 Testing program

Table 3.6 presents the testing program performed at the Dunkirk site aiming at assessing shear moduli at small strains.

Table 3.6 –Testing program performed at Dunkirk aiming at assessing shear moduli at small strains

Test	Depth (m)	Loop	p_{cav} (kPa)	Δp_{cav} (kPa)	$\Delta p_{cav}/p_{cav}$	Δt *(min)*
DKK6	6.0	L1	871	355	0.41	3.3
		L2	1425	512	0.36	5.2
		L3	1891	739	0.39	5.8
DKK8	8.0	L1	930	349	0.38	3.3
		L2	1450	569	0.39	5.5
		L3	1881	720	0.38	10.3
DKK11	11.0	L1	983	317	0.32	3.3
		L2	1451	487	0.34	6.4
		L3	1817	638	0.35	10.6

3.4.1.2 Results and analysis of a typical test

The interpretation of the test results is similar to what has been presented in Chapter 2, section 2.6.2. The process of transforming raw measurements into a cavity pressure versus cavity radial strain curve is exactly the same, and will not be repeated in this section. *In situ* experiments will be illustrated based on the typical test performed at eleven meters below ground level (DKK 11), which can be considered representative of all the others.

Two sets of parameters can be derived: (a) parameters derived from the virgin expansion curve, the same as could be derived from a standard pressuremeter test (the

Ménard modulus and the conventional limit pressure); (b) elasticity parameters derived from the unload loops, as presented in Chapter 2.

The result of test DKK 11 is presented in Figure 3.27. In this figure, the range for the evaluation of standard Ménard pressuremeter modulus and the conventional limit pressure, effectively measured in this case, are indicated. For the other tests (DKK 6 and DKK 8, interrupted prematurely for performing complementary testing procedures), limit pressure was obtained by extrapolation according to the method proposed in AFNOR (2015).

The detail of each loop, corrected for membrane compliance, is presented in Figure 3.28 a to c. In Figure 3.28d, each of the unload paths are presented, evidencing the effect of the cavity pressure before unloading on the measured stiffness. Hyperbolic fit of each loop is also presented in this figure.

For the tests performed, the evaluation of maximum shear moduli from each loop could not be done using Byrne *et al.* (1991) method. In fact, the chart proposed by these authors is valid for ratios between cavity pressure before unloading and the soil's horizontal stress at rest, $p'_{cav}/\sigma'_{h,0}$, varying from one to twelve. On site, because the horizontal stress at rest is relatively low with respect to the soil limit pressure, the first loop was performed at $p'_{cav}/\sigma'_{h,0} = 15.7$, value which is greater than the limits of the quoted chart. Therefore, only Briaud *et al.* (1983) method could be used to evaluate the maximum shear modulus for each loop. Figure 3.29 illustrates the application of this method to loop L2 in DKK 11.

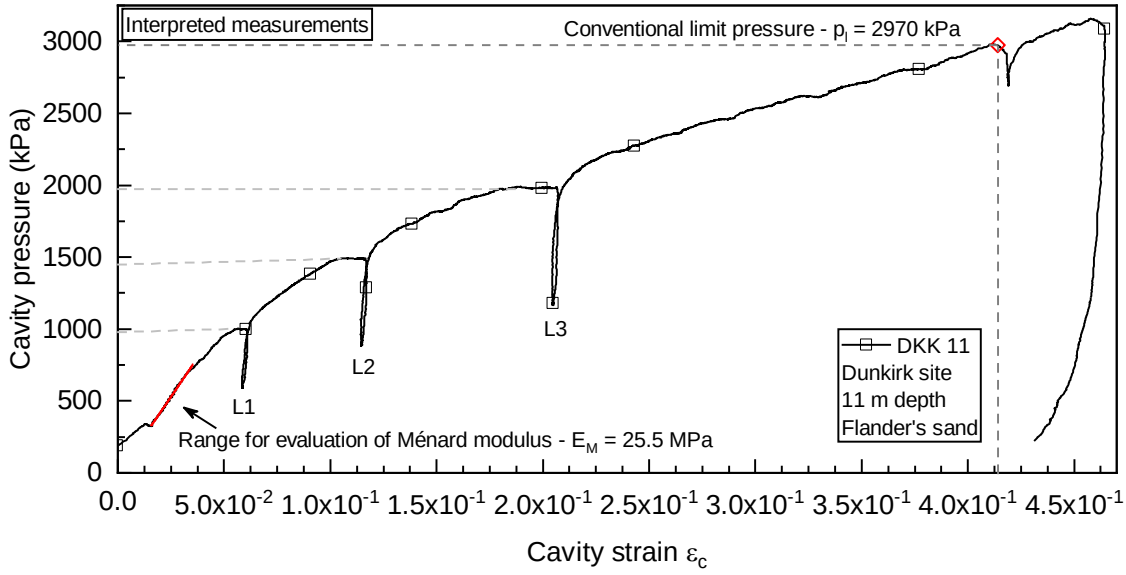

Figure 3.27 – Result of test DKK 11 performed at Dunkirk site at eleven meters depth

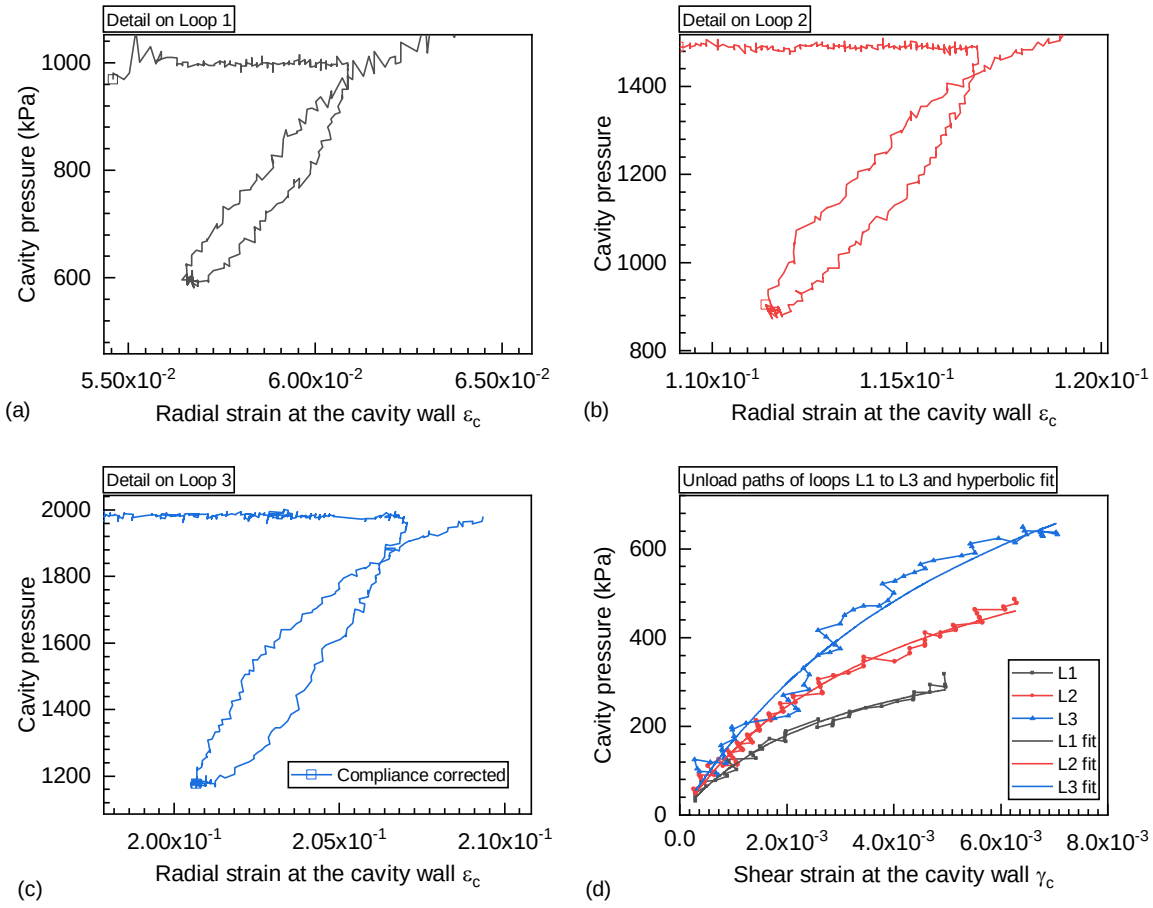

Figure 3.28 – Details on loops L1, L2 and L3 performed in test DKK 11

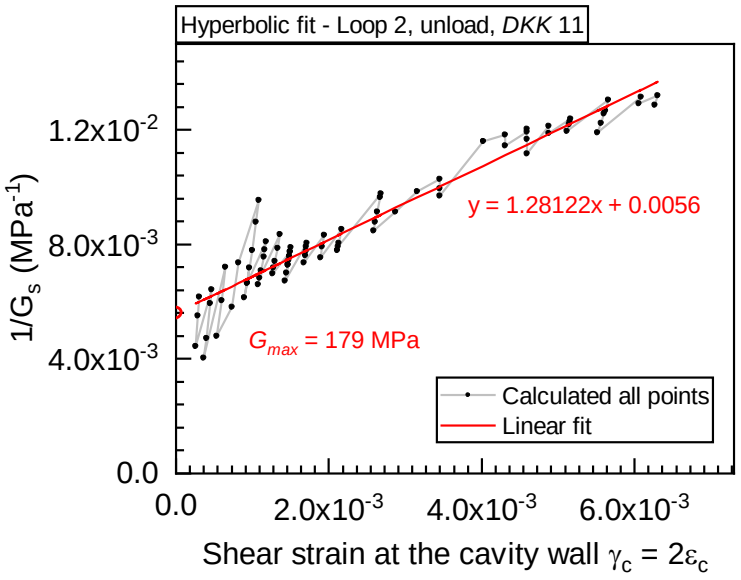

Figure 3.29 – Example of hyperbolic fit for the unload path of loop L2 performed in DKK11 test

The evaluation of the secant shear modulus decay is performed as presented in Chapter 2, section 2.6.2.2. Shear strains at the cavity wall are transformed into average shear strain through a transformed strain approach. Bellotti *et al.* (1989) approach (equations 1.36 and 1.37) is used to transform strains. For the application of these equations, the horizontal stress at rest and the effective friction angle of the soil need to be known. The horizontal stress at rest was estimated considering the bulk unit weights of the soil and, the position of the water table (at 5.4 meters-depth) and K_0 = 0.40, as presented in section 3.2.1. An effective friction angle of 31º was considered. For the case of loop L2, this transformed strain approach leads to a ratio between the average shear strain and the shear strain at the cavity wall $\gamma_{av}/\gamma_c = 0.124$.

A plot of secant shear moduli in function of shear strain at the cavity wall and its further transformation into average shear strain is presented in Figure 3.30. From this figure, it can be seen that there is relatively more measurement noise in this case than in those presented in Chapter 2, in the laboratory (Figure 2.53). This is due only to the measurement resolution of the pressure-volume controller used *in situ*, which is lower than that of the device used in the laboratory. Nevertheless, the relative errors with respect to the fitted curve are of ±7.5% for a domain of average shear strains greater than $2 \cdot 10^{-4}$, which is considered satisfying for the aim of this research.

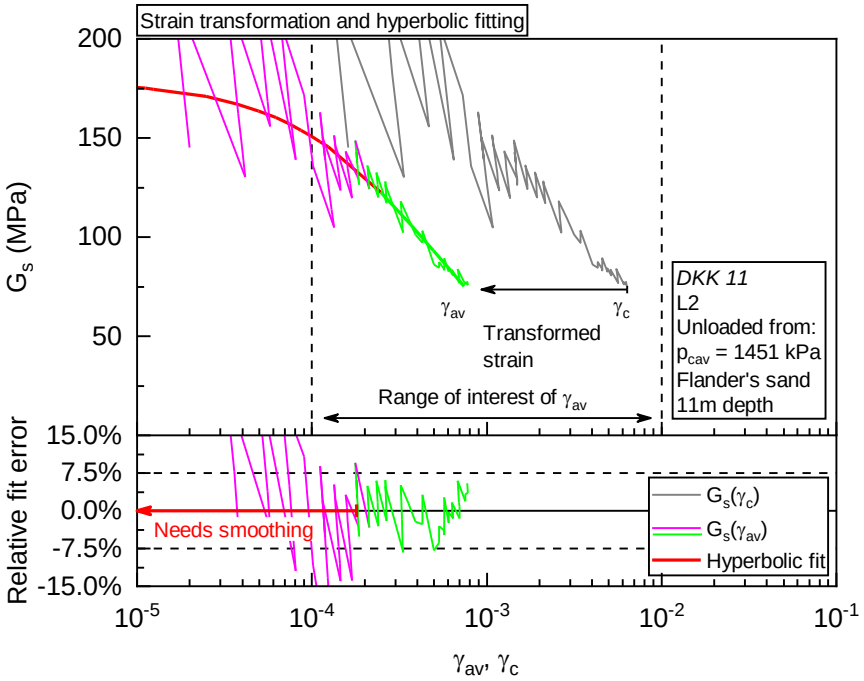

Figure 3.30 – Example of the strain transformation and the derivation of G_s in function of γ_{av} for the second unload loop in *DKK 11* test, including an evaluation of the relative fit errors

3.4.1.3 Summary of results

Results of the cavity expansion curves obtained in tests DKK 8 and DKK 11 are presented in appendix C. The parameters derived from these curves are summarized in the forthcoming sections.

c) Standard pressuremeter parameters

The parameters derived from the virgin expansion curve (first expansion, disregarding the loops) are summarized in Table 3.7. With respect to these parameters, one should note that: (1) there is a trend of increase in the interpreted initial radius that is due to the increasingly difficulty found during performing the borehole; (2) there is a slight decrease in the limit pressure with depth, which is consistent with the CPT test profile presented in Figure 3.10; (3) moduli evaluated in the first linear portion of the expansion curve (Ménard modulus) also tend to decrease with depth, but decrease is more accentuated than for limit pressure.

Table 3.7 – Summary of the parameters interpreted from the virgin loading curve: r_0 the initial radius of the cavity, E_M the Ménard pressuremeter modulus, G_M the corresponding shear modulus, and p_l the pressuremeter limit pressure

Test	Depth (m)	r_0 (mm)	E_M (MPa)	G_M (MPa)	p_l (kPa)
DKK6	6.0	30.9	60.0	22.6	3890*
DKK 8	8.0	31.0	38.2	14.4	3100*
DKK 11	11.0	32.0	25.6	9.6	2970

(*) extrapolated value

d) Parameters derived from the unload loops

The influence of the cavity pressure before unloading on the maximum shear modulus derived using the Briaud *et al.* (1983) method is illustrated in Figure 3.31. The shear stiffness decay evaluated from all loops in all tests is presented in Figure 3.32.

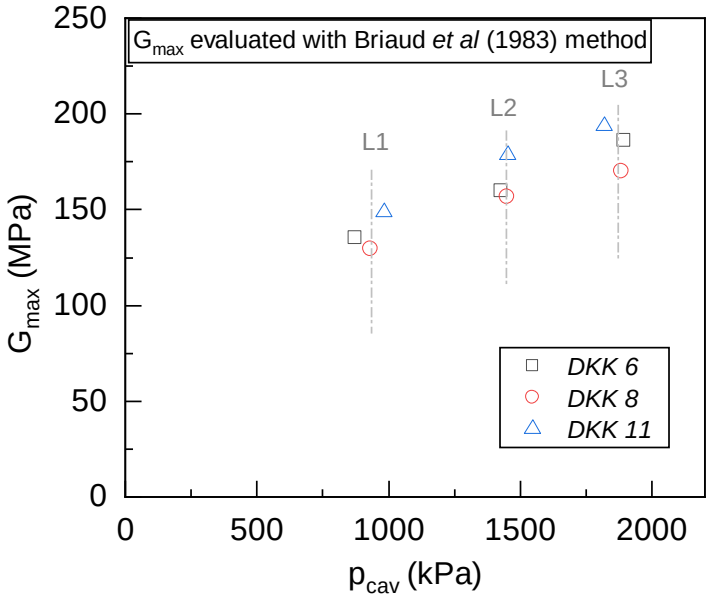

Figure 3.31 – Maximum shear modulus evaluated at Dunkirk site for each unload loop using Briaud *et al.* (1983) method in tests DKK 6, DKK 8 and DKK 11

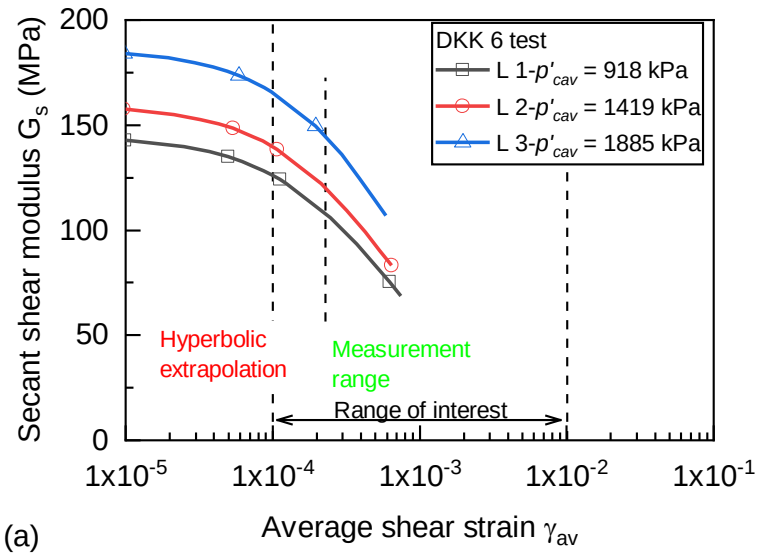

(a)

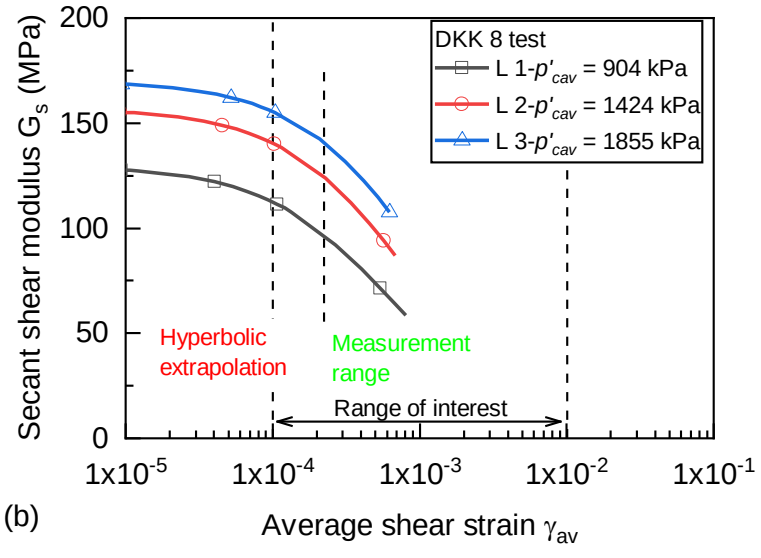

(b)

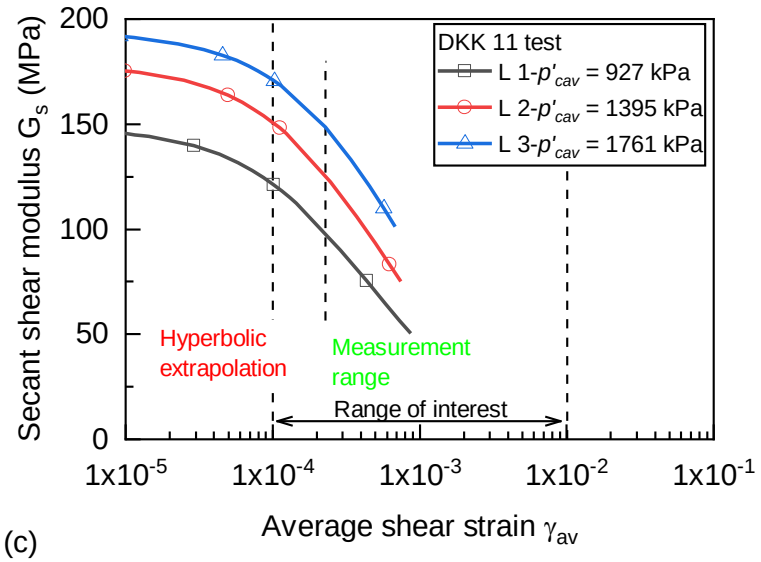

(c)

Figure 3.32 – Summary of the degradation curves of the secant shear moduli versus average shear strain obtained for all loops in (a) DKK 6, (b) DKK 8 and (c) DKK 11 tests

The hyperbolic parameters derived from the interpretation of all the unloading loops using the method of Briaud *et al.* (1983) are synthetized in Table 3.8. In this table, besides the total cavity pressure before unloading p_{cav}, the effective cavity pressure before unloading, ($p'_{cav} = p_{cav} - u$), is also presented. Porewater pressure u was calculated considering the water table at 5.4 meters depth. Full drainage was assumed in the sand for further interpretation of the tests (meaning that u remains constant during the complete cavity expansion test). Strain adjustment coefficients calculated using Bellotti *et al.* (1989) approach are also synthetized in this table.

Table 3.8 – Application of Briaud et al. (1983) method to the interpretation of the unload loops (hyperbolic fit) and Bellotti *et al.* (1989) to the calculation of the strain adjustment

		Hyperbolic fit					Strain adjustment
	Loop	p_{cav} (kPa)	p'_{cav} (kPa)	a (MPa^{-1}) 10^{-3}	b [-]	G_{max} *(MPa)*	γ_{av}/γ_c
DKK 6	L1	924	918	6.904	1.2720	145	0.124
	L2	1425	1419	6.257	0.9606	160	0.107
	L3	1891	1885	5.363	0.6649	186	0.098
DKK 8	L1	930	904	7.721	1.5683	130	0.134
	L2	1450	1424	6.370	0.8543	157	0.114
	L3	1881	1855	5.880	0.5690	170	0.104
DKK 11	L1	983	927	6.722	2.1844	149	0.145
	L2	1451	1395	5.598	1.2812	179	0.124
	L3	1817	1761	5.153	0.7895	194	0.114

3.4.1.4 Validation

a) Assessing Flander's sand elementary shear modulus

The validation of the shear moduli evaluated on site is done by comparing the results obtained with Flander's sand intrinsic properties that have been presented in section 3.2.1. The evolution of the maximum shear modulus with the average stress was evaluated using the equation given by Zdravković et al. (2018) for specimens isotopically consolidated.

Results are presented in Figure 3.33, Figure 3.34 and in Figure 3.35. Values of average stresses calculated using the different methods found in literature are also presented in these figures and further summarized in Table 3.9.

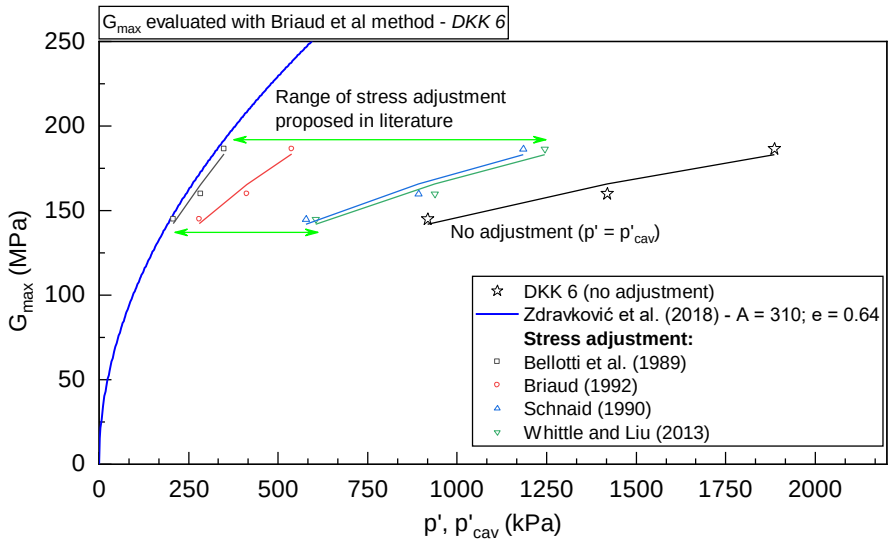

Figure 3.33 – Comparison between maximum shear modulus evaluated with the pressuremeter in *DKK* 6 test and intrinsic moduli of Flander's sand after Zdravković et al. (2018)

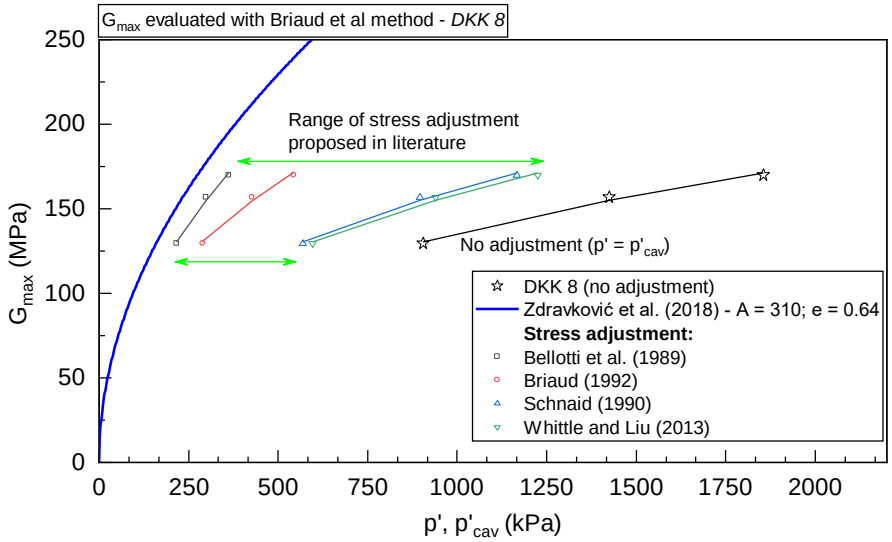

Figure 3.34 – Comparison between maximum shear modulus evaluated with the pressuremeter in DKK 8 test and intrinsic moduli of Flander's sand after Zdravković et al. (2018)

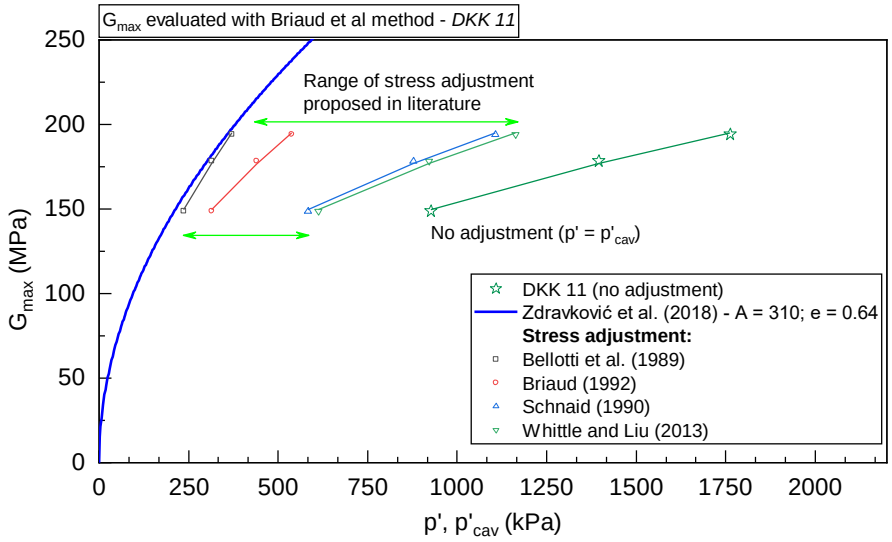

Figure 3.35 – Comparison between maximum shear modulus evaluated with the pressuremeter in DKK 11 test and intrinsic moduli of Flander's sand after Zdravković et al. (2018)

It can be seen that stress adjustment according to the method of Bellotti *et al.* (1989) leads to a trend of evolution of maximum shear moduli in function of average stress very close to that intrinsic of Flander's sand.

Table 3.9 – Cavity pressure and average stress around the cavity for each unload loop

	Loop	p'_{cav} (kPa)	Average stress around the cavity p' (kPa)			
			Bellotti *et al* (1989	Briaud (1992)	Schnaid (1990)	Whittle and Liu (2013)
DKK 6	L1	918	207	279	577	606
	L2	1419	283	413	892	937
	L3	1885	349	538	1185	1244
DKK 8	L1	904	217	289	568	597
	L2	1424	298	428	895	940
	L3	1855	362	543	1166	1225
DKK 11	L1	927	236	315	582	612
	L2	1395	314	440	877	921
	L3	1761	370	538	1107	1163

The evolution of the shear modulus with the shear strain was evaluated as previously, using the Oztoprak and Bolton (2013) model. Belotti *et al.* (1989) method was used to evaluate the average stress around the cavity for each loop. A comparison between shear stiffness decay curves assessed using the pressuremeter and those considered as elementary for Flander's sand is presented in Figure 3.36.

Results obtained in tests DKK 6 and DKK 11 (Figure 3.36a and c) show a good agreement between the degradation curves evaluated with the pressuremeter and the elementary behavior of Flander's sand. For DKK 8 test (Figure 3.36 b) one can observe a small offset in the values of shear modulus, especially in the extrapolation zone. The origin of this error can be understood by analyzing Figure 3.34: in this case the values of maximum shear modulus evaluated with the pressuremeter and adjusted to the mean effective stress state using Bellotti *et al*. (1989) method are slightly smaller than those expected from the intrinsic curve for Flander's sand.

The values of Ménard moduli represented by the dashed horizontal green line and the green area (precedent PMT campaigns) in Figure 3.36 are significantly smaller than the values of maximum shear modulus at the average stress states around the cavity during the unload loops. In general, G_M seems to correspond to the shear modulus of soil degraded to an average shear strain level of about $1 \cdot 10^{-2}$.

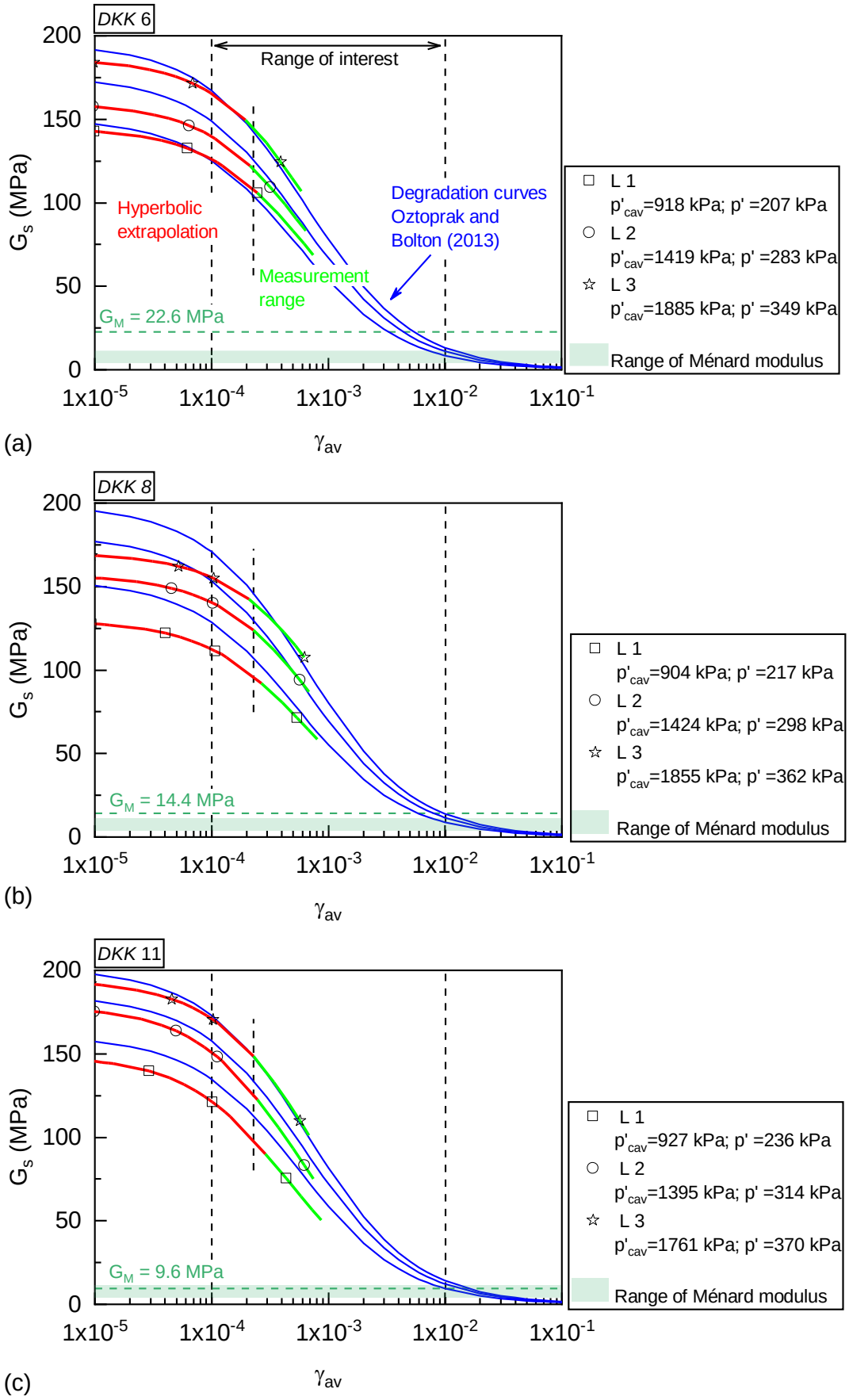

Figure 3.36 – Comparison between secant shear moduli decay in function of average shear strain assessed using the pressuremeter and the evaluated intrinsic curves for Flander's sand

b) Evaluation of the shear modulus in situ

Shear moduli evaluated for each unload loop presented in the previous section are associated to an average stress state imposed around the cavity before each loop is performed. This stress state does not necessarily correspond to the *in situ* stress state at rest. The evaluation of the *in situ* shear modulus $G_{max,0}$ using the pressuremeter requires: (1) estimating the average stress state in the ground at the testing depth and (2) adjusting the shear moduli evaluated with the pressuremeter test with respect to this reference stress state. Adjusting the average stress state around the cavity to the stress state *in situ* is done as follows:

- Define a trend of shear moduli dependency as a function of the average stress from the three values evaluated with the pressuremeter test. The stress dependency curve can be described by equation 3.4. For the matter of simplicity, the stress-dependency exponent *n* is supposed to be equal to 0.5, and coefficient *K* can be easily obtained by fitting the three points obtained from the pressuremeter test.

$$G_{\max} = K \cdot (p')^n \tag{3.4}$$

- The maximum shear modulus at rest $G_{max,0}$ can then be estimated by replacing the average stress *p'* by the average stress evaluated on site, p'_0. An evaluation of the stress state on site based on Flander's sand parameters is presented in Table 3.10.

Table 3.10 – Stress state evaluated *in situ* based on Flander's sand properties

Test	Depth (m)	$\sigma_{v,0}$ (kPa)	u (kPa)	$\sigma'_{v,0}$ (kPa)	K_0	$\sigma'_{h,0}$ (kPa)	p'_0 (kPa)
DKK6	6.0	104	6	98	0.4	39	59
DKK 8	8.0	144	26	118	0.4	47	71
DKK 11	11.0	204	56	148	0.4	59	89

Adjustment of shear moduli evaluated with the pressuremeter test to the stress state *in situ* for tests DKK 6, DKK 8 and DKK 11 is presented in Figure 3.37, Figure 3.38 and Figure 3.39, respectively. Table 3.11 summarizes adjustment coefficients obtained from the pressuremeter test results as well as the evaluated initial shear modulus at rest on site.

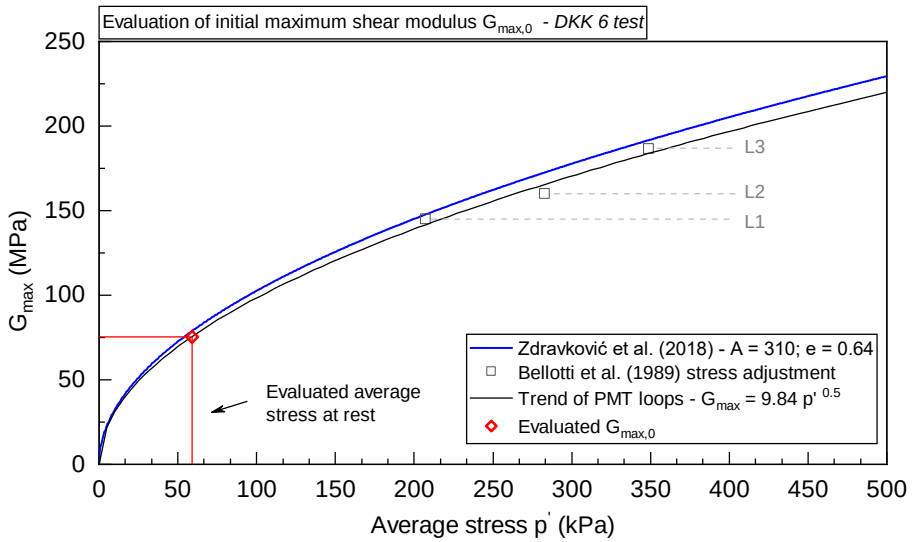

Figure 3.37 – Evaluation of the initial maximum shear modulus on site from the trend of shear moduli evaluated using the pressuremeter test DKK 6

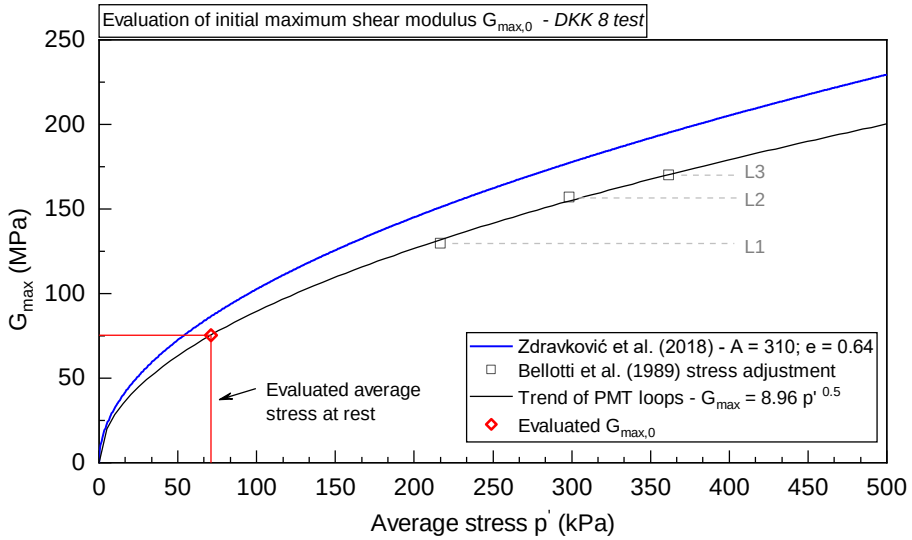

Figure 3.38 – Evaluation of the initial maximum shear modulus on site from the trend of shear moduli evaluated using the pressuremeter test DKK 8

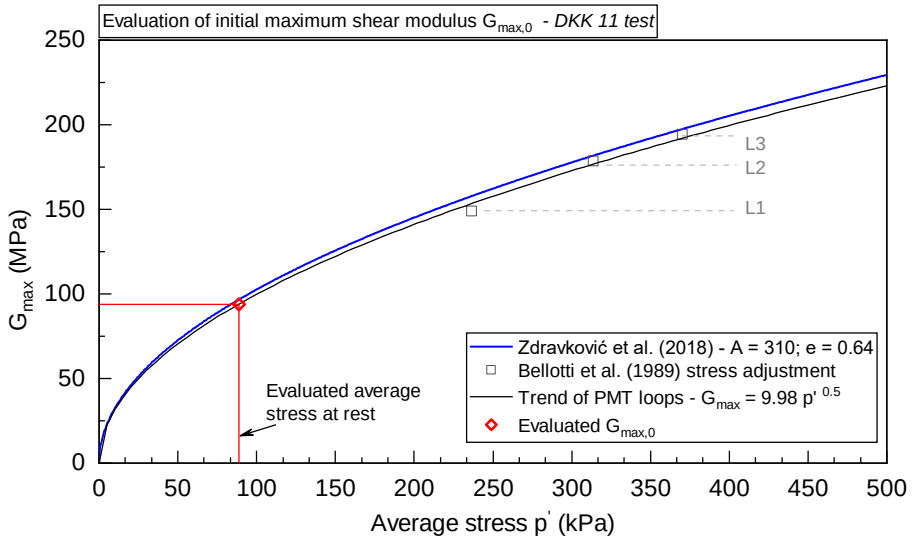

Figure 3.39 – Evaluation of the initial maximum shear modulus on site from the trend of shear moduli evaluated using the pressuremeter test DKK 11

Table 3.11 – Summary of the intrinsic stress adjustment coefficients and evaluated values of initial shear modulus at rest *in situ*

Test	**Depth** (m)	***n*** (-)	***K*** ($kPa^{1/n}$)	***p'0*** (kPa)	***Gmax,0*** (MPa)
DKK6	6.0	0.5	9841	59	76
DKK 8	8.0	0.5	8956	71	75
DKK 11	11.0	0.5	9979	89	94

The evaluated values of $G_{max,0}$ adjusted to the *in situ* stress state can then be compared to the profile of initial shear stiffness obtained on site presented in Zdravković et al. (2018). This comparison is presented in Figure 3.40. It can be noticed that values evaluated using the pressuremeter and the proposed loading and interpretation procedure lay on the lower boundary of the envelope of values presented by the previous mentioned authors. It is possible that this difference comes from a stiffness anisotropy in the Flander's sand. In fact, the stiffness profile presented was obtained using seismic cone penetrometer test, which is a dynamic wave propagation test in which the direction of wave propagation is mainly vertical. Cavity expansion tests, on the other hand, shear the horizontal plane.

Values of Ménard shear moduli are also presented in Figure 3.40. These values are much lower than at rest moduli measured on site. Yet, G_M values decrease sharply with depth, which could probably be, in this case, caused by the progressive disturbance during the borehole advancement (deeper tests resulted in larger initial cavity radius). This difficulty did not disturb the results obtained with the unload loops, which points out that this loading procedure is rather insensitive to drilling disturbance.

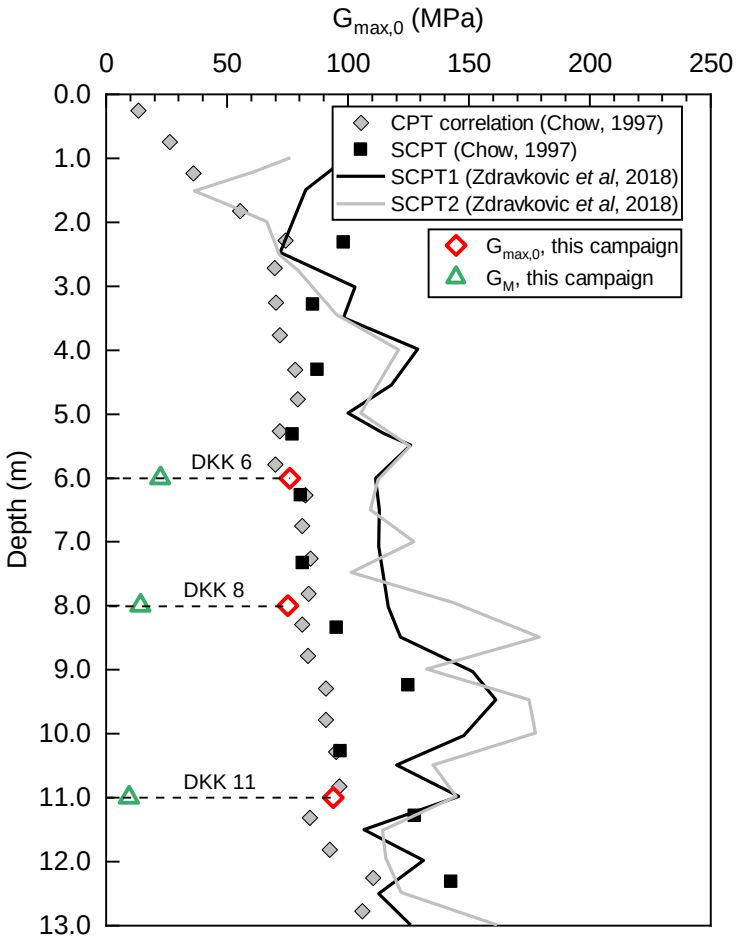

Figure 3.40 – Comparison between the initial shear modulus obtained in the present pressuremeter investigation campaign with values presented in Zdravković et al. (2018)

3.4.1.5 Concluding remarks

Shear moduli derived from the three loops performed at increasing cavity pressure showed a clear dependency between stiffness and cavity pressure. One major difficulty in test interpretation is the adjustment of the stress state (i.e. transforming the cavity pressure before unloading into an average stress state in the soil around the cavity). There is no consensus between the propositions found in literature, and the results obtained vary significantly amongst the existing methods. On the Dunkirk site, the previous knowledge of the elementary relationship between G_{max} and p'_c contributed to the determination of the most adequate method for stress adjustment: in this case, that of Bellotti *et al.* (1989). Generalizing this for all types of sands requires more studies.

With respect to the shear stiffness decay, the use of the transformed strain approach proposed by Bellotti *et al.* (1989) was successful. This approach requires the knowledge of the soil friction angle and the horizontal effective stress at rest, which can be challenging in sites where the soil tested is completely unknown.

Another important aspect is that the interpretation method requires that the effective cavity pressure be known. In this work, full drainage of the soil was assumed, which can be considered adequate given the known grain size distribution curve of the sand. The porewater pressure could be evaluated because the position of the water table was previously known. If soil properties are unknown, the measurement of the excess pore water pressure using pressure transducers on the probe is recommended to allow following up its evolution during the test.

The interpretation of each pressuremeter loop enables an evaluation of the maximum shear modulus and the secant shear modulus decay curve starting from a stress state imposed on the soil just before loop is performed. This stress state does not necessarily correspond to the initial stress state at rest on the site. Therefore, establishing the initial *in situ* shear modulus requires (1) evaluating the initial stress at rest and (2) adjusting shear moduli obtained with the pressuremeter to this stress state. It has been shown that evaluating initial shear stiffness with this procedure led to shear moduli close to those measured on site using seismic cone penetration tests (wave propagation tests).

3.4.2 Tests in clays: Merville site

3.4.2.1 Testing program

The testing program aiming at assessing shear moduli at small strains performed at the Merville testing site is presented in Table 3.12.

Table 3.12 –Testing program performed at Merville aiming at assessing shear moduli at small strains

Test	**Depth (m)**	**Loop**	p_{cav} **(kPa)**	Δp_{cav} **(kPa)**	$\Delta p_{cav}/p_{cav}$	Δt *(min)*
MVL9.1	9.0	L1	619	208	0.34	1.0
		L2	786	246	0.31	1.0
		L5	1110	480	0.43	2.0
		L7	1267	562	0.44	3.0
MVL11.1	11.0	L2	922	269	0.29	2.0
		L4	1101	365	0.33	2.7
		L5	1280	367	0.29	3.2
		L6	1426	1034(*)	0.73	3.2
MVL12.2	12.0	L1	933	347	0.37	3.2
		L2	1144	441	0.39	3.2
		L3	1336	518	0.39	3.2

(*) only the beginning of the unload was interpreted (400 kPa)

3.4.2.2 Results and analysis of a typical test

In situ measurements will be illustrated based on the typical test performed at twelve meters-depth in borehole BH2 (MVL 12.2). The sets of parameters derived are the same as previously presented for sands at Dunkirk. The result of test MVL 12.2 is presented in Figure 3.41.

The detail of loops one to three, corrected for membrane compliance, is presented in Figure 3.42a to c. Each of the unload paths are presented in Figure 3.42d. In this case, it can be observed that there is no evident effect of the cavity pressure before unloading on the measured stiffness: all the three loops plot approximately aligned. Hyperbolic fit of each loop is also presented in this figure. Loop L4, performed at the same pressure levels that L1, but after having unloaded the cavity, presents a similar slope.

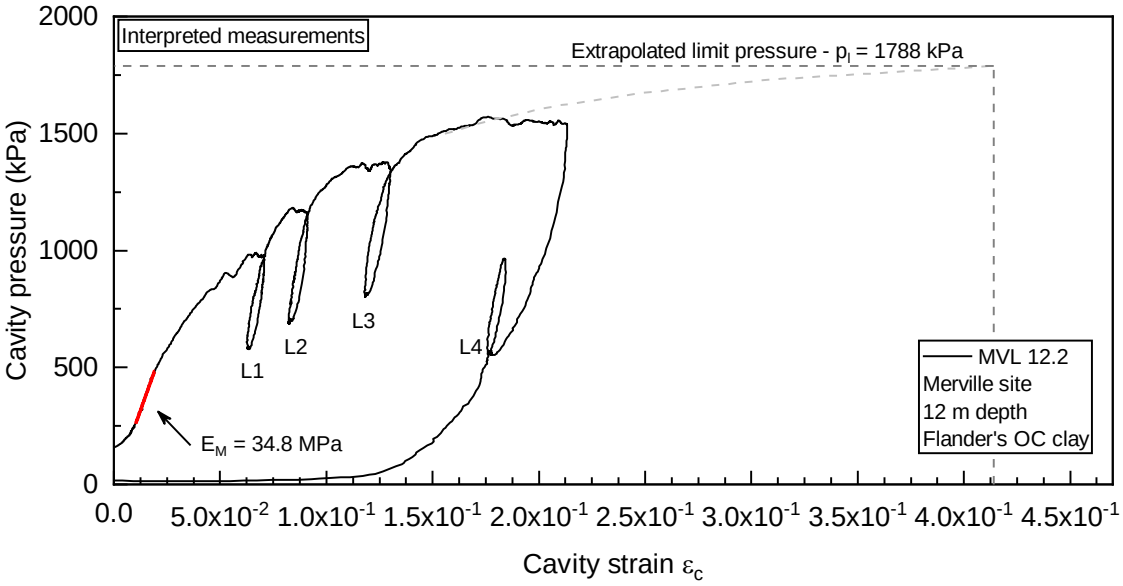

Figure 3.41 – Result of test MVL 12.2 performed in Merville site at twelve meters depth

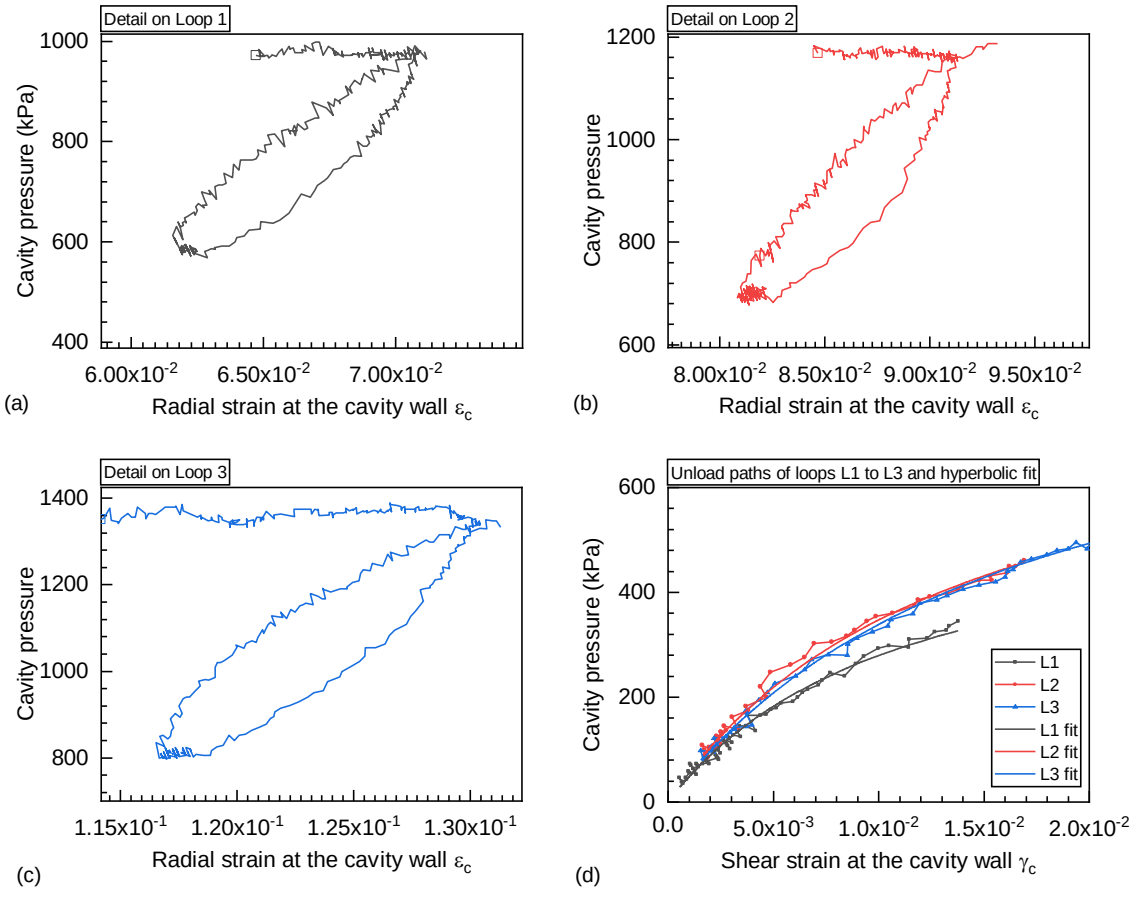

Figure 3.42 – Details on loops one to three performed in test MVL 12.2

The method of Briaud *et al.* (1983) was used to evaluate maximum shear moduli for each loop. The application of this method to loop L3 in MVL 12.2 is illustrated in Figure 3.43.

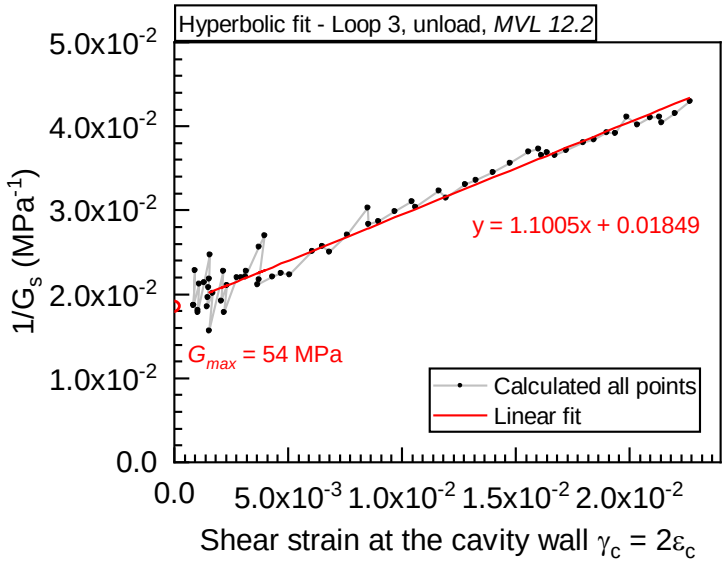

Figure 3.43 – Example of hyperbolic fit for the unload path of loop L3 performed in MVL 12.2 test

In the case of clays, the evaluation of the secant shear modulus decay is performed using Jardine (1992) transformed strain approach, rewritten in eq. 3.5, relating the shear strain at the cavity wall and the average shear strain in the soil around the cavity. A plot of secant shear moduli in function of shear strain at the cavity wall and its further transformation into average shear strain for loop L3 is presented in Figure 3.44.

$$\gamma_{av} = \frac{\gamma_c}{1.2 + 0.8 * log10\,(\gamma_c/10^{-5})} \tag{3.5}$$

By comparing the results presented in this figure with those presented in Figure 3.30 for an unload loop in Dunkirk sands, it can be easily seen that shear stiffness decrease in function of average strain is less accentuated in clays. This observation is in agreement with the fact that shear stiffness decreases slower for soils with higher plasticity indices (as presented in Vucetic and Dobry (1991), for example).

3.4.2.3 Summary of results

Results of the cavity expansion curves obtained in MVL 9.1 and MVL 11.1 tests are presented in appendix C. The parameters derived from these curves are summarized in the forthcoming sections.

a) Standard pressuremeter parameters

The parameters derived from the virgin expansion curve (first expansion, disregarding the loops) are summarized in Table 3.13.

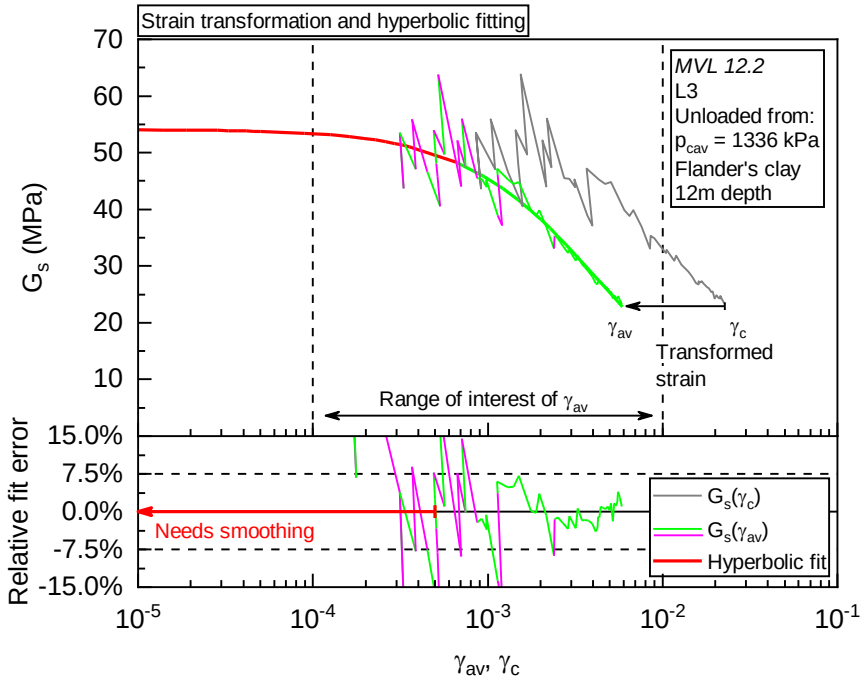

Figure 3.44 – Example of the strain transformation and the derivation of G_s in function of γ_{av} for the third unload loop in *MVL 12.2* test, including an evaluation of the relative fit errors

Table 3.13 – Summary of the parameters interpreted from the virgin loading curve: r_0 the initial radius of the cavity, E_M the Ménard pressuremeter modulus, G_M the corresponding shear modulus, and p_l the pressuremeter limit pressure

Test	Depth (m)	r_0 (mm)	E_M (MPa)	G_M (MPa)	p_l (kPa)
MVL9.1	9.0	32.1	25.0	9.4	1550*
MVL11.1	11.0	32.4	38.8	14.6	1586*
MVL12.2	12.0	30.9	34.8	13.1	1788*

(*) extrapolated value

b) Parameters derived from the unload loops

The influence of the cavity pressure before unloading on the maximum shear modulus derived using Briaud *et al.* (1983) method is illustrated in Figure 3.45. The shear stiffness decay evaluated from all the interpreted loops is presented in Figure 3.46. The hyperbolic parameters derived using the method of Briaud *et al.* (1983) are synthetized in Table 3.14.

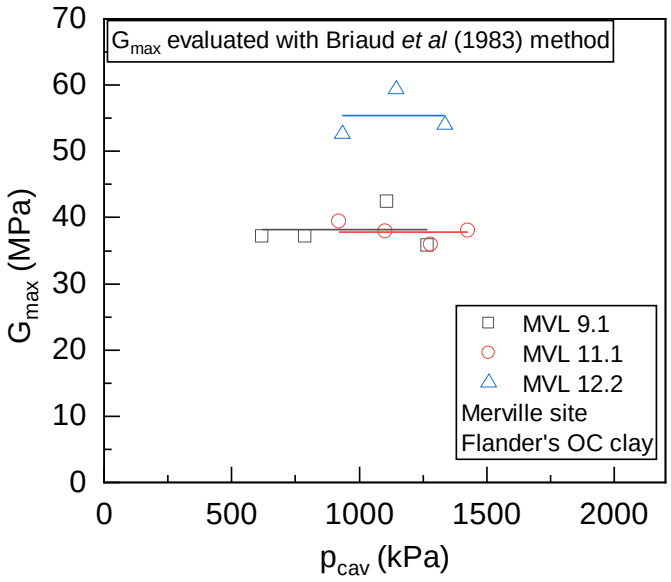

Figure 3.45 – Maximum shear modulus evaluated in Merville site for each unload loop using Briaud *et al.* (1983) method in MVL 9.1, MVL 11.1 and MVL 12.2 tests

From Figure 3.45 it can be observed that there is no trend of evolution of maximum shear moduli in function of the cavity pressure before unloading. This is different from what has been observed on the tests on sands. This may indicate that the effective stress around the cavity has not evolved during the cavity expansion test, meaning that the variations in porewater pressure were equal to the variation in total stress. It is not possible to verify this hypothesis, since there are no measurements of evolution of excess pore water pressure (EPWP) during the test, but it will be assumed valid for the further test interpretation. Thus, based on this assumption, the values of G_{max} obtained with the pressuremeter correspond to the initial shear modulus at rest on site, $G_{max,0}$.

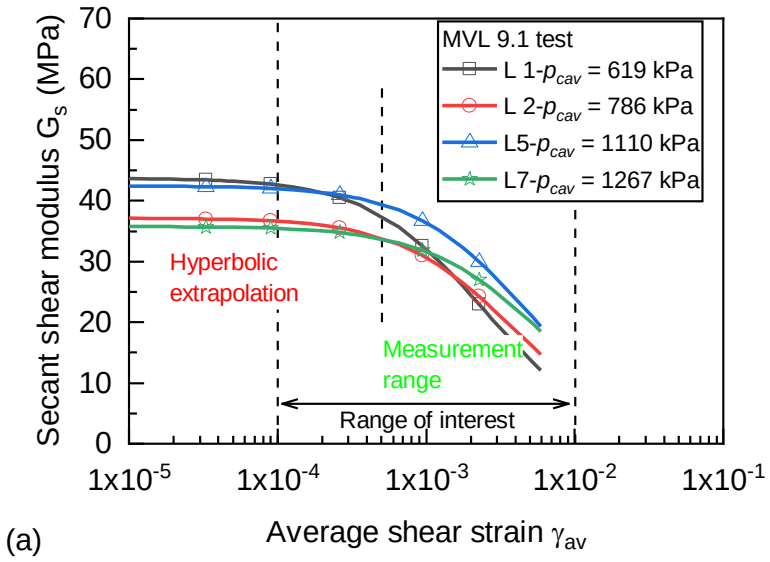

(a)

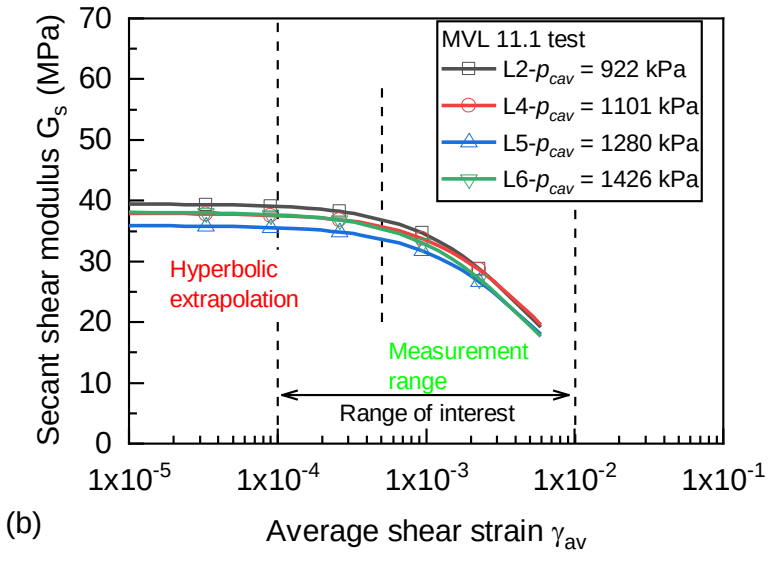

(b)

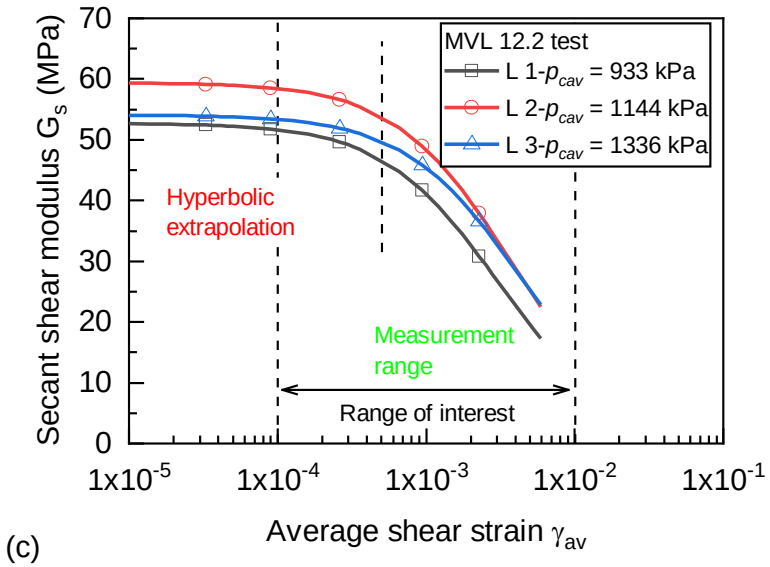

(c)

Figure 3.46 – Summary of the obtained degradation curves of the secant shear moduli versus the average shear strain obtained for all loops in (a) MVL 9.1, (b) MVL 11.1and (c) MVL 12.2 tests

Table 3.14 – Application of Briaud *et al.* (1983) method to the interpretation of the unload loops (hyperbolic fit). Strain adjustment calculated using Jardine (1992) approach

		Hyperbolic fit			
	Loop	p_{cav} **(kPa)**	**a** (MPa^{-1}) 10^{-3}	**b** [-]	G_{max} *(MPa)*
MVL9.1	L1	619	26.911	2.5946	37
	L2	786	26.911	1.7896	37
	L5	1110	23.560	1.2249	42
	L7	1267	27.962	1.1356	36
MVL11.1	L2	922	25.350	1.1680	39
	L4	1101	26.381	1.0718	38
	L5	1280	27.871	1.2046	36
	L6	1426	26.243	1.3292	38
MVL12.2	L1	933	18.974	1.6816	53
	L2	1144	16.836	1.1952	59
	L3	1336	18.489	1.1005	54

3.4.2.4 Validation

The validation of the shear moduli evaluated on site is done by comparing test results obtained with the pressuremeter with Flander's clay elementary properties that have been presented in section 3.2.2. Values of maximum shear moduli obtained for each loop were directly compared to values of G_{max} measured *in situ* through geophysical tests. The elementary degradation of maximum shear modulus with strain was evaluated using the Hardin and Drnevich (1972) model, as suggested by Borel and Reiffsteck (2006) for the site.

Figure 3.47 presents a comparison between values of maximum shear moduli obtained for each unload loop in the pressuremeter tests performed in this research and values obtained *in situ* using other investigation methods, such as down-hole and cross-hole geophysical tests and standard pressuremeter tests. From this figure, and similarly to what was observed for tests at Dunkirk, it can be noticed that the values of $G_{max,0}$ evaluated using the pressuremeter lay on the lower boundary of the envelope of values assessed on site using geophysical tests, tending to be slightly underestimated for tests MVL 9.1 and MVL 11.1.

Profiles of standard Ménard shear modulus obtained in precedent campaigns are also reported in Figure 3.47. Values of Ménard modulus obtained in the current campaign plot within the range of values previously obtained on site. This points out to the validation of the capability of the proposed test procedure and the Monocell FC probe

to provide equivalent values of Ménard modulus than in the standard Ménard procedures.

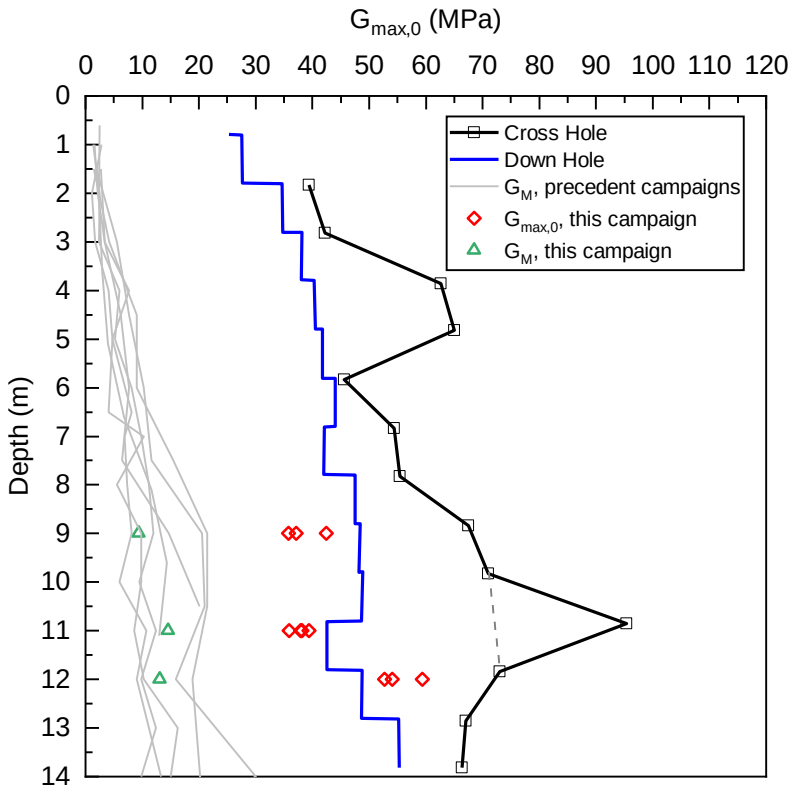

Figure 3.47 – Comparison between the initial shear modulus obtained in the present pressuremeter campaign with values obtained on site using other tests (after Borel and Reiffsteck (2006))

A comparison between shear stiffness assessed using the pressuremeter and those considered as intrinsic for Flander's clay assessed using cross-hole and down-hole tests, $G_{max,CH}$ and $G_{max,DH}$, respectively is presented in Figure 3.48. The range of standard pressuremeter modulus obtained in previous testing campaigns is also presented in this figure.

The theoretical shear modulus degradation curves plotted refers to the model of Hardin and Drnevich (1972) described by eq. 3.2, which was considered as adequate for describing strain dependency of Flander's clay stiffness by Borel and Reiffsteck (2006). On this equation, values of τ_{max} were evaluated from the undrained shear stiffness profile presented in Figure 3.19 ($\tau_{max} = 2c_u$).

The grey area delimited by the two envelope curves corresponds to the estimated possible values of shear stiffness that can be expected at the testing depths. The upper-bound limit starts from the higher value of initial shear modulus, that obtained by cross-

hole tests. The lower-bound starts from the lower initial shear modulus, obtained by down-hole test at a given depth.

From the results presented in Figure 3.48 it can be concluded that evaluating shear moduli using the proposed procedure within the range of interest of measurement leads to values close to the estimated elementary shear modulus of Flander's clay. For tests MVL 9.1 and MVL 11.1 there is a slight trend to underestimate *in situ* shear stiffness. Results of test MVL 12.2 lay fully inside the range of expected values. This result is considered satisfying for the aims of this research.

Similarly to what has been observed for tests in sands in Dunkirk site, the values of Ménard moduli G_M represented by the greened area seem to correspond to the shear modulus of soil degraded to an average shear strain level of about 5.10^{-3} and 1.10^{-2}. In this case, it could be observed that, on average, initial shear modulus of the soil evaluated by geophysical tests is approximately 4 to 6 times higher than Menard shear modulus obtained using standard pressuremeter tests.

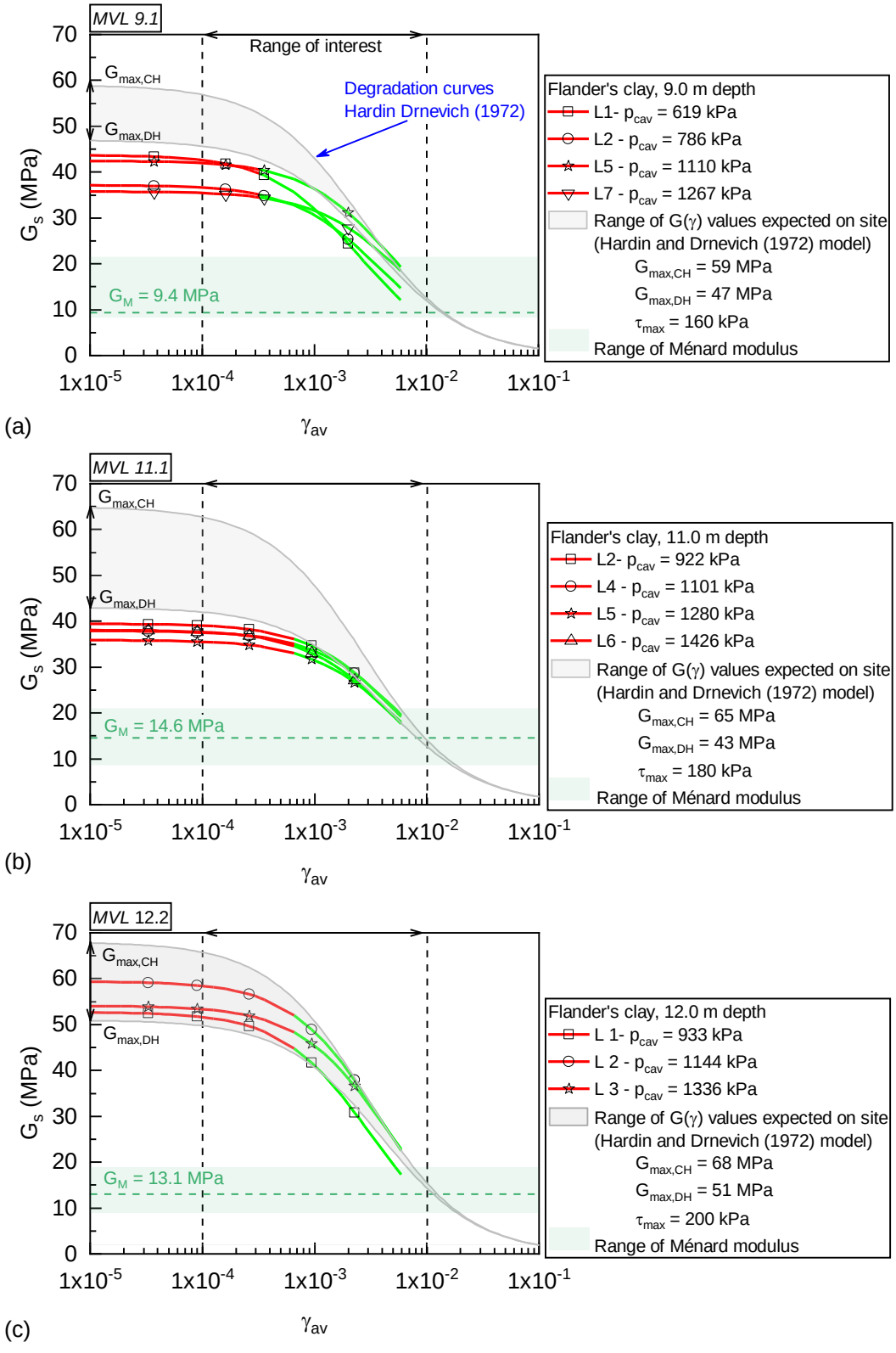

Figure 3.48 – Comparison between secant shear moduli decay in function of average shear strain assessed using the pressuremeter and a range of evaluated intrinsic curves for Flander's clay

3.4.2.5 Concluding remarks

In Merville site, shear moduli derived from three or more loops performed at increasing cavity pressure were approximately constant. This independency with respect to the cavity pressure points to the hypothesis of fully undrained behavior and that no variations in the effective stress state around the cavity took place during the cavity expansion. As previously discussed, measuring pore water pressure variation along the test could help to validate this assumption.

Test interpretation is easier under the hypothesis of fully undrained conditions, since there is no need to estimate the changes in average effective stress around the cavity. In that manner, shear moduli measured with the pressuremeter correspond to the elementary modulus of the soil. Comparison of moduli assessed with the method proposed herein with those obtained by geophysical tests on site yielded close results, considered as satisfactory for the validation purpose within this research. Yet, the degradation curves determined from the pressuremeter tests, adjusted using the strain transformed approach proposed by Jardine (1992), were in good agreement with those expected for the soil.

3.4.3 Other tests performed in this research

Besides the tests performed at Dunkirk and Merville sites, other tests have been performed using the Monocell FC probe during this research. Some of them were undertaken in the context of cross-validation campaigns (comparison with standard method) proposed within the National Project ARSCOP, and other for consulting projects in which Fugro France was involved. Some of these results were recently published in conferences (Lopes (2018), Lopes et al. (2018), (2019b)); presented in internal ARSCOP meetings and reports (Droniuc et al. (2019)), and analyzed during a master thesis project Hussein (2019). Amongst the testing sites, we can mention:

- Tests in soft clays at Cran site: eight tests performed following three different loading protocols (standard Ménard, continuous rate of shearing and protocol 1 with three loops). The resulting values of limit pressure of soil were similar to those obtained using standard pressuremeters (between 0.1 and 0.5 MPa).
- Tests in very stiff *molasse* clay in Toulouse: limit pressure of soil varying between 3.9 and 12.4 MPa, in good agreement with standard measurements.

- Tests in sandstone in Gouvieux: cross-validation campaign aiming to compare the performance of three different probes for tests at high pressures. Tests with the Monocell FC probe were carried-out up to 14 MPa. Moduli evaluated from unload-reload loops performed according to the procedure B of AFNOR (2013b) using the Monocell FC probe were shown to be in good agreement with respect to tests performed using flexible dilatometer with local measurement of strains.
- Tests in soils of the Parisian sedimentary basin (dense sands, overconsolidated clays, sandstone, chalk), performed by Fugro France in the context of consulting projects aiming at the optimization of deep foundations (measurement of soil limit pressure at high-pressures – up to 22 MPa in the chalk). Some of these tests were presented by Cour and Lopes (2018b), (2018a), Lopes et al. (2018).

Most of these tests were performed previously to the Dunkirk and Merville campaigns and they provided very important insights with respect to the improvement and development of the testing procedure *in situ*. However, the results of these tests will not be presented in this work

3.5 PRESENTATION OF RESULTS OBTAINED. ASSESSING CYCLIC PARAMETERS

This section presents the results of the cyclic tests performed at Dunkirk and Merville sites with the purpose of understanding soil behaviour under cyclic loading using the pressuremeter. The section is divided in four parts. First, the testing program is presented. Then, the interpretation procedure is illustrated through representative cases. Finally, the results of the other tests are summarized.

3.5.1 Tests in sands: Dunkirk site

3.5.1.1 Testing program

Table 3.15 presents the cyclic testing program performed at the Dunkirk site. Series performed after having pre-sheared the soil to a certain level are indicated with a (*). In tests DKK 6, DKK 10 and DKK 12 the minimum pressure for all cyclic series was

fixed near 550 kPa. In test DKK 7, the maximum cavity pressure was fixed at approximately 2400 kPa ($A + p_{min} = 2400$ kPa). As the cyclic series were manually controlled, it was difficult to keep the same period T for all series. The values presented are averaged.

Table 3.15 – Testing program performed at Dunkirk site aiming at assessing cyclic properties

Test	Depth (m)	Loading program	Series	A (kPa)	p_{min} (kPa)	p_{max} (kPa)	p_{mean} (kPa)	N	T (s)
DKK6	6.0	2*	S1	390	530	920	725	10	60
			S2	880	530	1410	970	8	90
			S3	1390	530	1920	1225	7	100
			S4	1860	530	2390	1460	13	120
DKK7	7.0	2*	S1	390	2000	2390	2195	6	60
			S2	870	1530	2400	1965	9	100
			S3	1870	530	2400	1465	5	180
DKK10	10.0	2	S1	370	580	950	765	10	70
			S2	860	580	1440	1010	10	100
			S3	1860	580	2440	1510	10	180
DKK12	12.0	2	S1	370	590	960	775	10	70
			S2	870	590	1460	1025	10	100
			S3	1850	590	2440	1515	11	180

On site, probe pressure was controlled based on raw readings of pressure at the ground level (without accounting for membrane self-resistance), which explains the small differences in series amplitude A and minimum cavity pressure p_{min} amongst the different tests.

3.5.1.2 Results and analysis of a typical test

The analysis of the accumulation of plastic strains due to cyclic loading is similar to that performed in Chapter 2. In the present case, it will be illustrated on test *DKK 10*, which result is presented in Figure 3.49. Three cyclic series of increasing amplitude were performed (S1 to S3) starting from a "virgin" state (the cavity has not been pre-loaded before performing the cyclic series).

It can be noticed that measurements on the third cyclic series present significantly more noise than those presented in section 3.4. This in caused by the higher water flow-rate that had to be imposed to perform the cyclic series under approximately constant frequencies. The pressure-transducer in the pressure-volume controller used is placed

near the injection pump and at high flow-rates the pump generates high-frequency peaks in water pressure. For this reason, the shear stiffness degradation curve cannot be determined from each cycle. This aspect needs to be improved in further developments of the controller device, but it is considered that the quality of the collected data is sufficient for the purposes of this research.

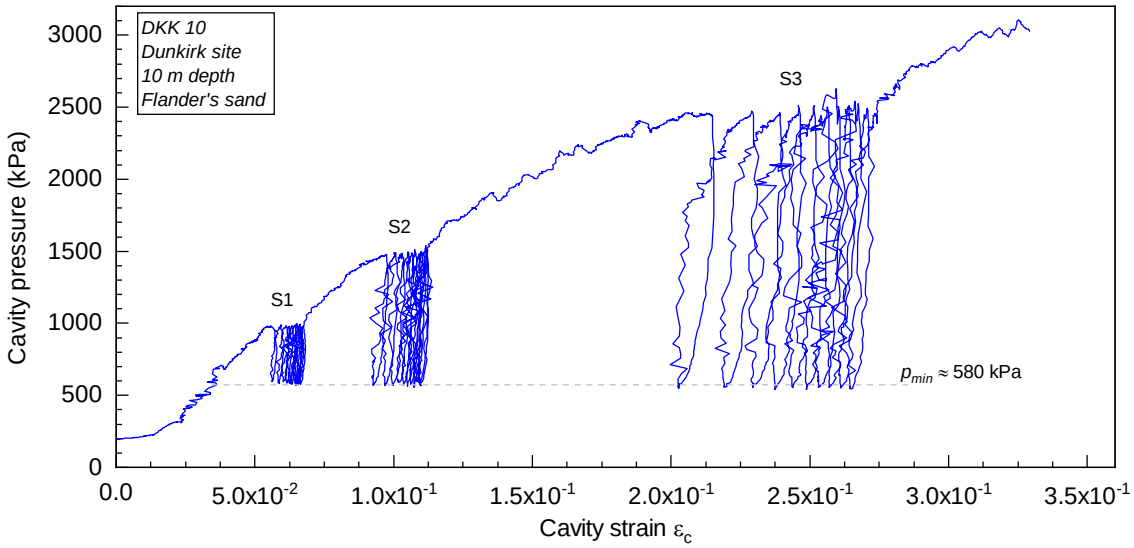

Figure 3.49 – Result of the cyclic series S1 to S3 in DKK 10 test

The cyclic series were interpreted in the same way as presented in Chapter 2. In the present case, since it was possible to derive cavity strains from the cyclic test results (no disturbance of geometric configuration as in the calibration chamber PCC), results are presented in terms of radial strain accumulation in function of the number of cycles. The interpretation of test DKK 10 is illustrated in Figure 3.50.

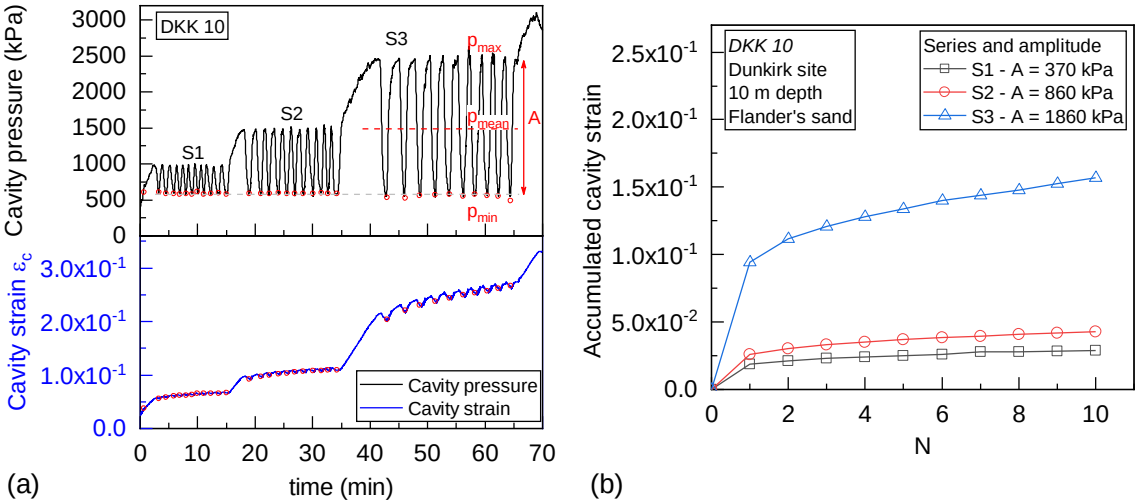

Figure 3.50 – Interpretation procedure for the determination of the accumulation of cavity strains in function of the number of cycles. Example of test DKK 10.

3.5.1.3 Summary of results

The accumulation of cavity strains obtained in tests DKK 6, DKK 7, DKK 10 and DKK 12 is summarized in Figure 3.51.

The cyclic series in tests DKK 6 and DKK 7 (Figure 3.51a and b) were performed after the soil had been pre-sheared to a cavity pressure level of approximately 3000 kPa. The cyclic series in tests DKK 10 and DKK 12 (Figure 3.51c and d) were performed from a "virgin" initial state of the soil. The difference in behavior from these two cases is evident from a first analysis of the results: series performed from a virgin state result in much higher strain accumulation.

With respect to the series performed after the soil has been pre-sheared, it can be noticed that for series S1 and S2 of amplitudes equal to 390 and 870 kPa respectively, there is near zero strain accumulation. However, the higher amplitude series S3 (A = 1860 kPa) lead to a "reactivation" of the accumulation of radial strains in the soil.

By comparing the results presented in Figure 3.51c with those in Figure 3.51d, one can notice that test DKK 12 resulted in more cyclic accumulation than test DKK 10. This result may seem contradictory because less accumulation should be expected for the test at greatest depth. However, this can be explained by analyzing the CPT profile presented in Figure 3.10. CPT resistance is lower at 12 meters depth than at 10 meters (in average, 20 MPa at 12 meters versus 30 MPa at 10 meters). The soil conventional limit pressure measured at these depths were of respectively 2.75 MPa and 3.35 MPa. This observation is in agreement with the fact that strain accumulation is dependent on soil resistance, which is related to its limit pressure.

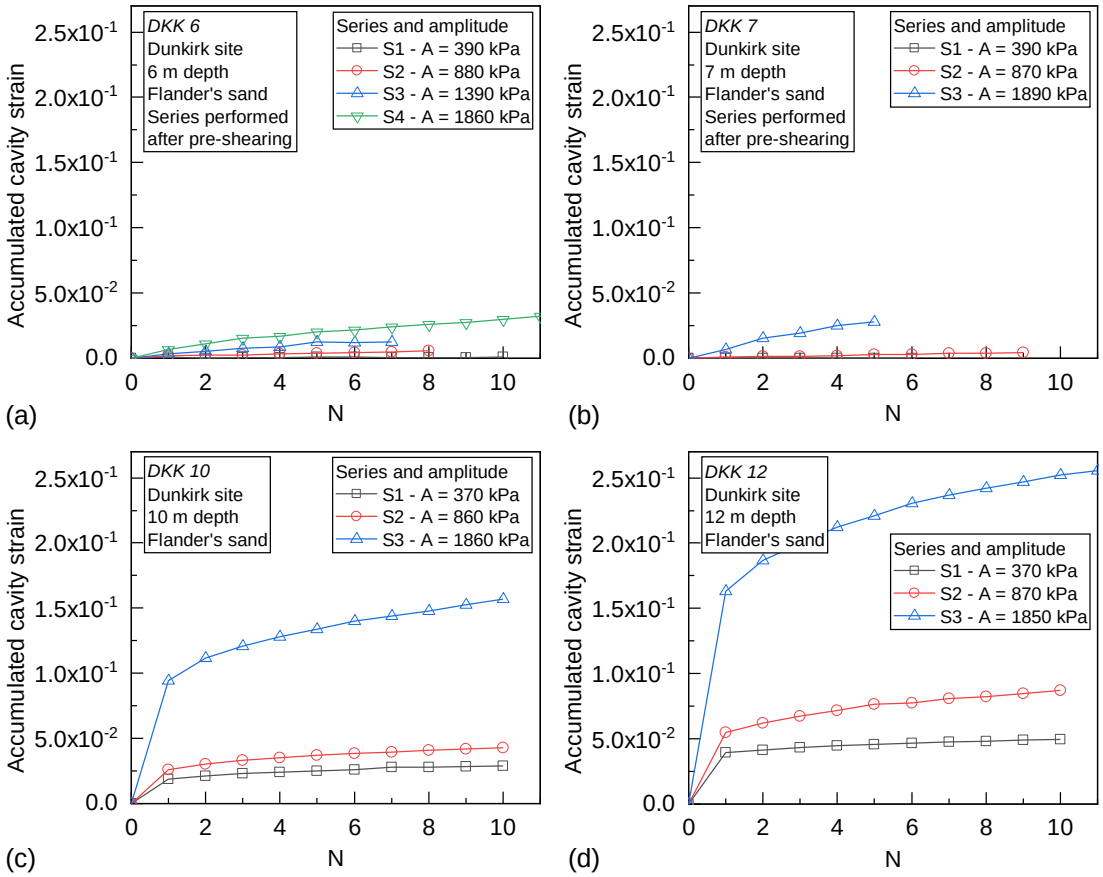

Figure 3.51 – Summary of accumulated strains during series of repeated cycles in tests DKK 6, DKK 7, DKK 10 and DKK 12

3.5.1.4 Concluding remarks

With respect to the tests aiming at assessing cyclic properties at Dunkirk site, it could be concluded that: (1) increasing cyclic amplitude leads to an increase in plastic strain accumulation in function of the number of cycles, which is consistent with what has been presented in literature and measured in the laboratory; (2) performing the same cyclic procedure after having pre-sheared the soil close to its limit pressure results in much less accumulation; (3) in cycles performed after the soil has been pre-sheared, increasing the cyclic amplitude can "reactivate" the plastic strain accumulation mechanism.

3.5.2 Tests in clays: Merville site

3.5.2.1 Testing program

Table 3.16 presents the cyclic testing program performed at Merville site. Different loading programs were performed on this site in comparison to those undertaken in the laboratory and at Dunkirk. The reason for this is that, due to schedule constraints, this testing campaign was performed only a few months after the laboratory tests, and before tests at Dunkirk site. The exact loading program enabling the evaluation of key differences on the behavior of overconsolidated clays and sands under cyclic loading had not yet been fully defined.

It should also be noted that the behavior of clays under cyclic pressuremeter loading had not yet been studied in the laboratory within the framework of this research. Furthermore, there are no existing guidelines on how to apply this type of solicitation to the design of piles. The loading program performed in Merville evolved on site according to the observations of soil response after each test. The testing program presented herein should be seen as an exploratory program, in which we aimed at answering the question, "what behavior do we obtain if we perform a given procedure?". Amongst the procedures performed, one can note:

- study of the influence of the sequence of loading on the strain accumulation (increasing or decreasing amplitude at a constant p_{max}), from tests MVL 10.1 and MVL 10.2, series S3 and S1, respectively;
- effect of progressively increasing p_{mean} on series of variable amplitude from test MVL 14.1 S1 to S4,
- effect of pre-shearing on the strain accumulation by comparing series S5 with S1 in test MVL 14.1. and effect of pre-shearing on high amplitude cycles (MVL 11.2);
- study of the effect of cyclic frequency on shear moduli obtained in tests performed after pre-shear (series S5.1 to S5.3 in MVL 14.1);
- study of the effect of cyclic frequency in tests performed under virgin conditions from series S1.1 to S1.3 in test MVL 15.1;

Table 3.16 – Testing program performed at Dunkirk site aiming at assessing cyclic properties

Test	Depth (m)	Loading program	Series	A (kPa)	p_{min} (kPa)	p_{max} (kPa)	p_{mean} (kPa)	N	T (s)
MVL10.1	10	2	S1	200	740	940	840	9	40
			S2.1	200	940	1140	1040	10	30
			S2.2	410	730	1140	935	10	30
			S3.1	200	1120	1320	1220	9	20
			S3.2	400	920	1320	1120	9	20
			S3.3	590	730	1320	1025	10	20
MVL14.1	14	2- (1)	S1	200	790	990	890	12	20
		2- (1)	S2	200	980	1180	1080	14	20
		2- (2)	S3.1	200	1170	1370	1270	17	14
		2	S3.2	410	970	1380	1175	18	14
		2- (3)	S4.1	200	1360	1560	1460	20	10
		2	S4.2	400	1160	1560	1360	11	20
		2- (3)	S4.3	200	1340	1540	1440	6	14
		2	S4.4	600	960	1560	1260	6	30
		2	S4.5	800	750	1550	1150	5	40
		2*	S5.1	200	790	990	890	10	20
		2*	S5.2	200	790	990	890	10	5
		2*	S5.3	200	790	990	890	2	160
MVL15.1	15	2	S1.1	200	790	990	890	10	170
			S1.2	200	790	990	890	10	30
			S1.3	200	790	990	890	12	10
			S2	200	1000	1200	1100	10	30
MVL10.2	10	2	S1.1	600	720	1320	1020	11	100
			S1.2	400	930	1330	1130	10	50
			S1.3	200	1130	1330	1230	10	30
		2*	S2	200	730	930	830		30
MVL11.2	11	2*	S1	990	120	1110	615	4	180
		2*	S2	1010	280	1290	785	4	160
		2*	S3	1140	320	1460	890	1	120
		2*	S4	200	1250	1450	1350	4	30

(1) - preceded by 60 second pressure-hold step at p_{max}
(2) - preceded by 90 second pressure-hold step at p_{max}
(3) - preceded by 240 second pressure-hold step at p_{max}

3.5.2.2 Summary of results

Cyclic tests performed on the Merville site followed loading procedures relatively variable so that results cannot be synthesized through one single representative test. Instead, the following paragraphs present important observations from the different tests performed.

c) On test repeatability and the influence of the loading sequence

Test repeatability was verified by comparing results obtained in MVL 10.1 and MVL 10.2, performed at the same depth, located 3 meters apart in the horizontal plane. Figure 3.52a presents the loading program of both tests superposed. Analyzing the strain accumulation during the cyclic series, it can be observed that the sequence of loading did not significatively affect the final soil response. After 45 minutes of test, the plastic strain accumulation was nearly the same in both cases. Figure 3.52b presents the cavity expansion response for both tests, showing a good repeatability. It can also be observed that the series S1, S2.1 and S2.2 of test MVL 10.1 do not seem to disturb the response of the series S3 of the same test.

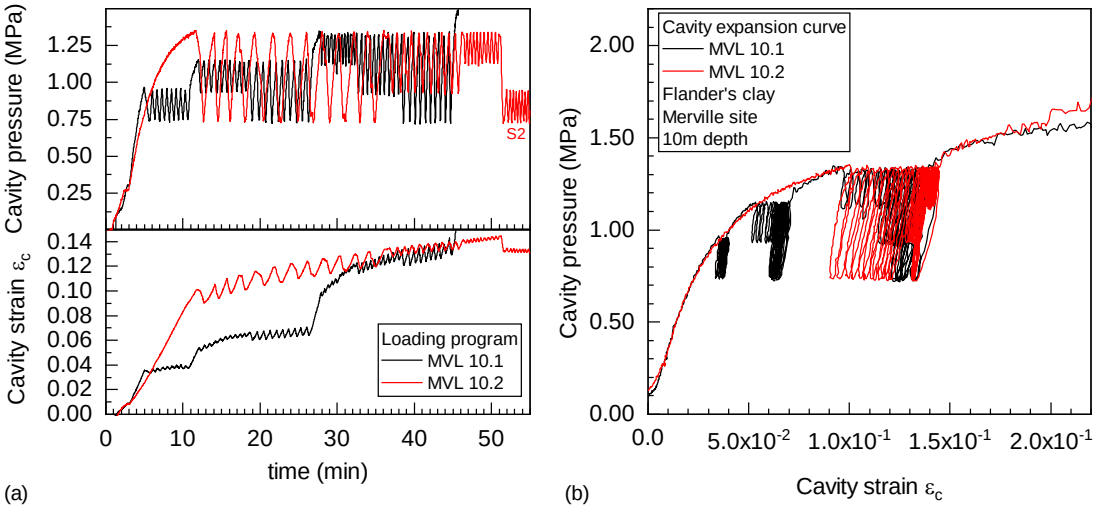

Figure 3.52 – Comparison between tests MVL 10.1 and MVL 10.2

It can also be observed that strain accumulation nearly ceases in series S2 in MVL 10.2, performed after the soil has been pre-sheared.

d) On the effect of increasing p_{mean} at constant amplitude

Figure 3.53 presents the strain accumulation for series MVL 14.1 S1, S2, S3.1, S4.1 and S4.3, all carried out at a constant amplitude of 200 kPa but at increasing mean pressure level. It can be observed that for this loading program the strain accumulation presents a quasi-linear trend with the number of cycles (Figure 3.53a), and that cycling at higher average pressures results in higher accumulation rates. In this plot, no trend of stabilisation could be observed. However, when the tests are analysed in function of the elapsed time since the maximum pressure before unloading has been reached

(Figure 3.53b), a behavior very similar to what is obtained during pressure-hold steps is observed.

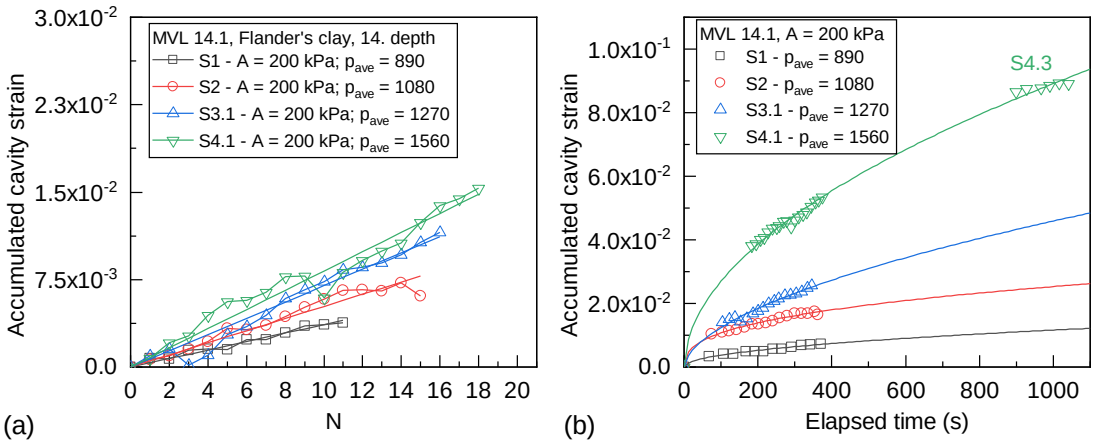

Figure 3.53 – MVL 14.1 test, series at constant amplitude of 200 kPa and increasing average pressure. (a) the influence of the number of cycles; (b) the influence of the elapsed time

e) On the effect of time

Figure 3.54 presents the loading program performed in test MVL 14.1 with a detail for the series S4. This series was preceded by a 240-second pressure-hold step and an intermediary pressure hold step was also performed between series S4.2 and S4.3. The cyclic strain accumulation presented in Figure 3.54b seems to follow an envelope similar to that of the plastic accumulation at a constant pressure p_{max}. Yet, increasing cyclic amplitude (which in this case means lowering the average load), seems to reduce the rate of strain accumulation over time. In this precise case, cycling seems not to induce more strain accumulation than time dependent phenomena.

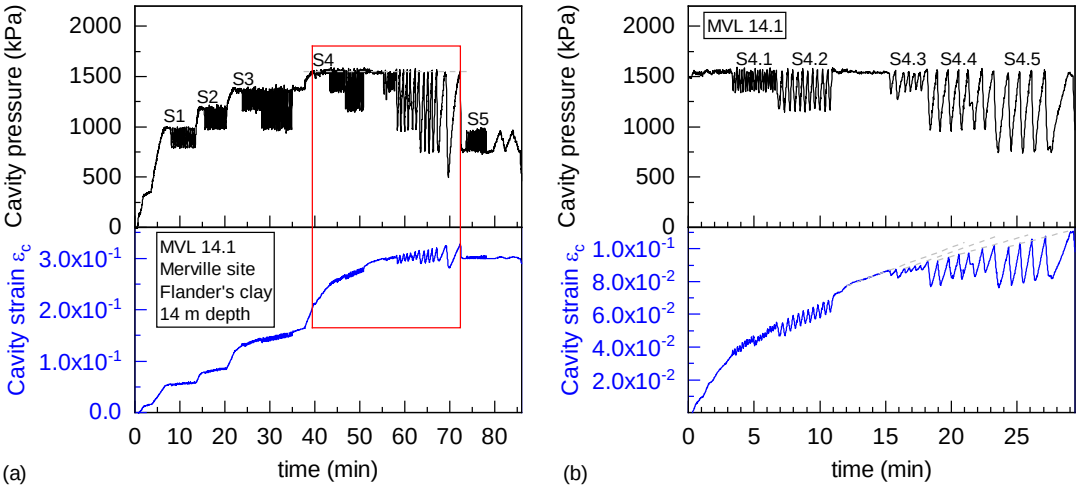

Figure 3.54 – Effect of time on the cyclic strain accumulation on test MVL 14.1. (a) the whole loading program; (b) detail of series S4 performed at a constant p_{max}

f) On the effect of cyclic frequency - after pre-shear

The effect of the shearing rate on the evaluated shear modulus was studied by performing cyclic series of same amplitude with different periods on test MVL 14.1 series S5. Cyclic series of periods T = 20 s, 5 s and 160 s were performed (in this order). Results are presented in Figure 3.55. Shear modulus was calculated as the average slope of all the points of the loops. It can be observed that cycles performed at shorter periods (higher frequency) result in higher shear modulus. This observation is in agreement with literature review on the behavior of clays. It could also be related to increases in PWP, which also reinforces the interest of having local measurement of PWP in the probe.

It can also be observed that series S5 did not present strain accumulation due to cyclic loading, differently from series S1, performed at the same stress level, but in a virgin soil state. This observation underlines the effect of the loading path on the strain accumulation.

These results show that using pressuremeters for assessing the relationship between soil stiffness and the rate of loading seems feasible. However, making measurements at shorter periods of time requires more developed sensors and data faster acquisition than those employed in this research. In that case, it would be recommended to: perform pressure and strain measurements locally on the probe instead of measurements at the ground level; improve measurement resolution; increase the rate of data acquisition.

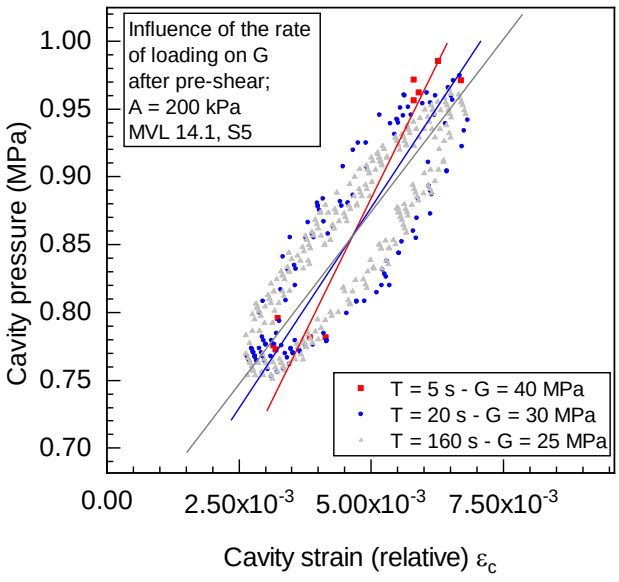

Figure 3.55 – Effect of the loading rate on the shear modulus evaluated from loops performed after pre-shearing the soil

g) On the effect of cyclic frequency - virgin loading

The effect of the loading rate was also studied in test MVL 15.1, series S1.1, S1.2 and S1.3. Results are presented in Figure 3.56. From the response versus time (Figure 3.56a), it can be observed that increasing the cyclic frequency does not change the rate of plastic strain accumulation.

Figure 3.56b presents the cavity expansion response during this cyclic series. Shear moduli were evaluated at each unload and reload path, as indicated by the red line and the green lines, respectively. It can be observed that the unload shear modulus G_U tends to decrease during cycling, and, inversely, the reload shear modulus G_R tends to increase as a function of the number of cycles. The evolution of shear moduli in function of the number of cycles is presented in Figure 3.57. From this figure it can be observed that the unload moduli and the reload moduli tend to converge after approximately 15 cycles. This is in agreement with what has been observed by Puech and Brucy (1982). In the present case, the cyclic shear modulus G_{UR} stabilizes at approximately 34 MPa. Evaluating the influence of the rate of loading on the shear modulus from this loading procedure is more difficult because of the superimposition of both strain accumulation and time dependency.

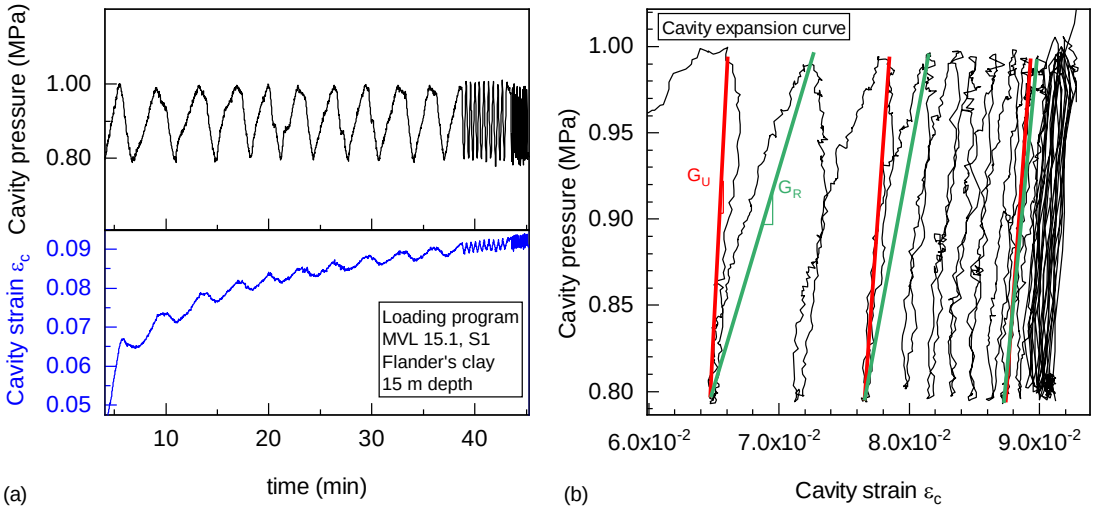

Figure 3.56 – MVL 15.1 test. (a) loading program and response of the cavity as a function of time; (b) cavity expansion response with detail to the unload and reload cyclic shear modulus, G_U and G_R

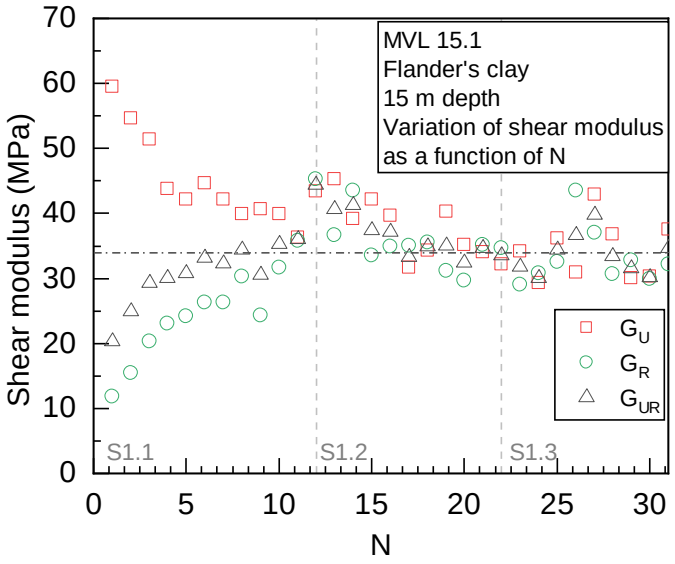

Figure 3.57 – Variation of cyclic shear modulus in function of the number of cycles for series S1 in MVL 15.1 test

h) On the effect of pre-shearing on strain accumulation

In order to investigate the influence of pre-shearing on strain accumulation, cycles of high amplitude were performed after having pre-sheared the soil to a pressure near its limit pressure in test MVL 11.1. Corresponding results are presented in Figure 3.58.

It can be observed that after the soil has been pre-sheared, the cyclic amplitude seems not to significatively contribute to the accumulation of cyclic strains. Instead, the proximity of the upper limit of the cyclic series (p_{max}) to the limit pressure seems to lead to significant accumulation. This can be easily observed by comparing series S1 with series S4 in the figure. Series S1 is of very high amplitude (higher than the limit of $2c_u$ mentioned by Wroth (1982)), but leads to no strain accumulation. On the other hand, series S4 of small amplitude (200 kPa) leads to severe accumulation. The importance of these results with respect to the perspectives of the evaluation of the behavior of piles under cyclic loading through pressuremeter tests will be discussed in Chapter 4.

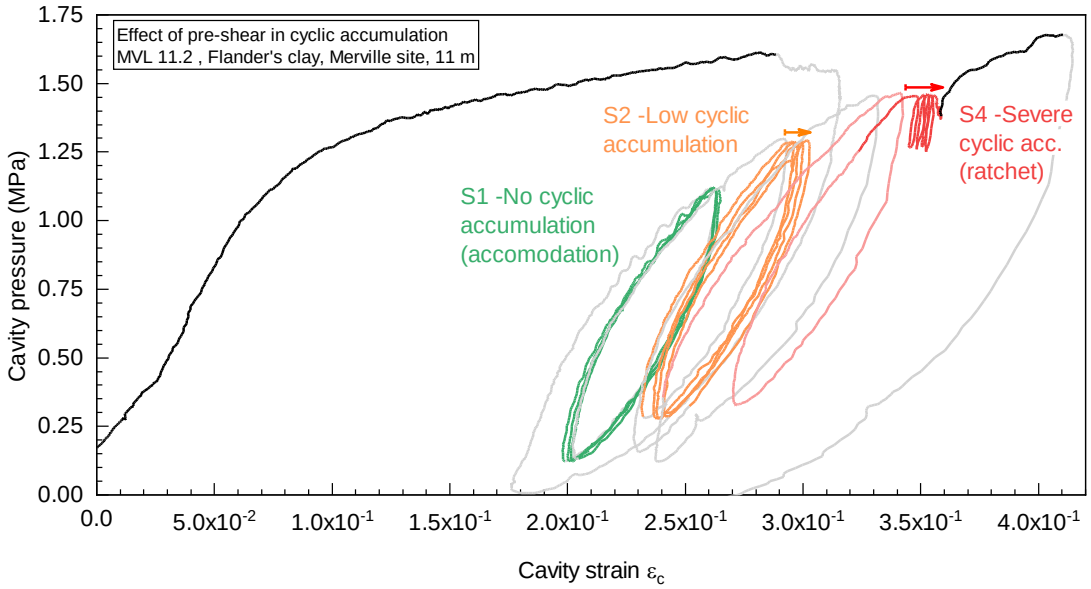

Figure 3.58 – MVL 11.2 test. Effect of pre-shearing on the cyclic strain accumulation

3.5.2.3 Concluding remarks

The cyclic tests performed at Merville site enabled understanding the behavior of clay under cyclic cavity expansion tests and confirming some aspects already presented in literature. With this exploratory campaign, it was possible to observe that (1) the cyclic loading sequence (increasing amplitude or decreasing amplitude) seems not to influence the final plastic strain accumulation. The independency on the loading sequence observed here is in agreement with what has been described by Puech and Garnier (2018) with respect to the elementary behavior of soils and piles under cyclic loadings. This observation opens perspectives to the applicability of damage laws to soil behavior, and that they can potentially be assessed using cyclic pressuremeter tests. This result also underlines the possible application of an "equivalent number of cycles approach" in pressuremeter loading programs (as schematized in Figure 1.7); (2) series of constant amplitude and increasing mean pressure result in increasing rates of plastic strain accumulation, similar to what is observed while performing pressure-hold steps at increasing pressure levels (time dependent behavior); (3) time dependent behavior (creep or consolidation) led to a higher rate of plastic strain accumulation than what could be induced by cycling. Differently from what has been observed in sands, increasing cyclic amplitude in clays did not "reactivate" strain accumulation. (4) pre-shearing the soil reduces significantly or even ceases accumulation. In series performed after pre-shearing, shear moduli dependency on loading frequency could be observed. The influence of loading frequency for cyclic series performed from a virgin state,

however, was shown to be masked by the mechanisms leading to cyclic mobility; (5) It has been shown that even very high amplitude cyclic series performed after the soil has been pre-sheared resulted in accommodated cycles. It seemed, however, that as p_{max} reaches the vicinity of the limit pressure, ratchet mechanism is triggered on. This behavior is fundamentally different from what has been observed in sands and provide meaningful insights with respect to the application of the pressuremeter test to the design of piles under cyclic loads.

SUMMARY AND PARTIAL CONCLUSIONS

The experimental procedures undertaken *in situ* in the context of the validation of the measurement capabilities of the Monocell FC ® probe to assess small strain shear modulus and cyclic properties of soils have been presented in this chapter. Tests were performed at two reference sites in which the soil layers had been previously characterized by other geotechnical investigation methods. The type of soils tested were dense sands at Dunkirk site and overconsolidated clays at Merville site. Two types of loading protocol were performed: 1) for assessing shear moduli at small strains and 2) for assessing cyclic properties.

It has been shown that standard Ménard pressuremeter parameters (Ménard modulus and limit pressure) could also be derived from the cavity expansion tests performed with the Monocell FC probe. These parameters were shown to be consistent with those derived from standard PMT tests performed in previous campaigns on the same sites. From this result, it can be concluded that the procedure proposed can be considered as complementary to the standard PMT procedure.

Loading protocol 1 led to satisfying results on both sites. The methods used for deriving the maximum shear modulus from each unload loop ($G_{max}(p_{cav})$), adjusting it to the average stress state around the cavity ($G_{max}(p')$) and then obtaining shear modulus degradation as a function of the average shear strain in the soil, $G_s(p',\gamma_{av})$, yielded consistent and representative results in comparison with the elementary properties of the soils found on site. In the case of sands, a strong dependency between modulus and cavity pressure before unloading was observed: higher pressure leading to higher modulus. This effect did not take place in tests in clays. Tests in sands resulted in stiffer

behavior, but a more accentuated stiffness degradation in function of the shear strain in comparison to results in clays.

With respect to the loading protocol 2, the latter enabled confirming the effect of cyclic amplitude, average pressure and loading path (pre-shearing or not) on the plastic strain accumulation, already observed in the laboratory for sands. The tests performed in clays showed fundamental differences with respect to those in sands, especially in what concerns the effect of cyclic amplitude after the soil has been pre-sheared.

It can be concluded that the proposed testing procedures associated with the testing equipment evaluated enable assessing elementary soil properties, reaching one of the goals of this research. As presented in the bibliographic review, these properties can be used for advanced geotechnical design. Examples of application of the pressuremeter tests proposed herein to engineering problems will be presented in Chapter 4.

CHAPTER 4

APPLICATION TO PILE DESIGN

INTRODUCTION

The study presented in the previous chapters has enabled confirming that assessing elementary elasticity properties of soils from pressuremeter tests is possible. This required the use of an innovative probe, presenting improved measurement capabilities, as well as the application of a special testing protocol and interpretation procedures. The practical aspects presented in the bibliographic review, that have historically made it difficult to obtain these parameters from standard PMT tests, could be overcome. It was also shown that this testing equipment can be used for performing series of repeated cyclic loads, yielding a soil response that is strongly correlated to the elementary behavior of soil under cyclic loading.

It has been shown in the bibliographic review that the design of piles under cyclic loading requires the determination of soil stiffness at small strain rates. At present, this was only possible through laboratory tests. The use of geophysical tests to characterize shear stiffness at very small strains is straightforward, but this method does not enable characterizing stiffness at intermediate strain levels and up to failure, which is also required for pile design.

In this chapter, it will be demonstrated how the pressuremeter procedures elaborated and tested in this work can be used for improving the design of piles under both static and cyclic axial loading. Focus will be put on the evaluation of pile head stiffness, local load transfer relationships and overall stability under cyclic loading.

4.1 OBTAINING PARAMETERS FOR CYCLIC PILE DESIGN

As presented in the bibliographic review, in French practice, the standard method used for the evaluation of the head load-displacement behavior of piles under monotonic loading is based on the results of standard Ménard pressuremeter tests. Despite the existence of other mobilization functions that depend on the elementary stiffness of the soil, such as those proposed by Randolph and Wroth (1978), Baguelin and Frank (1980), Kraft et al. (1981), practitioners have historically found it difficult to reliably obtain this parameter *in situ*.

In the recent SOLCYP recommendations for the design of piles under cyclic axial loading (Puech and Garnier, 2018), the behavior of the pile-soil interface is characterized as a function of the shear stiffness G of soil in the elastic domain (in the order of G_{max} to $G_{max}/2$).

It has been shown that this parameter can now be obtained using the pressuremeter procedure and equipment presented in the previous chapters. In this section, one will present how the results obtained with the pressuremeter at the reference testing sites (Dunkirk and Merville) can be used for the design of piles under monotonic and cyclic axial loading. Results obtained with the proposed approach will be compared with the results of full-scale monotonic and cyclic pile loading tests previously performed at these sites in the context of the SOLCYP project.

4.1.1 Description of the approach

When using pressuremeters to characterize soil behaviour with respect to the design of piles under cyclic axial loading, two different loading programs have to be performed, yielding two different sets of parameters. The first is the “Protocol 1”, including three or more unload loops, that enable deriving the shear stiffness of the soil at low strain levels. This protocol should allow obtaining parameters for characterizing the stiffness of the mobilization functions describing the pile-soil interaction. The second is the “Protocol 2”, that enables characterizing soil behaviour under series of repeated cycles. This should allow obtaining insights on the pile stability under cyclic loadings and parameters for the determination of the pile ultimate bearing capacity.

Protocol 1 has been well defined and validated for the determination of soil elementary stiffness in chapters 2 and 3. On the other hand, Protocol 2 (cyclic) enabled understanding soil response under cyclic loading, but it was not possible to quantify cyclic design parameters from it. As a consequence, in this chapter, focus will be given to what concerns the determination of pile stiffness under cyclic loading. Perspectives will be drawn with respect to stability domains.

The following approach is proposed for this study:

- The pressuremeter tests performed at limited testing depths on the reference sites enabled only partially characterizing the soils found on these sites. However, the study of pile behaviour requires that all soil layers crossed by the pile be characterized. In that manner, information gathered in precedent investigation campaigns held on the same sites will be used for complementing those obtained only with the pressuremeter;
- Values of pile ultimate skin friction and tip resistance were measured from static load tests performed on instrumented piles throughout the SOLCYP project (Benzaria (2013)). These values were adopted for the calculations presented herein, in which focus was brought to the determination of stiffness properties;
- Based on the previous statements, a soil profile reassembling stiffness and strength parameters was defined for each site. The stiffness parameters were those relative to the maximum shear modulus and Ménard modulus (enabling the application of the traditional approach). The strength parameters were the ultimate skin friction and the tip resistance;
- The established soil model was used to simulate pile behaviour using the load transfer method. Two types of mobilization laws were used: (1) Frank and Zhao (1982) mobilization laws, in which Ménard modulus is an input parameter and which has been successfully used by French practitioners in the past decades to simulate pile behavior under monotonic loading; (2) Randolph and Wroth (1978) and Baguelin and Frank (1980) mobilization laws, which are expressed in function of the elementary shear modulus of soil;
- The geometrical and mechanical properties of the real piles installed and tested on the sites (after Benzaria (2013)) were used for these simulations;

- The global pile responses (pile head load versus displacement) calculated with both approaches are compared with measurements obtained on piles subject to monotonic and cyclic loadings.

4.2 APPLICATION TO PILES INSTALLED IN SANDS – DUNKIRK AND LOON-PLAGE SITES

4.2.1 Description of the adopted soil model

Pile tests were performed at Loon Plage testing site, which is a neighbouring site (about 10 km apart) to Dunkirk, where the pressuremeter tests were performed in the context of this thesis. The same sand is found at both sites, and their mechanical properties can be considered as similar at depths between 6 and 12 meters, as presented in Chapter 3.

It has been shown that the pressuremeter tests performed at Dunkirk yielded values of maximum shear moduli close to the lower bound of the values obtained in other campaigns. It could be seen in Figure 3.40 (page 192) that moduli evaluated using the Monocell FC probe were close to those evaluated by Chow (1997) using seismic cone penetration test (SCPT), which, in turn, are close to those obtained by correlation with CPT q_c profile using Baldi *et al.* (1989) equation (3.1). For this reason, in this chapter the profile of maximum shear modulus at Loon Plage site will be evaluated by application of Baldi *et al.* (1989) correlation with the CPT profile available. It is assumed with a reasonable level of confidence that this profile is representative of what would be measured on site if the new pressuremeter approach had been applied to its characterization.

The soil profile considered for the calculation model at Loon-Plage is presented in Figure 4.1. The CPT profile and the averaged values of q_c per layers are presented in Figure 4.1a. Figure 4.1b presents the profile of shear modulus evaluated using standard Ménard pressuremeter tests from precedent campaigns on site and the maximum shear modulus derived from the CPT correlation. Figure 4.1c presents the ultimate skin friction derived from local measurements on the instrumented pile F4. In the case of pile B2, ultimate skin friction was not directly measured using local instrumentation. It was estimated in this study based on the results of dynamic pile driving analysis presented by Benzaria (2013).

Table 4.1 – Summary of the model parameters for pile F4 at Loon Plage site

Layer base (m)	Ult. skin friction (pile F4) (kPa)	*(pile B2)* ***(kPa)***	*Tip resistance* (pile F4) *(kPa)*	*Ave. E_M* (MPa)	*Ave. G_M* (MPa)	*Ave. q_c* *(MPa)*	*Ave. G_{max}* (MPa)
-1.0	62	30		9	3.4	16.5	29
-2.5	84	30		4	1.5	1.7	29
-4.0	32	30		4	1.5	4.3	48
-5.5	28	30		9	3.6	13.9	74
-6.3	40	30		14	5.1	8.0	68
-7.5	44	50		14	5.1	18.4	87
-12.0	70	150	3300	19	7.1	33.7	118
<-13.0		60		2	0.8	1.7	46

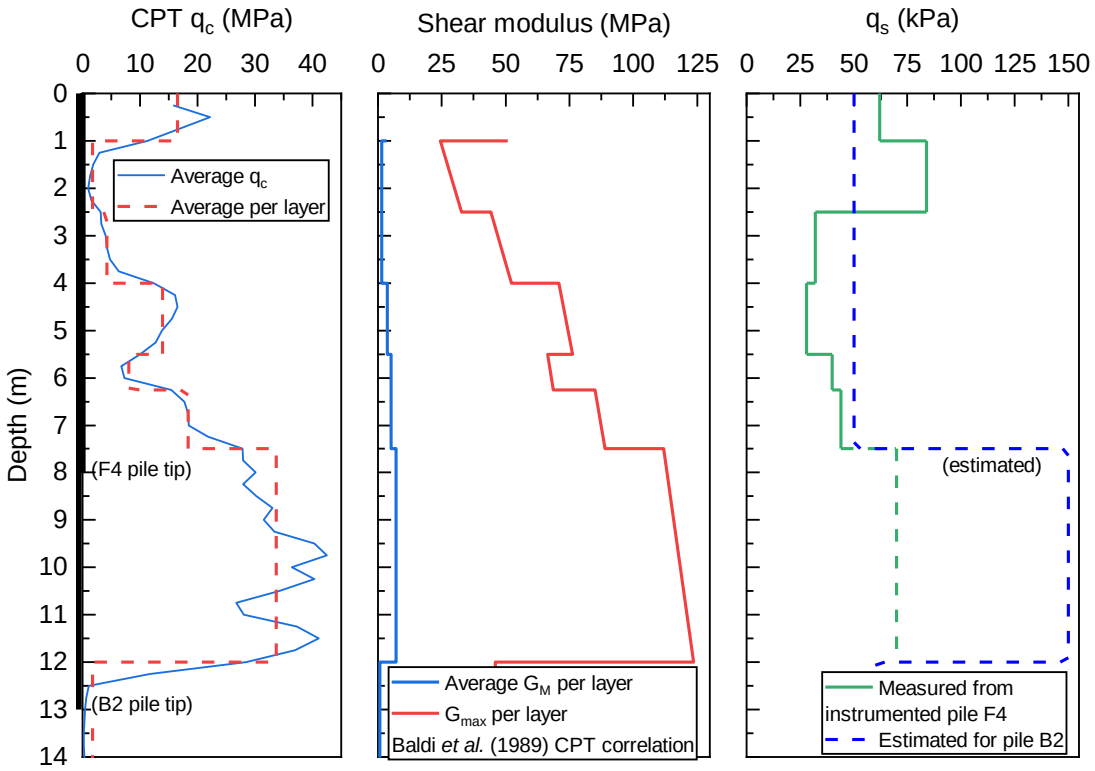

Figure 4.1 – (a) CPT averaged profile; (b) Ménard modulus (measured) and *G_{max}* (from CPT correlation) profile; (c) ultimate skin friction measured from instrumented pile load test (pile F4)

4.2.2 Presentation of the studied piles

Benzaria (2013) presented the results obtained from several cyclic axial loading tests performed in bored and driven piles built at the Loon Plage site. In this study, the results of pile F4 and B2 presented by this author will be analysed.

Pile F4 is a continuous flight auger (CFA) pile (reinforced concrete), of diameter B = 420 mm and embedded depth of L = 8 meters. The pile was first submitted to a static compression load test and, after being unloaded, it was submitted to several cyclic series. Other static load tests were performed in order to verify the effect of the cyclic loading on the pile bearing capacity. The loading program performed is presented in Table 4.2 and the resulting pile response in Figure 4.2.

Pile B2 is a driven closed-end steel tube, of diameter B = 406 mm, 15 mm thickness and embedded length of L = 13 meters. Pile was submitted to the loading program presented in Table 4.3. Static tests were performed according to French standard on pile load testing (NF P94-150-1, -2), including long load steps; in tests indicated as "rapid", load steps were 180 seconds long, and load was increased in 20 seconds between them. The resulting response is presented in Figure 4.3.

Table 4.2 – Loading program (compression) performed on pile F4 at Loon Plage site after Benzaria (2013)

Test	**Type**	***f*** (Hz)	V_m (kN)	V_c (kN)	***N***	V_r (kN)
L-F4/CS1	Static					980
L-F4/CC1	Cyclic	0.5	180	130	1879	
L-F4/CR1	Static (rapid)					973
L-F4/CC2	Cyclic	0.5	280	140	200	
L-F4/CC3	Cyclic	0.5	270	200	200	
L-F4/CC4	Cyclic	0.5	330	200	100	
L-F4/CC5	Cyclic	0.5	330	260	200	
L-F4/CR2	Static (rapid)					975
L-F4/CR3	Static (rapid)					1500
L-F4/CC6	Cyclic	0.5	500	400	38	
L-F4/CC7	Cyclic	0.5	500	300	300	
L-F4/CR4	Static (rapid)					

Table 4.3 – Loading program (tension) performed on pile B2 at Loon Plage site after Benzaria (2013)**.**

Test	**Type**	***f*** (Hz)	V_m (kN)	V_c (kN)	***N***	V_r (kN)
L-B2/TC1	Cyclic	0.5	500	380	20	
L-B2/TC2	Cyclic	0.5	500	300	750	
L-B2/TC3	Cyclic	0.5	500	380	500	
L-B2/TC4	Cyclic	0.5	500	450	1105	
L-B2/TS1	Static (rapid)					

In the tables above, V_m is the average load applied at the pile head, V_c is the cyclic component of the load, V_r is the bearing capacity assessed from static loading, f is the frequency and N is the number of cycles.

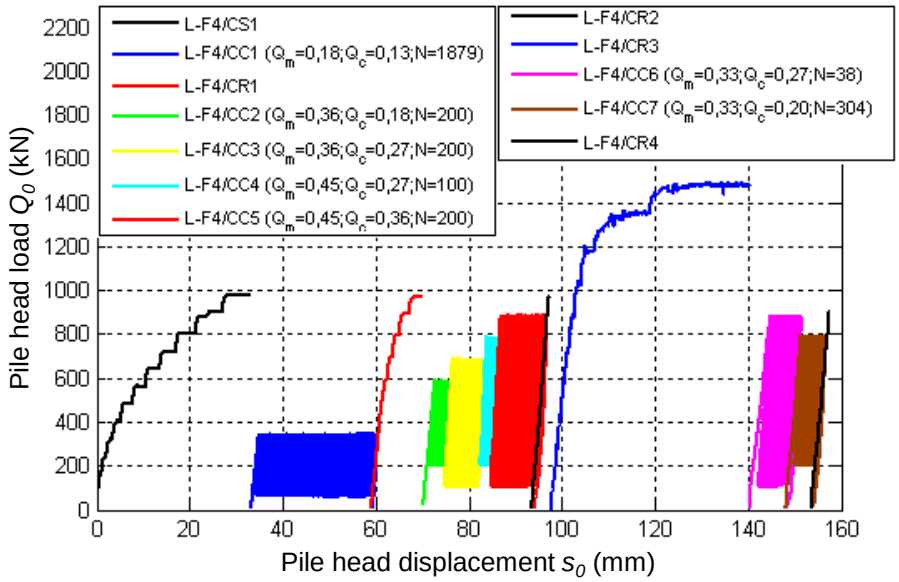

Figure 4.2 – Loading program performed on CFA pile F4 at Loon Plage site (Benzaria, 2013)

With respect to the stiffness of the pile F4 head load-displacement behaviour, it can be noticed that the first static loading (CS1) is significantly less stiff than the subsequent ones (CR1, CR2, CR3 and CR4). The pile response obviously stiffens due to the cyclic loading. With respect to the bearing capacity, it was observed that pile tip has progressively mobilized as the pile settled due to cyclic loading, leading to an increase in bearing capacity, but associated to very high values of head displacements.

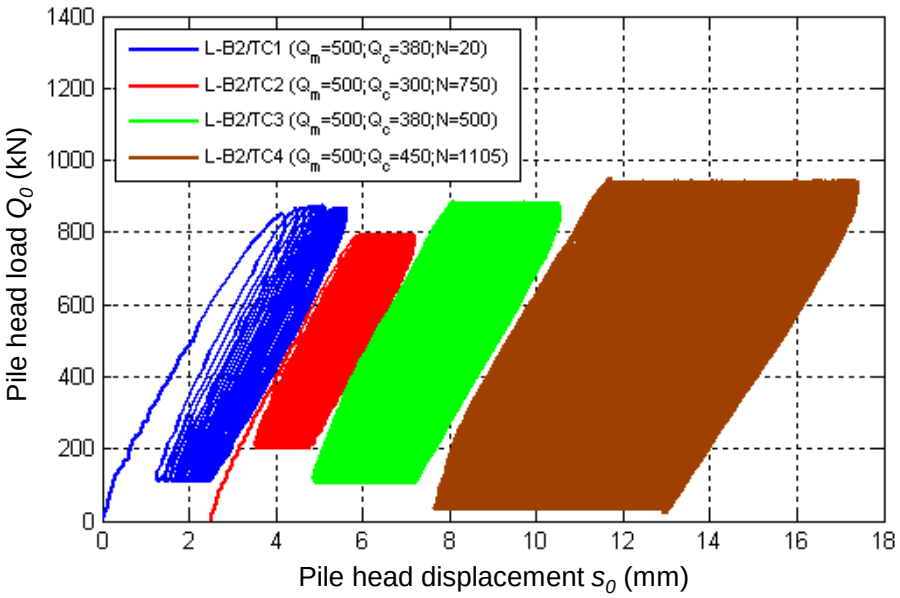

Figure 4.3 – Loading program performed on driven pile B2 at Loon Plage site (Benzaria, 2013)

4.2.2.1 Aspects related to the pile stiffness

Benzaria (2013) calculated the stiffness of the pile head response K_c within each cyclic series and its evolution with the number of cycles. K_c is defined for each cycle according to eq. 4.1, in which $Q_{0_{min,N}}$ and $Q_{0_{max,N}}$ are the minimum and maximum load applied at the pile head at a cycle N, and $s_{0_{min,N}}$ and $s_{0_{max,N}}$ are the associated pile-head displacements.

$$K_{c,N} = \frac{Q_{0_{max,N}} - Q_{0_{min,N}}}{s_{0_{max,N}} - s_{0_{min,N}}} \tag{4.1}$$

In the case of the CFA pile F4, the author obtained a general trend of increase (in average between 5 % to 10 %) in the stiffness of the pile-head response within the first 30 cycles followed by a stabilization. It was not possible to establish a reliable relationship between pile-head stiffness and the loading level, because it is likely that one cyclic series has influenced the results of the following one. The average cyclic stiffness obtained during the first series (CC1) was approximately $K_{c,cc1}$ = 290 kN/mm; the average stiffness obtained during the last cyclic series (CC7) was $K_{c,cc7}$ = 380 kN/mm. Averaging all the cyclic series, $K_{c,ave}$= 340 kN/mm.

The evolution of pile-head stiffness during this series of tests in pile F4 is presented in Figure 4.4. In this figure, the static load tests CS1, CR1 to CR3 were superposed starting from the same origin point. A red dashed line of slope $K_{c,ave}$= 340 kN/mm is also represented.

From this figure, it can be noticed that the pile head stiffness increases, tending to an "average cyclic stiffness".

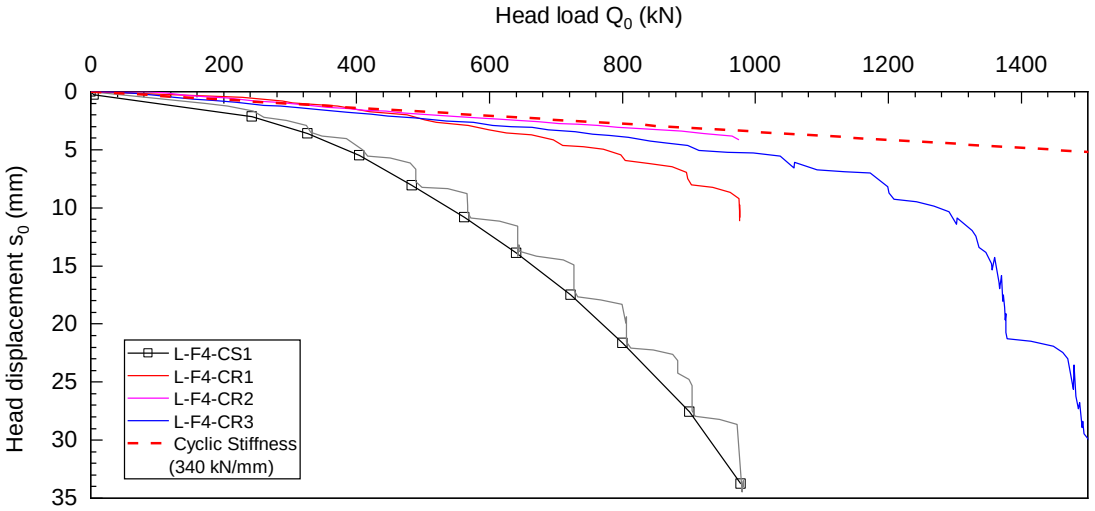

Figure 4.4 – Comparison between the different static compression load tests performed in F4 pile (adapted from Benzaria (2013))

In the case of pile B2, there was a slight reduction of the pile-head stiffness in function of the number of cycles. The average stiffness of all the cyclic series was $K_{c,ave}$ = 230 kN/mm.

Figure 4.5 presents a comparison between the first tension loading in pile B2 (L-B2-TC1) and the last static tension load test (series L-B2-TS1, not presented in the previous figure). It can be seen that in this case, the stiffness obtained in the first loading, in the last loading and the average cyclic stiffness are similar.

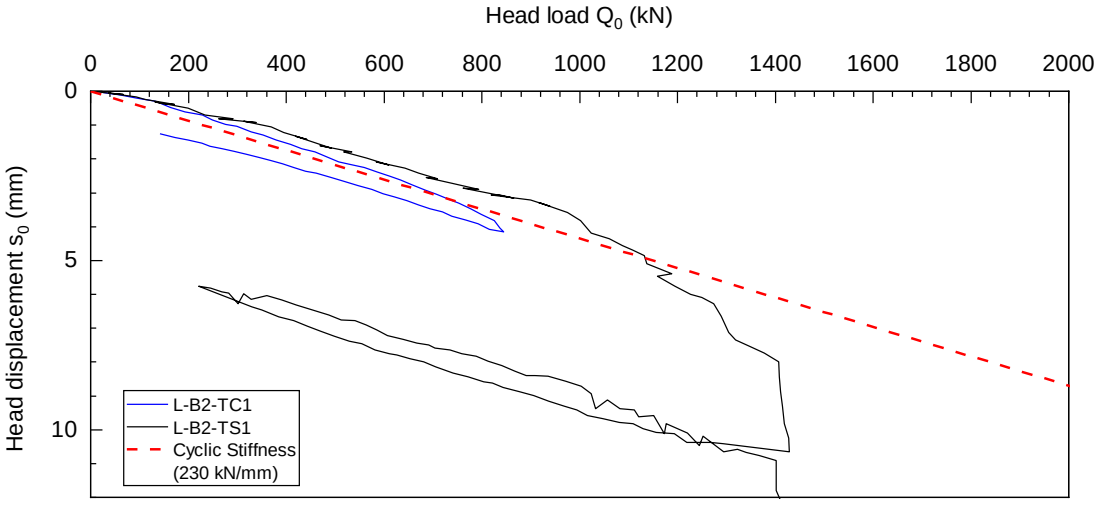

Figure 4.5 – Comparison between the first and the last tension load tests performed in pile B2 (adapted from Benzaria (2013))

4.2.2.2 Aspects related to the pile stability

Cyclic stability charts obtained by Benzaria (2013) for the bored piles under one-way compression tests at Loon-Plage site are presented in Figure 4.6. In that case, the failure criteria under cyclic axial loading is associated to a pile head displacement of 3% of the pile diameter after N_f cycles. If this criterion is reached for a number of cycles N_f smaller than 100, the pile is considered as unstable; if it is reached between 100 and 1000 cycles it is considered as metastable; and if it is not reached within 1000 cycles, it is considered as stable. From Figure 4.6,it can be noticed that the stable domain is very narrow.

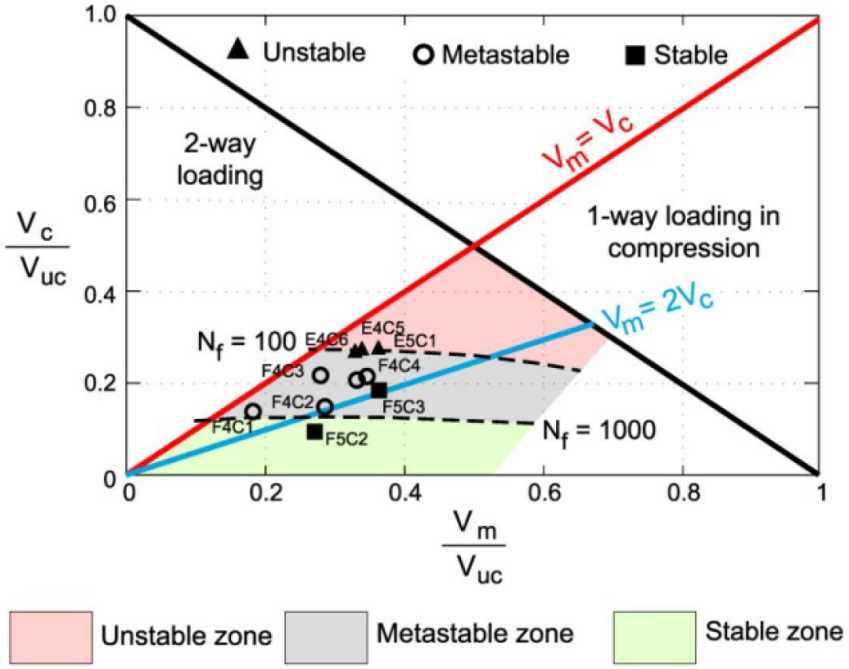

Figure 4.6 – Cyclic stability diagram for bored piles under one-way compression tests at Loon-Plage (from Puech and Garnier, 2018)

A stability diagram for driven piles in sands was established by Jardine and Standing (2012) based on the piles tested at Dunkirk site, here considered as having equivalent soil properties as Loon-Plage. The resulting chart is presented in Figure 4.7.

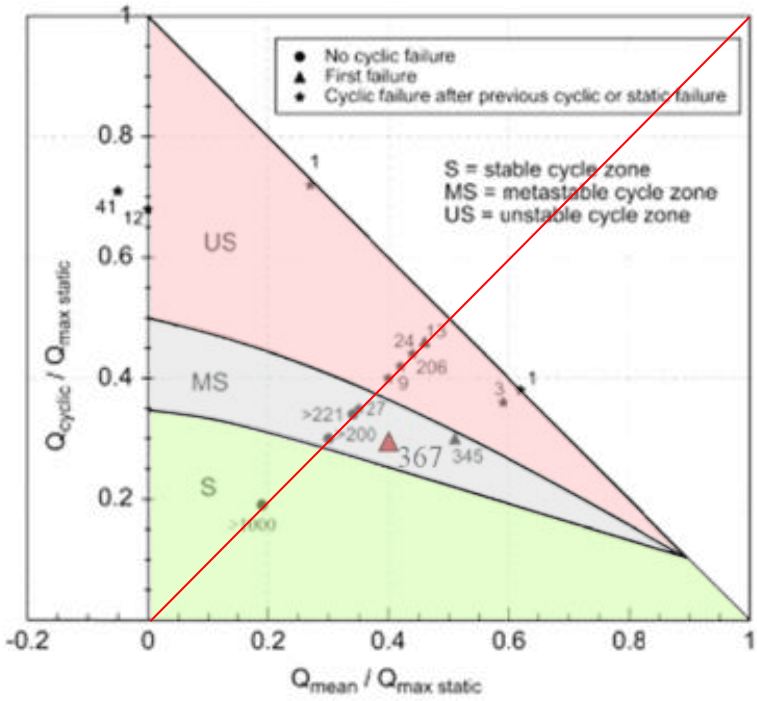

Figure 4.7 – Cyclic stability diagram for driven piles installed at Dunkirk site (adapted from Jardine and Standing, 2012 and Benzaria, 2013)

One very clear difference that can be observed between the two diagrams is that the stability zone is increased in the case of driven piles with respect to bored piles.

Parameters related to the rate of degradation and the generation of permanent displacements were calibrated within the framework of the SOLCYP project (Puech and Garnier, 2018), based on the pile response to tension cyclic loading measured at Dunkirk and Loon-Plage sites. The parameters calibrated are those that can be used as input for calculations using the SCARP software (Poulos, 1989b)), as described in the bibliographic review. These parameters will be reminded in section 4.2.4, in which a similar exercise was performed based on the results of the pressuremeter tests.

4.2.3 Modelling the pile-head response under monotonic and cyclic loading

4.2.3.1 Local analysis

Benzaria (2013) presented the skin friction and tip resistance mobilization functions derived upon the first monotonic static load test performed on pile F4, which had its shaft instrumented with removable extensometers enabling measurements of deformation along pile depth. The results obtained are presented in Figure 4.8. It can

be seen that the local measurements confirm that the pile behaviour was relatively soft: relative displacements of the order of 20 mm were necessary to fully mobilize skin friction in pile segments between 3 to 7 meters depth. On the other hand, the mobilization of skin friction on the two first meters of the pile shaft was much stiffer, possibly related to the peak in CPT cone resistance on the first meters.

In the present study, pile F4 was modelled using the load transfer method applying the mobilization functions proposed by Frank and Zhao (1982) (using standard Ménard pressuremeter modulus E_M as input) and those by Randolph and Wroth (1978) (using the $G_{max,0}$ profile that could have been established with the new pressuremeter procedures as input). Those mobilization functions were computed along the entire pile shaft profile and at its tip. Figure 4.9 illustrates the mobilization functions computed at 2 m, 5m, 7m and at the pile tip. There were no mobilization functions measured for pile B2.

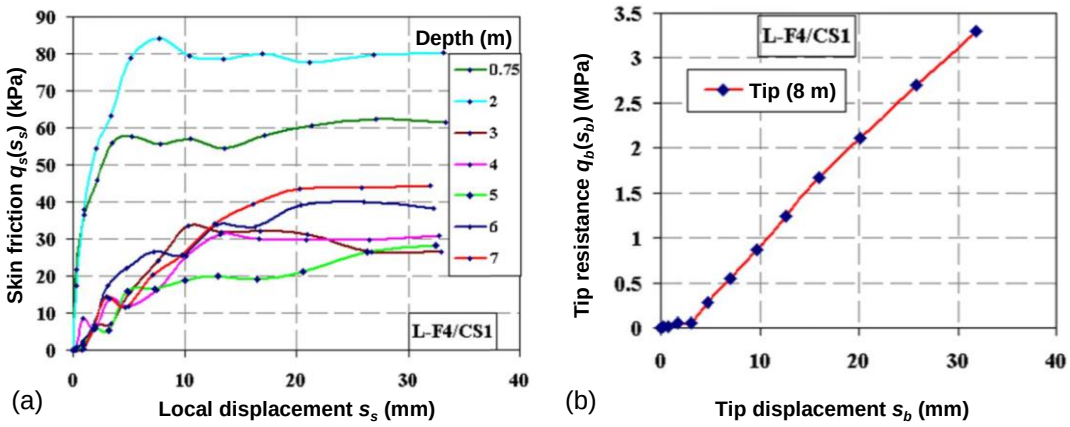

Figure 4.8 – (a) Skin friction and (b) tip resistance mobilization functions measured under monotonic static load test on instrumented pile F4 in dense sand, after Benzaria (2013)

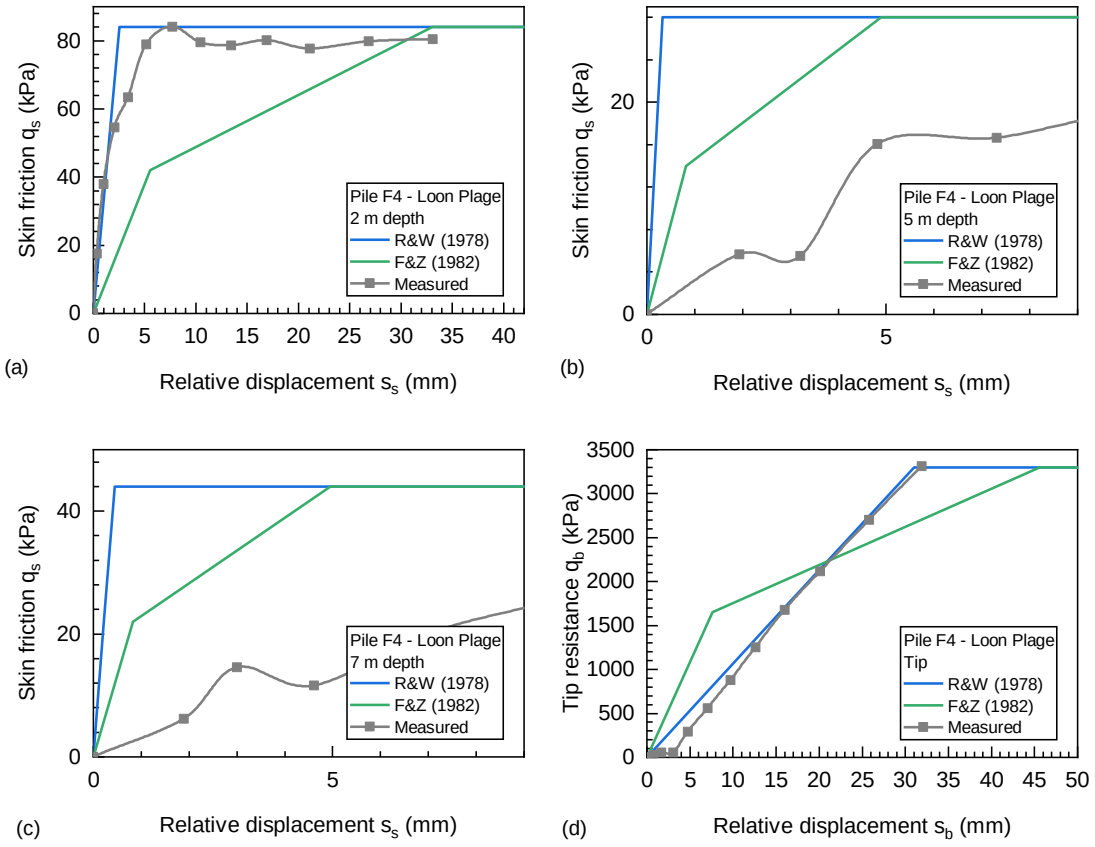

Figure 4.9 – Computed mobilization functions at 2m, 5m, 7m and at pile tip. Comparison with measurements on pile F4 obtained by Benzaria (2013)

Comparing the computed mobilization functions, it can be concluded that, with the exception of the pile tip, Frank and Zhao (1982) functions provide a softer local response. Between 5 and 7 meters, the friction mobilization measured was much softer than that computed at these same depths. This observation is general for the rest of the pile shaft, even if the curves are not presented herein. At 2 meters depth and at the pile tip, Randolph and Wroth (1978) model provided a local stiffness close to the measured one.

This analysis leads to conclude that, for the CFA pile installed in sand, the simulation of the measured local behaviour at virgin loading using the two types of mobilization functions is uncertain. In next section, the global behaviour will be simulated by integrating local responses along the shaft. It should also be noticed that there were no measured mobilization functions available for pile behaviour during cyclic loading.

4.2.3.2 Global analysis

a) Case of pile F4

The pile head load-settlement behaviour was simulated using a finite difference software that implemented the mobilization functions previously presented. For these calculations the Young's modulus of the pile was considered E_b = 20 GPa, B = 0.42 m and L = 8 m for pile F4. Results are presented in Figure 4.10.

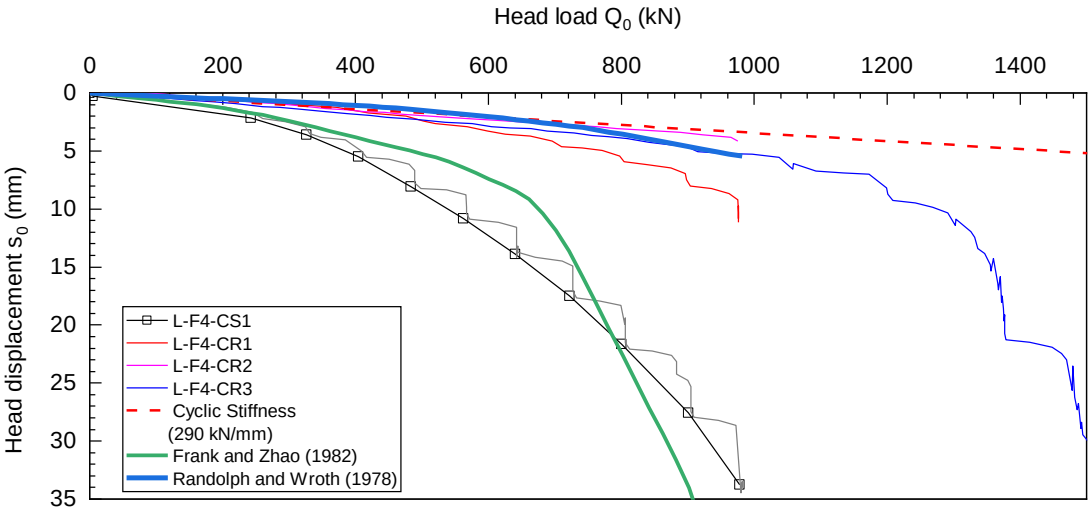

Figure 4.10 – Results of the global analysis of the pile F4 head load-displacement response compared to measurements

From the presented results, it can be noticed that the response obtained using Frank and Zhao (1982) mobilization function is close to that of the pile under first static loading. This was expected after the bibliographic review and confirms the adequacy of this method for evaluating the behaviour of piles under monotonic loading. On the other hand, the global stiffness obtained using Randolph and Wroth (1978) mobilization functions is closer to that of the pile under cyclic loading.

b) Case of pile B2

Pile B2 was modelled considering the Young's modulus of steel equal to 210 GPa, $B = 0.406$ m, a wall thickness of 15 mm and $L = 13$ m. The obtained response is presented in Figure 4.11.

In this case, since the pile-head stiffness does not evolve (or very little) along the cyclic loading, Randolph and Wroth (1978) mobilization function, yielding a stiffer response, seems better suitable for modelling the pile behaviour. It appears in that case that the pile installation process (driving) has stiffened the pile response, similarly to a pre-loading.

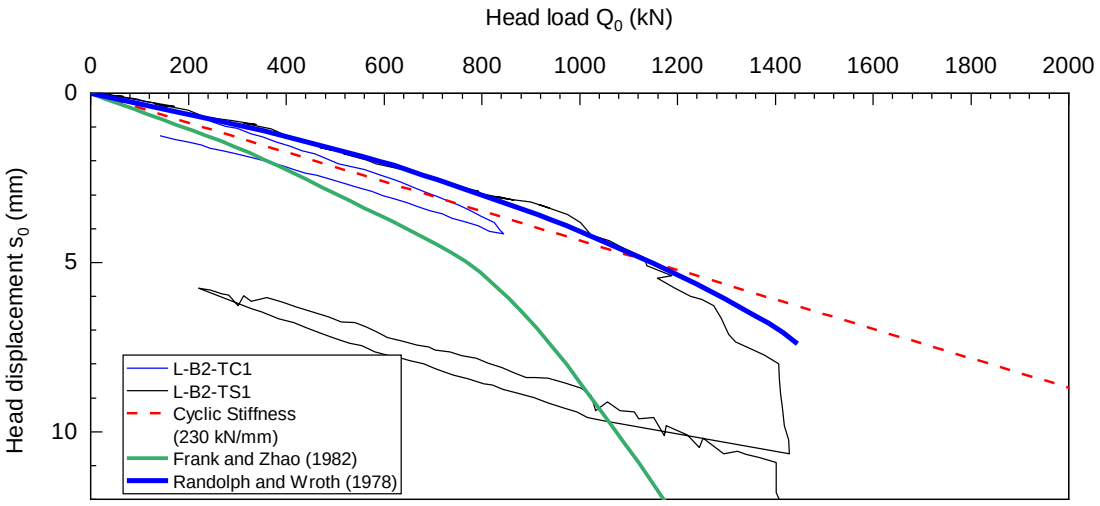

Figure 4.11 – Results of the global analysis of the pile B2 head load-displacement response compared to measurements

If a structure is supported by piles and transmit a cyclic load to the pile head, pile response will be governed by the so-called cyclic stiffness. With reference to Figure 4.10 and to Figure 4.11, the cyclic stiffness is represented by the slope of the red dashed line. Simulating global pile response using soil stiffness at small strains and mobilization functions defined for elastic properties seems to be better suited for problems involving soil-structure interaction under cyclic loading

4.2.4 Aspects related to pile stability and pressuremeter results

In this section, an attempt is made to correlate the behavior assessed using cyclic pressuremeter tests and the pile response observed under cyclic axial loading. The cyclic pressuremeter tests performed in sands, either in calibration chamber or on site,

presented in Chapters 2 and 3 highlighted the following important aspects related to plastic strain accumulation along the tests:

- Increasing the cyclic pressure amplitude starting from an initial at-rest state leads to an increase in the rate of plastic strain accumulation as a function of the number of cycles;
- Cyclic series of small amplitude performed after having pre-sheared the cavity yield no or very limited plastic strain accumulation. Increasing the cyclic pressure amplitude after having pre-sheared the soil can 'reactivate' the accumulation mechanisms;

These observations could be represented in an analogue of a cyclic stability chart in Chapter 2. Actually, this behavior can be explained using cylindrical cavity expansion theory in elasto-plastic soils respecting a Mohr-Coulomb failure criterion. According to the theory, plasticity will develop around the cavity if the following criteria are reached:

- On the first loading, if the cavity pressure reaches a value greater than p_y (pressure for start of yielding around the cavity). In granular soils starting from a horizontal pressure at-rest p_0, it can be shown (see Yu (2000), for example) that the initiation of yielding takes place according to eq. (4.2);

$$p_y = p_0(1 + sin\varphi') \tag{4.2}$$

- During unloading from a given cavity pressure p_{cav} greater than p_y, if the unloading factor reaches a value k x p_{cav}, soil fails in extension. Wroth (1982) presented the solution for calculating the limit amplitude $A_l = k$ x p_{cav}, eq. (4.3).

$$A_l = \frac{2sin\varphi'}{1 + sin\varphi'} p_{cav} = k\, p_{cav} \tag{4.3}$$

These domains can be represented on a schematic pressuremeter cavity expansion curve and translated into limits in an analogous stability chart, as presented in Figure 4.12. Analytical solution of cavity expansion problem enables drawing the four following limits in the quoted figure: **(1)** the average pressure must be higher than the horizontal pressure at-rest ($p_{mean} > p_0$); **(2)** Soil yields when the maximum cavity pressure exceeds p_y defined in eq. (4.2). It happens if ($p_{mean} + A/2 = p_y$); **(3)** there exist a lower bound

limit for the minimum cyclic pressure below which soil fails in extension. This limit is given by eq. (4.3), knowing that $p_{cav} = p_{mean} + A/2$. **(4)** There is a maximum cyclic amplitude for which either the upper or the lower boundary will be touched. It can be calculated with eq. (4.3) for $p_{cav} = p_l$. It corresponds to the maximum pressuremeter amplitude that the soil can support before failing.

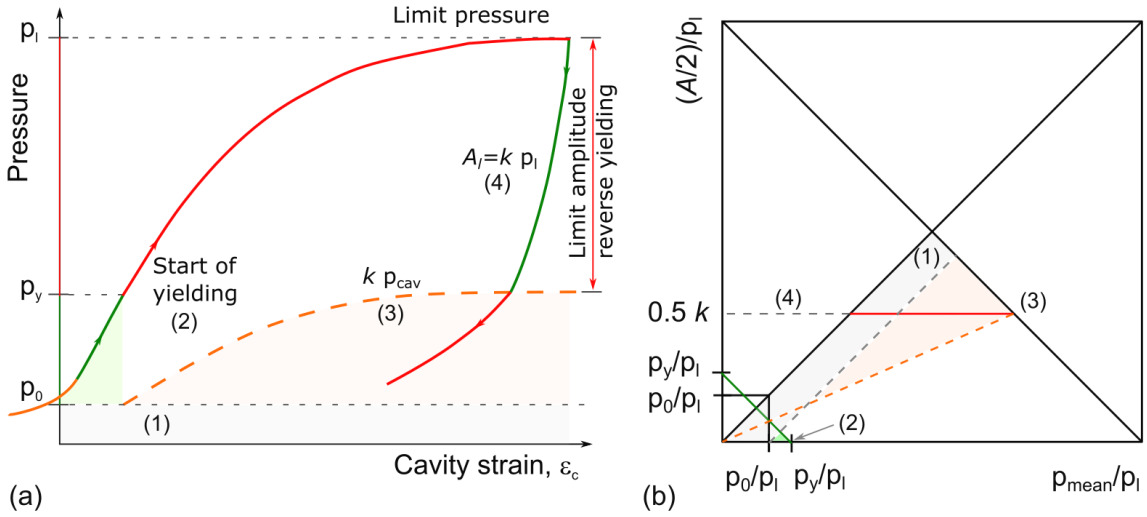

Figure 4.12 – Representation of a schematic pressuremeter curve into an analogous stability chart

The representation of the elasticity domains in the analogous stability chart of Figure 4.12b should be read as follows: the grey zone (1) comprises pressure levels lower than the initial pressure at-rest and it is likely that it will not be tested with pressuremeters. The narrow green zone (2) represents the elastic domain at-rest. The green zone can be expanded through the white adjacent zone by loading and unloading the cavity. The orange zone (3) represents the zone at which soil fails in extension, due to excessive unloading.

It has been observed from the pressuremeter tests carried out in this thesis that cyclic series performed in the elastic domains will lead to little strain accumulation. On the other hand, cyclic series that are adjacent to the plasticity boundaries (2, 3 or 4) will lead to significative accumulation. Yet, series crossing from one domain to the other will also lead to strain accumulation. Some of these experimental observations are presented in Figure 4.13

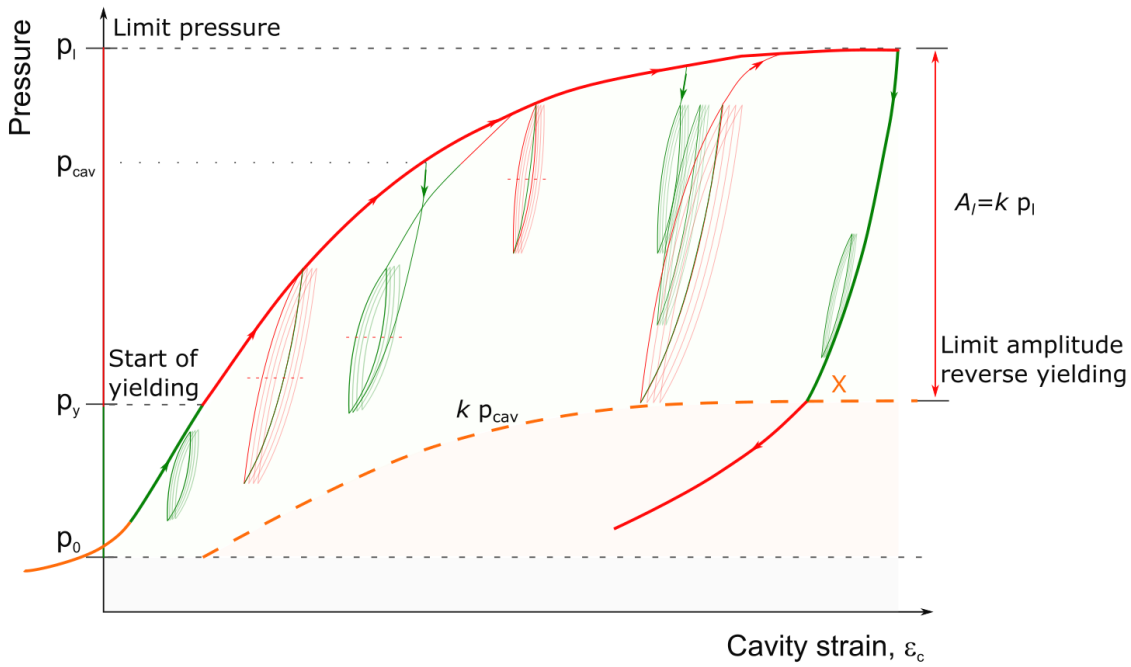

Figure 4.13 – Elastic domains for a pressuremeter test in granular soil. Green cycles: elastic domain; Red cycles: tangent to plasticity boundary

The evolution of the theoretical elastic domains presented in Figure 4.13, given the boundaries delimited by equations 4.2 and 4.3, can be translated into an analogous stability chart, as illustrated in Figure 4.14. With reference to this figure, (a) refers to the soil state at-rest. The cavity can be elastically loaded only within a very narrow domain, delimited between the horizontal pressure at-rest p_0 and the pressure for initial yielding p_y. It can be seen in (b) that when the cavity is progressively loaded to pressure levels $p_{cav,i}$ greater than p_y, the elastic domain for cyclic loading is extended. It reaches its maximum extent in (c), when the cavity is brought to failure. At this point, the cyclic amplitudes that can be supported within the elastic domain are maximum. If the cavity is unloaded to pressure levels outside this elastic domain, the stability zone will move back, leading to the initiation of a new plastic zone around the cavity, as presented in (d). After full deflation, it is not possible to know, based only on the presented equations, if the lower boundary is "erased".

From the elements presented above, it can be concluded that cyclic loading paths starting from a virgin state will lead to soil yielding at very small amplitudes. Pre-shearing the soil extends the area in which elastic cycles can be performed. This conclusion is analogous to the results measured in non-displacement and displacement piles in sands at Loon Plage site: the CFA pile presented a small stability zone and an

important bearing capacity degradation, while the stability zone of the driven pile was larger.

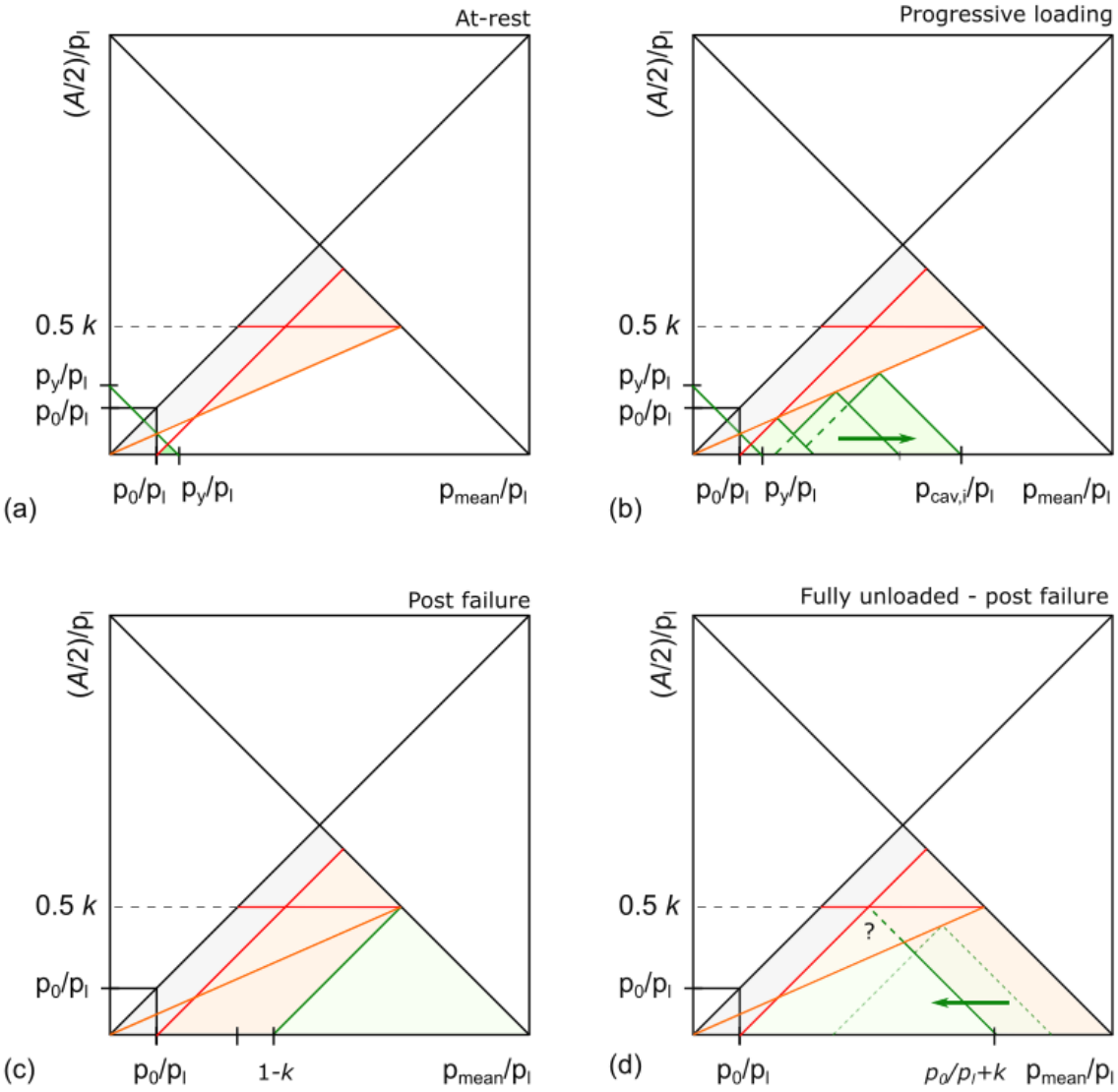

Figure 4.14 – Elastic and plastic zones in an analogous stability chart for cyclic pressuremeter test

Based on what has been exposed, it can be noticed that the elasticity (or stability) domain in sands evolves according to the cyclic loading path. It reaches a maximum when the soil is loaded near failure, but it can be reduced after unloading. Moving from elastic domain to plastic one initiates strain accumulation. If this logic is to be applied to pile-soil interaction, it can be inferred that local strain accumulation will generate displacement accumulation at a global level and thus, should be avoided in order to ensure pile safety.

With respect to the determination of the ultimate pile resistance under cyclic loading based on pressuremeter tests, the problem is more complex than in the case of piles

under monotonic loading. While in the case of piles under monotonic loading the ultimate skin friction and tip resistance can be directly (empirically) related to the limit pressure of the soil, in the case of piles under cyclic loading, these parameters must be related to the size of a stability zone, for a given loading level.

In this manner, pile design for cyclic loads in sands should be carried out as a way to answer the following question: for a given local average skin friction, which is the maximum skin friction amplitude that can be supported without slipping? The stability domains obtained with the pressuremeter could thus be related to the pile local cyclic capacity, as presented in Figure 4.15. The maximum cyclic amplitude is that represented by the red arrow (a).

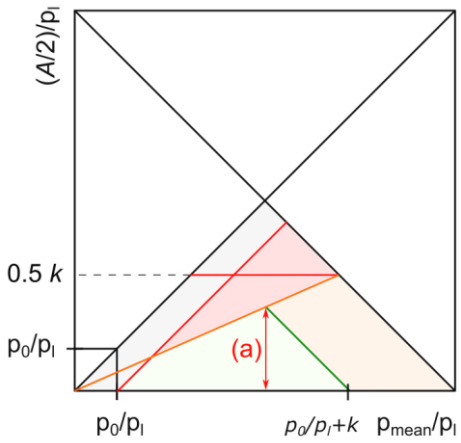

Figure 4.15 – Insight on how using cyclic pressuremeter tests to evaluate the loss in bearing capacity of piles

The limits of the areas in the graphics of Figure 4.14 can be analytically determined if the friction angle of the soil and the horizontal pressure at-rest are known. When those parameters are unknown (most cases), the results of cyclic pressuremeter tests can be used as an estimate. As an example, Figure 4.16 presents the cavity strain accumulated after the five first cycles of the pressuremeter tests performed in Dunkirk. The position of the lines was estimated, given the known effective friction angle of Flander's sands ($\varphi' = 31^o$). In all the cases, strain accumulation increases as the loading path approaches a plasticity boundary (dashed lines). By comparing Figure 4.16a (after pre-shearing) and Figure 4.16 c (at virgin loading) it can be observed that pre-shearing reduces the strain accumulation: there is more accumulation in graphic (c) than in (a).

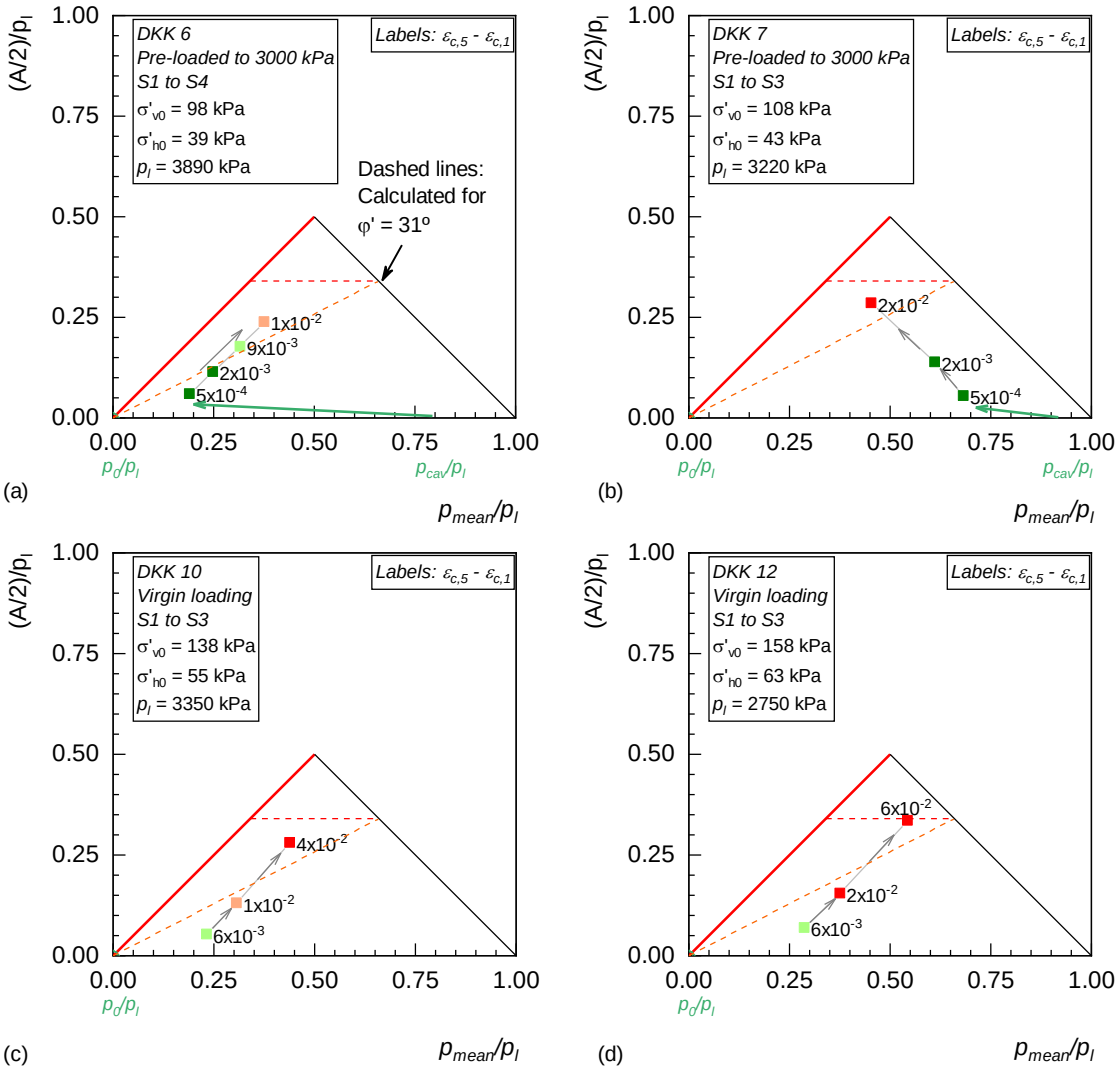

Figure 4.16 – Accumulated cavity strain after the five first loops of the pressuremeter tests performed in Dunkirk site

An attempt was made to correlate the plastic strain accumulation measured with the pressuremeter with parameters describing permanent displacement accumulation on the pile head. For this, a power law function similar to that described by equation (1.15) used in software SCARP was fitted for each cyclic series, relating the accumulated plastic strain $\varepsilon_{c,N}$ to the number of cycles N using a power law depending on a coefficient m (eq. 4.4).

$$\varepsilon_{c,N} = \varepsilon_{c,1} N^m e^{n\, p_{max}/p_l} \tag{4.4}$$

A similar exercise had been done in the SOLCYP project for piles installed in sand. With respect to the accumulation of permanent displacements at the pile head, it was found that (1) for stable driven piles: 0.10 < m < 0.15; (2) for unstable or metastable

driven piles: 0.30 < m < 0.40; and (3) for unstable bored (non-displacement) piles: m = 0.6.

The values obtained for the exponent *m* by fitting eq. 4.4 to the accumulation curves obtained with the pressuremeter were plotted in the cyclic stability diagrams presented in Figure 4.17. It can be seen that values of *m* for tests performed after pre-shear (figure a) and at low cyclic amplitudes are relatively low and comparable to that obtained for stable driven piles. As cyclic amplitude is increased, *m* increases. In the case of tests performed starting from a virgin state (figure b), the parameter *m* is high for all series. Its values compare to that obtained for the global response of unstable non-displacement piles.

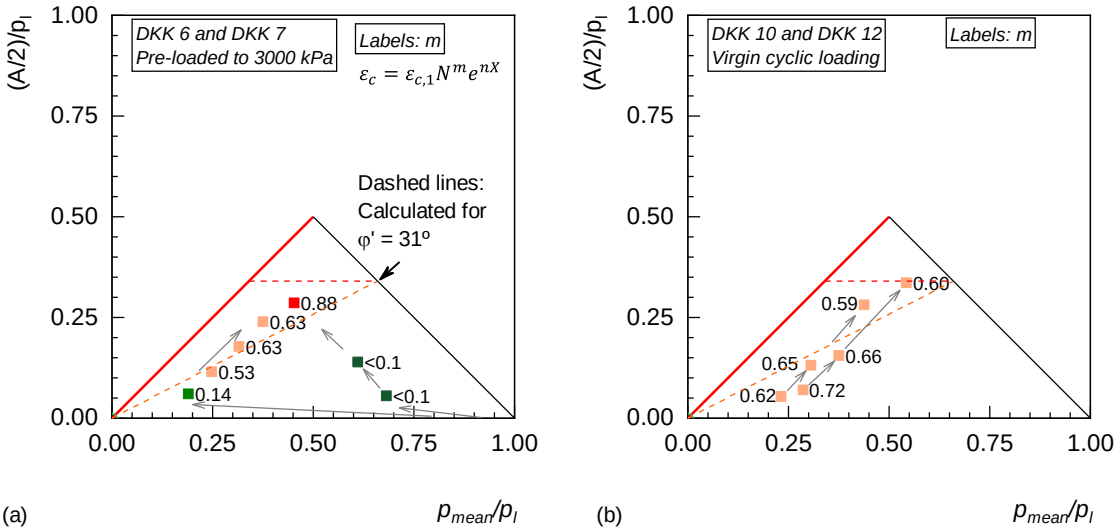

Figure 4.17 – Values of the parameter *m* for (a) tests performed after having pre-sheared the soil and (b) for tests starting from a virgin soil state

The trends presented showing the evolution of cavity strain accumulation finds an interesting correlation with the global behavior of piles installed in sands. Further research would be necessary to validate this observed correlation between local pressuremeter cavity strain accumulation and the global pile-head displacement accumulation. If confirmed, a similar procedure could be used for evaluating the number of cycles necessary for reaching failure or to estimate the displacement accumulation as a function of the number of cycles. It would require integrating the local response to a global level, which was not done here.

4.3 APPLICATION TO PILES INSTALLED IN CLAYS – MERVILLE SITE

4.3.1 Description of the adopted soil model

The pile load tests performed at Merville site were approximately 1500 m distant from the place where the pressuremeter campaign was carried-out. Given the site geology and the geotechnical information gathered on site, the soil properties measured with the pressuremeter can be considered as similar to those where the piles were installed (same clay, same geological history, sedimentary basin).

The pressuremeter tests performed following Protocol 1 at Merville site at 9 m, 11 m and 12 m depths yielded values of maximum shear moduli close to those obtained using down-hole geophysical tests. Therefore, the profile of maximum shear modulus obtained by the down-hole (lower bound) tests will be considered as representative of what could have been measured using the pressuremeter along the entire pile depth.

The soil profile considered for the calculation model is presented in Figure 4.18. It was discretized in twelve layers in order to incorporate the variations in ultimate skin friction that have been measured through instrumented pile load tests presented by Benzaria (2013). Figure 4.18a presents the CPT profile and the average values of q_c discretized by layers. Figure 4.18b presents the profile of shear modulus evaluated using standard pressuremeter tests from precedent campaigns on site and maximum shear modulus obtained from down-hole test. Figure 4.18c presents the calculation parameters per soil layer.

Table 4.4 – Summary of the model parameters for piles F2 and B1 at Loon Plage site

Layer base (m)	**Ult. skin friction (pile F2)** (kPa)	**(pile B1)** (kPa)	***Tip resistance (pile F2)*** *(kPa)*	***(pile B1)*** *(kPa)*	***Ave. E_M*** (MPa)	***Ave. q_c*** *(MPa)*	***Ave. G_{max}*** (MPa)
-2.4	26	20			5.0	0.8	37.8
-3.4	21	20			8.0	1.3	39.2
-4.4	19	20			14.0	1.9	40.6
-5.4	48	20			14.0	2.4	42.0
-6.4	42	28			18.0	2.8	43.4
-7.4	42	67			19.0	3.0	44.8
-8.4	46	155			23.0	3.2	46.2
-9.4	23	155			25.0	3.4	47.6
-10.4	34	160			25.0	3.5	49.0
-11.4	30	180			26.0	3.7	50.4
-13.0	47	180	1420	910	30.0	4.1	52.4

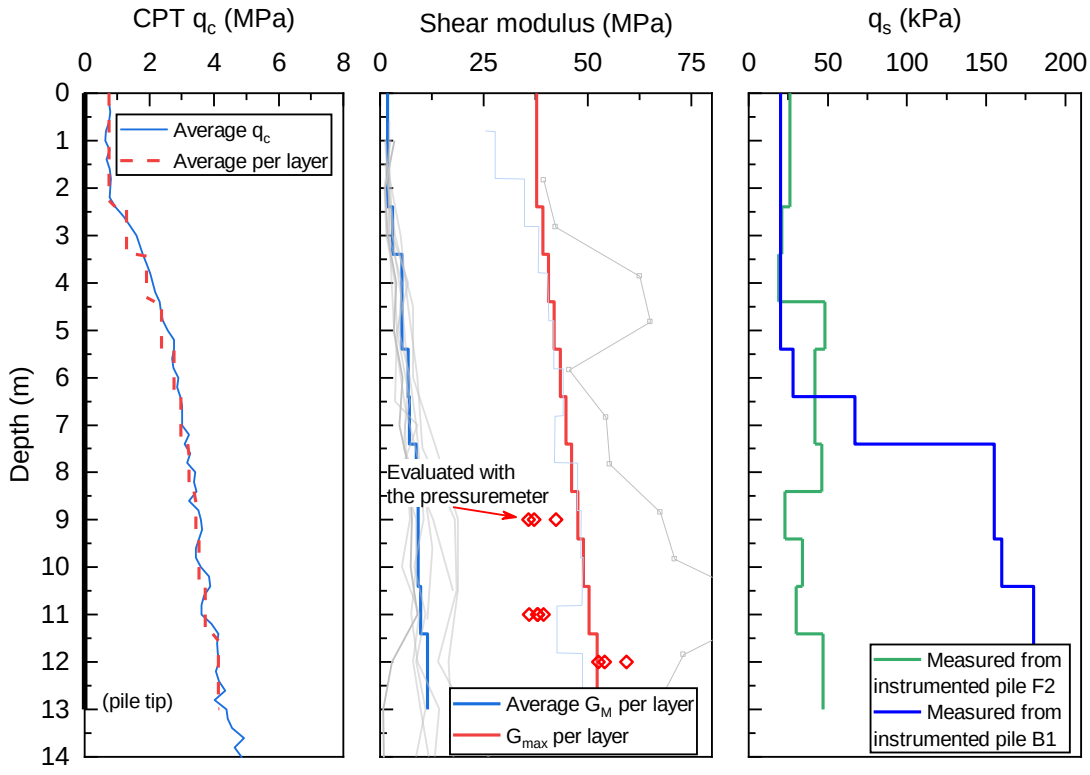

Figure 4.18 – (a) CPT averaged profile; (b) Ménard modulus G_M (measured) and G_{max} (calibrated from Down-Hole tests) profile; (c) ultimate skin friction measured from piles F2 and B1

4.3.2 Presentation of the studied piles

Benzaria (2013) presented the results obtained from several cyclic axial loading tests performed on bored, driven and screwed piles built at the Merville site. We propose to analyse the response of the non-displacement pile F2 and the displacement pile B1 in this thesis.

Pile F2 is a continuous flight auger (CFA) pile (reinforced concrete), of diameter B = 420 mm and embedded depth of L = 13 meters. It was submitted to the loading program presented in Table 4.5. The resulting response is presented in Figure 4.19.

Pile B1 is a driven closed-end steel tube, of diameter B = 406 mm, 15 mm thickness and embedded length of L = 13 meters. The pile was submitted to the loading program presented in Table 4.6. The resulting response is presented in Figure 4.20.

Table 4.5 – Loading program performed on CFA pile F2 at Merville site after Benzaria (2013)

Test	**Type**	f (Hz)	V_m (kN)	V_c (kN)	N	V_r (kN)
M-F2/CC1	Cyclic	0.5	450	225	3408	
M-F2/CC2	Cyclic	0.5	525	225	4834	
M-F2/CC3	Cyclic	0.5	525	300	2021	
M-F2/CR1	Static (rapid)					900
M-F2/CC4	Cyclic	0.5	225	180	1013	
M-F2/CC5	Cyclic	0.5	360	180	1000	
M-F2/CC6	Cyclic	0.5	360	270	1088	
M-F2/CC7	Cyclic	0.5	450	270	602	
M-F2/CC8	Cyclic	0.5	450	360	81	
M-F2/CC9	Cyclic	0.1	450	360	24	
M-F2/CC10	Cyclic	0.5	450	360	85	
M-F2/CR2	Static (rapid)					900
M-F2/CC11	Cyclic	0.1	360	350	502	
M-F2/CC12	Cyclic	0.5	360	350	478	
M-F2/CC13	Cyclic	0.5	540	270	159	

Table 4.6 – Loading program performed on driven pile B1 at Merville site after Benzaria (2013)

Test	**Type**	f (Hz)	V_m (kN)	V_c (kN)	N	V_r (kN)
M-B1/CS1	Static					1535
M-B1/CR1	Static (rapid)					1281
M-B1/CC1	Cyclic	0.5	260	187.5	10000	
M-B1/CC2	Cyclic	0.5	400	255	2000	
M-B1/CC3	Cyclic	0.5	400	380	1200	
M-B1/CC4	Cyclic	0.5	520	370	1000	
M-B1/CC5	Cyclic	0.5	500	470	1000	
M-B1/CR2	Static (rapid)					

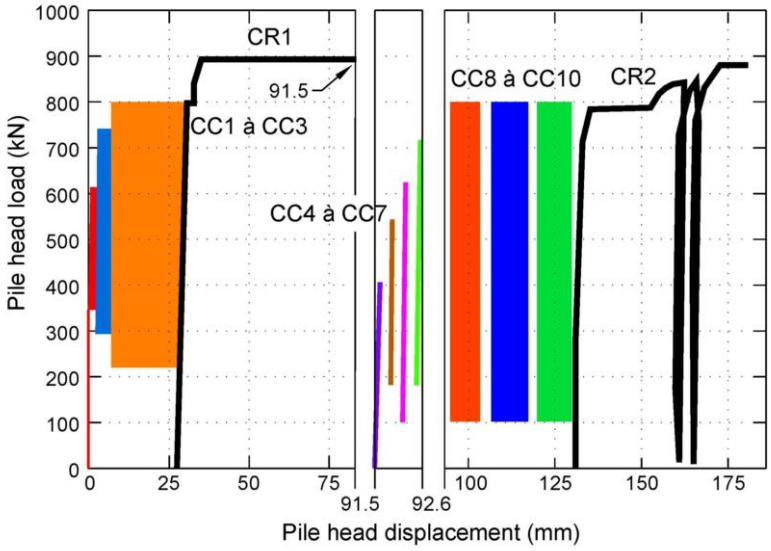

Figure 4.19 – Loading program performed on pile F2 at Merville site, after Benzaria (2013)

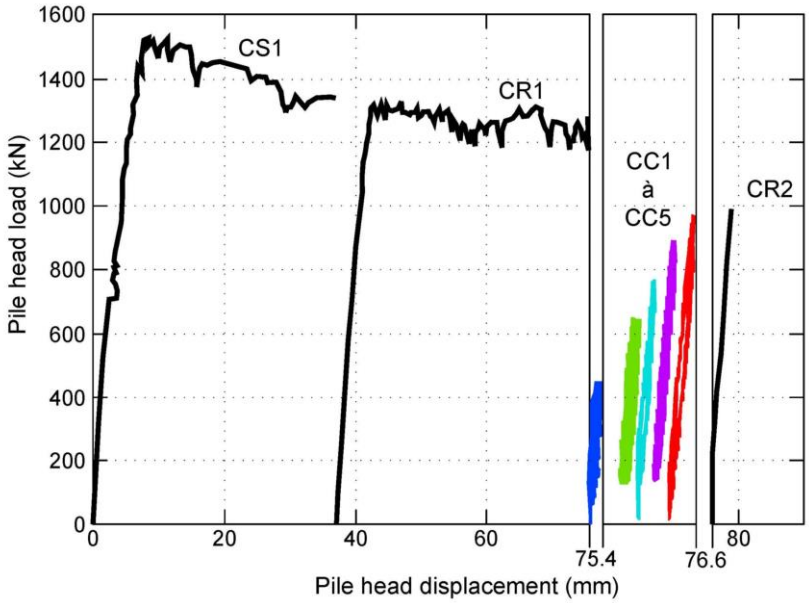

Figure 4.20 – Loading program performed on driven B1 at Merville site, after Benzaria (2013)

4.3.2.1 Aspects related to the pile stiffness

With respect to the stiffness of the pile head load-displacement behaviour, it was observed that, for both piles, this parameter did not significantly evolve during cyclic loading. The stiffness obtained during the cyclic series performed on pile F2 varied from approximately $K_{c,cc11}$ = 310 kN/mm to $K_{c,cc5}$ = 375 kN/mm. Averaging all the cyclic series, $K_{c,ave}$= 340 kN/mm is obtained.

4.3.2.2 Aspects related to the pile stability

Puech and Garnier (2018) presented the interaction diagrams of the piles tested at Merville site. The authors also presented a comparison between a larger database of pile tests in overconsolidated clays. The result is presented in Figure 4.21. It can be seen that for Merville piles (red line), the degradation of pile capacity under one-way loading is of about 20% of the pile bearing capacity under static loading.

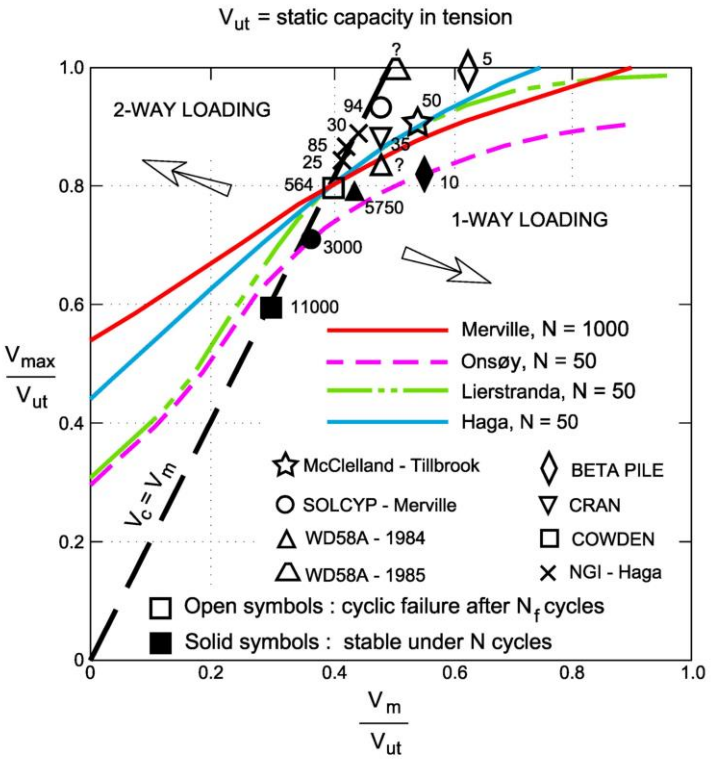

Figure 4.21 – Overview of cyclic stability diagrams obtained in clays (from Puech and Garnier, 2018)

By performing different combinations of cyclic loadings of average load Q_m and cyclic load Q_c, Benzaria (2013) observed that the response of the piles installed in the highly overconsolidated Merville clays was much influenced by the maximum load applied to the pile head ($Q_{max} = Q_m + Q_c$). Despite the pile installation procedure has an influence over the maximum capacity under monotonic loading, there was no clear difference in the capacity degradation for bored, driven or screwed piles, in Merville clays.

4.3.3 Modelling the pile-head response under monotonic and cyclic loading

4.3.3.1 Local analysis

Mobilization functions were derived from the first monotonic static load test performed on piles F1 and B1 at the Merville site. Although not presented here, pile F1 has the same technical characteristics as pile F2. The results obtained by Benzaria (2013) are presented in Figure 4.22 and in Figure 4.23. There is a clear difference with respect to what has been measured in sands (Figure 4.8): in overconsolidated clays, skin friction and tip resistance fully mobilize at much smaller displacements (between 1 to 2 mm).

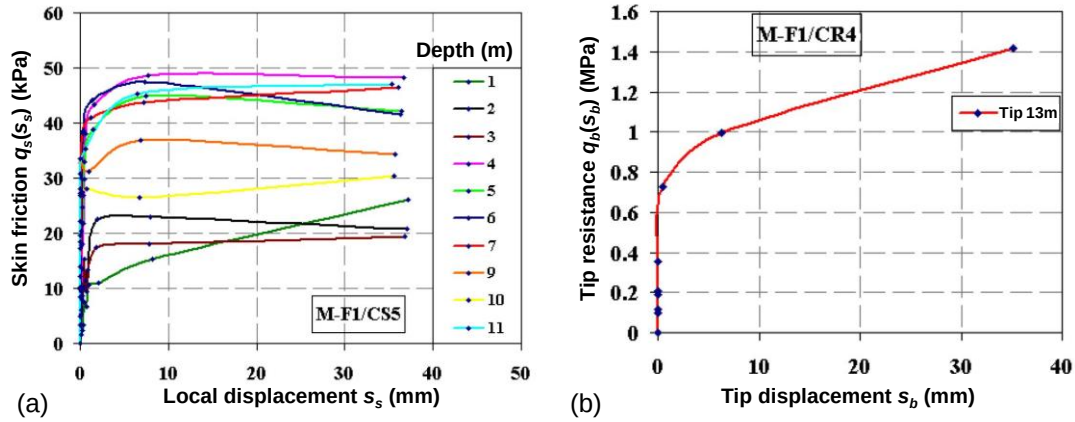

Figure 4.22 – (a) Skin friction and (b) tip resistance mobilization functions measured under monotonic static load test on instrumented pile F1 in OC clay, after Benzaria (2013)

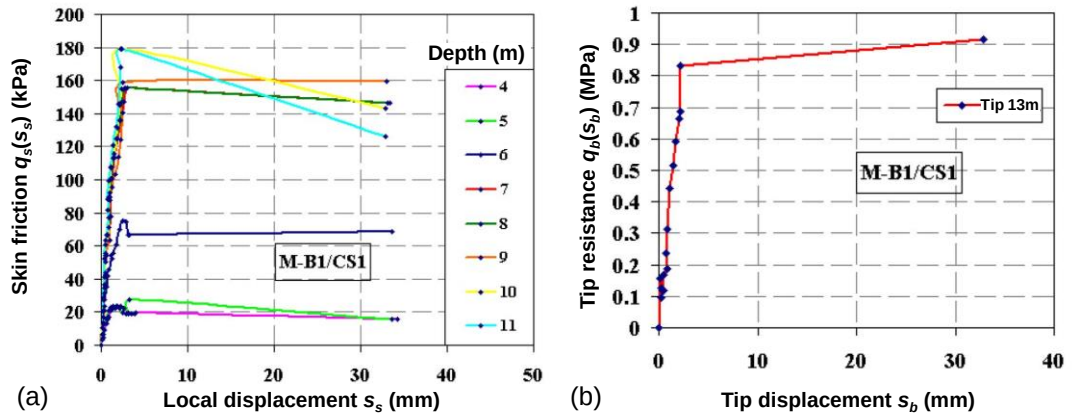

Figure 4.23 – (a) Skin friction and (b) tip resistance mobilization functions measured under monotonic static load test in instrumented pile B1 in OC clay, after Benzaria (2013)

The computed mobilization functions were then compared with the measured ones at certain depths. Figure 4.24 presents the result of this comparison for the CFA pile F1. Results of pile B1 are similar and not presented herein.

In this case, it can be observed that the initial slope of the mobilization functions proposed by Frank and Zhao (1982) are much closer to those proposed by Randolph and Wroth (1978) than when this same comparison was performed in sands. The local computed stiffness is also closer to the measured one. In this case there is a better consistency between the models themselves and between the models and the measurements.

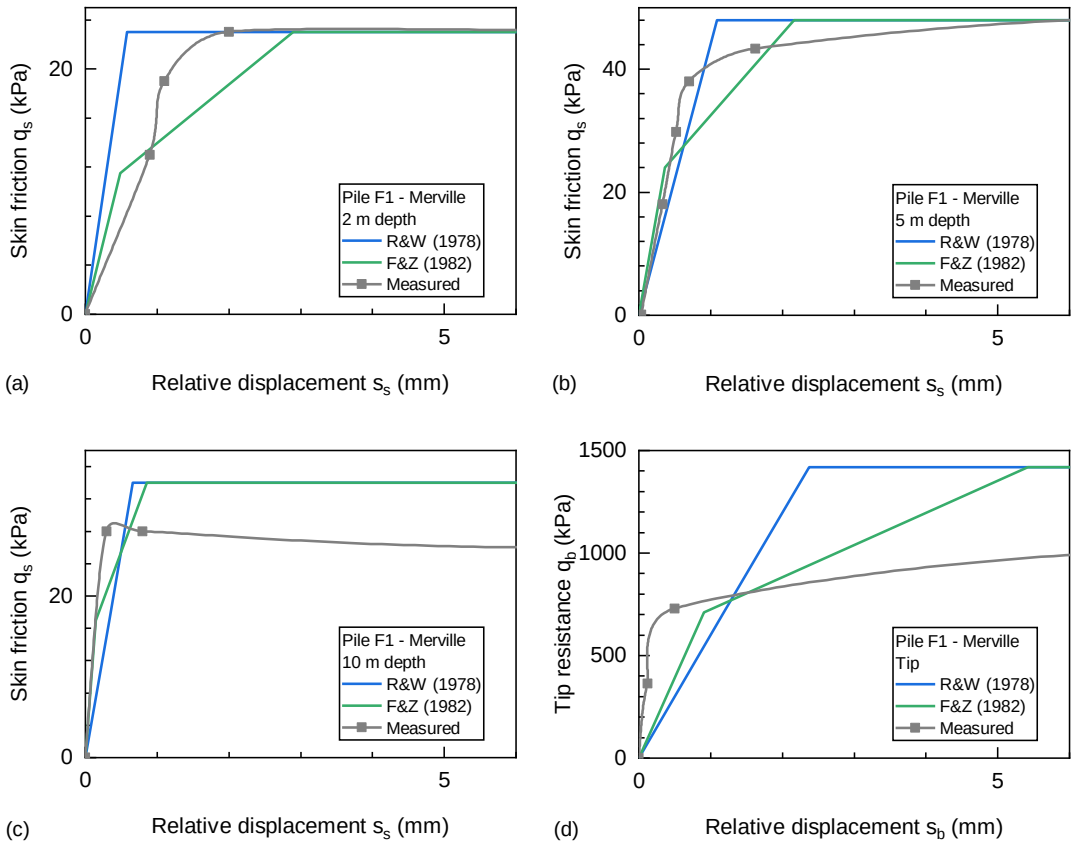

Figure 4.24 – Computed mobilization functions at 2m, 5m,10m and at pile tip. Comparison with measurements on pile F1 obtained by Benzaria (2013)

4.3.3.2 Global analysis

a) Case of pile F2

The pile head load-settlement behaviour was simulated using the method previously described, considering the Young's modulus of the pile was E_b = 20 GPa, B = 0.42 m and L = 13 m. Results are presented in Figure 4.25.

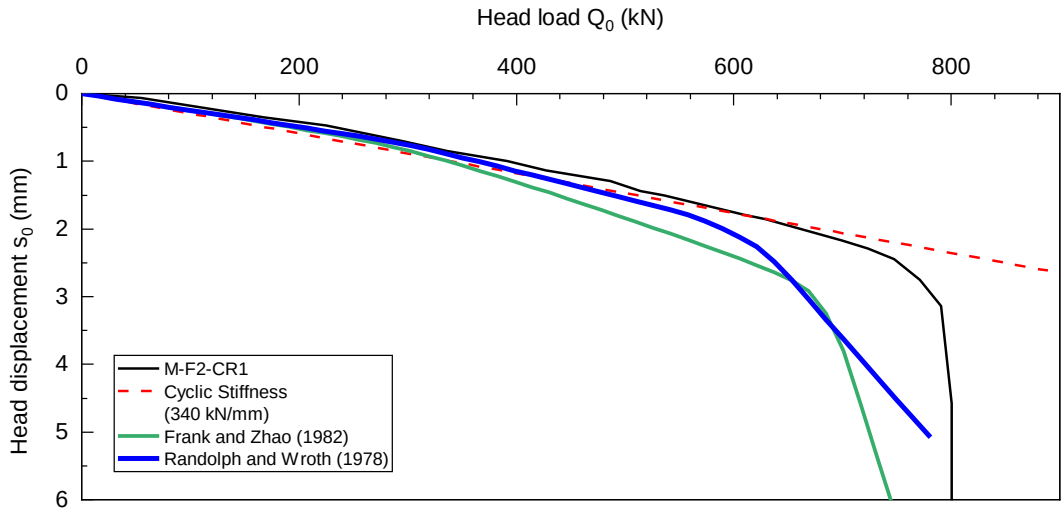

Figure 4.25 – Results of the global analysis of the pile head load-displacement response compared to measurements of pile F2

b) Case of pile B1

Pile B1 was modelled considering the Young's modulus of steel equal to 210 GPa, $B = 0.406$ m, a wall thickness of 15 mm and $L = 13$ m. The response obtained is presented in Figure 4.26.

For piles installed in clays, it can be noticed that the responses obtained using both Frank and Zhao (1982) and Randolph and Wroth (1978) mobilization functions are equally close to that of the pile under first static loading. It can also be observed that the pile stiffness under first monotonic loading is similar to that obtained during cyclic loading (red dashed line). The effect of the installation procedure (displacement or non-displacement) with respect to the pile-head stiffness is not as pronounced as in the case of piles installed in sands.

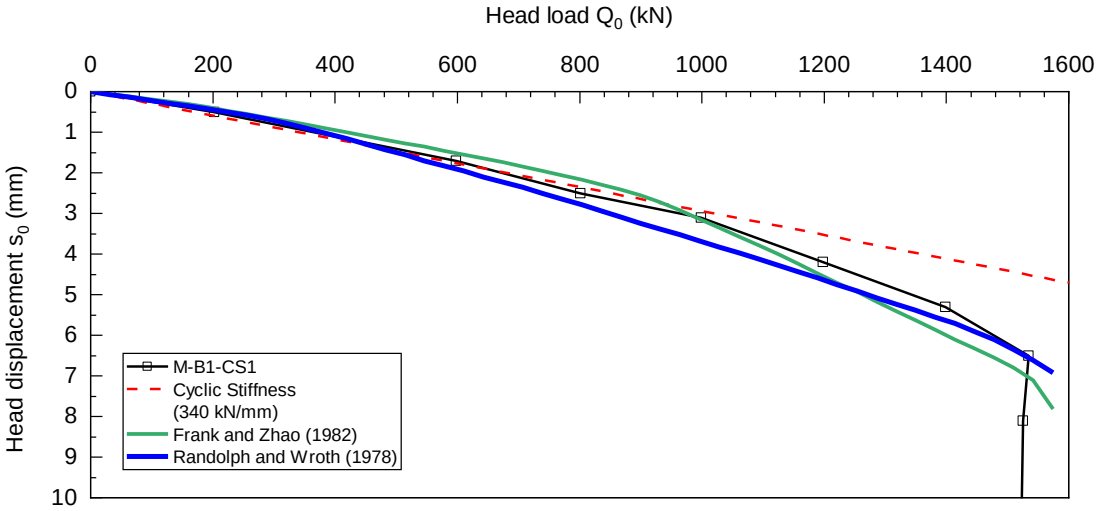

Figure 4.26 – Results of the global analysis of the pile head load-displacement response compared to measurements of pile B1

4.3.4 Aspects related to pile stability and pressuremeter results

Pressuremeter test MVL 11.2 presented in Chapter 3 (Figure 3.58) presented a behavior very similar to that of the piles under cyclic loading previously described. In this test, cyclic series were performed after the soil was loaded near failure. The detail of the cyclic series, normalized by the soil limit pressure, is presented in Figure 4.27b. The cyclic stability chart for piles in clays is presented in parallel and at same relative vertical scale at the left side of it (figure a).

The threshold for cyclic mobility measured in the pressuremeter test is very close to the threshold for pile stability in clays. It seems that in the pressuremeter test, it is also the maximum pressure within the cyclic series that governs the cyclic mobility: for p_{max} near 80% p_l there begins to occur plastic accumulation.

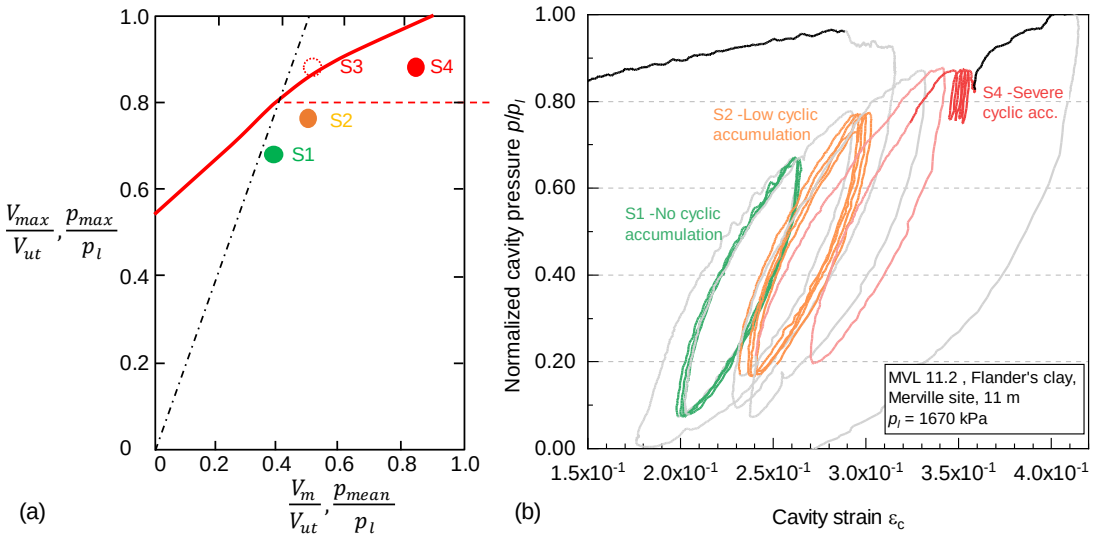

Figure 4.27 – Comparison between cyclic accumulation in pressuremeter test MVL 11.2 (b) and that measured on piles under cyclic loadings installed in clays (a)

The cyclic series presented above can also be represented in a normalized stability chart as it has been done for sands. Result is qualitatively presented in Figure 4.28. Series S3 and S4, which generated most severe accumulation, lie within a zone in which $p_{mean} + A/2 = 0.8\ p_l$, meaning that p_{max} is higher than 0.8 times p_l.

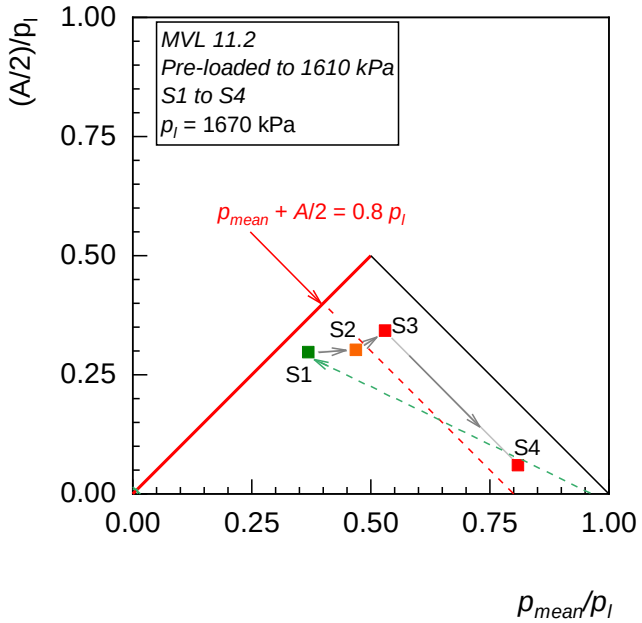

Figure 4.28 – Analogue of cyclic stability chart for pressuremeter test MVL 11.2

As a perspective, the test results presented above could be used for the evaluation of a degraded pile skin friction. In the present case, while the soil limit pressure is associated to the ultimate skin friction under monotonic loading, the maximum cavity pressure before triggering strain accumulation should be associated to the ultimate cyclic skin

friction (in between 70 and 80% p_l). Beyond this limit, plastic accumulation develops locally, and may result in instability at a global level.

SUMMARY AND PARTIAL CONCLUSIONS

In this chapter we have presented how the pressuremeter test can be used for assessing soil properties necessary for cyclic pile design. One first aspect concerned the determination of the shear modulus of soil at small strain rates and its application to determine the pile-head stiffness under cyclic loading. Local measurements of soil stiffness using the pressuremeter were integrated in a global pile analysis using the load transfer ("t-z") method. The second aspect concerned the pile stability issues, and assessing a loss of bearing capacity through the pressuremeter test. This chapter provided insights on how the local behavior measured with the pressuremeter correlated to the global behavior of the pile. However, integrating the local cyclic cavity expansion behavior to obtain a global degraded pile response was not yet attempted.

With respect to the **pile-head stiffness**, the results presented in sections 4.2.3 and 4.3.3 lead to the following conclusions:

- In sands, the behavior of the non-displacement pile under virgin monotonic static loading is governed by a weak soil stiffness. In the case of this type of piles, it is likely that this weakness can be associated to a "degradation" of the elastic properties resulting from the pile installation procedure. After being submitted to several series of cyclic loads, the pile response stiffens;
- The displacement pile studied in sands did not present this same hardening behavior. Pile-head stiffness was approximately the same in the first loading and after several series of cycles and was in any case much stiffer than for CFA piles. This behavior is likely related to the installation procedure, which pre-loads the soil around the pile;
- In overconsolidated clays, pile-head stiffness measured under monotonic or cyclic loading was similar. There was no trend of evolution of stiffness in function of the number of cycles or due to pre-loading the pile. There was no clear difference in the load-displacement behavior between the CFA and the driven piles. This result also shows a very close correlation with respect to measurements with the pressuremeter in clays;

- In a certain manner, the pressuremeter test mimics the disturbance during the probe insertion process (borehole drilling). It has been shown in the literature review that moduli derived on the first part of the expansion curve are strongly influenced by the probe insertion method. Yet, this disturbance is more pronounced in cohesionless soils than in fine soils. This is a possible reason for which the slope of Frank and Zhao (1982) mobilization functions, calibrated by relating the response of full-scale pile tests and pressuremeter modulus, was found 2.5 times higher in fine soils than in granular ones.
- The pile-head response obtained in unload paths seems to be predominantly governed by soil elementary elasticity properties. Pile modeled using mobilization functions based on elasticity theory (Randolph and Wroth, 1978)) and considering $G_{max,0}$ presented a good agreement with the measured unloading-reloading and the cyclic response of the pile.

With respect to **pile stability**, the local soil behavior measured with cyclic pressuremeter tests presented a strong correlation with the global behavior of piles under cyclic axial loading.

In the case of sands, performing cyclic series starting from a virgin state and of increasing amplitude with the pressuremeter leads to an increasing amount of plastic strain accumulation in function of the number of cycles. This behavior is analogous to that of CFA piles cyclically loaded, in which the stability zone is narrow. On the other hand, performing pressuremeter cyclic series after having pre-sheared the soil leads to reduced amount of strain accumulation. Accumulation can be "reactivated" if the soil fails in extension. The increased stability zone found in post-shear pressuremeter test is analogous to the improved stability zone of driven piles in sands.

In the case of overconsolidated clays, the accumulation of plastic strains due to cyclic loading seemed to be predominantly governed by the maximum pressure of the cyclic series. Cycling starting from a virgin state and increasing cavity average pressure and amplitude led to a behavior similar to that of creep tests (cavity pressure held constant). The behavior obtained when cycling after having pre-sheared the soil was found to be analogous to that of piles installed in overconsolidated clays. A threshold maximum cavity pressure of about 80% p_l obtained from pressuremeter tests is very close to that measured from pile tests.

GENERAL CONCLUSION AND PERSPECTIVES

The objective defined for this Ph.D. thesis was **the development of a new methodology for the design of deep foundations under cyclic axial loading using the pressuremeter test**. The definition of this goal arose from a lack of practical recommendations regarding cyclic pile design using soil parameters determined from *in situ* tests, specially the pressuremeter, which is the investigation method most commonly used for pile design in France. Whereas existing guidelines on the design of cyclically loaded piles refer mainly to the characterization of soil properties through laboratory tests, outlooks have been found in literature indicating the high potential of pressuremeter testing for this purpose.

The first set of parameters required for cyclic pile design is the same as that for piles under monotonic loading. Present practice shows that it can be satisfactorily evaluated using standard Ménard pressuremeter tests. The second set is related to pile behavior under cyclic loading and includes two main components: pile head stiffness under small shear strains and degradation of the pile-soil interface under repeated loading. There are currently no standard procedures enabling the evaluation of these properties from pressuremeter tests.

This work has evidenced that, beyond the lack of special testing procedures, the most critical issues for obtaining small strain parameters came from the **technological limitations of existing testing equipment**. The currently available Ménard type tricellular probes present very few technological enhancements if compared to the original models conceived some decades ago. It is recognized that improvements have taken place concerning data acquisition and automatization of the on-site operations, but the practical problems faced in day-to-day practice related to the conception of the

probe, the properties of the membranes, and the assessment of cavity strains have not found satisfactory answers since then. The use of modern technology for controlling the test at the ground level is definitely not sufficient to ensure quality measurements at the probe level several meters below the surface. The most critical aspects identified are: (1) premature membrane burst; (2) lack of control of the relationship between the volume injected in the measuring cell and the actual radial expansion of the probe and (3) difficulties related to the tricellular operation principle, such as the impossibility to make a reliable simultaneous control of water and gas, variations in the differential pressure between gas and water and progressive dissolution of gas into water.

Other types of probes, developed in parallel schools of thoughts, implement local and punctual strain measurement sensors. It has been claimed in literature that these probes can be used to measure the small strain behavior of soils and soft rocks. However, the maximum radial expansion that can be reached by this equipment is limited, preventing them to measure the limit pressure of soil in most cases. Without this parameter, the test cannot be used for the evaluation of the ultimate pile resistance, limiting its interest in daily practice.

An important part of this research was devoted to (a) studying and understanding the sources of uncertainties inherent to the most accessible pressuremeter probes and (b) selecting and validating a testing equipment potentially able to measure, in a same test, moduli at small strain range, and failure parameters at high strain range. In this context, **the innovative Monocell FC® probe has been chosen**. This probe implements an enhanced membrane technology, including the so-called “restraining sheath”. Its main function is to impose a predetermined geometry to the probe membrane during its inflation. By controlling the membrane geometry, this sheath enables establishing a reliable relationship between the volume of water injected inside the probe and its external diameter, which can be verified through calibration tests.

The validation of this equipment’s capabilities was carried out in two stages. The first stage consisted in performing tests under fully controlled test conditions in the laboratory. Specific calibration devices were developed to help evaluating the adequacy of the probe to assess cavity strains and cavity pressure variations. This first application yielded positive results. Then, tests were performed in dry Fontainebleau NE34 sand in calibration chamber. A parametric study conducted on the influence of the density index

of sand and the cavity pressure before unloading on the evaluated shear modulus showed that variations of these properties could be detected with the proposed testing procedures. Shear moduli obtained from unload loops using the pressuremeter and interpreted within a theoretical background of non-linear elasticity were found to be consistent with the elementary shear moduli of the tested sand. Yet, testing procedures including series of repeated cycles were developed and resulted in a soil response consistent with findings available in the literature.

As a practical result of the experiments conducted in the laboratory, **testing protocols could be defined** to assess the desired soil parameters. Procedures involve three steps: (1) probe calibration, (2) loading program in soil and (3) theoretical interpretation.

(1) **Probe calibration:** using calibration cylinders of variable diameters is a simple and efficient solution for obtaining a reliable relationship between probe volume and its external diameter. Membrane compliance tests were shown to be mandatory for the correct evaluation of soil shear modulus;

(2) **Loading program in soil**: tests aiming at determining shear modulus at small strains should include at least three unload-reload loops, performed at increasing cavity pressure, and always preceded by a pressure-hold step maintained a sufficient time to significantly reduce time dependent behavior. Loop amplitude should be carefully designed: large enough to enable capturing the non-linear response of the soil, but without generating soil failure in extension during unloading;

(3) Rough shear moduli are directly evaluated from the unload-reload response of loops performed in accordance with the previously defined protocols. They should be submitted to a **full interpretation procedure** aimed at transforming a basic cavity expansion response into an elementary soil response. This involves two steps: (a) in the case of drained tests, adjusting the pressure level imposed at the cavity wall at the moment of the start of the loop to an equivalent elementary average stress level; (b) in both drained and undrained cases, adjusting the radial strains measured at the cavity wall to an elementary averaged value of shear strain in the soil. By applying such interpretation procedure, any value of secant shear modulus derived within the pressuremeter

unload loop can be transformed into intrinsic soil shear modulus, at a given state of stress and strain.

The second part of the validation of this new testing equipment and procedures consisted in **performing *in situ* tests under real operational conditions** on sites where the soil layers had been previously characterized by other soil tests. The application *in situ* of the previously described procedure resulted in shear moduli that were found consistent with the elementary properties of the soils determined using other well-known laboratory testing or geophysical methods. This demonstrates the feasibility of assessing an equivalent elementary stress-strain dependency of the shear modulus of soils from properly designed pressuremeter tests. In our work the procedure was validated within a range of shear strains compatible with the requirements of pile design under cyclic loading.

In line with the initial objective of this work, **engineering application was focused on the design of piles under axial loading.**

Shear moduli measured on the two experimental sites of Dunkirk (dense sands) and Merville (overconsolidated clay) were used to derive mobilization functions for pile skin friction (t-z) and tip resistance (Q-z). The global load-displacement behavior of the piles was modelled and compared to the response of instrumented CFA and driven piles tested within the SOLCYP project.

By comparing the calculated local (t-z) and global (pile head stiffness) response of the piles with the actual measured response, one can conclude that:

- The French traditional approach, using the Frank and Zhao (1982) transfer functions based on standard Ménard pressuremeter data, provides a sound basis for simulating the monotonic response (first loading) of CFA piles in sands;
- The first loading of CFA or driven piles in clays is equally simulated by using the Frank and Zhao (1982) or the Randolph and Wroth (1978) transfer functions, the last calling for the introduction of the elasticity shear modulus;
- The cyclic response (cyclic stiffness) of both the CFA and driven piles should be based on the use of load transfer curves derived from elasticity theory using the elementary soil shear modulus as an input parameter.

These results can be potentially explained by the disturbance effects of probe insertion into the soil. In sands, the soil decompression generated by the pre-boring of the borehole mimics the boring process of the pile installation. Decompression results in fast degradation of shear modulus. In the case of overconsolidated clays, the disturbance induced due to pre-boring is less accentuated. In pressuremeter tests in clays, there is no effect of cavity pressure on the measured shear stiffness. This is comparable with the fact that both non-displacement and displacement piles responded with similar stiffnesses under monotonic axial loading in clays.

This is confirmed by the analysis of the accumulation of permanent cavity strains measured with cyclic pressuremeter tests which were found strongly correlated to the global degradation of the response of the piles under cyclic axial loading. In sands, cyclic series initiated with the pressuremeter in the virgin state result in a continuous and progressive accumulation of strains similar to the evolution of pile head displacements observed on a cyclically loaded CFA pile. The effect of pre-shearing the soil prior to performing cyclic series with the pressuremeter was shown to be analogous to the effect of pile driving, resulting in a reduced rate of strain accumulation with respect to tests starting from a virgin state. In the case of overconsolidated clays, the maximum cavity pressure applied during the pressuremeter cyclic series governed the strain accumulation. This behavior was also strongly correlated to the response of piles, non-displacement or displacement, installed in the same soil. In this case, the pile installation mode did not lead to significant changes in the overall pile stability under cyclic load.

The following **perspectives for future research** related to the interpretation methods, the applications for foundation design and the testing equipment may be listed:

- With respect to the **interpretation procedure**, it has been shown that presently there is no consensus in the literature concerning the calculation of the average stress around the cavity for tests in sands. There is still room for improvements in the theoretical background for the non-linear elastic solution of the cavity expansion problem;
- Whereas in this work the **engineering applications** of the proposed testing procedures were focused on the particular case of pile design, many other applications may be identified which require a complete and accurate

determination of the shear modulus of soils. One can mention *inter alia* the evaluation of the settlement of shallow foundations, the design of large structures for which the response is sensitive to shear stiffness decay (such as retaining walls and tunnels) and more generally the parametrization of elaborated constitutive models for soil-structure interaction modelling.

- We can also mention applications in which the consequence of cyclic repeated loads must be considered, such as the evaluation of the degradation of bearing capacity of piles, and of liquefaction properties of soils. For these applications, the test interpretation methods shall be further developed, aiming at better translating the accumulation of plastic strains measured at the pressuremeter test to parameters that can be used in practical applications;
- Concerning the **current limitations of the probe** used in this work, improvements on its measuring capabilities at low pressure levels are still desirable. More generally speaking, practitioners and clients should keep in mind that the measurement chain behind a pressuremeter test is complex. Heavy investments in automated controller and data acquisition, without improving the probe capabilities, are not sufficient to provide reliable data.

- With respect to the **testing equipment**, we can expect that the future implementation of sensors for measuring pore water pressure evolution during the test will provide precious information for test interpretation. Yet, there is ongoing development with respect to a new technique for locally assessing the radial expansion of the probe within the ARSCOP project. This technique, based on measuring the variation of the inductance of a hybrid elastic-conductor wire surrounding the probe, enables increasing the accuracy of radial strain measurements without limiting the probe's maximum expansion. It may help reducing the amount of time and efforts spent in probe calibration required at present.

BIBLIOGRAPHIC REFERENCES

Abchir, Z., Burlon, S., Frank, R., Habert, J., and Legrand, S. 2016. t-z curves for piles from pressuremeter test results. Géotechnique, **66**(2): 137–148.

AFNOR. 1999. Sols : Reconnaissance et Essais - Essai Pressiométrique Ménard. Partie 2: Essai Avec Cycle. French standard XP P 94-110-2. : 8 pages.

AFNOR. 2009. Calcul géotechnique - Ouvrages de soutènement - Ecrans. French standard NF P 94-282.

AFNOR. 2012. Justification des ouvrages géotechniques - Normes d'application nationale de l'Eurocode 7 - Fondations profondes. French standard NF P94-262.

AFNOR. 2013a. Justification des ouvrages géotechniques - Normes d'application nationale de l'Eurocode 7 - Fondations superficielles. French standard NF P 94-261.

AFNOR. 2013b. Geotechnical investigation and testing - Field testing - Part 5: Flexible dilatometer test. French standard NF EN ISO 22476-5. : 31 pages.

AFNOR. 2015. Geotechnical investigation and testing — Field testing — Part 4: Ménard pressuremeter test. French standard NF EN ISO 22476-4. : 55 pages.

Aghakouchak, A. 2015. Advanced laboratory studies to explore the axial cyclic behaviour of driven piles. Ph.D Thesis. Imperial College of London.

Ajalloeian, R., and Yu, H.S. 1998. Chamber studies of the effects of pressuremeter geometry on test results in sand. Géotechnique, **48**(5): 621–636.

Andria-Ntoanina, I. 2011. Caractérisation dynamique de sables de référence en laboratoire. Application à la réponse sismique de massifs sableux en centrifugeuse. Ph.D Thesis. Université Paris Est.

API. 2000. Recommended practice for planning, designing and constructing fixed offshore platforms-working stress design. API Recommended Practice 2A-WSD,: 71 pages.

Arsonnet, G., Baud, J.P., and Gambin, M. 2005. Realisation du forage pour essais pressiometriques par un système de tube fendu auto-foré (Staf). *In* 50 ans de pressiomètre. Presses des Ponts et Chaussées. pp. 31–45.

Atkinson, J.H., and Sallfors, G. 1991. Experimental determination of stress-strain-time characteristics in laboratory and-in-situ tests. *In* Proc. of the 10th European Conf. on Soil Mechanics and Foundation Engineering. *Edited by* A.G.I.R.; B.: A.A. Balkema. Florence, 26-30 May 1991. pp. 915–956.

Aubeny, C.P., Whittle, A.J., and Ladd, C.C. 2000. Effects of disturbance on undrained strengths interpreted from pressuremeter tests. Journal of Geotechnical and Geoenvironmental Engineering, **126**(12): 1133–1144.

Baguelin, F., and Frank, R. 1980. Theoretical studies of piles using the finite element method. *In* Numerical methods in offshore pilling. Institution of Civil Engineers. pp. 83–91.

Baguelin, F., Jézéquel, J., Le Mée, E., and Le Méhauté, A. 1972. Expansion de sondes cylindriques dans les sols cohérents. Bulletin de Liaison du Laboratoire des Ponts et Chaussées, **61**(1195).

Baguelin, F., Jézéquel, J., and Shields, D. 1978. The pressuremeter and foundation engineering. *In* First Edit. Trans Tech Publications, Clausthal.

Baldi, G., Bellotti, R., Ghionna, V.N., Jamiolkowski, M., and Lo Presti, D.C.F. 1989. Modulus of sands from CPT's and DMT's. *In* Proc. 12th Int. Conf. Soil. Mech. & Fndn Engng. Rio de Janeiro. pp. 165–170.

Bellotti, R., Ghionna, V., Jamiolkowski, M., Robertson, P.K., and Peterson, R.W. 1989. Interpretation of moduli from self-boring pressuremeter tests in sand. Géotechnique, **39**(2): 269–292.

Benoit, J., and Clough, G.W. 1986. Self-boring pressuremeter tests in soft clay. Journal of Geotechnical Engineering, **112**(1): 60–78.

Benoît, J., and Howie, J.A. 2014. View of pressuremeter testing in north america. Soils and Rocks, **37**(3): 211–231.

Benzaria, O. 2013. Contribution à l' étude du comportement des pieux isolés sous chargements cycliques axiaux. Ph.D. thesis. Université Paris Est.

Bohn, C., Lopes, A., and Frank, R. 2017. Development of Axial Pile Load Transfer Curves Based on Instrumented Load Tests. Journal of Geotechnical and Geoenvironmental Engineering, **143**(1): 04016081–1 to 15.

Bolton, M.D., and Whittle, R.W. 1999. A non-linear elactic/perfectly plastic analysis for plane strain undrained expansion test. Géotechnique, **49**(1): pages 133-141.

Borel, S. 2000. Caractéristiques géotechniques du site de Merville (Nord). 1.21.04.9. LCPC report. Thème 21. Caractérisation de la déformabilité des sols au moyen d'essais en place.

Borel, S., and Reiffsteck, P. 2006. Caractérisation de la déformabilité des sols au moyen d'essais en place. Laboratoire Central des Ponts et Chaussées.

Briaud, J.L. 1992. The pressuremeter. A.A. Balkema/Rotterdam/ Brookfield.

Briaud, J.L. 2013. Ménard Lecture. The pressuremeter test: Expanding its use. *In* 18th International Conference on Soil Mechanics and Geotechnical Engineering - Challenges and Innovations in Geotechnics. pp. 107–126. Available from http://www.geotech-fr.org/sites/default/files/congres/cimsg/107.pdf.

Briaud, J.L., Lytton, R.L., and Hung, J.T. 1983. Obtaining moduli from cyclic pressuremeter tests. Journal of Geotechnical Engineering, **109**(5): 657–665.

Briaud, J.L., Riner, K.B., and Ohya, S. 1984. Cyclic Pressuremeter Tests for Cyclic Lateral Loads. *In* 16th Offshore Technology Conference. Houston, Texas.

Briaud, J.L., Tucker, L.M., and Makarim, C.A. 1985. Pressuremeter standard and pressuremeter parameters. *In* Pressuremeters and its marine applications. Second International Simposium on Pressuremeters. pp. 303–323.

Brucy, F., Meunier, J., and Nauroy, J. 1991. Behavior of Pile Plug in Sandy Soils During and After Driving. *In* Offshore Technology Conference. Houston. p. 145 to 154.

Burlon, S., Thorel, L., and Mroueh, H. 2013. Proposition d'une loi t-z cyclique au moyen d'expérimentations en centrifugeuse. *In* Proceedings of the 18th International Conference on Soil Mechanics and Geotechnical Engineering. Paris. pp. 2335–2338.

Byrne, P.M., Salgado, R., and Howie, J.A. 1991. Gmax from pressuremeter tests - Theory, chamber tests and measurements. *In* International Conferences on Recent Advances in Geotechnical Earthquake Engineering and Soil Dynamics. 23. University of Missouri-Rolla, St. Louis, Missouri, March 11, 1991. pp. 57–63. Available from https://scholarsmine.mst.edu/icrageesd/02icrageesd/session01/23/.

Cambefort, H. 1964. Essai sur le comportement en terrain homogène des pieux isolés et des groupes de pieux. Annales de l'lnstitut Technique du Bâtiment et des Travaux Publics,: 1479–1518.

Cassan, M. 1960. Méthode pressiométrique d'étude des sols. L'ingénieur constructeur,: 3–16.

CEN. 2004. Eurocode 7: Geotechnical design—Part 1: General rules, EN 1997-1:2004. *In* European Committee for Standardization (CEN). Brussels.

CEN. 2007. Eurocode 7: Geotechnical design—Part 2: Ground investigation and testing, EN 1997-2:2007. *In* European Committee for Standardization (CEN). Brussels.

CFMS. 2019. Recommendations for planning and designing foundations of Offshore Wind Turbines. Comité Français de Mécanique des Sols et de Géotechnique. Workgroup "Foundations of Offshore Wind Turbines."

Chow, F. 1997. Investigations into the behaviour of displacement piles for offshore foundations. Ph.D. thesis. Imperial College of London.

Clarke, B.G. 1995. Pressuremeters in geotechnical design. *In* First Edit. Blackie Academic and Professional, Glasgow.

Clarke, B.G., and Smith, A. 1992. Self-boring pressuremeter tests in weak rocks. Construction and Building Materials, **6**(2): 91–96.

de Cock, F., and Legrand, C. 1997. Design of axially loaded piles: European practice. *In* Proceedings of the ERTC3 Seminar. Balkema, Rotterdam, Brussels, 17-18 April 1997. p. 377 pages.

Combarieu, O., and Canépa, Y. 2001. L'essai cyclique au pressiomètre. Bulletin des Laboratoires des Ponts et Chaussees, **233**: 37–65.

Cour, F. 2006. Controllably-Deformable Inflatable Sleeve, production method thereof and use of same for pressuremetering applications. Manchon Gonflable à Déformation Controlée. Procédée de Fabrication et Application à la Pressiométrie.

Cour, F. 2014. Hybrid elastic cable and process for manufacturing such a cable. Institut National de la Propriété Industrielle. Patent.

Cour, F. 2016. Drilling method, method for performing a pressuremeter test, and corresponding assembly. Organisation Mondiale de la Propriété Intellectuelle. Patent.

Cour, F. 2017. Measurement device by pressurizing the subsoil and method for carrying out an associated pressurization test. Patent.

Cour, F., and Lopes, A. 2018a. Paramètres de forage pour un positionnement judicieux de la sonde pressiometrique. (Using Borehole Drilling Parameters for Improving Probe Positioning and Results Interpretation - in French). *In* Journées Nationales de Géotechnique et de Géologie de l'Ingénieur. Champs-sur-Marne.

Cour, F., and Lopes, A. 2018b. Sonde monocellulaire innovante pour la réalisation d'essais d'expansion de cavité cylindrique (Innovative Monocell probe for performing cylindrical cavity expansion tests - in French). *In* Journées Nationales de Géotechnique et de Géologie de l'Ingénieur. Champs-sur-Marne.

Cour, F., and Rouet, A. 2017. La sonde pressiométrique monochambre FC. Du packer … au packer. Available from https://www.lathp.fr/la-thp-fabricant-de-sonde-pressiometrique-francis-cour/ [accessed 17 July 2019].

Coyle, H.M., and Reese, L.C. 1966. Load transfer for axially loaded piles in clay. J. Soil Mech. Found. Div., **92**(2): 1–26.

Cunha, R.P. 1994. Interpretation of self-boring pressuremeter tests in sand. Ph.D. thesis. University of British Columbia.

Delfosse-Ribay, E., Djeran-Maigre, I., Cabrillac, R., and Gouvenot, D. 2004. Shear modulus and damping ratio of grouted sand. Soil Dynamics and Earthquake Engineering, **24**(6): 461–471.

Droniuc, N., Lopes, A., and Puech, A. 2019. ARSCR004-AI-Charges cycliques. Rapport de recherche / Livrable. Axe 2. Méthodes de calcul des ouvrages géotechniques.

Duncan, J.M., and Chang, C.-Y. 1970. Nonlinear Analysis of Stress and Strain in Soils. Journal of the Soil Mechanics and Foundations Division, **96**(SM5): 1629–1653.

Dupla, J.C. 1995. Application de la sollicitation d'expansion de cavité cylindrique à l'évaluation des caractéristiques de liquéfaction d'un sable. Ph.D. thesis. Ecole Nationale des Ponts et Chaussées.

Dupla, J.C., and Canou, J. 2003. Cyclic pressuremeter loading and liquefaction properties of sands. Soils and Foundations, **43**(2): 17–31.

Elton, D.J. 1981. Effect of elastic tube strength on the pressure-meter modulus. Technical note. Geotechnical Testing Journal, **4**(3): 130–134.

Erbrich, C.T., O'Neill, M.P., Clancy, P., and Randolph, M.F. 2010. Axial and lateral pile design in carbonate soils. *In* Proc., 2nd International Symposium on Frontiers in Offshore Geotechnics (ISFOG II). pp. 125–154.

Fahey, M., and Carter, J.P. 1992. A finite element study of the pressuremeter test in sand using a nonlinear elastic plastic model. Canadian Geotechnical Journal, **30**(2): 348–362.

Fahey, M., and Jewell, R. 1990. Effect of pressuremeter compliance on measurement of shear modulus. *In* Proceedings of the Third International Symposium on Pressuremeters. Thomas Telford Publishing, Oxford. pp. 115–124.

Fahey, M., and Randolph, M.F. 1984. Effect of disturbance on parameters derived from self-boring pressuremeter tests in sand. Géotechnique, **34**(1): 81–97.

Ferber, V., and Abraham, O. 2002. Apport des méthodes sismiques pour la détermination des modules élastiques initiaux : application au site expérimental de Merville. *In* PARAM 2002 - Symposium international identification et détermination des paramètres des sols et des roches pour les calculs géotechniques. p. 8 pages.

Frank, R. 2014. Eurocode 7 on 'Geotechnical design': a code for soil-structure interaction. J. Appl. Eng. Sci. Technol., **1**(1): 1–10.

Frank, R. 2017. Some aspects of research and practice for pile design in France. Innovative Infrastructure Solutions, **2**(1): 32. Springer International Publishing.

Frank, R., Cuira, F., and Burlon, S. 2019. Calcul des Fondations Superficielles et Profondes. *Edited By*Presses des Ponts.

Frank, R., and Zhao, S.R. 1982. Estimation par les paramètres pressiométriques de l'enfoncement sous charge axiale de pieux forés dans sols fins. Bulletin des Laboratoires des Ponts et Chaussees, **119**(2712): 17–24.

Gambin, M. 1963a. Calcul du tassement d'une fondation profonde en fonction des résultats pressiométriques. Sols Soils, **7**: 11–28.

Gambin, M. 1963b. Le Pressiomètre et l'Art des Fondations. *In* Journées des Fondations. *Edited by* Laboratoire Central des Ponts et Chaussées. p. 17 pages.

Gibson, R.E., and Anderson, W.F. 1961. In-situ measurement of soil properties with the pressuremeter. Civil Engineering and Public Works Review, **56**(658): 615–618.

Haberfield, C.M. 1997. Pressuremeter Testing in Weak Rock and Cemented Sand. Proceedings of the Institution of Civil Engineers-Geotechnical Engineering, **125**: 168–178.

Hardin, B.O., and Drnevich, V.P. 1972a. Shear Modulus and Damping in Soils - Measurement and Parameter Effects. Journal of the Soil Mechanics and Foundation Division, **98**(SM6): 603–624.

Hardin, B.O., and Drnevich, V.P. 1972b. Shear Modulus and Damping in Soils - Design Equations and Curves. Journal of the Soil Mechanics and Foundation Division, **98**(SM7): 667–692.

Hoang, M.T., Cuira, F., Dias, D., and Miraillet, P. 2018. Estimation Du Rapport E / E M : Application Aux Radiers De Grandes Dimensions. Journées Nationales de Géotechnique et de Géologie de l'Ingénieur - Champs-sur-Marne,: 1–8.

Houlsby, G.T., and Withers, N.J. 1988. Analysis of the cone pressuremeter test in clay. Géotechnique, **38**(4): 575–587.

Howie, J.A. 1991. Factors affecting the interpretation and analysis of full-displacement pressuremeter tests in sands. Ph.D. thesis. University of British Columbia.

Huang, A.B., Holtz, R.D., and Chameau, J.L. 1991. Laboratory Study of Pressuremeter Tests in Clays. Journal of Geotechnical Engineering, **117**(10): 1549–1567.

Hughes, J.M.O., and Robertson, P.K. 1985. Full-displacement pressuremeter testing in sand. Canadian Geotechnical Journal, **22**: 298–307.

Hughes, J.M.O., Wroth, C.P., and Windle, D. 1977. Pressuremeter tests in sands. Géotechnique, **27**(4): 455–477.

Hussein, M. 2019. Use of a new monocell pressuremeter probe for the determination of soil shear modulus at small strains. Master thesis. Ecole des Ponts Paristech.

Jacquard, C., Rispal, M., Puech, A., Geisler, J., Durand, F., Cour, F., Burlon, S., and Reiffsteck, P. 2013. Une nouvelle sonde permettant de mesurer sans extrapoler la pression limite pressiométrique des sols. *In* Proceedings of the 18th International Conference on Soil Mechanics and Geotechnical Engineering. Paris. pp. 1–4.

Jacquard, C., and Varaksin, S. 2018. Rapport d 'analyse de l 'enquête relative à la pratique des essais pressiomètriques. National Project ARSCOP - Axe 2 - Research report.

Jardine, R.J. 1992. Nonlinear stiffness parameters from undrained pressuremeter tests. Canadian Geotechnical Journal, **29**: 436–447.

Jardine, R.J., Chow, F., Overy, R., and Standing, J. 2005a. ICP Design Methods for Driven Piles in Sands and Clays. *In* ICP Design Methods for Driven Piles in Sands and Clays. Thomas Telford, London.

Jardine, R.J., Potts, D.M., Fourie, A.B., and Burland, J.B. 1986. Studies of the influence of non-linear stress–strain characteristics in soil–structure interaction. Géotechnique, **36**(3): 377–396.

Jardine, R.J., and Standing, J.R. 2000. Pile load testing performed for HSE cyclic loading study at Dunkirk, France. Offshore Technology Report; OTO, **1** and **2**.

Jardine, R.J., Standing, J.R., and Kovacevic, N. 2005b. Lessons learned from full scale observations and the practical application of advanced testing and modelling. *In* Proceedings of the International Symposium on Deformation Characteristics of Geomaterials. Lyon. pp. 210–245.

Jézéquel, J., Lemasson, H., and Touze, J. 1968. Le pressiomètre Louis Ménard - quelques problèmes de mise en oeuvre et leur influence sur les valeurs pressiométriques. Bulletin de Liaison du Laboratoire des Ponts et Chaussées, **32**(537): 97–120.

Kerner, L. 2018. Interaction sol-structure sous sollicitations cycliques dynamiques : Application aux éoliennes offshore fondées sur monopieu. Ph.D. thesis. Université Paris Est.

Kjartanson, B.H. 1986. Pressuremeter creep testing in laboratory ice. Ph.D. thesis. University of Manitoba.

Le Kouby, A. 2003. Etude du comportement mécanique de micropieux sous chargements monotones et cycliques verticaux . Application aux effets de groupe. Ph.D. thesis. Ecole Nationale des Ponts et Chaussées.

Kraft, L.M., Ray, R.P., and Kagawa, T. 1981. Theoretical t-z Curves. Journal of the Geotechnical Engineering Division, Proceedings of the American Society of Civil Engineers, **117**: 1543–1559.

Kuwano, R. 1999. The stiffness and yielding anysotropy of sands. Ph.D. thesis. Imperial College of London.

Ladanyi, B. 1972. Determination of Undrained Stress-strain Behavior of Sensitive Clays with the Pressuremeter. Canadian Geotechnical Journal, **9**(3): 313–319.

Ladanyi, B. 1987. Suggested Methods for Deformability Determination Using a Flexible Dilatometer. International Journal of Rock Mechanics, **24**(2): 123–134.

LCPC. 1971. Essai Pressiométrique Normal. Modes Opératoires du Laboratoire Central des Ponts et Chaussées. DUNOD,: 49 pages.

Le, V.C. 2014. Étude Sur Modèle Physique Du Renforcement Des Sols Par Colonnes En « Soil-Mix» Application Aux Plates-Formes Ferroviaires. Ph.D. thesis. Université Paris Est.

Little, R.L.R.L., and Briaud, J.L. 1988. Full scale cyclic lateral load tests on six single piles in sand. Miscelaneous Paper GL-88-27. Geotechnical Division. Civil Engineering Department. Texas A&M University.

Lopes, A. 2013. Development of mobilization functions for skin friction and tip resistance without pressuremeter parameters. Master thesis. Ecole Nationale des Ponts et Chaussées.

Lopes, A. 2018. Cyclic Pressuremeter Tests - Shear Modulus Determination at Low Strain Rate. *In* Proceedings 26th European Young Geotechnical Engineers Conference. Graz. pp. 1–10.

Lopes, A., Dupla, J.C., Canou, J., and Droniuc, N. 2019a. Laboratory validation of an innovative mono-cell pressuremeter probe : test procedures and first results. *In* Proceedings of the XVII European Conference on Soil Mechanics and Geotechnical Engineering. Reykjavik. pp. 1–8.

Lopes, A., Puech, A., and Droniuc, N. 2019b. In-situ validation of an innovative mono-cell pressuremeter probe : first results. *In* Proceedings of the XVII European Conference on Soil Mechanics and Geotechnical Engineering. Reykjavik. pp. 1–8.

Lopes, A., Puech, A., Droniuc, N., Geisler, J., and Cour, F. 2018. Mesures de G à faibles déformations à partir d'une sonde préssiometrique monocellulaire. *In* Journées Nationales de Géotechnique et de Géologie de l'Ingénieur. Champs-sur-Marne.

Lunne, T., Lacasse, S., and Rad, N.S. 1989. General report / Discussion session 2: SPT, CPT, pressuremeter testing and recent developments in in-situ testing - Part 1 : All tests except SPT. *In* Proceedings of the 12th International Conference on Soil Mechanics and Foundation Engineering. Taylor and Francis, Rio de Janeiro, 13-18 August 1989. pp. 2339–2403.

Mair, R.J., and Wood, D.M. 1987. Pressuremeter Testing: Methods and Interpretation. Construction Industry Research and Information Association.

Manassero, M. 1989. Stress-strain relationships from drained self-boring pressuremeter tests in sands. Géotechnique, **39**(2): 293–307.

Ménard, L. 1956. Brevet d'invention - Pressiomètre. Service de la Propriété Intelectuelle, France.

Ménard, L. 1957. Mesures in situ des proprietes physiques des sols. Annales des Ponts et Chaussées, **14**: 357–377.

Ménard, L. 1961. Influence de l'amplitude et de l'histoire d'un champ de contraintes sur le tassement d'un sol de fondation. *In* Proc. of the 5th International Conference on Soil Mechanics and Foundation Engineering. Paris. pp. 249–253.

Ménard, L. 1963. Tendances Nouvelles en Mécanique des Sols. Bulletin A.I.A., (1): 1–12.

Ménard, L. 1965. Application du vibro-fonçage aux sondages sous-marins hydraulique. Sols Soils, (14): 24–41.

Ménard, L. 1967. Règles d'utilisation des techniques pressiometriques et d'exploitation des résultats obtenus pour le calcul des fondations. Notice Générale D-60.

Ménard, L., and Rousseau, J. 1962. L'évaluation des tassements. Tendances Nouvelles. Sols Soils, **1**(1): 13–29.

Muhammed, R. 2015. Étude en chambre d'étalonnage du frottement sol-pieu sous grands nombres de cycles. Application au calcul des fondations profondes dans les sols fins saturés. Ph.D. thesis. Université Pierre et Marie Curie.

Nutt, N.R.F. 1993. Development of the Cone pressuremeter. Ph.D. thesis. University of Oxford.

Oztoprak, S., and Bolton, M.D. 2013. Stiffness of sands through a laboratory test database. Géotechnique, **63**(1): pages 54-70.

Palmer, A.C. 1972. Undrained plane-strain expansion of a cylindrical cavity in clay: a simple interpretation of the pressuremeter test. Géotechnique, **22**(3): 451–457.

Payan, M., Khoshghalb, A., Senetakis, K., and Khalili, N. 2016. Small-strain stiffness of sand subjected to stress anisotropy. Soil Dynamics and Earthquake Engineering, **88**: pages 143-151. Elsevier.

PLAXIS. 2015. Performance of the GHS model in excavation projects. Documentation of the GHS constitutive model.

Poulos, H.G. 1989a. Cyclic Stability Diagram for Axially Loaded Piles. Journal of Goetechnical Engineering, **114**(8): 877–895.

Poulos, H.G. 1989b. SCARP Users' Manual. Centre of Geotechnical Research, Sydney, Australia.

Poulos, H.G., and Davies, E.H. 1968. The Settlement Behavior of axially loaded incompressive piles and piers. Géotechnique, **18**: 351–371.

Puech, A., and Brucy, E.M. 1982. Calcul de la capacité axiale des pieux de fondations marines à partir du pressiomètre autoforeur. *In* Symposium sur la pressiométrie et ses applications en mer. Institut Français du Pétrole. Laboratoires des Ponts et Chaussées. pp. 373–388.

Puech, A., and Garnier, J. 2017. Design of piles under cyclic loading: SOLCYP recommendations. John Wiley & Sons.

Randolph, M. 2013. McClelland lecture. Analytical contributions to offshore geotechnical engineering. *In* Proceedings of the 18th International Conference on Soil Mechanics and Geotechnical Engineering. pp. 85–105.

Randolph, M.F. 1986. RATZ: Load transfer analysis of axially loaded piles, Report no.GEO: 86 033.

Randolph, M.F., and Wroth, C.P. 1978. Analysis of deformation of vertically loaded piles. Journal of the Geotechnical Engineering Division, **GT12**: 1465–1488.

Rangeard, D., Hicher, P.Y., and Zentar, R. 2003. Determining soil permeability from pressuremeter tests. International Journal for Numerical and Analytical Methods in Geomechanics, **27**: 1–24. doi:10.1002/nag.258.

Reiffsteck, P., Lossy, D., and Benoît, J. 2012. Forages, sondages et essais in situ géotechniques. Presses des Ponts.

Robertson, P.K. 1982. In-situ testing of soil with emphasis on its application to liquefaction assessment. Ph.D. thesis. University of British Comumbia.

Robertson, P.K., and Hughes, J.M.O. 1986. Determination of properties of sand from self-boring pressuremeter tests. *In* Pressuremeters and its marine applications. Second International Simposium on Pressuremeters. pp. 283–302.

Salgado, R., J.K., M., and Jamiolkowski, M. 1998. Calibration chamber size effects on penetration resistance in sand. Journal of geo, **124**(9): 878–888.

Schnaid, F. 1990. A study of cone-pressuremeter test in sand. Ph.D. thesis. University of Oxford.

Schnaid, F., and Houlsby, G.T. 1990. Chamber size effects in the calibration of in-situ tests in sand. Report number OUEL 1849/90. University of Oxford, Department of Engineering Science.

Seed, H.B., and Reese, L.C. 1957. The action of soft clay along friction piles. Trans. Am. Soc. Civ. Eng., **122**: 731–754.

Shuttle, D.A., and Jefferies, M.G. 1995. A practical geometry correction interpreting pressuremeter tests in clays. Géotechnique, **45**(3): 549–553.

Silvestri, V. 2004. Disturbance effects in pressuremeter tests in clay. Canadian Geotechnical Journal, **41**(4): 738–759.

Tali, B. 2011. Comportement de l'interface sol-structure sous sollicitations cycliques. Application au calcul des fondations profondes. Ph.D. thesis. Université Paris Est.

Tani, K. 1995. General report: Measurement of shear deformation of geomaterials in the laboratory. *In* Pre-failure Deformation of Geomaterials. *Edited by* Shibuya Mitachi & Miura. Balkema, Rotterdam. pp. 1115–1131.

Tsuha, C.H.C., Foray, P.Y., Jardine, R.J., Yang, Z.X., Silva, M., and Rimoy, S. 2012. Behaviour of displacement piles in sand under cyclic axial loading. Soils and Foundations, **52**(3): 393–410.

Vucetic, M., and Dobry, R. 1991. Effect of soil plasticity on cyclic response. Journal of Geotechnical Engineering, **117**(1): 89–107.

Wedekin, V.M., Kastner, R., Guilloux, A., Bezuijen, A., Standing, J., and Negro, A. 2012. Urban tunnels in soft ground. Geotechnical Aspects of Underground Construction in Soft Ground,: 1047–1064.

Whittle, R. 1999. The myth of the finite pressuremeter geometry correction. CITR1003. Cambridge In Situ Technical Reference. Cambridge Insitu Limited.

Whittle, R., and Liu, L. 2013. A method for describing the stress and strain dependency of stiffness in sand. *In* 18th International Conference on Soil Mechanics and Geotechnical Engineering. Paris. pp. 1–5.

Whittle, R., Palix, E., and Donaghy, D. 2017. The influence of insertion process on determining the stiffness characteristics of chalk, using pre-bored, self-bored and pushed pressuremeters. *In* Offshore Site Investigation and Geotechnics. pp. 308–315. doi:10.1145/2505515.2507827.

Withers, N.J., Howie, J., Hughes, J.M.O., and Robertson, P.K. 1989. Performance and analysis of cone pressuremeter tests in sands. Géotechnique, **39**(3): 433–454.

Withers, N.J., Schaap, L.H.J., and Dalton, C.P. 1986. The development of a full displacement pressuremeter. *In* Pressuremeters and its marine applications. Second International Simposium on Pressuremeters. ASTM. pp. 38–56.

Wood, D.M. 1990. Strain-dependent moduli and pressuremeter. Géotechnique, **40**(3): 509–512.

Wroth, C.P. 1982. British experience with the self boring pressuremeter. *In* Proc. of Int. Symp. Pressuremeter and its Marine Applications. Institut Français du Petrole, Laboratoires des Ponts et Chaussees, Paris, 1982. Editions Technip, Collections Colloques et Seminaires 37, Paris, 1982. pp. 143–164.

Wroth, C.P., and Hughes, J.M.O. 1972. An Instrument for the in situ measurement of properties of clays. Technical report. CUED/C - SOILS TR13. University of Cambridge, Department of Engineering,.

Wroth, C.P., and Windle, D. 1975. Analysis of the pressuremeter test allowing for volume change. Géotechnique, **25**(3): 598–604. doi:10.1680/geot.1975.25.3.598.

Yu, H.-S. 2000. Cavity expansion methods in geomechanics. Springer-Science + Business Media, B.V.

Zdravković, L., Jardine, R.J., Taborda, D.M.G., Abadias, D., Burd, H.J., Gavin, K., Houlsby, G.T., Igoe, D., Liu, T., Martin, C.M., McAdam, R.A., Muir Wood, A., Potts, D.M., Gretlund, Skov, J., and Ushev, E. 2018. Ground characterisation for PISA pile testing and analysis. Géotechnique,. doi:10.1680/jgeot.18.pisa.001.

Zhang, J., Andrus, R.D., and Juang, C.H. 2005. Normalized shear modulus and material damping ratio relationships. Journal of Geotechnical and Geoenvironmental Engineering, **131**(4): 453–464.

APPENDICES

APPENDIX A.

REVIEW ON THE EXISTING TESTING EQUIPMENT AND STANDARDS

A.1 THE MÉNARD PRESSUREMETER

A.1.1 Principle and historical development

The first prototype of a Ménard type pressuremeter probe was operational in 1955 according to Baguelin et al. (1978). It had the particularity of having three independent expandable cells, stacked one above the other. Each cell was delimited by a rubber membrane. The three cells were inflated simultaneously and to the same pressure. The top and the bottom chambers were conceived to protect the middle one from the end effects caused by the finite length of the equipment. They were entitled the "guard cells" and, besides avoiding end effects, they had the role to avoid that the central cell expands axially into the void of the cylindrical cavity. On this manner, the middle chamber was induced, in principle, to expand only in radial direction, as if the probe had an infinite length expanding under plane strain conditions. The cavity deformation was assessed from the measurements of volume variations of this cell, thus entitled the "measuring cell". A scheme of the first Ménard pressuremeter probe is presented in Figure A.1. Since in theory the longitudinal dimensions of the probe do not change during pressurization, all the injected volume of water in the measuring cell is consumed by a diametrical expansion. Thus, considering water as an incompressible fluid, any variations of volume would be related to a variation of diameter. Since the guard cells had no measuring purposes, it has been further decided to fill it only with gas.

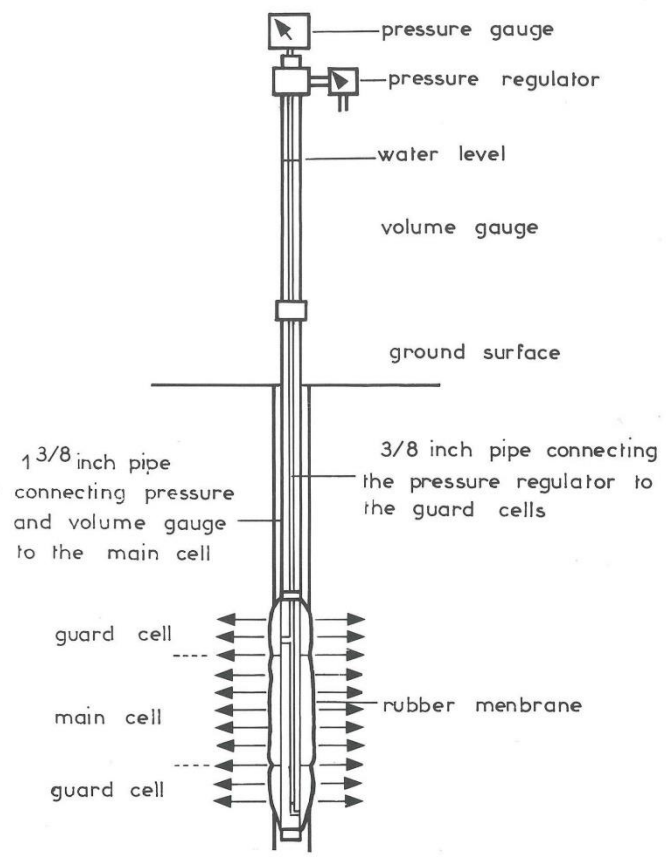

Figure A.1 – Sketch of the first Ménard pressuremeter, extracted from Ménard (1957)

As practitioners from all around the world began to get on with the pressuremeter test, some practical aspects evolved in regard to cavity expansion tests. Despite those general evolutions, the so-called "Ménard pressuremeter test" has undergone very few changes since its invention. Baguelin et al. (1978) describe some practical aspects that are fundamental for the success of the pressuremeter tests. Almost all of those aspects are still up to date and they are summarized in next item.

A.1.2 Practice

Baguelin et al. (1978) suggest that the following points need to be carefully performed so that to obtain successful results:

- Choosing the testing equipment better adapted for the soils that will be tested. This includes the choice of the probe's membranes, the external protective sheath and metallic protection, adequate tubing length, adequate sensitivity for pressure gauges and adequate gas pressure supply;
- Filling and saturating the circuits. Special care should be taken to avoid trapped air bubbles that may affect the volumetric measurements;

- Proceeding to calibration procedure. Calibrating the device (which includes the fully equipped probe, the tubing and the control unit) enables accounting for inherent pressure and volume losses when interpreting test results.

Volume losses correspond to the compressibility of any of the pressurized parts of the circuit, including the membranes, the protective sheath and external metallic protection, the tubing, the control unit and the fluid. Calibration for volume losses is done by placing the probe inside a thick-walled steel cylinder, considered as infinitely rigid. The pressure is raised until the probe membrane is in full contact with the tube. Then a series of pressure increments are applied up to the maximum working pressure. The curve of pressure in function of the injected volume after full contact corresponds to the system compressibility, in units of [volume/pressure].

Pressure losses[1] correspond to the amount of pressure needed to overcome the resistance of the membrane and the sheath at a given volume. The pressure actually applied to the soil cavity walls is equal to the pressure applied to the probe minus the pressure necessary to dilate its membranes in open-air, at a given volume. Calibrating for pressure losses (also called "membrane inertia" or "membrane correction") consists in inflating the probe in open-air conditions and keeping records of pressure and volume. The probe should be placed in upright position (vertical position as for tests in soil) and inflated using several pressure increments.

- Drilling the borehole and positioning the probe. Adequate techniques for drilling should be used, including the use of support fluids (e.g. bentonitic slurry) when needed. Probe insertion should be done as soon as possible to avoid cavity contraction or other time-dependent phenomena which could bring prejudice to test results.

The vertical spacing between tests performed in a same borehole is generally adopted as 1.0 meter and should not be inferior to 0.5 meters to avoid interference between tests. This spacing must be adjusted in multilayered geological contexts. The probe should not be located on an interface of two materials of different properties, since this may

[1] Pressure losses on this paragraph are associated to membrane mechanical resistance. This is different from "hydraulic pressure losses" which are discussed further on this text

generate a high risk of probe bursting or provide a cavity expansion curve hardly interpretable.

- Running the test. The Ménard type test is performed following a loading program in general with about 10 load steps. Each load step pressure is held constant for 60 seconds. Pressure and volume readings are recorded at 15 s., 30 s. and 60 s. after the beginning of each load step. The loading program can be adapted in function of the engineering needs for the test. For example, unload-reload loops can be performed. A typical loading program is presented in Figure A.9a.
- Deflating the probe and moving it to the next position or out of the borehole.

A.1.3 Equipment

The most common pressuremeters currently used in French practice are an evolution of the first tools developed by Ménard. A recent quiz promoted by the ARSCOP National Project (Jacquard and Varaksin (2018)) involving French professionals familiar with pressuremeter testing in daily practice pointed out the most used equipment and techniques. This chapter summarizes some of the major changes that have taken place in the last sixty years, focusing on equipment currently used in practice.

A.1.3.1 The probe

Since the first developments, Ménard named his different probe models by single alphabet letters. The first prototype was entitled type “A”, then “B”, “C”, “D”, “E”, “F” and “G”. Gambin (1990) and Cassan (2005) present some details of these pioneering probes. Amongst them, types “E” and “G” prevailed and were used in practice for a long time. Nowadays, type “G” is the most widespread.

Probes of type “E” have three independent cells, each one delimited by an independent membrane. These probes present some drawbacks with regard to maintenance and frequent bursting problems and are almost extinguished in current practice. Conversely, “G” type probes, also called “fitted” or “self-contained” probes, have been the subject of major design evolutions. The membranes isolating the guard cells were suppressed. The guard cells are nowadays delimited by the empty space between the external protective sheath ant the central measuring cell. A differential pressure between the water and the pressurized air is needed so that the measuring central cell can follow the

external sheath. The development of this type of probe allowed performing tests at greater depths and at higher pressures Gambin (1990).

Probes of type "G" are currently available in two diameters: 60 mm and 44 mm, entitled types "BX" and "AX", respectively. "BX" probes (Figure A.2a) are usually inserted into the ground without a rigid external protection. The expanding sheath is either in direct contact with the surrounding soil or protected by a flexible "*Chinese lantern"* (thin metallic stripes placed around the sheath). "AX" probes are usually placed inside a rigid steel slotted tube, which is an external membrane protection against gravelly soils. The slotted tube enables probe insertion through driving without damaging it. The most used slotted tubes have an outside diameter of 56 mm of 63 mm. Yet, "AX" probes are available in two lengths, with a 210 mm or 370 mm length measuring cell (Figure A.2b).

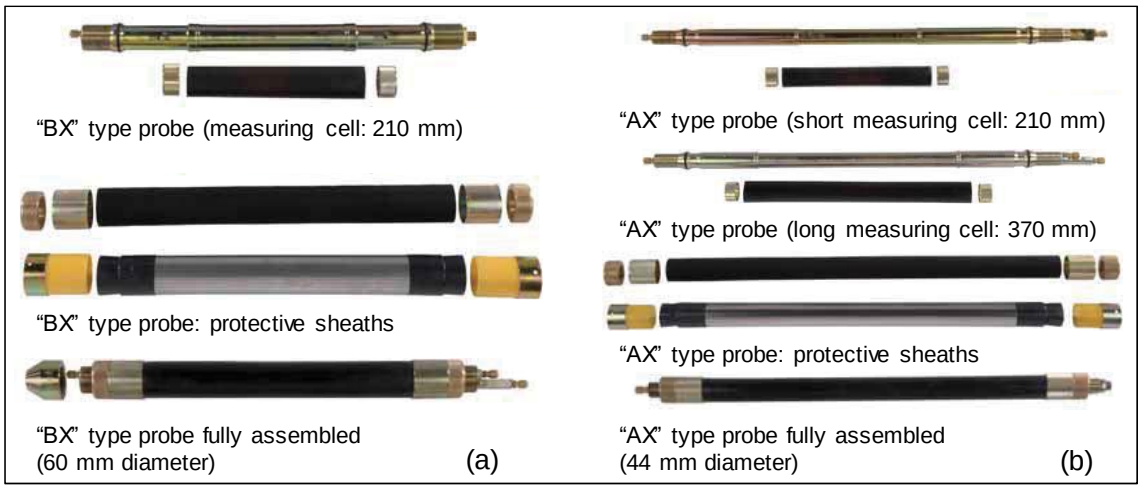

Figure A.2 – Examples of "G" type probes and its different protective sheaths (fabricant catalog available on internet APAGEO (2017)). (a) "BX" Ménard probe (60 mm external diameter). (b) "AX" Ménard probe (44 mm external diameter) of measuring cell lengths 210 mm and 370 mm.

A.1.3.2 The tubing

Different types of tubing can be used to connect the probe to the control unit. The most relevant technical aspects are the internal diameter, the stiffness and its sensitivity to temperature variations. For "G" type probes, two types of tubing can be distinguished: parallel and coaxial. In the first case, two parallel tubes link the probe to the control unit, one of them carrying water and the other, pressurized gas. In the case of coaxial tubing, the one carrying water is internal to the one for pressurized gas. This presents one major advantage: the tubing carrying water is subject to much less volumetric variation due to total pressure increases, because its walls are submitted to a constant pressure only equal to the difference between water and gas pressures (the so-called differential pressure), all along the test. Figure A.3 presents some types of tubing currently in use for Ménard pressuremeter tests.

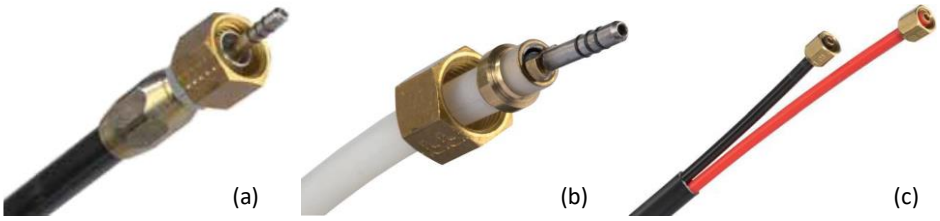

Figure A.3 – Different types of tubing. (a) Coaxial tubing for high pressure tests, (b) coaxial tubing for low pressure tests, and (c) parallel tubing (fabricant catalog available on internet APAGEO (2017)

A.1.3.3 The control unit

The control unit (C.U.) is the device that enables controlling the pressure on the water and gas circuits, managing the differential pressure between those circuits and measuring the injected volume of water. The pressure required for the realization of the test is provided by a pressurized air bottle connected to the C.U. The water reservoir is connected to a scaled volumeter enabling readings of the injected volume. Historically, none of the Ménard type control units provide a physical separation between air and water: pressurized air directly pushes water.

In early developed devices, all measurements were manual. It was up to the operator to write down the readings of pressure and volume all along the test. Figure A.4 presents the evolution of the most used types of control units. Most recent devices are equipped with sensors and data loggers. Acquisition is automatically done following pre-determined protocols. Printers were developed as a manner to prevent fraud in test

results by printing test results directly on site. Figure A.5 shows how the data acquisition systems are usually installed near the control unit, some of them with an integrated printer, and some in a more modern shape, including colored and touch screens.

The first attempt to fully automate the test was done during the eighties. The first automatic control unit was called the PAC (standing for Computer Assisted Pressuremeter, in French), presented by Baud (1985) and shown in Figure A.6(a). At that time, it was difficult to perform the numerical processing in a computational cost-effective way due to the limited existing technology. Some most recently developed devices are currently used in practice, such as those presented in Figure A.6(b to e).

The development of a control unit capable of performing pressuremeter tests containing several series of cycles was reported by Reiffsteck (2010). The claimed objective of that device was to assess liquefaction properties of soils. This equipment was further used by Reiffsteck (2014) applying different cyclic loading protocols at two reference testing sites, one with over consolidated clays and the other with dense sands. The author reports experimental difficulties in defining an adapted frequency for the cyclic loading, since drainage conditions are unknown. The need for pore-pressure measurements is pointed out.

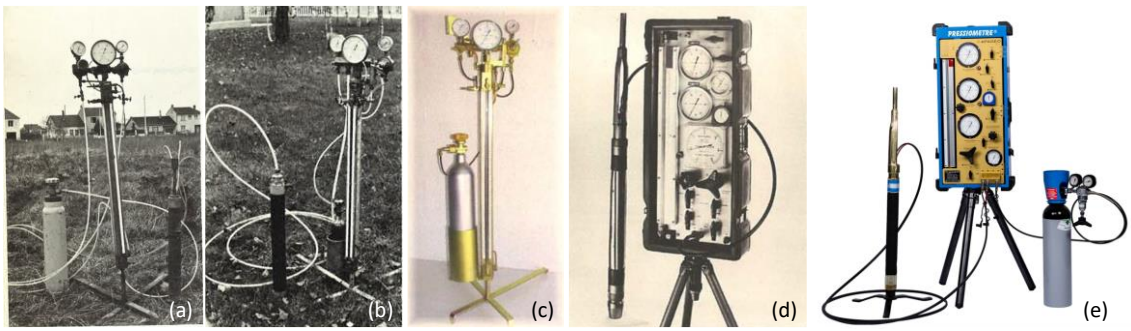

Figure A.4 – Evolution of the most common control unities. (a) Early "E" type pressuremeter and control unit LCPC (1971). (b, c) Early "G" type pressuremeter and c.u. (d) "G" type control unity integrated to a casing in 1975 Gambin (2005). (e) Fully assembled "G" type probe, control unit and gas bottle, as currently commercialized APAGEO (2017)

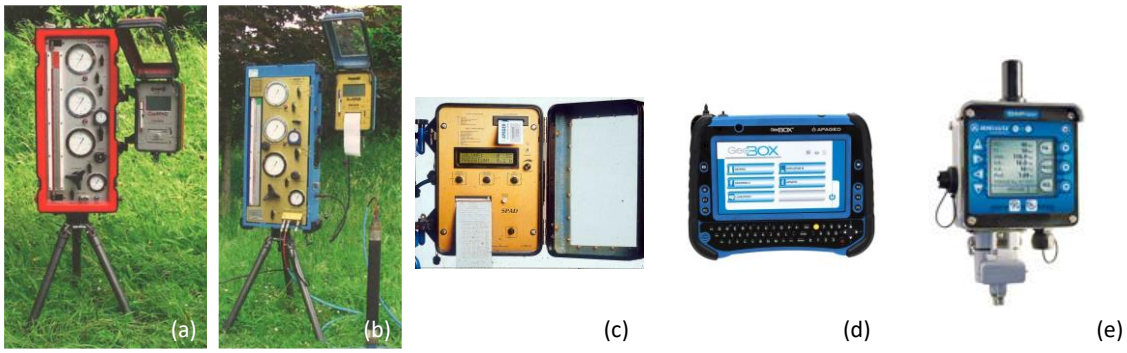

Figure A.5 – Data acquisition devices. (a, b) GeoSPAD system, enabling data acquisition and printing on site Gambin (2005). (c) Detail of the first series of data loggers with printer. (d) GeoSPAD 2 APAGEO (2017) and (e) BAP LUTZ (2014) currently used devices for data acquisition

Figure A.6 – Examples of automatic control units. (a) PAC Baud (1985), (b) PREVO LUTZ (n.d.), (c) GeoPAC APAGEO (2017), (d) PresioLIM AUTO LIM (n.d.), (e) Auto-Pression Logic (2019)

A.1.4 Limits of application

Jézéquel, Lemasson and Touze (1968) examine some inherent implementation problems that may limit the performance of the pressuremeter tests. Amongst other factors, the authors analyze the influence of the loading rate, the borehole convergence after drilling and the cavity swelling before the probe insertion, probe orientation (vertical or horizontal), the probe's measuring cell deformability, the distance between the actual test and the ground surface and the influence of the soil average stress on monotonic tests. Amongst the analyzed factors, the most significative seem to be related to the creation of borehole and disturbances that can take place before the probe is inserted. Regarding the influence of the stress state, it is concluded that the creation of the borehole disturbs the initial stress state *in situ* and thus, inherently, avoids any monotonic pressuremeter test to assess soil's intrinsic stress dependent properties. The authors also comment that some limitations of the pressuremeter tests are related to the measuring cell membrane. Ideally, they are expected to behave, at the same time, as

infinitely rigid (to minimize volume losses), infinitely flexible (so that they oppose low inertia to self-inflation) and to be resistant to bursting (for matters of durability and productivity).

Baguelin et al. (1978) also highlight critical issues related to the membranes. At the time of the publication, it was considered difficult to comply with the minimum quality requirements for probe's membranes and sheaths. Special concern was given to the homogeneity of the membrane thickness and the availability of the membranes, which were not standardized. The authors point out that membrane burst was the main cause of delays during on site operations. The situation has unfortunately not improved since that time.

The authors discuss the influence of parasite tubing effects on the test accuracy. The first source of error is related to the variation of the tubing compressibility coefficient with temperature. The authors measured a variation of the compressibility coefficient of a polyamide tube (mostly employed at that time for "E" type pressuremeters) of 4 mm internal diameter and 6 mm external diameter (length is not mentioned). The volumetric compressibility varied from 0.03 cm^3/100 kPa at 10°C to 0.05 cm^3/100 kPa at 40°C. Through a simplified calculation, authors conclude that such variability is unacceptable for tests performed in hard soils or rocks, and that coaxial tubing is more adequate for this case. The same study is unfortunately not done for coaxial tubing.

Another source of error regards the hydraulic pressure losses that may take place when there is water flowing inside the tubing. One example is presented for a semi-rigid plastic tubing of 4 mm internal diameter and 6 mm external diameter, 50 meters long, which has a hydraulic head loss of 60 kPa for a flow-rate of 100 cm^3/s. Authors do not explicit the temperature at which the test was performed. It is concluded that hydraulic pressure losses must be considered when interpreting the non-linear portion of the test, near the limit pressure, especially in tests performed in soft soils and when long tubing is used. One serious effect of the pressure losses is that it can make it very difficult to control water and air pressure simultaneously, affecting the differential pressure between the guard and the measuring cells.

Baguelin et al. (1978) presented limitations related to the maximum expansion capacity of the probes, both in terms of pressure and volume. Reaching those limits cause a test

to be terminated prematurely, i.e without reaching the limit pressure. Limits on pressure are due to the risk of bursting or damaging the control unit. Limits on volume are due to water supply limit (insufficient reservoir capacity).

At the time of the publication of the book, the authors considered that a pressure capacity 2.5 MPa was sufficient to most foundation studies. This is no more the case to date. According to the ARSCOP quiz (Jacquard and Varaksin (2018)), more than 50% of the participants are solicited by clients to perform tests to pressures higher than 5.0 MPa. It is usual to reach pressures up to 8.0 MPa. Thus, it seems that reaching “high” pressures is a current engineering need.

Regarding the volume capacity, Baguelin et al. (1978) consider that this is a more serious issue. Within a database of 67 tests randomly chosen by the authors, the limit volume (associated to the limit pressure) was effectively reached in only 2 tests. Two reasons presented by the authors for this are: (1) when approaching the limit pressure, there is an increasing risk of burst. This risk is associated to membrane failure, but also to it pulling out of the fittings that hold it on place. Operators, though, hesitate to continue the test, any failure being detrimental for the workday performance. (2) In the vicinity of the limit pressure, as soil yields, water flows rapidly out of the control unit. Operator becomes alarmed that the reservoir may empty completely, and the water circuits may desaturate. This is often the case for soils presenting fragile behavior, such as overconsolidated clay and loess.

The authors accept that the limit pressure can be obtained by extrapolation methods in cases where the test has been stopped prematurely. They discuss the relative errors that can be brought by extrapolation and discourage extrapolating more than 25% or 30% of the volumetric expansion.

Baguelin et al. (1978) list other technological limitations of the test. Some of them were overcome thanks to improvements and automatization of the control unit. One particular problem cited, inherent to three-cellular probes, is that tests with cycles are difficult to carry out. Performing unload-reload loops with three-cell probes requires managing two very different fluids at a same time: water and air. It is also noted that gas tends to dissolve into water during the test, since there is no physical separation in the C.U. Gas goes into the circuit and reappears as bubbles in the measuring circuits.

Few developments providing enhancements in measurement accuracy took place between the invention of the three cellular pressuremeter and now. The states of practice presented by Clough et al. (1990), Gambin (1990) and by Cassan (2005) showed that most of the recent developments were related to data acquisition and automatization of the pressure-volume controller. Three-cellular probes remained almost unchanged since the invention of the "G type" Ménard probe in the seventies.

The success of these probes for practical applications may be perceived as a proof of their adequacy to provide design parameters for standard geotechnical structures. However, the concept of three-cell probes brings some inherent limitations that prevent them to be used for recent engineering needs, such as the assessment of small strain moduli. Few works have dealt with the practical limitations due to membrane problems, such as frequent bursting at high expansion rates and the low accuracy of volumetric measurement due to bad membrane behavior. Cour et al. (2005) pointed that frequent membrane burst has been the origin of the degradation of test quality. According to the authors, an average of 20 tests can be performed before bursting. The ARSCOP quiz in 2018 Jacquard and Varaksin (2018) confirmed the frequent probe bursting problem: 50% of the practitioners report probe bursting in an average of 18 tests.

A closer look at the measuring chain involved in the pressuremeter test based on volumetric measurements reveals that all the following parts can have an influence in the measurement quality:

- The probe, its membranes and working principle;
- The tubing carrying water;
- The water (or other fluid used to assess volume changes);
- The pressure-volume controller;

On such type of probes, cavity strain is assessed through water volume changes measured in a pressure-volume controller placed on the ground surface. The probe is supposed to expand cylindrically, and all volume changes are supposed to be due to soil deformations. Any disturbances in the relation between the probe's real radial expansion and the injected volume of water will lead to errors in the assessment of the cavity strain. The accuracy on the evaluation of the cavity strain is intrinsically related to the membrane behavior, the volume losses in the tubing and in the control unit, and

not just to the resolution of the volume measurement device. Accurate volumetric readings at the control unit will not necessarily help enhancing the device's accuracy, since errors will be hidden in all the measuring chain. Calibration tests enable only correcting repeatable behavior, but cannot provide corrections for random uncertainties, such as those related to dissolution of air into water, bad membrane behavior, or temperature changes.

A.1.5 Standards

A.1.5.1 Historical background

From the early beginning of the pressuremeter test, Ménard has defined the detailed procedures for the test implementation and interpretation. The testing protocol has evolved in time. According to Cassan (2005), when the test was created in 1955, the duration of the load-steps was of four minutes. This was determined by Ménard in order to better follow the creep behavior during all the test steps. In 1957 and in 1958, the duration of the load steps was reduced to two minutes, and then, in 1965, it was finally defined as one minute, as presented in the general rules D60 Ménard (1967). In 1971, the first attempt to standardize the test at a national level was done by the *Laboratoire Central des Ponts et Chaussées* (LCPC (1971)) with the document entitled "*Modes opératoires des Laboratoires des Ponts et Chaussées – Essai pressiométrique normal*". This document was the main reference until the nineties. It has been progressively substituted by more modern French and European standards published by AFNOR (1991), (2000), (2015). A standard covering tests with one unload-reload loop was published by AFNOR (1999).

Parallel standardization for the pre-bored pressuremeter test was undertaken in the United States following the works of Briaud et al. (1985). The authors considered that the pre-bored pressuremeter standard should be written in such a way that it could be readily extended for other types of pressuremeters under fast development at that time, such as the self-bored, the pushed-in and the cone-pressuremeter. The authors discuss the following key issues regarding the PMT performance: (1) Mono cell probes compared to three cell probes, and the influence of the ratio between the probe length and its diameter; (2) Comparison between pressure or volume increment loading procedures; (3) Volume losses and membrane calibration; and (4) Data reduction and

test interpretation. The authors suggest that the test results should be plotted in terms of cavity pressure versus cavity radial strain, so that any pressuremeter test result could be directly compared, independently on probe dimensions (and thus independent of the probe volume). This work provided the fundamentals of the ASTM standard D 4719-07 (ASTM International (2007). The American standard is more flexible than the French one regarding some aspects, such as the concerned probe types (monocellular and three cell) and the loading protocols (imposed pressure or imposed volume).

The most recent European standard is NF EN ISO 22476-4 by AFNOR (2015). According to Jacquard and Varaksin (2018), most French practitioners still refer to older versions of the standard, and also to ancient Ménard recommendations. ASTM standard is not used by French practitioners.

A.1.5.2 The European standard – standard tests and definitions

In the following, the procedures imposed or recommended by the most recent European standard for the performance of a Ménard test are presented.

A.1.5.2.1 On the testing Equipment

According to AFNOR (2015), the pressuremeter testing equipment is composed of the following elements: (1) the three cellular probe; (2) rods for inserting the probe on the borehole; (3) the control unit; and (4) the tubing.

Probes can have a flexible membrane or be equipped with a slotted tube for protection. Its fully-assembled outside diameter (d_c) and the length of the measuring and guard cells (l_c and l_g, respectively) are tabulated, and it is required that the probe can accommodate a volumetric expansion of at least 700 cm^3 (for "BX" or "AX" long types) or 550 cm^3 (for "AX" short type probe). A scheme is presented in Figure A.7. There are no specific details on the type of membranes regarding material, quality and durability. There is an exigence that the membrane inertia should be a percentual lower than the limit pressure of the soil to be studied. Fluid to be used should be water or an equivalent one that would present the same viscosity but improved properties against freezing. There is no technical specification for the tubing diameter. It is mentioned that the compressibility coefficient obtained in calibration tests, if using a long tubing, should not be greater than 6 cm^3/MPa.

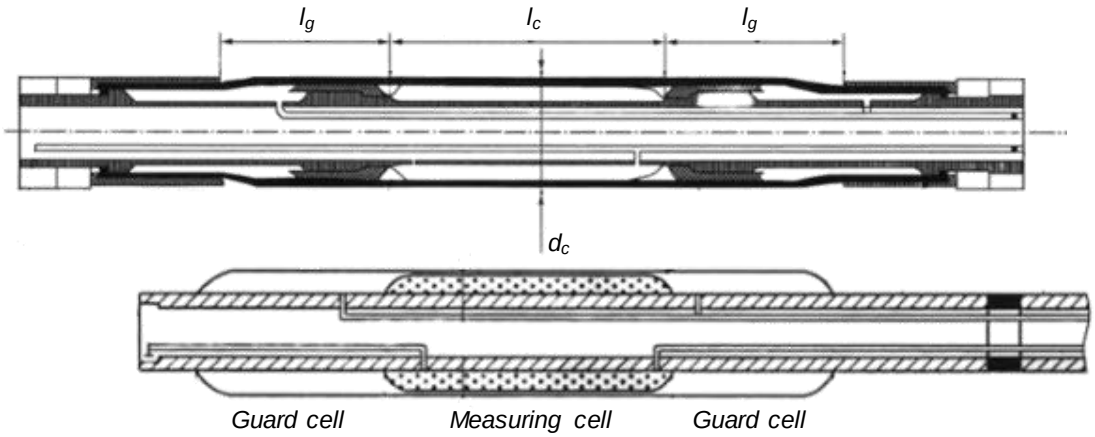

Figure A.7 – Plan and scheme of a tri-cellular pressuremeter probe according to AFNOR (2015)

A.1.5.2.2 On the calibration and measurement corrections

Readings of pressure and volume during a pressuremeter test are obtained on the control unit located at the ground level. Neither the measured pressure nor volumes are obtained precisely at the soil cavity walls. The following corrections must then be applied to the readings at the control unit:

- Hydrostatic pressure correction due to the vertical distance between the c.u. and the probe;
- Self-expansion volume correction, due to the compressibility of the whole device, including the CU, the tubing, the fluid and the probe with its membranes
- Probe membrane pressure correction due to the resistance opposed by the membrane to inflation;

Items b and c on the above list are obtained by calibration tests that must be undertaken for every probe, at every membrane or tubing changing, before performing tests in soil. The calibration procedure is described in the standard as follows;

- Measuring cell calibration: the central cell membrane must be inflated in open-air by 10 kPa pressure increments of 60 seconds duration each. The self-resistance of the measuring cell membrane is defined as the pressure corresponding to an injected volume of 700 cm^3 (for "BX" or "AX" long probe types) or 550 cm^3 (for "AX" short probe types); Once this test is performed, the probe can be fully assembled (protective sheath and external dressing). It must be pre-inflated at

least three times to this same volume for ensure membrane setting. Then, the measuring devices can be set to zero.

- The self-expansion calibration consists in placing the probe inside a thick steel cylinder, one-meter long, with a minimum thickness e of 8 mm and a diameter d_c inferior to 66 mm, and inflating it up to the maximum allowed pressure. The probe must be replicate the test conditions in the soil (flexible membrane or slotted tube, same tubing, same C.U.). After the probe touches the internal walls of the steel tube it is blocked against any radial expansion and thus, any volume variations due to pressure increases is expected to be due to device self-compressibility. An example of calibration curve is presented in Figure A.8a from which the following parameters can be determined:

Compressibility coefficient a [cm^3/MPa], calculated as the slope of the linear portion of the expansion curve. Remark: it is not precisely specified how to define the beginning of the linear part. Other methods, including non-linear hyperbolic laws to fit the calibration curve, can be used to derive the compressibility coefficient;

Contact volume V_p, equals to the interception of the straight-line portion with the *Y* axis;

This test enables estimating the initial volume of the central cell, V_c, which is further used to estimate the borehole cavity volume. V_c is calculated as the difference between the calibration cylinder volume along the central cell height (generally 21 cm for "BX" probes) and the injected volume to contact, V_p;

$$V_c = 0.25\,\pi l_c d_i^2 - V_p \qquad (A.1)$$

- The membrane resistance calibration consists in inflating the probe in open-air. The probe should be placed in vertical position in the same vertical plane than the control unit. Inflation is performed by applying constant pressure load steps of 60 seconds duration as for a test in soil. It is recommended that the pressure increment is equal to $1/5^{th}$ of the estimated value of the membrane resistance and that expansion is performed up to a minimum volume of 700 cm^3 (for "BX" or "AX" long probe types) or 550 cm^3 (for "AX" short probe types). The membrane resistance p_{el} is defined as the pressure associated to this limit volume, and it is noted that it can vary between 50 kPa and 200 kPa. Figure A.8b presents an

example of open-air calibration curve and the determination of p_{el} according to this standard.

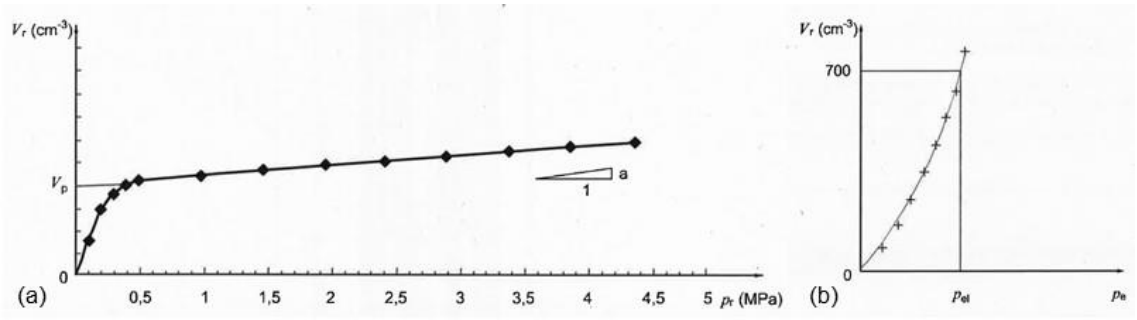

Figure A.8 – (a) Example of self-expansion calibration test and the definition of the coefficient of self-expansion a and the contact volume V_p. Extracted from AFNOR (2015). (b) Example of open-air calibration test and the definition of the membreane limit resistance p_{el}. Extracted from AFNOR (2015)

A.1.5.2.3 On the probe installation on the ground

The standard covers the following installation methods: pre-bored, driven and pushed (or vibro-pushed). Driving and pushing is mainly applicable to probes protected by a slotted tube. A table defining the recommended, tolerated and forbidden installation methods according to different types of soil is presented. Minimum and maximum borehole diameter are imposed in function of the probe outer diameter (Table A.1). The minimum vertical spacing between consecutive tests is of 0.75 meters and it is indicated that the usual spacing between tests is one meter. There is no guidance for adapting the placement of the probe in the borehole to cope with local heterogeneities, marked layering or high strength contrasts.

Table A.1 – Minimum and maximum borehole diameter in function of the probe dimensions AFNOR (2015)

Probe Type	***Diameter (mm)***	***Borehole diameter (mm)***	
		min	***max***
AX	*44*	*46*	*52*
BX	*58*	*60*	*66*
NX	*70/74*	*74*	*80*

A.1.5.2.4 On the testing protocol

Pressure should be applied to the cavity walls through constant-pressure load steps of 60 seconds duration. The operator should be able to apply a pressure increment in less than 20 seconds. If the tubing is longer than 50 meters, the time to increase the pressure

should be adjusted (but not specified). The pressure increment should be defined before the beginning of the test in order to obtain about 10 measuring points before reaching the end criteria. This should be done based on previous experiences, information collected while drilling the borehole or on specific engineering instructions. Operator can adjust the pressure increase a maximum of two times during the test if needed.

The pressure in the guard cells must be less than the pressure in the measuring cell: the difference should be typically twice the central cell membrane inertia. The differential pressure must be adjusted at the control unit before the beginning of the test and controlled during all the load steps. It is of major importance that the operator adjusts the differential pressure at the control unit in function of the probe depth to ensure that the differential pressure at the probe level remains constant. The standard imposes that the operator should be provided with a table establishing the differential pressure in function of the test's depth, such as that presented in the LCPC operation manual LCPC (1971).

The expansion process during the test is stress controlled, as presented in Figure A.9A. During each load step, volumetric readings are performed at predefined time intervals. If data is collected manually, intervals are of 15 s, 30 s and 60 s after the beginning of the load step. If electronic data acquisition is performed, readings at 1 s are also recorded. Expansion should continue until the end of test criteria are satisfied, which are defined as:

- A maximum pressure of 5.0 MPa is reached, or,
- The volume injected in the measuring cell is greater than 600 cm^3 (for "BX" or "AX" long probe types) or 450 cm^3 (for "AX" short probe types) or,
- The probe bursts;

It is accepted that even if the above-mentioned criteria are not reached, the test can be interpreted if there are at least three load steps beyond the creep pressure. It should be noticed that the end-of-test criteria are related to equipment limitations, and not necessarily aiming at effectively assessing the test parameters.

A.1.5.2.5 Data reduction and test interpretation

The collected data is reduced to produce a curve of corrected probe volume in function of cavity pressure. Only the values corresponding to the end of the load steps are presented. The so-called creep curve should be presented in the same graph in a secondary Y axis. It is obtained by calculating the difference between the volumes measured at 60 seconds and 30 seconds after the beginning of the load step. A recommended graphical representation is presented in Figure A.9B.

Pressure corrections include the hydraulic charge correction and the membrane resistance correction. Hydraulic pressure correction is due to the vertical distance between the probe and the control unit, as defined in Figure A.10, as can be calculated as:

$$p_h = \gamma_i(z_c - z_s) \qquad (A.2)$$

Membrane resistance correction is calculated by subtracting the membrane pressure p_e obtained at a given probe volume V_r in the open-air calibration from the gross pressure p_r obtained in the test in soil at the same volume V_r.

$$p = p_r(V_r) - p_e(V_r) \qquad (A.3)$$

Volumetric corrections due to device's self-expansion are calculated using the self-expansion coefficient *a* obtained in the calibration test. The corrected volume is calculated as:

$$V = V_r(p_r) - ap_r \qquad (A.4)$$

The corrected pressuremeter curve is obtained by the following equations:

$$p = p_r + p_h - p_e(V_r) \qquad (A.5)$$

$$V = V_r - V_e(p) \qquad (A.6)$$

From the pressuremeter corrected test curve the following numerical results should be derived: (1) the pressuremeter creep pressure; (2) the pressuremeter limit pressure; and (3) the Ménard modulus. Creep pressure is determined either from graphical analysis of the creep curve or from the expansion curve. It defines the changing from the pseudo-

elastic phase (quasi-linear) to the plastic phase. The limit pressure is defined as the pressure associated to doubling the cavity volume, at which the limit volume V_L is assigned. It can be calculated as:

$$V_L = V_C + 2V_1 \qquad (A.7)$$

In which V_c is the volume of the probe evaluated from calibration tests and V_1 is the injected volume corresponding to the beginning of the pseudo-elastic phase. If the limit volume has not been reached during the test the limit pressure can be obtained by extrapolation using two mathematical curve fitting methods and extrapolating the obtained curve up to the theoretical limit volume. Extrapolation methods can be used only it there are at least two measuring point beyond the pressuremeter creep pressure. In the case else, it should be noted only $p_l > p$, on this case p being the maximum pressure reached on the test.

The pressuremeter modulus is defined as the slope of the pseudo-elastic portion of the pressuremeter curve. This portion, delimited by pressure and volume values denoted (p_1, V_1) and (p_2, V_2), is defined by a mathematical expression, but the standard allows it to be modified following engineering judgment. The pressuremeter modulus is calculated using the following equations. A different formula is proposed for probes equipped with a slotted tube, which considers the tube dimensions:

$$E_M = 2(1+\nu)\left[V_c + \left(\frac{V_1 + V_2}{2}\right)\right]\left(\frac{p_2 - p_1}{V_2 - V_1}\right) \qquad (A.8)$$

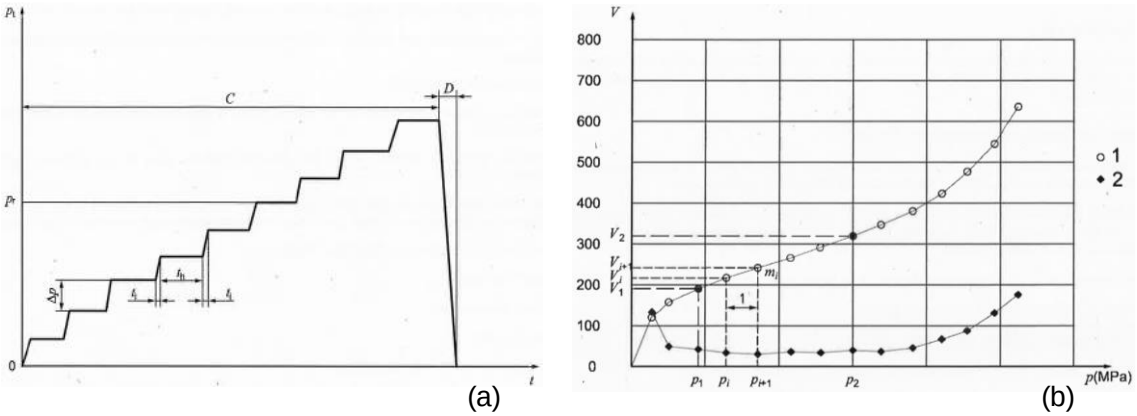

Figure A.9 – (A) Loading program as defined by AFNOR (2015). (B) Recommended representation of the pressuremeter test curve according to AFNOR (2015)

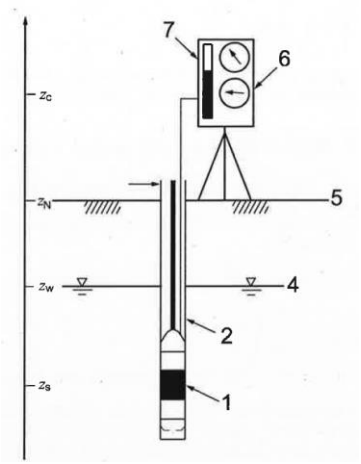

Figure A.10 – Definition of the altimetric levels according to AFNOR (2015)

The recommended practice for tests including one single unload-reload loop is presented in AFNOR (1999). It comprises the same testing specifications as for monotonic tests, but a reloading loop is also interpreted. The same formulation for the evaluation of modulus is used, but on this case, it is denoted E_R, standing for reload Ménard pressuremeter modulus. The suggested load program is presented in Figure A.11a and a representation of the test results after data reduction is presented in Figure A.11b. According to the proposed procedure, the unload phase should be performed in the load step preceding g the end of the pseudo-elastic phase. The duration of the unloading is of one minute until reaching a pressure corresponding to the beginning of the quasi-linear phase. Reloading is performed following constant-pressure load steps adopting the same pressure increment used on the virgin loading.

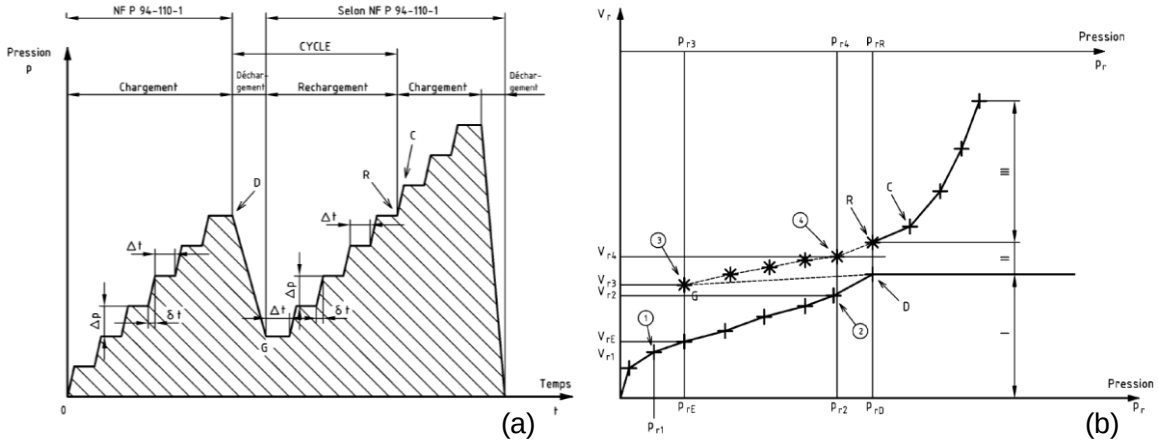

Figure A.11 – (a) Loading protocol suggested by AFNOR (1999) for tests containing one unload-reload loop. (b) Expansion curve for tests containing one unload-reload loop. Extracted from AFNOR (1999)

A.2 OTHER TYPES OF PROBES

Mechanical development of most of the alternative pressuremeter probes took place in the 70's as reported by Clough et al. (1990). Two leading directions can be distinguished regarding the recently developed equipment: (1) those concerning the probe it-self, the measuring cells geometry, the injected fluid and the measuring method (through volumetric measurements or using punctual displacement transducers); and (2) those concerning the insertion method, such as the pushed-in and self-bored probes. Figure A.12 from Clough et al. (1990) presents a scheme of the different probes commonly used in the 90's. Some of the most relevant aspects concerning these developments are discussed hereafter.

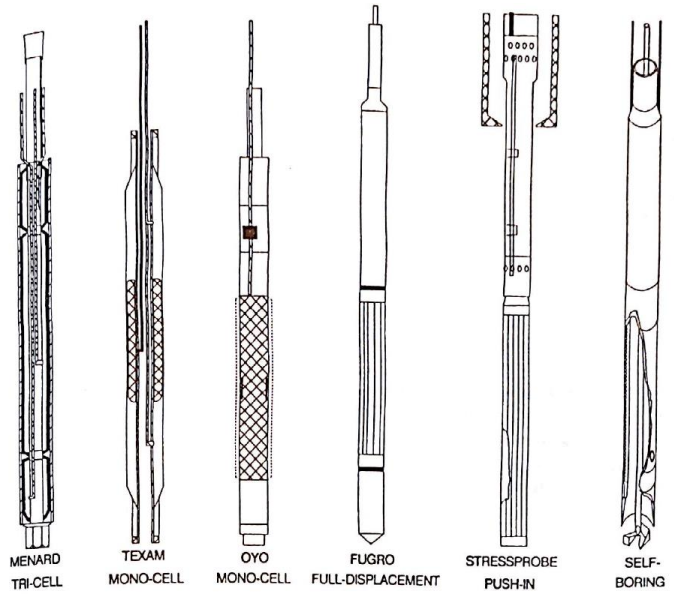

Figure A.12 – Scheme of the different types of probes developed between the 70's and the 80's Clough et al. (1990)

A.2.1 Pre-bored pressuremeter

A.2.1.1 Parallel developments

Briaud (1992) and Clarke (1995) present an overview of the historic development of pre-boring pressuremeter probes. Most developments took place between the 60's and the 80's, with different types of probes produced in different countries. Amongst them, only few are still being used for practitioners and cited in literature. They are briefly presented in the following text. They had their origins due to parallel development in the domain of pre-bored pressuremeters from three main fronts: (1) works in France due to Ménard as discussed on the previous section, (2) in Japan, from 1959, with the

works of Fukuoka and then Suyama leading to the invention of the *Oyometer* (OYO Corporation), and (3) in the United States, with the development of the TEXAM probe in the University of Texas A&M in 1981 Briaud (2005), further described in the book "The Pressuremeter", Briaud (1992). The main difference between the OYO and TEXAM type probes and the Ménard type probes was that the two first ones were mono-cellular (no guard cells).

According to Clarke (1995), three different instruments were developed by the OYO Corporation, usually called *Oyometers*. The Lateral Load Tester, LLT presented in Figure A.13 A and B, was developed in the late 50's for designing horizontally loaded piles. It is a single-cell probe, in which radial displacement is assessed from volumetric readings (such as in Ménard probes). It can be supplied in three different diameters (60 mm, 70 mm and 80 mm), and the cell length is of 600 mm. The maximum pressure capacity is 2.5 MPa, depending on the borehole diameter. Still according to this author, Elastometer 100 and Elastometer 200, developed by the same Japanese company, were the first commercially available probes equipped with displacement transducers for local readings of radial displacement. They were designed for testing rocks and can operate up to pressures of 10 MPa and 20 MPa, respectively. Probe diameter can be 62 mm or 72 mm, and the expanding cell measures 520 mm. It employs an 8 mm thick rubber membrane, of same type as those used in expandable packers, to ensure resistance to high pressures and to prevent the membrane from axially expanding into the void annulus between the probe and the borehole. The displacement transducer is a mechanical assembly of two spring-loaded arms, which follow the inner part of the membrane and that are connected to an LVDT (Figure A.14A and B). Pressure is measured by a transducer placed inside the probe. Measurements of pressure and displacement are sent to the surface by an electric cable running parallel to the hydraulic hose that feeds the probe. The probe is inflated through a high-pressure hand pump and there is no need for a pressurized air bottle, which makes the test safer. Both OYO monocell type probes have their own control units, which can be very simple, such as the hand pump (Figure A.14A).

Figure A.13 – (a) OYO Lateral Load Tester (LLT-M) monocell pressuremeter probe for low pressure applications (2.5 MPa). Extracted from fabricant website. OYO (2019a). (b) OYO AUTO LLT 2. Improved control unit with automatic test control OYO (2019b).

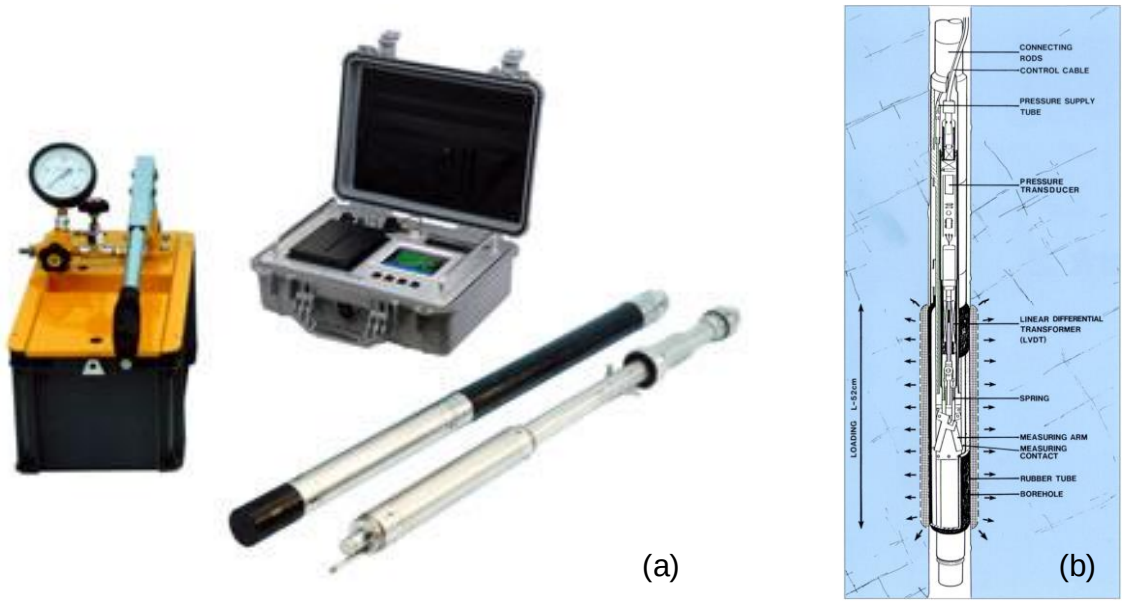

Figure A.14 – (a) OYO Elastmeter monocell pressuremeter probe for high-pressure applications (up to 20 MPa). Radial displacement transducers used to assess radial strain. (b) Probe scheme showing the displacement transducers OYO (2019c), (2019d)

Other type of monocellular probe frequently used in practice is the TEXAM probe. As extracted from Briaud (2005), "*The TEXAM pressuremeter (…) was developed in 1981 at Texas A&M University to simplify and make safer (no pressurized gas bottle) the operation and the repairing of the Ménard pressuremeter while allowing for more versatility in the types of possible PMT tests (e.g.: cyclic tests). The TEXAM probe is monocellular with a 6.5 length to diameter ratio to minimize end effects and the test is performed in equal volume increments*".

According to the manufacturer's instruction manual, the TEXAM has a pressure capacity of 10 MPa, a volume resolution of 0.01 cm^3, a pressure resolution of 1 kPa and

allows assessing a range of soil moduli up to 2000 MPa. Tests can be run in stress or strain-controlled manner. The control unit is composed of a mechanical actuator used to displace a piston which travels within a cylinder filled with the inflation fluid. Probe diameter can be 70 mm or 44 mm, for use in a slotted casing. The probe consists of a cylindrical metallic body covered with an inflatable rubber sheath protected or not with metallic strips. Radial expansion is measured through volumetric readings in the control unit, such as in Ménard type probes.

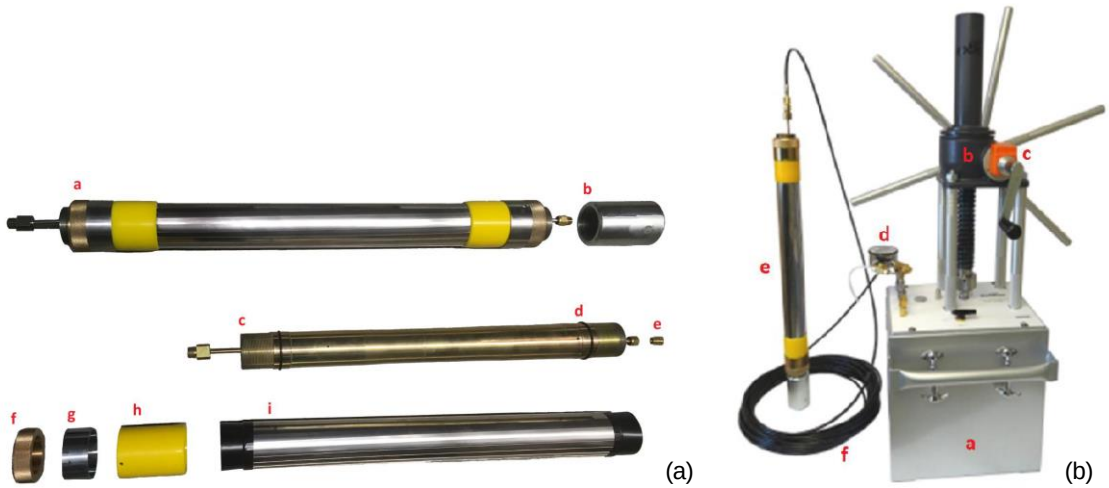

Figure A.15 – (a) TEXAM probe components (a – complete PMT probe; b – probe shoe; c – probe's body; d – O-ring; e – saturation plug; f – brass knurled nut; g – steel ring; h – vulcolan collar; i – metallic sheath); (b) Fully assembled TEXAM probe and control unit (a - the control unit; b - the actuator: c - volumetric counter; d - digital pressure gauge; e - the probe; f - the tubing) (adapted from TEXAM pressuremeter instruction manual RocTest Limited (2017a))

The manufacturer presents a calibration procedure based on inflating the probe into a steel thick cylinder, just like for Ménard type probes, It is recommended, however, that if a special test procedure is to be performed in soil (such as cyclic tests, creep tests, stress level influence test), a special calibration is also performed, mimicking the test procedure in soil. There are no further details on how to correct the test results afterwards. An abacus for the calculation of probe limits in terms of pressure and expansion volume is given, as presented in Figure A.16. It is of invaluable importance for operators for deciding the end-of test criteria.

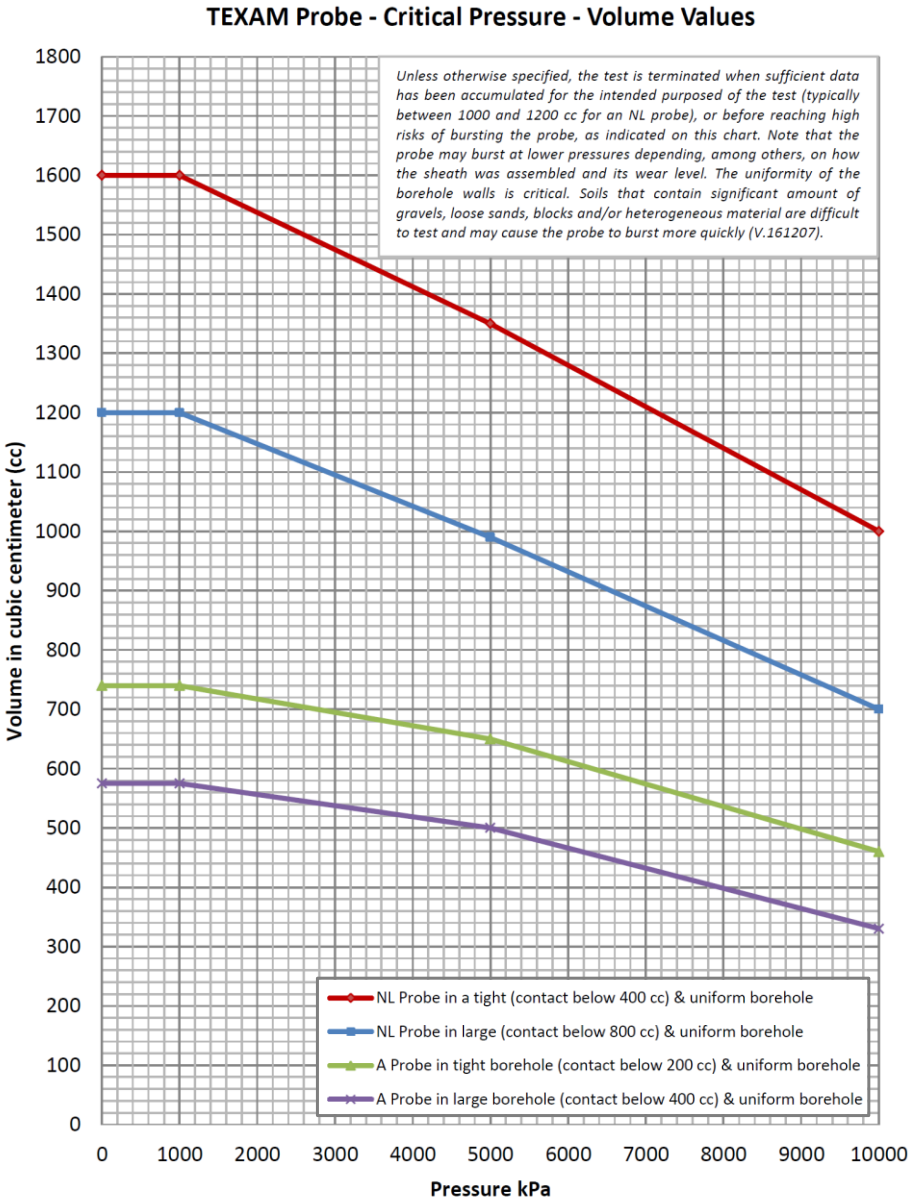

Figure A.16 – TEXAM probe limits in pressure and volume (extracted from TEXAM pressuremeter instruction manual RocTest Limited (2017a)

A.2.1.2 Technological innovations in Ménard type probes

Besides the parallel development carried out in outside of France, few innovations took place with respect to improving the current Ménard type probes. On this subject, one can mention the so-called **FC 60** probe, which is a tri-cellular probe respecting AFNOR (2015) standards. Its development took place in the past decade in France.

Its main originality consists on the fact that the external elastomer sheath, which defines the guard cells, has been surrounded by a textile restraining sheath (patented design and

production method by Cour (2006)). The textile sheath has a cylindrical profile at rest and the property of being able to dilate by opposing a very weak resistance until reaching a limit profile following a beveled shape. This shape was chosen to reduce stress concentrations near the probe ends, avoid undesirable deformation shapes and improve membrane durability. A scheme is presented in Figure A.17.

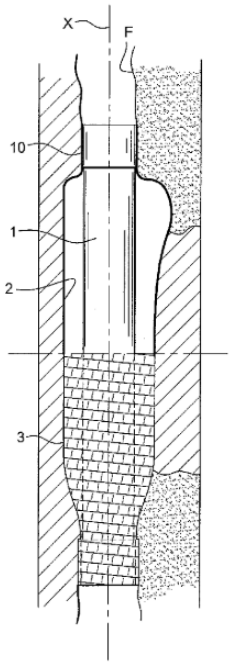

Figure A.17 – Scheme of the controllably-deformable inflatable sleeve Cour (2006) **showing (1) the mandrel that extends along the longitudinal axis (X), an inflatable jacket (2) connected to the mandrel and sealed through (10), and the restraining sheath (3) covering the inflatable jacket.**

A second textile device, which has been further patented by Cour (2013), is placed surrounding the membrane of the central measuring cell. This textile sheath has the main objective of controlling the expansion of the measuring cell, ensuring that its expansion is deployed following a quasi-cylindrical geometry, and thus, reducing longitudinal deformations. This invention had as main objective the increase of the accuracy of the measurement of the radial expansion by eliminating longitudinal deformation in the measuring cell. According to the fabricant THP (2015), a maximum volume of 1200 cm^3 can be injected in the central measuring cell. When this limit value is reached, membrane expansion is blocked by the textile sheath.

An external polyurethane sheath is placed surrounding textile sheath to protect it from abrasion when in contact with the soil. The probe is placed inside a metallic strip protection, which avoids it to be pierced when used in gravelly soils.

Probe is composed by intercalated layers of impervious rubber membranes and textile sheaths. Those layers are presented in Figure A.18 and described in the sequence.

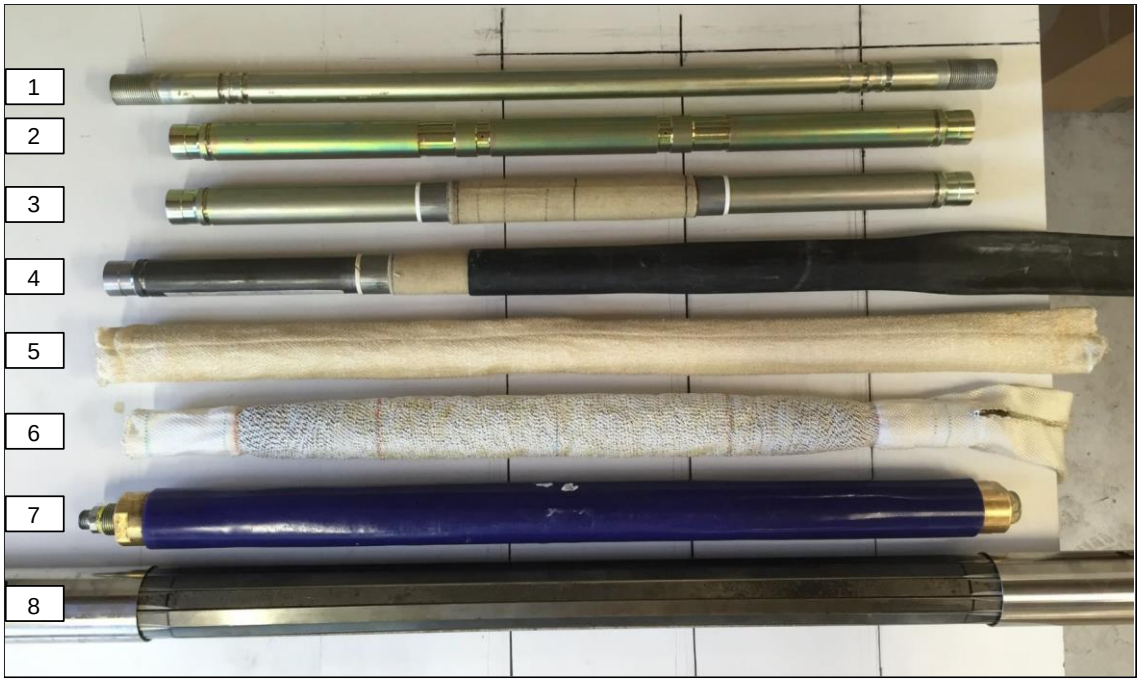

Figure A.18 – Component layers of a FC 60 probe (adapted from Cour and Rouet (2017))

1. Probe core: piece in which pressurized water and air are connected;
2. Sleeve in which all the membranes are crimped. This sleeve is further slipped over the probe core;
3. Central measuring cell surrounded by its textile membrane (controlled expansion), crimped on the sleeve;
4. Rubber membrane which defines the guard cells;
5. Longitudinal textile sheath. This sheath has no structural role. It protects the rubber membrane from being pinched by the external restraining sheath;
6. Restraining sheath (controlled deformation);
7. Polyurethane protection;
8. External protection, metallic stripes.

Figure A.19 presents the inflated profile of the probe. The beveled ends are imposed by the external restraining sheath. Figure A.20 presents the inflated profile of the central measuring cell, inflated inside a transparent plexiglass cylinder.

Figure A.19 – External textile restraining sheath employed in FC 60 probe THP (2015)

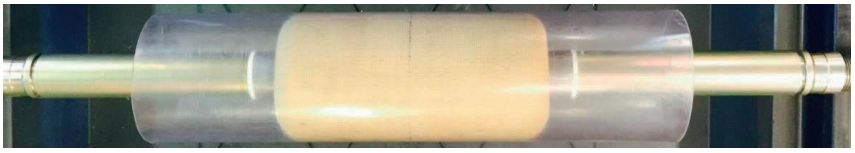

Figure A.20 – Textile sheath applied to the central measuring cell in FC 60 probe, imposing its cylindrical geometry THP (2015)

This innovative design presents two advantages regarding traditional Ménard type probes. The first is that all the membranes are industrially crimped to the probe mandrel. This reduces the tolerances on the cells dimensions and avoids any uncertainties due to operator's assembling skills on the working site. This assemblage mode type "mandrel-over-core" enables a quick replacement in case of probe bursting. The second advantage is that the rubber membrane has the only role to provide weathertightness; it is the restraining sheath that resists to the internal pressure. This contributes to increasing probe durability and its capabilities in pressure and maximum expansion. According to the fabricant, probe can be inflated up to 1000 cm^3 at 8 MPa (Figure A.21).

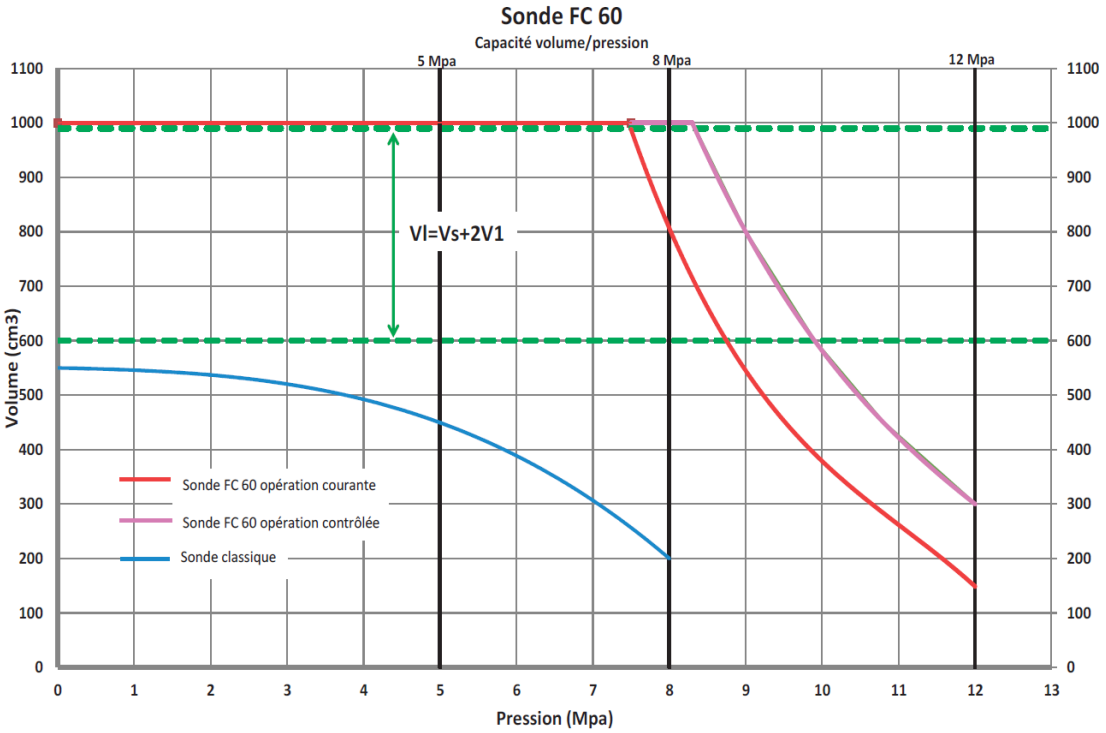

Figure A.21 – Limits of operation of the FC60 tri-cellular pressuremeter probe THP (2015)

FC 60 probe has been applied in practice since a few years Jacquard et al. (2013). Its increased capacities enable the effective measurement of soil conventional limit pressure, without the need of extrapolation methods. According the authors, results obtained using this probe have been proved to be similar to the ones obtained with other standard Ménard type probes.

A.2.2 Pushed-in pressuremeter

Pushed-in pressuremeter probes (PIP) are pushed into the ground. Soil can be fully displaced or partially displaced, depending on the probe toe section. The development of this type of probe took place mainly in the 80's, starting in France with a pressio-penetrometer developed for offshore use, first presented in 1982, and further in 1986 with the works of Withers et al. (1986) about the full displacement pressuremeter, a Dutch and British cooperation. The French device was a monocellular probe, volumetric displacement-measurement type, with a pressure capacity of 2.5 MPa and a 100% theoretical volumetric expansion capacity. The full displacement probe was equipped with sensors for locally assessing radial displacement up to a maximum capacity of 50% radial expansion, and a maximum pressure of 10 MPa.

Inserting the probe by pushing it into the ground has advantages and drawbacks. Main advantages are that, specifically for very soft soils, it is almost impossible to create a borehole and keep it open until a pre-bored probe can be inserted. Inserting a probe by pushing avoids any potential difficulties related to borehole stability. The installation mode is less sensitive to operator's drilling ability and practice and thus should lead to better test repeatability. Conversely the insertion mode by pushing may fail in gravelly or stiff soils. Furthermore, special theoretical considerations have to be done for this insertion method, since the soil stress state at-rest is strongly disturbed due to soil displacement when pushing the probe. The development of the pushed-in pressuremeters was accompanied by theoretical considerations providing a background for the interpretation of the test, especially with respect to the influence of disturbance due to insertion in the obtained parameters.

A.2.3 Self-bored pressuremeter

Since the early beginning of the pressuremeter practice it has been known that the installation process can change the soil response on the first part of the monotonic pressuremeter curve. According to Baguelin et al. (1978), the first self-boring probe was developed in France following the works of Jézequel in 1968. The probe was called the *pressiomètre autoforeur* (PAF). It aimed to eliminate the main factors that could alter the initial state of the soil during probe installation. Self-boring probes basically consist of probes assembled over a thin walled sampler, as shown on the scheme in Figure A.22. The grinder destroys the soil inside the sampler, reducing drastically soil disturbance due to the cavity formation.

French self-boring pressuremeters are monocellular probes using volumetric measurements to assess radial strain. Three models were developed: PAF-68, PAF-72 and PAF-76. A most recent version, entitled PAF 2000 was presented by Reiffsteck (2003). The main difference between this new version and the previous ones is the inclusion of sensors for local measurement of probe expansion (three lines of sensors).

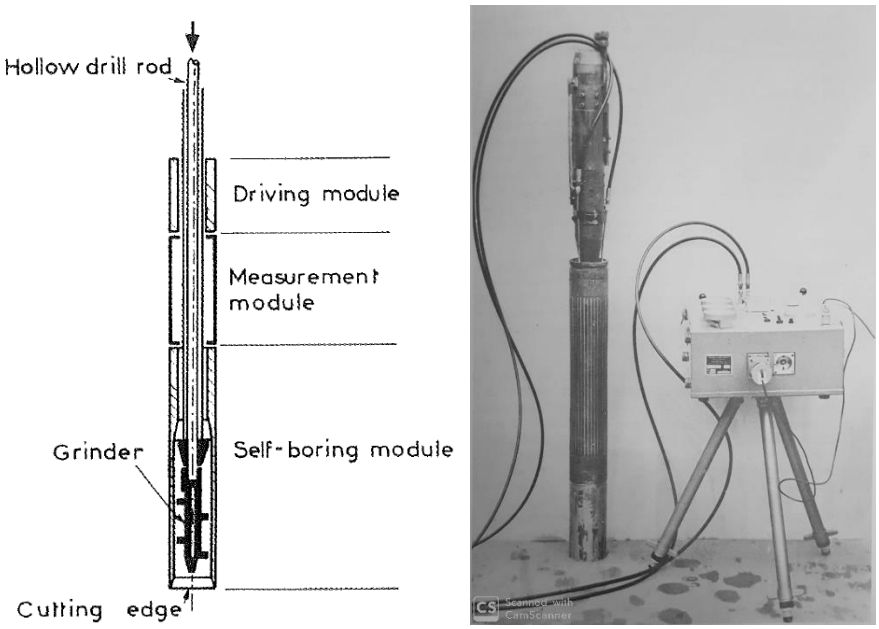

Figure A.22 – Principle of the self-boring pressuremeter probe and a photo of the PAF 72 (extracted from Baguelin et al. (1978)

Parallel developments took place in England, first presented by Wroth and Hughes (1972). The main difference from probes developed in France within the same decade was the presence of sensors for punctual measuring of radial expansion. Three feeler arms radially spaced of 120° were present, each one mechanically connected to strain gauges. The inventors used this solution to increase the accuracy in the assessment of soil moduli and of the earth pressure at-rest. The instrument was further named the *Camkometer*, denomination which is not in use anymore. Many modifications of the original equipment can be found in literature, including changes in the displacement arms to improve measurements, increases in the number of arms (6 instead of 3), installation of pore-pressure transducer.

Figure A.23 – Cambridge self-boring pressuremeter. Extracted from fabricant's catalog: Cambridge Insitu Ltd (2015)

The presence of local displacement transducers seems to limit the equipment's expansion capability. According to Cambridge Insitu Ltd (2015), the currently commercialized equipment has a maximum expansion rate of 15% of the probe's initial radius at-rest. Thus, the equipment cannot be used to assess soil limit pressure.

A.3 FLEXIBLE DILATOMETERS

A.3.1 Principle

Flexible dilatometer is the usual denomination of a pressuremeter adapted for measuring high pressure levels; Mair and Wood (1987). They are generally employed for testing rocks or very stiff soils. In principle, both tests (pressuremeters and flexible dilatometers) share the same working principle, that of cylindrical cavity expansion. There is, however, a fundamental difference regarding the requirements for measuring the radial displacement. In the case of flexible dilatometers, generally, measurements are made on the probe by punctual displacement transducers.

Care should be taken not to confuse the flexible dilatometers with flat dilatometers neither with borehole jacks. The stress field generated by those devices is not the same as that imposed by flexible membrane pressuremeters (uniformly distributed pressure), and thus different interpretation methods are used. A brief description of dilatometers that are not of concern for this thesis is presented in A.3.6.

A.3.2 Practice

According to Ladanyi (1987), first successful applications of flexible dilatometer tests for rock mechanics were reported by Panek et al. in 1964 in the United States and by Rocha et al. in 1966 in Portugal. According to the author, dilatometers presented the main advantage to be faster than other methods available at that time to evaluate rock properties. This is especially true for jointed rocks for which core drilling gives poor samples that cannot be adequately investigated through laboratory tests.

Ladanyi (1987) presents the suggested methods for determining deformability properties using flexible dilatometers. Author distinguishes two types of dilatometers: those based on volumetric changes (like pressuremeter probes) and those based on radial displacement measurement. It is stated that the principal use of this instrument is to obtain deformability properties, but that it can also be used for the determination of *in situ* stress state, rock's tensile strength, for the field determination of creep properties and for the determination of the short-term strength of weak rocks.

Despite large similarities between dilatometers and pressuremeters, some practical aspects are different from one to the other. For creating the boreholes in the required diameter in rocks, Ladanyi (1987) states that rotary diamond coring is usually done, instead of the destructive techniques usually employed for pressuremeters. Whether the borehole walls are unstable, casing should be used for stabilizing the cavity walls down to the test pocket. A common practice to enable successful tests to be performed in weak fragmented rocks consists in grouting the cavity after drilling it. Then, core drilling is performed into the grouted zone, resulting in a smooth walled drill hole. It is also recommended to check the walls of the drill hole using a camera and to make the rock cores available to the operating crew as a supplementary resource for evaluating rock quality before placing the probe in the cavity. In brief, much attention is given to the quality of the cavity walls.

In case of volumetric measurement probes, Ladanyi (1987) states that very high stiffness tubing and volumetric controller are required to avoid errors due to system deformability. This is not the case when the volumetric readings are done down hole. A calibration program like that of pressuremeters is required. The author states that ambient air temperature should be recorded during calibrations and that calibrations should be repeated if temperature changes by more that 5°C. The same author also presents a note stating that some probes are provided with radial strain measurement sensors that are in contact with the internal face of the expandable rubber membrane. On this case, special calibration procedure should be performed to determine the membrane change in thickness in function of the internal pressure.

Concerning the testing protocol and the determination of rock deformability properties, Ladanyi (1987) states that the a test should be pushed up to reaching the equipment's maximum allowed pressure. Performing multiple unload-reload loops present two major interests: the first is to identify moduli changes in function of stress changes. The second is that performing tests at very high pressure enables mobilizing a greater volume of rock, thus obtaining values more representative of the global rock behaviour.

A.3.3 Equipment

Some of the currently available dilatometric equipment are presented further. The main difference to be underlined between the probes concerns the strain measuring method, which can be: (1) volumetric measurement with volumeter embedded on the probe; (2) radial strain sensor crossing the membrane and touching the cavity wall; (3) radial strain sensor touching the interior face of the rubber membrane.

The Probex borehole dilatometer / pressuremeter, commercialized by RocTest is an example of the first type. Cavity strains are assessed through measurement of the probe volume. The fluid reservoir is placed above the probe core and goes down the hole. Measuring the volume this way has the advantage to avoid errors due to tubing compressibility and temperature variations. Pressure is measured at the ground surface, by a pressure transducer placed near the pressure source (hydraulic pump). Hydrostatic pressure corrections and membrane inertia corrections must be applied (same as for pressuremeters). According to the product technical description, maximum pressure is 30 MPa, minimum and maximum diameters are 73.7 mm (deflated) and 85.5 mm (fully inflated). This corresponds to a maximum expansion of 16% of the probe's initial radius, which means that this equipment cannot be used for assessing conventional limit pressure. A diametrical change measuring resolution of 0.001 mm is announced by the manufacturer RocTest Limited (2017b). The length of the expandable membrane is of 460 mm. The probe scheme as well as its photo are presented in Figure A.24.

The same manufacturer commercializes the model entitled DMP (usually called DMP 95, due to its external diameter of 95 mm). This probe's membrane is equipped with three pairs of metallic inserts spaced of 120°. Each of these inserts is connected to an inductive displacement sensor placed on the interior of the probe. It allows assessing cavity displacement without the influence of the membrane compressibility, in principle. According to the TELEMAC (2018) manual, displacement sensors are calibrated for a maximum expansion of 20 mm and a resolution of 1 μm. Expandable membrane length is 1000 mm. Pressure transducer is installed inside the probe. Inflation is controlled using compressed air (no need to use incompressible fluids such as water). Only membrane inertia corrections must be performed. Probe diameter is 95 mm, to be used in 101 mm borehole. Given the maximum possible expansion, this type

of probe cannot be used to assess conventional limit pressure. One example of such device is presented in Figure A.25.

Other examples of dilatometers are those commercialized by Cambridge In Situ, called HPD73 and HPD95 Cambridge Insitu Ltd (2015). Those probes have an external diameter of 73 mm and 95 mm respectively. They are equipped with punctual strain sensing at 6 points equally spaced around the center of the expanding region. On these probes, displacement sensors are in contact with the internal face of the inflatable membrane. Announced displacement resolution is better than 1 micrometer. Maximum expansion capacity is of 38% and 58% of the probe's initial diameter, respectively, for models 73 and 95. Pressure measurement is inside the probe and pressure capacity is of 20 MPa. Example of this type of probe is presented in Figure A.26.

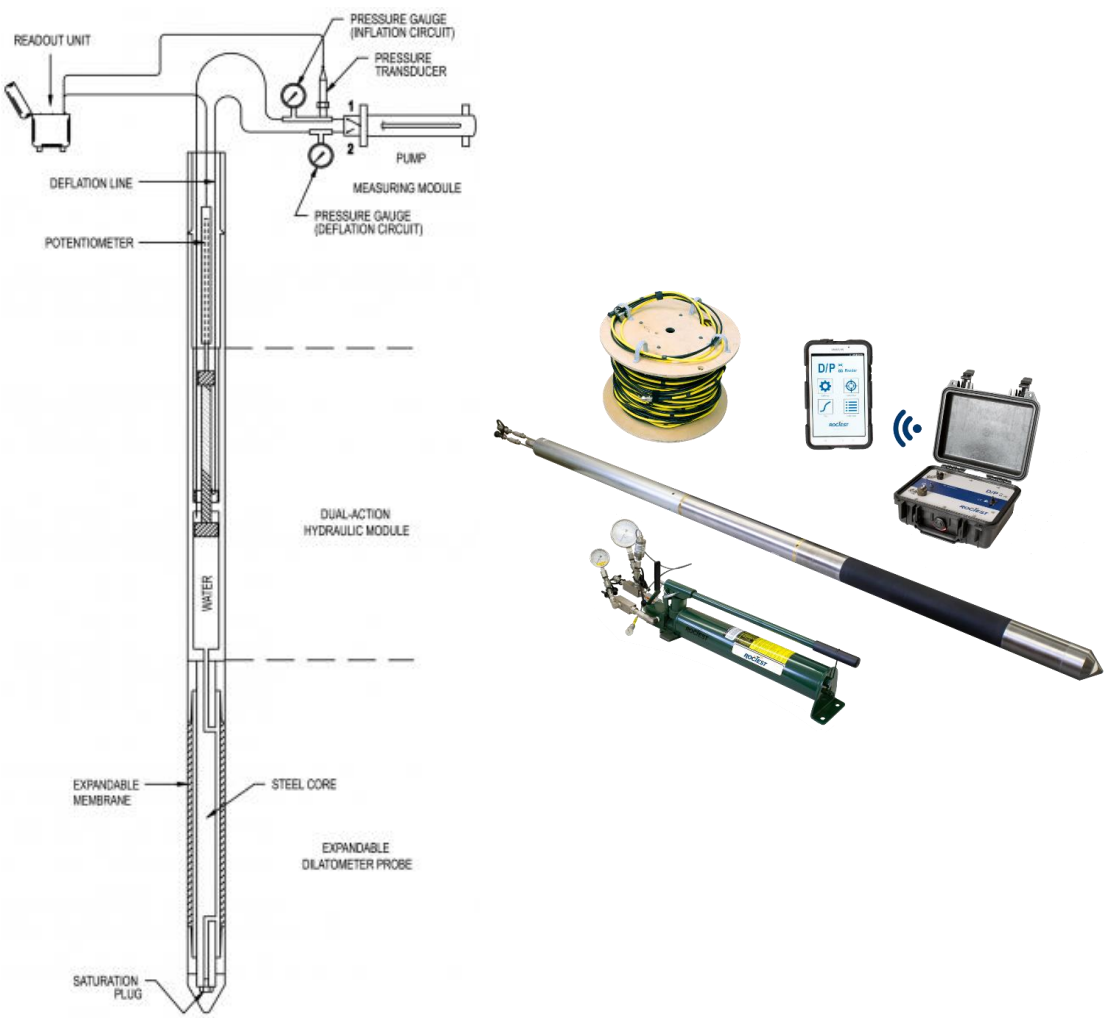

Figure A.24 – Probex borehole dilatometer/ pressuremeter. Extracted from user's guide: RocTest Limited (2017b)

Figure A.25 – DMP 95 mm dilatometric probe. Radial strains are assessed through induction sensors connected to metallic insertions trespassing the membrane. TELEMAC (2018)

Figure A.26 – High pressure dilatometers HPD73 and HPD95 by Cambridge In Situ: Cambridge Insitu Ltd (2015)

A.3.4 Limits

Most limits associated to dilatometer tests are the same as those for pressuremeters, regarding probe installation and disturbance of soil's initial state. For rocks, it is expected that disturbance due to drilling is much less that that provoked when drilling soil because of rock's greater strength and stiffness. Another limit inherent of dilatometric probes is that of the maximum allowable expansion, as mentioned in the previous examples. The presence of sensors for local assessment of radial displacement reduces the expansion capability of the membrane for mechanical reasons.

Dilatometric probes are of more complex implementation on site, since the equipment is technically more advanced than pressuremeter probes (electronic circuits embedded on the probe) and thus more expansive. As described by Baguelin et al. (1978), and especially taking into consideration the cost of the equipment, operators tend to be alarmed when high pressures and high expansion rates are achieved during the test, and it is likely that they stop the test prematurely in order to avoid damages to the test equipment.

A.3.5 Standards

Most recent standard on dilatometer tests is the European ISO NF 22476-5 AFNOR (2013). This standard is an evolution of the several suggested practice manuals published, as the one by Ladanyi (1987).

A.3.5.1 On the testing equipment

The standard imposes that the expansion of the borehole walls is monitored by three or more electric transducers. Variant A type probes are equipped with displacement transducers that penetrate the membrane and directly bear on the borehole wall. Those probes are more adapted to tests in rocks. Type B probes have displacement transducers placed at the inner wall of the membrane. Those probes require special calibration procedure to account for membrane compressibility. Figure A.27 presents a scheme of a dilatometric probe according to AFNOR (2013). According to this definition, equipment such as that presented in Figure A.24 cannot be considered as a dilatometer.

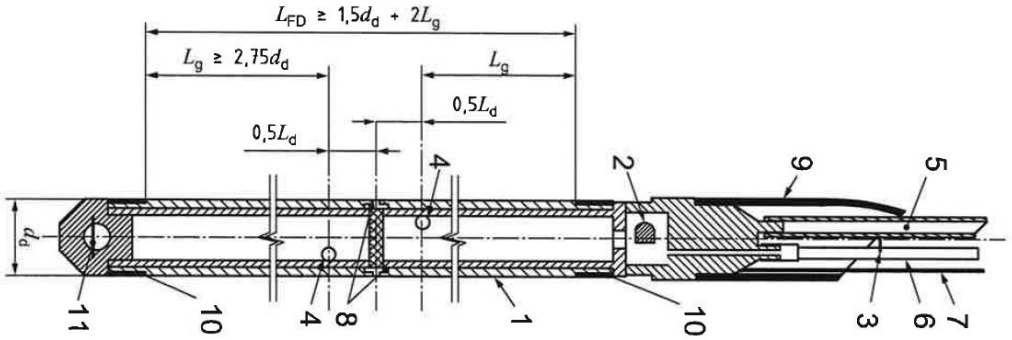

Figure A.27 – Dilatrometric probe scheme according to AFNOR (2013)

The control unit should allow applying pressures of at least 20 MPa, implementing a pressure increase of 0.5 MPa in less than 20s and stopping the injection when necessary. Probe can be inflated using gas or liquid.

A.3.5.2 On the calibrations and measurement corrections

Probes must be calibrated for pressure losses due to membrane stiffness at each change of membrane and at appropriate intervals to the use of the probe, and at least once a year. Before proceeding to the open-air calibration, probe must be inflated at least three times to its maximum capacity. It should be connected to the injection controller using a short line (less than 2 meters). For the open-air calibration test, probe should be inflated as if it was in the ground, in vertical position, using pressure increments sufficiently small so that to properly define the complete range of diameters of the membrane. Once the open-air calibration curve is obtained, pressure loss correction is done the same way as for pressuremeters.

"B" type dilatometers (those having the strain sensors bearing the internal walls of the membrane) require calibration for the membrane compression. The procedure is quite similar to that for pressuremeters: the probe is placed into a thick steel cylinder and then pressurized to cover all the pressure ranges attained during tests in soil. Membrane compression corrections can be done in two ways: the first is similar to that for pressuremeters, by calculating the slope of the calibration curve after probe is in contact with calibration cylinder. This can be done if the calibration curve is linear. The second way is correcting point by point, calculating the compressibility coefficient *a* between any pressure holds p_1 and p_2. It is suggested to take the steel cylinder deformability into account for calibration interpretation. For instruments with multiple displacement transducers, the mean value of the compressibility coefficient *a* is to be calculated.

A.3.5.3 On the probe installation on the ground

Samples should be taken of the drilled rock at the desired testing depth. They should be identified, classified and shall be available for every separate ground layer within the desired investigation depth. After the test pocket is drilled (about 3 m length), the dilatometric probe should be placed no later than 2 hours after finishing the pocket. Exception is for the case of hard rocks. If no core has been recovered or when the stability of the borehole wall is not guaranteed, the decision of performing a test shall be evaluated by the operator. This remark regards the risk of probe burst or to get the equipment permanently blocked into the borehole.

A.3.5.4 On the testing protocol

Four loading procedures are proposed by AFNOR (2013), entitled procedures A to D. Procedure A comprises loading, unloading and reloading paths, data are recorded manually. Procedure B is similar, but data is recorded automatically. Procedure C comprises only a loading phase with manual data recording. And procedure D comprises only one loading phase, followed by an unload reload loop which is then followed by a long pressure hold step. Data is recorded manually.

In procedure A (Figure A.28*a*), both the loading and unloading parts shall be carried out in steps with pressure holds at each step. The minimum pressure in each reload loop shall be the contact pressure between the probe and the rock. After reaching the maximum pressure during the test, load shall be decreased in steps with readings continued as before.

In procedure B (Figure A.28*b*), the unloading and reloading phases of each loop shall be carried out either by steps or continuously. The loop sizes are normally smaller than in case of procedure A, and the pressure amplitude can be adjusted according to design specifications of the test. A pressure-drop of about one third of the pressure at the start of the unload loop is recommended. Before commencing the descent phase of a loop, enough time shall be allowed for time-dependent effects to become insignificant (no fixed criterium).

For both procedures A and B, it is suggested that the maximum applied pressure during the test is decided by considering the maximum stress expected to be applied to the ground by the structure considered.

In procedure C (Figure A.28*c*), pressure shall be increased in steps until either the ground fails or the capacity of the equipment is reached. Operator is authorized to adjust the pressure increment according to soil behaviour to obtain enough points to evaluate the pseudo-elastic behaviour and to obtain at least three pressure-holds beyond this phase. This procedure is very similar to that of pressuremeter tests.

In procedure D (Figure A.28*d*), AFNOR (2013) recommends that the loading program be individually designed according to design requirements.

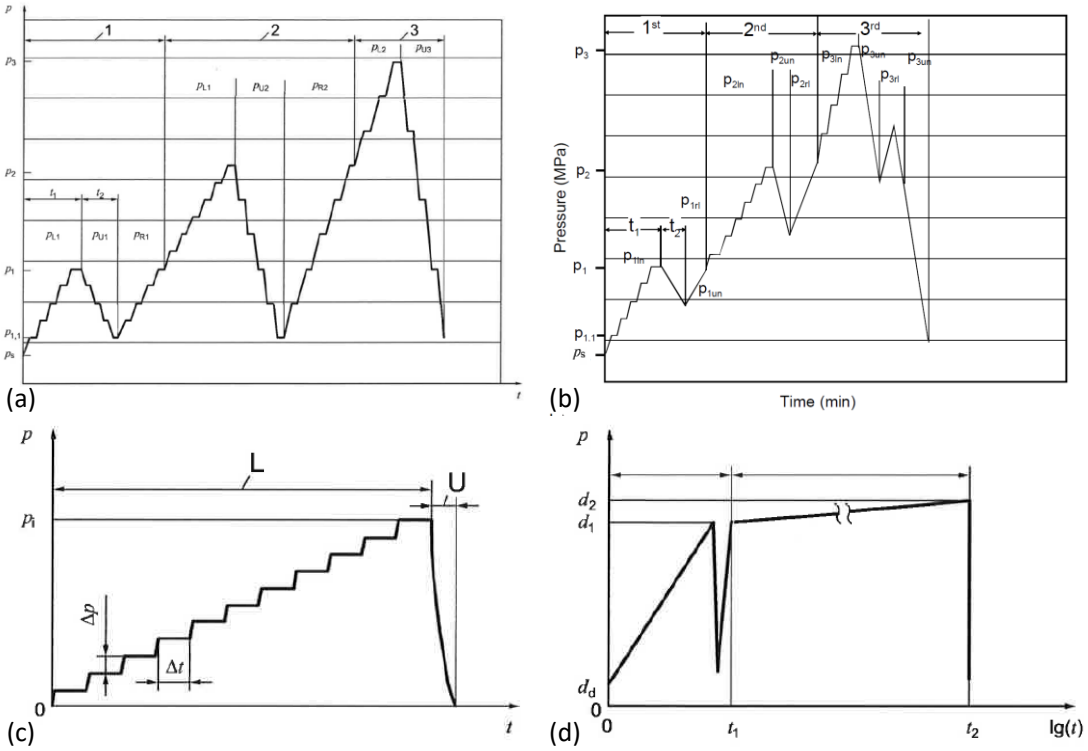

Figure A.28 – Four testing procedures as suggested in AFNOR (2013) (adapted)

A.3.5.5 Data reduction and test interpretation

Data correction regarding pressure losses and membrane compressibility must be performed. The basic problem equations are presented in the standard. The approach is different from that of pressuremeter tests. For dilatometers, a shear modulus is first

calculated and then transformed into a compressibility modulus. Flexible Dilatometer Test shear modulus (G_{FDT}) is calculated as follows:

$$G_{FDT} = \Delta p \left[\frac{0.5 d_s}{\Delta d}\right] \qquad (A.9)$$

where d_s is the nominal diameter of the test pocket, determined by extrapolating the early linear portion of the expansion graph to meet the horizontal line through the pressure axis at which the pocket expansion first begins; Δd is the additional diametral displacement of the borehole due to Δp; and Δp is the increment of applied pressure above the contact pressure. It is recommended that the shear modulus be determined using the average value of the pocket diametral displacement measured at least in three diametral directions for a given loading path. However, if values differ much from each other indicating anisotropy of the rock mass, the G value shall be determined separately for each direction. The standard does not clearly define limits for the application of this second procedure.

Shear modulus can be transformed into elasticity modulus E_{FDT} using the following equation, based on linear elasticity:

$$E_{FDT} = 2G_{FDT}(1 + \nu) \qquad (A.10)$$

An assumption needs to be made on the Poisson's coefficient ν, but the standard does not provide guidance

Pressure and strain ranges used to determine G or E moduli are defined according to the test procedure used. For procedures A to C, moduli G shall be calculated as schematically presented in Figure A.29 (*a* to *c*). Procedure D is suggested for assessing rock creep parameters and there is no recommended procedure for deriving a shear modulus from this procedure.

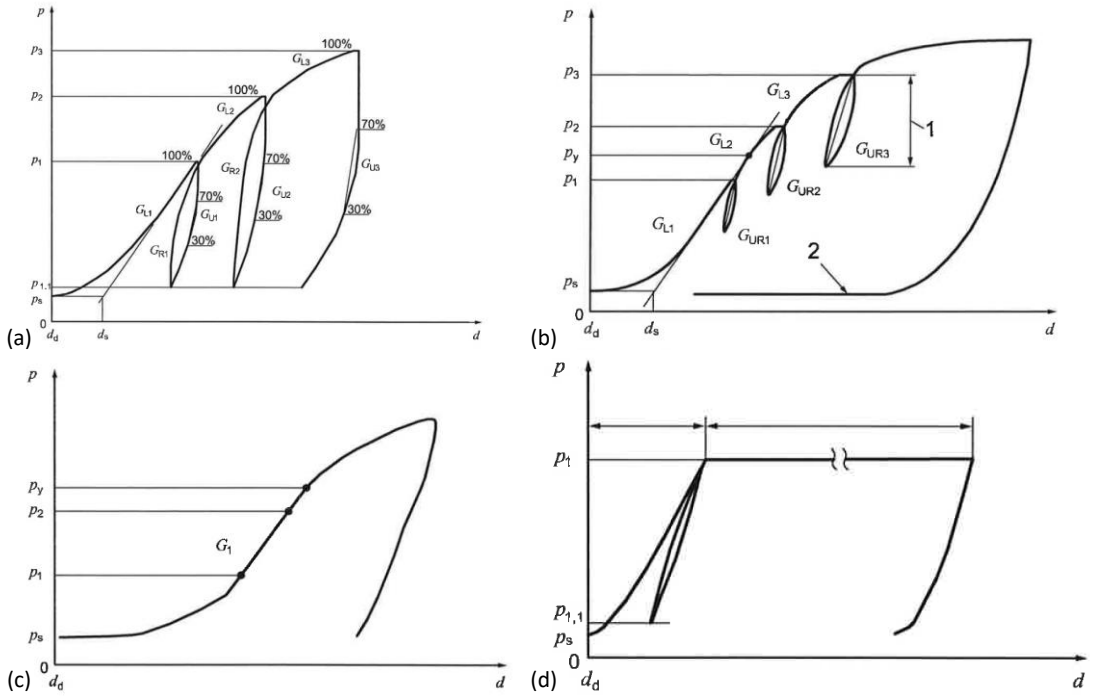

Figure A.29 – Theoretical curves obtained after data reduction and corrections when performing the test procedures AFNOR (2013)

A.3.6 Other types of dilatometers not covered by this work

This chapter focused on the similarities between flexible dilatometers and pressuremeters and presented a brief overview of flexible dilatometers principles, practice and existing equipment. There exist other types of probes for performing expansion tests in soil, but they have fundamental difference regarding the expansion mode in comparison to cylindrical cavity expansion tests, reason for which they are not covered by this text. Two examples of these types of dilatometers are the rigid dilatometers and the flat dilatometers.

Rigid dilatometers are composed of two semi-circular rigid plates separated by a hydraulic jack. The most renowned equipment of this type is the Goodman Jack (Figure A.30). The test principle is very similar to pressuremeter or flexible dilatometer tests: the jack is inserted into a borehole in the rock. The main difference is that the stress field generated by the rigid platens is not cylindrically homogeneous, such in the case of flexible-membrane probes.

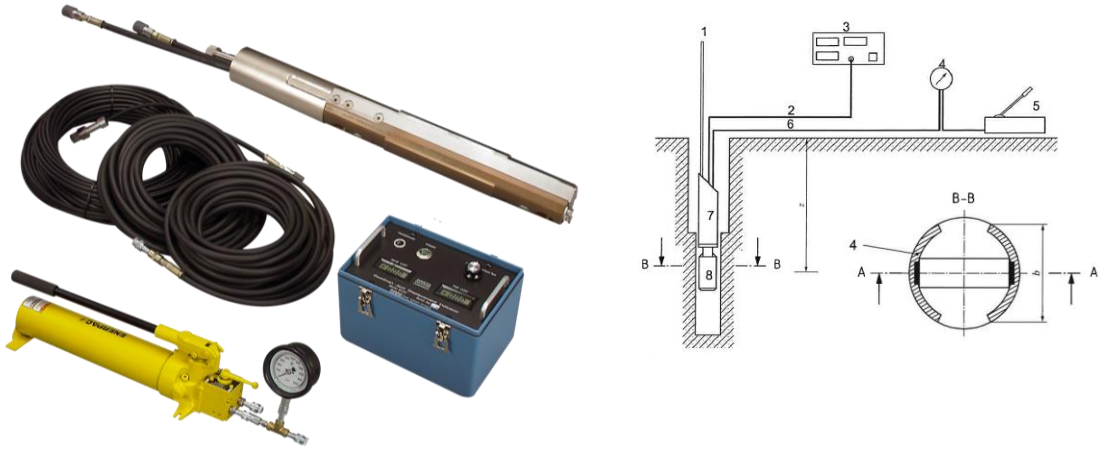

Figure A.30 – Example of rigid dilatometer: The Goodman Jack (DGSI (2013)). Pressure is applied to the cavity walls through rigid platens, generating a non-homogeneous cylindrical stress field. Not covered by this work

Flat dilatometers, amongst which the most known is the so-called Marchetti dilatometer (Figure A.31), consists of a steel blade with a circular, thin steel membrane mounted flat on one face. The blade is driven vertically into the soil using pushing rigs Schnaid (2009). Penetration is halted every 20 cm and a test is performed by inflating the membrane and taking a series of pressure readings at prescribed displacements. The test is suitable for a wide variety of soils such as clay, sand, silt and hard formations. Membrane expansion is not cylindrical since its expansion is more likely to approach to half a sphere. For this clear reason, interpretation methods are different from those proposed for pressuremeters and flexible dilatometers.

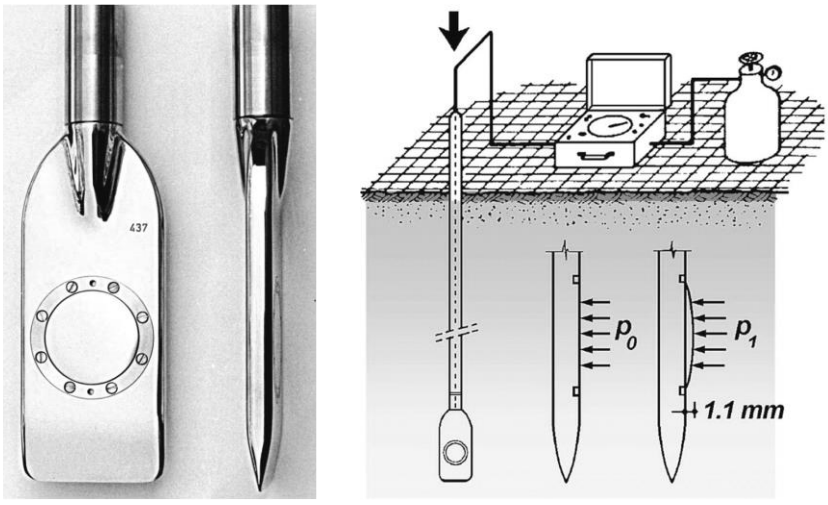

Figure A.31 – Example of flat dilatometer (Marchetti dilatometer, extracted from Schnaid, 2009), not considered on this work

A.4 COMPARISON BETWEEN THE EXISTING PROCEDURES AND THE DIFFERENT TYPES OF PROBES

The previous sections presented a quick overview on the existing equipment and the usual test procedures for cylindrical cavity expansion tests. Most of them have a common origin which was Ménard's works in the late 50's and the 60's. It is evident that the testing procedures are influenced by the available testing equipment, its capabilities and limitations.

From the analyzed documents, it appears that in French practice the pressuremeter test result is used as a direct input for foundation design, using empirical rules that have first been established by Ménard and then evolved always following the same testing methodology. For this reason, testing protocols have not significantly evolved since their creation in the 60's, in an effort to keep tests compatible with those present in the database used for the development of the design rules still in use nowadays. French standards are the most detailed and restrictive ones. Only one type of loading procedure is authorized, and only three-cellular probes are concerned. Much effort has been undertaken to fully standardize the test to keep it fully automatable, from execution to interpretation. End-of-test criteria in terms of maximum pressure or volume are strictly imposed, enabling straightforward way to check if the test was completed. Formulas for the determination of the so-called pseudo-elastic range also facilitate the definition of the range for the calculation of modulus.

However, it seems that this high level of detail brings some prejudice regarding some practical aspects. The end-of-test criteria are frequently compliant to tests that are stopped prematurely, which recomforts operators, frequently afraid to push the test up to its limits due to risk of probe bursting and loss of productivity. Since extrapolations are formally authorized, prematurely stopped tests have been widely accepted and there has been no practical reason for improving equipment capability. This seems to have recently changed as high-pressure tests have been frequently demanded by engineers in order to optimize their projects. The standard will have to evolve to comply with the recent practitioners needs.

The American standard on pre-bored pressuremeter test is much more flexible on what concerns the testing equipment and the loading protocol. This standard considers

monocellular probes equivalent to three-cellular ones since the minimum length to diameter ratio equals six is verified. Loading program can be either stress controlled, volume controlled or in a continuous rate of increase. End-of-test criteria are related to each equipment capabilities and it is up the operator to identify its occurrence during a test. Test interpretation is much more sensitive to engineer's judgment since there is no mathematical formulation to help defining the pseudo-elastic phase. The use of this standard by practitioners requires a higher level of expertise by the staff involved, from the one who operates the test, the one who interprets it and to the final client who needs to evaluate its applicability and acceptability to design.

Standards applicable to flexible dilatometer tests are yet more flexible on what concerns the testing procedures. It seems that those standards are more focused in obtaining soil's or rock's fundamental properties instead of ensuring that a specific and well stablished testing procedure to be followed. On this manner, engineers who apply this standard have more flexibility to adapt the loading program according to specific engineering needs of a project. On what concerns the testing equipment, flexible dilatometer's standards are very rigorous by imposing the use of displacement transducers inside the probe in order to ensure high precision. Despite requirements for measurement resolution are very rigorous (in the order of 5 μm), there are no further exigences in terms of probe calibration.

The appraisal of new types of probes brought to light new possibilities regarding the way the probe is inserted on the ground, the way the cavity expansion is carried out, how measurements are performed and how accurate measurements are. Amongst the main evolutions one can cite the invention of probes with punctual measurement of strains, the invention of the self-boring and the push-in capability, the data logging devices and the development of fully automated control units. Few or none improvements were made concerning the expandable membrane. Two distinct groups of probes became evident: those enabling high expansion rates to the detriment of the measurement accuracy, and those conceived to measure very small strains, to the detriment of the assessment of the strength properties. Mair and Wood (1987) and Clarke (1995) synthetize the limits of the probes existing at that time. Table A.2 presents a synthesis of the characteristics of the pre-bored pressuremeters and dilatometers presented on the previous paragraphs. The measurement capacities

presented herein are theoretical and do not take into consideration the equipment performance, fatigue over time and operator's sensibility.

Table A.2 – Examples of the characteristics of some of the most currently used pressuremeters and dilatometers. Characteristics obtained from manufacturer's catalogs or from literature where indicated

Probe name	Manufacturer	Capacity Pressure (MPa)	Deformation	Measurement method		Diameter (mm)	Length (measuring / total) (mm)
				Pressure	Deformation		
Ménard "AX" short	APAGEO, Geomatech (*)	10.0 (1)	100% $V_{0, probe}$ (depending on pressure) (2)	Water, at surface	Volume, at surface	44	210 / 610 (2)
Ménard "AX" long	APAGEO, Geomatech (*)	10.0 (1)	100% $V_{0, probe}$ (depending on pressure) (2)	Water, at surface	Volume, at surface	44	370 / 590 (2)
Ménard "BX"	APAGEO, Geomatech (*)	10.0 (1)	100% $V_{0, probe}$ (depending on pressure) (2)	Water, at surface	Volume, at surface	60	210 / 450 (2)
TEXAM	RocTest Limited	10.0 (3)	68% to 90% $V_{0, probe}$ (depending on pressure)	Water, at surface	Volume, at surface	44 / 70	540 / 460
FC60	La THP	8.0 to 12.0 (4)	110% of the initial radius	Water, at surface	Volume, at surface	60 (metallic stripes)	210 / 450 (2)
LLT-M	OYO Corporation	2.5	> 65% $D_{0, probe}$	Water, at surface	Volume, at surface	60 / 70 / 80	600 / 600
Elastmeter 100 / 200	OYO Corporation	20.0	12 % (1)	Fluid, at surface	Caliper arm, average of two points on the probe	62 / 72	520
PROBEX	RocTest Limited	30.0	= 16% $D_{0, probe}$	Fluid, at surface	Volume, reservoir near the probe	73.7	457 / 457
DMP 95	RocTest Limited	20.0	= 21% $D_{0, probe}$	Fluid, in the probe	Three inductance transducers, trespassing the membrane	95	1000
HPD 73	Cambridge Insitu Ltd	20.0	= 38% $D_{0, probe}$	Fluid, in the probe	Six strain arms in the probe	73	450 (1)
HPD 95	Cambridge Insitu Ltd	20.0	= 58% $D_{0, probe}$	Fluid, in the probe	Six strain arms in the probe	94	-

(*) - Also available from other manufacturers
(1) - According to Clarke (1995). Notice from manufacturer not found
(2) - Established on the European standard (AFNOR, 2015)
(3) – According to manufacturer (Figure A.16)
(4) – According to manufacturer (Figure A.21)

Despite pressuremeters and flexible dilatometers provide essentially the same type of mechanical solicitation, current standards and equipment are unexchangeable for both reglementary reasons and for technical reasons. For example, dilatometers cannot be used to perform pressuremeter tests because they are limited on expansion capability.

Even if they could achieve the expansion requirements, the European standard imposes that the probe must have three-cells so that it can be considered as a pressuremeter.

From the bibliographical analysis presented herein, it seems that the development of a methodology for the design of deep foundations under cyclic loads based on the pressuremeter test will have to overcome the limits imposed by the current practice and the existing standards. For this new application, both properties related to small strains (cyclic loading) and to soil strength (limit pressure, related to pile bearing capacity) are required. A new framework for cavity expansion tests, more general and more flexible must be developed.

A.5 BIBLIOGRAPHIC REFERENCES FOR APPENDIX A

AFNOR. 1991. Sols : Reconnaissance et Essais - Essai Pressiométrique Ménard. French standard NF P 94-110.

AFNOR. 1999. Sols : Reconnaissance et Essais - Essai Pressiométrique Ménard. Partie 2: Essai Avec Cycle. French standard XP P 94-110-2. : 8 pages.

AFNOR. 2000. Sols : Reconnaissance et Essais - Essai Pressiométrique Ménard. Partie 1: Essai sans cycle. French standard NF P 94-110-1.

AFNOR. 2013. Geotechnical investigation and testing - Field testing - Part 5: Flexible dilatometer test. French standard NF EN ISO 22476-5. : 31 pages.

AFNOR. 2015. Geotechnical investigation and testing — Field testing — Part 4: Ménard pressuremeter test. French standard NF EN ISO 22476-4. : 55 pages.

APAGEO. 2017. Product catalog - Matériels & services pour la géotechnique, le forage et le laboratoire. Available from https://www.apageo.com/upload/catalogue_apageo_fr.pdf [accessed 15 July 2019].

ASTM International. 2007. Standard Test Methods for Prebored Pressuremeter Testing in Soils. D 4719 - 07. : 9 pages.

Baguelin, F., Jézéquel, J., and Shields, D. 1978. The pressuremeter and foundation engineering. Trans Tech Publications.

Baud, J.P. 1985. Le PAC - Pressiomètre Assisté par Calculateur. Travaux,: 8 pages.

Briaud, J.L. 1992. The pressuremeter. A.A. Balkema/Rotterdam/ Brookfield.

Briaud, J.L. 2005. The preboring pressuremeter: some contributions. *In* 50 ans de pressiomètre. pp. 1–22.

Briaud, J.L., Tucker, L.M., and Makarim, C.A. 1985. Pressuremeter standard and pressuremeter parameters. *In* Pressuremeters and its marine applications. Second International Simposium on Pressuremeters. pp. 303–323.

Cambridge Insitu Ltd. 2015. Using pressuremeters. A guide to pressuremeter testing,. Available from https://www.cambridge-insitu.com/system/files/files_trackable/pressuremeters_web.pdf.

Cassan, M. 2005. Les essais pressiométriques et leurs applications en france - rappels historiques et état des connaissances. *In* 50 ans de pressiomètre. Vol. 2. Presses de l'ENPC/LCPC. p. 76 pages.

Clarke, B.G. 1995. Pressuremeters in geotechnical design. *In* First Edit. Blackie Academic and Professional.

Clough, G.W., Briaud, J.L., and Hughes, J.M.O. 1990. The development of pressuremeter testing. *In* Proc. of the 3rd Int. Symp. on Pressuremeters. ISP3. pp. 25–45.

Cour, F. 2006. Controllably-Deformable Inflatable Sleeve, production method thereof and use of same for pressuremetering applications. Manchon Gonflable à Déformation Controlée. Procédée de Fabrication et Application à la Pressiométrie.

Cour, F. 2013. Inflatable sleeve with controlled expansion. Manchon Gonflable à Expansion Controlée. Organisation Mondiale de la Propriété Intellectuelle. Bureau International.

Cour, F., Puech, A., and Durand, F. 2005. A new generation Ménard pressuremeter equipment. *In* 50 ans de pressiomètre. pp. 63–74.

Cour, F., and Rouet, A. 2017. La sonde pressiométrique monochambre FC. Du packer … au packer. Available from https://www.lathp.fr/la-thp-fabricant-de-sonde-pressiometrique-francis-cour/ [accessed 17 July 2019].

DGSI. 2013. Product catalog - Goodman jack. Available from https://durhamgeo.com/product/goodman-jack/ [accessed 15 July 2019].

Gambin, M. 1990. The history of pressuremeter practice in france. *In* Proceedings of the 3rd International Symposium on Pressuremeters. ISP3. pp. 5–24.

Gambin, M. 2005. Je me Souviens. *In* 50 ans de pressiomètre. p. 4 pages.

Jacquard, C., Rispal, M., Puech, A., Geisler, J., Durand, F., Cour, F., Burlon, S., and Reiffsteck, P. 2013. Une nouvelle sonde permettant de mesurer sans extrapoler la pression limite pressiométrique des sols. *In* Proceedings of the 18th International Conference on Soil Mechanics and Geotechnical Engineering. Paris. pp. 1–4.

Jacquard, C., and Varaksin, S. 2018. Rapport d ’analyse de l ’enquête relative à la pratique des essais pressiomètriques. National Project ARSCOP - Axe 2 - Research report.

Jézéquel, J., Lemasson, H., and Touze, J. 1968. Le pressiomètre Louis Ménard - quelques problèmes de mise en oeuvre et leur influence sur les valeurs pressiométriques. Bulletin de Liaison du Laboratoire des Ponts et Chaussées, **32**(537): 97–120.

Ladanyi, B. 1987. Suggested Methods for Deformability Determination Using a Flexible Dilatometer. International Journal of Rock Mechanics, **24**(2): 123–134.

LCPC. 1971. Essai Pressiométrique Normal. Modes Opératoires du Laboratoire Central des Ponts et Chaussées. DUNOD,: 49 pages.

LIM. (n.d.). Product catalog - PressioLIM AUTO Pressiomètre / CPV Automatique Pres. Available from https://lim.eu/pdf/pressioAUTO-FR.pdf [accessed 15 July 2019].

Logic. 2019. Product catalog - Auto-Pression - L’essai pressiométrique vraiment automatique. Available from https://logicingenierie.com/fr/cpv-auto-pression/ [accessed 15 July 2019].

LUTZ, J. (n.d.). Users manual - Prevo - Enregistrement d’essais pressiométriques - version BP5PVO136FR. Available from http://www.jeanlutzsa.fr/public/DocPREVO/DUCBP5PVO136FR.pdf [accessed 15 July 2019].

LUTZ, J. 2014. Users manual - BAP 160 - Version LB2 EPF 563 FrEn. Available from http://www.jeanlutzsa.fr/public/temp/LB2EPF/LB2EPF563FrEn.pdf [accessed 15 July 2019].

Mair, R.J., and Wood, D.M. 1987. Pressuremeter Testing: Methods and Interpretation. Construction Industry Research and Information Association.

Ménard, L. 1957. An apparatus for measuring the strength of soil in place. University of Illinois.

Ménard, L. 1967. Règles d'utilisation des techniques pressiometriques et d'exploitation des résultats obtenus pour le calcul des fondations. Notice Générale D-60.

OYO, C. 2019a. Product catalog - Lateral Load Tester LLT Type M. Available from https://www.oyo.co.jp/english/wp-content/uploads/2014/09/Model-4189_LLTM_C1410.pdf [accessed 15 July 2019].

OYO, C. 2019b. Product catalog - Auto LLT2. Available from https://www.oyo.co.jp/english/products_lists/276-2/ [accessed 15 July 2019].

OYO, C. 2019c. Product catalog - Elastmeter-2 Model 4180. Available from https://www.oyo.co.jp/english/wp-content/uploads/2014/09/Model-4180_Elast_Sonde_And_Acce_C1410.pdf [accessed 15 July 2019].

OYO, C. 2019d. Product catalog - Elastmeter-2 and Elast Logger-2. Available from https://www.oyo.co.jp/english/wp-content/uploads/2014/09/Model-4022_Elast_Logger2_C1410.pdf [accessed 15 July 2019].

Reiffsteck, P. 2003. Cahier des charges du P.A.F. 2000. Partie 1 : sonde - Version 4. Caractérisation de la déformabilité des sols au moyen d'essais en place. Opération 11J9922. LCPC.

Reiffsteck, P. 2010. Conception d'un CPT cyclique et études de conception et d'adaptation et réalisation d'un pressiomètre autoforeur pour essais cycliques. Rapport de recherche SOLCYP. Thème 2: Essais Spéciaux. R/09/SOL/01.

Reiffsteck, P. 2014. Réalisation d'essais PMT et PAF cyclique sur les sites d'essais de chargement de pieux du projet SOLCYP. Rapport de recherche SOLCYP. Thème 2: Essais Spéciaux. R/09/SOL/04.

RocTest Limited. 2017a. Texam Pressuremeter Instruction Manual. Available from https://roctest.com/fr/product/pressiometre-texame/ [accessed 15 July 2019].

RocTest Limited. 2017b. Instruction Manual - Probex - Borehole dilatometer (Rock pressuremeter). Available from https://roctest.com/fr/product/dilatometre-de-forage-probex/.

Schnaid, F. 2009. In Situ Testing in Geomechanics. Taylor and Francis.

TELEMAC. 2018. Manuel d'instructions. Dilatomètre flexible. Modèle DMP.

THP. 2015. Product catalog. Sonde Pressiométrique Francis Cour FC 60. Available from https://www.lathp.fr/la-thp-fabricant-de-sonde-pressiometrique-francis-cour/ [accessed 17 July 2019].

Withers, N.J., Schaap, L.H.J., and Dalton, C.P. 1986. The development of a full displacement pressuremeter. *In* Pressuremeters and its marine applications. Second International Simposium on Pressuremeters. ASTM. pp. 38–56.

Wroth, C.P., and Hughes, J.M.O. 1972. An Instrument for the in situ measurement of properties of clays. CUED/C - SOILS TR13 - University of Cambridge,.

APPENDIX B.

PRESSUREMETER PROBE QUALIFICATION TESTS

There is currently no or limited documentation regarding the measurement accuracy of the standard tri-cellular pressuremeter probes. A testing program was established to verify if the most used testing equipment can potentially enable the assessment of the small strain domain of soils and rocks.

B.1 TESTING EQUIPMENT

The equipment tested consists of the most commonly employed equipment in French practice, recently summarized by Jacquard and Varaksin (2018). Three types of probes, assembled in different configurations, were tested. They were:

- Probe type Ménard “AX” 44, short cell, diameter 44 mm, equipped with external slotted tube, external diameter 56 mm (AX 44, ST 56);
- Probe type Ménard “AX” 44, short cell, diameter 44 mm, equipped with external slotted tube, external diameter 63 mm (AX 44, ST 63);
- Probe type Ménard “BX” 60, diameter 60 mm, without external dressing (BX 60);
- Probe type Francis Cour “FC” 60, diameter 44 mm, equipped with external metallic stripes, external diameter 60 mm (FC 60, mts);
- Probe type Francis Cour “FC” 60, diameter 44 mm, without external protection (FC 60, nue);

All the Ménard type probes were equipped with reinforced sheaths.

The employed tubing was of type coaxial, resistant to 10 MPa, type “Tecalan” of 3 millimeters internal diameter. Three different lengths were tested: two meters, twenty-five meters and fifty meters.

The pressure-volume controller used was of type “Ménard” certified and calibrated by the manufacturer according to standard specifications. The control unit was equipped with sensors for data acquisition. Data acquisition was performed using a commercial equipment model “BAP 160” and according to standard protocols (1s, 15s, 30s and 60s after the beginning of each load-step).

B.2 TESTING PROGRAM

The following tests were performed:

- Calibration of the three lengths of tubing without the probe (closed end);
- Hydraulic head loss tests;
- Probe open-air calibration tests;
- Probe calibration tests in thick steel tubes of variable diameter;
- Photos of the central measuring cell (cmc) during its inflation;

The testing program performed is summarized in Table B.1 to Table B.3.

B.3 LOADING PROGRAM AND TEST DESCRIPTION

The loading program was established in order to test the equipment in a large range of working pressures and volumes. For all the cases, the equipment was fully saturated before the start of a testing series following good practice recommendations. After a series of tests was launched, the equipment was not reset even though it sometimes deviates from zero. This procedure enables to put in evidence the possible accumulation of errors inherent to equipment.

The following procedures were applied:

- For the closed-end tubing calibration:
  - Tubing was fully saturated and then its end was closed;
  - Pressure-hold steps of one minute were performed at 0.1 MPa, 0.5 MPa, 1.0 MPa, 2.0 MPa, 3.0 MPa, 4.0 MPa, 5.0 MPa, 6.0 MPa, 7.0 MPa, 8.0 MPa. Standard data acquisition system was used. Only values at 60 s (end of the loading step) were interpreted.
  - After the last load step, pressure was released, and the test was repeated.

Table B.1 – Synthesis of the tests performed with the coaxial tubing

Equipment	Type of test	Test condition	Tubing length	Number of tests	Remark
Tubing	Calibration	Closed end	2 m	4	
Tubing	Calibration	Closed end	25 m	5	
Tubing	Calibration	Closed end	50 m	5	
Tubing	Hydraulic head loss	Open end	2 m	5	
Tubing	Hydraulic head loss	Open end	25 m	5	
Tubing	Hydraulic head loss	Open end	50 m	5	

Table B.2 – Synthesis of the calibration tests performed with different three-cellular probe

Equipment	Type of test	Test condition	Tubing length	Number of tests	Remark
AX 44, ST 56	Calibration	Open air	2 m	5	
		Tube ϕ 60 mm	2 m	5	
		Tube ϕ 66 mm	2 m	3	
		Tube ϕ 75 mm	2 m	3	
		Tube ϕ 85 mm	2 m	1	No contact
AX 44, ST 63	Calibration	Open air	2 m	5	
		Tube ϕ 66 mm	2 m	5	
		Tube ϕ 75 mm	2 m	3	
		Tube ϕ 85 mm	2 m	2	
BX 60	Calibration	Open air	2 m	5	
		Tube ϕ 66 mm	2 m	5	
		Tube ϕ 75 mm	2 m	3	
		Tube ϕ 85 mm	2 m	6	
FC 60, mts	Calibration	Open air	2 m	5	
		Tube ϕ 66 mm	2 m	4	
		Tube ϕ 75 mm	2 m	5	
		Tube ϕ 85 mm	2 m	5	
		Tube ϕ 95 mm	2 m	1	No contact
FC 60, nue	Calibration	Open air	2 m	5	
		Tube ϕ 60 mm	2 m	3	
		Tube ϕ 66 mm	2 m	5	
		Tube ϕ 66 mm	25 m	3	
		Tube ϕ 66 mm	50 m	3	
		Tube ϕ 75 mm	2 m	3	
		Tube ϕ 85 mm	2 m	1	No contact

Table B.3 – Synthesis of the photos of the central measuring cells

Equipment	Type of test	Test condition	Tubing length	Number of tests	Remark
AX 44, cmc	Central cell photo at variable pressures	Tube ϕ 50 mm	2 m	1	
		Tube ϕ 64 mm	2 m	1	
		Tube ϕ 70 mm	2 m	1	
		Tube ϕ 80 mm	2 m	1	
BX 60, cmc	Central cell photo at variable pressures	Tube ϕ 64 mm	2 m	1	
		Tube ϕ 70 mm	2 m	1	
		Tube ϕ 80 mm	2 m	1	
		Tube ϕ 90 mm	2 m	1	
FC 60, cmc	Central cell photo at variable pressures	Tube ϕ 50 mm	2 m	1	
		Tube ϕ 64 mm	2 m	1	
		Tube ϕ 70 mm	2 m	1	
		Tube ϕ 80 mm	2 m	1	

- For the hydraulic head loss tests:
  - The end of the tubing was left open. The system was filled with pure water, at environmental temperature (7 degrees Celsius for all tests);
  - Water pressure was imposed at 100 kPa (1 bar). The volume of water flown after 5 seconds was manually recorded. This was repeated five times. The device was refilled with water and the same procedure was repeated for 10 seconds and for 15 seconds intervals;
  - The above procedure was repeated for pressures of 200 kPa and 300 kPa (which comprises the common interval of differential pressures applied in standard tests);
- For the probe open air calibration tests:
  - Probe was connected to the tubing and to the controller device. The saturation procedure was performed;
  - Pressure was applied in 60 seconds hold steps, following the procedure described in AFNOR (2015). Standard data acquisition system was used.
- For the probe diametrical calibration tests:
  - Probe was connected to the tubing and to the controller device. The saturation procedure was performed.;
  - Probe was inserted into the calibration cylinder;
  - Pressure hold steps of 0.1 MPa, 0.3 MPa, 0.5 MPa, 1.0 MPa, 2.0 MPa, 3.0 MPa, 4.0 MPa, 5.0 MPa were applied, following the procedure described in AFNOR (2015). Standard data acquisition system was used.

- Test was repeated three to five times, comprising at least the load steps of 0.5 MPa, 1.0 MPa, 2.0 MPa, 3.0 MPa, 4.0 MPa, 5.0 MPa.

- For the photos of the central measuring cell:
  - The external sheath that defines the guard cells was removed. Only the central measuring cell was assembled on the probes;
  - Probe was placed into a transparent plexiglass tube. The measuring cell was inflated and volume readings were manually recorded for pressure steps of 50 kPa, 100 kPa, 150 kPa, 200 kPa, 250 kPa, 300 kPa (also 400 kPa for the FC probe).
  - Once the maximum pressure was reached, probe was deflated in load steps of 300 kPa, 200 kPa, 100 kPa. This procedure was repeated three times.
  - A photo of the probe was taken at each load step.

B.4 INTERPRETATION AND RESULTS

B.4.1 Closed-end tubing calibration

The interpretation of the closed-end tubing calibration had the only objective to better understand the influence of the tubing length on the system compressibility. The parameter calculated was the so-called "compressibility coefficient", *a*, which is obtained through the slope of the curve of volume and pressure [cm^3/MPa].

It has been noticed that when releasing the pressure after the last load step, the water volume displayed on the pressure-volume controller device did not come back to zero as it would be expected. For example, at the end of a test started at P = 0 MPa, V = 0 cm^3 readings of volume were found to vary between -4 cm^3 to +6 cm^3, displaying P = 0 MPa, V = -4 to +6 cm^3. The longer the tubing, the longer were the variations. Those volume variations cannot be attributed to any eventual leakages on the system, since it has been rigorously verified before the beginning of the tests and there were no variations of volume with time when the system was pressurized. One example of volume offset obtained with the 50 m tubing is presented in Figure B.1a. The main reason for this is attributed to progressive dissolution of gas into the water during the device's pressurization, which can mislead the volumeter readings. For interpreting the results, all the measured curves were reset to zero following the procedure presented in

Figure B.1b. The test results and the average compressibility coefficient calculated for each tubing length are presented in Figure B.2

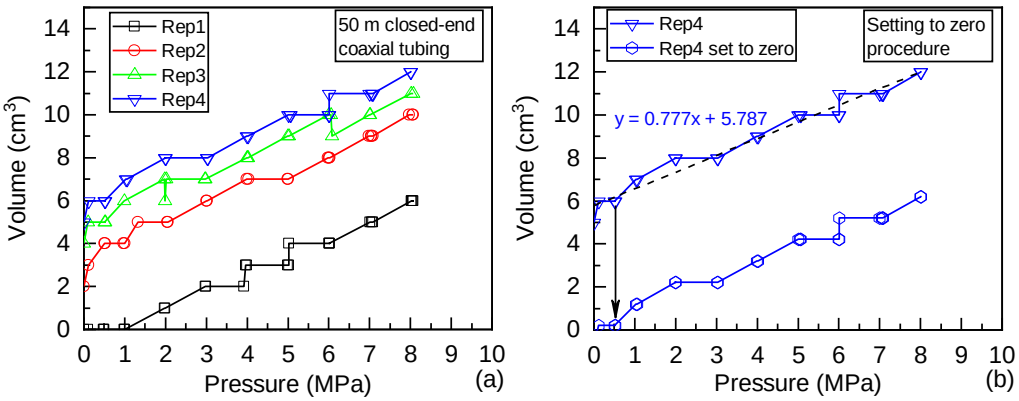

Figure B.1 – (a) Example of four repetitions the 50-meter closed end tubing calibration. (b) Procedure for setting measurements to zero to proceed to analysis

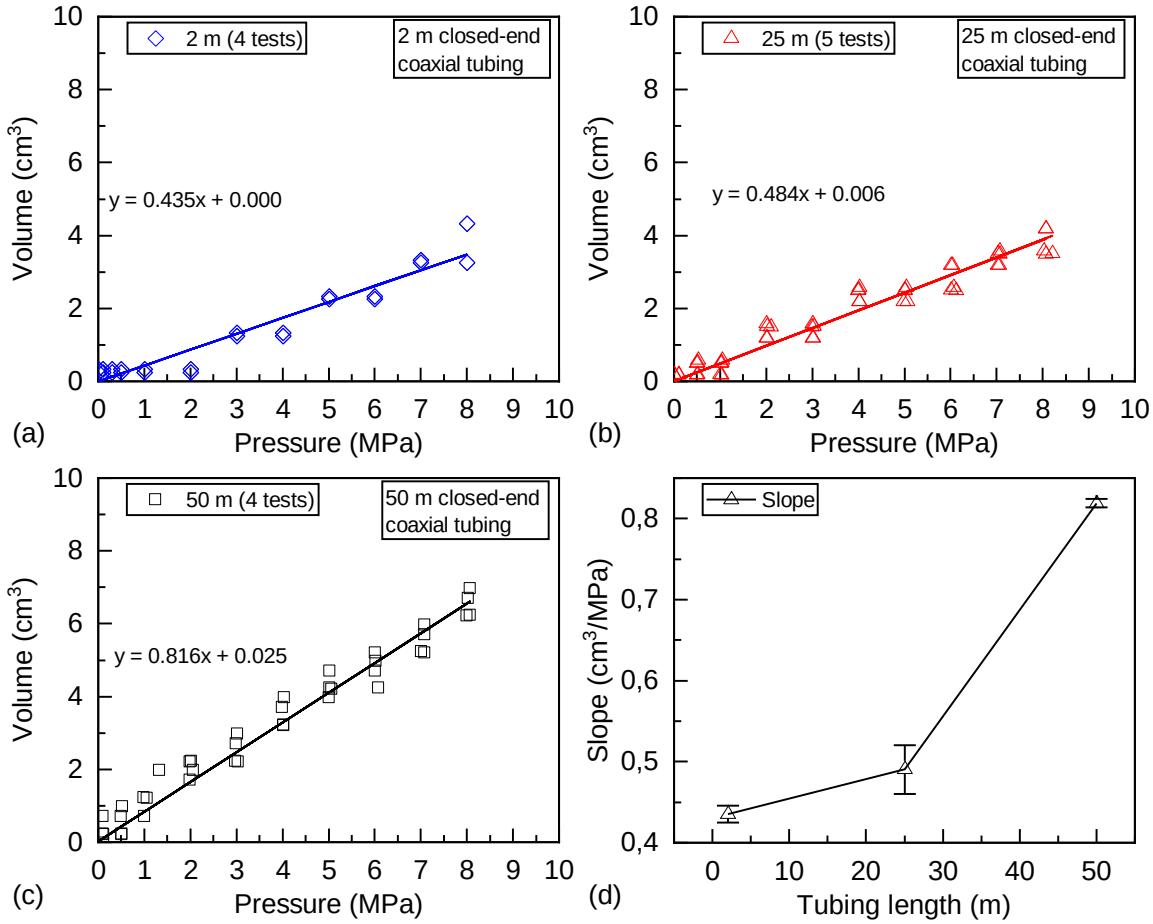

Figure B.2 – Results of tubing self-compressibility tests. (a) 2-meter-long tubing, (b) 25-meter-long tubing, (c) 50-meter-long tubing, (d) synthesis of the compressibility coefficient of all tubes.

Those results allow drawing the following conclusions:

- Tubing present a relatively stiff behavior, representing a volume loss lower than 1 cm^3/ MPa for lengths between 2 to 50 meters.

- The working principle of the coaxial tubing, in which the water line is surrounded by pressurized air is efficient;
- System frequently does not come back to zero at the end of a test. The main probable reason is that, since there is no separation between gas and water in the circuit, the pressurized air progressively dissolves into water during system pressurization;
  - Evidences of this phenomenon were the gas bubbles that were observed in the volumeter after the device's depressurization at the end of some tests (Figure B.3);
  - This inherent source of error may be a serious issue in the case of cyclic tests in which probe pressure is increased and decreased repeatedly during a same test. With a closed-end 50m long tubing, the magnitude of the volume offsets between the pressurization and relief was of **6 cm^3**.

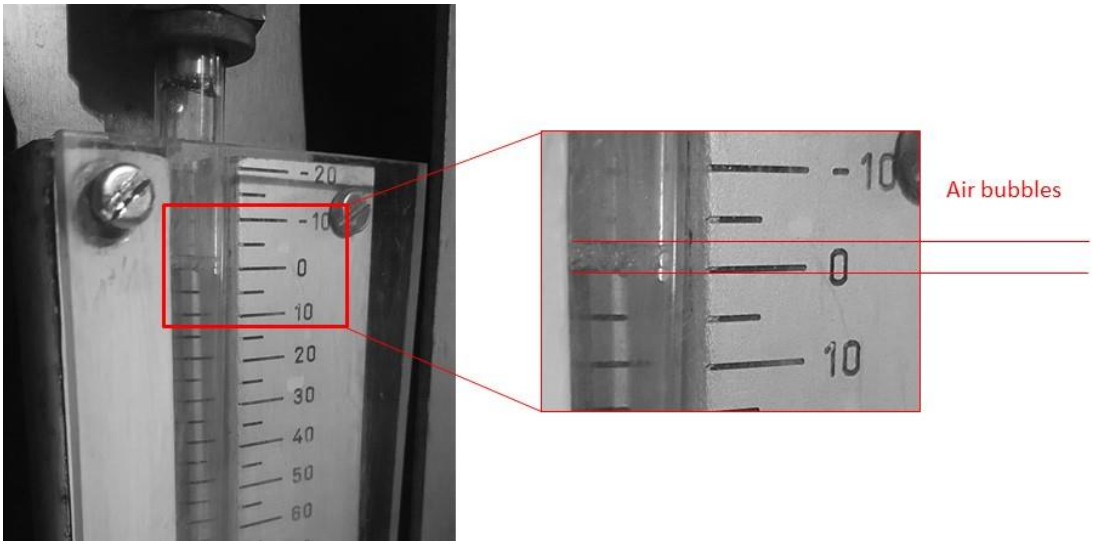

Figure B.3 – Gas bubbles observed in the control unit volumeter at the end of the test

B.4.2 Hydraulic head loss tests

Measurements of volume and time were used to calculate the water flow rate, for each pressure applied, and for each tubing length. This enabled plots of water-flow rate in function of the applied pressure to be done. Those graphics can be interpreted in two manners, to answer the following questions: (1) which is the maximum volume of water that can flow through a given tubing length in function of the input pressure? And (2) what is the hydraulic head loss in function of the water flow-rate, for various lengths of tubing?

Those tests are important because pressure losses can be significant when using long tubing of small internal diameter. When there is a water flow, the water pressure at the level of the probe will be different than that measured at the level of the pressure-volume controller. This difference will be bigger for longer tubing, for lower temperatures and if there is presence of anti-frozen fluid dissolved in the water (higher viscosity). For tri-cellular probes, in which air and water must be kept at the same differential pressure during the whole test (generally between 100 kPa and 200 kPa), this can be a serious issue. Results are presented in Figure B.4:

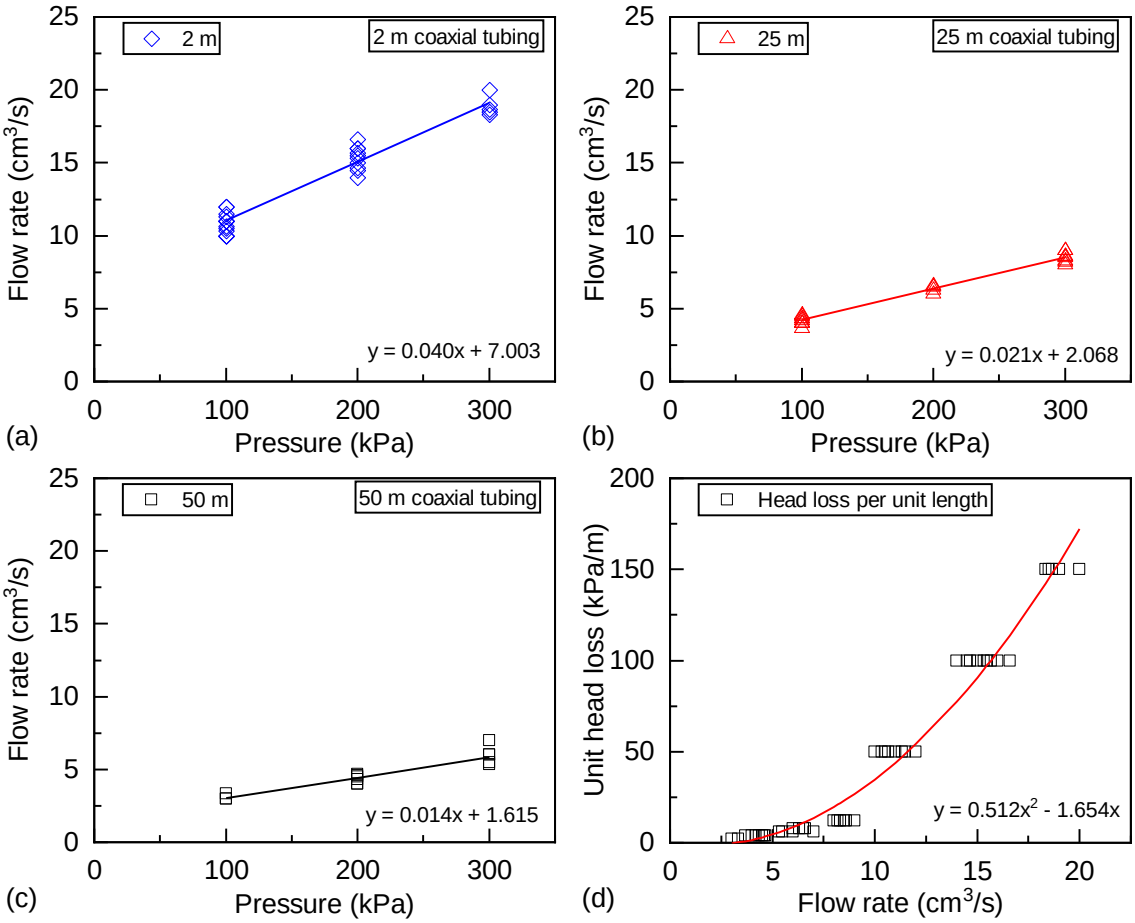

Figure B.4 – Results of the water head loss tests. (a) 2-meter-long tubing, (b) 25-meter-long tubing, (c) 50-meter-long tubing, (d) obtained unit head loss in function of the water flow-rate.

Those results enable drawing the following conclusions:

- Considering the example of a 50-meter-long coaxial tubing and a probe operating at 150 kPa differential pressure at 7°C, the maximum flow-rate possible is 3.7 cm^3/s. This implies that during a standard load step change (20 s) a maximum of approximately 74 cm^3 can be injected;

- During a pressuremeter test, near failure, there is a risk that the device cannot supply enough flow-rate to compensate soil creep. On this case, the operator can be misled by the device's delay in responding, and soil resistance can be overestimated;
- If gas flows faster than water, it is possible that probe be first pressurized by gas and that the water cell catches it up later, yielding misleading results of the cavity expansion.

B.4.3 Probe open air calibration tests:

The open-air calibration tests were interpreted to obtain the parameter p_{el}, which corresponds to the pressure necessary to inflate the probe to its conventional limit volume (conventionally defined as 550 cm^3 for AX type probes and 700 cm^3 for BX and FC60 ones). Open air calibration curves are used to correct pressures in the whole range of volume of the test. So, the scatter between each repetition gives an idea of the uncertainty brought by this calibration procedure to the interpretation of the test.

It has been observed that the standard testing procedure plays a role on the uncertainty obtained. The test is performed at constant pressure-hold steps during which the injected volume of water varies due to the progressive flow from the CPV to the probe. As seen on the previous section, the existence of a flow-rate implies that there is a hydraulic head loss during the test. For this reason, test results may be sensitive to all the factors affecting the hydraulic head losses: tubing length and diameter, temperature, the presence of anti-freeze fluid (fluid viscosity). The probe inflation will be time-dependent due to the water-flow and maybe also due to possible time-dependent properties of the membrane's material. It is though very difficult to obtain two identical results using a manually controlled CPV, because time-spans during step changings can easily vary. Better repeatability would probably be obtained if the duration of the load step change was fixed and if the total duration of the test was imposed. There are currently no standard specifications on this purpose: the current standards impose a minimum of load steps and the duration of the load step, without imposing the total duration of the test or the duration of the load step change. Test results are presented in Figure B.5 and synthetized in Table B.4. The following conclusions can be drawn from the presented results:

- Probe type BX 60 is the one which presented higher values of standard deviation for pressure values calculated at constant volume. It is also the probe that presented the lowest self-resistance. It is likely that both results come together, since a less resistant membrane will enable higher flow rates, and thus the results will be more dependent on the operator's reaction;
- Standard deviations are smaller when comparing FC60 probe equipped with metallic stripes and the same probe without the metallic dressing. The reason is the same;
- It can be noticed from the presented curves that there are small variations in pressure during a given load-step. The origin of those variations comes from the difficulty in keeping the pressure perfectly constant at the controller (there is certain inertia between acting on the gas regulator and the real change in probe pressure). It is possible that those small pressure variations affect the test results, but it was not possible to avoid them using the manual controller.

Table B.4 – Average values of pressure and standard deviation calculated at various volumes for the open-air calibration tests

	AX 44 ST 56		**AX 44 ST 63**		**BX 60**		**FC60**		**FC60 ms**	
Volume (cm^3)	**P_{avg}** (kPa)	**std** (kPa)	**P_{avg}** (kPa)	**std** (kPa)	**P_{avg}** (kPa)	**std** (kPa)	**P_{avg}** (kPa)	**std** (kPa)	**P_{avg}** (kPa)	**std** (kPa)
0	0	0	0	0	0	0	0	0	0	0
50	36	13	54	10	15	4	45	20	43	11
100	112	9	108	10	40	10	91	18	93	7
150	154	9	135	8	74	10	136	8	137	9
200	180	10	165	8	92	12	165	11	174	7
250	203	16	196	5	113	12	184	15	199	6
300	218	15	221	10	121	11	191	4	217	11
350	228	14	235	6	127	9	219	12	236	17
400	249	10	258	9	152	14	217	13	249	5
450	258	10	270	8	151	18	233	7	248	3
500	272	17	290	4	157	14	236	5	272	8
550	**284**	**17**	**309**	**5**	172	15	236	5	279	6
600	-	-	-	-	187	20	252	12	283	2
650	-	-	-	-	200	19	257	13	291	6
700	-	-	-	-	**217**	**19**	**261**	**13**	**301**	**6**

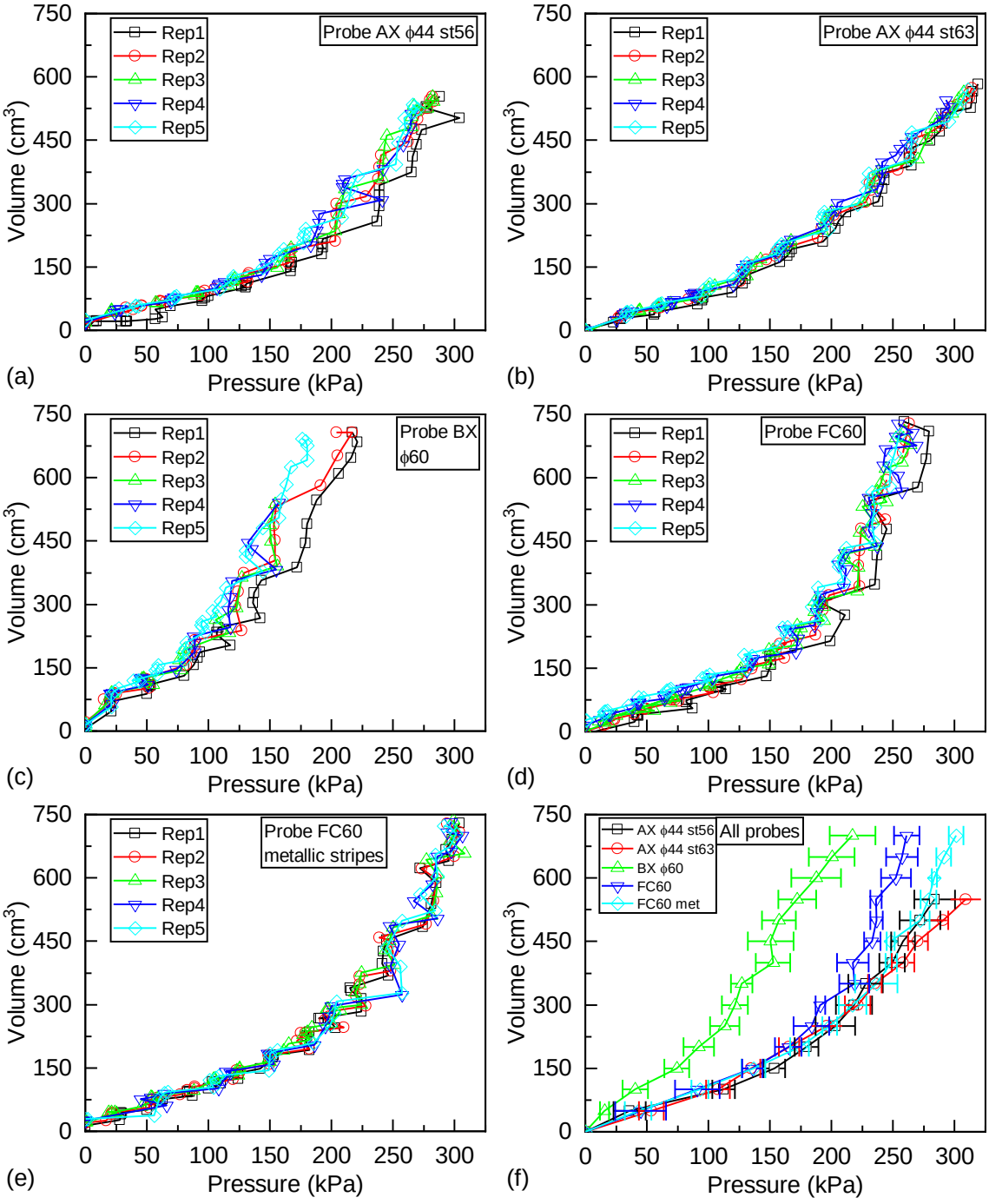

Figure B.5 – Results of open-air calibration tests for five probe configurations. (a) Ménard type AX 44 with slotted tube of external diameter 56 mm, (b) Ménard type AX 44 with slotted tube of external diameter 63 mm, (c) Ménard type BX 60 without metallic protection, (d) FC60 type without metallic protection, (e) FC60 type equipped with metallic stripes, (f) synthesis of all tests with indication of the standard deviation in pressure.

B.4.4 Probe diametrical calibration tests

All diametrical calibration tests were interpreted to obtain the compressibility coefficient *a* [cm3/MPa], calculated as the slope of the curve a range of pressures between 1 and 5 MPa. The so-called "probe volume" (V_c) was calculated according to the formula proposed by AFNOR (2015), considering the length of the central measuring cell equal do 210 mm. It should be noticed that, according to this standard, there is an acceptable tolerance of + 2 mm (or + 5 mm, according to the model) in the length of the measuring cell.

For investigating the influence of the tubing length on the determination of the compressibility coefficient, the FC60 probe was also calibrated using other two lengths of tubing: 25 meters and 50 meters. The results are presented in Figure B.11f:

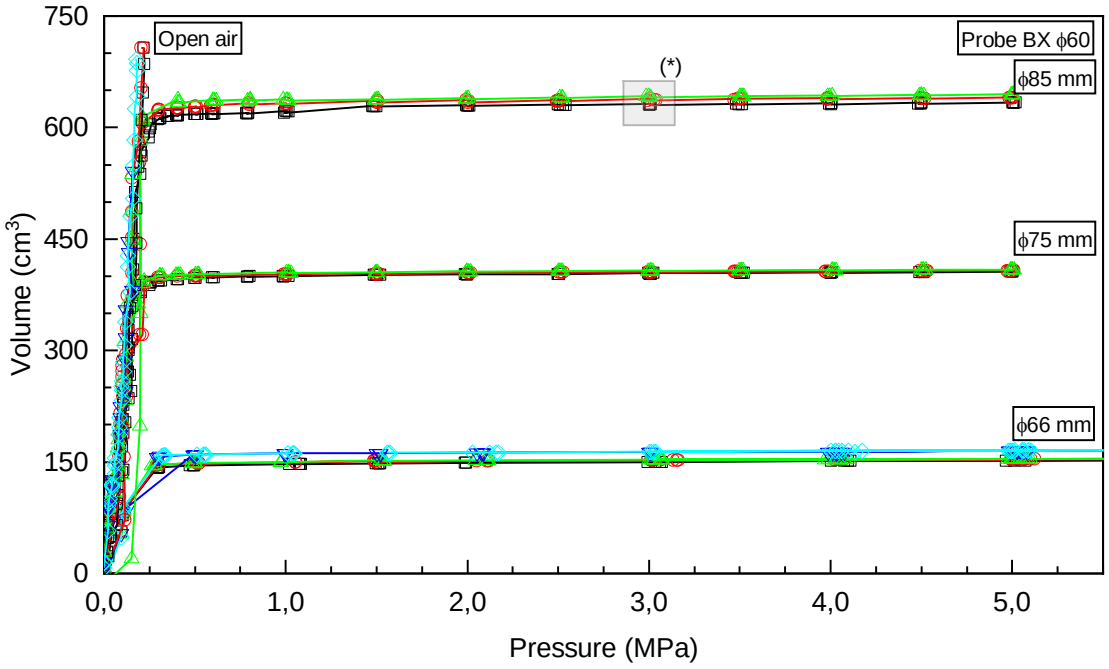

Figure B.6 – Calibration tests of Ménard type probe BX 60 using different calibration tubes. (*) Detail of volume changes during this load step presented in Figure B.13

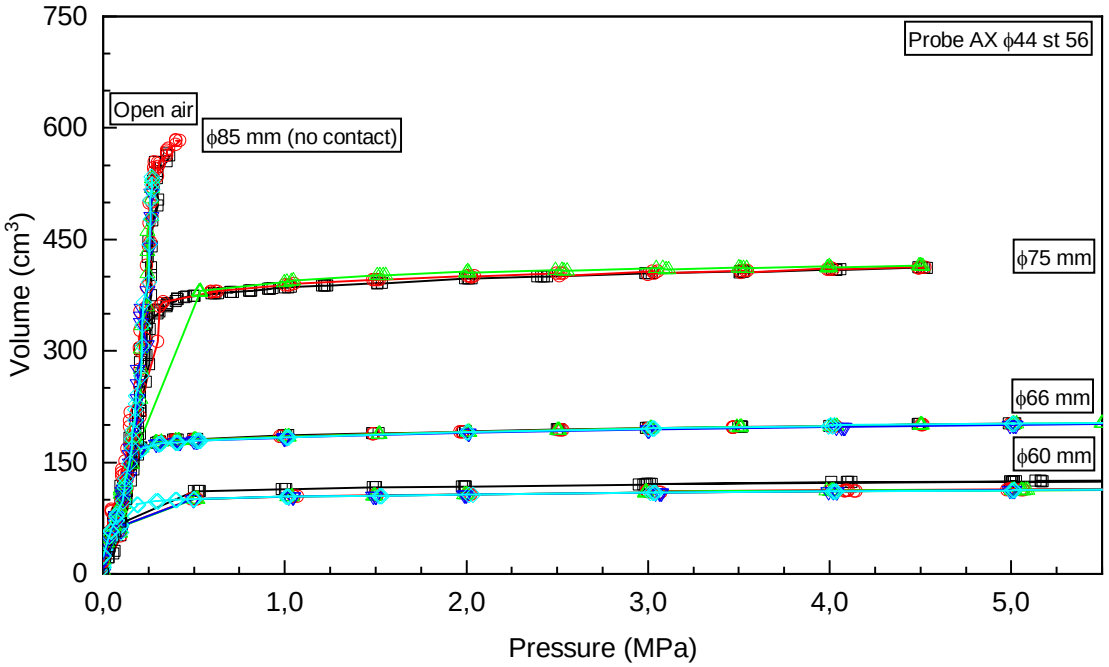

Figure B.7 – Calibration tests of Ménard type probe AX 44 equipped with slotted tube 56 mm using different calibration tubes

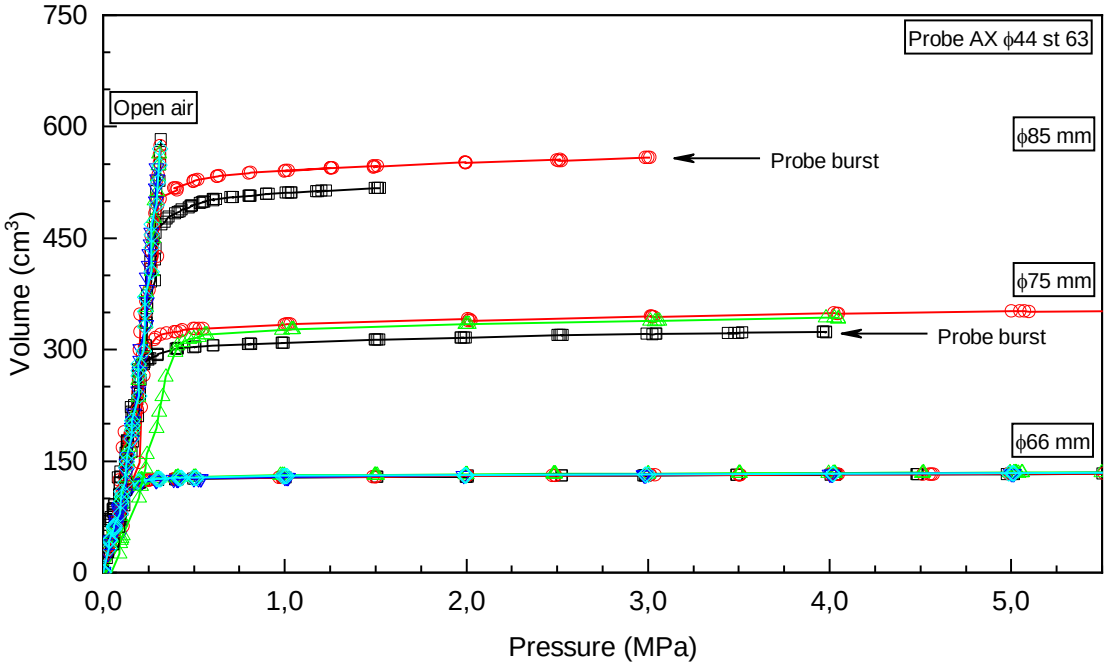

Figure B.8 – Calibration tests of Ménard type probe AX 44 equipped with slotted tube 63 mm using different calibration tubes

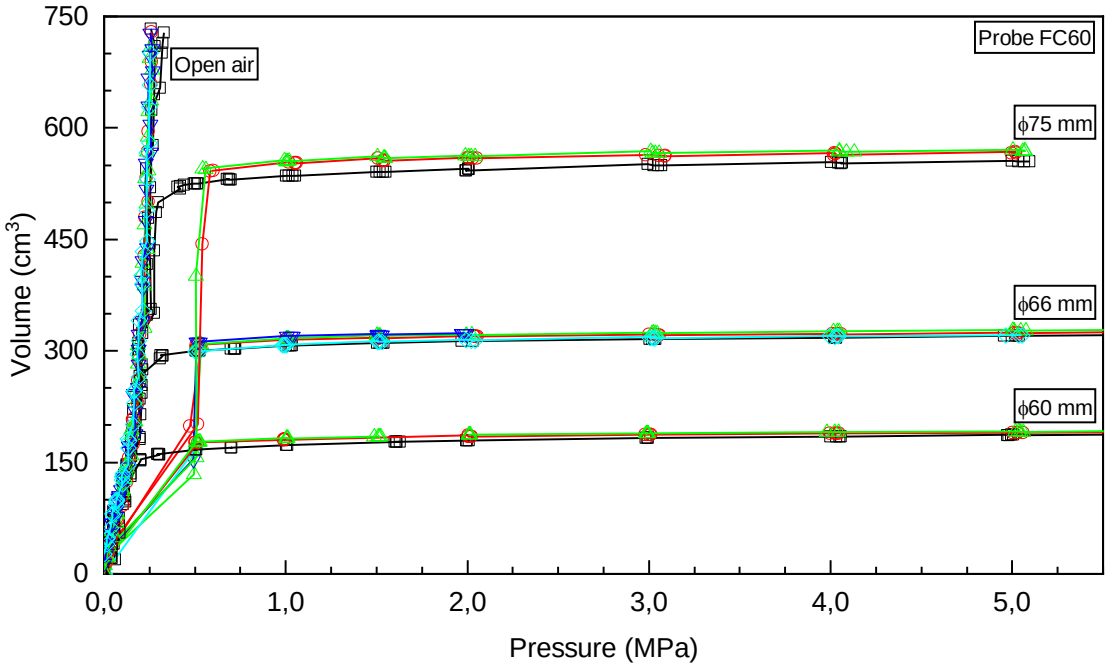

Figure B.9 – Calibration tests of FC60 type probe without external metallic protection using different calibration tubes

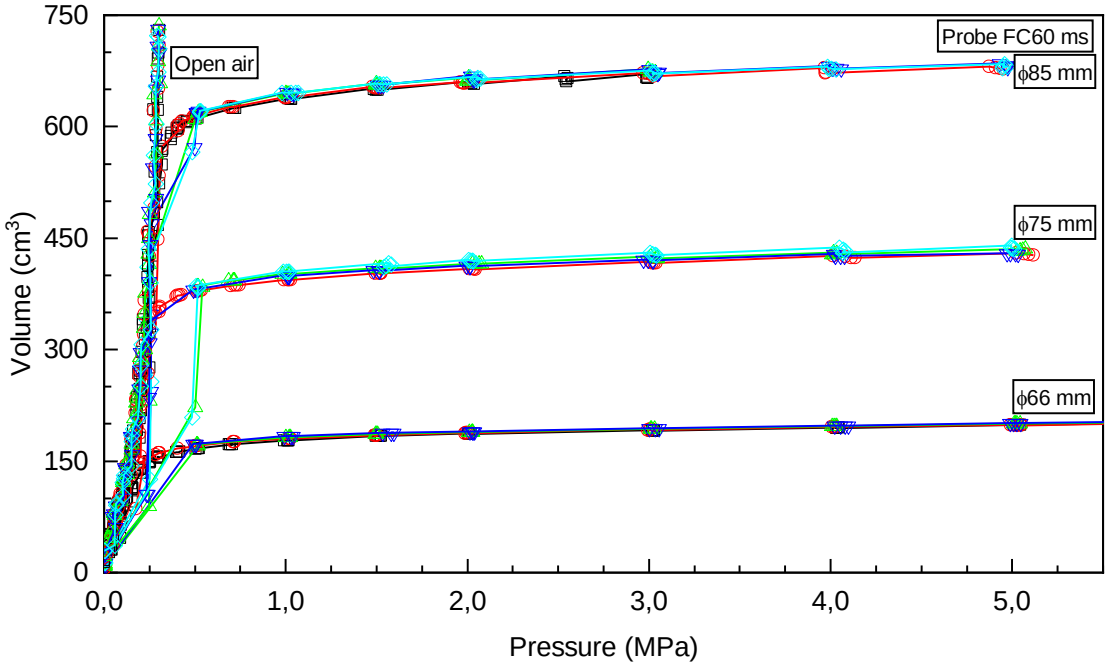

Figure B.10 – Calibration tests of FC60 type probe equipped with external metallic protection using different calibration tubes

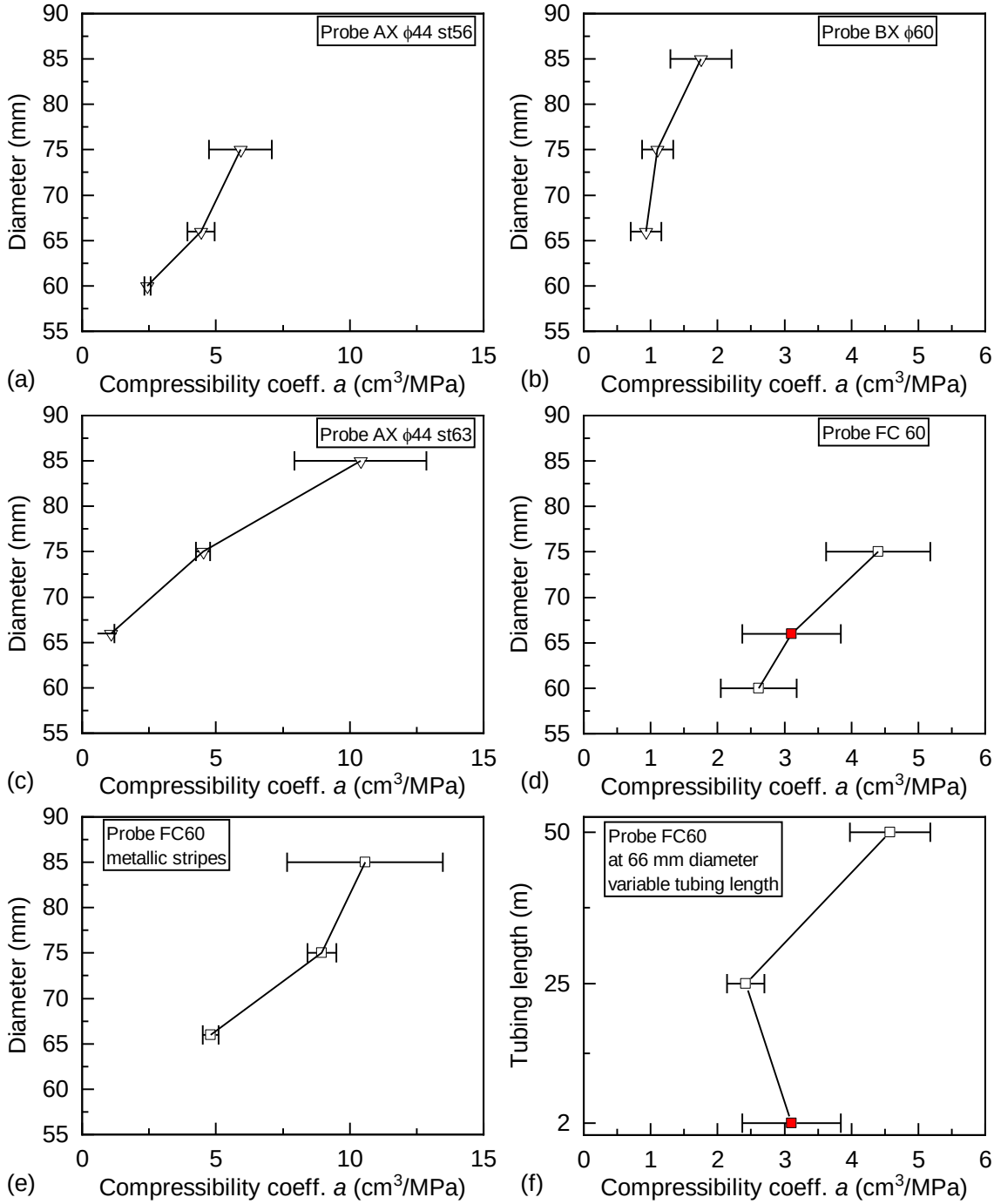

Figure B.11 – Synthesis of the calculated compressibility coefficients ("*a*") for five configurations of probes at variable calibration diameters. (a) AX 44 with slotted tube 56 mm, (b) BX 60 without metallic protection, (c) AX 44 with slotted tube 63 mm, (d) FC60 without metallic protection, (e) FC60 with metallic stripes, (f) study of the effect of changing the tubing length on the compressibility coefficient of FC60 probe at 66 mm calibration tube.

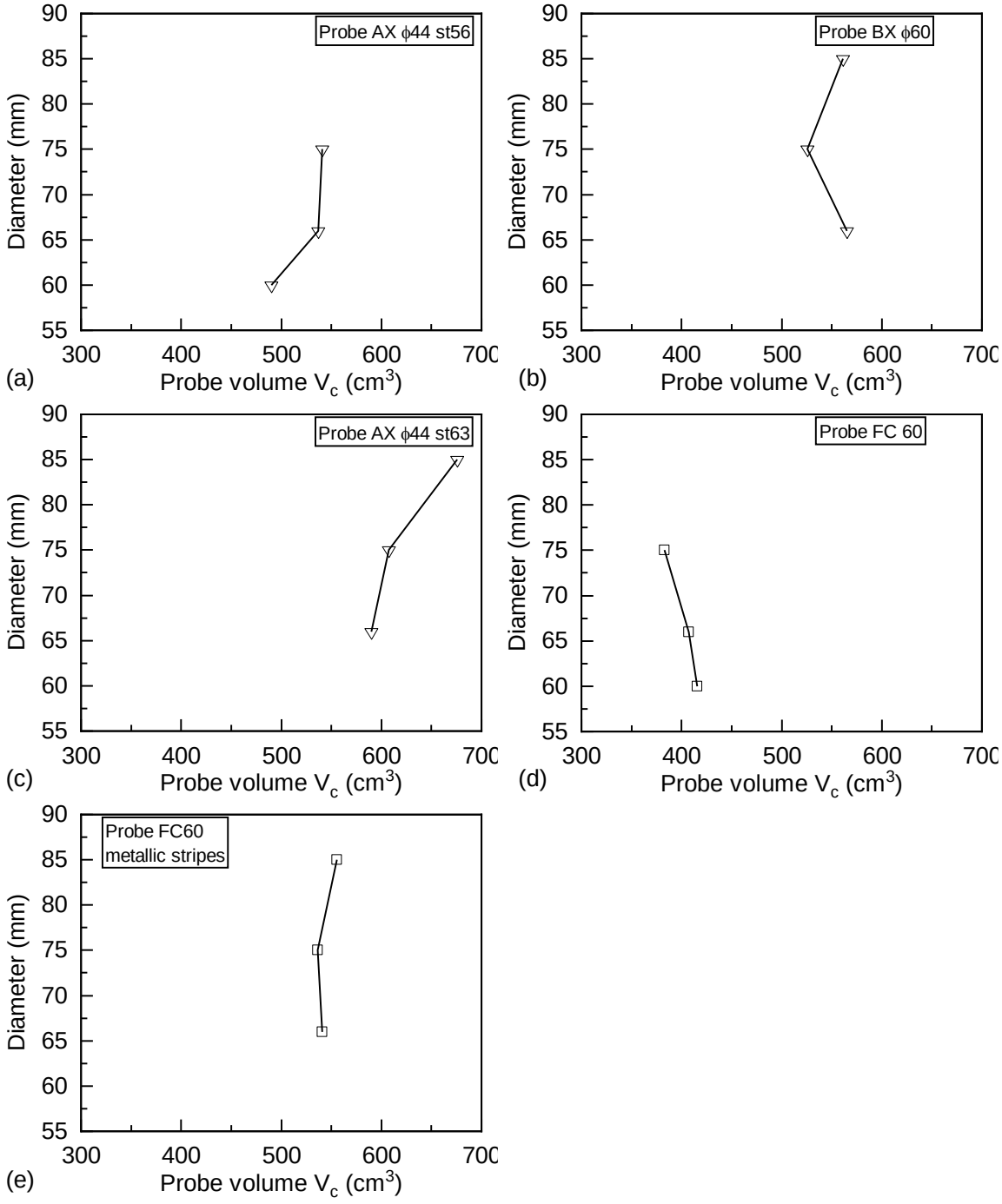

Figure B.12 – Synthesis of the calculated "probe volumes" ("V_c") for five configurations of probes at variable calibration diameters. (a) AX 44 with slotted tube 56 mm, (b) BX 60 without metallic protection, (c) AX 44 with slotted tube 63 mm, (d) FC60 type without metallic protection, (e) FC60 type equipped with metallic stripes.

The following conclusions can be drawn from the multiple calibration tests performed:

- All probes, but especially those equipped with external metallic protection, present a non-linear behaviour in the first portion of the calibration curve (between contact and 1.0 MPa). This is currently not considered by the standard interpretation methods, which propose calculating a constant compressibility coefficient *a*;

- The compressibility coefficient *a* calculated at a given pressure range, varies drastically with the variation of the calibration tube. This can introduce major uncertainty on the test interpretation if the borehole diameter is not identical to the diameter of the calibration;
- The calculated "probe volume" varies drastically for the AX type probes equipped with external protection. The variation is smaller, but yet significative, for probes BX and FC60.

From Figure B.11(f) it can be noticed that changing the tubing changes the compressibility coefficient. However, due to the large variability obtained (high standard deviations, possibly due to low measurement resolution or other random measurement errors), the experiment's results do not allow to separate the effect of tubing compressibility from that of the rest of the system's compressibility. This implies that for tests in soil, calibrations have to be performed using the fully assembled system. If tubing is changed, it is recommended to recalibrate the whole system.

Besides the calculation of the coefficients *a* and V_p, the calibration tests revealed some other sources of uncertainty possibly inherent to the three-cellular probes. Figure B.13 presents the detail of the variation of volume and the differential pressure during a given load step at 2.0 MPa for the BX type probe. It can be seen that there is a trend that probe volume varies during the 60-seconds load step. The greater is the probe volume (larger calibration tubes), the greater is the in-step volume variation. By taking a closer look at what happens during the pressure-hold step, it can be observed that the differential pressure may slightly vary over time. For bigger cell volumes (especially for the 85 mm calibration tube), it is clear that even very small variations in the differential pressure create variations in the measuring cell volume. In the example of the 85 mm tube, a variation of 25 kPa in the differential pressure caused a variation of 2 cm^3 in volume, which can be explained by longitudinal variations (length or curvature) of the measuring cell. The small variations in the differential pressure can be attributed to the pressure-volume controller device used, manually controlled and with mechanical regulation of pressures. This problem seems to be difficult to solve, since it demands regulating the pressure of two different fluids (water and gas) flowing through a compressible system

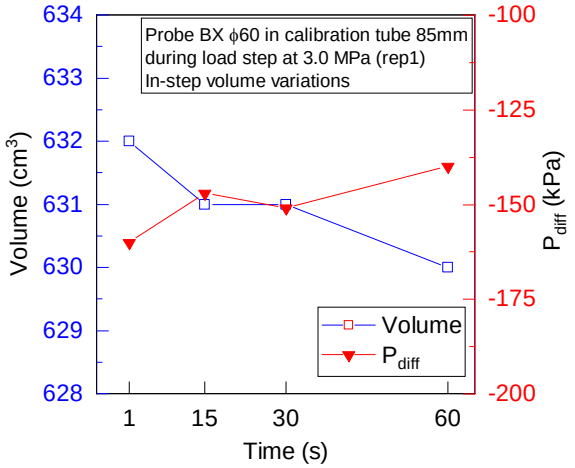

Figure B.13 – Observed relationship between variations in differential pressure and disturbances on the volume measurements during a constant load-step (probe BX 60, inside a calibration tube of 85 mm, at 3.0 MPa)

It has also been observed that some atypical volume variations happened between two load steps (pressure changing). AFNOR (2015) suggests that pressure increases may be performed at a maximum time span of 20 seconds. To verify the volume variations during a load-step change, the data was acquired during the 20 second interval and pressure and volume values were manually recorded. Results obtained for the Menard BX probe inside the 85mm tube, while changing load from 3 to 4 MPa are presented in Figure B.14:

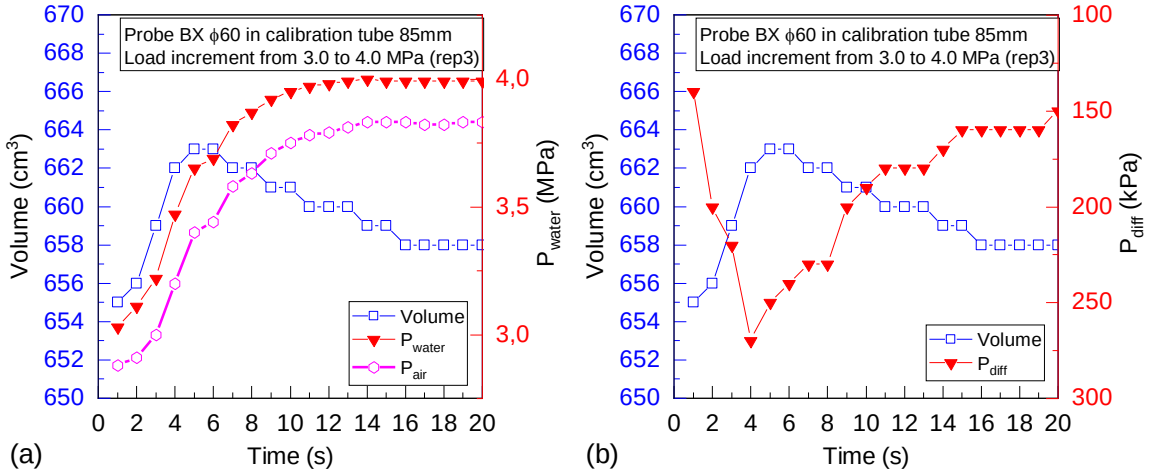

Figure B.14 – Observed variations in volume of a BX 60 type probe inside an 85 mm calibration tube during a pressure change between 3.0 to 4.0 MPa. (a) Readings of volume and pressure for 20 seconds during pressure augmentation. (b) Variations of the differential pressure during the same pressure-increment presented in (a).

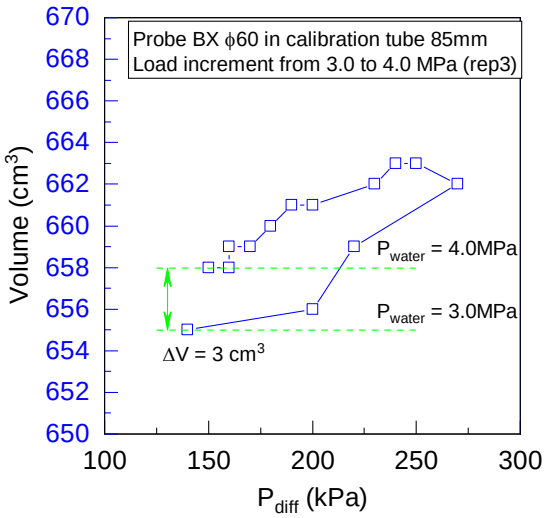

Figure B.15 – Variations of the measuring cell volume detected during calibration tests for a BX probe inside a 85mm steel tube, when changing pressure from 3.0 MPa to 4.0 MPa;

It can be observed that during pressure changes, the differential pressure is not constant. It varies considerably, from 150 kPa to 250 kPa. The change in differential pressure causes an important change in volume due to longitudinal elongations in the measuring cell. As the differential pressure stabilizes and reach the original value of 150 kPa, the measuring cell assumes back its shape. This behavior is schematized in Figure B.16.

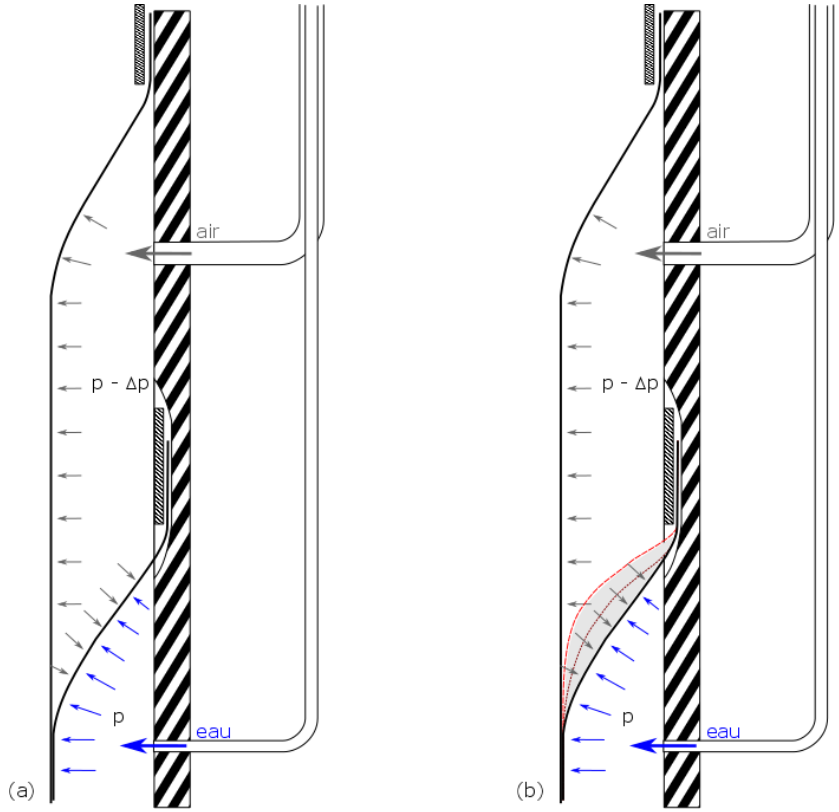

Figure B.16 – Scheme of the measuring cell longitudinal elongations that may take place when differential pressure varies (adapted from Cassan (2005))

B.4.5 Photos of the central measuring cell

The previously described phenomena was investigated by inflating the central measuring cells inside transparent plexiglass tubes of different diameters. As the central cells were inflated against external atmospheric pressure, the pressure inside the measuring cell is equivalent to the differential pressure ($P_{water} - P_{atm} = P_{diff}$). Thus, changing the measuring cell pressure allows simulating changes in the differential pressure. Plotting the volume against the pressure (in this case, representing the differential pressure) enables an evaluation of the sensitivity of the measured volume to variations of the differential pressure. At each change in probe pressure, a photo was taken, which helps understanding the origin of the problem. The assembled photo board is presented in Figure B.17. It appeared that the central cell extremities suffer longitudinal stretches, which constitute an important source of measurement error. As differential pressure variations may be random, this uncertainty cannot be corrected (as by calibration tests).

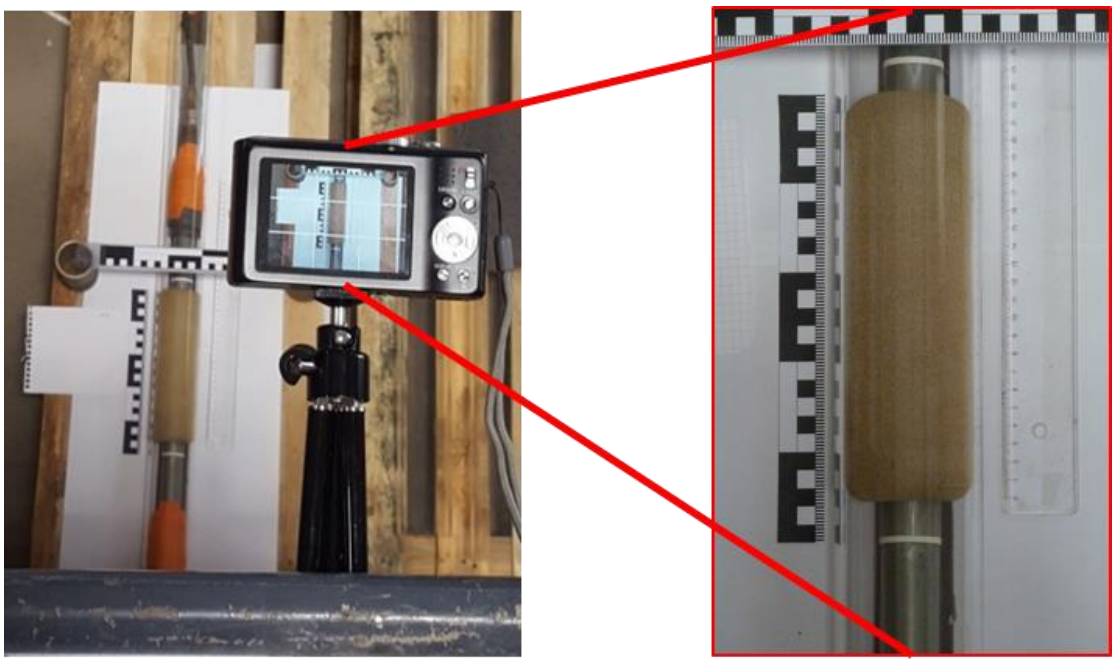

Figure B.17 – Scheme of the photo board for capturing the behavior of the central cells

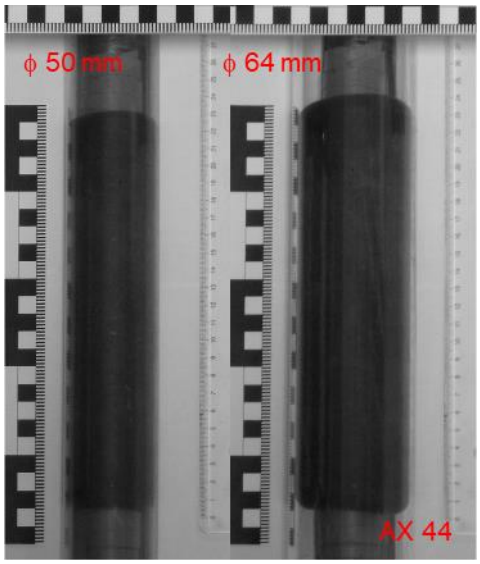

Figure B.18: Probe type Ménard AX 44 inflated inside transparent plexiglass tubes

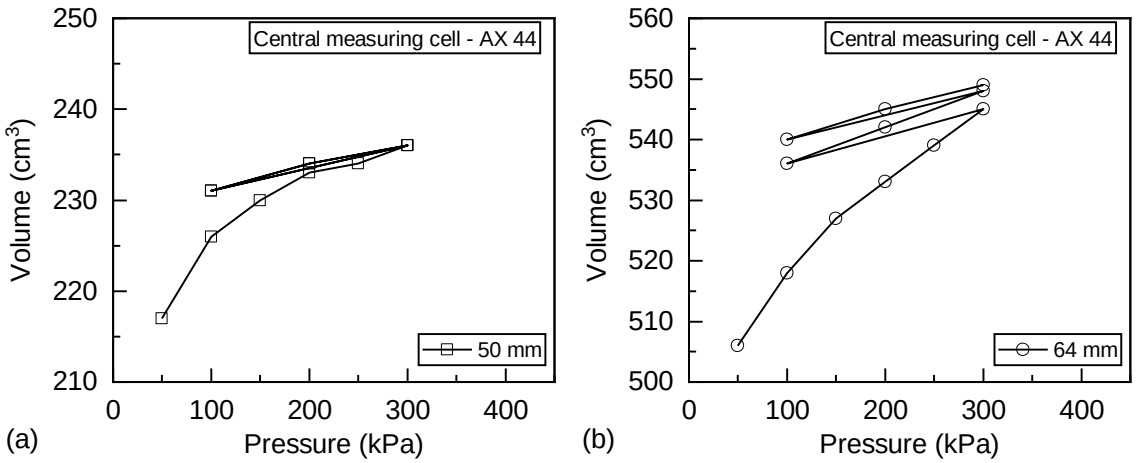

Figure B.19 – Variations of volume measurements due to pressure changes for the central cell of a Ménard type AX 44 probe inflated into transparent plexiglass tubes.

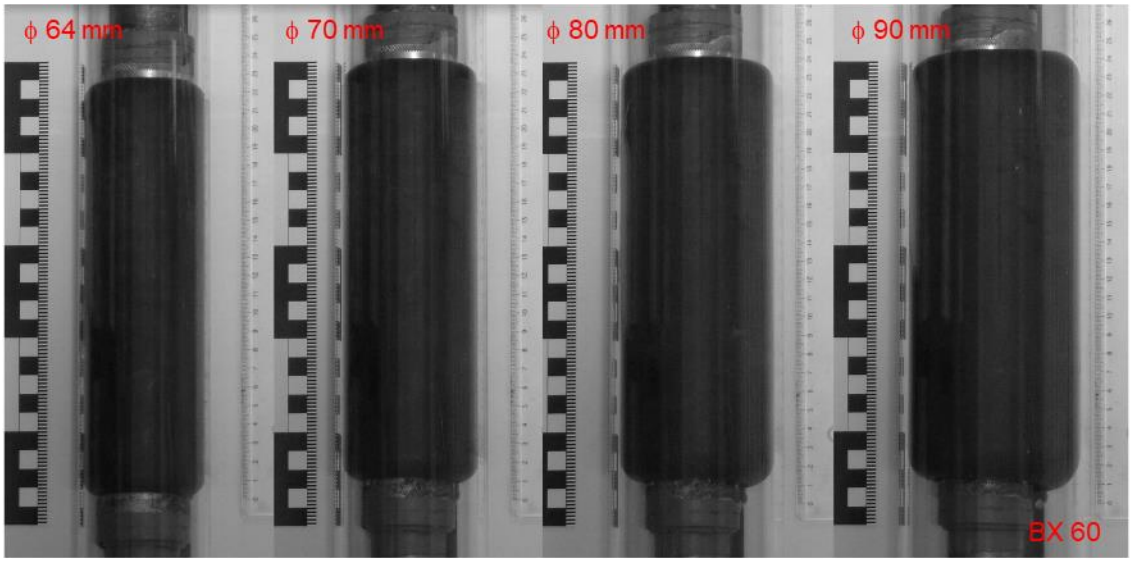

Figure B.20 – Probe type Ménard BX 60 inflated inside transparent plexiglass tubes

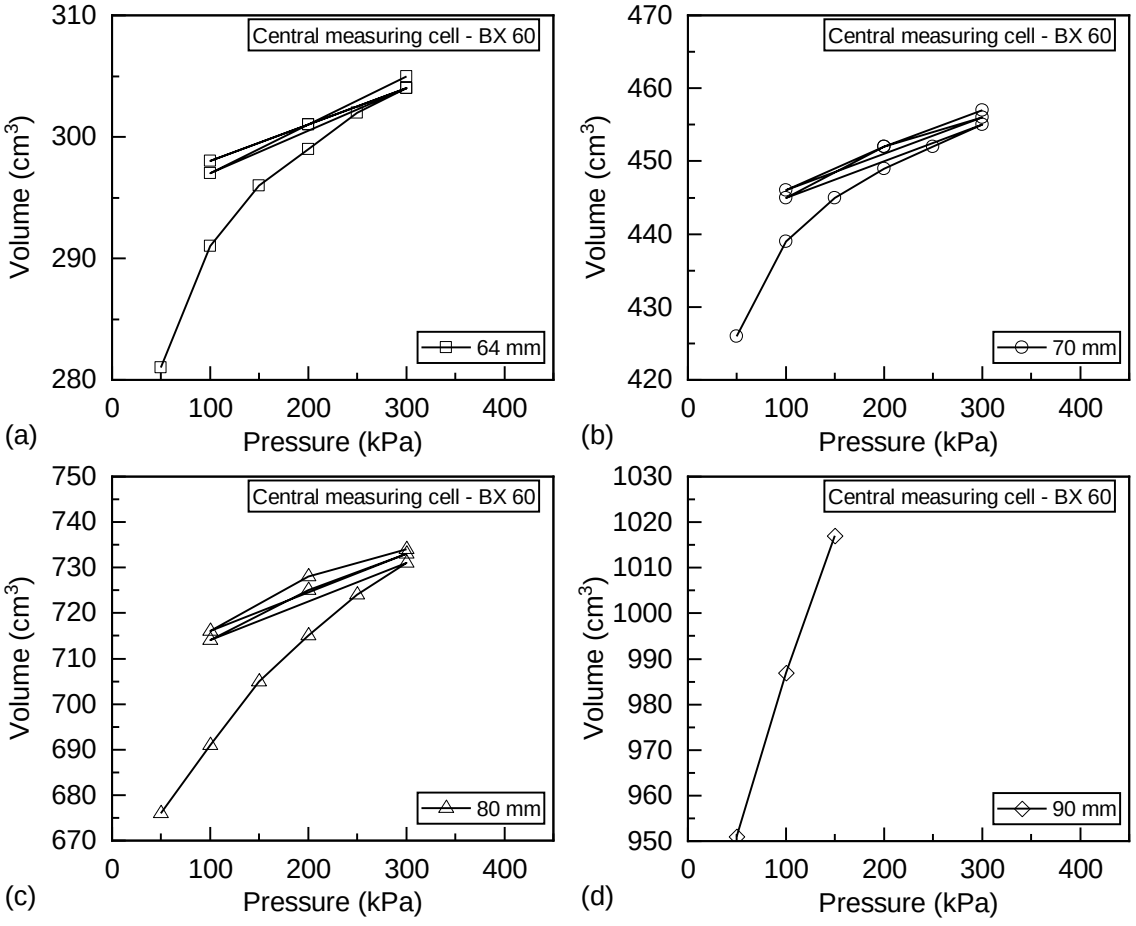

Figure B.21 – Variations of volume measurements due to pressure changes for the central cell of a Ménard type BX 60 probe inflated into transparent plexiglass tubes.

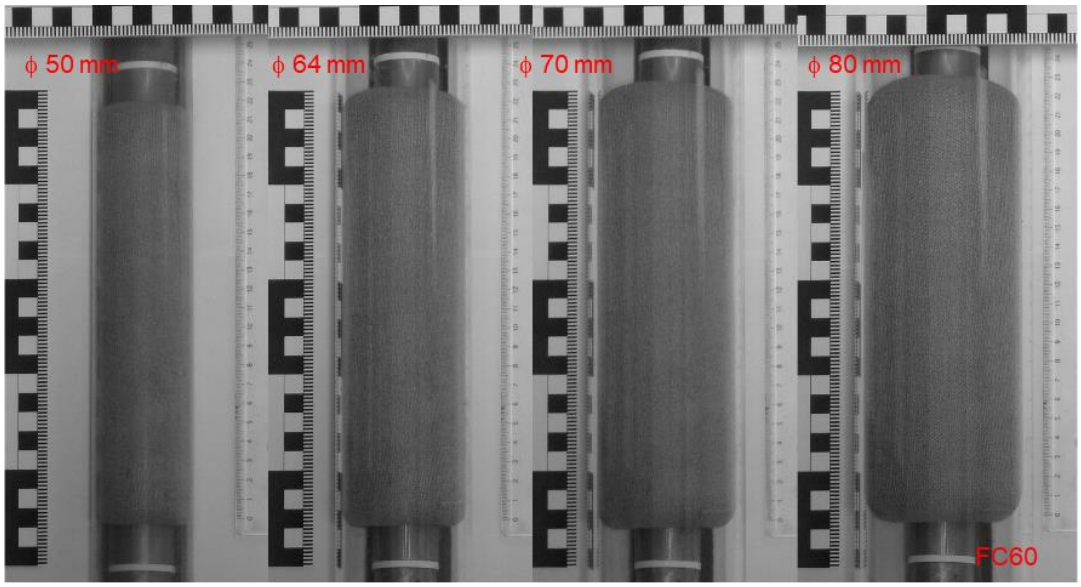

Figure B.22 – Probe type Ménard BX 60 inflated inside transparent plexiglass tubes

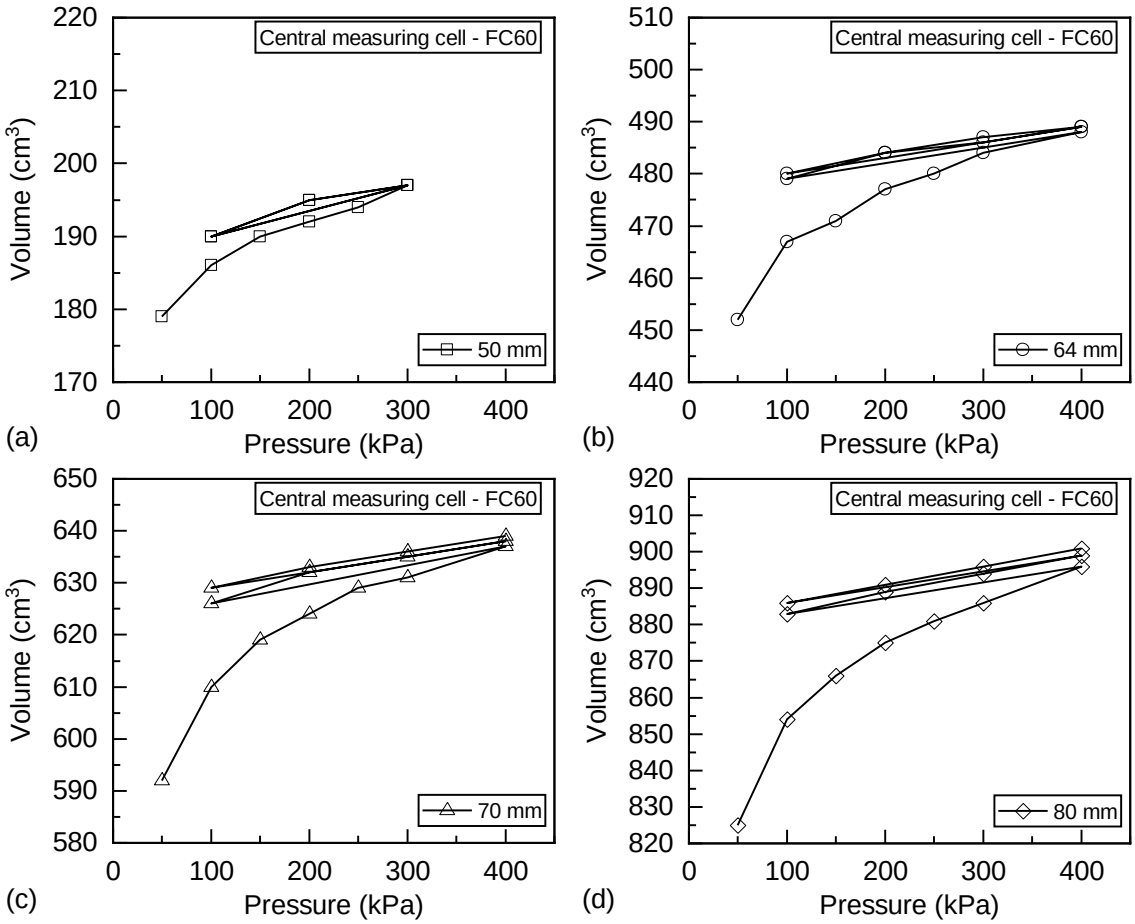

Figure B.23 – Variations of volume measurements due to pressure changes for the central cell of a FC60 type probe inflated into transparent plexiglass tubes.

In the above graphics, the slope dV/dP_{diff} represents the variation in volume measurements due to changes in differential pressure, at a constant external diameter. The following conclusions can be drawn:

- At constant external diameter, the measuring cell volume can fluctuate if the differential pressure varies. The results presented in Figure B.15 show dV/dp_{diff} = 7 cm^3/100 kPa at an average volume of 650 cm^3 (85 mm external diameter). This confirms that the relationship between the cell volume and the probe's external diameter is very sensible to variations in differential pressure;
- All the probes present variations of volume as the differential pressure varies. This is an intrinsic problem to the tri cellular probes;
- The higher is the cell volume, the most pronounced is the uncertainty. This happens because there is a bigger span between the membranes and the probe core, which gives more free space for the membrane to oscillate;
- Deflation and re-inflation do not follow the same path as the first inflation. There is a kind of "hardening" behavior;
- The analysis of the series of photos showed that this "hardening" is probably due to the interaction between the membrane and the plexiglass tube. In an assembled probe, it is probable that the central cell membrane will interact with the external sheath, but this experiment does not enable evaluating the rubber-to-rubber interaction.
- The magnitude of the volume variation in function of variation in differential pressure (dV/dp_{diff}) obtained with the BX probe in this simplified experiment is the same as that obtained during calibration tests using the fully assembled probe.
- Probe FC60 presented the lower dV/dp_{diff} values. This confirms that the restraining sheath contributes to minimize longitudinal elongations in the measuring cell.

B.5 GENERAL CONCLUSIONS FROM THE QUALIFICATION TESTS

The following main aspects regarding the measurement quality can be drawn from the qualification tests performed:

- Tubing compressibility does not seem to add uncertainty to measurements, independently on the tubing length. However, the data collected does not enable separating the tubing behavior from that of the whole system (probe + tubing + controller), which implies that the calibrations must be systematically performed for the fully assembled system. Changing any of its components (probe, tubing or controller) implies recalibrating the whole system.
- Tubing length, however, can be a source of uncertainty for two other reasons:
  - Temperature effects, which cannot be accounted for in calibration, since temperature changes may be random at the working site;
  - Water head losses, which will depend on the viscosity of the fluid being used (water or water with anti-freeze fluid) and on the temperature, and thus cannot be calibrated;
- Water head losses, associated to an imposed differential pressure during the entire test, are a critical aspect when using long tubing, especially in cold weather, since water viscosity is bigger at lower temperatures. This association ends up by imposing a maximum passing flow rate through the tubing. For solving this problem, priority should be given for tubing of larger diameters (at least 4 mm or larger) and working with absolute pressure (suppressing the tri cellular principle and the differential pressure).
  - If water flows slower than gas, it is likely that the guard cells will be pressurized faster than the measuring cell. This results in a probe that first expands by the action of gas pressure, and the measuring cell that catches it up after. This results in false readings of cavity volume that cannot be perceived by the operator at the ground level;
- The operational principle of the tri cellular probes presents serious drawbacks for tests including unload and reload paths. Critical sources of uncertainty are:

- Poor repeatability due to gas dissolution in water during pressurization, which makes the volumeter readings randomly deviate from zero in repeated tests. The magnitude of this error was evaluated in this study to reach up to 6 cm^3;
- Difficulties in keeping the differential pressure constant during a test, and especially during pressure increase or decrease. This point can add severe uncertainty to the test, because even small variations in the differential pressure can cause longitudinal elongations in the measuring cell, resulting in volume changes and in loss of the relation between the cell volume and its diameter. The magnitude of this error was observed to reach up to 7 cm^3/100 kPa p_{diff};
- Given the order of magnitude of the random error in volume measurement there is an impossibility to obtain a reliable relationship between the volume injected into the probe and its external diameter. Errors induced by variations in differential pressure are random and cannot be corrected through calibration tests. Yet, it is likely that these errors could not be avoided considering the numerous factors that trigger them: water flow-rate, tubing length, current volume of the measurement cell, rate of loading, membrane quality and others;
- Tri cellular probes were designed for operating under pressure-controlled procedures. Using these probes for performing volume-controlled procedures is difficult because it would require retro-controlling the gas pressure according to the response in water pressure

APPENDIX C.

IN SITU TEST RESULTS

C.1 DUNKIRK SITE

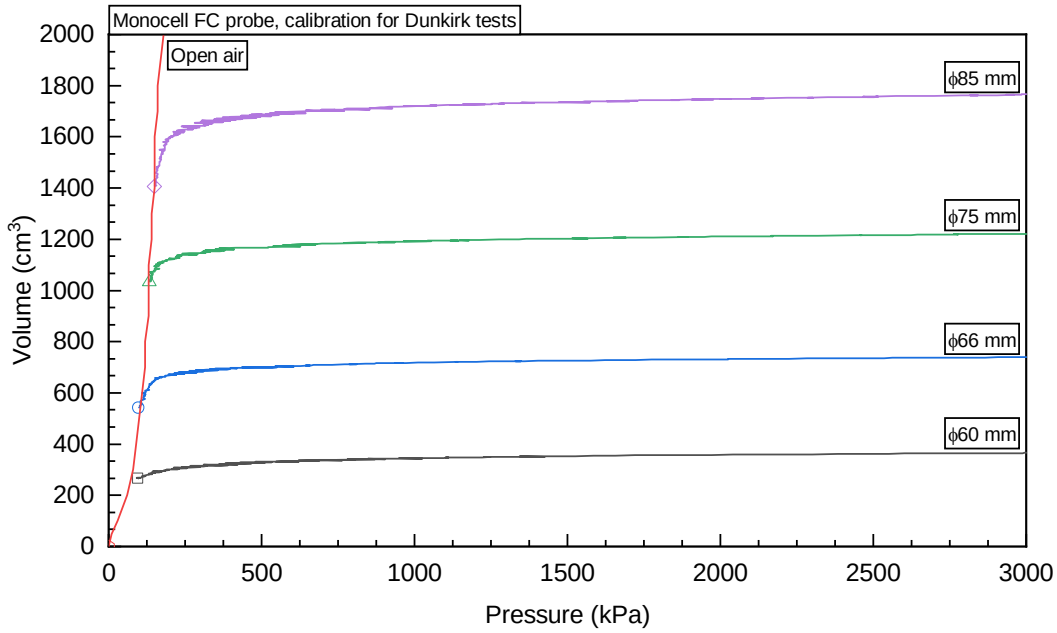

Figure C.1 – Calibration of the Monocell FC probe previous to the Dunkirk site tests

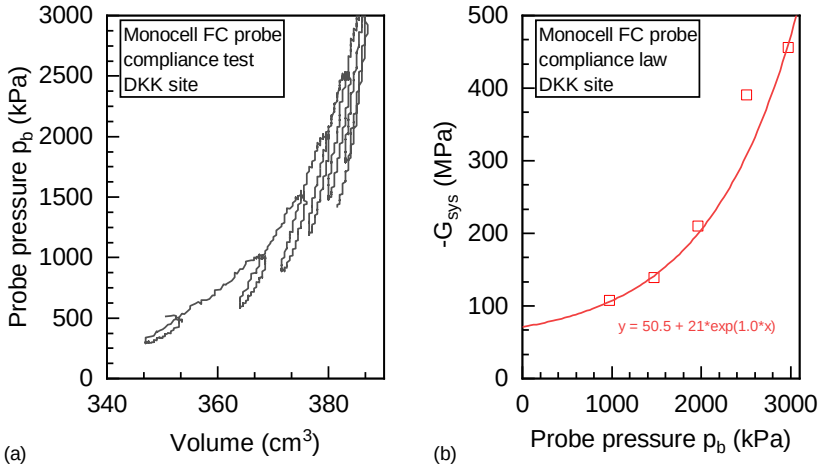

Figure C.2– (a) Compliance test in Dunkirk site; (b) compliance law established

C.1.1 Borehole BH1

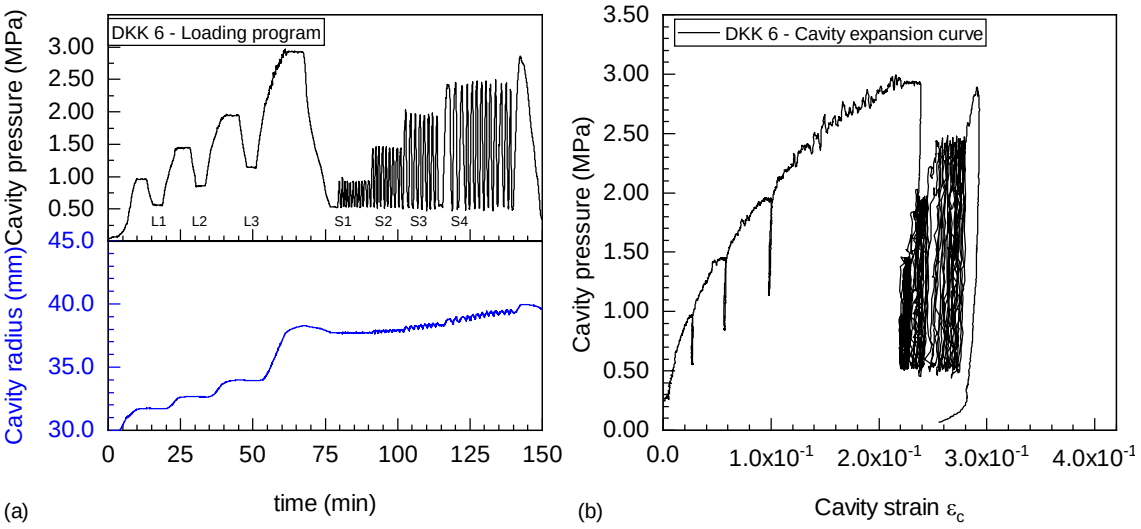

Figure C.3 – Loading program and cavity expansion response of test DKK 6

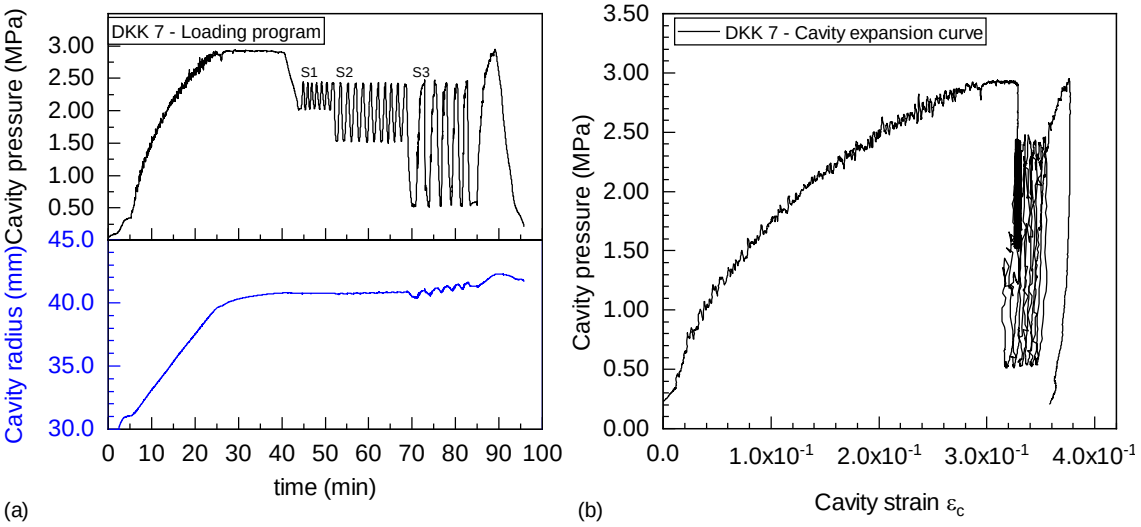

Figure C.4 – Loading program and cavity expansion response of test DKK 7

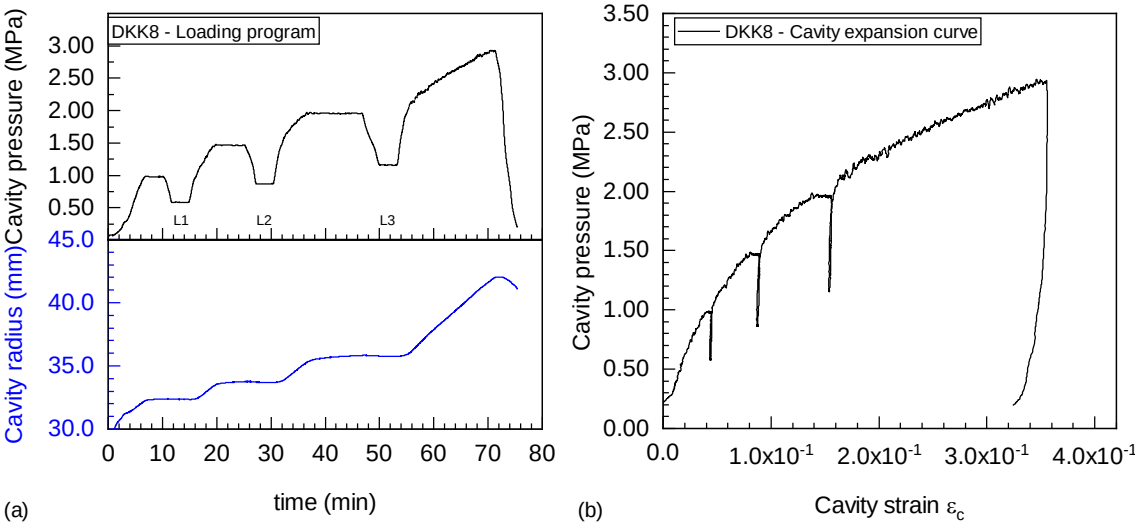

Figure C.5 – Loading program and cavity expansion response of test DKK 8

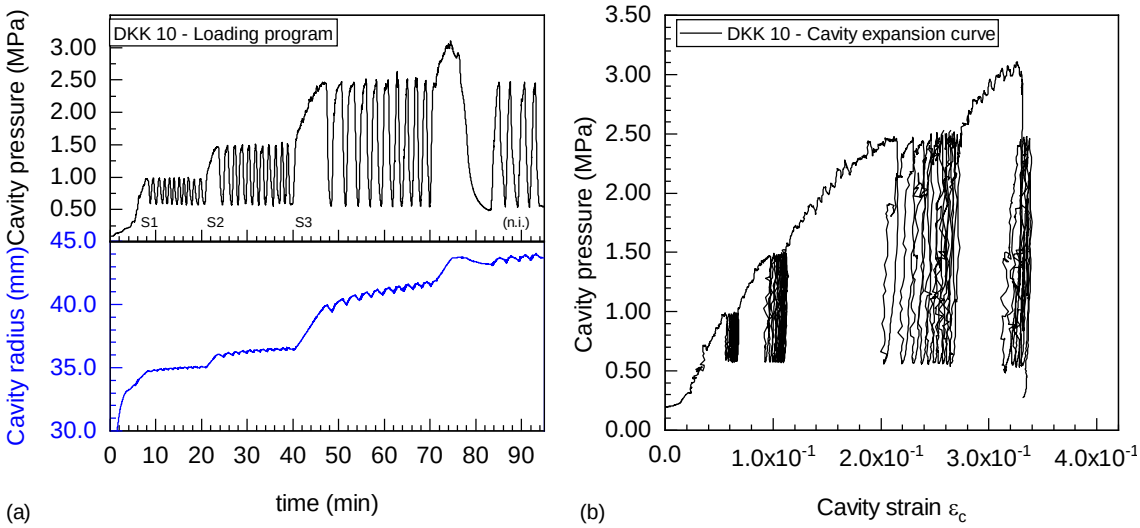

Figure C.6 – Loading program and cavity expansion response of test DKK 10

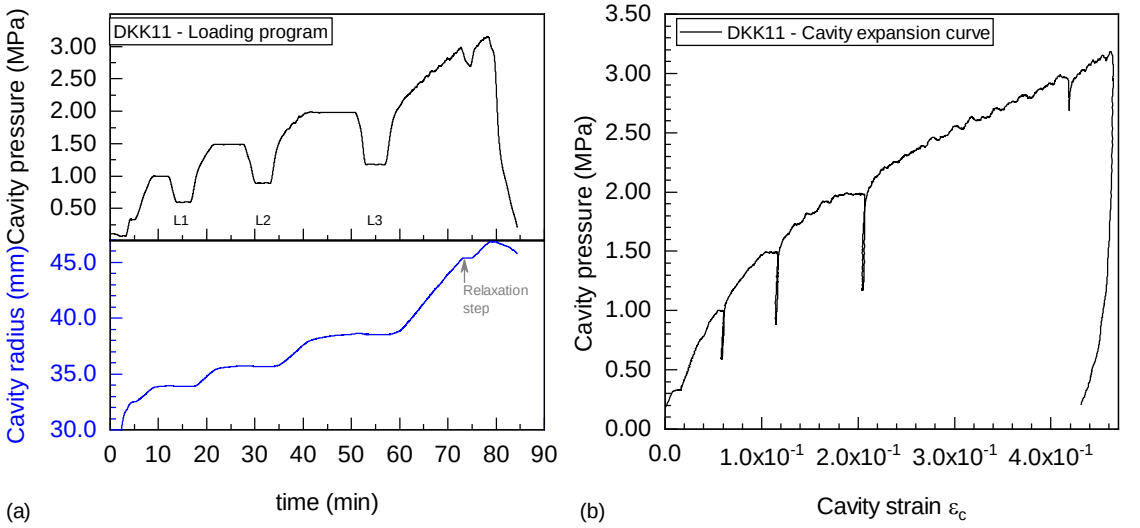

Figure C.7 – Loading program and cavity expansion response of test DKK 11

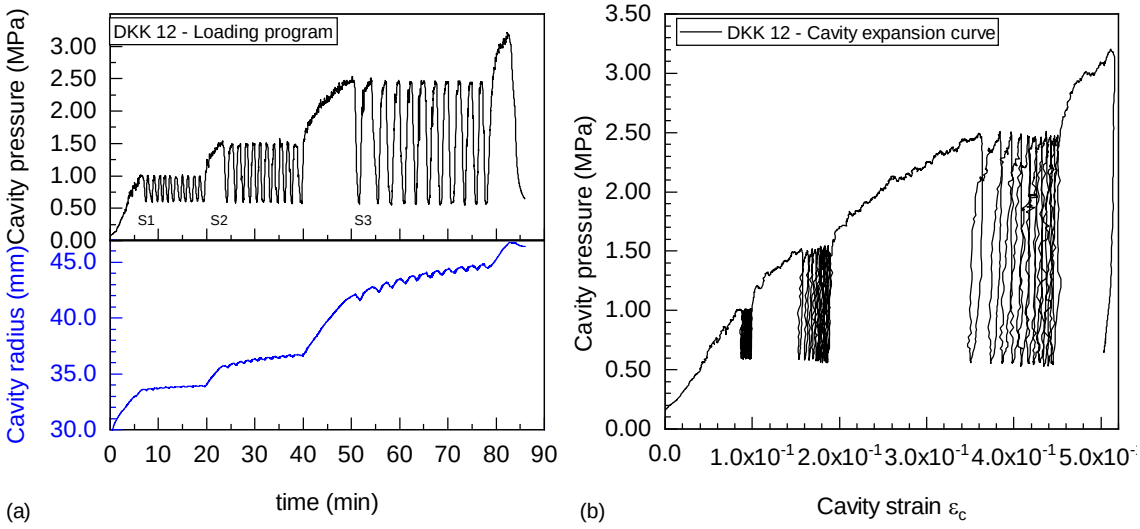

Figure C.8 – Loading program and cavity expansion response of test DKK 12

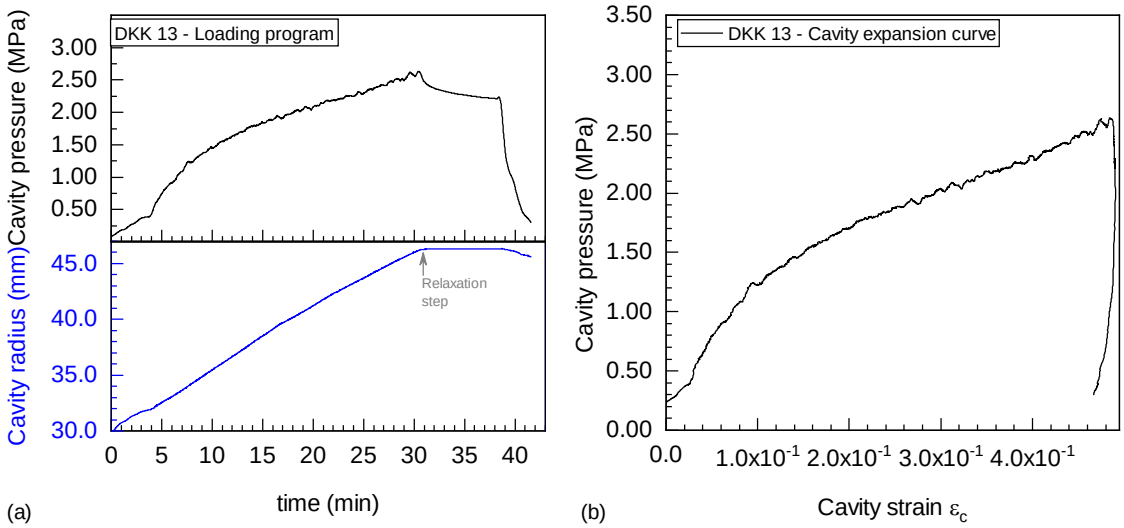

Figure C.9 – Loading program and cavity expansion response of test DKK 13

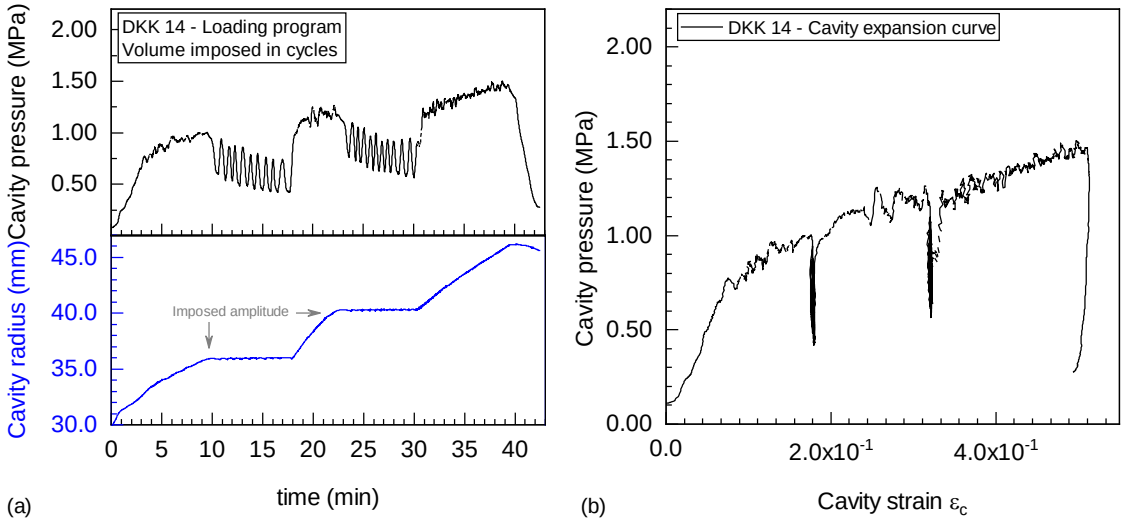

Figure C.10 – Loading program and cavity expansion response of test DKK 14 (not interpreted)

C.2 MERVILLE SITE

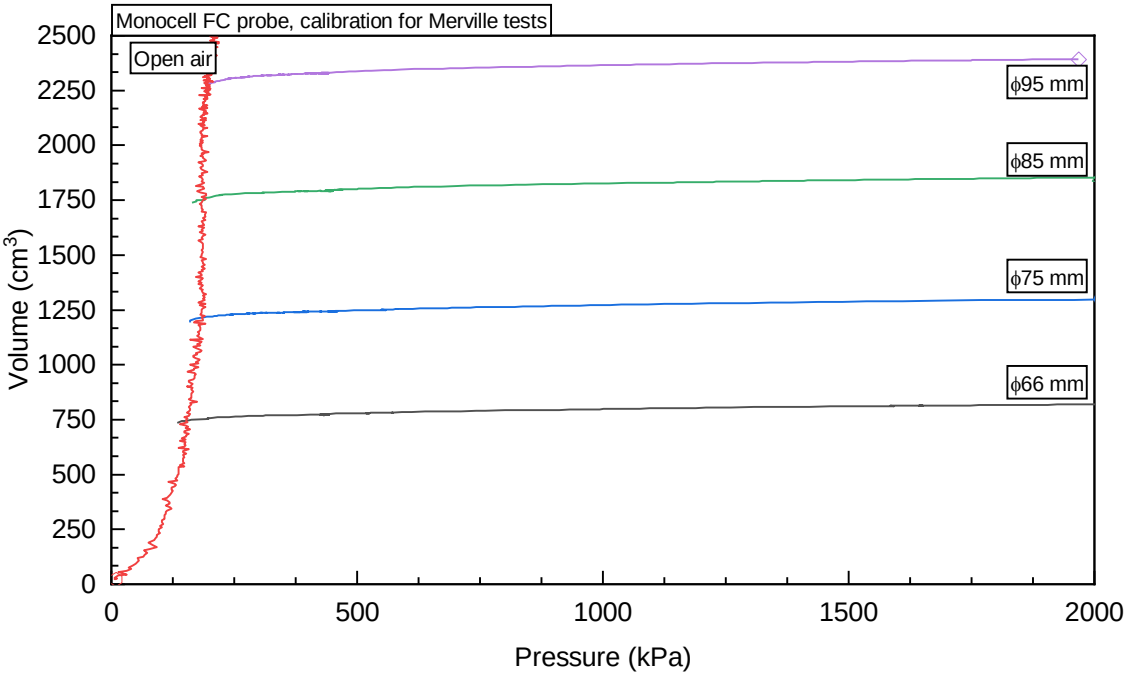

Figure C.11 – Calibration of the Monocell FC probe previous to the Merville site tests

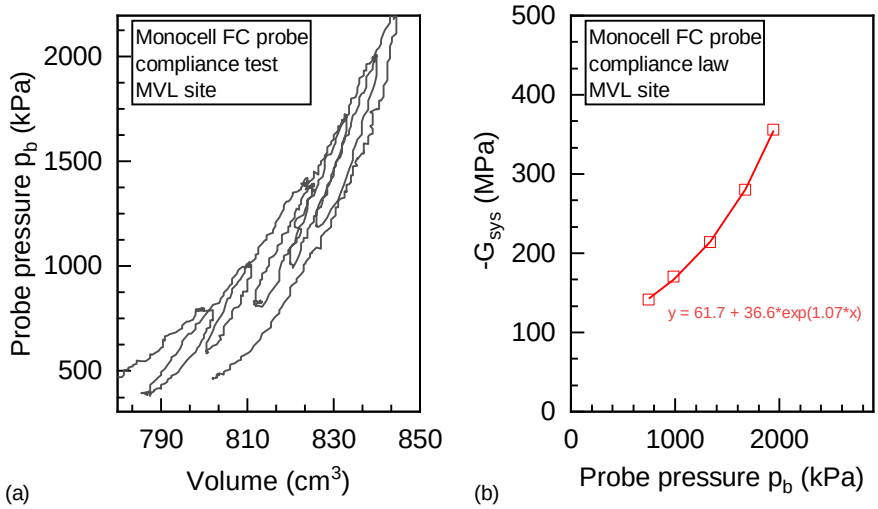

Figure C.12 – (a) Compliance test in Merville site; (b) compliance law established

C.2.1 Borehole BH1

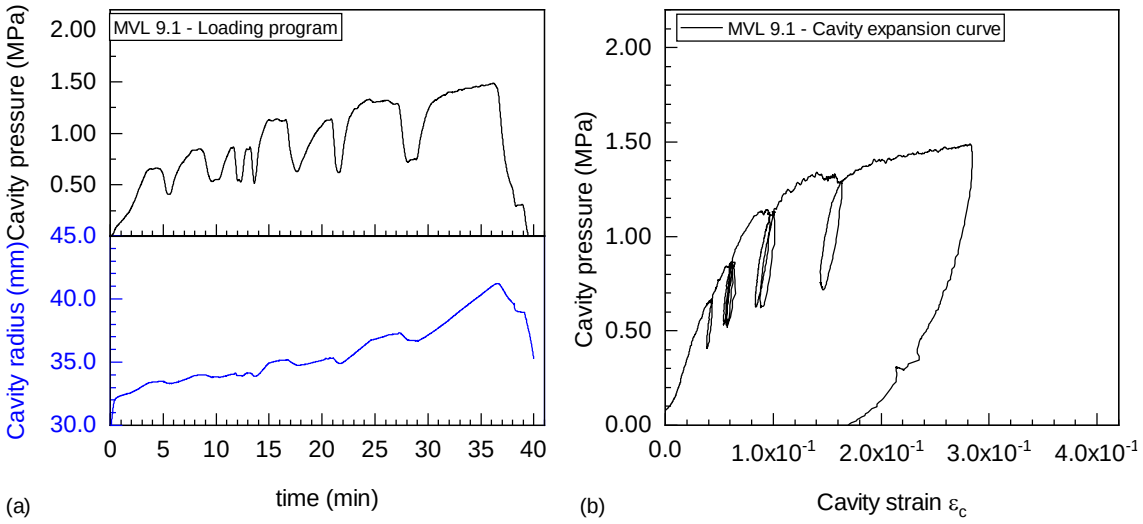

Figure C.13 – Loading program and cavity expansion response of test MVL 9.1

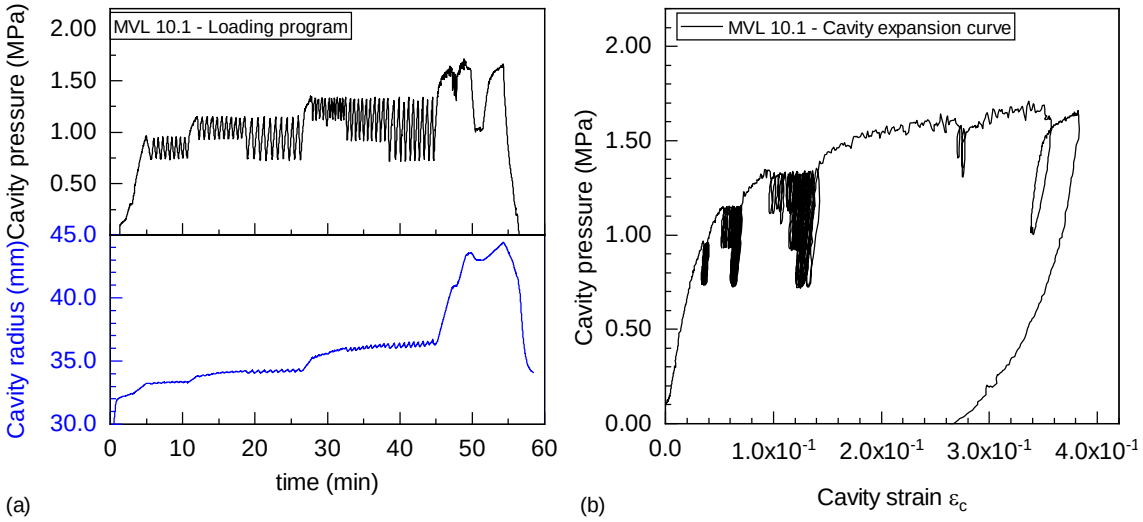

Figure C.14 – Loading program and cavity expansion response of test MVL 10.1

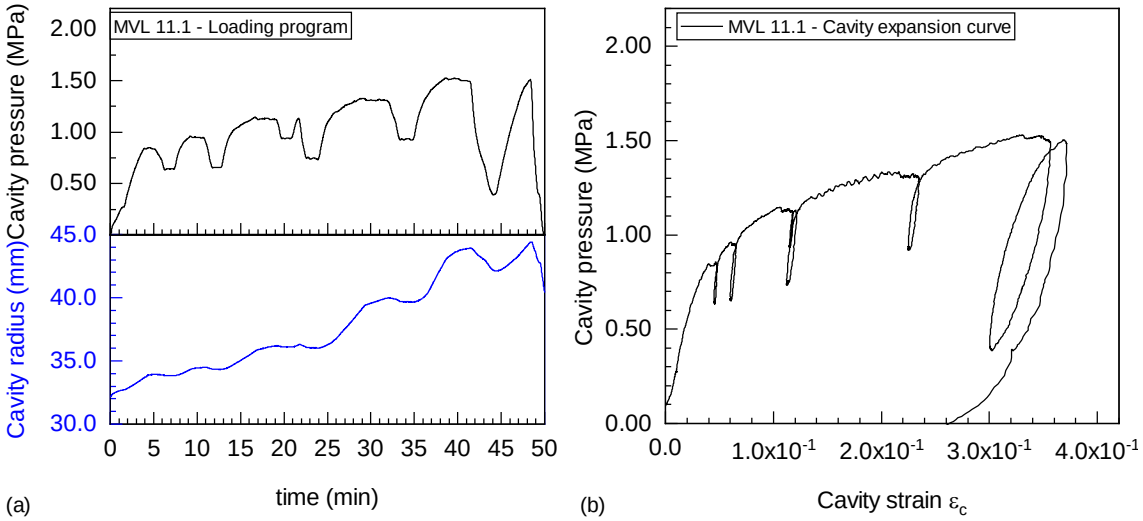

Figure C.15 – Loading program and cavity expansion response of test MVL 11.1

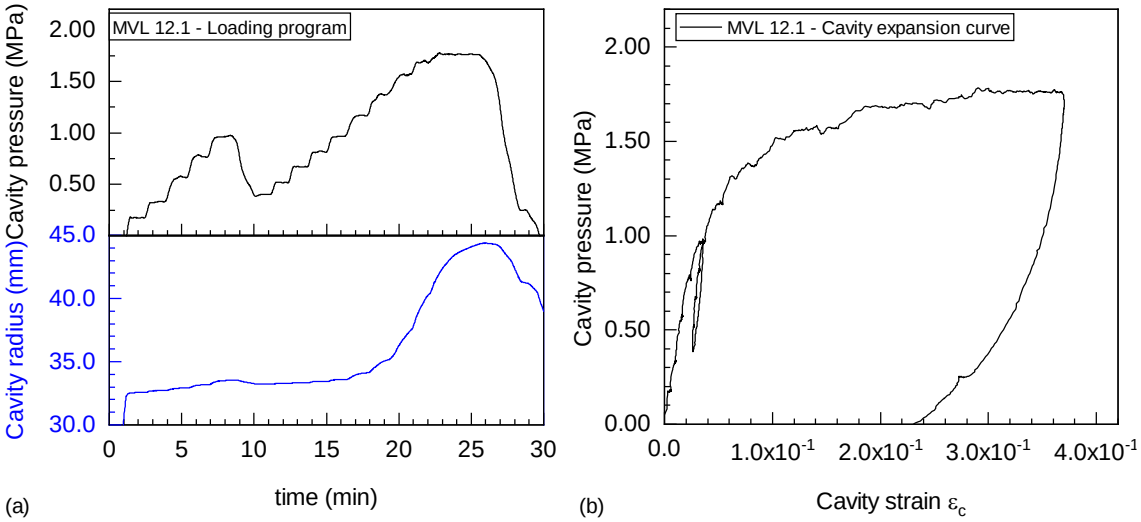

Figure C.16 – Loading program and cavity expansion response of test MVL 12.1

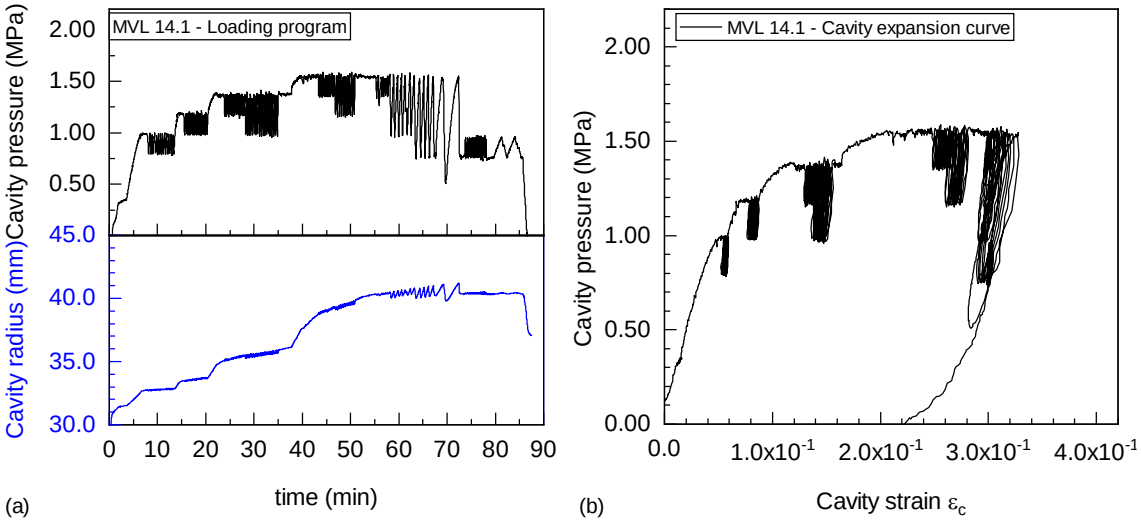

Figure C.17 – Loading program and cavity expansion response of test MVL 14.1

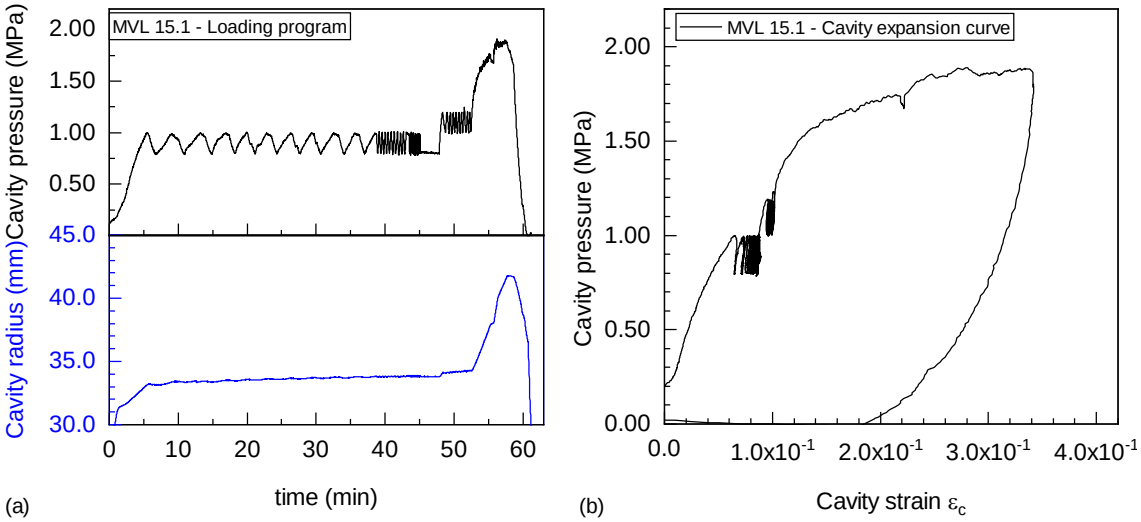

Figure C.18 – Loading program and cavity expansion response of test MVL 15.1

C.2.2 Borehole BH2

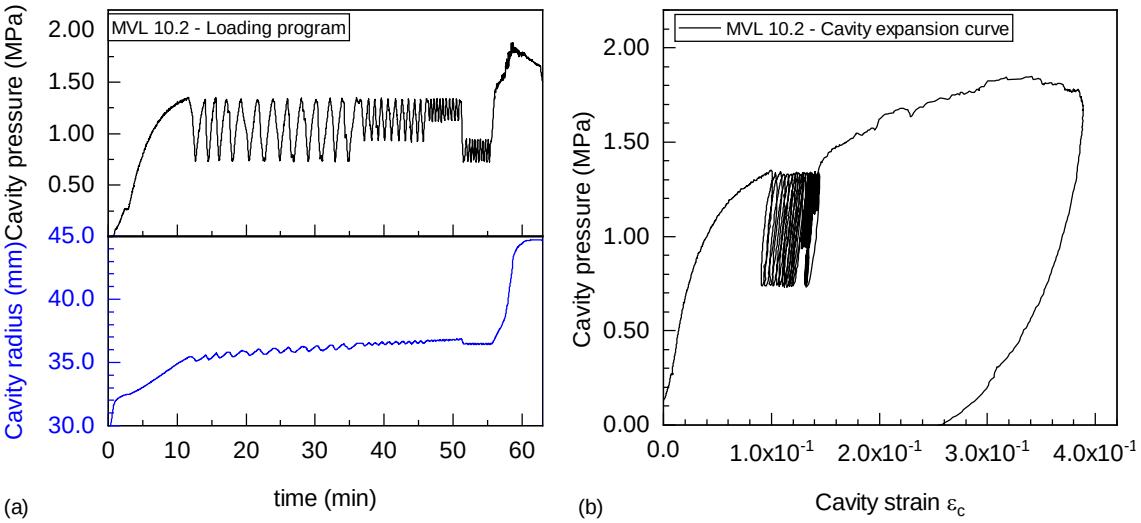

Figure C.19 – Loading program and cavity expansion response of test MVL10.2

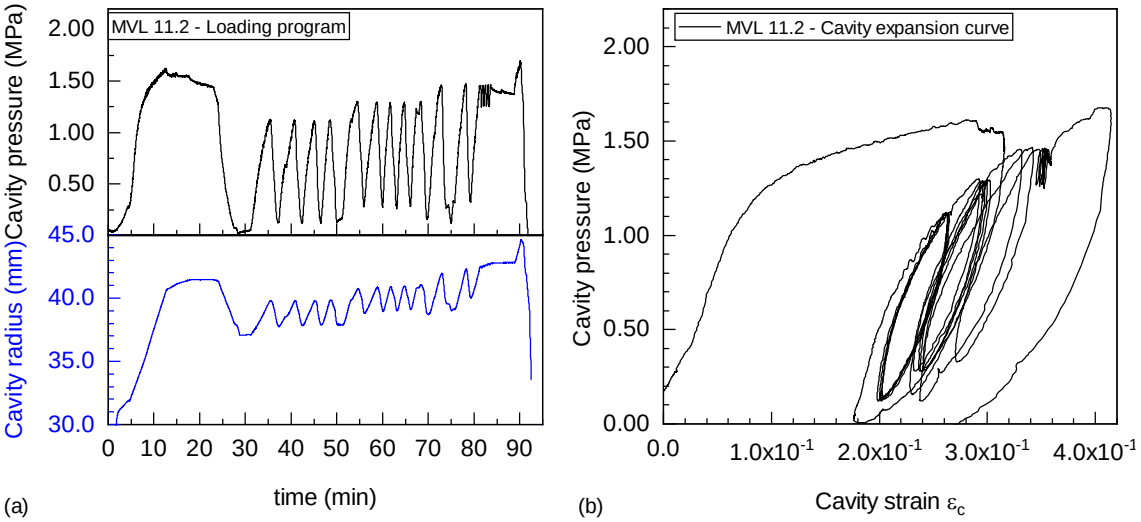

Figure C.20 – Loading program and cavity expansion response of test MVL 11.2

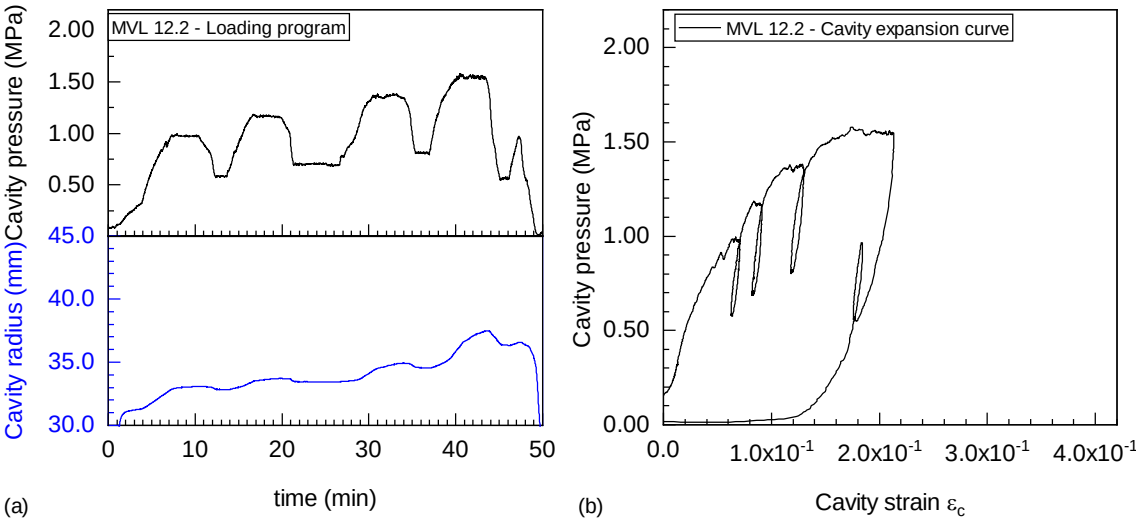

Figure C.21 – Loading program and cavity expansion response of test MVL 12.2

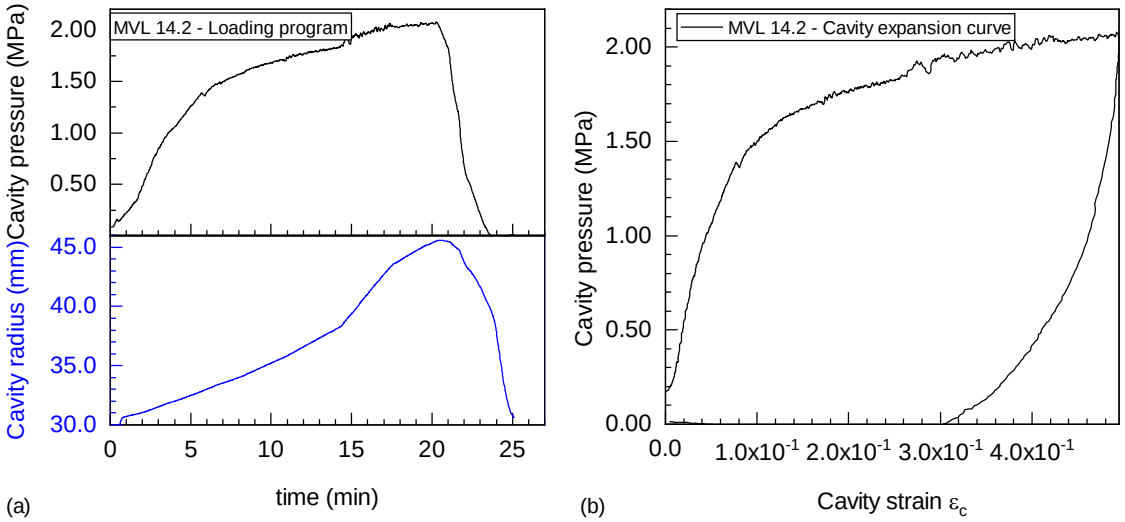

Figure C.22 – Loading program and cavity expansion response of test MVL 14.2